

Newcastle
University

School of
Civil Engineering
& **Geosciences**

An inverse predictive model for the design of functional textiles

A thesis submitted for the degree

Doctor of Philosophy

In the School of Civil Engineering and Geosciences

At the University of Newcastle upon Tyne

By

Christopher Iliffe

June 2016

Abstract

Coated woven fabrics are used for large scale structures including airports and sports stadia. Manufacturers produce a range of fabrics from which a single fabric is selected by the structural engineer based on design criteria such as stiffness, weight, strength and formability. Designs must therefore utilise a fabric with properties which may not be optimal for that particular application. This thesis develops and tests a model that allows a bespoke coated woven fabric to be designed with specified mechanical properties such as tensile stiffness, Poisson's ratio and shear stiffness.

A method is developed to 'invert' an existing predictive mechanistic 'unit cell' model using the derivatives of the equations defining the unit cell. The existing model is altered to enable the prediction of shear characteristics in addition to tensile properties by the inclusion of the coating using a finite element representation. The 'inverse' model is shown to accurately design a fabric for specific and attainable targets of Young's modulus, Poisson's ratio, and shear stiffness which have been derived using the predictive model for various fabric stress states.

The effect of variability in fabric parameters on the tensile response of a fabric is considered using both Monte Carlo and FORM analysis. The sensitivity of the fabric response to biaxial loading is calculated using the direction cosines defined in the FORM methodology. The calculation of fabric sensitivity also enables a detailed investigation of the sensitivity of fabric stress-strain behaviour to variation in individual fabric parameters. A method is developed to design fabrics with mechanical properties which are robust to changes in manufacturing parameters by altering the geometry of the fabric.

The model is validated by comparing the inverse model output to unit cell model input and also to biaxial test results. The inverse model shows excellent fidelity with results calculated using the unit cell model, but fails to adequately reproduce the actual fabric geometry when target stiffness values are based on biaxial test data. A method for the removal of yarns from fabrics and tensile testing of coated fabric yarn specimens is also developed.

It is common practice to use a plane stress formulation to approximate the stress-strain response of a coated woven fabric. Comparison of the model output with biaxial test results necessitated the creation of a method for the calculation of fabric tensile stiffness at multiple stress states instead of a single set of elastic constants. This approach takes into account the complex nonlinear behaviour of architectural fabrics by considering the variation in stress-strain behaviour at different biaxial stress states.

The final inverse model provides a novel tool for the design of coated woven fabric with prescribed mechanical responses at multiple stress states that is robust to variations in its constituent parameters, with scope for future application in textile architecture, medical textiles and industrial textiles.

Acknowledgements

I would like to thank my supervisors Ben Bridgens and Peter Gosling for their continual support, direction and understanding and Nicola Smithies and Alex Colman for their patience and help at the start and end of this project. Additionally I would like to thank William Cragie, Fred Beadle and Stuart Patterson for their assistance in Laboratory testing. Further I would like to thank the Engineering and Physical Sciences Research Council and the School of Civil Engineering and Geosciences for their funding of this project.

Lastly I would like to thank Nicola Iliffe and my parents, without whose unconditional encouragement and endless support I would never have started, let alone finished, this thesis.

Outline Contents

1. Introduction
 - 1.1. Context
 - 1.2. Aims and Objectives
 - 1.3. Outline Method
 - 1.4. Scope
 - 1.5. Structure of Thesis
 - 1.6. Publications
 - 1.7. Awards
2. Literature review
 - 2.1. Architectural fabrics
 - 2.2. Features of coated woven fabrics
 - 2.3. Types of fabric model
 - 2.4. Optimisation
 - 2.5. Statistical analysis and robustness of fabrics
3. Predictive model for the design of fabrics (Sawtooth)
 - 3.1. Introduction
 - 3.2. Aim
 - 3.3. The simple spring and arm case
 - 3.4. Sawtooth model inversion
 - 3.5. Implementation
 - 3.6. Yarn strength
 - 3.7. Model checking and initial validation
 - 3.8. Conclusions

- 4. Variability and robustness
 - 4.1. Introduction
 - 4.2. Aim
 - 4.3. Objectives
 - 4.4. Chapter overview
 - 4.5. Initial assumptions
 - 4.6. Normally distributed data
 - 4.7. Monte Carlo methodology
 - 4.8. FORM methodology
 - 4.9. Comparison of failure points
 - 4.10. Robust design of a fabric
 - 4.11. Discussion of application of the reliability index
 - 4.12. Conclusions
- 5. Model validation
 - 5.1. Model validation
 - 5.2. Methodology for testing of fabrics
 - 5.3. Validation study
 - 5.4. Structural design study
- 6. Conclusions and recommendations for future work
 - 6.1. Conclusions
 - 6.2. Recommendations for future work
- 7. Glossary
- 8. References
- A. Appendix

Contents

1. Introduction	1
1.1. Context	2
1.1.1. Background	2
1.1.2. Fabric modelling.....	5
1.2. Aims and Objectives	8
1.2.1. Aims.....	8
1.2.2. Objectives.....	8
1.3. Motivation	9
1.4. Outline method	14
1.5. Scope	15
1.6. Structure of Thesis.....	16
1.7. Publications	17
1.8. Awards	17
2. Literature Review.....	18
2.1. Architectural fabrics	19
2.1.1. Need for this work	19
2.1.2. Previous work.....	20
2.1.3. Further architectural and structural applications.....	20
2.1.4. Medical applications	21
2.2. Features of coated woven fabrics	22
2.2.1. Fibre geometry and properties	22
2.2.2. Yarn geometry and properties	29
2.2.3. Coating properties	34
2.2.4. Fabric Weaves	38
2.2.5. Creep and cyclic loading.....	40

2.2.6.	Fabric Manufacture	42
2.2.7.	Coated fabrics: Classification and response	43
2.2.8.	Uncoated fabrics: Classification and response	60
2.3.	Types of fabric model	61
2.3.1.	Biaxial and Uniaxial stress-strain behaviour representation	61
2.3.2.	Fabric modelling	65
2.3.3.	Summary, review and discussion of models	89
2.4.	Optimisation	91
2.4.1.	Stochastic and deterministic optimisation	91
2.4.2.	Overview of optimisation	91
2.5.	Statistical analysis and Robustness of Fabrics	103
2.5.1.	Correlation	103
2.5.2.	Robustness	105
3.	Predictive model for the design of architectural fabrics	109
3.1.	Introduction	110
3.2.	Aim	112
3.3.	The simple spring and arm model	113
3.3.1.	Modelling the spring and arm model	115
3.4.	Sawtooth model inversion	117
3.4.1.	The sawtooth model	117
3.4.2.	Inverting a simplified sawtooth model	123
3.4.3.	Full Sawtooth	129
3.5.	Implementation	150
3.5.1.	Sawtooth model	150
3.5.2.	Objective function	153
3.5.3.	Simple sawtooth	154
3.5.4.	Full sawtooth	157

3.6.	Yarn strength	161
3.7.	Model checking and initial validation	165
3.7.1.	Results for known feasible biaxial targets	165
3.7.2.	Results for known feasible shear targets.....	177
3.7.3.	Discussion of results.....	180
3.8.	Conclusions.....	183
4.	Variability and Robustness of Fabric Geometry and Constituent Parameters	184
4.1.	Introduction.....	185
4.2.	Aim.....	185
4.3.	Objectives.....	185
4.4.	Chapter overview	186
4.5.	Initial Assumptions	187
4.6.	Normally distributed data	189
4.7.	Monte Carlo Methodology:.....	194
4.7.1.	Methodology.....	194
4.7.2.	Constraint compliant Monte Carlo	201
4.7.3.	Analysis and discussion	204
4.8.	FORM Methodology:.....	217
4.8.1.	Background	217
4.8.2.	Methodology.....	219
4.8.3.	Constraint compliant FORM.....	224
4.8.4.	Example Results	227
4.9.	Comparison of failure points.....	229
4.10.	Robust design of a fabric	238
4.11.	Discussion of application to the reliability index.....	254
4.12.	Conclusions.....	259
5.	Model Validation	261

5.1.	Model validation.....	262
5.2.	Methodology for testing of fabrics.....	263
5.2.1.	Uniaxial testing.....	263
5.2.2.	Biaxial testing	265
5.2.3.	Yarn mechanical properties	294
5.2.4.	Tensile strength.....	310
5.3.	Validation study.....	311
5.3.1.	Comparison to known feasible targets	311
5.3.2.	Fabric design for five sets of targets	312
5.3.3.	Reducing model constraint by reducing the number of targets:	332
5.3.4.	Discussion of designed fabrics	335
5.3.5.	Robust fabric design.....	337
6.	Conclusions and Recommendations for future work.....	343
6.1.	Research Summary	344
6.2.	Conclusions.....	345
	To complete a full and in depth review of the state of the art of fabric modelling, design and analysis:	345
	Formulate an inverse material model:	345
	Incorporate variability of material parameters into the model and assess sensitivity of the resultant design:.....	346
	Complete a validation study:	347
	To attempt a structural design study using an FE simulation of a true structural design case:.....	348
6.3.	Recommendations for future work.....	349
	Inclusion of a yarn model	349
	Sinusoidal model.....	349
	Powerful computing	349
	Non-rectangular Geometry	350

Non-plain weave fabrics	350
Improvement to the shear model	350
Use in a finite element program.....	350
Structural design case study	351
Contents	351
7. Glossary.....	352
7. References	358
A. Appendix.....	372

Figures

Figure 1-1: Munich 1972 Olympic stadium roof (Tensinet, 2015)	2
Figure 1-2: The three principal anticlastic shapes. Reproduced from Bridgens <i>et al.</i> (2009)	3
Figure 1-3: Dynamic Earth Centre (Edinburgh) (Tensinet, 2015).....	4
Figure 1-4: De Montil NV (Belgium) (Tensinet, 2015).....	4
Figure 1-5: Finite element representation of filaments in shear (Durville, 2010).....	6
Figure 1-6: “Three-dimensional rendering of yarns within a unit cell” used by Glaessgen <i>et al.</i> (1996)	6
Figure 1-7: Finite element model of a Hypar (initial form found configuration) (Pargana <i>et al.</i> , 2010)	6
Figure 1-8: Standard Conic construction.....	9
Figure 1-9: Hypar geometry (Gosling <i>et al.</i> , 2013).....	11
Figure 1-10: Deformation of the Hypar under snow load (Plan)	12
Figure 1-11: Deformation of the hypar under snow load. Original (blue) and deformed geometry (grey).....	12
Figure 1-12: Fundamental sawtooth unit cell (Bridgens and Gosling, 2008)	14
Figure 2-1: Tensioning of a conic structure	19
Figure 2-2: PTFE-glass fibre image, in which the plys can be seen (Bridgens <i>et al.</i> , 2004)	22
Figure 2-3: Classification of technical yarns according to raw material (Alagirusamy and Das, 2010).....	23
Figure 2-4: Symbolic representation of Polyamide 6.6. (Osswald and Menges, 1996) ..	24
Figure 2-5: Symbolic representation of an Aramid (Osswald and Menges, 1996)	24
Figure 2-6: Effect of fibre diameter on tensile strength of fibre. Reproduced from Campbell (2010)	26
Figure 2-7: Symbolic representation of Polyethylene-terephthalate (PET) (linear polyester) (Osswald and Menges, 1996).....	27
Figure 2-8: Stress Strain responses for Glass fibres (Left) and Polyester fibres (right). Reproduced from Forster and Mollaert (2004)	28
Figure 2-9: Ply yarn. Reproduced from Alagirusamy and Das (2010).....	29
Figure 2-10: Calculation of twist angle (Lomov <i>et al.</i> , 2005; Alagirusamy and Das, 2010)	30

Figure 2-11: Microbuckling (right) and migration (left). Reproduced from Madhavan and Naik (2000)	32
Figure 2-12: F1202 warp cross section (fill yarn) (Colman, 2013a)	34
Figure 2-13: Symbolic representation of PVC (Polyvinyl chloride) (Osswald and Menges, 1996)	35
Figure 2-14: Symbolic representation of PTFE (Osswald and Menges, 1996)	36
Figure 2-15: Symbolic representation of Silicon coating (Forster and Mollaert, 2004) ..	36
Figure 2-16: Fabric weaves (BSI, 1971; WOO <i>et al.</i> , 2002; Forster and Mollaert, 2004; Rao <i>et al.</i> , 2008)	39
Figure 2-17: Polymer creep responses under constant load: Reproduced from Osswald and Menges (1996)	40
Figure 2-18: Creep Strength data for some polymers: Reproduced from Gerdeen <i>et al.</i> (2006)	41
Figure 2-19: Reduction in residual strength due to cyclic loading. Reproduced from Jones (1994)	41
Figure 2-20: Fabric Manufacture, 6m wide Loom. Reproduced from Verseidag (2011) ..	42
Figure 2-21: Crimp interchange, reproduced from (Lomov <i>et al.</i> , 2005)	48
Figure 2-22: Example of uniaxial response, reproduced from Testa <i>et al.</i> (1978). ϵ_1 and ϵ_2 are the strains in the warp and weft yarn respectively.	49
Figure 2-23: Example of nonlinearity of biaxial response, PTFE response planes produced from biaxial tests carried out on B18059 PTFE coated Glass-fibre fabric	50
Figure 2-24: Biaxial stress-strain curves for PTFE fabric (Bridgens and Gosling, 2004)..	50
Figure 2-25: simple (right) and pure (left) shear reproduced from Colman <i>et al.</i> (2014)	53
Figure 2-26: Diagram of the load–shear angle curve reproduced from Liu <i>et al.</i> (2004)	54
Figure 2-27: Test and prediction of in plane shear for a plain weave glass fabric using an FE method reproduced from Boisse <i>et al.</i> (2005a)	56
Figure 2-28: comparison between the response of coated and uncoated fabrics manufactured specifically for the tests (Skelton and Freeston, 1971)	56
Figure 2-29: Two zones that make up the Bi-linear model reproduced from Kageyama <i>et al.</i> (1988)	62

Figure 2-30: measured (dots) and fitted (line) modulus strain curve. The curves from which the fit was made are also shown (-----). Reproduced from (Lucas, 1983)	63
Figure 2-31: Biaxial response surface divided into discrete zones. Reproduced from Minami (2006).....	64
Figure 2-32: Unit cell representation (Plain Weave)	67
Figure 2-33: Geometry of circular yarns, reproduced from Peirce (1937)	69
Figure 2-34: Yarn elastic deformation, reproduced from Peirce (1937)	71
Figure 2-35: Non circular yarn geometry reproduced from Kemp (1957).....	72
Figure 2-36: The unit structure, a) unit structure, b) model, c) Notation for forces and deformation, reproduced from Kawabata <i>et al.</i> (1973)	73
Figure 2-37: The compression of a yarn, reproduced from Kawabata <i>et al.</i> (1973)	74
Figure 2-38: Model for calculating the biaxial strain characteristics, reproduced from Menges and Meffert (1976).....	75
Figure 2-39: Typical load extension diagram of coated and uncoated fabric, reproduced from Dimitrov and Schock (1986)	76
Figure 2-40: Free body diagram of the model of yarns, reproduced from Testa <i>et al.</i> (1978)	77
Figure 2-41: Typical fabric element (Stubbs and Fluss, 1980)	78
Figure 2-42: Truss model of fabric element, reproduced from Stubbs and Fluss (1980)	78
Figure 2-43: Trapezoidal lattice model (Kato <i>et al.</i> , 1999)	80
Figure 2-44: Unit cell representation of yarns (Pargana <i>et al.</i> , 2007)	81
Figure 2-45: 1:0 stress ratio comparing test (___) and model (- - -) results (Pargana <i>et al.</i> , 2007)	81
Figure 2-46: Response of crushing elements in the unit cell model produced by Pargana <i>et al.</i> (2007)	83
Figure 2-47: Sinusoidal representation of yarn cross-section, reproduced from Bridgens and Gosling (2008)	83
Figure 2-48: sinusoidal yarn model reproduced from Bridgens and Gosling (2008).....	84
Figure 2-49: Fundamental sawtooth unit cell, reproduced from Bridgens and Gosling (2008)	85
Figure 2-50: “Three-dimensional rendering of yarns within a unit cell” used by Glaessgen <i>et al.</i> (1996)	87

Figure 2-51: Deformed geometries for a shear angle of 54° demonstrating shear lock up (Badel <i>et al.</i> , 2007)	88
Figure 2-52: Initial configuration for the plain weave fabric (Durville, 2010)	89
Figure 2-53: $y = \tan(x)$ for $-5\pi < x < 5\pi$	94
Figure 2-54: Representation of TolX and TolFun. Reproduced from MathWorks (2012a)	99
Figure 2-55: Sensitivity of individual variables before and after robustness optimisation. (Kim <i>et al.</i> , 2010).....	107
Figure 3-1: Inverse method.....	111
Figure 3-2: Spring and arm case layout, a) prior to loading, b) deformed	114
Figure 3-3: Fundamentals of the full sawtooth model with springs representing the coating. Modified from Bridgens and Gosling (2008).....	118
Figure 3-4: Unit cell position within the sawtooth representation	119
Figure 3-5: Kite Shape yarn cross section reproduced from Bridgens (2005)	122
Figure 3-6: Fundamentals of the simple sawtooth model.....	124
Figure 3-7: Flow chart demonstrating how the derivative $\frac{d\epsilon_2}{d\epsilon_1}$ cannot be defined	137
Figure 3-8: Plane Rectangular Bilinear Element and Plane Bilinear Isoparametric Element	140
Figure 3-9: Fundamentals of the full sawtooth model with an Isoparametric Element representing the coating.....	140
Figure 3-10: Plane Isoparametric Element in xy and $\xi\eta$ space modified from Cook <i>et al.</i> (1989)	141
Figure 3-11: Order three Gauss Point locations in a quadrilateral element: Reproduced from Cook <i>et al.</i> (1989)	143
Figure 3-12: Equal geometry uncoated fabric, yarn lateral compaction, and yarn friction (Liu <i>et al.</i> , 2004)	145
Figure 3-13: Moment due to inter yarn friction calculation (Colman, 2012)	146
Figure 3-14: Calculation of shear force for a non-square geometry (Liu <i>et al.</i> , 2004) (Colman, 2014).....	148
Figure 3-15: Review of the positions of the elements that make up the shear model.	148

Figure 3-16: Calculation of the external shear force acting on the unit cell. Where M_S is the total moment resisting shear force, M_K is the moment due to the coating, M_F is the moment due to inter yarn friction	148
Figure 3-17: Overview of the process of solving the equilibrium sawtooth problem ..	152
Figure 3-18: Overview of the geometry optimisation for the unit cell minimisation (for a whole fabric)	155
Figure 3-19: Simple sawtooth optimisation process overview.....	156
Figure 3-20: Use of pattern search to inform gradient based optimisation.....	158
Figure 3-21: Overview of full sawtooth fabric design optimisation procedure.....	160
Figure 3-22: Published fabric strengths for Ferrari fabrics (Ferrari, 2013c; Ferrari, 2013a; Ferrari, 2013b).....	161
Figure 3-23: Inferred yarn strengths for Ferrari fabrics from published data (Ferrari, 2013c; Ferrari, 2013a; Ferrari, 2013b)	162
Figure 3-24: Published fabric strengths for Ferrari, Verseidag and ATEX fabrics (Verseidag, 2010a; Verseidag, 2010b; Atex, 2013a; Atex, 2013b; Ferrari, 2013c; Ferrari, 2013a; Ferrari, 2013b).....	162
Figure 3-25: Inferred yarn strengths for Ferrari, Verseidag and ATEX fabrics from published data (Verseidag, 2010a; Verseidag, 2010b; Atex, 2013a; Atex, 2013b; Ferrari, 2013c; Ferrari, 2013a; Ferrari, 2013b)	163
Figure 3-26: Results of the optimisation for the feasible solution of the F1202 PVC Polyester fabric	167
Figure 3-27: Results of the optimisation for the feasible solution of the B18089 PTFE glass-fibre fabric.....	168
Figure 3-28: Original geometry of the B18089 PTFE glass-fibre fabric.....	169
Figure 3-29: Optimised geometry of the B18089 PTFE glass-fibre fabric.....	169
Figure 3-30: Results of the optimisation for the feasible solution of the B18089 PTFE glass-fibre fabric.....	171
Figure 3-31: Optimised geometry of the B18089 PTFE glass-fibre fabric (Prior knowledge of original geometry)	171
Figure 3-32: Results of the optimisation for the feasible solution of the ATEX3000 Silicone glass-fibre fabric	173
Figure 3-33: Original geometry of the ATEX3000 Silicone glass-fibre fabric	173
Figure 3-34: Optimised geometry of the ATEX3000 Silicone glass-fibre fabric	174

Figure 3-35: Results of the optimisation for the feasible solution of the ATEX3000 Silicone glass-fibre fabric	175
Figure 3-36: Optimised geometry of the ATEX300 Silicone glass-fibre fabric (Prior knowledge of original geometry).....	176
Figure 3-37: Shear response of a F1202 fabric up to a 50 shear angle	178
Figure 3-38: Comparison between coating only and coating and friction shear response (green-full shear response, red-coating only)	180
Figure 4-1: Normal Distribution (Mean = 24.96, standard deviation = 3.010)	189
Figure 4-2: Probability plot of data used in Figure 4-1	190
Figure 4-3: Probability plot of warp yarn amplitudes for an F1202 fabric	191
Figure 4-4: Probability plot of weft yarn thicknesses for an F1202 fabric.....	191
Figure 4-5: Probability plot of warp yarn out of plane angles for an F1202 fabric	192
Figure 4-6: Linearly distributed data tested for normality (200 data points linearly distributed between 0 and 1)	192
Figure 4-7: Method for the comparison of results to the failure criteria $0.99 \cdot \text{Target} < E_{11} < 1.01 \cdot \text{Target}$	196
Figure 4-8: Convergence of Monte Carlo probability of failure	198
Figure 4-9: Mean probability of failure at increasing intervals	199
Figure 4-10: Mean standard deviation of failure at increasing intervals	200
Figure 4-11: Method of Monte Carlo implementation.....	203
Figure 4-12: Monte Carlo results where only E_{y1} and E_{y2} are considered to vary with a coefficient of variation of 0.1 for the inequality $0.95 \text{Target} < E_{11}$ (red = failed, blue = success)	206
Figure 4-13: Sensitivity of E_{11} to variation in unit cell parameters ($C_v = 0.01$) for 'test' description see Table 4-2	209
Figure 4-14: Sensitivity of E_{11} to variation in unit cell parameters ($C_v = 0.1$) for 'test' description see Table 4-2	210
Figure 4-15: Histogram and Normal fit of 'test 3' data	211
Figure 4-16: Effect of variation in E_{y1} with respect to E_{y2} and E_k on the value of E_{11} where the $C_v = 0.01$	213
Figure 4-17: Effect of variation in E_{y1} with respect to E_{y2} and E_k on the value of E_{11} where the $C_v = 0.1$	214

Figure 4-18: Effect of variation in θ_1 with respect to other variables on the value of E_{11} where the $C_v = 0.1$	215
Figure 4-19: Effect of variation in θ_1 on the value of E_{11} where the $C_v = 0.1$	215
Figure 4-20: Effect of variation in L_2 on the value of E_{11} where the $C_v = 0.1$	216
Figure 4-21: Marginal distribution in the space of the standardised normal variables (Melchers, 1999)	218
Figure 4-22: Probability density function contours and original (non-linear) and linearized limit state surfaces in the standard normal space (Melchers, 1999).....	218
Figure 4-23: Two random variable joint density function $f_{RS}(r, s)$, marginal density functions f_R and f_S and failure domain D (Melchers, 1999)	218
Figure 4-24: Distribution of safety margin $Z = R - S$ (Melchers, 1999)	221
Figure 4-25: Comparison of the value of the shortest distance β and $g(y)$ as an optimisation progresses for the inequality $0.95 \times \text{Target} < E_{11}$ where $C_v = 0.01$ for all variables	223
Figure 4-26: Method of FORM implementation	226
Figure 4-27: Monte Carlo results showing θ_1 and θ_2 where only θ_1 and θ_2 are considered to vary with a coefficient of variation of 0.1 for the inequality $0.95 \text{Targ} < E_{11}$ (red = failed, blue = success)	230
Figure 4-28: Monte Carlo results showing y_1 and y_2 where only θ_1 and θ_2 are considered to vary with a coefficient of variation of 0.1 for the inequality $0.95 \text{Targ} < E_{11}$ (red = failed, blue = success)	231
Figure 4-29: Comparison of FORM and Monte Carlo generated failure points (approximate point of likely failure Monte Carlo (green), and point of failure from FORM analysis (magenta))	232
Figure 4-30: Comparison of FORM and Monte Carlo generated failure points zoomed to failure point (approximate point of likely failure Monte Carlo (green), and point of failure from FORM analysis (magenta)). Points of maximum likelihood are shown as '+'.	233
Figure 4-31: Comparison of FORM and Monte Carlo generated failure points (approximate point of likely failure Monte Carlo (green), and point of failure from FORM analysis (magenta))	235
Figure 4-32: Comparison of FORM and Monte Carlo generated failure points zoomed to failure point (approximate point of likely failure Monte Carlo (green), and point of failure from FORM analysis (magenta)). Points of maximum likelihood are shown as '◇'.	236

Figure 4-33: Normality test for the results of the Monte Carlo analysis for the inequality $E_{11,target} \times 0.99 < E_{11}$, where E_1 and E_2 varied only with a coefficient of variation of 0.01.	237
Figure 4-34: Comparing robust and global optimisation	238
Figure 4-35: Methodology for robust design for a single target E_{11}	242
Figure 4-36: Original fabric geometry (F1202 PVC coated polyester)	244
Figure 4-37: Robustly optimised fabric geometry for two targets (F1202 PVC coated polyester E_{11} and E_{22})	245
Figure 4-38: Sensitivities of the variables to the E_{11} target	246
Figure 4-39: Sensitivities of the variables to the E_{22} target	247
Figure 4-40: Designed fabric geometry for two targets (F1202 PVC coated polyester E_{11} and E_{22})	249
Figure 4-41: Robustly optimised fabric geometry for two targets (Optimised designed geometry)	250
Figure 4-42: Sensitivities of the variables to the E_{11} target	251
Figure 4-43: Sensitivities of the variables to the E_{22} target	252
Figure 4-44: Design point and reliability index β according to the first order reliability method (FORM) for normally distributed uncorrelated variables (BSI, 2006)	254
Figure 4-45: relationship between individual partial factors (BSI, 2006)	256
Figure 4-46: Probability density function from Monte Carlo data where r_2 and θ_1 were varied with $C_v = 0.1$.	257
Figure 5-1: Uniaxial stress strain curve, showing hysteresis in the fabric response under repeated loading (F1202 Warp data (Colman, 2013b))	263
Figure 5-2: Uniaxial testing equipment for stress-strain response reproduced from (Newcastle_University, 2012)	264
Figure 5-3: Uniaxial test setup	265
Figure 5-4: Biaxial test apparatus used at Newcastle University, reproduced from: (Bridgens and Gosling, 2008)	266
Figure 5-5: MSAJ cruciform specification (Membrane Structures Association of Japan, 1995)	267
Figure 5-6: Example biaxial response for F1202 fabric	268
Figure 5-7: Characteristic load history, red = stress in warp direction, blue is the stress in the weft direction from the Tensinet Design Guide (Forster and Mollaert, 2004)	268

Figure 5-8: Radial load regime (Bridgens and Gosling, 2008, p. 4).....	269
Figure 5-9: Finite element representation of stress distribution in the cruciform specimen (Membrane Structures Association of Japan, 1995)	270
Figure 5-10: 3D representation of F1202 response data with biaxial data points which appear as the white lines in the figure. The data was obtained using a biaxial testing machine at Newcastle University.....	274
Figure 5-11: 3D representation of F1202 response data without biaxial data points. The data was obtained using a biaxial testing machine at Newcastle University.	275
Figure 5-12: F702 cut through the surface for surface fit checking along the weft direction	275
Figure 5-13:F702 cut through the surface for surface fit checking along the warp direction	276
Figure 5-14: 3D representation of B18089 response data without biaxial response data points shown in the figure	277
Figure 5-15: 3D representation of F702 response data without biaxial data points including the plane stress representation of the surface using unconstrained strain minimisation elastic constants.....	278
Figure 5-16: Data points in relation to biaxial test response surface, showing how a smaller area of points fits to the test data better than the larger are shown above...	279
Figure 5-17: Data points produced to populate the small surface area to be represented by the plane stress surface	279
Figure 5-18: Comparison of constrained and unconstrained differential strain and stress minimisation results. Blue– fabric biaxial stress-stress-strain response surface points, red – constrained/unconstrained differential stress/strain results. For a f702 fabric at 3.76kN/m (warp), 11.27kN/m (weft)	280
Figure 5-19: Area of 'patch' plotted against E_x at target point 1	282
Figure 5-20: Area of 'patch' plotted against E_x at target point 4	282
Figure 5-21: Density of 'patch' plotted against E_x at target point 1	283
Figure 5-22: Density of 'patch' plotted against E_x at target point 4	283
Figure 5-23: Number of points in the 'patch' plotted against E_x at target point 1	284
Figure 5-24: Number of points in the 'patch' plotted against E_x at target point 14	284
Figure 5-25: Area of 'patch' plotted against E_y at target point 1	285

Figure 5-26: Sum of R^2 plotted against the density of points for the plane stress representing the whole fabric	286
Figure 5-27: Plane stress response surfaces for each selected point on the surface for a PVC coated polyester fabric (F702) (using unconstrained strain minimisation) visualisation 1.....	290
Figure 5-28: Plane stress response surfaces for each selected point on the surface for a PVC coated Polyester fabric (F702) (using unconstrained strain minimisation) visualisation 2.....	291
Figure 5-29: Plane stress response surfaces for each selected point on the surface for a PTFE coated glass-fibre fabric (B18059) (using unconstrained strain minimisation) visualisation 1.....	292
Figure 5-30: Plane stress response surfaces for each selected point on the surface for a PTFE coated glass-fibre fabric (B18059) (using unconstrained strain minimisation) visualisation 2.....	293
Figure 5-31: Results of the virgin yarn (Tersuisse Multifils SA) tests with outliers removed	297
Figure 5-32: Yarn ravelling on a sample of PVC coated polyester fabric.....	298
Figure 5-33: Yarn ravelling on a sample of PTFE coated glass-fibre fabric.....	298
Figure 5-34: Testing equipment including failed F1202 yarn	298
Figure 5-35: Example result for PVC polyester fabric F702 in the warp direction	299
Figure 5-36: Example results for PTFE glass-fibre fabric B18089 in the warp direction	300
Figure 5-37: Example results for Silicone glass-fibre fabric ATEX3000 in the weft direction	300
Figure 5-38: Example of method of calculation of modulus for polyester yarns (F702 Warp) (blue = curve utilised for calculation, green = available data, red = fitted curve)	301
Figure 5-39: Calculation of yarn modulus as calculated for the early response from F702 (warp) yarn response curve (blue = curve utilised for calculation, green = available data, red = fitted curve)	302
Figure 5-40: Calculation of yarn modulus as calculated for the low stiffness response from F702 (warp) yarn response curve (blue = curve utilised for calculation, green = available data, red = fitted curve).....	303

Figure 5-41: Calculation of yarn modulus as calculated for the mid response from F702 (warp) yarn response curve (blue = curve utilised for calculation, green = available data, red = fitted curve)	303
Figure 5-42: Calculation of yarn modulus as calculated for the late response from F702 (warp) yarn response curve (blue = curve utilised for calculation, green = available data, red = fitted curve)	304
Figure 5-43: Example of method of calculation of modulus for glass-fibre yarns (ATEX3000 weft) (blue = curve utilised for calculation, green = available data, red = fitted curve).....	304
Figure 5-44: Example of repeatability of results from ATEX3000 warp data with outliers removed	306
Figure 5-45: All data produced from the F1202 tests in the warp direction	306
Figure 5-46: A selection of samples of F1202 warp data with the second change in gradient visible	307
Figure 5-47: Cross section of F1202 warp yarn showing the two discrete plies (Colman, 2013a)	308
Figure 5-48: F1202 warp yarn after failure	308
Figure 5-49: Results used for calculation of F1202 (warp) mechanical properties	308
Figure 5-50: Results of fabric design without variation in targets for F702 targets (1)	313
Figure 5-51: Results of fabric design without variation in targets for F702 targets (2)	314
Figure 5-52: Target (X) and designed fabric (.) stiffnesses at increasing values of allowable variation from original targets.....	316
Figure 5-53: Target (X) and designed fabric (.) Poisson's ratios at increasing values of allowable variation from original targets.....	317
Figure 5-54: Target (X) and designed fabric (.) stiffnesses at increasing values of allowable variation from original targets.....	318
Figure 5-55: Target (X) and designed fabric (.) Poisson's ratios at increasing values of allowable variation from original targets.....	319
Figure 5-56: Geometry of the designed fabric (F702 targets)	321
Figure 5-57: Results of fabric design without variation in targets for B18059 targets	321
Figure 5-58: Target (X) and designed fabric (.) stiffnesses at increasing values of allowable variation from original targets.....	322

Figure 5-59: Target (X) and designed fabric (.) Poisson's ratios at increasing values of allowable variation from original targets	323
Figure 5-60: Target (X) and designed fabric (.) stiffnesses at increasing values of allowable variation from original targets	324
Figure 5-61: Target (X) and designed fabric (.) Poisson's ratios at increasing values of allowable variation from original targets	325
Figure 5-62: Geometry of the designed fabric (B18059 targets).....	326
Figure 5-63: Results of fabric design without variation in targets for ATEX3000 targets	327
Figure 5-64: Target (X) and designed fabric (.) stiffnesses at increasing values of allowable variation from original targets	328
Figure 5-65: Target (X) and designed fabric (.) Poisson's ratios at increasing values of allowable variation from original targets	329
Figure 5-66: Target (X) and designed fabric (.) stiffnesses at increasing values of allowable variation from original targets	330
Figure 5-67: Target (X) and designed fabric (.) Poisson's ratios at increasing values of allowable variation from original targets	331
Figure 5-68: Geometry of the designed fabric (ATEX3000 targets).....	332
Figure 5-69: Designed Geometry for four targets (F1202)	333
Figure 5-70: Designed Geometry for eight targets (F1202).....	334
Figure 5-71: Designed Geometry for twelve targets (F1202)	334
Figure 5-72: Response surfaces for the sawtooth model and measured response for one geometry (F1202).....	336
Figure 5-73: Geometry of the robustly optimised F702 fabric	339
Figure 5-74: Comparison of original F702 and robustly optimised fabric sensitivities to E_{11}	340
Figure 5-75: Comparison of original F702 and robustly optimised fabric sensitivities to E_{22}	341

Tables

Table 2-1: Comparison of fibre properties, (Houtman and Orpana, 2000; Horrocks and Kandola, 2005)	25
Table 2-2: Technical Yarn Characteristics (Alagirusamy and Das, 2010)	30
Table 2-3: Some example coating properties (Colman, 2013b)	37
Table 2-4: PVC and PTFE coating properties (Osswald and Menges, 1996)	37
Table 2-5: Poison's ratios of coatings (O'Hara, 1983; Fillon and Glavatskih, 2008; McKeen, 2009; Ognedal <i>et al.</i> , 2012; AZO_Materials, 2014).....	37
Table 2-6: Properties of fabrics (Houtman and Orpana, 2000)	43
Table 2-7: Mechanical properties of common fabrics (Houtman and Orpana, 2000) B1 – Difficult to ignite. A2 – 98%% non-combustible.	44
Table 2-8: Indicative Design Working Life (Table NA.2.1.) (BSI, 2007)	45
Table 2-9: Classification of PVC coated polyester fabric (Forster and Mollaert, 2004)..	46
Table 2-10: Classification of PTFE coated glass-fibre fabric (Forster and Mollaert, 2004)	46
Table 2-11: General comparison of the properties of fabrics (Forster and Mollaert, 2004)	47
Table 3-1: 'Spring and arm' system nomenclature	114
Table 3-2: Geometry used to find feasible targets and resultant optimised geometry for F1202 fabric.....	166
Table 3-3: Feasible targets found at the applied loads P1 and P2 and results for F1202 fabric	166
Table 3-4: Geometry used to find feasible targets and resultant optimised geometry for B18089 fabric	167
Table 3-5: Feasible targets found at the applied loads P1 and P2 and results for B18089 fabric	168
Table 3-6: Geometry used to find feasible targets and resultant optimised geometry for B18089 fabric	170
Table 3-7: Feasible targets found at the applied loads P1 and P2 and results for B18089 fabric	170
Table 3-8: Geometry used to find feasible targets and resultant optimised geometry for ATEX3000 fabric	172

Table 3-9: Feasible targets found at the applied loads P1 and P2 and results for ATEX3000 fabric	172
Table 3-10: Geometry used to find feasible targets and resultant optimised geometry for ATEX3000 fabric	174
Table 3-11: Feasible targets found at the applied loads P1 and P2 and results for ATEX3000 fabric	175
Table 3-12: Initial targets and results for the design of shear properties	179
Table 3-13: Initial and optimised geometry for shear target optimisation	179
Table 4-1: Monte Carlo predicted probability of failure at different failure criteria for feasible targets for an F1202 fabric (10000 runs = 20000 data sets)	205
Table 4-2: Test definition for Figure 4-13 and Figure 4-14	207
Table 4-3: FORM predicted probability of failure at different failure criteria for feasible targets for an F1202 fabric (5000 runs = 10000 data sets).....	227
Table 4-4: Point of Maximum likelihood for an F1202 fabric compared to the inequality $0.95 \times \text{Target} < E_{11}$ where $C_v = 0.1$ for $\theta_{1,2}$ only	229
Table 4-5: Comparison of point of Maximum likelihood for an F1202 fabric compared to the inequality $0.95 \times \text{Target} < E_{11}$ where $C_v = 0.1$ for $\theta_{1,2}$ only.....	234
Table 4-6: comparison of FORM and Monte Carlo failure probability to different failure criteria for feasible targets for an F1202 fabric (5000 runs = 10000 data sets)	234
Table 4-7: Original and robustly optimised geometry for F1202 fabric.	244
Table 4-8: Original and robustly optimised geometry for F1202 fabric.	249
Table 4-9: Target reliability index β for Class RC2 structural members ¹⁾ (BSI, 2006) ..	255
Table 5-1: Example elastic constants calculated using a Plane Stress Representation (F1202 fabric)	273
Table 5-2: Example elastic constants calculated using a Plane Stress Representation (B18089 fabric).....	276
Table 5-3: Elastic constants calculated using a Plane Stress representation (F702 fabric)	278
Table 5-4: Target values of elastic constants at specified stress states produced from the F702 fabric using unconstrained differential strain minimisation.....	281
Table 5-5: Comparison of plane stress and multiple target representations of biaxial data (PTFE coated glass-fibre – B18059). The values (10:10) etc. refer to the warp:weft load respectively in kN/m	289

Table 5-6: Comparison of yarn modulus for different curve segments for selected tests (tests 1, 2, and 4 were removed as anomalous)	302
Table 5-7: Yarn test summary; showing the calculated values of stiffness using the central portion of the response	305
Table 5-8: Comparison of single yarn test results to previously carried out uniaxial tests for yarn modulus	309
Table 5-9: Targets from PVC coated Polyester fabric F702	313
Table 5-10: Targets from PTFE coated glass-fibre fabric B18059	321
Table 5-11: Targets from Silicone coated glass-fibre fabric ATEX 3000	326
Table 5-12: Targets for PVC coated polyester F1202 fabric	333
Table 5-13: Variation in geometry used in the robust optimisation of an F702 fabric	338
Table 5-14: F702 robustly optimised geometry	338

Nomenclature

Variable	MATLAB Designation	Units	Description
Universal designations			
$X_{1,2}$	-	-	Where X is any variable: subscripts '1' and '2' represent the Warp and Weft directions respectively.
X_y	-	-	Where X is any variable: subscript 'y' refers to a property of the yarn.
X_k	-	-	Where X is any variable: subscript 'K' refers to a property of the coating.
X_c	-	-	Where X is any variable: subscript 'c' (in some external sources referred to as 'z') refers to the compressive force between the warp and weft directions.
X_s	-	-	Where X is any variable: subscript 's' refers to shear.
X_F	-	-	Where X is any variable: subscript F refers to frictional forces, normally in relation to the calculation of shear forces.
X'	-	-	Where X is any variable: the apostrophe refers to a 'prime' value. This is the result after one iteration. Two apostrophes refer to a result obtained from a second iteration.
-	X1a	-	Where X is any variable, and 1 or 2 denote warp and weft (in most cases): the following letters such as 'a', 'b', 'c' etc. refer to multiple calculations of the same variable. This may be due to multiple calculations of the same variable at the same point, or multiple calculations of the same variable at differing points.
-	X_note		Where X is any variable: the addition 'note' refers to any extra note attached to the variable. E.g. 'SavedData_Run1_NoShear' would refer to some saved data in run 1 with no shear.
Forces and Strains			
P	Fm1 , Fm2	kN/m	The stress acting on the fabric which is equal to the force acting on the edge of a 1m length of fabric
F	F1 , F2	N	The force acting on the edge of a unit cell
F_k	Fk1 , Fk2	N	The force acting on the coating
F_y	FY1 , Fy2	N	The force acting on a single yarn
F_c	Fc1 , Fc2	N	The force acting on the coating
ϵ	e1 , e2	No units	Strains

Variable	MATLAB Designation	Units	Description
τ	Tor		Shear stress acting on a unit cell
γ	Gamma		Shear strain
M	M		Moment relating to the calculation of shear forces
Yarn and Coating Geometry and Mechanical Properties			
$E_{1,2}$	E1 , E2 or $\gamma(7), \gamma(8)$	kN/m	Yarn stiffness.
E_k	E_k or $\gamma(9)$	kN/m	Coating stiffness.
ν_k	ν_k	No units	Coating Poisson's ratio
Θ	Ph1 , Ph2 or $\gamma(1), \gamma(2)$	rad	Out of plane angle of the yarns.
L	L1, L2 or $\gamma(3), \gamma(4)$	mm	Quarter yarn wavelength.
Y	Y1, Y2	mm	Half the length of a yarn in a unit cell
r	r1, r2 or $\gamma(5), \gamma(6)$	mm	Yarn radius.
w	w1, w2	mm	Half yarn width.
$A_{1,2}$	A1 , A2	mm	Yarn amplitude.
Area _{1,2}	Area1 or Area2	mm ²	Yarn cross-sectional area.
$\delta_{1,2}$	d1 , d2	mm	Deflections in the plane of the fabric.
Spring and arm model			
F	F	No units	Load.
θ	Be	No units	Initial angle between the bar and the x-axis
K	K	No units	Spring constant
E	E	No units	Spring constant (stiffness)
A	A	No units	Spring constant (area)
L_{y0}	L_y	No units	Initial length of the spring
L_0	L_x	No units	Half the initial distance between the two roller supports
δ		No units	Displacement of the roller supports in the x-direction
Δ			Displacement of the pin joint in the y-direction
Biaxial and shear response characteristics			
$E_{11,22}$	E11 , E22	kN/m	Fabric Young's modulus
$\nu_{12,21}$	ν_{12}, ν_{21}	No units	Fabric Poisson's ratio
G	G		Fabric shear stiffness
Other nomenclature used in this report			
$\frac{\Delta y}{\Delta x}$	-	-	Used to symbolise an iterative calculation
$\frac{dy}{dx}$	-	-	A full derivative
$\frac{\partial y}{\partial x}$	-	-	A partial derivative

Variable	MATLAB Designation	Units	Description
N _{1,a}	-	-	The derivative of ‘N ₁ ’ with respect to ‘a’.
u	-	-	Displacements of the isoparametric element parallel to x and y.
v	-	-	
ξ	Eta	-	Axis for which an isoparametric element will appear rectangular.
η	xi	-	
Statistics			
μ	Mu	-	Population Mean
σ	Std	-	Population standard deviation
C _v	cov	-	Coefficient of Variation

1. Introduction

1.1. Context

1.1.1. Background

For thousands of years fabrics have been used to produce shelters in the form of tents or awnings. Animal skins or traditional fabrics such as wool were used until the advent of modern industrial processes in the nineteenth century when the mass production of fabric allowed for the creation of large spans such as circus tents using mass produced linen or hemp canvas (Forster and Mollaert, 2004). It is only in the last hundred years that modern doubly curved prestressed structures using modern architectural fabrics have been constructed. Possibly the most famous early example of a tensioned doubly curved structure is the cable net structure designed by Frei Otto in Munich for the 1972 Olympic games (Figure 1-1). Since the early examples of architectural fabric structures numerous examples have been produced across the world. These merge the requirement for shelter with distinct and unique architectural solutions that are organic in their appearance, and are a step change away from traditional rectangular construction.

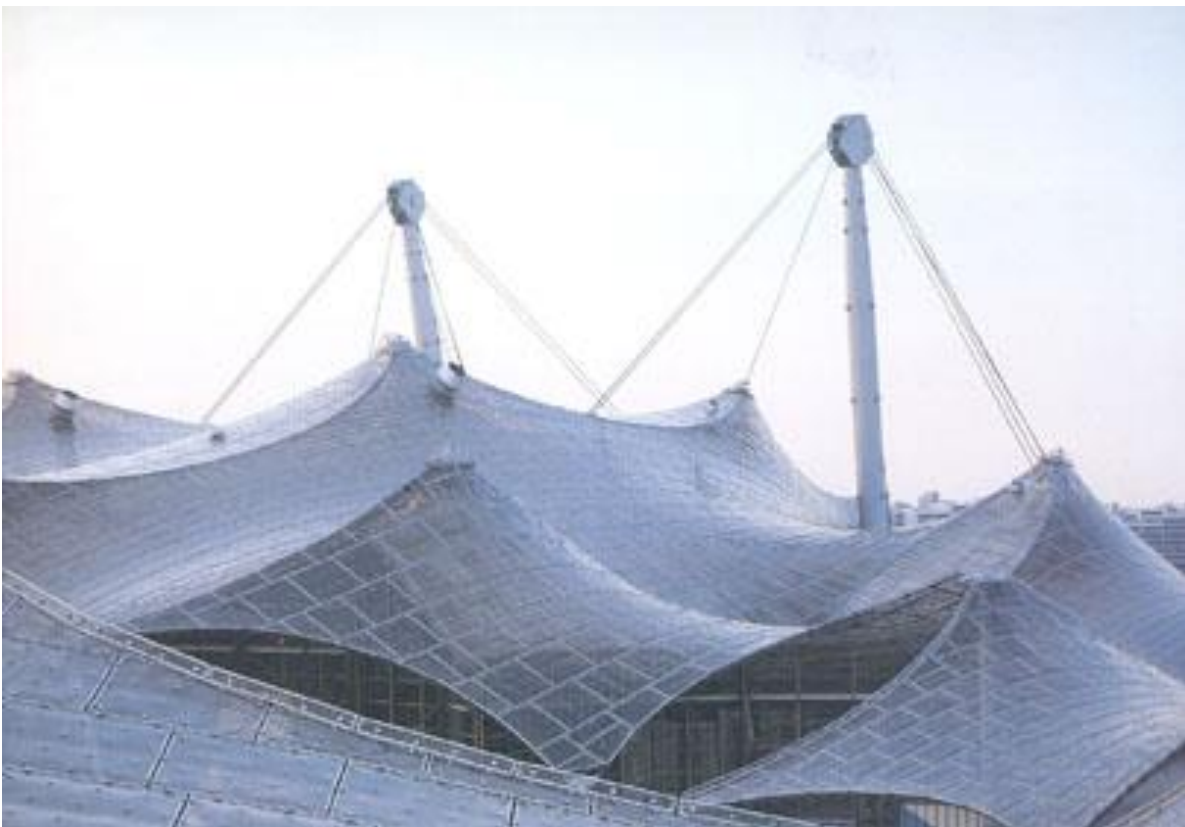


Figure 1-1: Munich 1972 Olympic stadium roof (Tensinet, 2015)

1. Introduction

Modern architectural fabrics are produced from a woven base cloth that is most often plain-weave. This base cloth is coated with polymers such as PTFE (Polytetrafluoroethylene) or PVC (Polyvinylchloride) which increases the fabric's shear resistance (Skelton and Freeston, 1971), stabilises the weave, and provides waterproofing. The resultant architectural fabric resists loading entirely through tensile and shear response in the plane of the fabric as the material has negligible bending and compressive stiffness (Bridgens *et al.*, 2004; Gosling *et al.*, 2013). Unlike standard construction materials which can resist loads through bending or compression the shape of a fabric structure is crucial to its ability to resist loads. Doubly curved prestressed surfaces allow for the transfer of both uplift and downward loads through the structure whilst prestressing ensures that under all loaded conditions the fabric does not become slack, or become wrinkled which results in stress concentrations in the wrinkles.

Three “*fundamental forms*” (Bridgens *et al.*, 2009, p. 2) exist from which all doubly curved shapes can be derived. These are the hypar (Figure 1-4), the barrel vault (Figure 1-3) and the conic which can be produced by manipulating the boundary conditions of an initial flat fabric (Figure 1-2) (Bridgens *et al.*, 2009).

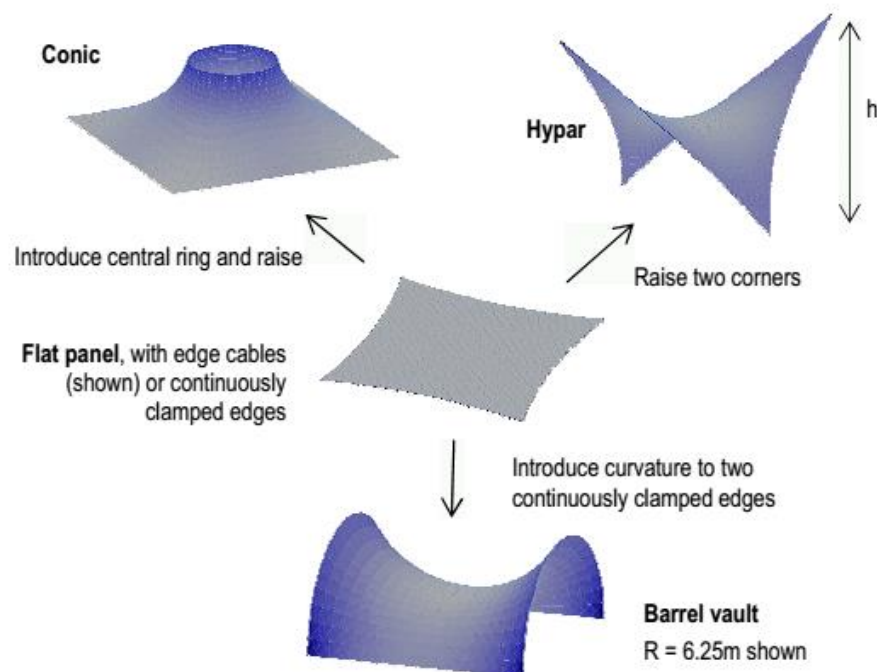


Figure 1-2: The three principal anticlastic shapes. Reproduced from Bridgens *et al.* (2009)

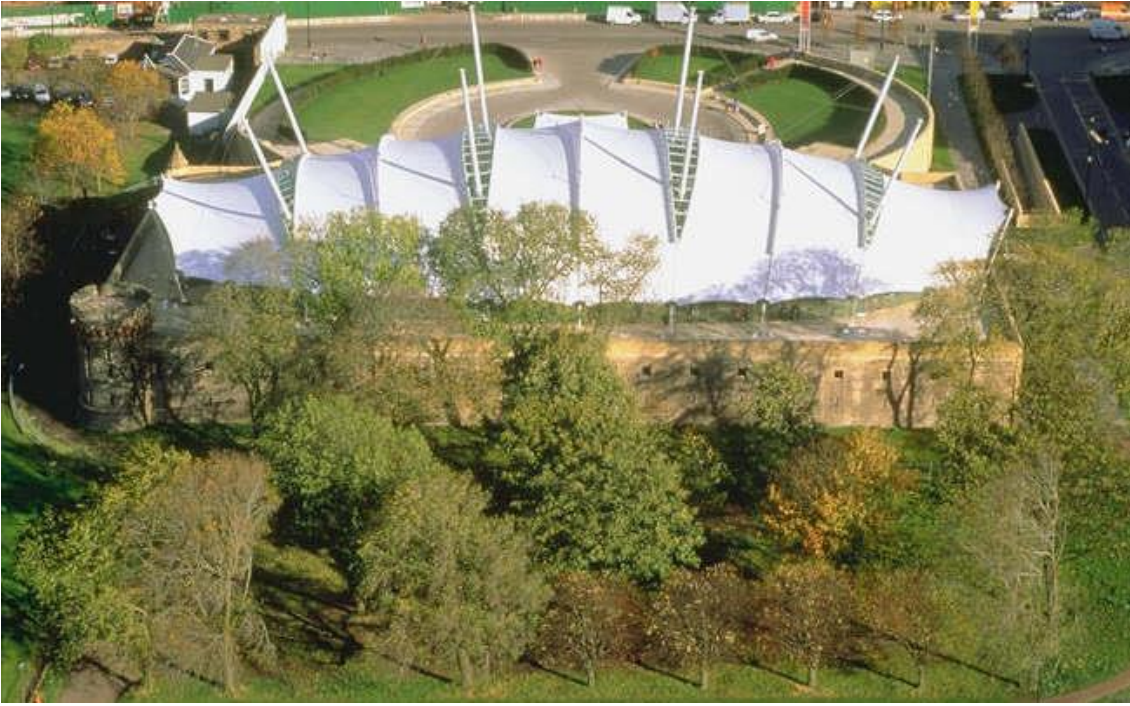


Figure 1-3: Dynamic Earth Centre (Edinburgh) (Tensinet, 2015)



Figure 1-4: De Montil NV (Belgium) (Tensinet, 2015)

Modern fabric structures are characterised by their anticlastic (doubly curved) surfaces, light weight, and high strength to weight ratio in the plane of the fabric. They also experience large deflections, large strains (up to ten percent) and large shear strains.

Due to their low weight and the need for relatively little in the way of hard structural supports fabric structures have a low environmental impact when compared to traditional construction methods. Modern techniques also allow for limited recycling of fabrics (Ferrari, 2014). In addition to anticlastic doubly curved fabric structures inflated membrane structures also exhibit many similarities to architectural fabric structures. These are however outside of the scope of this report (§1.4).

1.1.2. Fabric modelling

The first fabric material model was developed by Peirce (1937) in which plain weave fabrics are described in terms of their weave geometry and material properties and the equilibrium equations which are fundamental to further work are developed. In addition to describing the fabric's geometry the seminal work by Peirce (1937) also considers the response of fabrics to biaxial loading. Since then considerable work has been carried out with the aim to quantify the response of architectural fabrics to uniaxial, biaxial, and shear loads (Peirce, 1937; Kawabata *et al.*, 1973; Menges and Meffert, 1976; Wang, 2002; Bridgens and Gosling, 2008; Colman *et al.*, 2014).

The constitutive modelling of the fabric response can be broadly divided into two types; predictive and representative modelling. Predictive models attempt to predict the load-deformation of fabrics by considering their geometry and stiffness characteristics whilst representative models aim to represent known fabric response and attempt to describe this in terms of fitted equations or models. The important difference between these two methods is that the representative model becomes unreliable beyond the initial data set for which it has been calibrated. A predictive model should model all conditions for which it has been designed though may become unreliable when used outside of the range for which it has been checked. Material models can be split further to include mechanical material models which describe the material's weave and constituent properties to calculate load-deformation response. Finite element methods model the material using finite elements to represent yarns (Figure 1-6), filaments (Figure 1-5), or coating. They can also be used to model fabric as a whole (Figure 1-7). The model shown in Figure 1-5 considers the filaments that make up a yarn only. In summary Predictive models should be more broadly applicable to new design situations.

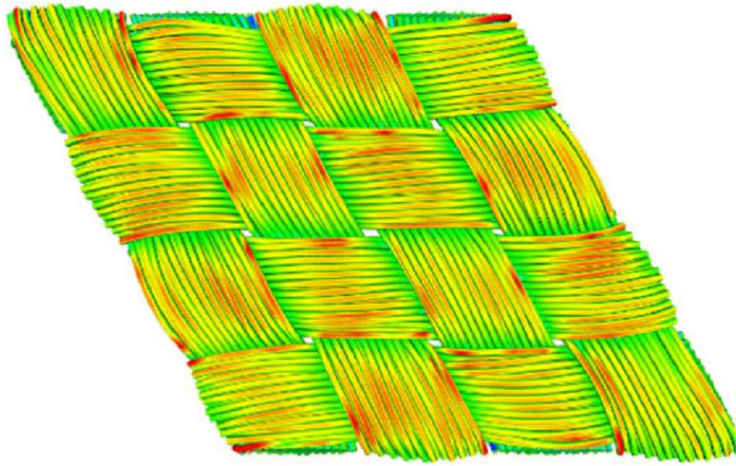


Figure 1-5: Finite element representation of filaments in shear (Durville, 2010)

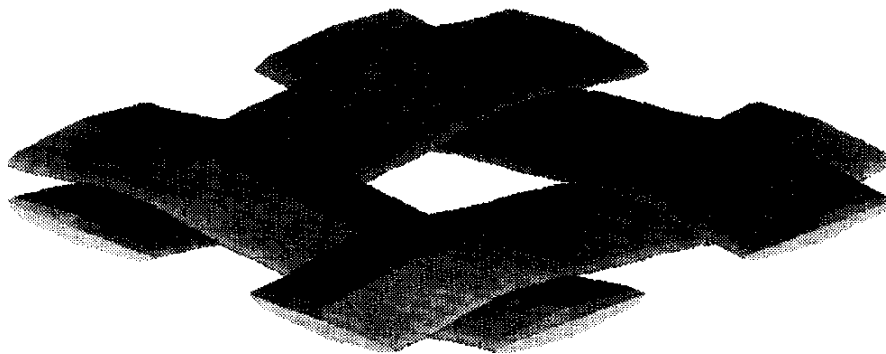


Figure 1-6: "Three-dimensional rendering of yarns within a unit cell" used by Glaessgen *et al.* (1996)

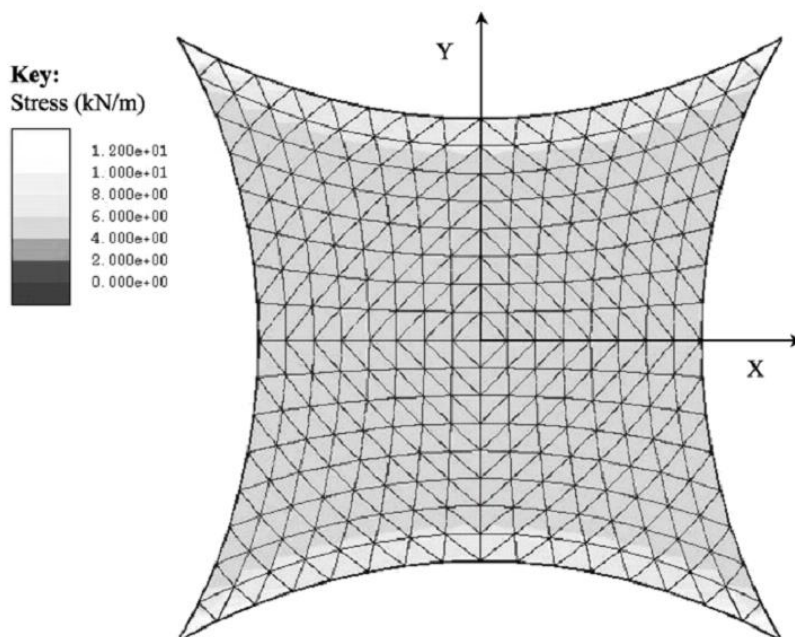


Figure 1-7: Finite element model of a Hypar (initial form found configuration) (Pargana *et al.*, 2010)

1. Introduction

In addition to the constitutive models, fabric test data might be represented in a number of ways. Current practice is to use the plane stress representation, describing a pair of stiffness's and Poisson's ratios for the entire fabric response (Blum and Bögner, 2002). These 'fits' can then be described as representative models, as they represent the data from which they were formed, but may not represent other data sets. Though other methods have been developed to represent fabric test data more accurately these have not yet been incorporated into standard analysis software (Day, 1986; Minami, 2006). Additionally Bartle *et al.* (2013) models fabric load-deformation response by using Neural Networks, which utilise data from one or more fabrics to build a representative model of behaviour, but then demonstrates the ability to predict the response of different fabrics.

1.2. Aims and Objectives

1.2.1. Aims

The aim of this research is to produce an inverse predictive material model for coated woven fabrics that is robust with respect to variability in material properties to be used to design bespoke architectural fabrics with specific properties at different loading conditions.

1.2.2. Objectives

1. To complete a full and in depth review of the state of the art of fabric modelling, design and analysis.
2. Formulate an inverse material model.
3. Incorporate variability of material parameters into the model and assess sensitivity of the resultant design.
4. Develop a methodology to design a material that is robust with respect to uncontrolled variations in parameters, such as manufacturing tolerance and constituent material variability. This should produce statistics to give confidence intervals for the likelihood of the attainment of the specified designed properties
5. Complete a validation study using biaxially tested samples of coated woven fabric.
6. To carry out a structural design study using an FE simulation of a true structural design case.

1.3.Motivation

The model developed in the following chapters might be used in the future to produce real structures for specific responses using a bespoke fabric. To this end a qualitative demonstration of how the method might be applied to a conic structure is detailed below:

Conics are constructed with the warp direction aligned upwards, and the weft direction aligned radially (Figure 1-8). This is done principally for aesthetic reasons. The structure is then prestressed by application of load at the edge of the material (Figure 1-8), or by the vertical displacement of the ring upwards. The loading in the warp direction induces loads in the weft (radial) direction and the structure then finds its shape.

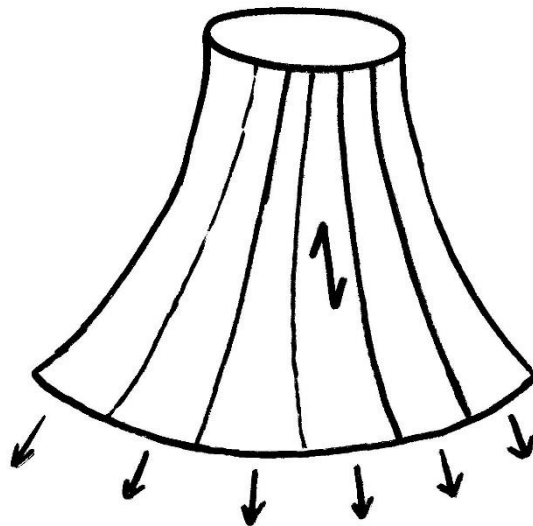


Figure 1-8: Standard Conic construction

This method of patterning the weft direction radially, whilst visually appealing, is not optimal for the purpose of prestressing. The warp yarns will have relatively little crimp, whilst the weft yarns will begin with a relatively large amount of crimp. Therefore inducing load in the weft direction through crimp interchange by stressing the warp yarns is inefficient. A more efficient method would be to pattern the warp yarn radially, however, this would result in an unappealing visual effect.

The method developed in the following chapters could therefore be used to apply a constraint on the initial response of the fabric at installation conditions. Namely that the warp yarn be relatively crimped, whilst the weft yarn is relatively flat. This would lead to a high stiffness in the weft direction with a lower stiffness in the warp direction.

1. Introduction

Therefore a lower load in the warp direction would lead to crimp interchange with the weft direction inducing higher stresses in that direction without initial high stress in the warp direction. It is noted that this would require a higher deformation in the warp direction.

At this point standard or nominally 'normal' response characteristics would be required for the further analysis of the fabric under normal loads. Therefore two design targets for the design of the fabric have been selected (Table 1-1). Other design requirements might be considered as well.

Condition	E_{11}	E_{22}
Installation	Low	High
Normal operation	Medium	Medium
Snow	High	Medium
Uplift	Medium	High

Table 1-1: Loading conditions and required responses

Thus the design of the fabric might be carried out. Under installation the high stiffness in the weft direction with respect to the warp direction should lead to lower prestress. Under snow load a high warp stiffness would lead to reduced possibility of ponding at corners or edges, whilst the radial stiffness should be less of a concern. Under wind loading a high radial stiffness should reduce billowing outwards.

Once the design criteria are identified the inverse model developed in the following chapters will then be run to produce a fabric that demonstrates the required mechanical response at the specified loads. This could then be used to produce a response surface for which response criteria could be identified for all loading scenarios similar to the method suggested by Bridgens *et al.* (2004). However, utilising detailed design information about a fabric is not currently possible with commercially available fabric structure analysis software.

A second, quantitative, application of the model is also made using exercise three as set out by Gosling *et al.* (2013) as the basis for the design of a hypar to be analysed. The structure is analysed in Oasys GSA (Oasys, 2014) similarly to Gosling *et al.* (2013) which utilises two fabric moduli and one Poisson's Ratio for the fabric. The details of the structure that was analysed are outlined below:

1. Introduction

Geometry:	6m x 6m square hypar with high points two meters above low points. The warp direction runs between high points. The edges are supported by cables.
Prestress:	Warp = 3kN/m, Weft = 3kN/m, Cable prestress = 30kN
Material properties:	A PVC coated polyester fabric is used. The warp and weft moduli are both 600kN/m, both Poisson's ratios are 0.3 and the shear modulus is 30kN/m. The cable is 12mm in diameter, with an elastic modulus of 205GPa.
Loading:	A wind uplift of 1kN/m ² and a snow load of 0.6kN/m ² are considered.

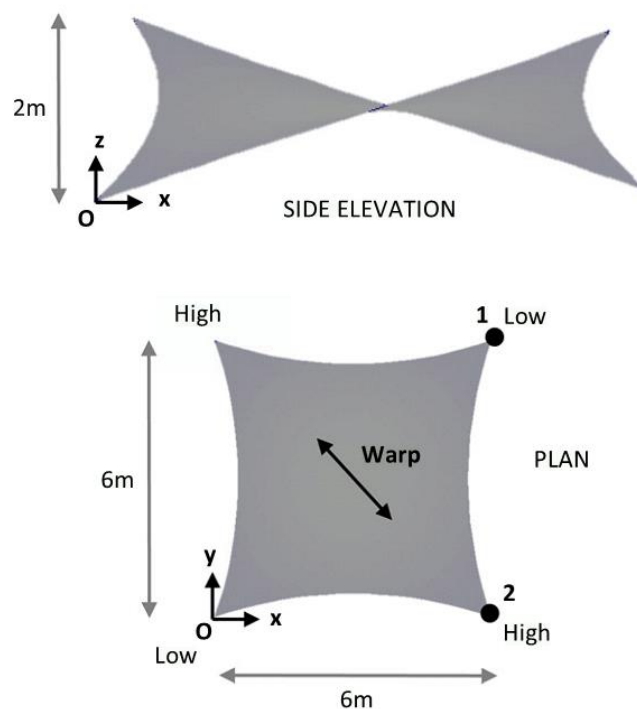


Figure 1-9: Hypar geometry (Gosling *et al.*, 2013)

The structure was analysed and the maximum deflection due to the snow load calculated to be 218mm (Figure 1-10 and Figure 1-11).

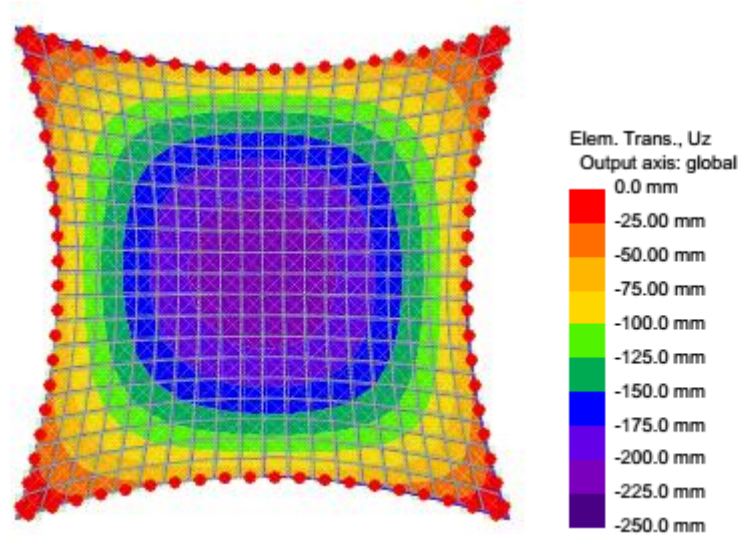


Figure 1-10: Deformation of the Hypar under snow load (Plan)

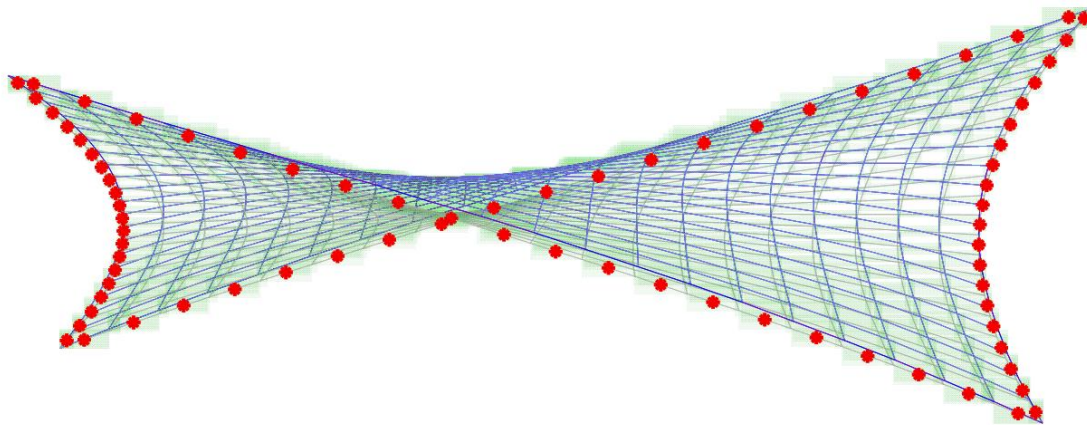


Figure 1-11: Deformation of the hypar under snow load. Original (blue) and deformed geometry (grey)

At this stage the artificial constraint might be placed upon the model. For instance, that the deflection under snow load must be reduced whilst maintaining the deflection under wind load. This would in this case require an increase in stiffness in the warp direction, that direction predominantly supporting the downwards load. Whilst maintaining the stiffness in the weft direction. Alternatively it might be decided that at a higher loading this deflection must be maintained with only a small increment of additional deflection.

These cases would form the basis of the design of a fabric, from which a response plane could be obtained. However, as current fabric design analysis software is unable to incorporate more than one set of moduli or response planes into the analysis

(Oasys, 2014) an analysis of any designed fabric for these conditions would be at the very least, extremely difficult.

1.4. Outline method

Initially this research focusses on the derivation of a number of equations that describe the biaxial response of a fabric. The constitutive model from which these equations are derived is the sawtooth model as developed by Bridgens and Gosling (2008) (Figure 1-12). The equations are built up in stages with an initial proof of concept used to demonstrate the applicability of the method. After the method's validity has been confirmed a simplified model and then the full model are considered from which equations for the stiffness and the Poisson's ratio of a fabric are derived.

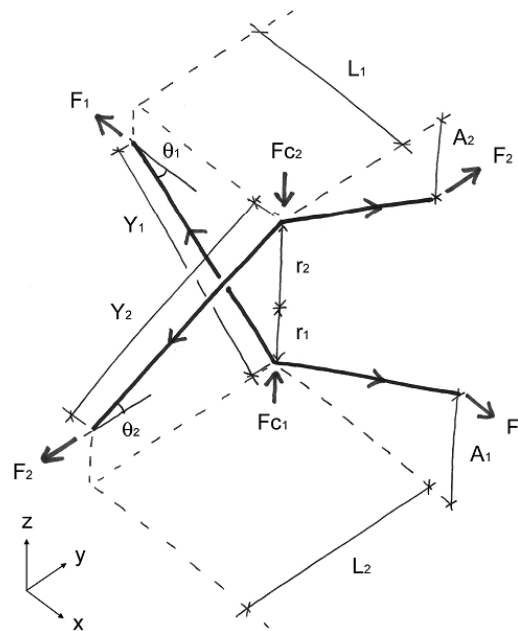


Figure 1-12: Fundamental sawtooth unit cell (Bridgens and Gosling, 2008)

After the model equations are derived a method for the consideration of the effect of variability in a fabric's constitutive properties is proposed. From this a method for the optimisation of a fabric's robustness to changes in its constitutive properties is produced.

Finally the various methodologies developed are compared to real test data from biaxial tests carried out at Newcastle University.

1.5.Scope

This thesis considers only the material model developed by Bridgens and Gosling (2008) with some alterations, and the inclusion of a shear model developed by Page and Wang (2000) and later Colman *et al.* (2014). This model was chosen because it reproduces fabric load-deformation characteristics accurately for architectural fabrics, and is presented in a fashion which should be applicable to the creation of an inverse material model. Biaxial and shear modelling, with the inclusion of data from uniaxial testing is therefore only considered in this thesis. Extensive testing of fabrics has been carried out at Newcastle University and is not predicted to be necessary as these results are available, and should be applicable. Manufacturing a bespoke fabric to corroborate the results of theoretical testing is also outside of the scope of this project. Only plain weave fabrics are considered in detail as they form the majority of architectural fabrics. Further; only PVC coated Polyester, PTFE coated glass fibre, and Silicone coated glass fibre fabrics are considered as test results and further specimens are available for these fabric types. PTFE coated PTFE fibre, Cotton, and other fabrics are beyond the scope of this project. Robust design of fabrics is carried out based on existing statistical data available at Newcastle University, and produced by Colman (2014). In situ testing of the accuracy of the robustness methodology is beyond the scope of this work. Linear yarn stiffness is also used in the project to remove the need to independently calculate and verify nonlinear yarn stiffness. As the tensile strength of fabrics and yarns is a field largely unrelated to the prediction of fabric tensile stiffness this is excluded after a short review of tensile strengths is made.

1.6. Structure of Thesis

Chapter 1, Introduction: Introduces the research project.

Chapter 2, Literature review: Reviews the current state-of-the-art of fabric material modelling and relevant information regarding the makeup and analysis of architectural fabrics. Key topics include: The features of coated woven fabrics, the response to biaxial load of fabrics, the modelling of fabrics, the determination of fabric properties through testing, and current statistical and optimisation methods.

Chapter 3, A predictive model for the design of functional textiles: Includes the formulation of the inverse material model based on the sawtooth model previously developed. This is then implemented into a design methodology for the design of a bespoke fabric.

Chapter 4, Variability and robustness: Discusses the Monte Carlo and FORM methodologies for the analysis of fabric variability and applies these methodologies to the design of a fabric's properties for the reduction of sensitivity to variation in fabric parameters.

Chapter 5, Validation: Attempts are made to design real fabrics based on a blind test in which the model attempts to reproduce a fabric utilising only knowledge of the fabric's response to biaxial loads. In addition a real fabric is optimised for the reduction of its sensitivity to variation in parameters, and a structural design study is proposed.

Chapter 6, Conclusions and recommendations for future work: An overview of the conclusions of the work is presented and further work necessary for the improvement of the model is set out.

Glossary: A list of terms relating to this thesis.

References: Have been listed alphabetically by author using the Harvard referencing system as used at Newcastle University

Appendix: Further information relevant to the thesis, including: Published conference paper, fabric data sheets, and further test data.

1.7. Publications

- A Predictive Model for the Robust Design of Functional Textiles – Draft, awaiting completion.
- Iliffe CN, Bridgens BN, Gosling PD. (2013) 'A Predictive Model for the Design of Functional Textiles', *VI International Conference on Textile Composites and Inflatable Structures*. Munich, Germany. Pp 395-406.

1.8. Awards

Newcastle University Post Graduate Research Conference – Best Poster in 'Infrastructure' section 2012.

2. Literature Review

2.1. Architectural fabrics

2.1.1. Need for this work

This research focusses entirely on the use of fabrics in architectural applications as a load bearing component such as a roof or awning. These are normally prestressed by the application of load during construction to avoid de-stretching which can lead to fabrics that flap in the wind, or wrinkles. Wrinkles lead to stress concentrations in the fabric which can lead to tears. Edge support, normally cables, and some solid support structure, often steel work, provide the support conditions for the structure. The fabric structure itself will be loaded entirely in tension and designed to remain in tension under all loading conditions as the fabric itself will have negligible compressive strength.

The need for the research is typified in the following example: Conic structures are designed to be installed with the warp yarns (down the fabric roll) aligned down the structure (Figure 2-1) which gives a more aesthetic appearance than having them aligned across the structure. The outside of the conic is tensioned after installation to achieve the required prestress. This tensioning results in the tensioning of the weft yarns (across the roll) due to the interaction between the yarns (Poisson's ratio) which tightens up the structure. However, as warp yarns are generally straighter than weft yarns (§2.2.4) a large amount of stress may need to be applied to the warp direction to achieve the required stress in the weft direction. It would be easier to align the fabric the other way.

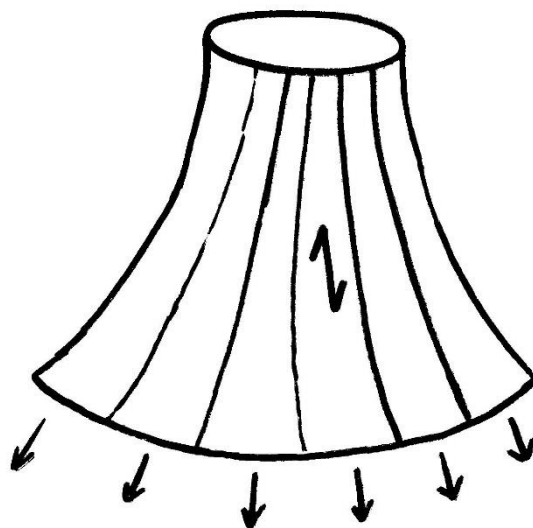


Figure 2-1: Tensioning of a conic structure

Companies such as Ferrari have developed technologies to allow them to vary the tension in the yarns during manufacture (and hence the ‘crimp’) which might help with this problem (Ferrari, 2014), but there is currently little available information on what level of crimp would be necessary. This research aims to change this.

2.1.2. Previous work

Only limited work has been carried out into the design of bespoke architectural fabrics, and at this time *“there is no standard or systematic design optimisation process”* (Behera and Muttagi, 2002, p. 315), though Behera and Muttagi (2002) describe how the current design methodology for fabrics is based on iterative testing and experience. Behera and Muttagi (2002) consider the use of an ‘Expert System’ which mimics the experience of an experienced engineer by applying the same principles and experience to the problem fabric design. However, these are described as complex IF, AND, OR statements that generally work in conjunction with some objective to produce a solution based on general rules. If the experience of the author were to be outside of the design situation proposed the system would struggle to find an adequate solution. Also discussed are neural networks, similar to those used by (Bartle *et al.*, 2013). Artificial Neural Networks mimic the behaviour of neurones by considering inputs in parallel to produce nonlinear representations of the outputs. They can adapt to new information, and will become more predictive the more information they receive. Work carried out in this field is very promising, but still in its infancy.

2.1.3. Further architectural and structural applications

Sørensen (2009, p. 1) discusses the design of wind turbines which are *“traditionally made of polymer matrix composite materials (laminates and sandwich structures)”*. As the laminate consists of a fibre matrix impregnated with a resin such as *“glass fibre/polyester [or] carbon fibre/epoxy”* the design methodology for fabrics may be applicable to the design of this laminate. Wind turbines fail in a number of ways, and Sørensen (2009, p. 2) identifies that *“Reliable modelling tools must be developed for modelling of the damage evolution in wind turbine blades”*. It is hoped that future work will demonstrate the applicability of this design method to the design of wind turbine blades. However, it is predicted that architectural fabrics will demonstrate considerably higher strains than solid composites, whilst solid composites will show a more complex biaxial behaviour, and possibly higher stresses.

Fabrics are also in use as permanent formwork. In this application the fabric cloth remains part of the structure after the setting of restrained material, providing permanent restraint to that material.

2.1.4. Medical applications

The “*design of a textile composite bone plate*” is relevant because of the large disparity between bone mechanical properties and response and the properties of metal plates (such as stainless steel) usually used in “*fracture fixations*” which are then removed later. This disparity causes bones to heal differently, and can lead to refracture after the plate is removed. Kharazi *et al.* (2010) produces a textile composite bone plate that aimed to, and achieved, properties close to those of the “*host material*” i.e. the bone. This was made more difficult as the “*longitudinal mechanical properties of cortical bones are higher than their transverse properties*”.

Here it can be noted how a designed fabric might enable a greater compliance to the host materials properties. The weft yarns might be orientated transversely, possibly with high crimp, reducing the stiffness whilst stiff yarns might be used in the other direction. In addition a designed fabric might be produced to generate a very high modulus at a higher load, to restrict extension beyond a certain point that would not aid healing. Lastly, unlike the standard bone plate the composite used is referred to as a “*partially resorbable*” as it does not need to be removed through surgery though the glass fibres remain in the body, having not been reabsorbed, the matrix is absorbed into the body.

“*It is estimated that 20 million prosthetic meshes are implanted each year worldwide*”, these are used in hernia repair, catheters, and heart valve repair (Sanders and Kingsnorth, 2012). However, the mechanical properties of the meshes (tensile and shear stiffness) do not necessarily meet the needs of individual patients, leading to discomfort and durability. Only limited work has been carried out on the optimisation of the mechanical properties of medical meshes, including the example above. It is hoped that further work will enable the use of this methodology in the design of woven mesh fabric for medical applications (Scheidbach *et al.*, 2004; Champault *et al.*, 2009; Sergent *et al.*, 2009).

2.2. Features of coated woven fabrics

How do the properties of the constituent components of a fabric affect the properties of a fabric as a whole?

“Textile composites are composed of textile reinforcements combined with a binding matrix (Long, 2005, p. xiii). This definition can include a wide array of “materials used for load bearing applications”, however this report will focus on architectural fabrics thus: The “textile reinforcement” considered here will be the regular woven pattern of yarns produced when a textile is manufactured (§2.2.1, 2.2.4). The “binding matrix” will generally be referred to as the coating used in the manufacture of architectural fabrics (§2.2.3).

2.2.1. Fibre geometry and properties

Yarns are produced from fibres, which are defined as *“textile raw material, generally characterised by flexibility, fineness and [a] high ratio of length to thickness”* (Lomov *et al.*, 2005, p. 1). Fibres are twisted together to form yarns and the twist of the yarn produces friction between fibres which holds the yarn together (Lomov *et al.*, 2005) though other means can be used to create cohesion (Lawrence, 2003, p. 21). Multiple yarns, or strands, can also be twisted together to produce a ply yarn (Lomov *et al.*, 2005). Cross-sections of fabrics show the individual fibres, and sometimes even the filaments (Figure 2-2).

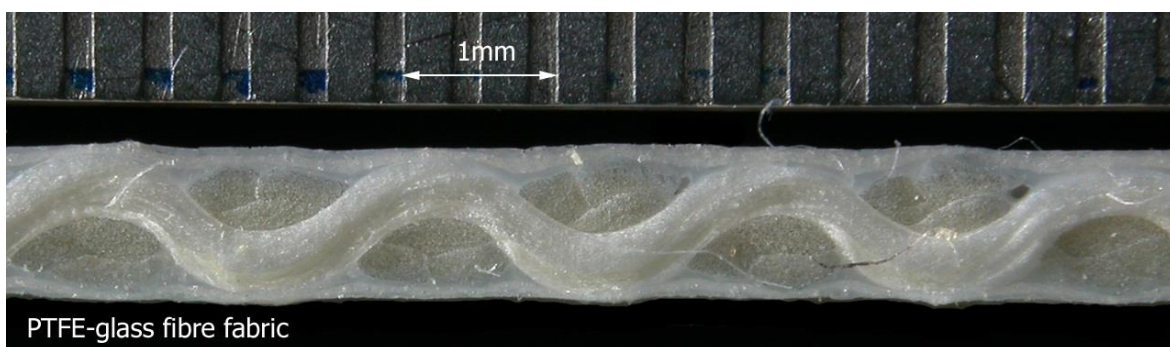


Figure 2-2: PTFE-glass fibre image, in which the plies can be seen (Bridgens *et al.*, 2004)

Yarns can be split into a number of subcategories, *“Yarns containing only one fibre are monofilaments. Untwisted, thick yarns are termed tows. Flat tows are called rovings”* (Long, 2005, p. 2). Yarns discussed as part of this work on architectural fabrics will generally be continuous filament twisted ply yarns. The multiple strands that make

up a ply yarn are visible above where three distinct sections can be seen in the yarn ends (Figure 2-2).

The properties of a finished fabric are intrinsically linked to the properties of the yarns that make up the fabric *“transformed by the textile structure”* (Lomov *et al.*, 2005, p. 2) and the strength of a coated fabric is mainly determined by the strength of the constitutive yarns (Forster and Mollaert, 2004). As such the properties of the yarns must be understood prior to the consideration of the fabric as a whole. The behaviour of yarns is *“non-linear and non-reversible owing to the fibrous nature and inter fibrous friction”* within the yarns (Lomov *et al.*, 2005, p. 5). Whilst the internal fibrous friction produces the non-linear response of the yarn *“the frictional properties of fibres on the outside of the yarn enable woven fabrics to maintain their weave pattern and structure”* (Bridgens, 2005, p. 22). This is referred to as the dimensional stability of the fabric (Bridgens, 2005).

A number of yarns and fibres are used in the manufacture of fabrics. Glass and polyester fibres are currently the most widely used yarns in the manufacture of architectural fabrics. Other yarns used in fabrics include cotton, Polyamide 6.6 (Nylon), Aramid (Kevlar) and more recently carbon fibres (Houtman and Orpana, 2000). Alagirusamy and Das (2010) classify yarns using a flow chart (Figure 2-3) from which it can be seen that artificial yarns tend to have a higher strength (Tenacity) than natural yarns though this is highly generalised.

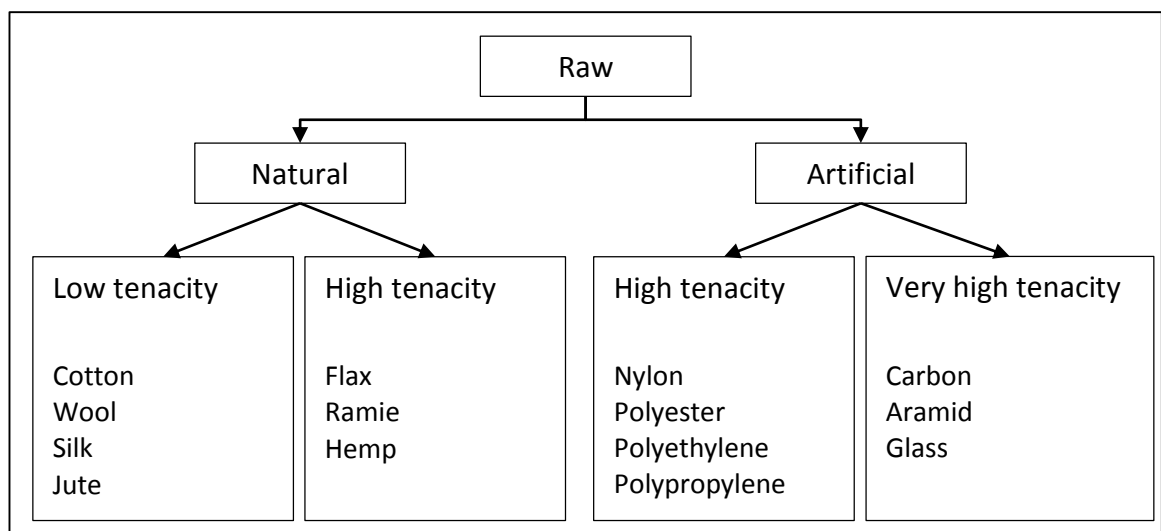


Figure 2-3: Classification of technical yarns according to raw material (Alagirusamy and Das, 2010)

Cotton fibres were used by Frei Otto in his early garden show structures. Cotton is seldom used nowadays except in limited applications because it is susceptible to fungal attack and moisture due to its organic nature (Houtman and Orpana, 2000).

Polyamide 6.6 (Nylon) has poor resistance to UV (ultraviolet) light and “*swells in length when it gets wet*” (Figure 2-4). It is used in the sailing industry due to its low weight and high strength but is of little use as an architectural fabric (Houtman and Orpana, 2000, p. 1).

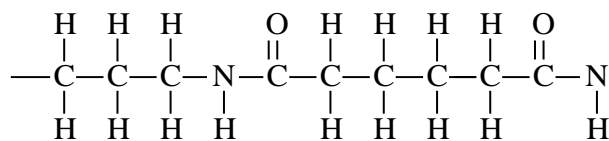


Figure 2-4: Symbolic representation of Polyamide 6.6. (Osswald and Menges, 1996)

Aramid fibres (Kevlar) are a class of thermoplastics referred to as liquid crystalline polymers (Osswald and Menges, 1996). Aramid fibres have high tensile strength and are chemically resistant. However, due to low elastic strain, poor UV resistance, poor resistance to high temperatures, and cost the material is not widely used in architectural fabric applications (Houtman and Orpana, 2000).

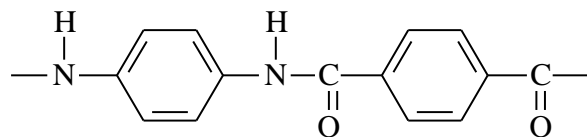


Figure 2-5: Symbolic representation of an Aramid (Osswald and Menges, 1996)

Carbon fibres are characterised by low density and high strength and stiffness. The mechanical characteristics of carbon fibres do not deteriorate up to temperatures of 450°C. These fibres are used mainly in aerospace engineering, and automotive engineering, or where exceptionally high temperatures are expected (Horrocks and Kandola, 2005). Carbon fibres have also found use in the sailing industry. Future work may therefore need to include carbon fibre fabrics.

Extruded PTFE fibres can also be used in architectural fabrics with a PTFE (Polytetrafluoroethylene) coating. PTFE fibres have inferior mechanical properties in comparison to polyester and glass fibres for most applications (Table 2-1). However PTFE

2. Literature Review

is highly resistant to chemical corrosion and UV and IR (Infrared) radiation. PTFE coated PTFE fabric also has good tear resistance (Houtman and Orpana, 2000; Forster and Mollaert, 2004). PTFE coated PTFE fabrics are also more expensive than other architectural fabrics, and difficult to weld (Bridgens, 2005).

Fibre	Density (g/cm ³)	Tensile Strength (GPa)	Tensile Strain (%)	Elasticity (GPa)
Cotton	1.5-1.54	0.35-0.7	6-15	4.5-9
Polyamide 6.6 (Nylon)	1.14	Until 1.0	15-20	5-6
Polyester fibre*	1.38-1.41	1.0-1.3	10-18	10-15
Glass fibre (E-glass)	2.4-2.6	2-6	2.0-3.5	50-100
Glass fibre (S-glass)	2.5	3.5	2.0-3.5	87
Aramid fibres (Kevlar)	1.45	Until 2.7	2-4	130-150
PTFE (Polytetra- fluoroethylene)	2.1-2.3	0.16-0.38	13-32	0.7-4.0
Carbon fibres**	1.7-2.0	2.0-3.0	<1	200-500
Carbon fibres ***	1.5-2.0	1.5-7.0	<1	150-800

*Trevira, Terylene, Dacron, Diolen **Celion, Carbolon, Sigrafil, Thornel *** Carbon and graphite fibres

Table 2-1: Comparison of fibre properties, (Houtman and Orpana, 2000; Horrocks and Kandola, 2005)

Glass fibres are one of the two principal fibres used in architectural fabrics. Glass filaments are supplied in various diameters, from 3 to 11 microns and the tensile strength of these filaments is highly dependent on their diameter (Forster and Mollaert, 2004) with smaller diameters resulting in higher tensile strengths (Figure 2-6). Glass fibres are incombustible, corrosion resistant, and have high strength at low densities. They are also low cost thanks in part to the abundant nature of the raw materials required for production (silicon) (Kostikov, 1995; Horrocks and Kandola, 2005). Whilst there is a wide variation in components and additives all glass fibres primary component is SiO₂ (Wallenberg and Bingham, 2010). Glass fibres are largely unsusceptible to ageing; however moisture will reduce the tensile strength of glass fibres (Houtman and Orpana, 2000). Further to this glass fibres are limited to small strains and demonstrate linear stress strain relationships with abrupt failures (Horrocks and Kandola, 2005).

2. Literature Review

Generally there are four distinct grades of glass fibre, E, S, R and C-glass fibres, of which the types commonly used in fabrics are E and S-glass (Electrical resistant and High Strength respectively) (Horrocks and Kandola, 2005). The generally more expensive S-glass fibre has a higher tensile strength, and can be elongated more than the generally cheaper E-glass before fracture (Wallenberg and Bingham, 2010). Glass fibres are drawn from a glass melt which produces the variability in strength based on the diameter of the fibre. The outside of the fibre will cool considerably faster than the inside, producing internal tension and external compression. The variation in internal forces will be less in lower diameter filaments (Forster and Mollaert, 2004) therefore producing a higher tensile strength (Figure 2-6). The contents of the melt from which the filament is drawn will also alter its properties.

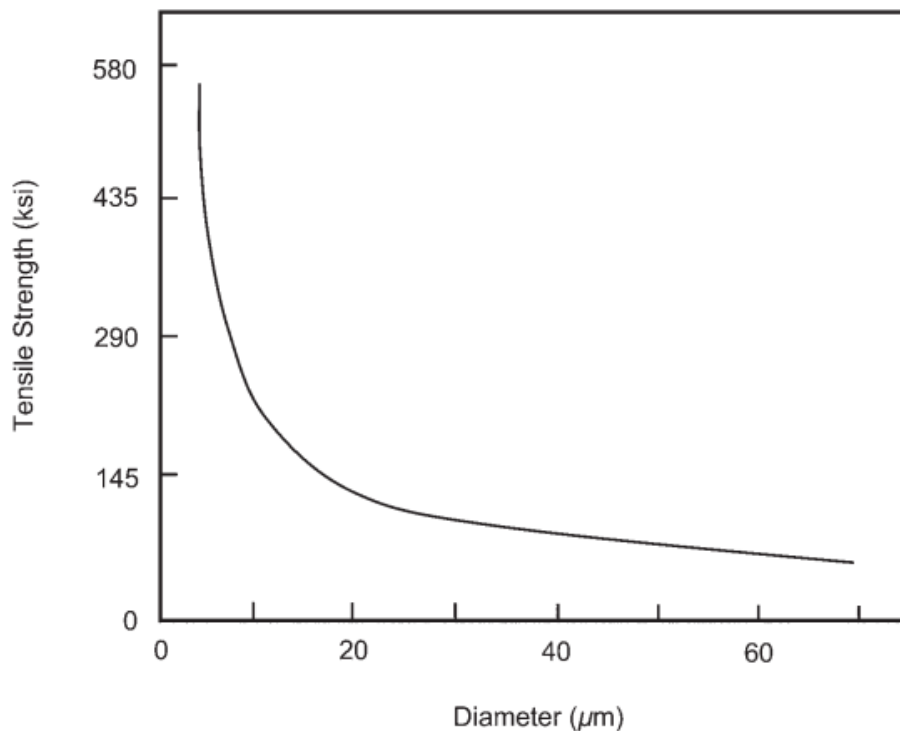


Figure 2-6: Effect of fibre diameter on tensile strength of fibre. Reproduced from Campbell (2010)

Polyester fibres are the other principal fibre used in architectural fabrics. Polyester fibres are produced from Polyethylene-terephthalate (PET) (Figure 2-7) (McIntyre, 2000). This is the same polyester (a thermoplastic) that is used in drinks bottles, although the forming process is different for the two applications (Margolis, 1985). *“Polyester exhibits good tensile strength, flexibility and significant elongation before yield”* (Chilton and Velasco, 2005, p. 426) differentiating it from glass fibres. Polyester fibre based fabrics

are therefore more suited to errors during manufacturing of the yarn because the yarns are more easily stretched to accommodate the manufacturing errors. Short or misshaped yarns can be stretched without being damaged to incorporate manufacturing errors. However, polyester fibres do demonstrate poor resistance to UV radiation. Thermoplastics such as polyester are not “*crosslinked*” and therefore derive their mechanical properties from the arrangement of the “*monomer units that form high molecular weight chains*” (Jones, 1994). This means that as a bundle of polyester molecules in chains extend they straighten out, resistance to which provides the fibres tensile strength.

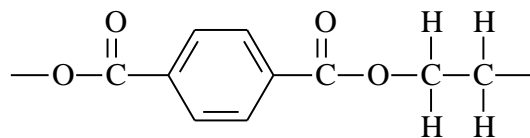


Figure 2-7: Symbolic representation of Polyethylene-terephthalate (PET) (linear polyester) (Osswald and Menges, 1996)

Polyester yarns display highly nonlinear behaviour (Figure 2-8). Bridgens (2005) compares two plots produced by (Forster and Mollaert, 2004) of this behaviour and notes that both plots show significant differences due to the complexity of the behaviour of PET yarns. This non-linearity is initially due to the ‘straightening’ of the chains that make up the fibre, followed by their elastic extension, and finally their plastic extension, and the failure of individual chains. The yarn’s long term non-linear behaviour is due to the creep response of the yarn under sustained load (§2.2.5).

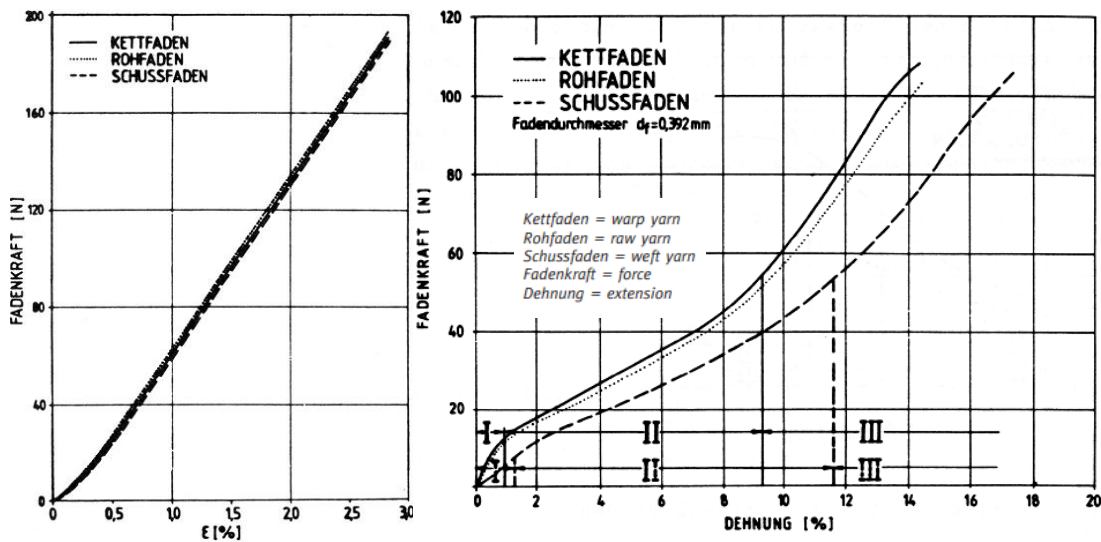


Figure 2-8: Stress Strain responses for Glass fibres (Left) and Polyester fibres (right). Reproduced from Forster and Mollaert (2004)

Polyester fibres are manufactured by melt spinning the polymer filaments which also allows for the crystallisation and orientation of the macromolecular chains within the yarns. This leads to a higher elastic modulus and tensile strength in the final yarn. Engineering grades of PET are generally highly crystalline, whilst grades used in bottles and other situations are generally amorphous. Macromolecular orientation and crystallisation have a large effect on the final properties of a yarn (Margolis, 1985; Forster and Mollaert, 2004). A higher degree of orientation means that more molecular chains are aligned in the direction of the applied load, and thus more of the polyester is 'available' to resist tension in that direction.

The mechanical differences between the responses of glass-fibres and polyester fibres is evident in the near linear response of glass fibres compared to the s-curved response of the polyester fibres (Figure 2-8 and Table 2-1). Glass fibres exhibit good chemical and environmental resistance, but have limited bending and strain characteristics when compared to those of polyester fibres. However polyester fibres are less environmentally resistant and more prone to damage due to repeat loading than glass fibres. The choice of yarn type is therefore clearly dependant on the situation the yarn will be employed in.

2.2.2. Yarn geometry and properties

“...Second only to fibres from which yarns are made, yarns are the basic building blocks of most textile fabrics. Many fabric properties will, in addition to the fibre properties and the fabric structure, depend on the structure and properties of the constituent yarns”(Lawrence, 2003, p. 21). Therefore understanding how the structure of the yarn affects its properties is essential.

The yarns used in this project are formed by twisting together fibres (though non-twist yarns also exist) which leads to tension and lateral forces in the yarn and the fibres are consolidated by the friction generated in the twist (Lomov *et al.*, 2005). Similarly several yarns can be twisted together to form a ply yarn (Figure 2-9). Ply yarns can be seen in Figure 2-2. The ply yarn shown in Figure 2-9 demonstrates how after the individual yarns have been weaved together the fibres that made up the independent yarns become aligned with the direction of load in the ply yarn. Yarns can be characterised by *“their dimensional, structural and constituent fibre parameters”* (Alagirusamy and Das, 2010, p. 26) along with their mechanical behaviour.

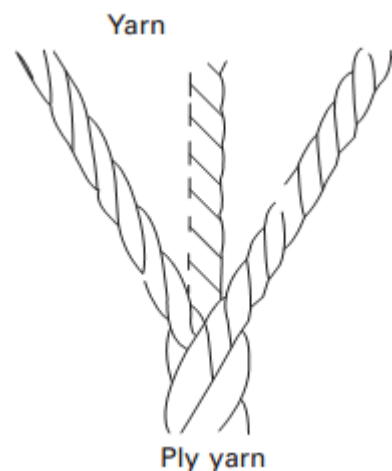


Figure 2-9: Ply yarn. Reproduced from Alagirusamy and Das (2010)

Alagirusamy and Das (2010) characterise the properties of a yarn according to dimensional, structural and constituent parameters (Table 2-2). In addition to these we are also interested in the mechanical properties of the yarn or how the structure of the yarn might affect the tensile strength; bending, tensile, and compressive stiffness of a yarn.

Parameters	Characteristics
Dimensional Parameters	Linear Density Diameter
Structural Parameters	Twist and its direction Wrap Density and its direction Number of plies, ply twist, and twist combination Core content, core-sheath ratio Blend Constituents and blend ratio Packing coefficient
Constituent fibre parameters	Number of filaments in cross-section Filament cross-sectional shape Length Linear density Crimp cross-sectional shape

Table 2-2: Technical Yarn Characteristics (Alagirusamy and Das, 2010)

The linear density is the measure of the mass of yarn per unit length and its SI value is the Tex (1 tex = 1 g/km). This also acts as the unit of yarn count. The variation in Linear density is the unevenness of the yarn (Lomov *et al.*, 2005; Alagirusamy and Das, 2010).

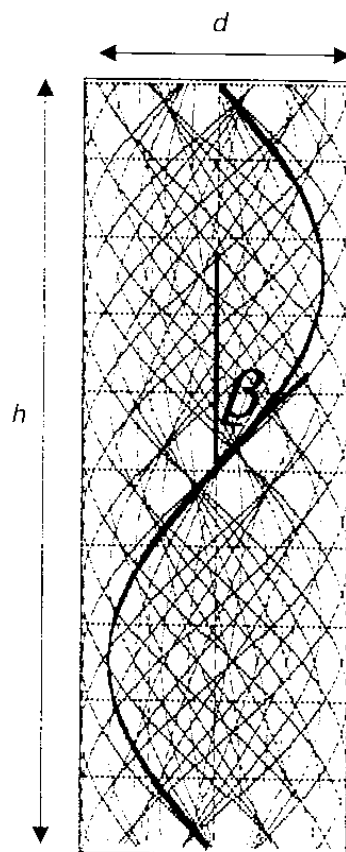


Figure 2-10: Calculation of twist angle (Lomov *et al.*, 2005; Alagirusamy and Das, 2010)

Assuming that the yarn is a cylinder and the fibre follows a helical pattern within the yarn the twist of the yarn can be calculated (Equation 2-1) (Lomov *et al.*, 2005). The twist angle is “Indicative of the intensity of frictional interaction inside a yarn” (Lomov *et al.*,

2005, p. 5) which is useful as a method of estimating the effective modulus of a fabric yarn. The estimated stiffness of the yarn will be the original stiffness multiplied by $\cos(\beta)$. Further to this the yarn diameter will not always be easily available as yarns do not have precise boundaries and as such the diameter must be estimated (Equation 2-2) (Madhavan and Naik, 2000; Lomov et al., 2005; Alagirusamy and Das, 2010).

$$\tan \beta = \frac{\pi d}{h} = \pi d K \quad \text{Equation 2-1}$$

Where β = twist angle, d = yarn diameter, h = length of the period of the twist, $K = 1/h$ = the twist of the yarn.

$$d = \sqrt{\frac{4T}{\pi \rho_f V_f}} = C \sqrt{T} \quad \text{Equation 2-2}$$

Where C = a coefficient for each yarn type, and T = the linear density, ρ_f = fibre density, V_f = the fibre volume.

Three further factors affect the calculation of twist and add to the complexity of defining a yarn, resulting in deviations from the idealised geometry of a perfect helix in a cylinder. Microbuckling and migration both contribute to deviation from this standard model. The outer fibres of the yarn follow a longer path than the internal fibres. Given that the fibres were all the same length at manufacture this creates an inward pressure from the outermost fibres which are now more highly stressed and have the greatest curvature. This radial force causes migration of the outermost fibres in towards the centre, and those less stressed fibres move outwards. Microbuckling occurs in the centre of the fibre where some twist is present in the central fibres. This effectively reduces the length of those fibres and, by introducing further twist, reduces the stiffness of the yarn (Madhavan and Naik, 2000). Migration can be accounted for in the numerical estimation of a yarn's properties by the introduction of a constant (Alagirusamy and Das, 2010).

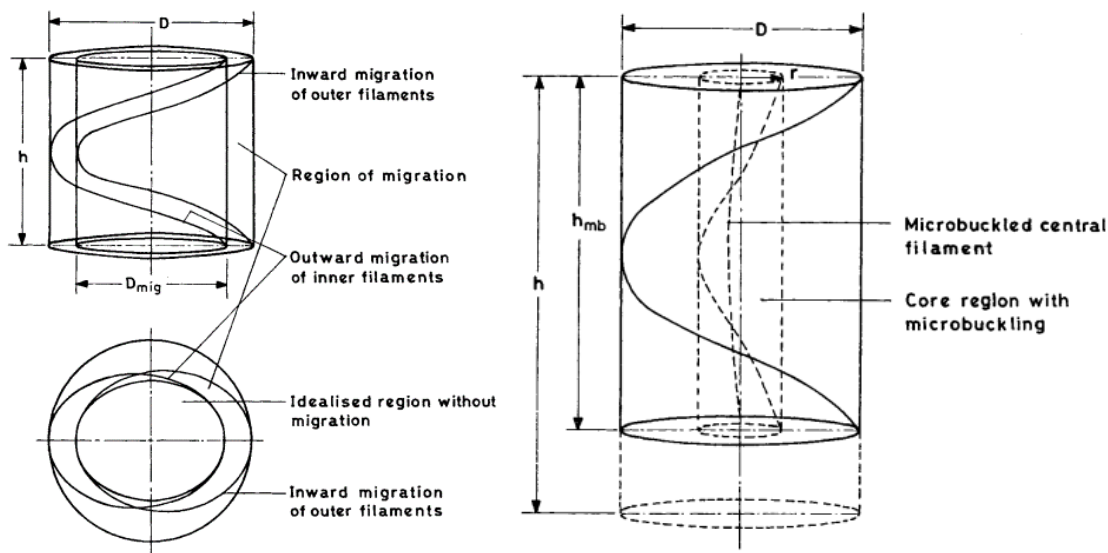


Figure 2-11: Microbuckling (right) and migration (left). Reproduced from Madhavan and Naik (2000)

Further complicating the calculation of the stiffness of a yarn is the possibility that some fibres will be broken, not all fibres will have equal properties, and other damage (such as ageing) may be present (Singh and Naik, 2001).

Crucially yarn properties are nonlinear due to their twist and the migration of fibres within the yarn (in addition to the properties of the fibres). The number of additional variables that would need to be considered to enable a complete modelling of the yarn would be considerable, so utilising a nonlinear stiffness for yarns is therefore beyond the scope of this project (§1.4).

Lomov *et al.* (2005, p. 5) states that the two “*most important yarn deformation modes [during manufacture] in determining the internal geometry of a fabric are bending [...] and compression*”, with bending allowing “*for yarn interaction forces in the fabric, and transverse compression which [...] define the shape of yarns in the fabric*”. However, bending is not often considered in the modelling of yarns and fabrics, although it is regularly mentioned as an important deformation mechanism (§2.3.2). Testa *et al.* (1978, p. 1028) states that bending is an important deformation mechanism but also states that in their model “*bending resistance of both coating and yarns is neglected*”.

Testa *et al.* (1978) and Tan and Barnes (1984) list the deformation mechanisms of coated fabrics, including for yarns specifically,:

- *Yarn rotations (or crimp interchange between warp and fill yarns)*
- *Bending and torsion of yarns*
- *Crushing (or flattening) of yarns at crossover point*
- *Yarn bending*
- *Yarn flattening*
- *Yarn extension*
- *Friction between filaments; friction between yarns at crossover*
- *Yarn nesting at crossover (the settling of one yarn into the other)*
- *Yarn swelling*
- *Yarn and fabric rupture*

However Tan and Barnes (1984), in common with Testa *et al.* (1978) do not include bending or yarn compression in their models (§2.3.2.2). Therefore whilst bending of the yarns may be an important deformation mechanism when considering unwoven yarns most models consider it unimportant for the calculation of fabric response. Contrary to this Dimitrov and Schock (1986, p. 858) describe the bending stiffness of fibres as influencing the Bedding-down effect which they state “*will probably contribute considerably to the load extension behaviour of fabrics*”.

The compression of the yarns, or the change of the shape of yarns, is a predominant yarn deformation mechanism, further to this Pargana *et al.* (2000, p. 2) suggests that “*particular attention has to be given to the modelling of the yarn crushing deformation mechanism*”. Therefore it is necessary to include some representation of yarn deformation if accurate modelling of yarn behaviour is to be achieved.

Bridgens (2005) states that there are three mechanisms which may result in a change in yarn radius, specifically:

- *Initial bedding down (inelastic)*
- *Yarn crushing due to contact with orthogonal yarn (elastic or partially inelastic)*
- *Reduction in yarn radius due to tensile extension, i.e. Poisson’s effect (elastic or partially elastic)*

Dimitrov and Schock (1986) suggest the following factors will influence the bedding down effect:

- *The slack in the yarn*
- *The coatings penetration into the yarn's internal space*
- *Bending stiffness of the fibres*
- *Lateral compressibility of the fibres, stiffness*
- *Spinning characteristic of the yarn.*

Yarns used in architectural fabrics vary in size in the range of approximately 0.1mm to 5mm. Versedag Duraskin PVC B4951 has a thickness of 0.6mm which means the yarn diameter can be estimated to be approximately 0.3mm, whilst a PTFE coated glass fibre fabric (B18059) has a thickness of 1.4mm (Verseidag, 2005). Comparing glass and polyester yarns shows that the shape of the glass yarn might be described as a squashed oval, whilst the PVC yarn might be more accurately described as a stretched oval (Figure 2-2 and Figure 2-12). Yarn dimension information will be essential in the design of bespoke fabrics, where maxima and minima will need to be set to ensure viable fabric properties are designed. It is also possible that discretisation may be necessary to allow only viable yarns to be produced, however, given the wide range and variability of yarns that are available this may not be necessary.

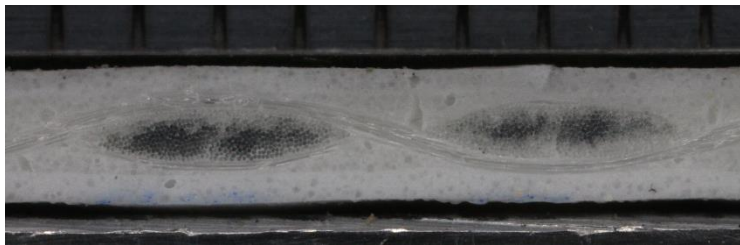


Figure 2-12: F1202 warp cross section (fill yarn) (Colman, 2013a)

2.2.3. Coating properties

Whilst the woven textile is the primary load-carrying component for roof structures the coating (sometimes referred to as the fabric matrix, but referred to as the coating throughout this thesis) protects the fabric from environmental effects and provides a weather tight enclosure (Chilton and Velasco, 2005), the coating also acts as the predominant method of shear resistance and stabilises the fabric weave. Impregnation of the yarns (migration of coating in between yarn filaments) by the coating can also affect the properties of the yarns. Farboodmanesh *et al.* (2005) demonstrate this by adding a coagulant to a rubber coating for a PET fabric, thus stopping the penetration of

the rubber into the yarns as the coagulant forces the rubber to *“bond with itself”*. This non-impregnated fabric demonstrated reduced shear stiffness (Farboodmanesh *et al.*, 2005), even given that the coating was two to three times thicker in the non-impregnated fabric than that of the comparison fabric. This paper shows that the properties of the coating will have a large effect on the properties of the fabric composite. However, as this is the only detailed study into this, and the materials used are not those used in architectural fabrics it is only possible to draw general conclusions from this work. No corroborating papers have been found to confirm this work.

Polyvinyl chloride (PVC) (Figure 2-13), is the most common coating used in conjunction with polyester fabric (Chilton and Velasco, 2005). PVC is formulated with various additives that alter its properties, and these must be selected for specific uses. Plasticisers are used to increase the softness of the coating, pigments give the coating its *“lustre and beauty”* and also *“play an important role in the colour, UV stability and opacity”* of the fabric. In addition PVC is stabilised with *“thermal stabilisers, oxidation stabilisers and UV/light stabilisers”* (Forster and Mollaert, 2004, p. 226).

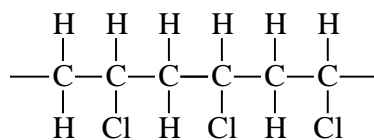


Figure 2-13: Symbolic representation of PVC (Polyvinyl chloride) (Osswald and Menges, 1996)

PTFE (Polytetrafluoroethylene) (Figure 2-14) is under normal conditions non-flammable and resistant to chemical attack. PTFE alone is a good electrical insulator, and also has excellent chemical resistance making it resistant to environmental effects such as mould growth and pollutants. In addition PTFE exhibits self-cleaning properties (repelling dirt) and as it is hydrophobic helps defend glass-fibre yarns against water damage that would otherwise reduce fabric strength. Finally PTFE is *“totally resistant to UV and IR-radiation”* (Forster and Mollaert, 2004, p. 228).

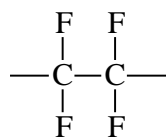


Figure 2-14: Symbolic representation of PTFE (Osswald and Menges, 1996)

Silicone (Figure 2-15) is used predominantly on glass fabric, gives a more flexible fabric, and offers greater translucency than PTFE coatings (Chilton and Velasco, 2005). Silicone coatings are based on silicone rubbers which are *“obtained by cross-linking during processing of silicone macromolecules”* (Forster and Mollaert, 2004, p. 229).

Silicone coatings have good *“elasticity and mechanical resistance”*, however in comparison to PTFE, silicone has poorer *“seamability”* and collects dirt faster (Forster and Mollaert, 2004, p. 229). It is suggested that surface treatments in development at the time of this reference may help *“counterbalance these defects”*. Bulut and Sular (2013) are currently working on this, however, their full paper was not available at the time of completion.

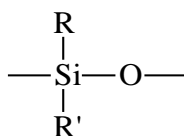


Figure 2-15: Symbolic representation of Silicon coating (Forster and Mollaert, 2004)

The properties of coatings can be examined using uniaxial bias tests in which no yarn connects both loaded points of a sample (Colman, 2013b) (Table 2-3). Uniaxial tests are carried out because the coating is difficult to remove to test independently, and any test on a coating not in situ would not be representative of the coating in use. The coating properties are heavily dependent on the type of coating and its thickness, with each individual fabric generally possessing different set of coating properties.

	Mean Tensile Stiffness (kN/m)
Ferrari PVC-polyester F702	33
Ferrari PVC-polyester F1202	37
Verseidag PTFE-glass fibre B18089	36
Verseidag PTFE-glass fibre B18059	54
ATEX Silicone-glass fibre ATEX3000	12
ATEX Silicone-glass fibre ATEX 5000	21

Table 2-3: Some example coating properties (Colman, 2013b)

It is important to note that fabric stiffness is calculated in kN/m. The fabric's thickness is negated when considering the stress as no consideration of out-of-plane deformation is made when considering fabric deformation, and the thickness is very small when compared to the width.

	PTFE	PVC
Tensile Strength (N/mm ²)	25-36	10-25
Elongation at break (%)	350-550	170-400
Modulus of elasticity (N/mm ²)	410	1000-3500

Table 2-4: PVC and PTFE coating properties (Osswald and Menges, 1996)

Farboodmanesh *et al.* (2005) describes how the coating thickness and impregnation, mentioned above, can drastically effect a fabric's properties although this specifically relates to shear properties which will be discussed in more detail below (§2.2.7.4).

Pavlidou *et al.* (2003, p. 1301) describes how the "*thickness of the coating should be kept as small as possible to eliminate the possibility of reduction in composite strength and modulus*" and how a large coating thickness may lead to "*Systematic decreases in flexural strength*". Additives are included in coatings for a variety of reasons: to effect flame retardation, to improve seamability or to alter the mechanical properties of coatings (Forster and Mollaert, 2004).

	Poisson's ratio
Flexible PVC	0.3 ⁴
PTFE	0.46 ^{2,3}
Silicone	0.47 - 0.4 ^{1,5}

Table 2-5: Poison's ratios of coatings (O'Hara, 1983; Fillon and Glavatskih, 2008; McKeen, 2009; Ognedal *et al.*, 2012; AZO_Materials, 2014)

The Poisson's ratios of the coatings were obtained from a number of sources. PVC used in fabrics is flexible PVC which includes plasticisers. PTFE is a standard well known

material and its properties are widely published. Lastly Silicone refers to Silicone rubber, rather than the other forms of Silicone which are available and have widely varying properties. There is some variation in the published properties of silicone coatings, although all of these are in the range presented in the table.

2.2.4. Fabric Weaves

There exist a variety of different weaves available for use in architectural fabrics (Figure 2-16). Different sources suggest that different weave patterns are more or less common than others: Bridgens (2005) suggests that plain weave fabrics are most common in architectural fabrics, whilst the Tensinet Design Guide (Forster and Mollaert, 2004) suggests that both plain weave and 2-2 basket weave (or panama) weaves are the most common. However, Chilton and Velasco (2005) focus on the basket or Panama weaves. Plain Weave fabrics are most commonly in use in architectural fabrics (all those discussed in Table 2-3), with every fabric available for testing at the time of writing being a plain weave fabric. As such all work within this report will focus exclusively on plain weave fabrics, and not attempt to produce inverse models, or design, for other weave types, these being outside of the scope of the project (§1.4). The weave of the fabric impacts on the mechanical properties of the fabric by altering the force distribution on the fibres and varying crimp interchange.

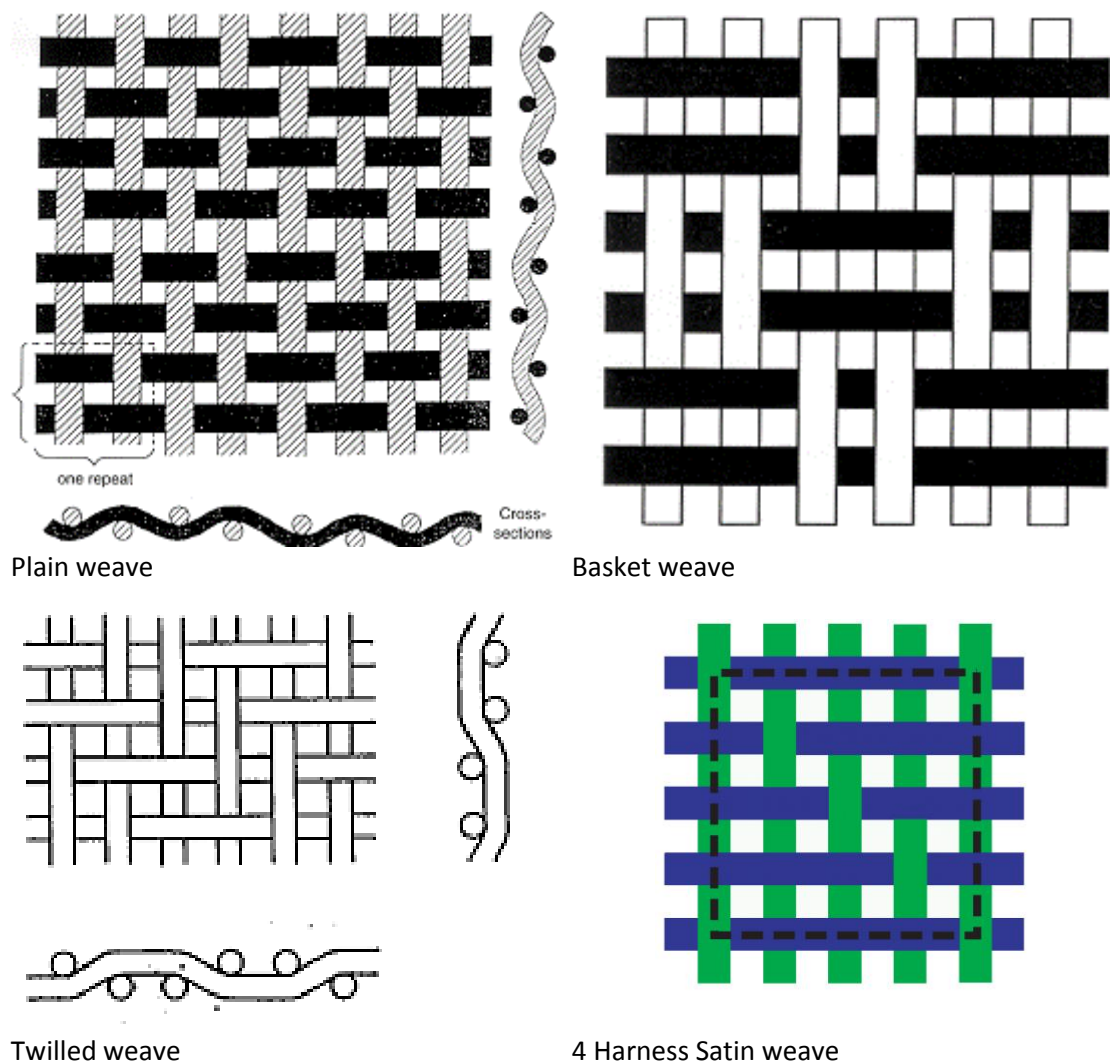


Figure 2-16: Fabric weaves (BSI, 1971; WOO *et al.*, 2002; Forster and Mollaert, 2004; Rao *et al.*, 2008)

The plain weave has the simplest weave geometry, whilst the panama weave exhibits less crimp in the yarns (Forster and Mollaert, 2004). Within a fabric two directions are normally defined; the warp and weft. The warp direction refers to the yarn down the length of the roll, whilst the weft yarn is across the roll (i.e. the shorter).

There also exists “*multi-layered weaves*” (Lomov *et al.*, 2005, p. 18), however this work is not concerned with these as they are used predominantly for “*heavy apparel and footwear*” (Lomov *et al.*, 2005, p. 18) which is beyond the scope of this work.

The testing for geometric properties of a fabric is carried out in accordance with independent institute’s test methods. Alternatively national standards offer guidance on methods to describe fabric geometry such as yarn count British Standards Institute (BSI, 1984). As fabric testing is outside of the scope of this thesis no further discussion will be carried out (§1.4).

2.2.5. Creep and cyclic loading

Creep is the “Time-Dependant deformation under a constant load” (Gerdeen *et al.*, 2006), and this can be expressed as the creep strength, or the creep under constant load (Figure 2-17 and Figure 2-18). Creep is the viscous (slow) deformation under constant load. As time increases the strain under constant load increases (Figure 2-18). The creep strength is dependent on time and ambient conditions, whilst the creep response can be represented as a function of the strain and time given that “most creep curves reduce to straight lines when plotted in a log-log graph” (Osswald and Menges, 1996, p. 271) (Equation 2-3).

$$\varepsilon(t) = M(\sigma, T)t^N \quad \text{Equation 2-3}$$

where M and N are material dependant properties, and T and t represent temperature and time respectively.

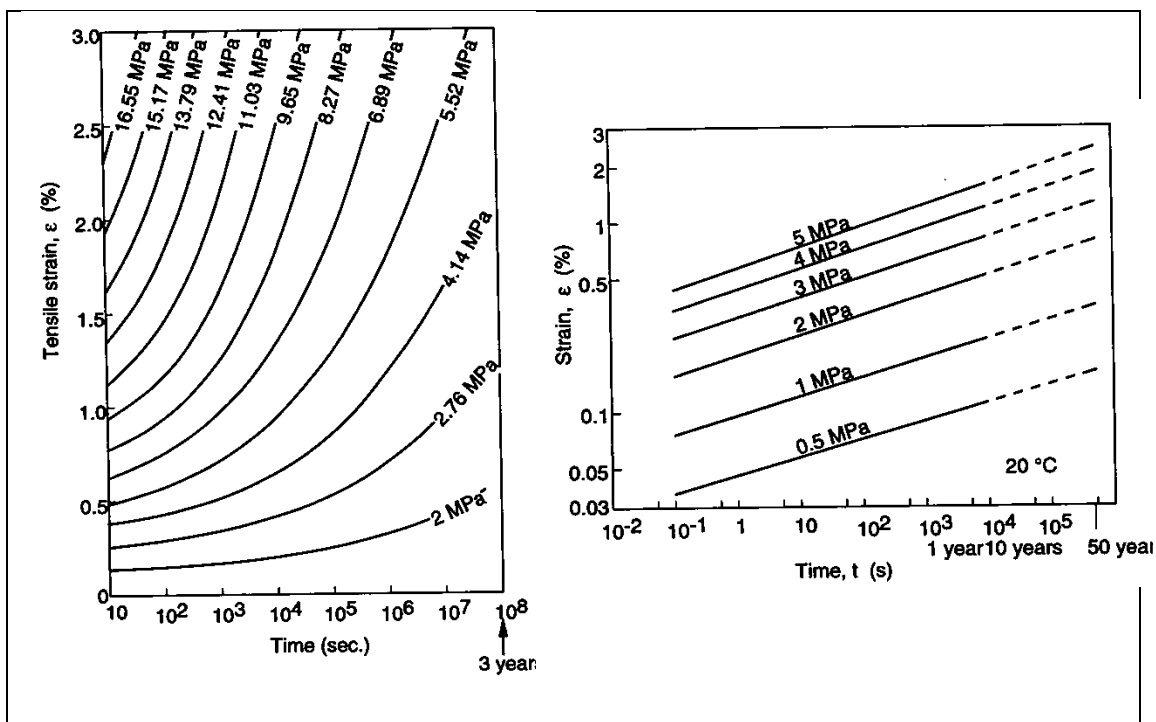


Figure 2-17: Polymer creep responses under constant load: Reproduced from Osswald and Menges (1996)

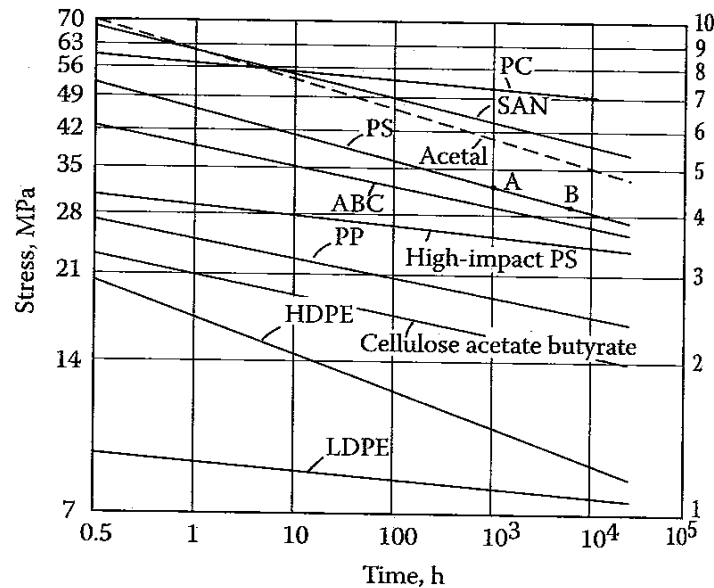


Figure 2-18: Creep Strength data for some polymers: Reproduced from Gerdeen *et al.* (2006)

Cyclic loading will damage fibres, reducing the residual strength of the composite (Jones, 1994) (Figure 2-19). This is referred to as the Load History of the fabric. *“The time dependence of the mechanical properties is especially evident in the creep failure of polymers”* (Gerdeen *et al.*, 2006).

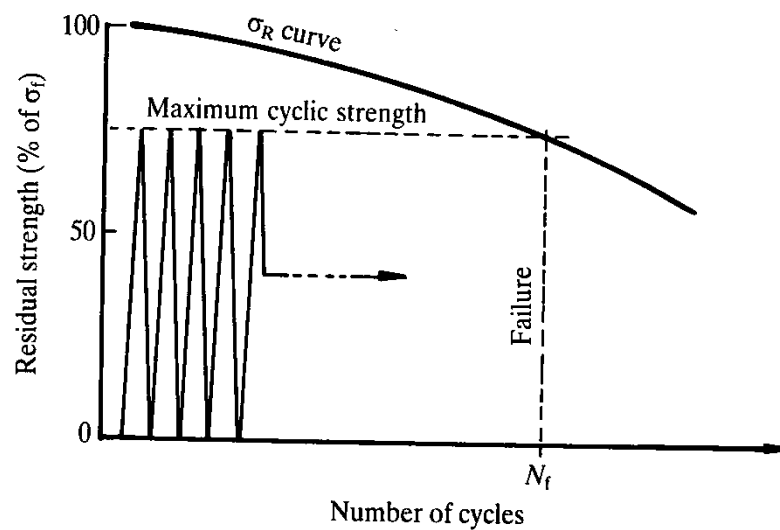


Figure 2-19: Reduction in residual strength due to cyclic loading. Reproduced from Jones (1994)

2.2.6. Fabric Manufacture

Yarns are woven on looms to form fabrics. The limiting factor to size in this process is the width of the loom. The looms used by Verseidag are up to six meters wide (weft direction) (Verseidag, 2011), however there is no limit to the length of the fabric in the warp direction, other than the availability of yarns of the required length which can be kilometres in length.



Figure 2-20: Fabric Manufacture, 6m wide Loom. Reproduced from Verseidag (2011)

Due to the tension in the yarns in the warp direction during manufacture there is 'generally' considerably more crimp in the weft direction due to manufacturing. This can lead to complications in the calculation of the required prestress, and fabric response as discussed above (§2.1). The crimp in the weft direction can be reduced to introduce stress in the warp direction by applying tension (increasing its crimp). However, if this is reversed, and the crimp in the warp direction is reduced to increase stress in the weft direction considerably more stress will be required in the warp direction to induce the required stress in the weft direction. Skelton and Freeston (1971) describe how differential tensions can develop during the process of transferring fabric from roll to roll which can lead to bowing in the weft direction yarns. Bowing in the weft yarns during manufacture can result in non-orthogonal fabric geometry.

Ferrari Précontraint is produced under warp and weft tension during coating (Ferrari, 2014) which should reduce any lack of stability in fabric properties due to weaving, or loss of tension prior to coating. Published advantages are:

- Exceptional dimensional stability
- Long-term strength
- Greater coating thickness at the top of the yarns
- Exceptional flatness

2.2.7. Coated fabrics: Classification and response

A wide variety of fabrics types exist, and within each type there is a wide range of different geometries available, leading to an extensive variety in the choice of fabric properties. These are covered in a series of Standards and codes of practice, and discussed below. Only certain fabric types will be prevalent in the discussion as these are the most commonly used fabrics in architectural and structural applications.

2.2.7.1. Fabric types and properties

Yarns are combined with coatings in a weave to produce a “*fabric composite material*” whose “*mechanical response is truly different from the simple sum of the behaviour of its two components*” (Farboodmanesh *et al.*, 2005, p. 198). The most common and their general published properties are listed in the tables below (Table 2-6 and Table 2-7).

	Polyester fabric			Fibreglass fabric	
Coating	PVC	PVC	PVC	PTFE	Si
Top coating	Acrylic	PVF-lamination	PVDF-merging		
Expected lifetime	8-10 years	12-15 years	12-15 years	>30 years	>30 years
Ageing Resistance	Average	Good	Good	Very good	Very good
Self-cleaning	Average	Good	Good	Very good	Average
Transparency	Good	Good	Good	Good	Very good
Fire-retardant	Good	Average	Good	Very good	Very good
Foldable	Very good	Average	Good	Bad	Average

Table 2-6: Properties of fabrics (Houtman and Orpana, 2000)

Fabric/Coating	Weight [g/m²]	Fire retardant	Tensile strength Warp/weft [N/50mm]	Tensile strain Warp/weft [%]	Tear strength [N]	Bending capacity
Polyester/PVC		B1				Very Good
Type 1	800		3000/3000	15/20	350	
Type 2	900		4400/3950	15/20	580	
Type 3	1050		5750/5100	15/25	950	
Type 4	1300		7450/6400	15/30	1400	
Type 5	1450		9800/8300	20/30	1800	
Fibreglass/PTFE	800	A2	3500/3000	7/10	300	Sufficient
	1270	A2	6600/6000	7/10	570	
Fibreglass/Si	800	A2	3500/3000	7/10	300	Good
	1270	A2	6600/6000	7/10	570	
Aramid/PVC	900	B1	7000/9000	5/6	700	Good
	2020	B1	24500/24500	5/6	4450	
PTFE/-	520	Non com- bustible	2000/2000	40/30	500	Very Good
Cotton-	350	B2	1700/1000	35/18	60	Very
Polyester/ -	520	B2	2500/2000	38/20	80	Good

Table 2-7: Mechanical properties of common fabrics (Houtman and Orpana, 2000) B1 – Difficult to ignite. A2 – 98% non-combustible.

Only two types of yarns which are commonly available and widely used will be considered in this project; glass-fibres and polyester. In addition only three types of coating will be considered; silicone, PTFE and PVC. Specifically PVC coated polyester, PTFE coated glass-fibre and silicone coated glass-fibre fabrics will be utilised in this project. These fabrics have been chosen as they represent the vast majority of fabrics widely used in architectural applications and are available to be tested. With the exception of Aramid /PVC and Cotton-polyester all the fabrics from Figure 2-6 are represented in the testing selection. As has already been discussed (§2.2.1) cotton fabrics are rarely used as architectural fabrics due to their limited longevity, and PTFE yarns are less available than polyester and glass-fibre yarns. Finally, these fabrics all share certain fundamental geometric properties that will allow for comparisons between different fabric types. This should enable a fabric to be designed for a specific situation with or without prior knowledge of what type of fabric would be preferred for the solution. Polyester base cloth fabrics demonstrate higher strain than glass fibre fabrics, but have a lower tensile strength and stiffness. Therefore, by considering multiple fabric types the model should be more widely applicable.

A comparison between Table 2-6 and Table 2-8 shows that PVC coated polyester fabric structures will be considered as having replaceable parts as their lives are limited to 15

years, however, PTFE fabric structures will be considered as category 4, where the fabric will be expected to last the lifetime of the structure.

Design Working life Category	Indicative design working life (years)	Examples
1	10	Temporary structures ^a
2	10-30	Replaceable structural parts e.g. gantry girders, bearings
3	15-25	Agricultural and similar structures
4	50	Building structures and other common structures, not listed elsewhere in this table
6	120	Monumental building structures, highway and railway bridges, and other civil engineering structures.
^a Structures or parts of structures that can be dismantled with a view of being re-used should not be considered as temporary		

Table 2-8: Indicative Design Working Life (Table NA.2.1.) (BSI, 2007)

Foldability is the ease with which fabric can be transported, glass fibres have a lower flexibility than polyester fibres, and hence polyester fabrics are more foldable. In addition, increased yarn flexibility generally results in reduced shear stiffness as yarns are able to bend more (§2.2.7.4), allowing for the creation of more highly doubly curved structures without wrinkling (Bridgens, 2005).

2.2.7.2. *Fabric classification*

The European Design Guide for Tensile Surface Structures (Forster and Mollaert, 2004) classifies PVC coated polyester fabric into five categories and PTFE coated glass-fibre fabric into the seven categories (Table 2-9 Table 2-10). Forster and Mollaert (2004) suggest that for comparisons between fabrics the latter five classifications for PTFE glass-fibre should be compared to the five categories for PVC coated polyester. However, in addition to PTFE coated glass-fibre and PVC coated polyester fabrics, silicone coated glass fibres fabrics will need to be considered, and the Tensinet Design Guide does not offer any classifications for these or other fabric types that are occasionally used.

2. Literature Review

Type	1	2	3	4	5
Surface weight (g/m ²)					
French design guide	720	1000	1200	1400	2000
WG Messe Frankfurt	800	900	1050	1300	1450
Tensile strength warp/weft (kN/m)					
French design guide	60/60	84/80	110/104	120/130	160/170
WG Messe Frankfurt	60/60	99/79	115/102	149/128	196/166
Trapezoidal tear warp/weft (N)					
WG Messe Frankfurt	310/350	520/580	800/950	1100/1400	1600/1800

Table 2-9: Classification of PVC coated polyester fabric (Forster and Mollaert, 2004)

Type	G1	G2	G3	G4	G5	G6	G7
Tensile strength warp/weft (kN/m)	26/22	43/28	70/70	90/72	124/100	140/120	170/158
Surface weight (g/m ²)	500	420	800	1000	1200	1500	1600
Trapezoidal tear warp/weft (N)	-	-	300/300	300/300	400/400	500/500	450/450

Table 2-10: Classification of PTFE coated glass-fibre fabric (Forster and Mollaert, 2004)

	PVC coated polyester fabrics	PTFE coated glass fabrics	Silicone coated glass fabrics	PTFE coated PTFE fabrics
Tensile strength warp/weft (kN/m)	115/302	124/100	107/105	84/80
Fabric weight (g/m ²)	1200 (type 3)	1200 (type G5)	110	830
Trapezoidal tear warp/weft (N)	800/950	400/400	960/700	925/925
Visible light transmission (%)	10-15	10-20	<80	19-38
Flexibility/crease recovery	High	Low	High	High
Fire reaction	M2 (NFP 92 503) B1 (DIN 4102)	M1 (NFP 92 503) B1/A2 (DIN 4102)	A (ASTM E-108) no toxicity of smokes	
Cleaning	Easier with top coats	Self-cleaning	Self-cleaning	Self-cleaning
How to make the seams	By high frequency	Thermally	Vulcanisation	Stitching
Life span (years)	>15-20	>25	>25	
Cost	Low	High	High	

Table 2-11: General comparison of the properties of fabrics (Forster and Mollaert, 2004)

Some detail is available in the Tensinet design guide for silicone coated glass-fibre fabrics, summarised above (Table 2-11) (Forster and Mollaert, 2004).

2.2.7.3. *In-plane tensile response*

“Fabric structures resist environmental loads as tensile stresses in the plane of the fabric” (Bridgens and Gosling, 2004, p. 1913). The tensile response of textile composites is highly non-linear due to the nonlinearity of the constituent material properties and the effect of the weave geometry. The non-linear response can be seen in uniaxial tests (Figure 2-22). The nonlinearity of the response is caused by both constituent material property nonlinearity (§2.2.1, 0, 2.2.3), and as a result of the interaction between the yarns and coating in the woven fabric.

Crimp interchange is the process by which fabrics alter their geometry prior to the extension of the yarns due to their stiffness. A force applied in one yarn direction straightens that yarn out, and forces the other direction to pull around it (Figure 2-21). This in turn results in some reaction to the original force, and will produce a contraction

of the unloaded direction. Due to the intricacies of this process it is possible to achieve a higher contraction in the unloaded direction than the extension in the loaded direction, and therefore Poisson's ratios of more than 0.5 are possible, and will be shown in later chapters.

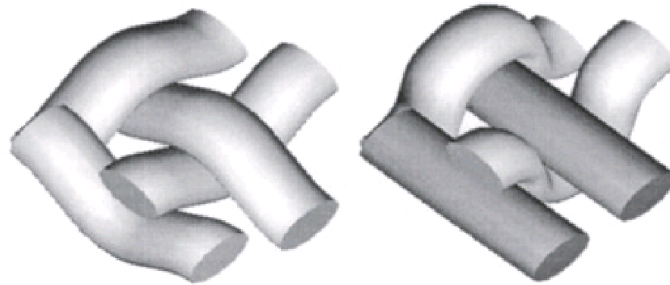


Figure 2-21: Crimp interchange, reproduced from (Lomov *et al.*, 2005)

At low loads the uniaxial tensile response is expected to have a shallower gradient (lower tensile stiffness) than at high loads, as the geometry of the fabric deforms in response to the load rather than the components extending (predominantly) by crimp interchange. After a new equilibrium geometry is reached where the yarns in tension have been (largely) straightened the yarns themselves will begin to deform under load. This results in a higher stiffness response dominated by the yarn response (§2.2.1).

There will be some component of both of these deformation mechanisms at all times during the deformation process in addition to the response of the coating at all loads. However the problem is simplified by Kageyama *et al.* (1988) to suggest that deformation followed by yarn extension is present in discrete response 'zones'.

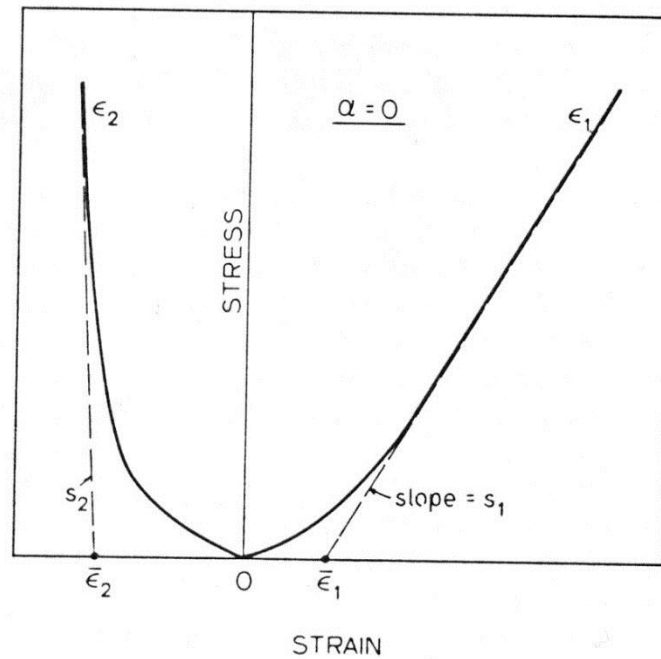


Figure 2-22: Example of uniaxial response, reproduced from Testa *et al.* (1978). ϵ_1 and ϵ_2 are the strains in the warp and weft yarn respectively.

Biaxial response further complicates the uniaxial response by introducing stress in both the warp and weft direction. The ratio between the loads in the different directions and the magnitude of the loads will alter the fabric stiffness, with crimp interchange or yarn extension remaining the dominant deformation mechanisms at different loads.

Applying a load in one direction will cause the yarns in that direction to straighten out (Figure 2-21), leading to a positive strain in that direction and a negative strain in the other direction. It then follows that if there was originally more crimp in the loaded direction that a higher degree of crimp interchange will occur as the fabric settles into a new equilibrium position. When the response of fabrics to biaxial load is visualised the high degree of nonlinearity this generates in conjunction with other deformation mechanisms becomes apparent (Figure 2-23 and Figure 2-24).

Crimp interchange was first noted by Peirce (1937) as being the principal deformation mechanism of fabrics under biaxial load. In 'as produced fabric' (or virgin fabric) crimp will generally be high in the weft direction with warp yarns demonstrating less crimp due to manufacturing processes. This may be varied by manufacturing techniques (§0)

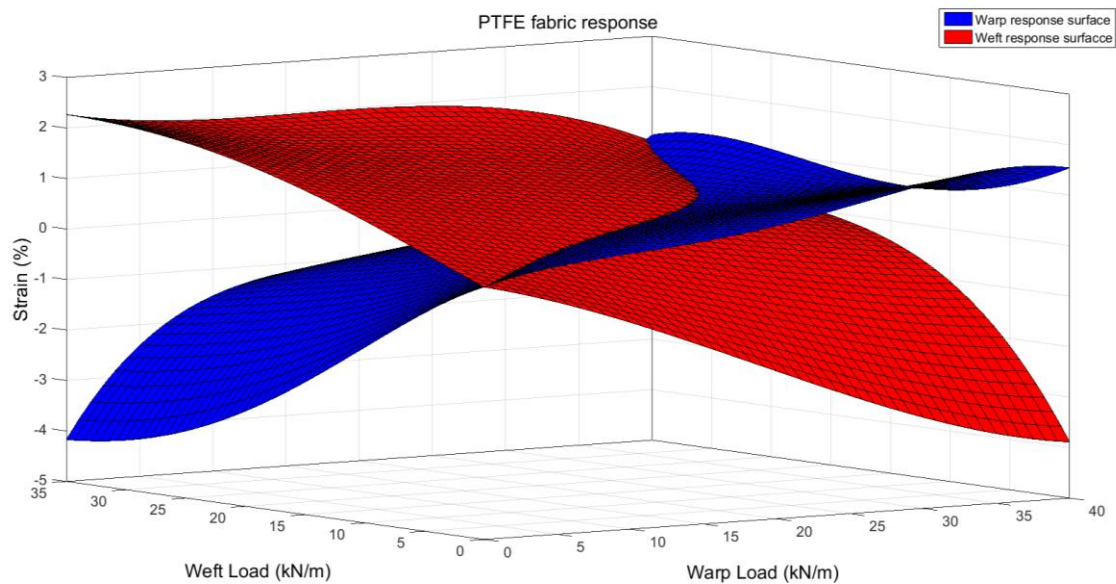


Figure 2-23: Example of nonlinearity of biaxial response, PTFE response planes produced from biaxial tests carried out on B18059 PTFE coated Glass-fibre fabric

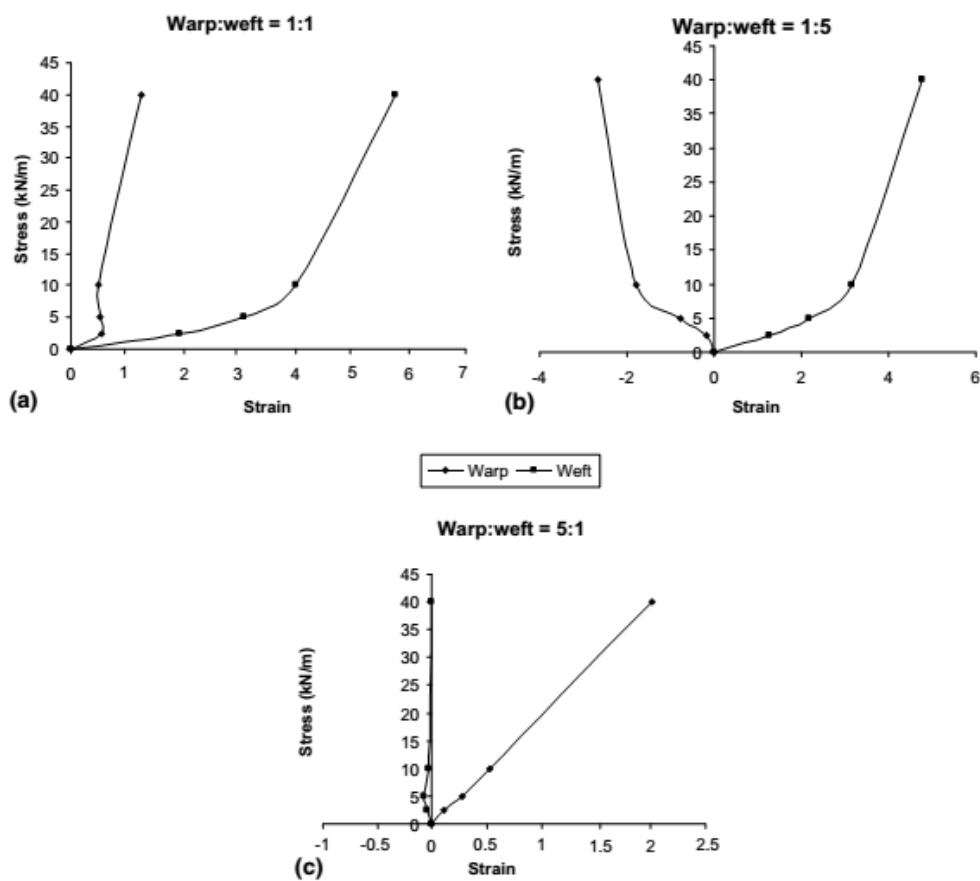


Figure 2-24: Biaxial stress-strain curves for PTFE fabric (Bridgens and Gosling, 2004)

The key features of fabric response as described by Bridgens and Gosling (2004, p. 1914) are: *“sudden changes in gradient (a and c), gradient reversal (i.e. multiple values of stress for a given strain) (a) and negative strain (band c) (Figure 2-24).*

These characteristics cause difficulties in establishing a single function which can fit all of the data and be developed into a response surface.” And as such numerous descriptions of the surface (§2.3.1) and constitutive models of the fabric (§2.3.2) have been developed to attempt to predict or represent the response of fabrics.

Fabrics also exhibit creep over time, time dependant hysteresis, and variability within batches and between batches and rolls (§2.2.5).

The Poisson’s ratio is the contraction of a fabric in one direction due to an extension in the other direction. Plane stress theory requires that Poisson’s ratio cannot exceed 0.5, however tests carried out on multiple different fabrics have shown that it can in fact be as high as “2.02” (PTFE glass G6 fabric) (Gosling and Bridgens, 2008). These higher values are required to *“model the high level of warp-fill interaction and large negative strains which occur in woven fabrics under biaxial load”* (Gosling and Bridgens, 2008, p. 216). It is therefore possible that a contraction in say the warp direction might be greater than the elongation it resulted from.

For a linear elastic materials the orthotropic constitutive model holds that the Young’s moduli (E_w and E_f refer to warp and fill directions respectively) are related to the Poisson’s ratios (ν_{wf} and ν_{fw} refer to the warp-fill and fill-warp ratios respectively) (Equation 2-4).

$$\frac{\nu_{wf}}{E_w} = \frac{\nu_{fw}}{E_f} \quad \text{Equation 2-4}$$

Using this theory may not be consistent with fabric behaviour, as interactions between the coating and yarns means that the complex fabric behaviour may not be adequately represented by elastic constants in this fashion. Gosling and Bridgens (2008, p. 220) state that as *“coated woven fabrics are not homogenous materials”* and therefore there is no requirement for the reciprocal relationship to be held (Equation 2-4). They should be considered to be more like mechanisms. To this end they offer an alternate

calculation for the Poisson's ratio (Equation 2-5) where 'C' is a constant related to the fabric type.

$$\frac{\nu_{wf}}{E_w} = C \left(\frac{\nu_{fw}}{E_f} \right) \quad \text{Equation 2-5}$$

The value of C is an empirical constant calculated from test data Gosling and Bridgens (2008, p. 219) (PVC coated polyester = 1.51, PTFE coated glass fibre = 1.40).

If fabrics are considered more like mechanisms it is possible to consider how the linear elastic relationship may hold for the yarns or coating, but not for the entire fabric.

2.2.7.4. *Shear*

"In-plane (or intra-ply) shear is generally considered to be the primary deformation mechanism during forming [finding the form the structure will take]" so must be considered for the design of a fabric (Boisse *et al.*, 2005b, p. 63). The double curvature in a fabric will be dependent on the supporting structure, but the amount that can be achieved will be related to the shear the fabric can undergo. However, calculating shear forces in a fabric, and the effect of biaxial loading on shear forces is complex. Whilst shear stiffness is known to be an important parameter in the analysis of doubly curved fabric structures *"shear behaviour remains absent from some analysis methodologies used by industry"* (Colman *et al.*, 2014, p. 163).

Unlike the simple engineering shear used in the analysis of plates and laminas the shear observed in woven fabrics is 'pure shear'. The side lengths are considered constant unlike in *"simple or 'engineering' shear"* where the area remains constant, and side lengths are allowed to vary (Colman *et al.*, 2014, p. 165) (Figure 2-25). Fabrics deforming in this way deform in a *"Trellis-like manner"*, with yarns rotating relative to the fulcra at the cross overs (Buckenham, 1997, p. 33). The importance of this can be demonstrated by considering the yarns as inextensible members (Nguyen *et al.*, 1999; Sun and Pan, 2005) and considering the large shear deformation often found in fabrics (typically up to 15°) (Bridgens, 2005; Colman *et al.*, 2014). In uncoated fabrics this can be even higher, exceeding 50° (Colman *et al.*, 2014), which suggests that the addition of a coating reduces the observable shear by 35°, confirmed by an observation made by Gosling *et*

al. (2013, p. 314): “The woven yarns provide tensile strength, whilst the coating stabilises and protects the weave and provides waterproofing and shear stiffness”.

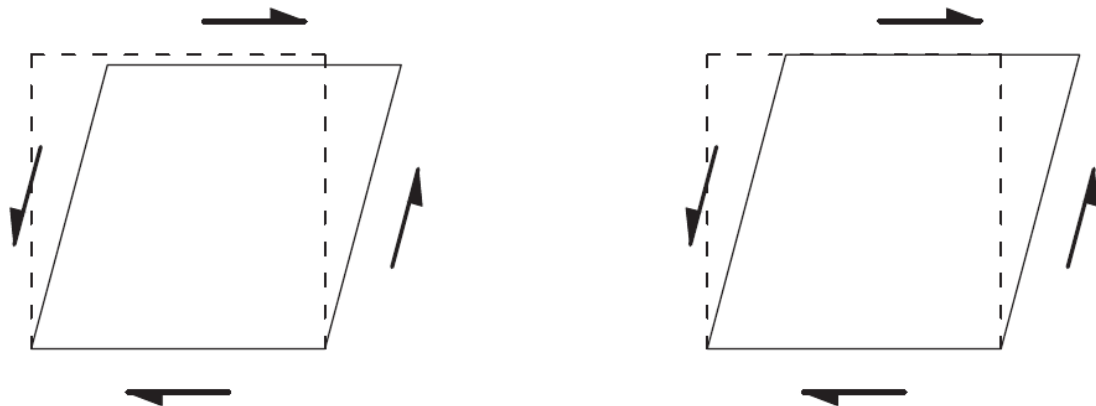


Figure 2-25: simple (right) and pure (left) shear reproduced from Colman *et al.* (2014)

Liu *et al.* (2004) consider three distinct states of (uncoated) fabric response to shearing for “*balanced plainweave*” fabrics. The initial state determines the geometry of the fabric which is then described as deforming in a “*trellis shear*” deformation mode. Two shear resisting mechanisms are then considered: Intra yarn friction (Figure 2-26 region 1) is the result of the friction between yarns at cross over due to tension in the fabric (and therefore a function of the out of plane force). Whilst yarn compaction occurs at lock up (γ_L in Figure 2-26) and resists considerably more load than yarn friction. A number of shear deformation mechanisms have been identified, some of which are shown in Figure 2-26:

- fibre rotation (Nguyen *et al.*, 1999)
- fibre slip (Nguyen *et al.*, 1999)
- yarn lock up (Nguyen *et al.*, 1999)
- yarn bending (Grosberg and Park, 1966)
- intra yarn friction (Liu *et al.*, 2004)
- yarn compaction (Liu *et al.*, 2004)
- coating shear resistance (Testa and Yu, 1987)

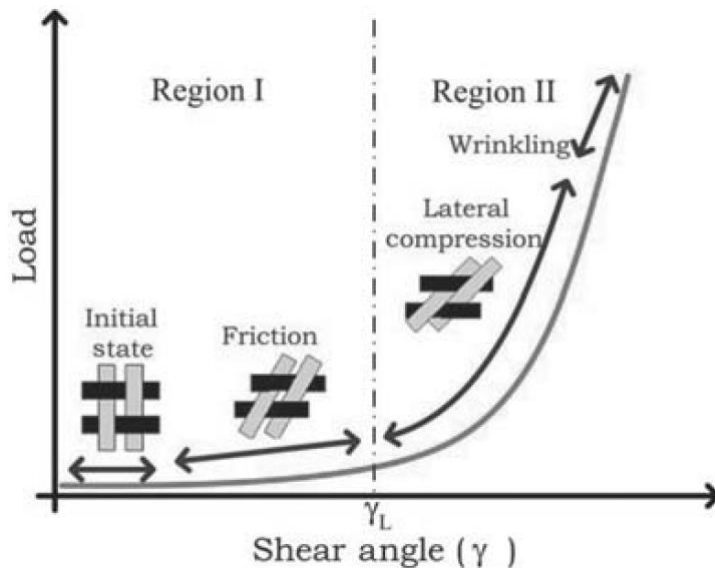


Figure 2-26: Diagram of the load-shear angle curve reproduced from Liu *et al.* (2004)

A more detailed investigation of this, and use of the formulation supplied by Liu *et al.* (2004) with its revision by Colman (2014) is made in the following chapter (§3.4.3).

Fibre slip is unlikely to occur in a coated fabric where the coating will restrain any lateral movement of the yarn at the fulcra, meaning that it will be necessary to consider the other deformation mechanisms. Matsudaira and Kawabata (1998) also model a gap between silk yarns that they consider to have a “*strong effect*” on the shear response of the fabric, but the applicability of this to coated fabrics would be limited as no gap can be observed to exist (Figure 2-12).

Grosberg and Park (1966) established that for uncoated fabrics in the early stages of deformation the response is predominantly due to yarn bending where no slippage has occurred (at very low shear angles). Following this the yarns begin to slide (rotate) about the fulcra (crossovers) producing friction between yarns and possibly elastic compaction forces between adjacent yarns. Lastly jamming occurs leading to wrinkling (Buckenham, 1997; Page and Wang, 2000).

However, having noted the above deformation mechanisms for uncoated fabrics, Testa and Yu (1987, p. 1636) state that “*resistance to shear deformation arises almost entirely from the coating*”. This may be important, but considering the underlying fabric architecture to have no input into the response of a fabric would seem to be an oversimplification where coated fabrics are known to have complex nonlinear responses.

It may be the case that the coating is principal in determining fabric response, but consideration of yarn interaction should also be noted. This is discussed in detail in the following chapter (§3.7.2), where the coating will be shown to be the principal method by which fabrics resist shear deformation, however, the underlying fabric geometry also affects the shear stiffness.

Woven fabrics may only shear to a limited degree after which further shear strain will lead to increased shear stiffness and wrinkling (Liu *et al.*, 2004; Gosling *et al.*, 2013; Colman *et al.*, 2014). Wrinkling (fabric lock-up or yarn lock-up) (Jones and Pickett, 2005) occurs when parallel yarns become ‘jammed’ against each other, and is characterised by rapid increases in shearing force, which leads to wrinkling, though this may not be entirely the case in coated fabrics (Nguyen *et al.*, 1999). Wrinkling must be avoided in construction as it is unsightly and leads to stress concentrations in the ridges.

Yarn lock-up would seem most readily applicable to finite element analysis where yarn lock up is expected to occur, given the complex interaction between yarns, and this has resulted in a number of FE methods that aim to quantify shear deformation in terms of finite element modelling (Page and Wang, 2000; Boisse *et al.*, 2005a; Badel *et al.*, 2007). These methods have the advantage of being able to calculate the frictional area between perpendicular yarns and the area of resistance between perpendicular yarns (Figure 2-27). However, these methods requires detailed knowledge of the yarn prior to analysis so does not lend themselves to predictive calculations. Lastly, none of the FE methods noted later (§2.3.2.4) consider coated fabrics.

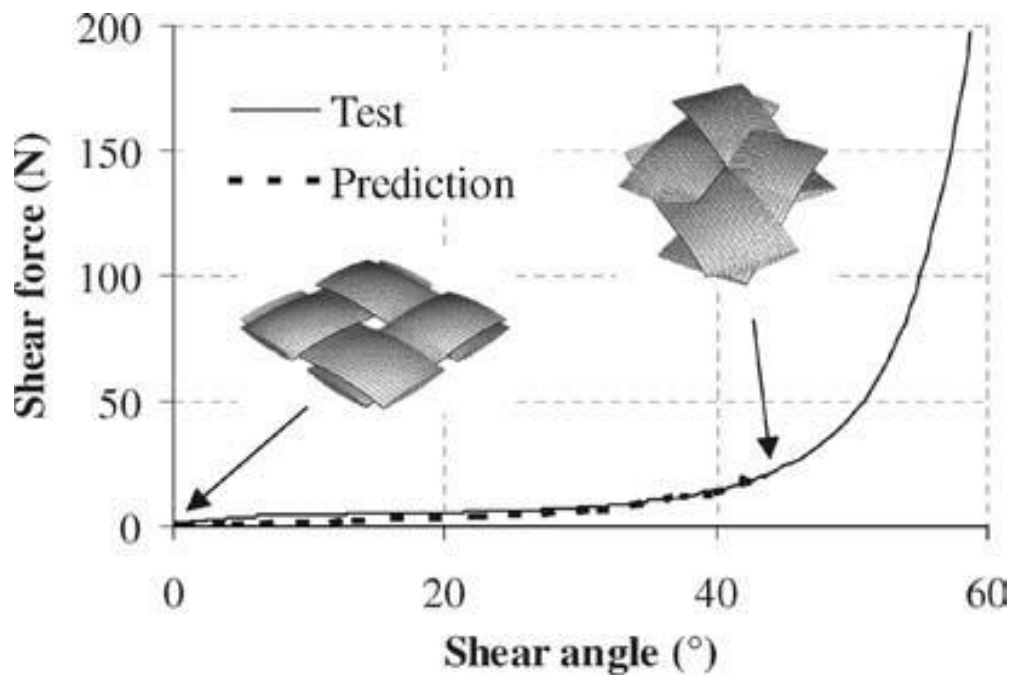


Figure 2-27: Test and prediction of in plane shear for a plain weave glass fabric using an FE method reproduced from Boisse *et al.* (2005a)

Coated fabric shear response, similarly to tensile response is characterised by hysteresis with the response curves shape being related to the stages of deformation discussed above.

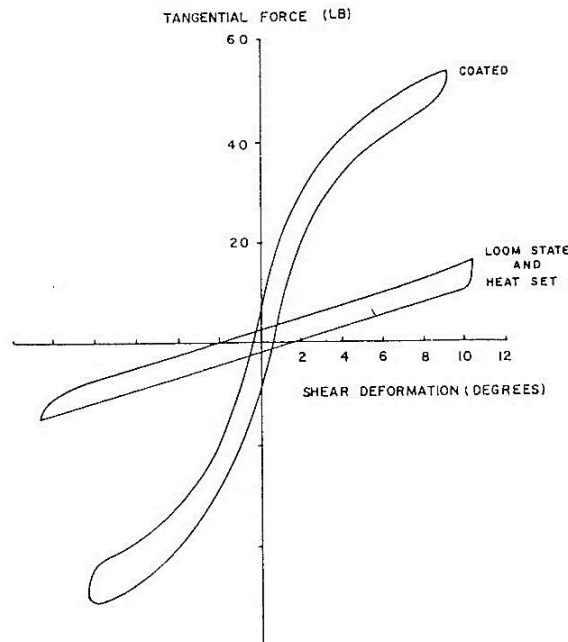


Figure 2-28: comparison between the response of coated and uncoated fabrics manufactured specifically for the tests (Skelton and Freeston, 1971)

The shear stiffness of a coated fabric was found to be ten to a hundred times greater than the uncoated substrate (Skelton and Freeston, 1971) (Figure 2-28).

Farboodmanesh *et al.* (2005, p. 197) states that shear behaviour in rubber coated fabrics is “*governed by the interaction of its two components*” in contrast to the earlier statement by Testa and Yu (1987) who state that shear response is governed by the coating. The work by Farboodmanesh *et al.* (2005) considers an altogether different type of fabric where the coating is formed from a neoprene latex to those normally employed in architectural structures. Whilst neoprene latex is not directly applicable to architectural fabric this paper is the only available source that considers the thickness of coating and impregnation of coating into the fabric base cloth with relation to shear stiffness. This difference may result in the different conclusion, namely that coating dominates the response at low shear angles with the fabric dominating at higher angles. Further to this Farboodmanesh *et al.* (2005) demonstrates that increased thickness of coating increases the load required for a particular shear angle. Whilst this is not unexpected it is the only available clear demonstration of this through test data. Testa and Yu (1987, p. 1636) consider coated fabrics and describe how that “*for both Teflon coated and silicone coated fabrics the shear response is elastic and nearly linear*” though this is for low shear angles it appears to be in contradiction to the response curves presented by Colman *et al.* (2014).

Current best practice is to use the plane stress orthotropic equations (Equation 2-6) (Colman *et al.*, 2014). It is important to note that in the plane stress orthotropic equations the shear response is entirely uncoupled from the tensile stiffnesses (E_w , E_f). The zero values in the cells [...]1,3, [...]2,3, [...]3,1, and [...]3,2 ensure that the in-plane tensile response is not linked to the in-plane shear response. This is not confirmed by work by Liu *et al.* (2004), who links the extension of yarns to an increased area of friction between yarns, resulting in a higher shear stiffness. However, if Testa and Yu (1987) are correct and the coating is only responsible for a fabric’s shear stiffness then this assumption will be accurate.

$$\begin{Bmatrix} \varepsilon_w \\ \varepsilon_f \\ \varepsilon_{wf} \end{Bmatrix} = \begin{bmatrix} \frac{1}{E_w} & \frac{-\nu_{fw}}{E_f} & 0 \\ \frac{-\nu_{wf}}{E_w} & \frac{1}{E_f} & 0 \\ 0 & 0 & \frac{1}{G_{wf}} \end{bmatrix} \cdot \begin{Bmatrix} \sigma_w \\ \sigma_f \\ \sigma_{wf} \end{Bmatrix}$$

Equation 2-6

Where $\epsilon_{w,f,wf}$ are the warp, weft, and shear strains respectively. $E_{w,f}$ are the in-plane tensile stiffnesses, $\nu_{fw,wf}$ are the in-plane Poisson's ratios, G_{wf} is the shear modulus, and $\sigma_{w,f,wf}$ are the stresses.

2.2.7.5. *Bending and compression*

“Architectural fabrics have negligible [out-of-plane] bending and [in-plane] compression stiffness” (Gosling *et al.*, 2013, p. 314). As such, whilst the small scale consideration of the bending of individual yarns in the case of shear has been dealt with in the previous section (§2.2.7.4) no detailed discussion of fabric unit cell bending will be made in this section. Fabrics are known to respond to loading by large deformations, biaxial tensile response, and shearing. As such bending stiffness is never considered in the analysis of a fabric.

Further to this fabrics have negligible in plane compressive stiffness in both of the principal yarn directions, so this too will be given no further consideration.

2.2.7.6. *Tensile strength*

The strength of a fabric is an important characteristic of fabric's, though may be difficult to consider within a unit cell representation of a fabric (§2.3.2.2). A fabric's strength is determined by the strength of the yarns as part of the constituent material, and reduced to less than the sum of the strength of the yarns by the interaction of each yarn with perpendicular yarns (Forster and Mollaert, 2004). Whilst the yarns may have a tensile strength when tested individually the deformations they undergo within a fabric will alter this, reducing it as the yarns are bent around each other. Similarly Pan (1996, p. 313) notes that *“the tensile behaviour of a fabric would be identical to that of its constituent yarns if all yarns were uniform in their tensile properties, and if the interactions between the two perpendicular yarn systems were negligible”*. However, given that this is not the case a method of calculating the strength of the material is then proposed. Using the strength of the yarns excluding the interaction with the perpendicular direction as an initial approximation Pan (1996) then calculates a ‘critical length’, or effective length taking into account out of plane curvature, of a yarn for a given maximum strength. The critical length is described as the equivalent yarn length of a virgin (non-woven) yarn to that of a woven yarn and takes account of inter-yarn interactions. This allows a virgin yarn's properties to be used in strength calculations,

whilst ignoring the inter-yarn interactions. This critical length can then be applied to the original strength calculation based on non-interacting perpendicular yarns to give a fabric strength. It is also noted that whilst this is the case for plane weave fabrics weave structure will affect this value.

The procedure to determine fabric strength as published by the BSI (1998b) is to apply a load along the axis of interest, measuring the extension and load of the sample until break. The maximum load and maximum strain at break are recorded, and correspond to the strength of the material. This is a uniaxial strip test, although biaxially tested fabric exhibit lower values of tensile strength (Happold *et al.*, 1987).

2.2.7.7. Tearing and Tear propagation

Fabric failure will often be due to an existing tear rather than loads exceeding fabric strength. In tear propagation the *“force which originally passed directly through [a tear] before the tear existed, has now been “led around the tear”* (Forster and Mollaert, 2004, p. 239). This leads to a stress concentration at the pinnacle, or tip, of the tear, which if large enough will continue to propagate the tear. Forster and Mollaert (2004) suggest that an initial tear length (critical tear length) should be assumed and the fabric’s resistance to this tear analysed, but do not specify what this should be. More generally the tearing strength is approximately 16% of the tensile strength of a fabric when analysed using a wide strip test (Happold *et al.*, 1987). A wide strip test is a tensile load-extension test performed in an Instron or similar test machine which measures the load-extension characteristics of a wide strip of fabric, 400mm wide.

A number of test methods exist for the calculation of fabric tear resistance including the Tongued (double-tear), the Trouser-shaped (single-tear), the trapezoidal method, and by putting an initial cut into a uniaxial sample (BSI, 1982; BSI, 1998a; BSI, 2003; Forster and Mollaert, 2004).

2.2.7.8. Environmental impact and Recyclability

“The recycling of PVC coated fabrics is possible using a process (patented by Solvay and applied by Ferrari) which allows the separate recycling of the PVC resin and the polyester fibres by selective chemical dissolving.” (Forster and Mollaert, 2004, p. 227). Whilst some companies offer to repurpose fabrics after their return, for instance as floor coverings (Verseidag, 2011) .

The relatively low weight of fabric structures compared to other roofing solutions does generally also result in a reduction of foundation mass and superstructure with a resultant decrease in both cost and material. This in itself increases the environmental performance of fabric structures as they require less embodied carbon in the superstructure and foundations.

The final point of note with relation to the environmental impact of fabric is that the fabric's low mass leads to a high conductivity of external environment to internal surfaces, and low insulation (Forster and Mollaert, 2004). It follows therefore that heating and internal airflow must be carefully monitored for spaces enclosed by a fabric structure.

The generally short life span of architectural fabrics, especially PVC coated polyester fabrics means that they need to be replaced regularly in structures that are constructed for a design life of more than 30 years. Where the fabrics are non-recyclable, the use of architectural fabrics is therefore not sustainable.

2.2.8. Uncoated fabrics: Classification and response

Uncoated fabrics will not be tested or designed in this thesis, however, there is a great body of work that has been carried out on uncoated fabrics, including work by Peirce (1937), and Kawabata *et al.* (1973), Nguyen *et al.* (1999), Grosberg and Park (1966), Testa and Yu (1987) to model uncoated fabrics. The difference between coated and uncoated fabrics is the lack of any restraint provided by the coating on the yarns.

Fabrics are generally classified in terms of their tensile strength, linear density of fibres (Tex or denier), weight and other relevant properties. Tex is "*the unit of linear density, equal to the mass in grams of 1000 meters of fiber, yarn, or other textile strand, that is used in a direct yarn numbering system*" (ASTM, 2013).

2.3. Types of fabric model

Or how can a model be used to design fabrics, and what properties are needed?

This section reviews current methods for the modelling of fabrics, focussing on what is needed to produce a fabric model and later how these might be used to produce an inverse model. Pargana *et al.* (2007, p. 1323) states that “*the accurate and reliable modelling of fabrics is of paramount importance for the successful and realistic design and analysis of these structures*”. The accuracy of models to be used in the description of plane weave fabrics will also be considered. Many models are available, all of which consider different properties of the fabric and make different assumptions regarding its geometry and how loads are distributed. These can be summarised as:

- Result modelling
 - linearizing results
 - curve fitting
 - discretisation
- Yarn modelling
- Unit cell modelling
 - Finite element models
 - Physically based models

2.3.1. Biaxial and Uniaxial stress-strain behaviour representation

The representation of fabric test data has been attempted in a number of ways. Though the complex nonlinear response of fabrics to uniaxial, biaxial, and shear loading means numerous models have been developed to represent fabric response to tensile and shear loads.

Bi-linear representations of fabric response have been widely used to represent test data, the initial crimp interchange dominated response and the later yarn extension dominated response are each represented by a linear relationship (Figure 2-29). However, the linear relationships must be reset for each stress ratio (Testa *et al.*, 1978; Kageyama *et al.*, 1988).

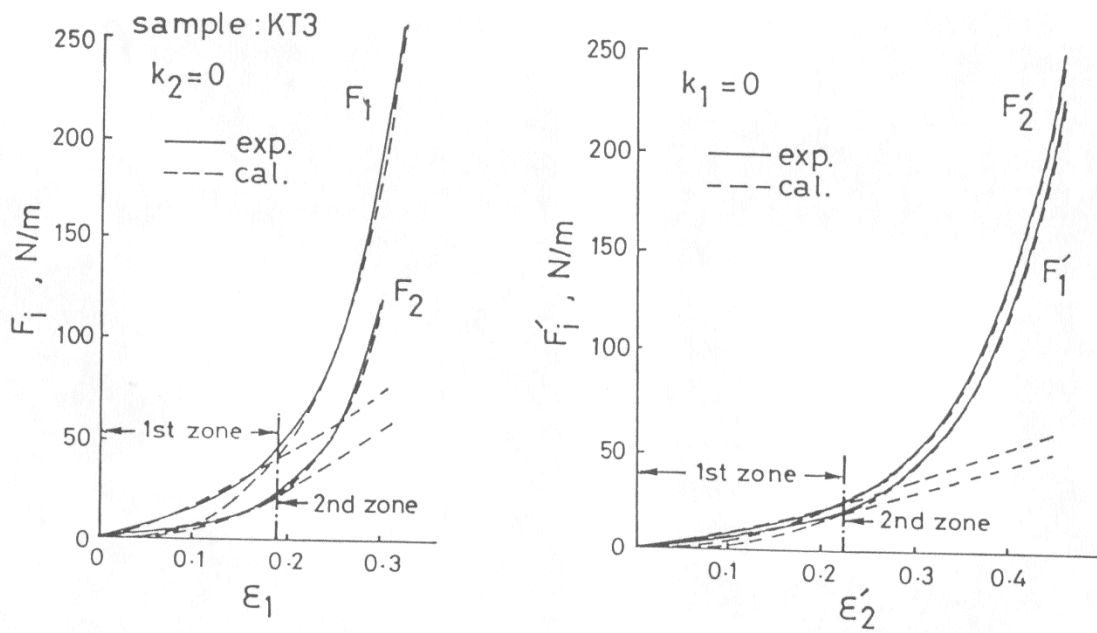


Figure 2-29: Two zones that make up the Bi-linear model reproduced from Kageyama *et al.* (1988)

Modulus-strain curves, using the derivative of the stress strain curve, can also be used to show fabric response, and can show more clearly small differences in mechanical properties. This is often seen as distinct peaks rather than the slight steepening or flattening often noted in stress-strain data. Lucas (1983) produces a fitted polynomial to modulus-strain curves for yarns using the sum of three “*modified Pearson VII lines*” (Figure 2-30). The same modified curves are also used to predict force elongation responses for yarns (Zimlik *et al.*, 2000). The accuracy of this method in reproducing initial moduli, whilst described as being “*better*” than previous models, is highly variable with published percentage differences between measured and predicted response being between 0.4 and 28%.

Chen *et al.* (1995) used “*polynomial functions*” to represent tensile and shear data to enable the calculation of strain energy. Biaxial properties were represented by second order polynomials and shear data represented by third order polynomials. The advantage of this method is that the moduli (derivatives of each curve) could be found quickly and in a single step. However, whilst the published r^2 values are high (greater than 0.98) the data appears to fail to represent sharp changes in stiffness as crimp is removed and yarn extension becomes the dominant deformation mechanism.

The problem with fitted curves which are not based on any physical model is that they give no useful information about the response beyond the points for which test data is

available. Though the data and its visualisation might be used for the range of results already obtained. In particular the noting of the peaks in stiffness at certain strains might be relevant in design (Figure 2-30).

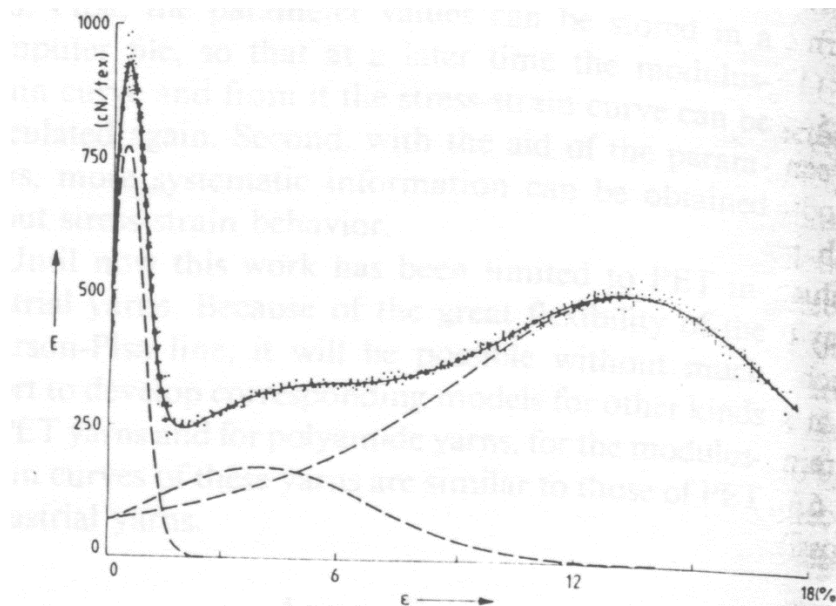


Figure 2-30: measured (dots) and fitted (line) modulus strain curve. The curves from which the fit was made are also shown (-----). Reproduced from (Lucas, 1983)

Strain energy functions produced from the “*complementary strain energy function*” have also been used to represent fabric biaxial response (Testa and Yu, 1987). This method requires the calibration of a number of parameters for any fabric found using uniaxial tensile testing, whilst the model itself appears to show only limited success in predicting response.

Current practice is to use the plane stress representation to represent fabric data with “*Fabric behaviour [] typically defined using elastic constants based on plane stress assumptions*” (Bridgens and Gosling, 2004, p. 1913). The plane stress representation defines the fabric in terms of two Young’s moduli and Poisson’s ratios, reducing the response to a simple representation, and largely ignoring the complex nonlinearity of fabric response.

Three methods of presenting fabric stress-strain behaviour in this way are presented by Bridgens et al. (2004): First is to represent the response in terms of two Young’s Moduli and one Poisson’s ratio which “*remain constant throughout the structural analysis*”.

Second is the “*Use of elastic and interaction moduli*” (Equation 2-7). The Poisson’s ratios can also be determined (Equation 2-8).

$$\begin{bmatrix} \sigma_{11} \\ \sigma_{22} \end{bmatrix} = \begin{bmatrix} E_{1111} & E_{1122} \\ E_{2211} & E_{2222} \end{bmatrix} \begin{bmatrix} \varepsilon_{11} \\ \varepsilon_{22} \end{bmatrix}$$

Equation 2-7

$$v_{12} = \frac{E_{1122}}{E_{1111}}$$

$$v_{21} = \frac{E_{2211}}{E_{2222}}$$

Equation 2-8

For which the subscripts 11 and 22 represent the warp and weft directions respectively. σ =stress, ε =strain, v =Poisson’s ratio, and E = elastic modulus (Blum and Bögnér, 2002) These equations (Equation 2-7 and Equation 2-8) are then solved by considering stresses and strains as small increments at points of interest. “*This procedure will be repeated for every part of the load history. Thus we can get an impression of the elastic moduli over the range of loading*” (Blum and Bögnér, 2002, p. 3).

Thirdly a method for the determination of elastic constants from response surfaces has been developed by Minami *et al.* (1997, p. 598) which “*employs multi step linearized approximation*” (Figure 2-31). In this method biaxial test data is discretised into a number of surfaces for which the response characteristics can be calculated (Figure 2-31).

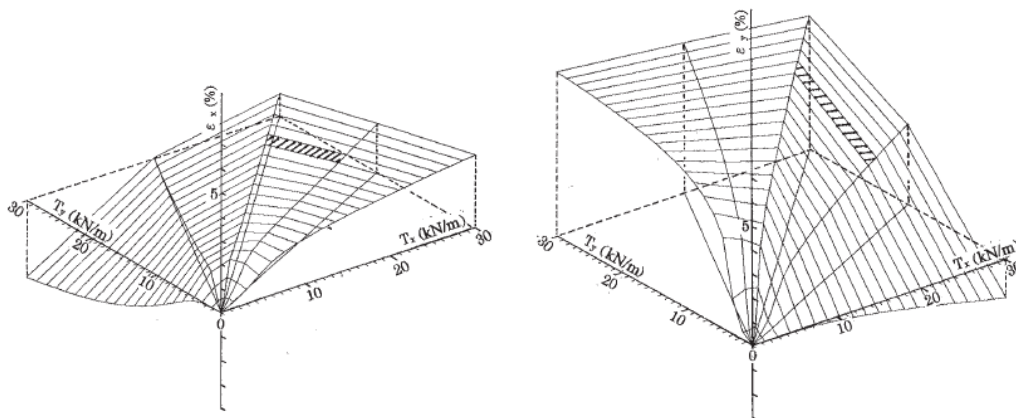


Figure 2-31: Biaxial response surface divided into discrete zones. Reproduced from Minami (2006)

Day (1986, p. 18) uses an alternate method to describe the fabric response based on soil mechanics and “*relating the mean and difference of the principal stresses, to the mean*

and difference of the principal strains". The material is considered to be orthotropic as *"the shear stiffness of a typical woven fabric is low"* and thus the principal stresses and strains are taken to be the warp and weft stresses. The shear stress is derived separately. Arbitrary stress strain curves are used in the relationships between stresses and strains as polynomials proved unusable because of *"discontinuities in the material"*. When comparing these equations to test data *"systematic adjustments"* are made to the curves until the accuracy cannot be improved. And the material (and its nonlinearity) can therefore be represented by two simultaneous equations.

Bridgens *et al.* (2004) suggests a new approach to the use of response surfaces: That a surface should be fitted to fabric data and the stress-strain response surface used to allow a *"direct correlation between stresses and strains [] for structural analysis"*. In the suggested method *"A 'look-up' table of warp and weft stresses and strains replaces elastic constants in the analysis"*. And therefore the stress at a given displacement would not need to be recalculated, rather 'looked up' from the available test data, *"consequently, a differentiable surface function does not need to be defined"* (Gosling and Bridgens, 2008, p. 225). Splines are used to represent the fabric surface in later work.

2.3.2. Fabric modelling

A detailed discussion of fabric models has been made below. Special consideration is given to mechanical models.

Mechanical models endeavour to represent the response of a fabric to loading by considering a model that in some way represents the physical reality of the fabric, which was first demonstrated by Peirce (1937). In this fashion the extrapolation of the model beyond initial testing can be carried out by considering how the various properties of the model physically change under new conditions. The properties of such models can be modified easily and those that are representative require only minimal testing and no calibration for the model properties to be changed. A detailed discussion of a number of mechanical fabric models is made in this report (§2.3.2.3), though all of these models consider a unit cell, the response of which can be used to represent the response of an entire fabric (§2.3.2.2).

Parameters used in mechanical models include yarn geometry, yarn spacing, fabric crimp, and coating and yarn moduli. These can be determined from uniaxial or biaxial

testing and physical measurement. Where constants or calibrations from biaxial test data are required the model must be considered to be representing the data set from which these are derived, and cannot be used beyond that initial range as with a predictive model (§2.3.2.3).

2.3.2.1. Yarn modelling

Numerous models exist that endeavour to predict the characteristics of yarns within fabrics: Singh and Naik (2001) have produced a method which predicts the longitudinal and transverse tensile strength of yarns with reference to (Hearle, 1969). Madhavan and Naik (2000) have produced models which predict the elastic properties of yarns and demonstrate how certain properties of yarns such as twist can affect the modulus of the yarn as a whole. Yarn modulus “*decreases substantially with increasing twist*” in the work by Madhavan and Naik (2000). Further work, including that discussed earlier (§2.2.1), also attempts to classify yarn mechanical properties using yarn characteristics and a great deal of work has been carried out in this area beyond the pieces discussed above (Ghosh, 2005; Palaniswamy and Mohamed, 2005; Nurwaha and Wang, 2011; Arain *et al.*, 2012).

However most unit cell and predictive methods outlined below do not make use of detailed yarn descriptions. Thus as the proposed work will be based on a unit cell model a detailed discussion of various yarn models is not considered necessary.

It is possible that the inclusion of yarn models may become necessary in future work to improve the reliability of the predictive model design. This is made more likely due to the nonlinearity of response of certain yarns (Figure 2-8), where linear representations of yarn properties may prove overly simplistic in the context of a complex nonlinear response system.

2.3.2.2. Unit cell modelling

In the modelling of fabrics a repeatable unit is almost always used to enable the consideration of a small component of the fabric that can then be repeated or expanded upon to give the response of an entire fabric. This principle is initially described by Peirce (1937, p. 54) who describes the fabric assuming yarns are “*flexible, circular cylinders interwoven in a regularly recurring pattern*”. This bears a great deal of semblance to later descriptions. The unit cell most often used and described as “*the smallest element that*

may be used to characterise the mechanical response of the fabric as a whole” (Pargana *et al.*, 2000, p. 4) is that of a half wavelength of each yarn centred at cross over (Figure 2-32). This representation allows for the small scale modelling of the interaction of the yarns at crossover, whilst considering the extension of the cell in both warp and weft directions. This can be extended to consider shear response.

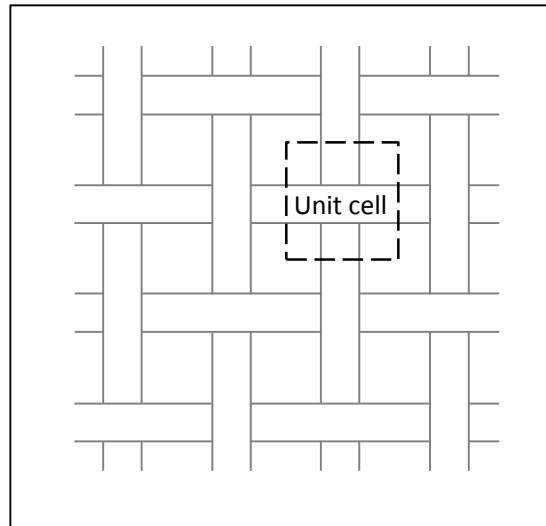


Figure 2-32: Unit cell representation (Plain Weave)

The idealisation of the unit cell can vary depending upon the model employed, however, in every case reviewed this cell is used as the basis of the model with the exception of the work by Badel *et al.* (2007) which uses two unit cells (§2.3.2.4).

2.3.2.3. Predictive models

Fabric models are generally developed using one of two methodologies. Models are developed to either represent biaxial data, or predict the biaxial stress-strain response.

Representative constitutive models utilise biaxial stress-strain response data to inform variables in the descriptive equations that then ensure the modelled response is within certain tolerances. Representative models are only reliable within the range of the data the original variables were informed from, as beyond this the variables have not been calibrated. This requires the testing of fabrics to obtain the data to calibrate the model against. Models utilising this approach which will be discussed in more detail below include: The model by Tan and Barnes (1984) which requires the “*Calibration of the material model*”, the model by Kato *et al.* (1999) which requires biaxial data to identify

“characteristic strains”. Pargana *et al.* (2000), and Uetani *et al.* (2002) both require that *“the constitutive parameters are obtained from bi-axial tests of membrane sheets”*.

A truly predictive models would require no biaxial or uniaxial testing to calibrate or calculate model parameters beyond those originally used to check the model, and calculate the stiffness of the yarns. Predictive models should only utilise readily available data about a fabric's constitutive properties that will allow for prediction of response beyond the original data sets for the different materials the model was tested against. The parameters required will be the geometry of the fabric, and the response of yarns and coating under load (such as young's modulus of the yarns). This will be particularly important for a model which is intended to be used to design fabrics which have not been manufactured yet, as biaxial data with which the model could be calibrated will be not be available.

A number of methods exist to describe the response of a fabric in terms of a unit cell or mechanical model with each offering innovative or improved methods in comparison to previous models. The methods used to describe fabric geometry and response in terms of unit cell formulations all have their route in the work carried out by Peirce (1937) who described a series of properties needed to compare fabrics or *“Geometrical Similarity”* and produced a model that describes *“The Geometry of the Plain Weave”*. The relevant geometrical properties introduced are listed below:

- *“Crimp”* is described as *“the percentage excess of length of the yarn axis over the cloth length”*.
- *“Weight”*
- *“The twist factor”* describes *“The angle of twist between surface fibres and yarn”* similar to the method used earlier (§2.2.1).
- *“Breaking Length”* gives the strength of the material.

“The Geometry of the Plain Weave” is described in terms of:

- *“Diameter of thread, $d_{1,2}$ ”*
- *“Spacing of thread, $p_{1,2}$ ”*
- *“Maximum angle of the thread axis to plane of cloth, $\vartheta_{1,2}$ ”*

2. Literature Review

- Length of thread axis between planes containing the axes of consecutive cross threads, $l_{1,2}$
- Maximum displacement of the thread axis, normal to the plane of the cloth, $h_{1,2}$
- Crimp (fraction), $c_{1,2}''$

(Peirce, 1937)

The geometrical properties identified can be used to accurately describe the geometry of a plain weave fabric assuming circular yarns, and forms the basis of yarn description methodologies used in this section (Figure 2-33). Similarly Peirce produces the first examples of equations that relate these properties to each other which form the foundation of the predictive models that will be used to design a fabric (Equation 2-9). Peirce's equations precede and inform the 'equilibrium equations' used by others (Kawabata *et al.*, 1973; Tan and Barnes, 1984; Wang, 2002; Bridgens and Gosling, 2008).

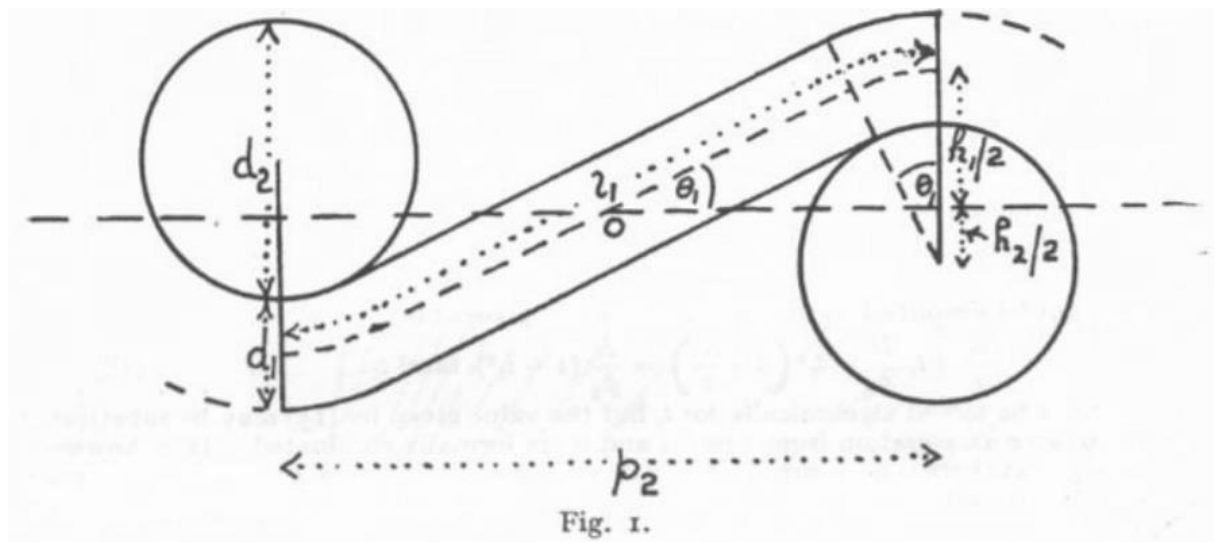


Figure 2-33: Geometry of circular yarns, reproduced from Peirce (1937)

$$D = d_1 + d_2$$

$$c_1 = \frac{l_1}{p_2} - 1$$

$$p_2 = (l_1 - D \theta_1) \cos \theta_1 + D_1 \sin \theta_1$$

$$h_1 = (l_1 - D \theta_1) \sin \theta_1 + D(1 - \cos \theta_1)$$

$$h_1 + h_2 = D$$

Reproduced from Peirce (1937)

Equation 2-9

The equation $d_1 + d_2 = h_1 + h_2$ requires that the sum of the yarn diameters is equal to the sum of the out of plane dimension, this also partly describes crimp interchange. Peirce also considers crimp interchange explicitly, and how the fabric might deform when *“ignoring any compression or extension of the threads themselves”*. Peirce also describes how the tension forces must be balanced at crossover (Equation 2-10). This is the first demonstration of the need for the out of plane forces to be balanced.

$$T_1 \sin \theta_1 = T_2 \sin \theta_2$$

$$F_1 p_1 \tan \theta_1 = F_2 p_3 \tan \theta_2$$

Equation 2-10

(where T is the tension and F is the load/inch)

The flattening of yarns (*“Compression of Threads”*) and the elastic deformation of yarns (*“The Crimped Form of an Elastic Thread”*) are also investigated. The threads are considered to *“have the form of an ellipse”* although as Kemp (1957, p. 44) notes the assumption of circular cross sections *“is invalid except possibly for very open weaves”*. This leads to his suggestion of an improvement to the above work: The elliptical yarn is also considered to be a *“homogeneous elastic material”* which, as has been shown earlier (§2.2.1) is not necessarily the case. However Peirce does state that *“it is not seriously suggested that the assumption of perfectly elastic isotropic material describes actual textiles”*. The use of simplified properties allows for the computation of the response of the complex system. Yarn elongation, and its effect on vertical forces are

also included in Peirce's model (Figure 2-34, Equation 2-11), after crimp interchange has been considered without its inclusion.

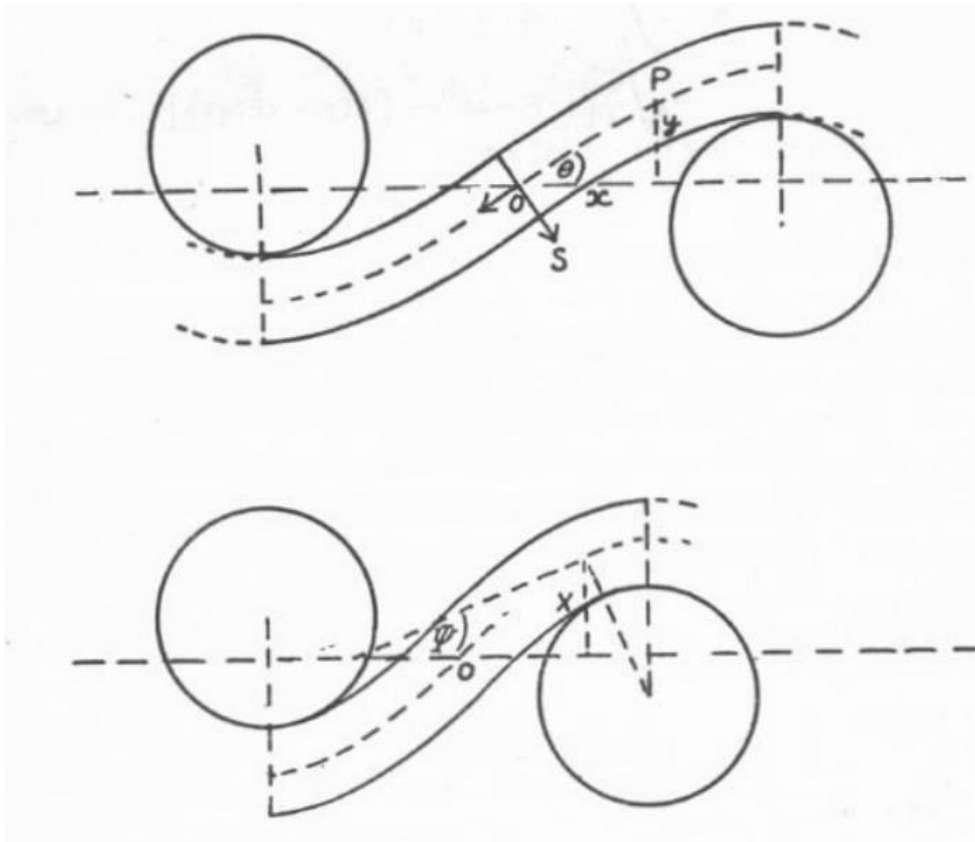


Figure 2-34: Yarn elastic deformation, reproduced from Peirce (1937)

$$\left(F_1 P_1 + 8 \frac{m_1}{p_2^2} \cos \theta_1\right) \tan \theta_1 = \left(F_2 P_2 + 8 \frac{m_2}{p_1^2} \cos \theta_2\right) \tan \theta_2 \quad \text{Equation 2-11}$$

(where m is the bending moment in the yarn)

An improvement on the circular cross section is suggested by Kemp who uses a “racetrack section” in an attempt to improve the description of the yarn. The racetrack section is described as being “*obviously closer to the actual shape of the thread section*”, and makes use of the equations and notation developed by Peirce (Figure 2-35). The racetrack formulation makes use of a compaction factor ‘ e ’ to describe the compaction of threads similar to that used by Peirce.

$$e = b/a \quad \text{Equation 2-12}$$

2. Literature Review

For the development of a predictive model the use of factors such as the thread flattening coefficient will be preferable to other methods of defining yarn compaction at crossover (often referred to as “crushing” in literature) such as those requiring constants or coefficients that have to be deduced from testing (Equation 2-12). However, coefficients require some testing to obtain, therefore methods not utilising coefficients will always be preferable.

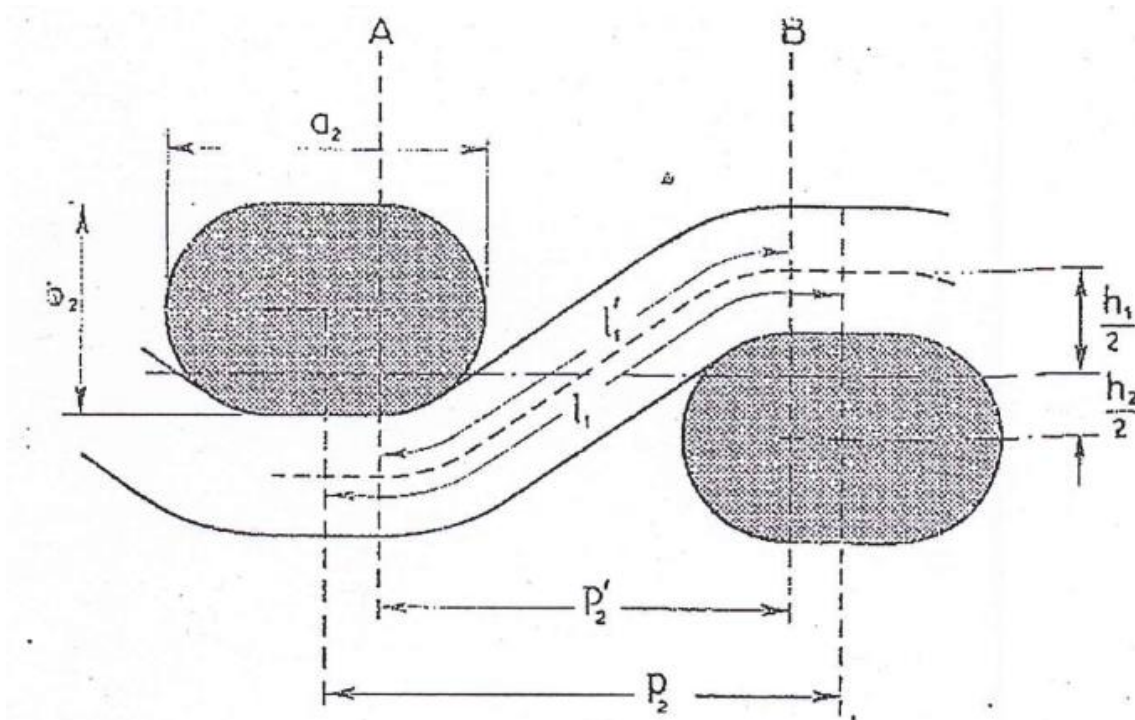


Figure 2-35: Non circular yarn geometry reproduced from Kemp (1957)

In 1973 Kawabata *et al.* (1973) redefined the problem of how to represent fabric geometry, and introduced a new way of visualising the geometry in terms of a centre line running through the centre of the yarn (Figure 2-36). This included a new method for considering yarn compaction at crossover, but no consideration of coating. This is the first ‘sawtooth’ method, described this way because of its appearance. A simple method similar to this will be used early in the next chapter (§3.3) to describe how the design of a fabric can be achieved and prove the theory of the concept without the inclusion of a number of more complex variables.

2. Literature Review

The yarn compaction at crossover is defined as “*merely that the thickness changes*” due to the out of plane force exerted between yarns at the point of contact (Kawabata *et al.*, 1973) (Figure 2-37). The property is measured experimentally using the “*parallel-plate method*” (Figure 2-37). The decrease in thickness, δ , is then used to calculate the change in geometry.

$$\delta_{D1,2} = \phi_{1,2}(F_c)$$

Equation 2-14

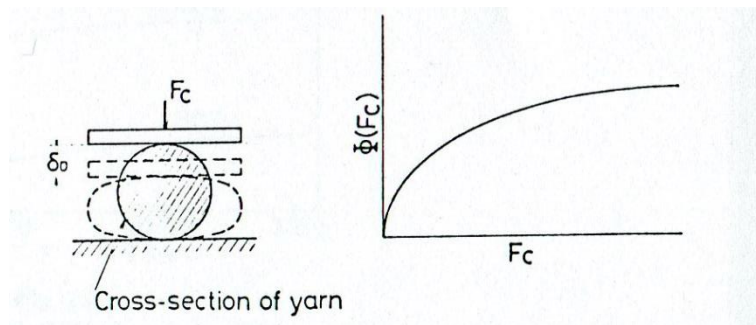


Figure 2-37: The compression of a yarn, reproduced from Kawabata *et al.* (1973)

The first true sawtooth model to be developed that includes both coating and yarn deformation was produced by Menges and Meffert (1976, p. 12). The model “*is considered to be a load bearing structure consisting of deformable bars that lie in the direction of the warp and woof [weft] axes*” (Figure 2-38). The work focusses on PVC coated polyester fabrics although this is extended to PTFE coated glass fibre fabrics by Dimitrov and Schock (1986). Others such as Pargana *et al.* (2000) improving the unit cell models with the addition of a yarn compaction at crossover mechanism, not included in the work by Menges and Meffert (1976).

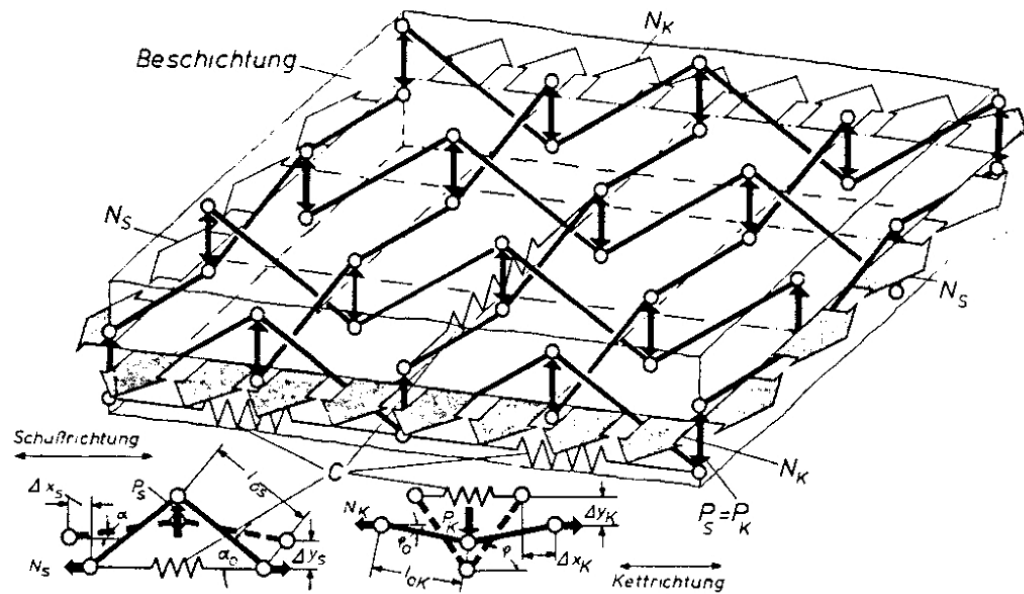


Figure 2-38: Model for calculating the biaxial strain characteristics, reproduced from Menges and Meffert (1976)

In this model however there is no consideration of yarn compaction at crossover. Yarn coating properties are considered to be linear, and the value of the coating response represented by the springs, C , is found to have little effect on the response. Such that *"If the value assumed for C varies by a factor of 10, the figures calculated for the strain are changed by an amount of only 1%"*. As such the author justifies the use of a single value of coating constant. A single value would be useful in the design of a fabric as this could be varied in the design and the value changed based on the type of coating chosen.

The author finds that it is the structure of the fabric which dominates the response to load for instantaneous loads with *"the amount contributed by individual components vary[ing] to an extent depending on the type of loading and the stress level"*. This is as might be predicted given knowledge of fabrics response.

For the fabric tested the results given in the paper appear to show excellent agreement to test data. However, only three sets of test results are presented for a single fabric and at relatively favourable stress ratios (2:1 and 1:1), other stress ratios (4:1, 1:0) would show less standard responses, and possibly negative strain. It is therefore unknown as to how well the model would respond at stress ratios where there is less equality between loading directions. Further to this the method is described as *"cumbersome"* (Tan and Barnes, 1984), as such whilst it may offer a good basis for a design method it would require the addition of a yarn deformation component and shear stiffness.

2. Literature Review

Dimitrov and Schock (1986) describe the fabric response, and also extend the “*Meffert theory*”, to include PTFE coated glass fibre fabrics. Initially the response characteristics of a fabric are defined within each section of the response (Figure 2-39), although the author admits that there will be some overlap, especially at the initial stages. Variations to the model employed by Meffert include the use of a variable yarn stiffness with “*progressive stiffness at low loads, which is due to the initial stretch of the yarn until fibres are in contact with each other*”. A parabola is fitted to the data making this model representative, and unlikely to be useable in the design of fabrics. Dimitrov and Schock (1986, p. 858) also consider a “*bedding down effect*”.

The model is found to give “*reasonable*” results for what is described as the “*natural stress state*” defined as the stress ratio “*which causes no crimp interchange for a particular fabric*”. However, results are found to be “*not so good*” for other ratios. Such descriptions of results offer no quantitative description of the quality of a model. Error in the model is possibly due to the lack of inclusion of any true description of yarn compaction at crossover in this model, which is significant at high loads experienced by PTFE glass fibre fabrics. The discretisation and inclusion of a progressive fit to the yarn response may also contribute to this error by reducing the effect of the yarn stiffness at the point where the response is increasingly defined by the yarn extension rather than crimp interchange or initial bedding down.

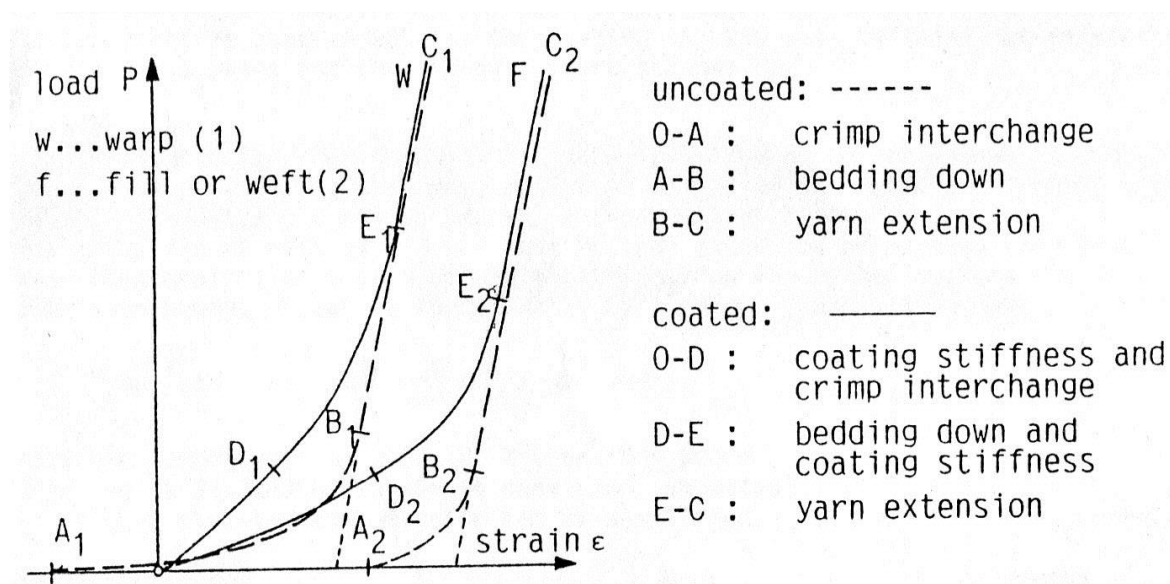


Figure 2-39: Typical load extension diagram of coated and uncoated fabric, reproduced from Dimitrov and Schock (1986)

Testa *et al.* (1978) also considers a sawtooth model for plain weave fabrics, however, as only “square fabrics” are used to reduce the number of parameters its applicability to the design of a fabric is limited. Though Tan and Barnes (1984) do suggest that this could be applied to other geometries “relatively” easily. The geometric constraints that ensure “continuity” in this model relate to the equilibrium equations used in other models and are (Equation 2-15):

- $h_1 + h_2 = 2t$ (sum of yarn amplitudes is equal to the sum of yarn thicknesses)
- $l_{1,2}^2 - d_{1,2}^2 = h_{1,2}^2$ (the triangle made up of the yarn amplitude, length and in plane length is right-angled)

Equation 2-15

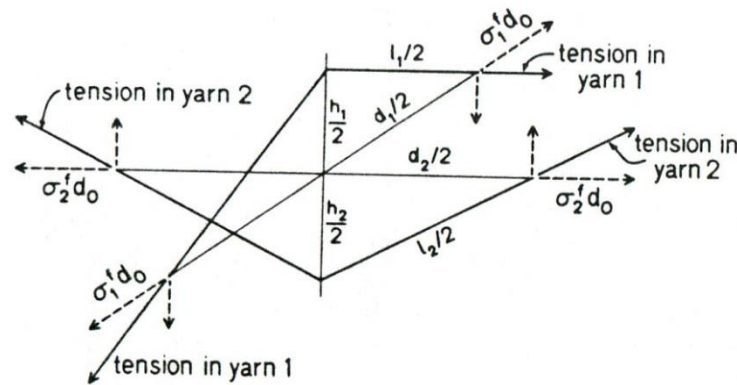


Figure 2-40: Free body diagram of the model of yarns, reproduced from Testa *et al.* (1978)

The bilinear model as well as the work of Dimitrov and Schock (1986) demonstrates how yarn properties might be obtained from tests, i.e. that the straight portion of the response in a uniaxial test is a region where only yarn extension and coating need be considered, and as such yarn mechanical properties can be derived from this section of the curve.

Stubbs and Fluss (1980) also make use of a sawtooth formulation describing it as a “space-truss” that can be used to investigate the “effect on the response due to geometric and elastic parameters such as yarn geometry, rotations and elastic parameters such as yarn geometry, rotations and crushing, as well as coating properties”. This model, as with others restricts the loading to the orthogonal direction.

2. Literature Review

The model developed by Stubbs and Fluss (1980, p. 52) utilises only linear elastic properties, or rather that “*all elements will be assumed to obey Hooke’s law and any nonlinearities introduced in the overall response will be considered a consequence of geometric nonlinearities*”. This use of only linear elastic properties to represent the nonlinear response is excellently suited to the process of designing a fabric, whereby the nonlinearities known to be found in fabric response might be designed for. This would allow a single parameter to be designed which in turn does not require the use of look-up tables to identify a response, and thus limits the design to known variable responses. This should lead to a more predictive design methodology, rather than a representative model of fabrics known to already exist. The typical element (Figure 2-41 and Figure 2-42) epitomises most sawtooth methodologies.

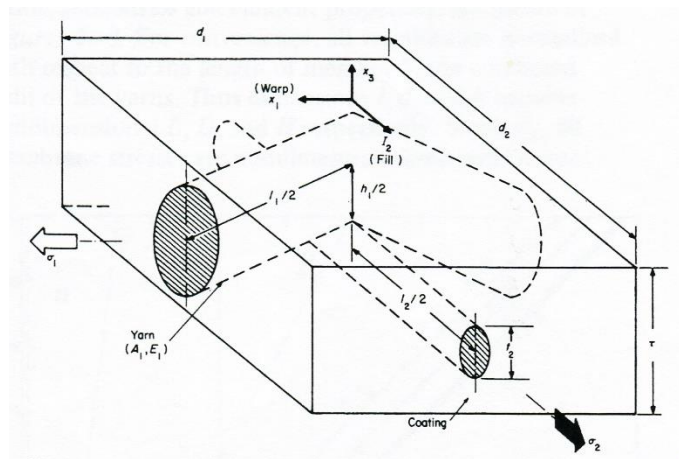


Figure 2-41: Typical fabric element (Stubbs and Fluss, 1980)

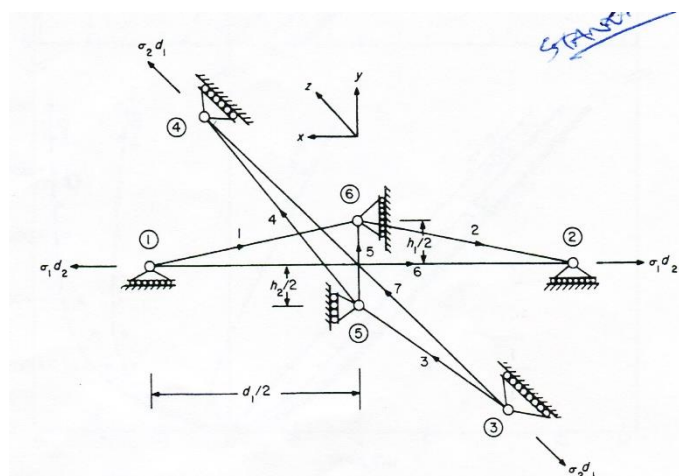


Figure 2-42: Truss model of fabric element, reproduced from Stubbs and Fluss (1980)

The continuous coating is only represented by the two elements 7 and 6 whilst the yarn compaction at crossover is modelled by element 5 (Figure 2-42). Thus this method includes all the components of the fabric generally considered to be necessary for accurate modelling. However, the response of this element is based on the variation of a value K_5/K_y (K_5 is the yarn resistance to cross-section deformation, K_y is the yarn stiffness) where a low value represents a low resistance to cross section deformation and a high value a high resistance to cross section deformation. The method used by Stubbs and Fluss (1980) involves carrying out uniaxial tests which inform the values K_y and N , which then represent the elastic properties of the fabric. Whilst this may accurately represent the response of a yarn's compaction at crossover for a specific fabric the use of only test data to find these values makes the model entirely representative, and means that such a method could not be introduced into a design methodology. However, were the bar element that represents the yarn interaction to be replaced by some means of predicting the response other than a simple representative relationship this method to predict the response of fabrics might be applicable to the design of fabrics.

This method demonstrates a number of important principles that will be used during the creation of the proposed method, and provides a basis for more advanced sawtooth methods. Its accuracy appears similar to that of the model produced by Testa *et al.* (1978) although higher accuracies are apparently seen in some cases there still appears to be error around the point where the change from crimp interchange to yarn extension occurs.

A further model similar to those above is also developed by Tan and Barnes (1984) however, as it is described as "*similar to that described by Testa and Stubbs*" no detailed discussion of it will be made here as it too is representative, requiring the "*Calibration of the material model*".

The final unit cell model to be reviewed takes an alternate view of the linearized model by considering a "*trapezoidal lattice model*". The model developed by Kato *et al.* (1999) (Figure 2-43) has two principal components: A warp and weft yarn are represented by two sets of elements each (A, AA, A and B, BB, B). Coating is represented by the elements

C, D, E, and F in addition to the element R_1 which represents the coating that has permeated into the yarns and an element, 'V', which represents compression.

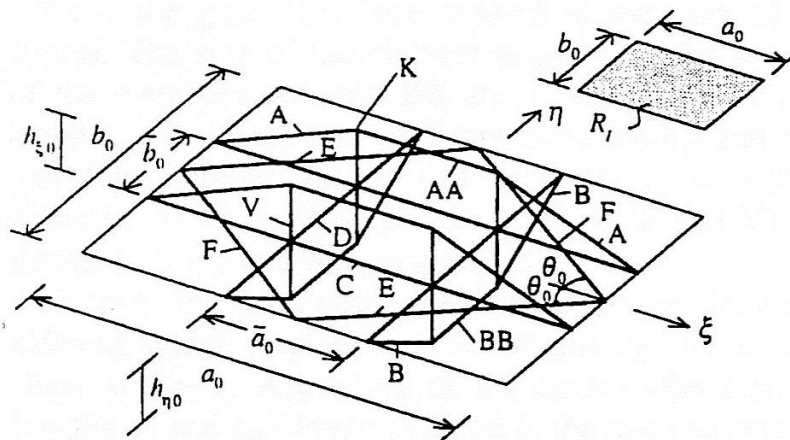


Figure 2-43: Trapezoidal lattice model (Kato *et al.*, 1999)

The model is then used as a component in an FE method and also utilises a hysteresis approximation to allow for the modelling of hysteresis. One problem with this is that the model becomes representative, in that certain parameters are found using “*trial and error*”. The model appears to show good correlation to test data however it requires estimation of calibration properties so would be unsuitable for the design of a fabric.

Another less simple model is developed by Pargana *et. al.* (Pargana *et al.*, 2000; Pargana *et al.*, 2007) where a number of nonlinear and rigid elements represent yarns, whilst coating is modelled as an isotropic plate. No creep is included in the model and there is no slip at yarn crossovers. Again the model requires calibration. Whilst the model appears more ‘realistic’ in its formulation results do not appear to be as accurate as might be expected, especially for unloading curves. Again the discussion does not quantify the accuracy of the model, but states that the model “*predicts realistically*” the response. Examination of the response curves presented does not necessarily hold this to be the case. Of particular concern might be the 1:0 stress ratio, where the lowest weft strain is underestimated by what appears to be approximately 50%.

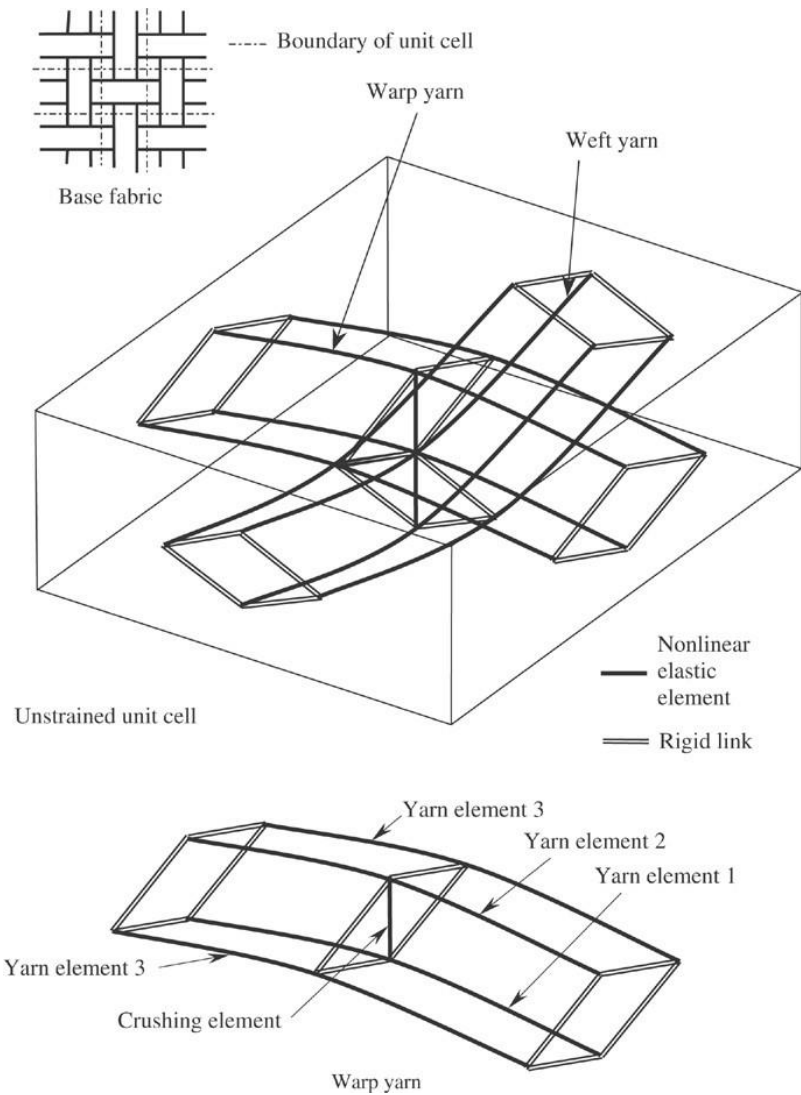


Figure 2-44: Unit cell representation of yarns (Pargana *et al.*, 2007)

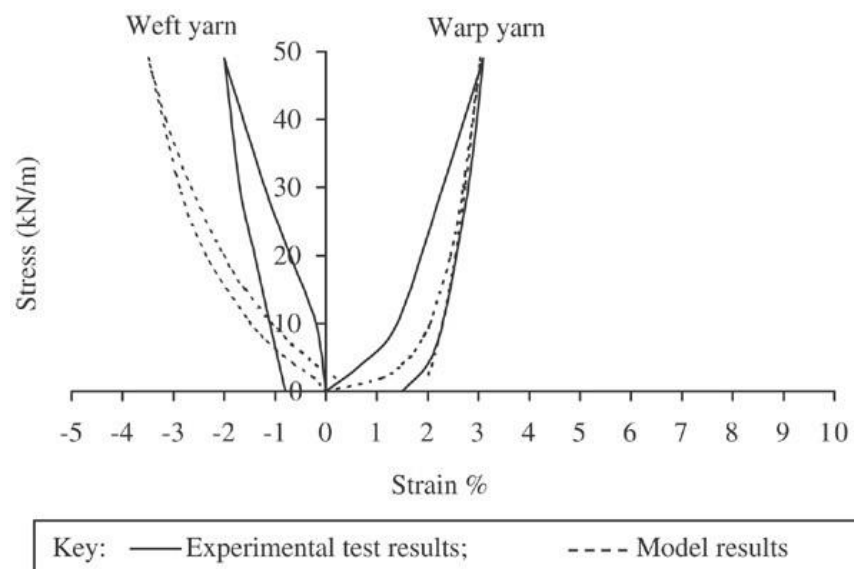


Figure 2-45: 1:0 stress ratio comparing test (—) and model (---) results (Pargana *et al.*, 2007)

Yarn compaction models are used to represent the crushing behaviour of yarns, first identified by Peirce (1937), which is important for the calculation of the fabric response

(Testa *et al.*, 1978; Skelton, 1980; Tan and Barnes, 1984; Dimitrov and Schock, 1986; Bridgens and Gosling, 2008). A number of these methods are covered in the following section (§2.3.2.4) as they relate to Finite Element modelling, and the model developed by Bridgens and Gosling (2008) whilst discussed briefly below is discussed in more detail in the following chapter (§3.4). *“Considering that a yarn typically contains 12000 or more filaments it is computationally efficient to consider the yarn as a continuum”* (Glaessgen *et al.*, 1996, p. 44), as considering the crushing and movement of each individual filament would require considerable computational outlay. As such most yarn deformation at crossover models consider a simplification of the problem.

Dimitrov and Schock (1986, p. 856) consider a bedding down effect rather than yarn crushing. Bedding down is described as described as *“the removal of slack between the yarns of opposite direction,”* where *“the associated lateral compression of the yarns will probably contribute considerably to the load-extension behaviour of the fabrics”*. They however describe the *“actual mode of behaviour”* as being *“rather complex”* and opt for a method to add an initial gap between the yarns, an assumption that is not borne out in observations of real fabrics. They also list the following as affecting the bedding down:

- slack of yarn
- coating penetration into yarns internal space
- bending stiffness of fibres
- lateral compressibility
- spinning characteristics of yarn

Further to this it is also suggested that errors in the response surface might be improved with the use of *“a progressive spring”* (Figure 2-39). Though no mention of how this progressive spring might be implemented is made, nor how accurate a solution with a *“progressive spring”* might be in comparison to the published results.

A crushing element is used by Pargana *et. al.* (Pargana *et al.*, 2000; Pargana *et al.*, 2007) and is derived from the crushing force and crushing strain utilising yarn properties (Figure 2-46).

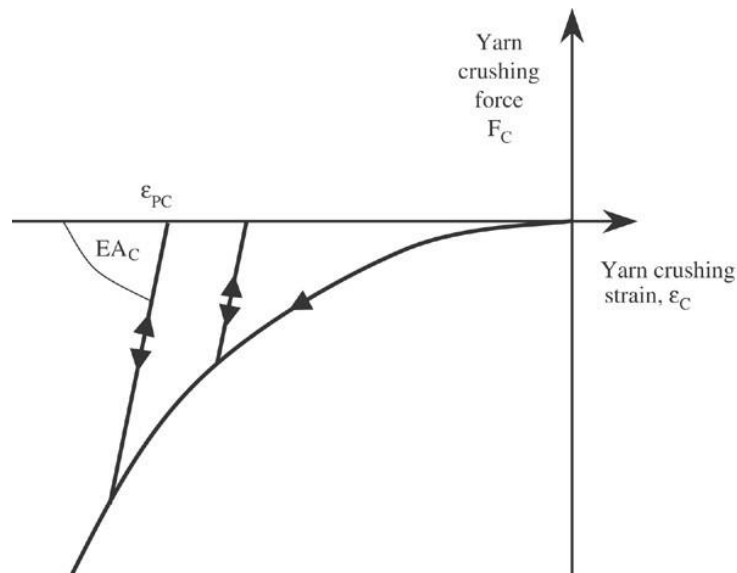


Figure 2-46: Response of crushing elements in the unit cell model produced by Pargana *et al.* (2007)

Additionally to the central yarn models presented above sinusoidal models have also been presented as an alternate method of representing the geometry of the yarn unit cell. Bridgens and Gosling (2008, p. 8) describes the sinusoidal representation as “*a more realistic representation than the ubiquitous sawtooth*”. This can be readily appreciated when diagrams of the model are considered (Figure 2-47) if compared to diagrams of the sawtooth model (Figure 2-38, Figure 2-40).

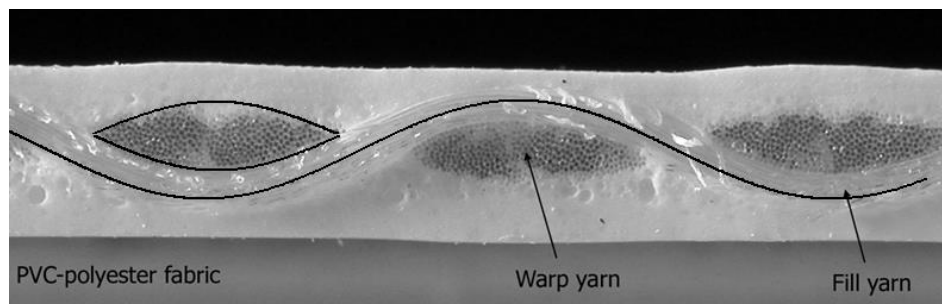


Figure 2-47: Sinusoidal representation of yarn cross-section, reproduced from Bridgens and Gosling (2008)

Wang (2002) developed a model based on the sine curve that is described as having “*extremely good*” agreement between calculated and measured curves. Sine curves are used to represent the fabric geometry, yet the constitutive equations bare close relation to the equations discussed above (Equation 2-9 and Equation 2-10). And the method still relies on the equilibrium equation (Equation 2-16).

$$b_{01} + b_{02} = A_{01} + A_{02} \quad \text{Equation 2-16}$$

b = yarn radius, A = yarn amplitude.

2. Literature Review

The model presented by Wang (2002) appears to show good correlation to measured data in the cases presented, however, in more than one case the “*straight line model*” [sawtooth model] used appears to show better correlation to measured data. Additionally both sets of data represent the shape of the measured response, and a largest measured error from the tested result of 10% is not as accurate as other model claim to be. Finally, whilst the model does appear to show good correlation, although not necessarily better than the “*straight line model*” it does not include a consideration of coating response.

Bridgens and Gosling (2008, p. 8) finds that the “*correlation of the simple sine curve [] is extremely good*” when compared to yarn geometry where “*the mean deviation from measured points is only 2.5%*”. In this model the yarn is modelled with a series of pinned bars (Figure 2-48). The vertical forces are applied at each node.

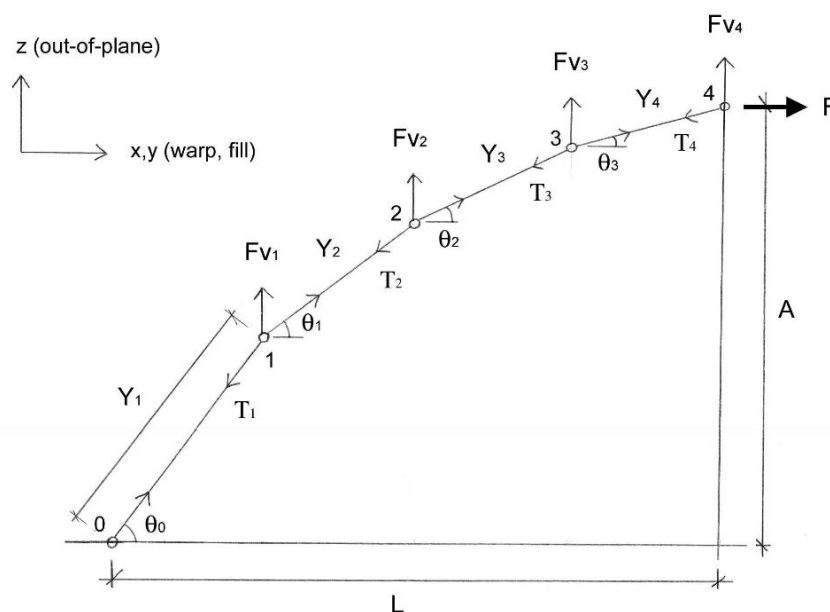


Figure 2-48: sinusoidal yarn model reproduced from Bridgens and Gosling (2008)

The sawtooth model is found to predict tested fabric strains more accurately than the sinusoidal model with “*the deviation of the sawtooth model from the mean of the viscoelastic test data [being] 5.3 to 5.9% of the strain range*”. However it is also noted that the deviation between repeat tests is 3.0% of the strain range. Bridgens and Gosling (2008, p. 13) state that the “*model output is considerably more accurate than the assumed material properties which are commonly used in industry*”. Thus the model appears to be of adequate accuracy to allow for the design of fabrics.

At this stage it has been shown that a number of models exist that offer to varying degrees a prediction of fabric response from initial geometry and constituent mechanical properties, but that only one of these offer exactly what is required. What is needed is a truly predictive model based on the geometry of a fabric rather than parameters obtained from testing. It must also accurately predict the response of coated fabrics and thus be useable as the basis of a method to design a fabric from the required mechanical properties of the fabric rather than the known geometry.

These problems are resolved by Bridgens and Gosling (2008, p. 1) who proposes a *“Predictive model for membrane structure design”*. The sawtooth model proposed in this work utilises a unit cell as with many of those above and includes two principal constraints, namely that:

1. *“The sum of the yarn radii must equal the sum of the yarn wave form amplitudes”* which is drawn from Peirce (1937)
2. *“Assuming negligible yarn bending stiffness, out-of-plane [due to yarn interaction] force must equal zero. For the sawtooth model these out of plane forces are a component of the yarn tension at crossovers”* (Bridgens and Gosling, 2008, p. 6)

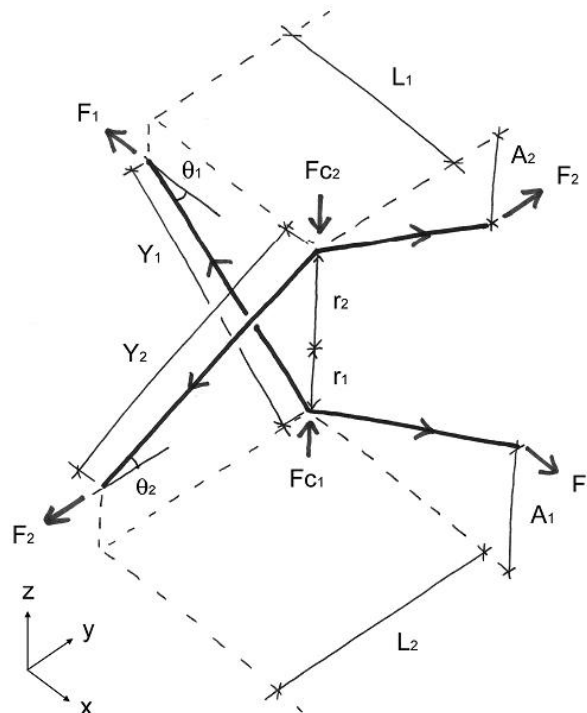


Figure 2-49: Fundamental sawtooth unit cell, reproduced from Bridgens and Gosling (2008)

The fundamental unit cell (Figure 2-49) is similar in many ways to those presented in models above e.g. the model produced by (Menges and Meffert, 1976), however, at crossover the yarn cross section is considered to be a rhombus with constant cross-sectional area. This removes the need *“to define the yarn crushing stiffness”* and allows *“the yarn cross-section to be modelled such that it is consistent with the wave-form of the orthogonal yarn”*. The rhombus yarn cross-section is covered in more detail later (§3.5) where a full discussion of this sawtooth model is made and consideration given to how the model can be used to design fabrics. At this it is possible to consider the effect of constituent properties (yarn length, out of plane angle, yarn radius, yarn width, loads and constituent component moduli) on a predictive model without the need for representative simplifications to be made.

The application of this method to the design process is discussed in detail in the following chapter (§3.5) where variations to the method are made to allow for non-orthogonal yarns and shear response to be analysed and designed for.

2.3.2.4. Finite element models

Finite Element (FE) methods reproduce the fabric response by considering the interaction of small elements that together represent the whole fabric or a unit cell. This can be a computationally expensive process due to *“their three dimensional structure, textiles tend to be computationally expensive to model with finite elements”* (Glaessgen *et al.*, 1996, p. 48). These models generally consider plain weave fabrics as part of a unit cell (Glaessgen *et al.*, 1996; Gasser *et al.*, 2000; Tarfaoui *et al.*, 2001; Badel *et al.*, 2007), although consideration of other weave geometries is also made (Bigaud and Hamelin, 1997; Durville, 2010). The unit cells used do not always correspond to the unit cell described earlier and used in the majority of mechanical models (§2.3.2.3), Glaessgen *et al.* (1996) for instance uses two crossing yarns as the basis of the unit cell (Figure 2-50). Finite element methods still reduce the complexity of the relationships defining a fabric's response, but unlike the mechanical models detailed above (§2.3.2.3) these allow for *“internal details”* of the response to be analysed (Glaessgen *et al.*, 1996).

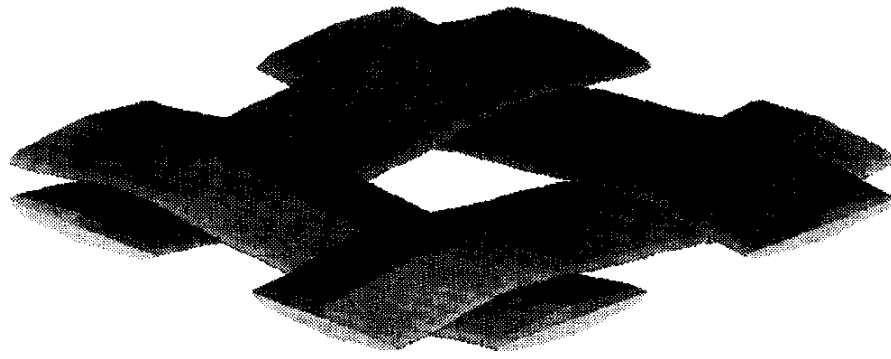


Figure 2-50: “Three-dimensional rendering of yarns within a unit cell” used by Glaessgen *et al.* (1996)

Circular yarns as used by Peirce (1937) have been the basis for two models (Glaessgen *et al.*, 1996; Tarfaoui *et al.*, 2001). Glaessgen *et al.* (1996) produces a model with a circular yarn and constant cross-sectional area (although not shape) in which a penalty function accounts for the changing shape of the yarn. This model requires eleven geometric parameters, and the shape itself is the result of a number of individual steps.

Gasser *et al.* (2000) produced a model that predicted the response of a balanced plain weave fabric at different load ratios, though when this was applied to unbalanced fabrics the errors, especially in the direction of the larger yarn became far greater. The correlation between test and model data is described as “good” giving no information as to the actual accuracy of the process. In this model the yarn deformation at crossover properties were calculated by comparison to biaxial data. The need for such calibrations makes it difficult to foresee FE methods being used to design a fabric as the designed fabric cannot be calibrated to any existing fabric, as biaxial test data for the fabric will be unavailable. It is however possible that the model could be calibrated to the sawtooth generated biaxial response data. This study does allow for the identification of the distribution of out of plane forces, and the effect of the out-of-plane force on the deformation of the yarn at crossover. Whilst the yarn is uncoated such information may prove useful in future work in the consideration of yarn friction for the purposes of shear response identification. The yarn contact area is required in the model produced by Liu *et al.* (2004) to calculate yarn friction. As such, detailed information about the yarn contact area at different hear angles might improve the accuracy of the model.

Shear response is considered by Badel *et al.* (2007) in which yarns are considered “as a continuous material”, ignoring the fibres that make them up. Again this method considers only uncoated fabrics, which experience relatively high levels of shear at low

loads when compared to coated fabrics. A lenticular yarn cross-section in two different unit cells (Figure 2-51) is used with yarns which rotate and deform to allow the analysis of shearing. Earlier (§2.2.7.4) it was noted that FE methods would allow better consideration of yarn lock up, and with this model that becomes apparent. The compaction forces at boundaries, and the areas of contact between yarns are more readily calculable where the area of contact is apparent as the area where two yarns meet (Figure 2-51). No quantifiable results are given for the accuracy of the method, though the graph presented does suggest that the method under predicts shear stiffness at low shear angles.

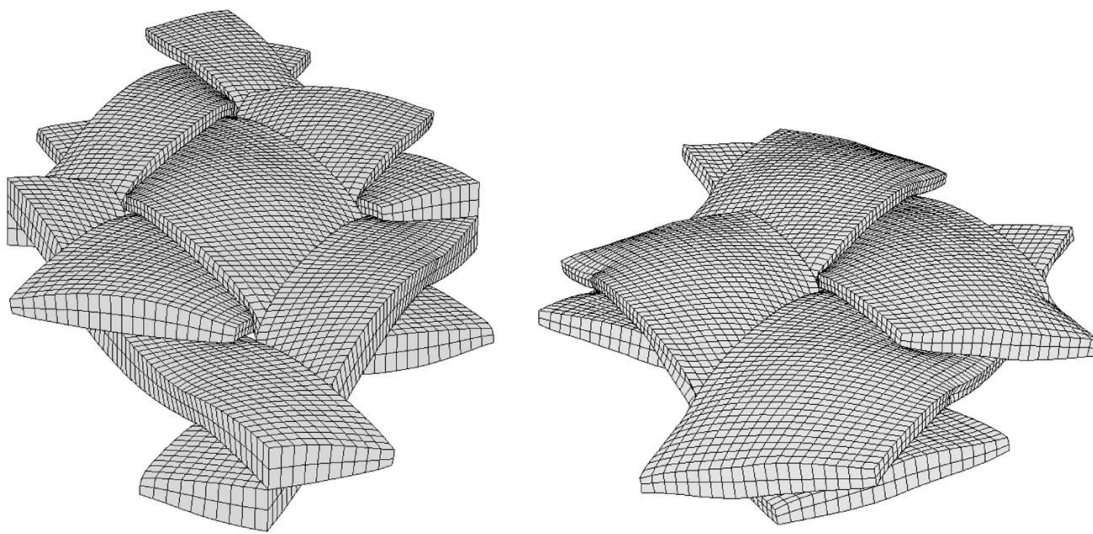


Figure 2-51: Deformed geometries for a shear angle of 54° demonstrating shear lock up (Badel *et al.*, 2007)

Durville (2010, p. 1246) considers the problem from the perspective of the interaction of the individual fibres of the yarn (Figure 2-52). Though the principle of the work is similar to the larger scale representations. Penalties are applied at contacts to model intra fibre friction, and an “*averaged binding condition*” is used to allow the fibres to move within the ‘yarn’ whilst still applying a boundary condition at the edge.

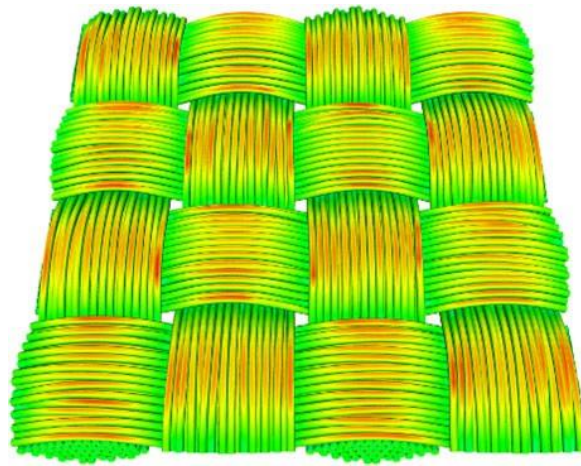


Figure 2-52: Initial configuration for the plain weave fabric (Durville, 2010)

Whilst the output of the model developed by Durville (2010, p. 1249) (Figure 2-52) might appear impressive no details as to its accuracy in predicting fabric response to biaxial load are given beyond saying that “*the loading curves exhibit the usual J-shape aspect at the beginning*”. Therefore the accuracy of the method in fact remains unproved. It is also noted that the yarns are untwisted, unlike in most structural fabrics.

The complexity of the creation of finite element models, the difficulty inherent in changing the geometry, and the computational expense, whilst generally allowing a more detailed inspection of intra yarn interactions does not lend itself to a design process. Such a process will require multiple different geometries to be tested quickly which would slow using FE models. The defining equations also do not lend themselves to manipulation towards an inverse methodology (given their complexity) and therefore a differing approach to design would be required. This might be an iterative process, altering the yarn structure in stages to attain a specific stiffness. This, coupled with often limited comparisons to actual test data means that at this stage the use of FE methods for fabric biaxial response design would be premature. Future work may prove to offer new insight at which point this should be re-examined.

2.3.3. Summary, review and discussion of models

In summary the models presented vary in complexity and accuracy, although the accuracy of many of those presented is only described in abstract terms such as ‘good’. Where such abstract definitions are used the presented figures sometimes appear to contradict even this. The model used as the basis of the design method is required to incorporate the coating’s response as well as the base cloth, and be as predictive as can

reasonably be achieved. Because of this, many of the models presented above cannot be considered for further use. Whilst FE models might conceivably be used in future to accurately describe and design fabrics the lack of coating consideration and difficulty in quickly modelling geometry during optimisation in current models means they are not the best choice available. The difficulty in varying the geometry and the inherent complexity of such models means that these have not been used in this work.

Sinusoidal models, whilst they appear to represent the geometry of a fabric more accurately, have been shown to be less accurate than sawtooth models produced by the same authors who proposed them (Bridgens and Gosling, 2008). However, should more accurate sinusoid models become available in the future replacing the choice of model made here with those might be advisable.

The last constraint on the choice of model to be used as the base for the fabric design process is that the equations be differentiable, discussed in more detail in the following chapter (§3.2). Therefore the model that best fulfils all these categories is the sawtooth as described by Bridgens and Gosling (2008). Additionally it is presented in a fashion that lends itself to the possibility of being differentiated.

An alternative to differentiating the defining equations might be to use a parametric study of a material model, for instance a finite element model, varying its properties to define relations between response to tensile or shear stress, and using these to design a new material. This is similar to the Neural Networks employed by Bartle *et al.* (2013) where the parallel optimisation of equations allows for the prediction of fabric properties.

2.4. Optimisation

How can the geometry of a fabric be optimised quickly and efficiently to give accurate robust and reproducible results?

Optimisation is an exceptionally wide area of study, and here refers specifically to numerical optimisation. In numerical optimisation we *“first identify some objective, a quantitative measure of the performance of the system”* (Nocedal and Wright, 2006, p. 2) which may be constrained, that we can optimise for a set of variables, which may also be constrained. The process of defining this objective, and the corresponding variables, is known as modelling. Recognising whether a model has been minimised or maximised is also important and this can often be found using optimality conditions. Numerical optimisation can be split up to include: constrained and unconstrained optimisation, continuous and discrete optimisation, global and local optimisation, and stochastic and deterministic optimisation (Nocedal and Wright, 2006).

2.4.1. Stochastic and deterministic optimisation

Optimisation problems can be either stochastic or deterministic. Stochastic optimisation allows the consideration of probability and differing scenarios in relation to the variables or objective. Stochastic models allow the optimisation of the expected performance of a model. It is therefore predicted that for the most part deterministic optimisation will be used during the development of the predictive model.

Related to this is Chance-constrained optimisation which allows for the optimisation of a given objective to some specified probability. And robust optimisation *“in which certain constraints are required to hold for all possible values of the uncertain data”* (Nocedal and Wright, 2006, p. 7).

2.4.2. Overview of optimisation

For the purpose of the design of a fabric the optimisation will be defined as the minimisation of the difference between some target and the calculated response given some constraints (i.e. the equilibrium equations). As part of this process tolerances are generally included in optimisation routines. These are the limits on accuracy or more generally *“a threshold which, if crossed, stops the iterations of a solver”* (MathWorks,

2012a). Without tolerances a solver might continue in its search for an optimal solution even though the solution has been found to an adequate number of decimal places.

Finding the solution to an optimisation problem requires the convergence of the answer towards a single value. This single value will be influenced by the initial guess especially where two or more solutions exist to the original problem. In this case, dependant on the routine in use, the initial guess may lead to a steepest gradient being followed that results in a non-optimal solution, or more generally it will normally lead to the closest solution to the original 'guess' being found. In global searches (i.e. where the entire population of results may be used to find a solution) this is more likely to occur.

Optimisation is typically carried out with design constraints defined as inequalities for some parameter (\mathbf{x}). A general optimisation might be defined as follows (Beyer and Sendhoff, 2007) (Equation 2-17):

$$\left. \begin{array}{l} \text{optimize: } f(\mathbf{x}), \\ \text{subject to: } g_i(\mathbf{x}) \leq 0, \quad i = 1, \dots, I \\ \quad \quad \quad h_j(\mathbf{x}) = 0, \quad j = 1, \dots, J \end{array} \right\} \quad \text{Equation 2-17}$$

The posing of the objective function, $f(\mathbf{x})$, is important. Should two functions need to be optimised simultaneously, where the value of one is very large and the value of the other very small, the large value can adversely affect the optimisation. Though both might be equally important if the objective is poorly posed the solution may not be optimal.

Normalising values removes the inherent bias of an optimisation towards larger values. When considering stress and strain the difference in values might be of the order of 10^5 , therefore the strain might be 'ignored' by an optimisation where the values have not been normalised to a single value range. This is often achieved by placing all values in the range of 0 – 1.

2.4.2.1. Unconstrained optimisation

Unconstrained optimisation problems are those where no external constraints are placed on the solution, where constraints can be safely ignored, or where constrained problems are reformulated "*in which the constraints are replaced by penalisation terms added to the objective function*" (Nocedal and Wright, 2006, p. 6). As such in an

unconstrained problem the result relies on the original guess point, and direction of search where more than one possible solution exists (MathWorks, 2014).

2.4.2.2. *Constrained optimisation*

Constraints might be simple inequalities ($0 < x < 100$), linear constraints or nonlinear constraints (Nocedal and Wright, 2006). In the case of the design of a fabric a number of constraints have been identified above, including the equilibrium constraint (§2.3.2). It is also clear that no yarn can overlap, and so the sum of the yarn widths cannot be greater than the sum of the in plane yarn lengths in the opposite direction. However, these might also include the necessity that no yarn may occupy the same space as another. The specifics of these choices will be reviewed in more depth in the following chapters. In the case of programming with MATLAB it is possible to create complex nonlinear constraints that in themselves contain optimisation routines (MathWorks, 2014). The 'fmincon' routine discussed below offers the following constraint options for the optimisation (Equation 2-18):

$$\min_x f(x) \text{ such that } \begin{cases} c(x) \leq 0 \\ ceq = 0 \\ A \cdot x \leq b \\ Aeq \cdot x = beq \\ lb \leq x \leq ub \end{cases} \quad \text{Equation 2-18}$$

Equation 2-18 describes two nonlinear inequalities, ' $c(x)$ ', and ' ceq ' which are formed from equations the result of which must be less than zero and zero respectively. The following two inequalities are linear, with ' A ', and ' Aeq ' representing the gradient and ' b ' and ' beq ' representing the y intercept. Finally the values ' lb ' and ' ub ' are the upper and lower bounds on the values of ' x '.

2.4.2.3. *Inverse Modelling*

The inverse of a function can be used as an analogy for the inverse of a more complex model. If a function $f(x)$ is considered to accept input x and produce the output $f(x)$ then the inverse of the function will produce x from the input $f(x)$ (Croft *et al.*, 2001). However, not all inverse functions produce unique answers. For instance, consider the function $\tan(x)$:

$$f(x) = \tan(x) = 0$$

One solution could be $x = 0$

$$\tan(0) = 0$$

However, if $x = 180$

$$\tan(180) = 0$$

Equation 2-19

This demonstrates an important principle, an inverse function will not necessarily produce the original input if it is constrained in such a way as to limit the output. But if these inverse functions are unconstrained, or else the result weighted in some fashion, no output may be obtained. In the case of the inverse tan function there is an infinite number of possible solutions to the inverse function $\tan^{-1}(x) = 0$. This would not be the case if the function was constrained for instance to $\frac{-\pi}{2} < y < \frac{\pi}{2}$.

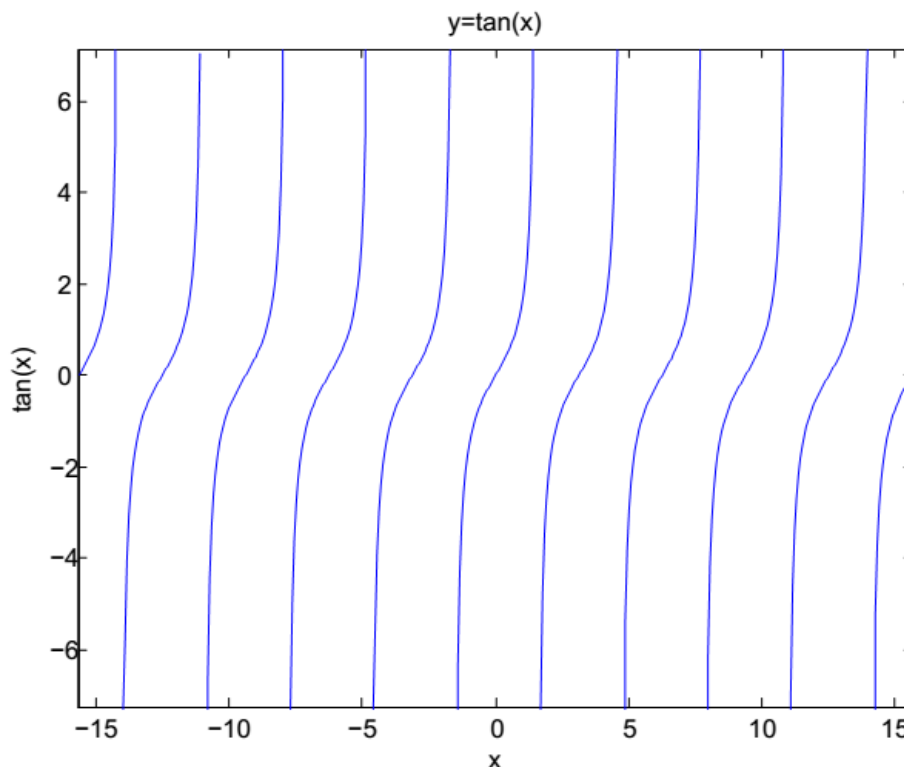


Figure 2-53: $y = \tan(x)$ for $-5\pi < x < 5\pi$

Combining and differentiating the equations that form the sawtooth model (§2.3.2.3) provides firstly a direct equation for the calculation of the values of tensile stiffness and

Poisson's ratio. This enables the construction of an objective function $f(\mathbf{x})$ that can be minimised to find a solution for target value of $f(\mathbf{x})$. Using one function removes the necessity of iteratively considering multiple functions and normalising them, as was done in the method employed by (Bridgens and Gosling, 2008). Secondly, demonstrating that the equations can be differentiated means that direct solution methods may be applicable to the equation, though this will be shown to not be the case in the next chapter (§3.5). Thirdly using differentiable equations means that FORM (First Order Reliability Method) methodologies can be employed to consider the statistical variance of the objective function. FORM uses derivative calculations to calculate the most probable failure point and therefore a probability of failure for an inequality. This is done by calculating the shortest distance to the failure region from the origin, for a given objective function, and is discussed in more detail in Chapter 4 (§4.8).

A number of inverse methodologies were reviewed with a view to ensuring that the most efficient and accurate methodology for the optimisation of multiple variables is used for the design of fabrics. In addition to this certain checks and balances needed in inverse optimisation are identified.

Faurholdt (2000, p. 472) describes the inverse method as fitting "*a mathematical model to a set of experimentally obtained parameters*". In the case of the design of a fabric this will be the sawtooth model, and fitting the fabric's properties to required mechanical properties for the fabric which match the user defined targets. A number of inverse methods are proposed and discussed with relation to the design model:

Initially the response is approximated as a Taylor series from which the objective function might be minimised in a single step (Equation 2-20), but as this would result in a representative model this is passed over at this point.

$$x_k^{min} = x_k^{cur} - \mathbf{H}^{-1} \frac{\partial f}{\partial x_k}$$

Where \mathbf{H} is the Hessian matrix

Equation 2-20

Following this it is suggested that a steepest descent method might be used (Equation 2-21). This is the principle used in the methodology discussed in the following chapter (§3.5), although modified through the use of internal MATLAB routines.

$$x_k^{min} = x_k^{cur} - \alpha \frac{\partial f}{\partial x_k} \quad \text{Equation 2-21}$$

Where the objective is to minimise the least squares problem:

$$f(x_k) = \sum_{i=1}^{MJ} [y_i - y(x_k)]^2$$

Equation 2-22

How the gradient might be calculated this is reviewed later. The method specifies the importance of the model being able to return to a given data set of design parameters (i.e. that the output of the inverse model is the same as the variables for the non-inverse model that would produce the input for the inverse model). This will initially be the requirement placed on the inverse model for a set of known targets, ensuring that both the inverse and non-inverse model ‘match’.

Gajewski and Garbowski (2014, p. 175) identify four requirements for the inverse model, “(a) the description of geometry, (b) the boundary conditions, (c) the initial conditions, (d) the properties of all the involved materials”. In the case of our model these will be fulfilled by:

- a) The geometry of the fabric components
- b) The applied loads and equilibrium equations
- c) Any prestress applied to a fabric
- d) The properties of the coating and yarns

Whereas this method only solves for the variables in (d) our model will optimise for the values in (a) and (d) which will affect the values in (b). Thus the situations are somewhat different. In addition this model uses a “vector of residua **R**” which is used to minimise the discrepancy between computed and experimental results. The value of ‘R’ is used to bring the optimisation in line with the results that were expected. This would clearly be impossible to implement in a model where the designed fabric does not exist, or where

representative models are being avoided. A least squares methodology is then used by Gajewski and Garbowski (2014, p. 175) to minimise the value of \mathbf{R} “*by adjusting the constitutive parameters*”. The method uses DIC (Digital Image Correlation) test data and optimises constitutive parameters from this.

The method presented appears to converge well to the experimental results in few iterations, but interestingly sensitivity of parameters are also investigated and computed “*using a calibrated FE model*” however little specific detail is offered on this process.

A medical application of an inverse modelling procedure has been developed that attempts to characterise elastic properties from a point indentation, necessary where not enough material was available to carry out strip tests. This model is then tested against strip test data. The model is created using latex rubber, not directly comparable to architectural fabrics, and an inverse FE method is used to calculate elastic properties from known physical properties. This process involved minimising the error between the model and test data by varying the constitutive parameters of the model. Again this process is not directly applicable to the problem of fabric design. (Aernouts *et al.*, 2010).

Multi objective optimisation will be the main problem associated with the design of a bespoke fabric where multiple parameters (geometry) are to be optimised for multiple targets (tensile stiffness at multiple stress states, Poisson’s ratios at multiple stress states). Yang and Xiao (2013) offer a method for the multi-objective optimisation of the parameters of a pump-turbine: The method uses a genetic algorithm to solve the optimisation problem (Equation 2-23).

$$\begin{aligned} \min y = f(\mathbf{x}) &= (f_1(\mathbf{x}), f_2(\mathbf{x}), \dots, f_n(\mathbf{x})) \\ \text{subject to } \mathbf{x} &= (x_1, x_2, \dots, x_m) \in X \\ \text{and to } \mathbf{y} &= (y_1, y_2, \dots, y_m) \in Y \end{aligned}$$

Equation 2-23

Here X represents the “*blade loading parameters* and Y represents the *hydraulic efficiencies*” which might be replaced by the yarn and coating properties and the shear properties in a fabric model. The objective function being four performance parameters.

The model integrates a number of codes together to enable the optimisation of the turbine parameters for specific requirements. The design model is expected to function in a similar fashion. The optimised pump is then compared to a baseline, where the efficiency must be higher than the baseline.

The statistical variances can be considered in parallel with the model parameters (Hendricks Franssen *et al.*, 2009) and the covariance of the parameters also included. However in inverse analysis these parameters must be estimated, given that there is no prior knowledge of the parameters and their statistical distributions. The methods given by Hendricks Franssen *et al.* (2009) principally relate to the inverse modelling of hydrological flow in aquifers, but may be useful to reference to if variability is to be modelled for unknown fabrics.

2.4.2.4. Review of MATLAB internal optimisation routines

Within MATLAB there exists a collection of pre-existing routines that can be used to achieve constrained and unconstrained optimisation. Not all of the optimisation functions available within MATLAB will be relevant to the project. A short review of optimisation routines that are predicted to be relevant and how they perform the optimisation is carried out here. For a full and complete review of optimisation in MATLAB the MATLAB 'help' literature (MathWorks, 2014) should be consulted with reference to published work on optimisation such as Nocedal and Wright (2006).

The following options allow a user to prescribe at what point an optimisation has reached a satisfactory result. Not all are available in every optimisation routine discussed below.

- 'TolFun' is the minimum change in the function value, or how close to zero the function needs to be (Figure 2-54).
- 'TolX' relates to the size of the last step, or change in the position being investigated (Figure 2-54).

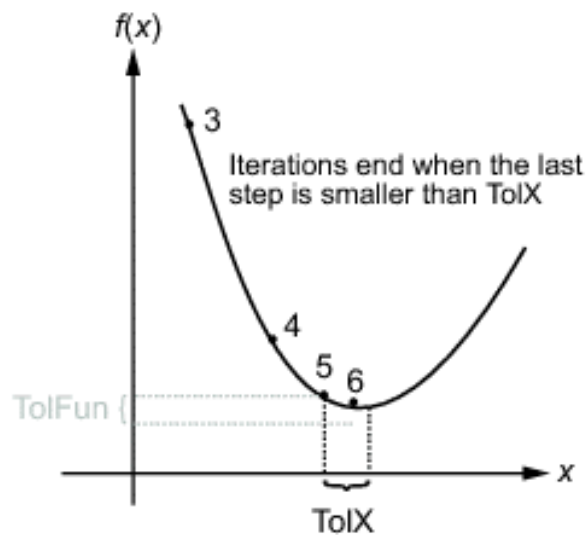


Figure 2-54: Representation of TolX and TolFun. Reproduced from MathWorks (2012a)

- 'MaxIter' is the maximum number of iterations an optimisation routine will run prior to termination.
- 'MaxFunEvals' is the maximum number of function evaluations an optimisation routine will run prior to termination.
- 'Tolcon' is the tolerance of the optimisation for the violation of constraints.
- 'ObjectiveLimit' is the value that will be considered acceptably close to the objective.
- 'DiffMinChange' is the minimum change that will be observed in a variable below which an optimisation routine will terminate.
- 'DiffMaxChange' is the maximum change possible in a variable beyond which an optimisation routine will terminate.

(MathWorks, 2012a)

Once the objective function is available for optimisation the above properties can then be modified to ensure an accurate result. For instance, if 'ObjectiveLimit' is increased the speed of the routine will be increased, but the accuracy of said routine may not be as high as the original optimisation.

A selection of relevant routines is reviewed in the following sections (§2.4.2.5 and §2.4.2.6):

2.4.2.5. *Unconstrained relevant MATLAB functions*

The function 'fsolve' can be utilised to "*solve a system of nonlinear equations*" of the form:

$$F(x) = 0 \quad \text{Equation 2-24}$$

"For x , where x is a vector and $F(x)$ is a function that returns a vector value" (MathWorks, 2014)

This function allows the solution of multiple equations, such as those set out in the sawtooth method (§2.3.2.3), to be found quickly and efficiently by iteratively optimising them. This method is unconstrained, and as such the result is unbounded. The speed of this method and, where multiple solutions are available, the solution found are highly dependent on the start point given to the function by the user. If there exists multiple possible solutions then the solution that is found will generally be the one closest to the initial point.

The function 'fzero' can be utilised to "*find [the] root of [a] continuous function of one variable*". This function considers zeros "*to be points where the function actually crosses, not just touches, the x-axis*". The algorithm used is described as being "*originated by T. Dekker [and] uses a combination of bisection, secant, and inverse quadratic interpolation methods*" (MathWorks, 2012a). This means that no derivatives are numerically calculated, but are calculated using interpolation methods.

2.4.2.6. *Constrained relevant MATLAB functions*

Constrained optimisation in MATLAB attempts to solve (Equation 2-25):

$$\min_x f(x) \text{ subject to } g(x) \leq 0, h(x) = 0$$

Equation 2-25

Where $f(x)$ is the function and $g(x)$ and $h(x)$ are the constraints.

This is represented as a solvable function using the Karush-Kuhn-Tucker (KKT) conditions (Equation 2-27) (Nocedal and Wright, 2006; MathWorks, 2014) which describe "*how the first derivatives of f and the active constraints [] are related to each other at a solution*" (Nocedal and Wright, 2006, p. 330).

$$L(x, \lambda) = f(x) + \sum \lambda_{g,i} g_i(x) + \sum \lambda_{h,i} h_i(x)$$

Equation 2-26

The KKT conditions use the “*auxiliary Lagrangian function*” (Equation 2-26) were “*the vector λ is [] the Lagrange multiplier vector*”(MathWorks, 2014).

$$\nabla L(x, \lambda) = 0,$$

$$\lambda_{g,i} g_i(x) = 0 \forall i,$$

$$\begin{cases} g(x) \leq 0 \\ h(x) = 0 \\ \lambda_{g,i} \geq 0 \end{cases}$$

Equation 2-27

Where these conditions are solved the gradient will be zero, however, this does not necessarily mean that solution is at a minimum, the solution could be at either a maximum, minimum or a plateau. As such the second order derivatives are calculated to check the solution is at a minimum. In practice this is carried out using a gradient approximation of the Hessian matrix (Equation 2-28).

$$H = \nabla^2 L = \nabla^2 f + \sum \lambda_{g,i} \nabla^2 g_i(x) + \sum \lambda_{h,i} \nabla^2 h_i(x)$$

Equation 2-28

(MathWorks, 2014)

The function ‘patternsearch’ uses a pattern search algorithm to find the minimum of a function. The entire results spectrum is polled at intervals, and this information is used to target a finer density of polls on the best function value. This function initially considers the whole results spectrum, and stores the results of previous iterations to inform future iterations. The actual method of polling will depend on the search method employed.

This function can be constrained with bounds, inequalities, equalities, and nonlinear constraints. (Kozola, 2009; MathWorks, 2012a)

2. Literature Review

Possibly the most relevant routine will be 'fmincon' which is an internal function designed to allow for the constrained minimisation of a function. This function can be constrained with bounds, inequalities, equalities, and nonlinear constraints, and minimises equations utilising one of a number of algorithms:

The interior point algorithm, which *"handles large, sparse problems, as well as small dense problems"* (MathWorks, 2014) will be used as it is the recommended algorithm for initial optimisations, being widely resilient to problems that might occur (infinite or NaN, 'Not-a-Number', numbers). As each optimisation will generally be new, and in an unknown space, this should ensure a methodology that is robust to poor choices of initial point or errors in search direction.

(MathWorks, 2012a; Mathworks, 2012b; MathWorks, 2014)

2.5. Statistical analysis and Robustness of Fabrics

How can fabric data be used to demonstrate the statistical distribution of fabric properties and what is the effect of this on the robustness of fabrics?

Statistical analysis is the use of data about the distribution of a variable to inform decisions made about the use of that variable, or information relating to it. Knowing a fabric achieves an average tensile stiffness of 810kN/m is useful information, but knowing that it will only achieve this 10% of the time to an accuracy of +/- 5% informs the use of that information. As part of this correlation considers how well certain functions agree with the fits that are applied to them.

A function may be considered to be robust if it is not susceptible to small changes in its defining variables. Robustness analysis attempts to quantify this, and look for methods to reduce the susceptibility of functions to these small changes.

2.5.1. Correlation

Correlation analysis is the process of inferring the strength of some relationship between two variables (Ayyub and McCuen, 1997). The two methods of this analysis discussed here are graphical analysis and the 'coefficient of determination'. Graphical analysis allows for a visual inspection of the available data and allows for the identification of the following:

1. Degree of common variation or how much two variables are related
2. Range and distribution of data points
3. Presence of extreme events or outliers
4. Form of the relationship
5. Type of relationship (Ayyub and McCuen, 1997)

It is generally assumed that where there is a "*high degree of association*" a causal relationship exists, however, care should be taken to not assume this where no evidence of interaction exists. Additionally it does not hold that where a relationship for a sample exists that this relationship holds for an entire population. This is the basis of the importance of the use of predictive models, that might represent the entire population of a variable without prior knowledge of the distribution, rather than representative models which represent the sampled data only.

2. Literature Review

The total variation in a sample (TV) (Equation 2-29) can be described as the sum of the variation that is explained by the variation in the second variable (EV) (Equation 2-30) and the unexplained variation (UV) (Equation 2-31) which is summarised in Equation 2-32.

$$TV = \sum_{i=1}^n (y_i - \bar{Y})^2 \quad \text{Equation 2-29}$$

y_i = an observation

\bar{Y} = the mean of the observations on Y

$$EV = \sum_{i=1}^n (\hat{y}_i - \bar{Y})^2 \quad \text{Equation 2-30}$$

\hat{y}_i = the value of Y estimated from the best relationship with X

$$UV = \sum_{i=1}^n (y_i - \hat{y}_i)^2 \quad \text{Equation 2-31}$$

$$TV = EV + UV \quad \text{Equation 2-32}$$

A measure of correlation is the coefficient of determination or the ratio EV/TV. Given that the relationship for UV holds then where the total variation is due only to the explained variation the square of the coefficient of variation might be calculated (Equation 2-34). As such where the variation is almost entirely unexplained the ratio will approach zero and the correlation is “null”, whereas where all variation is explained the coefficient will be one. (Ayyub and McCuen, 1997)

$$1 = \frac{EV}{TV} + \frac{UV}{TV} \quad \text{Equation 2-33}$$

$$R^2 = \frac{EV}{TV} = \frac{\sum_{i=1}^n (\hat{y}_i - \bar{Y})^2}{\sum_{i=1}^n (y_i - \bar{Y})^2} \quad \text{Equation 2-34}$$

2.5.2. Robustness

Any measure that characterises a distribution might be *“said to be robust if slight changes in distribution have a relatively small effect on their value”* (Wilcox, 2005).

A comprehensive overview” of the state of the art of robust optimisation is carried out by Beyer and Sendhoff (2007) who review the state of the art of robust optimisation in a succinct manner. Given a standard optimisation for a function $f(x)$, subject to certain constraints $g_i(x) \leq 0$ and $h_j(x) = 0$ which are inequality constraints on ‘ x ’. Robust design optimisation leads to *“solutions and performance results [that] remain relatively unchanged when exposed to uncertain conditions”*.

Taguchi’s robust design methodology utilised a three point design process:

1. System design in which the basic performance and product parameters are identified.
2. Parameter design, in which the design parameters are optimised to meet quality requirements.
3. Tolerance design, or fine tuning of the second stage.

Two kinds of parameter are used, noise factors (ξ) and control parameters (x) which are difficult to control and used to tune optimality respectively. These are then encapsulated in a series of equations that allow for the calculation of the deviation from some target value. Taguchi methods use design of Experiments (DOE) to evaluate different designs rather than using any optimisation (Beyer and Sendhoff, 2007).

To complete the DOE method the parameters are systematically changed according to a lattice, or *“control array”* with the noise factors varied at each point. Thus the best point can be defined. The greatest problem with the Taguchi method is that all possible (even bad) points are considered throughout the control array. Thus a high number of dimensions leads to an exponential increase in time to compute an answer (Wu and Wu, 2000; Beyer and Sendhoff, 2007).

Three types of robustness can be defined; deterministic robustness *“defines parameter domains in which the uncertainties α, δ , etc can vary”* whilst probabilistic robustness *“defines probability measures describing the likelihood by which a certain event occurs”*.

2. Literature Review

The last type, possibilistic robustness, uses “*fuzzy measures*” to define some possibility, membership, or grade (Beyer and Sendhoff, 2007). Further to this four different types of uncertainty are considered: Environmental and operating conditions e.g. material properties, angle of attack, or operating temperature. Production tolerances e.g. the accuracy of the machinery, this might relate to the precision of a yarn area for instance. System output uncertainty, which includes “*all kinds of approximation errors due to the use of models*”. And lastly Feasibility uncertainties which take into account uncertainty in the constraints, or whether they will be fulfilled (Beyer and Sendhoff, 2007). It is therefore possible to conclude that whilst uncertainty in fabric design will probably be due to production tolerances we will in all likelihood be unable to alter these. However, we can alter design values (the first type of uncertainty) thus attempting to achieve robustness through the alteration of the design.

An example of the application of robustness to a design problem is given by Kim *et al.* (2010) who produce a robust design methodology for an electromagnetic device. The method utilises a gradient index formulation which minimises the maximum gradient of the objective function with respect to uncertain variables. The objective function and gradient index (GI) value are given below (Equation 2-35 And Equation 2-36) (Kim *et al.*, 2010).

$$\text{Minimise } f(x) \quad \text{Equation 2-35}$$

$$\text{Subject to } g_j \leq 0, \quad j = 1, 2, \dots, m \\ x_L \leq x \leq x_U$$

$$GI = \max_i |df/du_i|, \quad i = 1, 2, \dots, N, \quad u_i \in x \quad \text{Equation 2-36}$$

The value u_i is some uncertain value.

The gradient index is then minimised to produce a new optimum (Equation 2-37).

$$\text{Minimise } GI_f = \max_i |df(x)/du_i| \quad i = 1, 2, \dots, N \quad \text{Equation 2-37}$$

$$\text{Subject to } g_j(x) + \Psi_j(g_j(x)) \leq 0, \quad j = 1, 2, \dots, m \\ f(x) \cong M$$

Here M is the target value of the objective function and Ψ_j is a penalty function added to the constraints.

The results given for the method for multiple uncertain variables are excellent. The sensitivity of each variable at the target is given to be considerably lower than a “deterministic design” (Figure 2-55).

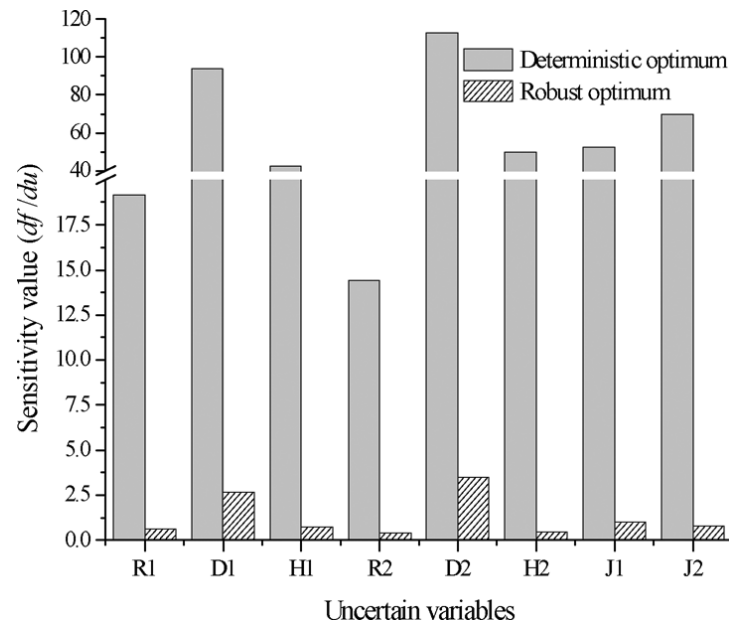


Figure 2-55: Sensitivity of individual variables before and after robustness optimisation. (Kim *et al.*, 2010)

This would seem to be a good basis for a robust design methodology for a fabric. Similarly to this the designed fabric will relate to a single target (mechanical property) that is calculated using a number of variables. The reduction of the sensitivity of the function to these variables will increase the robustness of the whole solution.

Gunawan and Azarm (2004a) consider a sensitivity region for robust optimisation for multiple objectives based on their previous work (Gunawan and Azarm, 2004b). In this method only a particular amount of variation is allowed in a function, $f(x, p)_i$ for which the parameters may vary only the amount Δp . The allowable variation in ‘ p ’ is then described as the sensitivity region. The advantage of this is that the new function value will be close to the original. The sensitivity is then calculated by considering the maximum amount of change in ‘ p ’ that can be accommodated for a given variation $f(x, p)_i$. The worst case value of Δp can then be used to give the sensitivity region. This method’s consideration of a worst case however should result in an

underrepresentation of the sensitivity, insensitivity to other parameters having not been totally taken into account.

3. Predictive model for the design of architectural fabrics

3.1. Introduction

An architectural fabric's mechanical properties vary depending on the properties of the yarns, coating and weave geometry. Given these physical characteristics it is possible to predict a fabric's response to biaxial and shear loading (Peirce, 1937; Kawabata *et al.*, 1973; Menges and Meffert, 1976; Testa *et al.*, 1978; Stubbs and Fluss, 1980; Tan and Barnes, 1984; Pargana *et al.*, 2000; Bridgens and Gosling, 2008). Various methods of achieving this have been discussed in the literature review (§2.3) including finite element, sinusoidal and sawtooth models. However as a simple method was needed for which derivatives could be calculated and geometry easily varied a sawtooth model was selected as the model for this work. Ensuring the model is differentiable allows for the values of Young's modulus and Poisson's ratio to be calculated directly which should allow for quicker optimisation of geometry. This chapter lays out a method for the design of a bespoke fabric with specific mechanical properties based on the inverse of the sawtooth model.

Given that the sawtooth model provides a reasonable prediction of fabric behaviour (Bridgens and Gosling, 2008) and thus allows for the calculation of the mechanical properties of a fabric it follows that the opposite should be achievable. I.e. that a fabric's geometry might be determined from specified tensile stiffness characteristics (mechanical properties). This model will be referred to in the following sections as the 'inverse sawtooth'. Producing this inverse sawtooth model is the aim of this chapter.

The sawtooth model is defined by a number of equations that represent the load elongation characteristics of a fabric (§3.4.1) and which once solved for a specific loading condition give the fabric's deformed geometry. From this the mechanical properties of the fabric are then calculated. As the Young's modulus (E_{11}) can be defined as a change in stress divided by a change in strain, E_{11} for a specific loading condition can be defined as the gradient of the stress and strain curves or $d\sigma/d\varepsilon$. In other words E_{11} is equal to the derivative of stress with respect to strain. Therefore the derivative of the equations that define the sawtooth model with respect to stress and strain will reproduce E_{11} at a specific load. This is the fundamental principle behind the requirement for the equations to be differentiable, and this property allows for the creation of an inverse sawtooth model by reversing the equations (Figure 3-1).

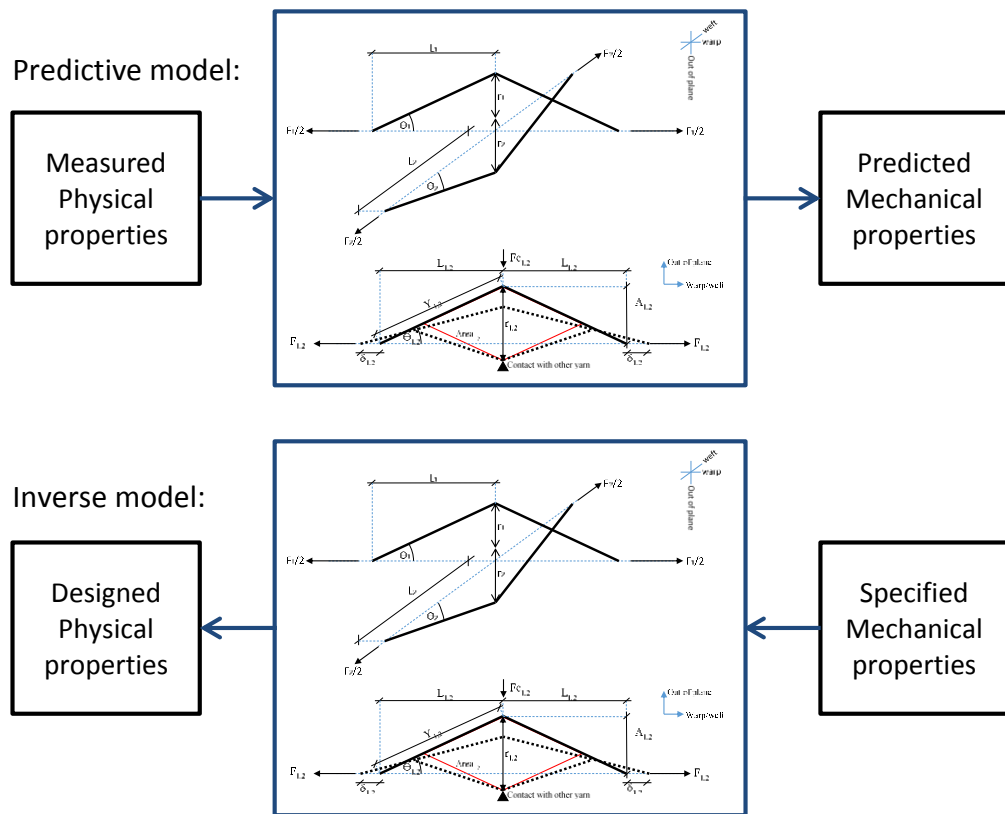


Figure 3-1: Inverse method

The response characteristics to be considered are the Young's moduli in both warp and weft directions (E_{11} and E_{22}), the Poisson's ratios of the fabric (ν_{12} and ν_{21}) and the shear modulus (G). Equations defining these responses at all loads (where the loads on a unit cell are calculated as F_1 and F_2) are produced in this chapter. These are then utilised as the objective function for a gradient based optimisation routine that is used to design a fabric for specified tensile stiffnesses. Optimisation will be shown to be necessary to solve situations where more than one, or zero, possible designs exists to solve the equations. In this chapter the formulation, modelling and use of these equations will be covered.

The methodology of inverting the model to enable it to be used for design is developed and demonstrated in a simple situation before more complex calculations are made. This is done to demonstrate that the method of differentiation is applicable to a series of nonlinear equations.

Following the demonstration of the method of inversion the inverse sawtooth model will be built up in parts. Only the effects of changes in unit cell geometry under load will

3. Predictive model

be considered at first, ignoring the effects of the coating, yarn extensions and yarn crushing forces. Once the principle has been demonstrated in this simple scenario the full sawtooth model will be considered, and equations that determine the fabric parameters which correspond to specific mechanical properties produced. The sawtooth model developed by Bridgens and Gosling (2008) will be used as the basis for the model with the additional inclusion of the consideration of the coating Poisson's ratio. This model was chosen because it is predictive, the importance of which has already been covered (§2.3.3), the geometry can easily be varied (unlike finite element models), and the equations are presented in a form that enables differentiation.

Finite difference calculations will be used to compare the inverse model to the predictive sawtooth model from which it was originally derived, whilst comparisons to real fabric responses should demonstrate the utility of the model.

The method of optimisation chosen is a gradient based solver from the available MATLAB solvers (Mathworks, 2012b). Internal MATLAB functions were used to expedite the model's development, and were found to fulfil the requirements of the design method. The modelling was carried out in MATLAB (Mathworks, 2012b) with MATLAB functions used to perform optimisations and complex derivations (MathWorks, 2012a).

3.2. Aim

To create an inverse model of the sawtooth model developed by Bridgens (2005), Kawabata *et al.* (1973), Menges and Meffert (1976) and Peirce (1937). This will lead to:

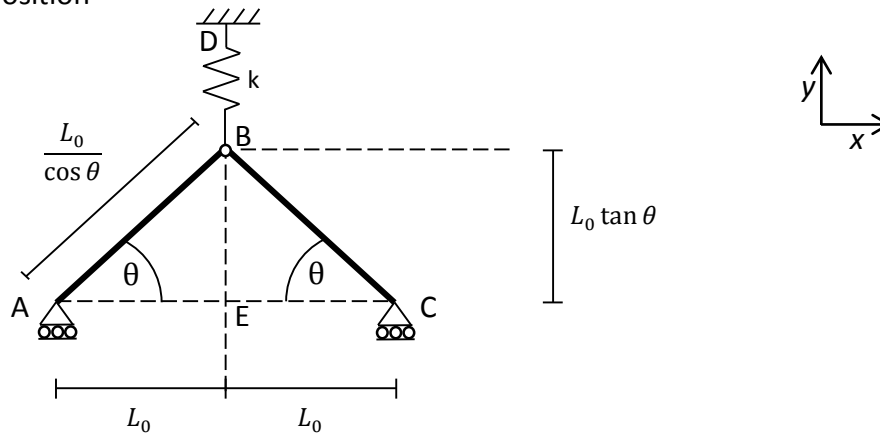
- Equations that define the material response based on the initial geometry and mechanical properties of the yarns and coating, and the applied loads.
- A computationally efficient optimisation routine to produce a designed fabric.
- A methodology to produce a 'designed fabric' (bespoke fabric) for specified elastic constants at multiple stress states.

3.3. The simple spring and arm model

To demonstrate the feasibility of using the proposed method of differentiation to calculate mechanical properties this method was first applied to a simple 'spring and arm' system. This was used to ensure that possible problems with the principle of the methodology were identified early on where known relationships could be used to calculate stresses and strains. Unlike the sawtooth model which represents the complex nonlinear behaviour of a fabric this system could be modelled using simple relationships to demonstrate the accuracy of the results. The simple relationships necessary were the load-extension response of a spring and the calculation of bar member loads. The source of any errors identified could be more easily tracked to its source where the number of variables was limited.

The simple spring and arm case consists of two inextensible bar members connected by a frictionless pin joint (B), and supported by a spring at the pin joint. The spring is connected to a fixed support (D) and can only deform downwards, the free ends of the members are supported by rollers (A and C), and can only move in the x-direction. The load applied is equal and opposite at both ends of the supports and acts in the x-direction (Figure 3-2).

a) Initial position



b) Deformed geometry

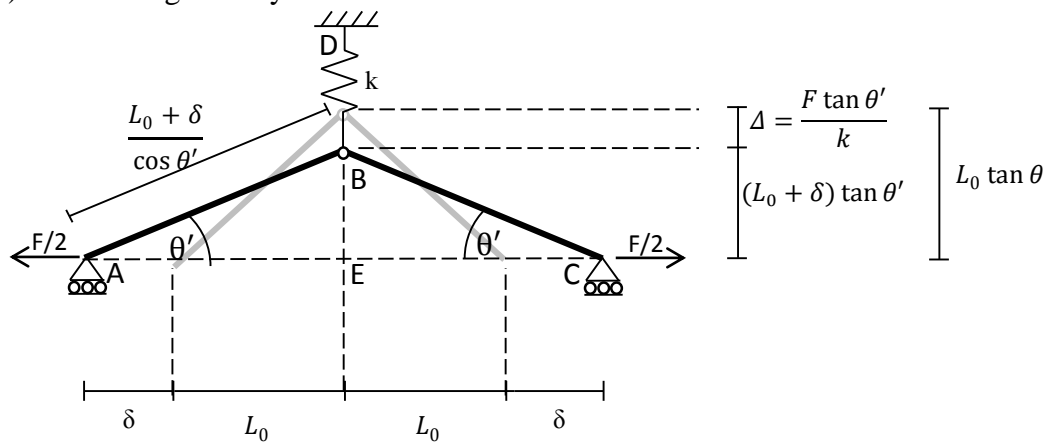


Figure 3-2: Spring and arm case layout, a) prior to loading, b) deformed

Term	Description
k	The spring stiffness (constant)
L_0	Half the distance between the two roller supports in the unloaded system
θ	The angle between the X-axis and the member in the unloaded system
θ'	The angle between the X-axis and the member in the loaded system
δ	The displacement of the roller supports from their original position
Δ	The displacement of the pin-joint at which the members connect to the spring
F	The force applied to the system (constant)

Table 3-1: 'Spring and arm' system nomenclature

3.3.1. Modelling the spring and arm model

The 'spring and arm' model also represents the behaviour of a single inextensible yarn where the response of the other yarn direction and the crushing of both yarns is embodied in the spring's load extension characteristics. In this simplification there is no consideration of coating. As such the response of this system should inform the formulation of further models.

The sawtooth model includes geometric and force equilibrium constraints (Kawabata *et al.*, 1973; Bridgens and Gosling, 2008), and these will be similarly found in this model:

Considering the deformation of triangle ABE (Figure 3-2) with inextensible members gives:

$$\frac{L_0}{\cos \theta} = \frac{L_0 + \delta}{\cos \theta'} \quad \text{Equation 3-1}$$

Rearranging Equation 3-1, substituting in the equation for ' k ', and considering the vertical resultant force at B (§A.6) gives the equations for F and θ' (Equation 3-2 and Equation 3-3).

$$F = \frac{k}{\tan \theta'} \left[\left(\frac{\delta + L_0}{\cos \theta'} \right)^2 - L_0^2 \right]^{0.5} - k(\delta + L_0)$$

*Note all $F = f(\theta', \delta)$

Equation 3-2

$$\theta' = \cos^{-1} \left(\frac{(L_0 + \delta) \cos \theta}{L_0} \right)$$

Equation 3-3

Thus the Force (F) has been written in terms of δ and θ' such that $F = f(\theta', \delta)$ (Equation 3-2). Similarly θ' has been written in terms of δ such that $\theta' = f(\delta)$ (Equation 3-3). At this point it is now possible to produce the full differential for $F = f(\theta', \delta)$. Croft *et al.* (2001) describes how all the partial derivatives of a differential equation must be calculated prior to the calculation of a full derivative (Equation 3-4).

3. Predictive model

It is necessary to find the derivative of force with relation to strain in the sawtooth model to calculate the stiffness of the unit cell. In the sawtooth model the reaction is influenced by a number of changes to the unit cell geometry (yarn extension, yarn crushing, and changes in the yarn angle) and therefore the response needs to be calculated to include these changes. Thus the solution is calculated as the full derivative with relation to a number of partial derivatives. In this simple case the number of variables is less, simplifying the process of finding the derivative. The full derivation is shown in the appendix (§A.6).

The full derivative may be calculated by considering the partial derivatives of the functions $F = f(\theta', \delta)$, and $\theta' = f(\delta)$ (Equation 3-2, Equation 3-3).

$$\frac{dF}{d\delta} = \frac{\partial F}{\partial \delta} + \frac{\partial F}{\partial \theta'} \cdot \frac{\partial \theta'}{\partial \delta} \quad \text{Equation 3-4}$$

The full derivative of the force with respect to the deformation is:

$$\frac{dF}{d\delta} = \frac{\partial F}{\partial \delta} + \frac{\partial F}{\partial \theta'} \cdot \frac{\partial \theta'}{\partial \delta} =$$

$$\left[\cos \theta \left\{ \frac{k(\tan^2 \theta' + 1) \cdot Q}{\tan^2 \theta'} - \frac{k \sin \theta' (L_0 + \delta)^2}{\cos^3 \theta' \tan \theta' \left(1 - \left(\frac{\cos^2 \theta (L_0 + \delta)^2}{L_0^2} \right) \right)^{0.5}} \right\} \right] + \frac{k(2L_0 + 2\delta)}{(2 \cos^2 \theta' \tan \theta' \cdot Q) - k} - k$$

$$\left[L_0 \left(\frac{1 - (\cos^2 \theta' (L_0 + \delta)^2)}{L_0^2} \right)^{0.5} \right]$$

Equation 3-5

The validity of using the derived equations is demonstrated by solving the equations within MATLAB (Mathworks, 2012b) and comparing the results to analytically calculated values of $dF/d\delta$. The results showed excellent fidelity (§A.7), and in addition demonstrated the need for all terms within the objective function to be considered. The full validation is given in the appendix (§A.7).

3.4. Sawtooth model inversion

Initially only a simplified model was used to further demonstrate the applicability of the method (§3.4.2). Following this the full sawtooth model was considered, and this was then modified to include the coating Poisson's ratio (§3.4.3). Lastly a shear component is developed. The equilibrium equations defining the sawtooth model (§3.4.1) are necessary to calculate displacements of a specific geometry and this is briefly reviewed before the inverse sawtooth is developed.

3.4.1. The sawtooth model

The sawtooth model as previously developed (Peirce, 1937; Kawabata *et al.*, 1973; Menges and Meffert, 1976; Bridgens and Gosling, 2008) is needed to calculate strains which will be used later to calculate the accuracy of the inverse model using a central finite difference method.. The justification for this choice of model has been briefly reviewed (§3.1), but will be considered in more depth here.

Firstly a predictive unit cell model has been chosen as it allows for the input and variation of geometry with relative ease, and considers only those properties that are obtainable with standard tests. Were a finite element method to have been chosen the use of a mesh would have made the variation of geometry difficult and computationally expensive because each new geometry would require re-meshing. Representative models naturally could not have been selected for the prediction of fabric tensile response outside of their initial data set. Those models that require calibration would also be unsuitable as the basis for the design of a bespoke architectural fabric as any designed fabric may not exist for the model to be calibrated to.

The sawtooth model was chosen for the inverse modelling as it fulfilled the following required criteria:

- It is predictive, inclusive of designs that are outside of the data range the model was originally tested in.
- It is accurate (Bridgens and Gosling, 2008). The model will be used on a wide variety of fabric types. In addition any inaccuracy in the initial model may be compounded during the inversion, where the model moves further away from the original data.

3. Predictive model

- The model is 'invertible'. The model is formulated such that its constitutive equations can be differentiated and thus make it possible to produce equations defining a fabrics tensile stiffness.
- The model represents plain-weave fabrics that are most often used as architectural fabrics.

Having fulfilled these criteria the sawtooth model, as presented by Bridgens and Gosling (2008), was chosen as the original model to be inverted (Figure 3-3). The sawtooth model is a unit cell representation of two yarns where twice the value of 'L' is equivalent to half the wavelength of a yarn (Figure 3-4). The unit cell is *"the smallest element that may be used to characterise the mechanical response of the fabric as a whole"* (Pargana et al., 2007, p. 1327).

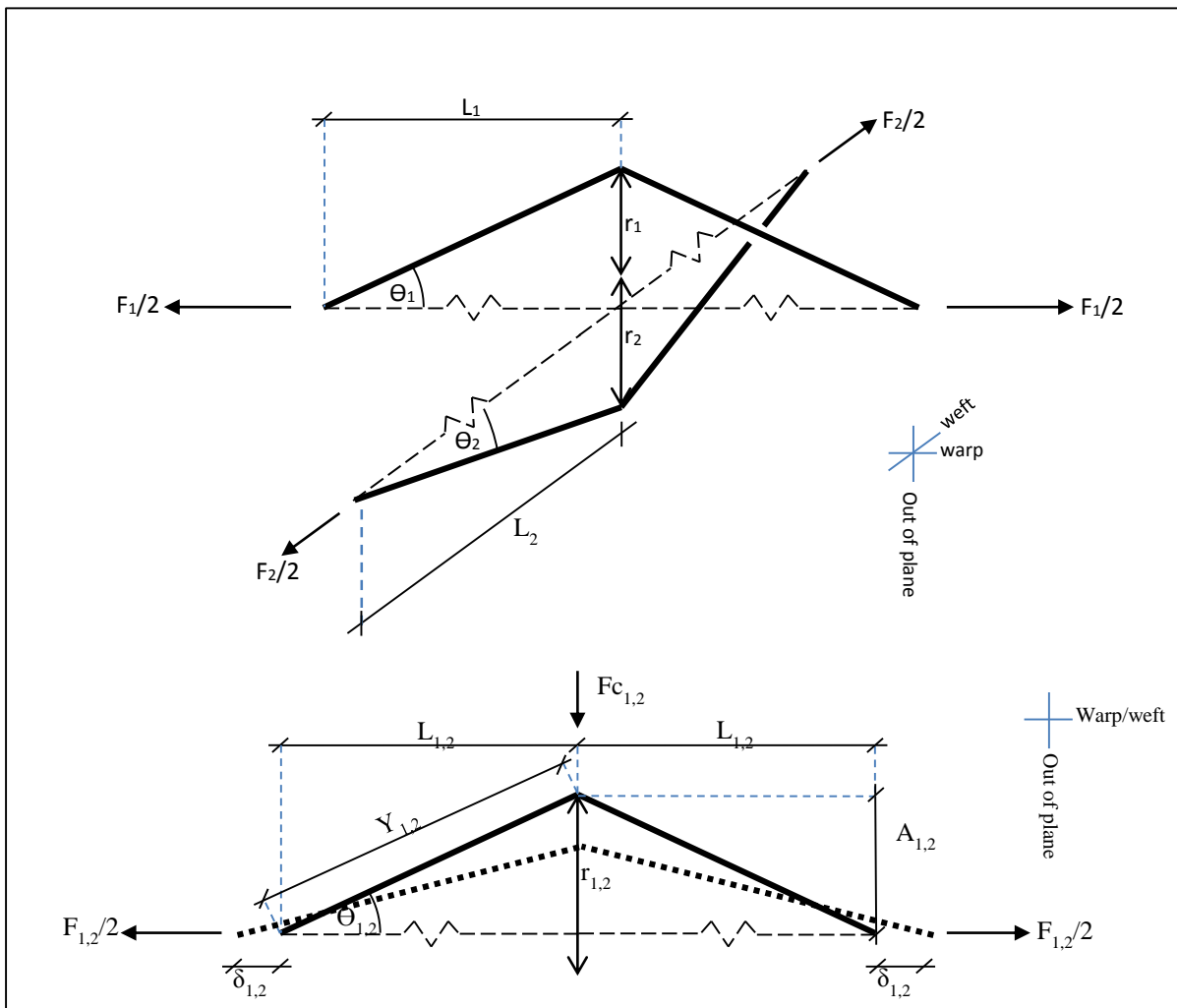


Figure 3-3: Fundamentals of the full sawtooth model with springs representing the coating. Modified from Bridgens and Gosling (2008)

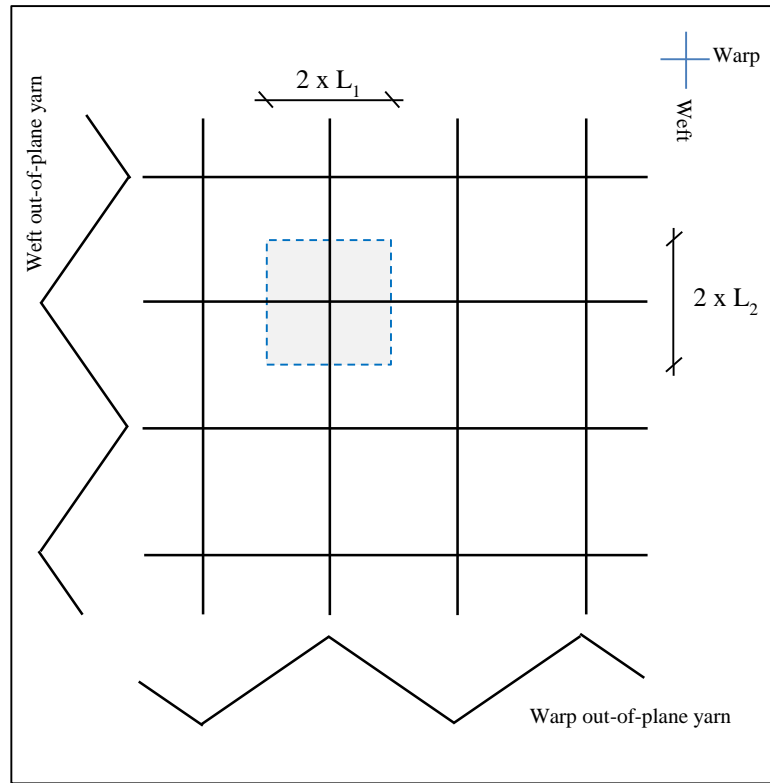


Figure 3-4: Unit cell position within the sawtooth representation

The equations needed to define the response of the sawtooth model as used by Bridgens and Gosling (2008) are detailed below:

$$(r_1 + r_2) = (A_1 + A_2) \quad \text{Equation 3-6}$$

Where $r_{1,2}$ are the yarn radii, and $A_{1,2}$ are the yarn amplitudes (crimp) in the warp and weft directions respectively.

This will be referred to as the equilibrium equation and is based on the equation produced by Peirce (1937). This ensures that there can never be any discrepancy between the thickness of the fabric, calculated from the yarn thicknesses, and the thickness of the fabric calculated from the yarn amplitudes. One result of this is that no 'gap' may exist between yarns, as suggested in some literature, though with the fabric being coated and therefore the yarns restricted this is deemed unlikely to occur.

$$F_{c1} = F_{c2} \quad \text{Equation 3-7}$$

The out-of-plane forces must be equal ($F_{c1,2}$ are the compaction forces at the warp/weft yarns respectively) (Equation 3-7).

3. Predictive model

$$F_{y1,2} \sin \theta_{1,2} = F_{c1,2} \quad \text{Equation 3-8}$$

The out-of-plane force (F_c) is produced by the interaction of the yarn tension force (F_y) with the yarn in the other direction (Equation 3-8). The out-of-plane angle is θ .

$$F_{k1,2} = 2E_k L'_{2,1} \varepsilon_{1,2} \quad \text{Equation 3-9}$$

Where F_k is the force in the coating spring and E_k is the coating stiffness

*when using springs to represent the coating (Figure 3-3).

The coating response to load (Equation 3-9) is governed by a 'spring representation of the coatings deformation. This has previously used a linear value of coating stiffness.

$$F_{y1,2} \cos \theta'_{1,2} + F_{k1,2} = F_{1,2} \quad \text{Equation 3-10}$$

The sum of the forces in the fabric must be equal to the applied load (Equation 3-10).

$$\varepsilon_{1,2} = \frac{L'_{1,2} - L_{1,2}}{L_{1,2}} \quad \text{Equation 3-11}$$

The strain (ε) is calculated using the original and deformed quarter yarn wavelength (yarn in-plane length) (Equation 3-11).

$$F_{1,2} = \frac{P_{1,2}}{2L_{2,1}} \quad \text{Equation 3-12}$$

The force (F) used is always considered in relation to the original geometry, $L_{2,1}$, (Equation 3-12) as within a stressed fabric the force applied to each unit cell will be in relation to the original shape of the fabric. Unit cells do not disappear as the fabric is stretched, and thus the force applied to each cell is presumed to remain the same, whilst the load on the fabric might change. The stress in the fabric per metre (P) is also considered constant.

$$Y'_{1,2} = Y_{1,2} \left[1 + \frac{F_{y1,2}}{2E_{y1,2} L'_{2,1}} \right] \quad \text{Equation 3-13}$$

The extension of a yarn has also previously used a linear value of yarn stiffness. Linear yarn stiffness's, especially in polyester yarns may grossly under represent the response of the yarn to load (§2.2.2).

A kite shaped yarn deformation mechanism as described by Bridgens and Gosling (2008) is used during this project. In earlier work by Menges and Meffert (1976) and Dimitrov and Schock (1986) springs are used to represent yarn deformation at the point of crossover, which has the distinct disadvantage of requiring “*precise knowledge of the local geometry and associated elastic and viscous properties of the yarn and coating*” (Dimitrov and Schock, 1986, p. 858). This requirement for detailed knowledge regarding the yarn properties does not lend itself to the design of a bespoke fabric for specific mechanical properties. As such the kite shaped mechanism (Figure 3-5) is preferable, and can be defined below (Equation 3-14, Equation 3-15 and Equation 3-16):

$$r'_{1,2} = \frac{Area_{1,2}}{2 * w'_{1,2}} \quad \text{Equation 3-14}$$

$$w'_{1,2} = \frac{w_{1,2}}{L_{2,1}} L'_{2,1} \quad \text{Equation 3-15}$$

$$Area_{1,2} = 2w_{1,2}r_{1,2} \quad \text{Equation 3-16}$$

The kite shaped mechanism represents the deformation of the yarn at the point of crossover due to compaction forces generated as a result of the tensile forces in the yarns in both directions. These forces will deform the yarns to some extent, and this is represented by the constant area kite. The kite deforms in proportion to the extension of the orthogonal yarn, and therefore represents the deformation of the yarn cross-section without the need for any detailed knowledge of the compaction stiffness of the cross section. This therefore acts as a geometric constraint, which allows for the consideration of yarn cross section deformation without any detailed analysis of the actual yarn deformation mechanism.

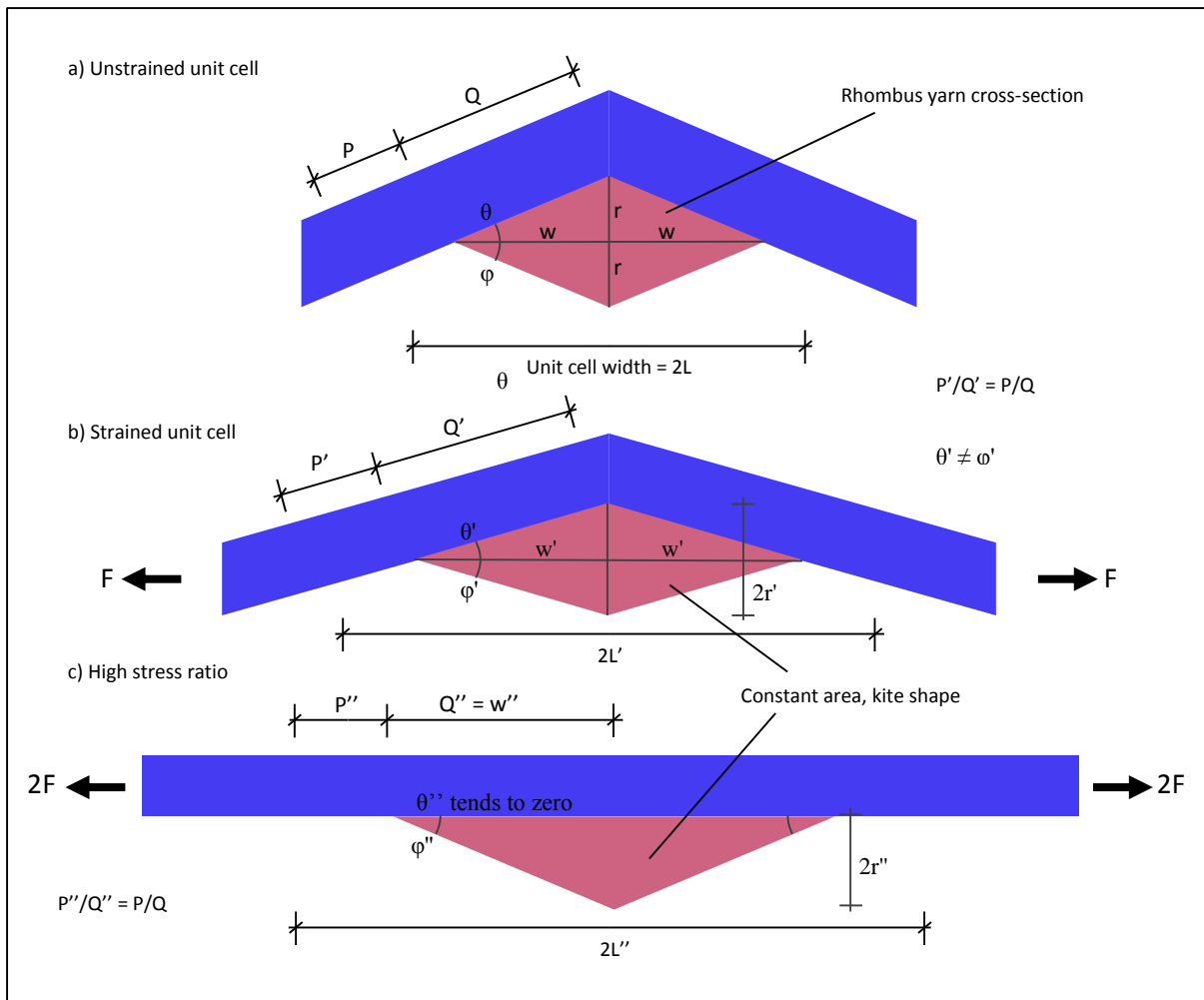


Figure 3-5: Kite Shape yarn cross section reproduced from Bridgens (2005)

The 'kite shape yarn cross section' can be defined as follows: *"as yarn 1 extends the ratio $P:Q$ is kept constant [and] the width of yarn 2 increases as yarn 1 extends."* It is noted that this is not *"intended to model inter-yarn friction"* and that accurately measuring the actual yarn deformation is infeasible as this would *"mean cutting the sample, which would profoundly affect the state of stress and balance of forces in the fabric"* (Bridgens, 2005, p. 229). It may be possible to measure this deformation, but this is outside of the scope of this project. Further to this a decision has been made to limit the scale of the work to the unit cell, and not to extend the model to the design of the constituent yarns in and of themselves which would require considerable further work. The response of the yarns is discussed in the Literature review (§2.2.2), and relies on spinning mechanism, angle of spin, inter filament friction and cohesion, and material type. Inclusion of all these parameters would greatly increase the model complexity and require the addition of a separate module to enable the design of the yarns.

The sawtooth model is, in essence, an equilibrium problem that must be solved given certain initial values of geometry to find the equilibrium state of the fabric after biaxial force has been applied. The defining equations must all be solved simultaneously and iteratively for the values of $\theta'_{1,2}$ and $Y'_{1,2}$ (Equation 3-6, Equation 3-7, Equation 3-8 and Equation 3-13). Once these values have been calculated it is possible to calculate the strain and other properties of the fabric at its stressed state.

The 'FSolve' (MathWorks, 2012a) routine is used for the iterative solving of the equations, and from this the deformations and hence strains can be calculated, which are vital to the following stages.

3.4.2. Inverting a simplified sawtooth model

The concept of the 'simple sawtooth' was developed to refine the method used to find the derivatives necessary to calculate the fabric's response parameters. It is also used to demonstrate that these can be used as the objective functions for an optimisation of the fabric's physical parameters towards a set of target moduli. Whilst the concept of using derivatives to find the tensile stiffness has been shown to work in the sections above (§3.3.2) it was also necessary to demonstrate feasibility in three dimensions.

3.4.2.1. Definition of the simple sawtooth

Whilst a true architectural fabric is a complex system made up of many components the objective of this portion of the project is to demonstrate the utility of the method to be used on more complex systems. This simple case (Figure 3-6) varies from the full sawtooth in that it does not consider the following properties:

- No yarn extension – the yarns are considered rigid except at the joints ($Y'_{1,2} = Y_{1,2}$)
- No yarn crushing – the yarn radii remain constant ($r'_{1,2} = r_{1,2}$)
- No coating – the coating provides no resistance in compression or tension ($F_k = 0$)

This model can be considered as a purely mechanical problem, similar to the proof of concept. The evolution of the system from that initial problem allows for small errors to be caught and modified prior to further more complex improvements.

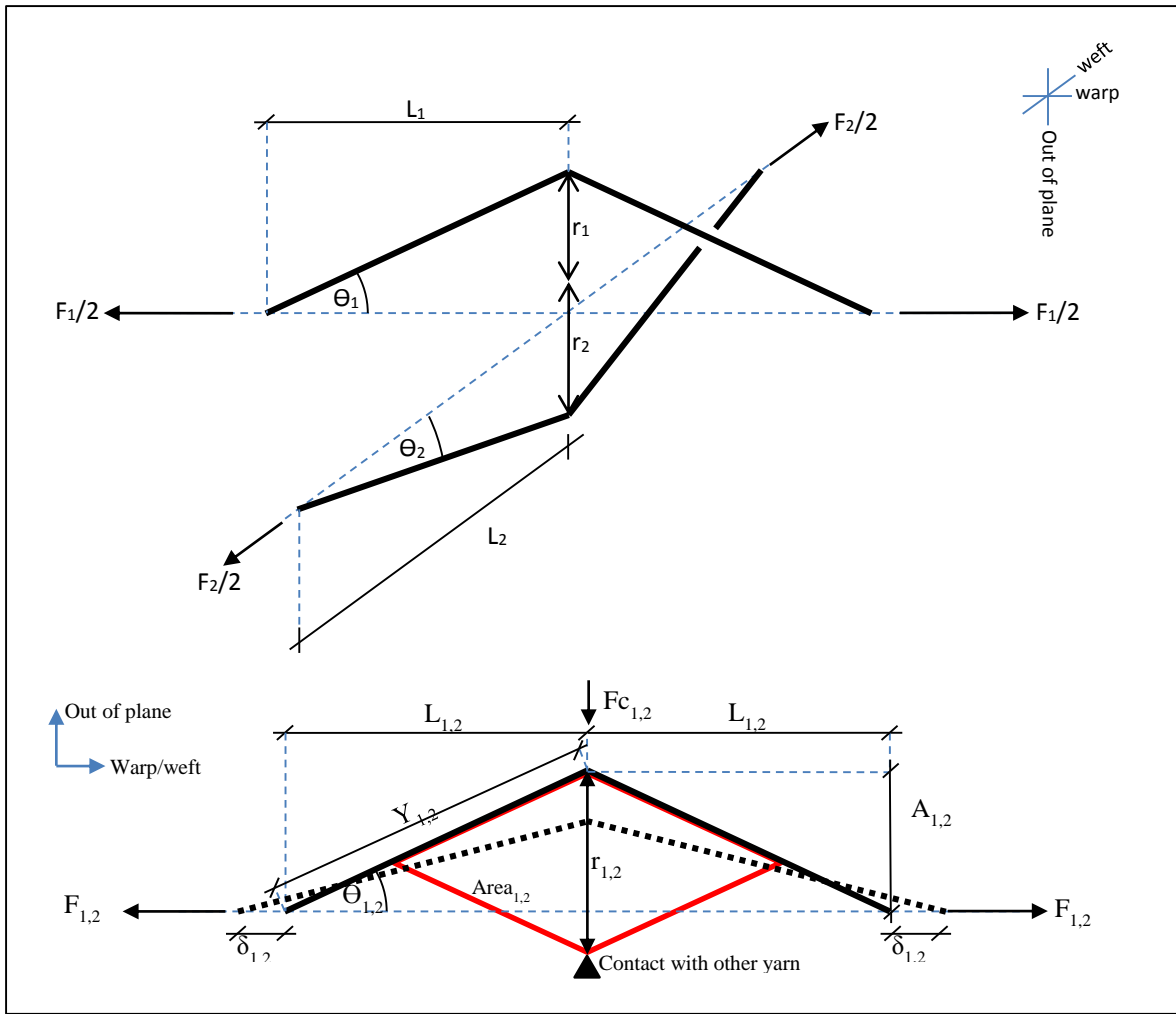


Figure 3-6: Fundamentals of the simple sawtooth model

3.4.2.2. Equations defining the response of the simple sawtooth

The equilibrium equations for the system state that the sum of the yarn radii must equal the sum of the yarn amplitudes (Equation 3-17) and the out of plane forces must be equal (Equation 3-18). Given that there can be no variation in yarn radius all deformation occurs in the movement of the yarns through the change in the yarn angle. The equilibrium equations are the base of all further equations shown.

$$(r_1 + r_2) - (A_1 + A_2) = 0 \quad \text{Equation 3-17}$$

$$F_{c1} - F_{c2} = 0 \quad \text{Equation 3-18}$$

$$F_{y1,2} \sin \theta_{1,2} - F_{c1,2} = 0 \quad \text{Equation 3-19}$$

3. Predictive model

From the equations above it is possible to define the equations used to calculate the derivatives below. The differential equations were produced in accordance with the method of combining partial derivatives outlined in the 'spring and arm' model (§3.3.2).

$$\frac{dF_1}{d\varepsilon_1} = \frac{\partial F_1}{\partial \varepsilon_1} + \frac{\partial F_1}{\partial \theta'_{1,1}} \cdot \frac{\partial \theta'_{1,1}}{\partial \varepsilon_1} + \frac{\partial F_1}{\partial \varepsilon_2} \cdot \frac{\partial \varepsilon_2}{\partial \varepsilon_1}$$

Equation 3-20

$$\frac{dF_2}{d\varepsilon_1} = \frac{\partial F_2}{\partial \varepsilon_1} + \frac{\partial F_2}{\partial \theta'_{2,1}} \cdot \frac{\partial \theta'_{2,1}}{\partial \varepsilon_1} + \frac{\partial F_2}{\partial \varepsilon_2} \cdot \frac{\partial \varepsilon_2}{\partial \varepsilon_1}$$

Equation 3-21

$$\frac{dF_1}{d\varepsilon_2} = \frac{\partial F_1}{\partial \varepsilon_2} + \frac{\partial F_1}{\partial \theta'_{1,1}} \cdot \frac{\partial \theta'_{1,1}}{\partial \varepsilon_2} + \frac{\partial F_1}{\partial \varepsilon_1} \cdot \frac{\partial \varepsilon_1}{\partial \varepsilon_2}$$

Equation 3-22

$$\frac{dF_2}{d\varepsilon_2} = \frac{\partial F_2}{\partial \varepsilon_2} + \frac{\partial F_2}{\partial \theta'_{2,1}} \cdot \frac{\partial \theta'_{2,1}}{\partial \varepsilon_2} + \frac{\partial F_2}{\partial \varepsilon_1} \cdot \frac{\partial \varepsilon_1}{\partial \varepsilon_2}$$

Equation 3-23

The derivatives of equations that relate to each partial derivative are required to produce $dF_{1,2}/d\varepsilon_{1,2}$ and $dF_{1,2}/d\varepsilon_{2,1}$ (Equation 3-25, Equation 3-26, and Equation 3-27). The derivations of the following equations are shown prior to the equation. Displacement (δ) is converted to strain in the following sections (Equation 3-24).

$$\delta_{1,2} = \varepsilon_{1,2} \cdot L_{1,2}$$

Equation 3-24

The derivation of a single formula that relates the force applied (F) to the out of plane angle ($\theta'_{1,2}$) and strain ($\varepsilon_{2,1}$) (Equation 3-25) is shown in the appendix (§A.8).

$$F_{1,2} = \frac{F_{2,1}((r_1 + r_2) - (L_{1,2} + (\varepsilon_{1,2} \cdot L_{1,2})) \tan \theta'_{1,2})}{(L_{2,1} + (\varepsilon_{2,1} \cdot L_{2,1})) \tan \theta'_{1,2}}$$

Equation 3-25

Once this has been achieved $\theta'_{1,2}$ can be defined in terms of only initial geometry and strain, as shown below (Equation 3-26):

$$\theta'_{1,2} = \cos^{-1} \left(\frac{(L_{1,2} + (\varepsilon_{1,2} \cdot L_{1,2})) \cos \theta_{1,2}}{L_{1,2}} \right) = f(\varepsilon_{1,2}) \quad \text{Equation 3-26}$$

And $\varepsilon_{2,1}$ can be defined in terms of only initial geometry and $\varepsilon_{1,2}$ (Equation 3-27).

$$\varepsilon_{2,1} = \frac{\cos \left(\sin^{-1} \left(\left(\frac{(r_1 + r_2) - (L_{1,2} + (\varepsilon_{1,2} \cdot L_{1,2})) \tan(\theta'_{1,2})}{L_{2,1}} \right) \cos \theta_{1,2} \right) \right)}{\cos \theta_{2,1}} - 1 \quad \text{Equation 3-27}$$

With the above equations it is possible to produce the derivatives $dF_{1,2}/d\varepsilon_{1,2}$ and $dF_{1,2}/d\varepsilon_{2,1}$, which can then be used to optimise a set of initial geometries for a set of targets. The derivatives are shown below:

$$\frac{dF_1}{d\varepsilon_1} = \frac{\cos \theta_1 \left(\frac{F_2 a (\tan^2 \theta'_1 + 1)}{b \tan \theta'_1} + \frac{F_2 (\tan^2 \theta'_1 + 1) (r_1 + r_2 - a \tan \theta'_1)}{b \tan^2 \theta'_1} \right)}{c} - \frac{F_2 L_1}{b} + \frac{F_2 a \cos \theta_1 \cos \theta_2 (r_1 + r_2 - a \tan \theta'_1) * (r_1 + r_2 - \frac{L_1 c}{\cos \theta_1})}{L_2 c b^2 e \tan \theta'_1} \quad \text{Equation 3-28}$$

$$\frac{dF_2}{d\varepsilon_2} = \frac{\cos \theta_2 \left(\frac{F_1 b (\tan^2 \theta'_2 + 1)}{a \tan \theta'_2} + \frac{F_1 (\tan^2 \theta'_2 + 1) (r_1 + r_2 - b \tan \theta'_2)}{a \tan^2 \theta'_2} \right)}{d} - \frac{F_1 L_2}{a} + \frac{F_1 b \cos \theta_1 \cos \theta_2 (r_1 + r_2 - b \tan \theta'_2) (r_1 + r_2 - \frac{L_2 d}{\cos \theta_2})}{L_1 d a^2 f \tan \theta'_2} \quad \text{Equation 3-29}$$

$$\frac{dF_2}{d\varepsilon_1} = \frac{F_1 \cos \theta_1 \cos \theta_2 \left(r_1 + r_2 - \frac{L_1 c}{\cos \theta_1} \right)}{L_2 c e} - \frac{F_1 L_1 (r_1 + r_2 - b \tan \theta'_2)}{a^2 \tan \theta'_2} - \frac{a \cos \theta_1 \cos^2 \theta_2 \left(\frac{F_1 b (\tan^2 \theta'_2 + 1)}{a \tan \theta'_2} + \frac{F_1 (\tan^2 \theta'_2 + 1) (r_1 + r_2 - b \tan \theta'_2)}{a \tan^2 \theta'_2} \right) (r_1 + r_2 - \frac{L_1 c}{\cos \theta_1})}{L_2^2 c e \left(1 - \frac{\cos^2 \theta_2 \left(L_2 - \frac{L_2 \cos \theta_2 - L_2 e}{\cos \theta_2} \right)^2}{L_2^2} \right)^{\frac{1}{2}}} \quad \text{Equation 3-30}$$

$$\frac{dF_1}{d\varepsilon_2} = \frac{F_2 \cos \theta_1 \cos \theta_2 \left(r_1 + r_2 - \frac{L_2 d}{\cos \theta_2} \right)}{L_1 df} - \frac{F_2 L_2 (r_1 + r_2 - a \tan \theta'_1)}{b^2 \tan \theta'_1} -$$

$$\frac{\cos^2 \theta_1 \cos \theta_2 b \left(\frac{F_2 a (\tan^2 \theta'_1 + 1)}{b \tan \theta'_1} + \frac{F_2 (\tan^2 \theta'_1 + 1) (r_1 + r_2 - a \tan \theta'_1)}{b \tan^2 \theta'_1} \right) \left(r_1 + r_2 - \frac{L_2 d}{\cos \theta_2} \right)}{L_1^2 df \left(1 - \frac{\cos(\theta_1)^2 \left(L_1 - \frac{L_1 \cos \theta_1 - L_1 f}{\cos \theta_1} \right)^2}{L_1^2} \right)^{\frac{1}{2}}}$$

Equation 3-31

Where the values a, b, c, d, e, and f are calculated separately (Equation 3-32, Equation 3-33, Equation 3-34, Equation 3-35, Equation 3-36, and Equation 3-37 respectively).

$$a = (L_1 + L_1 \varepsilon_1)$$

Equation 3-32

$$b = (L_2 + L_2 \varepsilon_2)$$

Equation 3-33

$$c = \left(1 - \frac{a^2 \cos^2 \theta_1}{L_1^2} \right)^{\frac{1}{2}}$$

Equation 3-34

$$d = \left(1 - \frac{b^2 \cos^2 \theta_2}{L_2^2} \right)^{\frac{1}{2}}$$

Equation 3-35

$$e = \left(1 - \frac{\cos^2 \theta_2 \left(r_1 + r_2 - \frac{L_1 c}{\cos \theta_1} \right)^2}{L_2^2} \right)^{\frac{1}{2}}$$

Equation 3-36

$$f = \left(1 - \frac{\cos^2 \theta_1 \left(r_1 + r_2 - \frac{L_2 d}{\cos \theta_2} \right)^2}{L_1^2} \right)^{\frac{1}{2}}$$

Equation 3-37

At this stage it becomes clear that the values of $dF_{1,2}/d\varepsilon_{1,2}$ and $dF_{1,2}/d\varepsilon_{2,1}$ are not suitable for use as engineering values, as they relate only to the unit cell (Figure 3-4). Thus it is necessary to demonstrate how these values will relate to true engineering values.

$dF_{1,2}/d\varepsilon_{1,2}$ and $dF_{1,2}/d\varepsilon_{2,1}$ can be used to produce values for E_{11} , E_{22} , ν_{12} and ν_{21} as shown below:

3. Predictive model

v_{12} can be defined as the contraction in direction 2 due to extension in direction 1 (Equation 3-38).

$$v_{12} = -\frac{d\varepsilon_{trans(2)}}{d\varepsilon_{axial(1)}} = -\frac{d\varepsilon_2}{d\varepsilon_1} \quad \text{Equation 3-38}$$

This can be used to show how the Poisson's ratios can be derived (Equation 3-39) (Long, 2005).

$$\begin{Bmatrix} \varepsilon_1 \\ \varepsilon_2 \end{Bmatrix} = \begin{bmatrix} \frac{1}{E_{11}} & -\frac{v_{12}}{E_{11}} \\ -\frac{v_{21}}{E_{22}} & \frac{1}{E_{22}} \end{bmatrix} \begin{Bmatrix} \sigma_1 \\ \sigma_2 \end{Bmatrix}$$

Equation 3-39

$$E_{11,22} = \frac{dF_{1,2}}{d\varepsilon_{1,2}}$$

$$v_{12} = -\frac{d\varepsilon_2}{d\varepsilon_1}$$

$$-\frac{v_{12}}{E_{11}} \propto E_{12}$$

$$-\frac{v_{12}}{\left(\frac{dF_1}{d\varepsilon_1}\right)} \propto \left(\frac{dF_1}{d\varepsilon_2}\right)$$

Using the definitions of E_{12} and E_{11} it is possible to show that $E_{11}/E_{12}=v_{12}$.

$$-\frac{\left(\frac{dF_1}{d\varepsilon_1}\right)}{\left(\frac{dF_1}{d\varepsilon_2}\right)} = -\frac{d\varepsilon_2 dF_1}{d\varepsilon_1 dF_1} = -\frac{d\varepsilon_2}{d\varepsilon_1}$$

$$-\frac{v_{12}}{E_{11}} = \frac{1}{E_{12}}$$

Equation 3-40

This is confirmed by Bridgens *et al.* (2004).

And to convert the derivatives between unit cell and fabric or global values it is necessary to implement the following (Equation 3-41):

$$F_{1,2} = P_{1,2} \times L_{2,1} \times 2$$

$$E_{11}^{unit\ cell} = E_{11}^{global} \times L_2 \times 2$$

$$E_{12}^{unit\ cell} = E_{12}^{global} \times L_2 \times 2$$

$$E_{22}^{unit\ cell} = E_{22}^{global} \times L_1 \times 2$$

$$E_{21}^{unit\ cell} = E_{21}^{global} \times L_1 \times 2$$

Equation 3-41

Using these definitions it is now possible to allow input in terms of Poisson's ratios and Young's moduli for a whole fabric rather than only a unit cell.

3.4.3. Full Sawtooth

The full sawtooth considers all the variables identified by Bridgens (2005); (Bridgens and Gosling, 2008) as governing the behaviour of the fabric. This will be shown to allow the design of a fabric for specific properties, including shear behaviour under biaxial loading, where additional components are added (§3.4.3.3). Other deformation mechanisms have been identified but the sawtooth model adequately predicts fabric biaxial stiffness without specific inclusion of these. Those identified by other references include:

- Yarn bending (Tan and Barnes, 1984)
- Changes in filament geometry (Tan and Barnes, 1984)
- Friction between yarns (although this is considered separately in 3.4.3.4) (Pargana *et al.*, 2007)

3.4.3.1. Definition of the full sawtooth model

The primary deformation mechanisms that allow a fabric to be analysed are listed:

- Yarn extension – the yarns are considered to follow a linear elastic stress strain relationship (Equation 3-10 and Equation 3-13).

3. Predictive model

- Yarn cross-section deformation – the yarn radii can vary (Equation 3-14 to Equation 3-16).
- Yarn friction – the friction between the yarns is considered to resist shear deformation when the shear model is developed (Equation 3-74).
- Coating – Initially the coating was represented by two springs which resist biaxial loads. Following this an isoparametric element is used to represent both biaxial and shear loading (Figure 3-9). The isoparametric element will also allow for the use of non-orthogonal yarns in future work.

Considering all of these response mechanisms within a single model will allow for the design of a fabric through the use of the equations defined herein.

3.4.3.2. Equations defining the response of the full sawtooth

This section establishes the process that was used to produce E_{11} , E_{22} , ν_{12} and ν_{21} . The coating is no longer represented by ‘spring’ coating equations used by Bridgens (2005). These are replaced by a method utilising the Poisson’s ratios of the coating within a finite element.

$$F_{1,2} = \frac{(F_{2,1} - F_{k2,1}) \left((r'_{1,2} + r'_{2,1}) - L_{1,2}(1 + \varepsilon_{1,2}) \tan \theta'_{1,2} \right)}{L_{2,1}(1 + \varepsilon_{2,1}) \tan \theta'_{1,2}} + F_{k1,2}$$

Equation 3-42

The equation defining the force in terms of the unit cell properties is produced in the same fashion as for the simple sawtooth (§3.4.2.2) and combines the equations defining the full sawtooth response (§3.4) (Equation 3-6, Equation 3-7, Equation 3-9 and Equation 3-10).

Following the method set out earlier (§3.4.2.2) it can be shown that the necessary derivatives of $F_{1,2}$ are given below (Equation 3-43 and Equation 3-44):

$$\begin{aligned} \frac{dF_{1,2}}{d\varepsilon_{1,2}} = & \frac{\partial F_{1,2}}{\partial \varepsilon_{1,2}} + \frac{\partial F_{1,2}}{\partial \theta'_{1,2}} \cdot \frac{\partial \theta'_{1,2}}{\partial \varepsilon_{1,2}} + \frac{\partial F_{1,2}}{\partial r'_{1,2}} \cdot \frac{\partial r'_{1,2}}{\partial \varepsilon_{1,2}} + \frac{\partial F_{1,2}}{\partial r'_{2,1}} \cdot \frac{\partial r'_{2,1}}{\partial \varepsilon_{1,2}} + \frac{\partial F_{1,2}}{\partial \varepsilon_{2,1}} \cdot \frac{\partial \varepsilon_{2,1}}{\partial \varepsilon_{1,2}} + \frac{\partial F_{1,2}}{\partial F_{k1,2}} \\ & \cdot \frac{\partial F_{k1,2}}{\partial \varepsilon_{1,2}} + \frac{\partial F_{1,2}}{\partial F_{k2,1}} \cdot \frac{\partial F_{k2,1}}{\partial \varepsilon_{1,2}} \end{aligned}$$

Equation 3-43

3. Predictive model

$$\begin{aligned} \frac{dF_{1,2}}{d\varepsilon_{2,1}} = & \frac{\partial F_{1,2}}{\partial \varepsilon_{2,1}} + \frac{\partial F_{1,2}}{\partial \theta'_{1,2}} \cdot \frac{\partial \theta'_{1,2}}{\partial \varepsilon_{2,1}} + \frac{\partial F_{1,2}}{\partial r'_{1,2}} \cdot \frac{\partial r'_{1,2}}{\partial \varepsilon_{2,1}} + \frac{\partial F_{1,2}}{\partial r'_{2,1}} \cdot \frac{\partial r'_{2,1}}{\partial \varepsilon_{2,1}} + \frac{\partial F_{1,2}}{\partial \varepsilon_{1,2}} \cdot \frac{\partial \varepsilon_{1,2}}{\partial \varepsilon_{2,1}} + \frac{\partial F_{1,2}}{\partial F_{k1,2}} \\ & \cdot \frac{\partial F_{k1,2}}{\partial \varepsilon_{2,1}} + \frac{\partial F_{1,2}}{\partial F_{k2,1}} \cdot \frac{\partial F_{k2,1}}{\partial \varepsilon_{2,1}} \end{aligned}$$

Equation 3-44

The equations for the derivatives can be used to produce E_{11} , E_{22} , ν_{12} and ν_{21} in this new more complex case as per the method employed in the simple sawtooth (Equation 3-41).

Therefore, as was demonstrated for the simple sawtooth, to define E_{11} we must first define all the partial derivatives detailed above (Equation 3-43 and Equation 3-44). The first partial derivatives with respect to the load and strain can be calculated as follows (Equation 3-45 and Equation 3-46):

$$\frac{\partial F_1}{\partial \varepsilon_1} = - \frac{L_1(F_2 - F_{k2})}{L_2(\varepsilon_2 + 1)} \quad \text{Equation 3-45}$$

$$\frac{\partial F_1}{\partial \varepsilon_2} = - \frac{(F_2 - F_{k2})(r'_1 + r'_2 - L_1(\varepsilon_1 + 1) \tan \theta'_1)}{L_2(\varepsilon_2 + 1)^2 \tan \theta'_1} \quad \text{Equation 3-46}$$

Further partial derivatives relating to the load can also be calculated:

$$\begin{aligned} \frac{\partial F_1}{\partial \theta'_1} = & - \frac{(F_2 - F_{k2})(\tan^2 \theta'_1 + 1)(r'_1 + r'_2 - L_1(\varepsilon_1 + 1) \tan \theta'_1)}{L_2(\varepsilon_2 + 1)^2 \tan^2 \theta'_1} \\ & - \frac{L_1(F_2 - F_{k2})(\tan^2 \theta'_1 + 1)(\varepsilon_1 + 1)}{L_2(\varepsilon_2 + 1) \tan \theta'_1} \end{aligned}$$

Equation 3-47

$$\frac{\partial F_1}{\partial r'_1} = \frac{\partial F_1}{\partial r'_2} = \frac{(F_2 - F_{k2})}{L_2(\varepsilon_2 + 1) \tan \theta'_1} \quad \text{Equation 3-48}$$

$$\frac{\partial F_1}{\partial F_{k1}} = 1 \quad \text{Equation 3-49}$$

$$\frac{\partial F_1}{\partial F_{k2}} = - \frac{r'_1 + r'_2 - L_1(\varepsilon_1 + 1) \tan \theta'_1}{L_2(\varepsilon_2 + 1) \tan \theta'_1} \quad \text{Equation 3-50}$$

The coating is no longer represented with springs, and is instead represented by the isoparametric element to define the coating response, the biaxial extension of which

3. Predictive model

includes the coating's Poisson's ration (Equation 3-51). The Isoparametric element is connected to the sawtooth model at the midpoint nodes of the element (§3.4.3.3):

$$F_{k1,2} = 2 \cdot L_{2,1} \left(\frac{E_k}{1 - \nu_k^2} \right) (\varepsilon_{1,2} + \nu_k \varepsilon_{2,1}) (1 + \varepsilon_{2,1}) \quad \text{Equation 3-51}$$

The derivatives of which then follow:

$$\begin{aligned} \frac{\partial F_{k1,2}}{\partial \varepsilon_{1,2}} &= \frac{\delta F_{k1,2}}{\delta \varepsilon_{1,2}} + \frac{\delta F_{k1,2}}{\delta \varepsilon_{2,1}} \frac{\delta \varepsilon_{2,1}}{\delta \varepsilon_{1,2}} \\ &= \frac{2E_k L_{2,1}}{\nu_k^2 - 1} \left[-\frac{\delta \varepsilon_{2,1}}{\delta \varepsilon_{1,2}} ((\varepsilon_{1,2} + \nu_k \varepsilon_{2,1}) + \nu_k (\varepsilon_{2,1} + 1)) - (\varepsilon_{2,1} + 1) \right] \end{aligned}$$

Equation 3-52

$$\begin{aligned} \frac{\partial F_{k1,2}}{\partial \varepsilon_{2,1}} &= \frac{\delta F_{k1,2}}{\delta \varepsilon_{2,1}} + \frac{\delta F_{k1,2}}{\delta \varepsilon_{1,2}} \frac{\delta \varepsilon_{1,2}}{\delta \varepsilon_{2,1}} \\ &= \frac{2E_k L_{2,1}}{\nu_k^2 - 1} \left[-(\varepsilon_{1,2} + \nu_k \varepsilon_{2,1}) - \frac{\delta \varepsilon_{1,2}}{\delta \varepsilon_{2,1}} (\varepsilon_{2,1} + 1) - \nu_k (\varepsilon_{2,1} + 1) \right] \end{aligned}$$

Equation 3-53

Similarly the yarn radius is considered (Equation 3-54):

$$r'_{1,2} = \frac{r_{1,2}}{(1 + \varepsilon_{2,1})} \quad \text{Equation 3-54}$$

$$\frac{\partial r'_{1,2}}{\partial \varepsilon_{1,2}} = \frac{\delta r'_{1,2}}{\delta \varepsilon_{1,2}} + \frac{\delta r'_{1,2}}{\delta \varepsilon_{2,1}} \frac{\delta \varepsilon_{2,1}}{\delta \varepsilon_{1,2}} = -\frac{\delta \varepsilon_{2,1}}{\delta \varepsilon_{1,2}} \frac{r_{1,2}}{(\varepsilon_{2,1} + 1)^2} \quad \text{Equation 3-55}$$

$$\frac{\partial r'_{1,2}}{\partial \varepsilon_{2,1}} = -\frac{r_{1,2}}{(\varepsilon_{2,1} + 1)^2} \quad \text{Equation 3-56}$$

And also the out of plane yarn angles:

$$\theta'_{2,1} = \cos^{-1} \left((1 + \varepsilon_{2,1}) \cos \theta_{2,1} - \left(\frac{(F_{2,1} - F_{k2,1})}{2E_{2,1} L_{1,2} (1 + \varepsilon_{1,2})} \right) \right) \quad \text{Equation 3-57}$$

$$\begin{aligned}
\frac{\partial \theta'_{2,1}}{\partial \varepsilon_{1,2}} &= \frac{\delta \theta'_{2,1}}{\delta \varepsilon_{1,2}} + \frac{\delta \theta'_{2,1}}{\delta \varepsilon_{2,1}} \frac{\delta \varepsilon_{2,1}}{\delta \varepsilon_{1,2}} + \frac{\delta \theta'_{2,1}}{\delta F_{k2,1}} \frac{\delta F_{k2,1}}{\delta \varepsilon_{1,2}} \\
&= \frac{1}{\sqrt{1 - \left(\cos \theta_{2,1} (\varepsilon_{2,1} + 1) - \frac{F_{2,1} - F_{k2,1}}{2E_{2,1}L_{1,2}(1 + \varepsilon_{1,2})} \right)^2}} \\
&\quad \cdot \left[\frac{\frac{2E_k L_{1,2}}{v_k^2 - 1} \left((\varepsilon_{2,1} + v_k \varepsilon_{1,2}) + \frac{\delta \varepsilon_{2,1}}{\delta \varepsilon_{1,2}} (1 + \varepsilon_{1,2}) + v_k (1 + \varepsilon_{1,2}) \right)}{2E_{2,1}L_{1,2}(1 + \varepsilon_{1,2})} \right. \\
&\quad \left. - \frac{(F_{2,1} - F_{k2,1})}{2E_{2,1}L_{1,2}(1 + \varepsilon_{1,2})^2} - \frac{\delta \varepsilon_{2,1}}{\delta \varepsilon_{1,2}} \cos \theta_{2,1} \right]
\end{aligned}$$

Equation 3-58

$$\begin{aligned}
\frac{\partial \theta'_{2,1}}{\partial \varepsilon_{2,1}} &= \frac{\delta \theta'_{2,1}}{\delta \varepsilon_{2,1}} + \frac{\delta \theta'_{2,1}}{\delta \varepsilon_{1,2}} \frac{\delta \varepsilon_{1,2}}{\delta \varepsilon_{2,1}} + \frac{\delta \theta'_{2,1}}{\delta F_{k2,1}} \frac{\delta F_{k2,1}}{\delta \varepsilon_{2,1}} \\
&= \frac{1}{\sqrt{1 - \left(\cos \theta_{2,1} (\varepsilon_{2,1} + 1) - \frac{F_{2,1} - F_{k2,1}}{2E_{2,1}L_{1,2}(1 + \varepsilon_{1,2})} \right)^2}} \\
&\quad \cdot \left[\frac{\frac{2E_k L_{1,2}}{v_k^2 - 1} \left(\frac{\delta \varepsilon_{1,2}}{\delta \varepsilon_{2,1}} \left((\varepsilon_{2,1} + v_k \varepsilon_{1,2}) + v_k (1 + \varepsilon_{1,2}) \right) + (1 + \varepsilon_{1,2}) \right)}{2E_{2,1}L_{1,2}(1 + \varepsilon_{1,2})} \right. \\
&\quad \left. - \cos \theta_{2,1} - \frac{\frac{\delta \varepsilon_{1,2}}{\delta \varepsilon_{2,1}} (F_{2,1} - F_{k2,1})}{2E_{2,1}L_{1,2}(1 + \varepsilon_{1,2})^2} \right]
\end{aligned}$$

Equation 3-59

$$\theta'_{1,2} = \tan^{-1} \left(\frac{(r'_1 + r'_2) - L_{2,1}(1 + \varepsilon_{2,1}) \tan \theta'_{2,1}}{L_{1,2}(1 + \varepsilon_{1,2})} \right)$$

Equation 3-60

$$\begin{aligned}
\frac{\partial \theta'_{1,2}}{\partial \varepsilon_{1,2}} &= \frac{\delta \theta'_{1,2}}{\delta \varepsilon_{1,2}} + \frac{\delta \theta'_{1,2}}{\delta r'_{1,2}} \frac{\delta r'_{1,2}}{\delta \varepsilon_{1,2}} + \frac{\delta \theta'_{1,2}}{\delta r'_{2,1}} \frac{\delta r'_{2,1}}{\delta \varepsilon_{1,2}} + \frac{\delta \theta'_{1,2}}{\delta \varepsilon_{2,1}} \frac{\delta \varepsilon_{2,1}}{\delta \varepsilon_{1,2}} + \frac{\delta \theta'_{1,2}}{\delta \theta'_{2,1}} \frac{\delta \theta'_{2,1}}{\delta \varepsilon_{1,2}} \\
&= \left(L_{1,2} \left(\frac{\left(r'_{1,2} + r'_{2,1} - L_2 \tan \theta'_{2,1} (1 + \varepsilon_{2,1}) \right)^2}{L_{1,2}^2 (1 + \varepsilon_{1,2})^2} + 1 \right) (1 + \varepsilon_{1,2}) \right)^{-1} \\
&\left\{ \left(\frac{L_{2,1} (\tan^2 \theta'_{2,1} + 1) (\varepsilon_{2,1} + 1)}{\sqrt{1 - \left(\cos \theta_{2,1} (1 + \varepsilon_{2,1}) - \frac{(F_{2,1} - F_{k2,1})}{2E_{2,1}L_{1,2}(1 + \varepsilon_{1,2})} \right)^2}} \left[\frac{\delta \varepsilon_{2,1}}{\delta \varepsilon_{1,2}} \cos \theta_{2,1} + \frac{(F_{2,1} - F_{k2,1})}{2E_{2,1}L_{1,2}(1 + \varepsilon_{1,2})^2} \right. \right. \right. \\
&\quad \left. \left. \left. - \frac{\frac{2E_k L_{1,2}}{v_k^2 - 1} \left((\varepsilon_{2,1} + \varepsilon_{1,2} v_k) + \frac{\delta \varepsilon_{2,1}}{\delta \varepsilon_{1,2}} (1 + \varepsilon_{1,2}) + v_k (1 + \varepsilon_{1,2}) \right) \right]}{2E_{2,1}L_{1,2}(1 + \varepsilon_{1,2})} \right] \right) - \frac{(r'_{1,2} + r'_{2,1} - L_2 \tan \theta'_{2,1} (1 + \varepsilon_{2,1}))}{(1 + \varepsilon_{1,2})} - L_{2,1} \frac{\delta \varepsilon_{2,1}}{\delta \varepsilon_{1,2}} \tan \theta'_{2,1} \right. \\
&\quad \left. - \frac{\frac{\delta \varepsilon_{2,1}}{\delta \varepsilon_{1,2}} r_{1,2}}{(1 + \varepsilon_{2,1})^2} - \frac{r_{2,1}}{(1 + \varepsilon_{1,2})} \right\}
\end{aligned}$$

Equation 3-61

$$\begin{aligned}
\frac{\partial \theta'_{1,2}}{\partial \varepsilon_{2,1}} &= \frac{\delta \theta'_{1,2}}{\delta \varepsilon_{2,1}} + \frac{\delta \theta'_{1,2}}{\delta \varepsilon_{1,2}} \frac{\delta \varepsilon_{1,2}}{\delta \varepsilon_{2,1}} + \frac{\delta \theta'_{1,2}}{\delta r'_{1,2}} \frac{\delta r'_{1,2}}{\delta \varepsilon_{2,1}} + \frac{\delta \theta'_{1,2}}{\delta r'_{2,1}} \frac{\delta r'_{2,1}}{\delta \varepsilon_{2,1}} + \frac{\delta \theta'_{1,2}}{\delta \theta'_{2,1}} \frac{\delta \theta'_{2,1}}{\delta \varepsilon_{2,1}} \\
&= \left(L_{1,2} \left(\frac{(r'_{1,2} + r'_{1,2} - \tan \theta'_{2,1} (\varepsilon_{2,1} + 1))^2}{L_{1,2}^2 (1 + \varepsilon_{1,2})^2} + 1 \right) (1 + \varepsilon_{1,2}) \right)^{-1} \\
&\quad \cdot \left\{ \frac{L_{2,1} (\tan^2 \theta'_{2,1} + 1) (\varepsilon_{2,1} + 1)}{\sqrt{1 - \left(\cos \theta_{2,1} (1 + \varepsilon_{2,1}) - \frac{(F_{2,1} - F_{k2,1})}{2E_{2,1} L_{1,2} (1 + \varepsilon_{1,2})} \right)^2}} \right. \\
&\quad \cdot \left(\cos \theta_{2,1} - \frac{\frac{2E_k L_{1,2}}{v_k^2 - 1} \left(\frac{\delta \varepsilon_{1,2}}{\delta \varepsilon_{2,1}} ((\varepsilon_{2,1} + \varepsilon_{1,2} v_k) + v_k (1 + \varepsilon_{1,2})) + (1 + \varepsilon_{1,2}) \right)}{2E_{2,1} L_{1,2} (1 + \varepsilon_{1,2})} + \frac{\frac{\delta \varepsilon_{1,2}}{\delta \varepsilon_{2,1}} (F_{2,1} - F_{k2,1})}{2E_{2,1} L_{1,2} (1 + \varepsilon_{1,2})^2} \right) \left. - \frac{r_{1,2}}{(1 + \varepsilon_{2,1})^2} \right. \\
&\quad \left. - \frac{\frac{\delta \varepsilon_{1,2}}{\delta \varepsilon_{2,1}} r_{2,1}}{(1 + \varepsilon_{1,2})^2} - \frac{\frac{\delta \varepsilon_{1,2}}{\delta \varepsilon_{2,1}} (r'_{1,2} + r'_{1,2} - \tan \theta'_{2,1} (\varepsilon_{2,1} + 1))}{(1 + \varepsilon_{1,2})} - L_{2,1} \tan \theta'_{2,1} \right\}
\end{aligned}$$

Equation 3-62

Using two different formulae for the out of plane angle ensures that the calculation of the derivatives is not looped as happens below, but irreconcilably, with the calculation of the derivatives of the strains (Equation 3-57 and Equation 3-60).

After extensive work it was found that $\delta\varepsilon_{1,2}/\delta\varepsilon_{2,1}$ could not be defined analytically. A circular problem presents when the calculation of the analytical derivative is attempted (Figure 3-7). To calculate the derivative other derivatives must first be known, the calculation of which requires the partial derivative of the strains (Equation 3-63).

$$\frac{dr'_2}{d\varepsilon_1}, \frac{d\theta'_1}{d\varepsilon_1}, \frac{dr'_1}{d\varepsilon_1}, \frac{d\theta'_2}{d\varepsilon_1} \quad \text{Equation 3-63}$$

Given that these derivatives are themselves not independent they must be calculated from other derivatives, the aim of which is to find a solution where independent variables form the basis of the solution. This must be defined in terms of the dependant variables chosen to define the model. Therefore it is shown that for the most part only dependant variables exist within the formulation which cannot be refined down to the few independent calculations.

As part of an effort to find an entirely analytical solution the original equations were repeatedly redefined and an effort was made to express the equilibrium equations differently. However, where the equilibrium equations are defined in some form, necessary for the definition of the sawtooth model, the interdependencies persists, and cannot be resolved to an entirely analytical solution.

The problem of dependency only persists where yarns are considered extensible though as this is intrinsic to the nature of fabrics, i.e. that the yarns extend under load, and that this is the predominant deformation mechanism at higher loads, this mechanism cannot be ignored for the full fabric design case. It is possible that a complete analytical derivative might be formed for the initial fabric deformation, where yarn extension is considered to be minimal, and thus might be ignored, but this would ignore an important portion of the response, and thus be inappropriate for use in a design methodology.

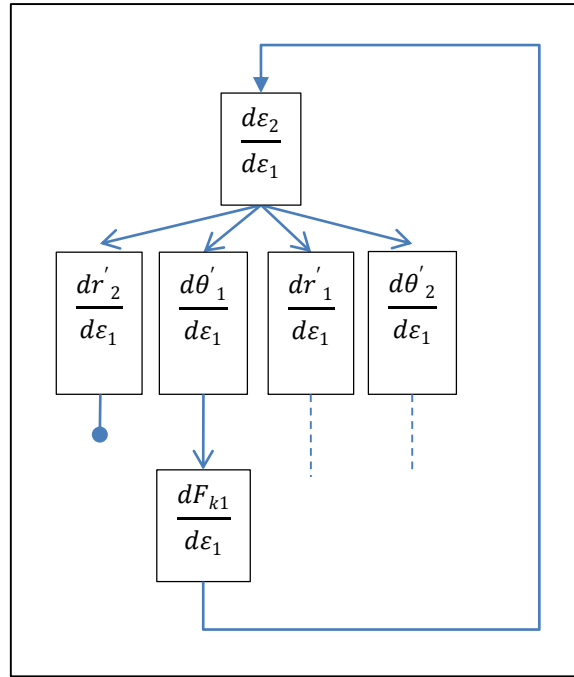


Figure 3-7: Flow chart demonstrating how the derivative $\frac{d\epsilon_2}{d\epsilon_1}$ cannot be defined

$\frac{\delta\epsilon_1}{\delta\epsilon_2}$ can be defined in terms of $\frac{\delta\epsilon_2}{\delta\epsilon_1}$ and reciprocally, but neither can be defined without the requirement for another derivative to be calculated. The equations defining the response are circularly interconnected, at some point a break has to be made in the circular interdependency, and this was made at the partial derivative $\frac{\delta\epsilon_{2,1}}{\delta\epsilon_{1,2}}$. This is then calculated iteratively, and therefore referred to as $\frac{\Delta\epsilon_{1,2}}{\Delta\epsilon_{2,1}}$, using the sawtooth model and a central finite difference calculation with a variable value of the force applied (Equation 3-64).

Where: $F_{1,2} = 0$

$$increment_{1,2} = 0.001$$

Where: $F_{1,2} \neq 0$

$$increment_{1,2} = F_{1,2}/1000 \text{ or } 0.1\% \text{ of } F_{1,2}$$

Equation 3-64

Therefore $\frac{dF_{1,2}}{d\varepsilon_{1,2}}$ can be calculated (Equation 3-65).

$$\begin{aligned} \frac{dF_1}{d\varepsilon_1} = & \left(\frac{(J)(\tan(\cos^{-1} B)^2 + 1)D}{L_2 \tan(\cos^{-1} B)^2 (\varepsilon_2 + 1)} + \frac{L_1(J)(\tan(\cos^{-1} B)^2 + 1)(\varepsilon_1 + 1)}{L_2 \tan(\cos^{-1} B) (\varepsilon_2 + 1)} \right) \\ & \cdot \left(\frac{1}{L_1 \left(\frac{E^2}{L_1^2 (\varepsilon_1 + 1)^2} + 1 \right)} \left(\frac{r_2}{(\varepsilon_1 + 1)^3} + \frac{E}{(\varepsilon_1 + 1)^2} + \frac{L_2 \frac{\Delta \varepsilon_2}{\Delta \varepsilon_1} \tan(\cos^{-1} C)}{(\varepsilon_1 + 1)} + \frac{\frac{\Delta \varepsilon_2}{\Delta \varepsilon_1} r_1}{(\varepsilon_1 + 1)(\varepsilon_2 + 1)^2} \right. \right. \\ & \left. \left. - \frac{L_2 (\tan(\cos^{-1} C)^2 + 1)(\varepsilon_2 + 1) \left(\frac{\frac{\Delta \varepsilon_2}{\Delta \varepsilon_1} \cos(\theta_2)}{\sqrt{1 - (C)^2}} + \frac{J}{2E_2 L_1 \sqrt{1 - (C)^2} (\varepsilon_1 + 1)^2} - \frac{\frac{2E_k L_1 (\varepsilon_2 + \varepsilon_1 v_k)}{v_k^2 - 1} + \frac{2E_k L_1 \frac{\Delta \varepsilon_2}{\Delta \varepsilon_1} (\varepsilon_1 + 1)}{v_k^2 - 1} + \frac{2E_k L_1 v_k (\varepsilon_1 + 1)}{v_k^2 - 1}}{2E_2 L_1 \sqrt{1 - (C)^2} (\varepsilon_1 + 1)} \right)}{(\varepsilon_1 + 1)} \right) - \frac{\Delta \varepsilon_2}{\Delta \varepsilon_1} \right) \\ & \cdot \left(\frac{2E_k L_2 (\varepsilon_1 + \varepsilon_2 v_k)}{v_k^2 - 1} + \frac{2E_k L_2 v_k (\varepsilon_2 + 1)}{v_k^2 - 1} \right) - \frac{2E_k L_2 (\varepsilon_2 + 1)}{v_k^2 - 1} - \frac{L_1(J)}{L_2 (\varepsilon_2 + 1)} + \frac{\left(\frac{2E_k L_1 (\varepsilon_2 + \varepsilon_1 v_k)}{v_k^2 - 1} + \frac{2E_k L_1 \frac{\Delta \varepsilon_2}{\Delta \varepsilon_1} (\varepsilon_1 + 1)}{v_k^2 - 1} + \frac{2E_k L_1 v_k (\varepsilon_1 + 1)}{v_k^2 - 1} \right) D}{L_2 \tan(\cos^{-1} B) (\varepsilon_2 + 1)} \\ & - \frac{r_2(J)}{L_2 \tan(\cos^{-1} B) (\varepsilon_1 + 1)^2 (\varepsilon_2 + 1)} - \frac{\frac{\Delta \varepsilon_2}{\Delta \varepsilon_1} r_1(J)}{L_2 \tan(\cos^{-1} B) (\varepsilon_2 + 1)^3} - \frac{\frac{\Delta \varepsilon_2}{\Delta \varepsilon_1} (J)(D)}{L_2 \tan(\cos^{-1} B) (\varepsilon_2 + 1)^2} \end{aligned}$$

Where:

$$\begin{aligned}
 A &= \left(\frac{r_1}{1 + \varepsilon_2} \right) + \left(\frac{r_2}{1 + \varepsilon_1} \right) \\
 B &= \left((1 + \varepsilon_1) \cos(\theta_1) - \left(\frac{F_1 - \left(\left(\frac{E_k}{1 - v_k^2} \right) (\varepsilon_1 + v_k \varepsilon_2) 2L_2 (1 + \varepsilon_2) \right)}{2E_1 L_2 (1 + \varepsilon_2)} \right) \right) \\
 C &= \left((1 + \varepsilon_2) \cos(\theta_2) - \left(\frac{F_2 - \left(\left(\frac{E_k}{1 - v_k^2} \right) (\varepsilon_2 + v_k \varepsilon_1) 2L_1 (1 + \varepsilon_1) \right)}{2E_2 L_1 (1 + \varepsilon_1)} \right) \right) \\
 D &= \left(A - L_1 \tan \left(\cos^{-1} \left((1 + \varepsilon_1) \cos(\theta_1) - \left(\frac{F_1 - \left(\left(\frac{E_k}{1 - v_k^2} \right) (\varepsilon_1 + v_k \varepsilon_2) 2L_2 (1 + \varepsilon_2) \right)}{2E_1 L_2 (1 + \varepsilon_2)} \right) \right) \right) (\varepsilon_1 + 1) \right) \\
 E &= \left(A - L_2 \tan \left(\cos^{-1} \left((1 + \varepsilon_2) \cos(\theta_2) - \left(\frac{F_2 - \left(\left(\frac{E_k}{1 - v_k^2} \right) (\varepsilon_2 + v_k \varepsilon_1) 2L_1 (1 + \varepsilon_1) \right)}{2E_2 L_1 (1 + \varepsilon_1)} \right) \right) \right) (\varepsilon_2 + 1) \right) \\
 H &= F_1 - \left(\left(\frac{E_k}{1 - v_k^2} \right) (\varepsilon_1 + v_k \varepsilon_2) 2L_2 (1 + \varepsilon_2) \right) \\
 J &= F_2 - \left(\left(\frac{E_k}{1 - v_k^2} \right) (\varepsilon_2 + v_k \varepsilon_1) 2L_1 (1 + \varepsilon_1) \right)
 \end{aligned}$$

Equation 3-65

At this point all necessary derivatives have been derived and can be used to design a fabric's geometry for the tensile stiffnesses and Poisson's ratios with respect to biaxial load (§3.5).

3.4.3.3. Isoparametric formulation for coating

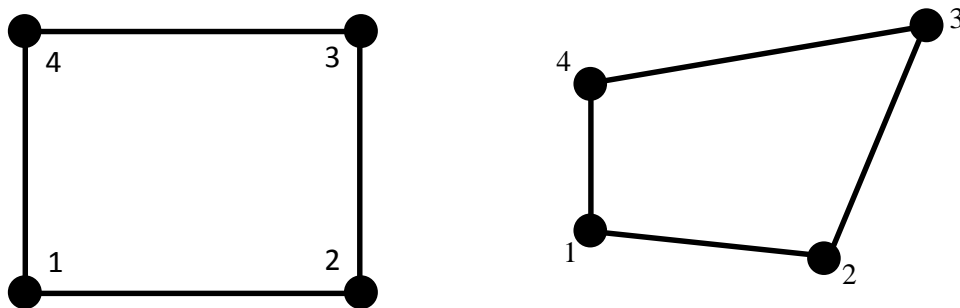
With the derivatives calculated it is possible to optimise a fabric's geometry for the response to biaxial load although not for response to shear loading. As has been mentioned the 'springs' that were used to represent the coating stiffness in the model used by Bridgens (2005) have been replaced by a finite element this is similar to the method employed by Kato *et al.* (1999). The material properties used in the element were taken from the literature review (§2.2.3). The practical effect of this thus far has been to make a slight alteration to the calculation of the coating force, but this is to be used to demonstrate how a fabric's response to shear can also be designed.

Two types of finite elements were considered to replace the springs representing the coating deformation in earlier models. The simpler 'Plane Rectangular Bilinear Element' and the more complex 'Plane Bilinear Isoparametric Element' (Figure 3-8). The

3. Predictive model

advantage of the isoparametric formulation lies in its ability to represent non-rectangular geometry, which may be useful if fabrics with fibres that are non-perpendicular are to be considered in future work, or to have curved sides (Cook *et al.*, 1989). Whereas the 'Plane Rectangular Bilinear Element' will restrict any future iterations of this work to standard rectangular geometries.

As such the Isoparametric formulation will be used to ensure the model can be used with non-perpendicular fabric geometries. The element replaces the springs in the structure (Figure 3-9).



Plane Rectangular Bilinear Element
(Cook *et al.*, 1989)

Plane Bilinear Isoparametric Element

Figure 3-8: Plane Rectangular Bilinear Element and Plane Bilinear Isoparametric Element

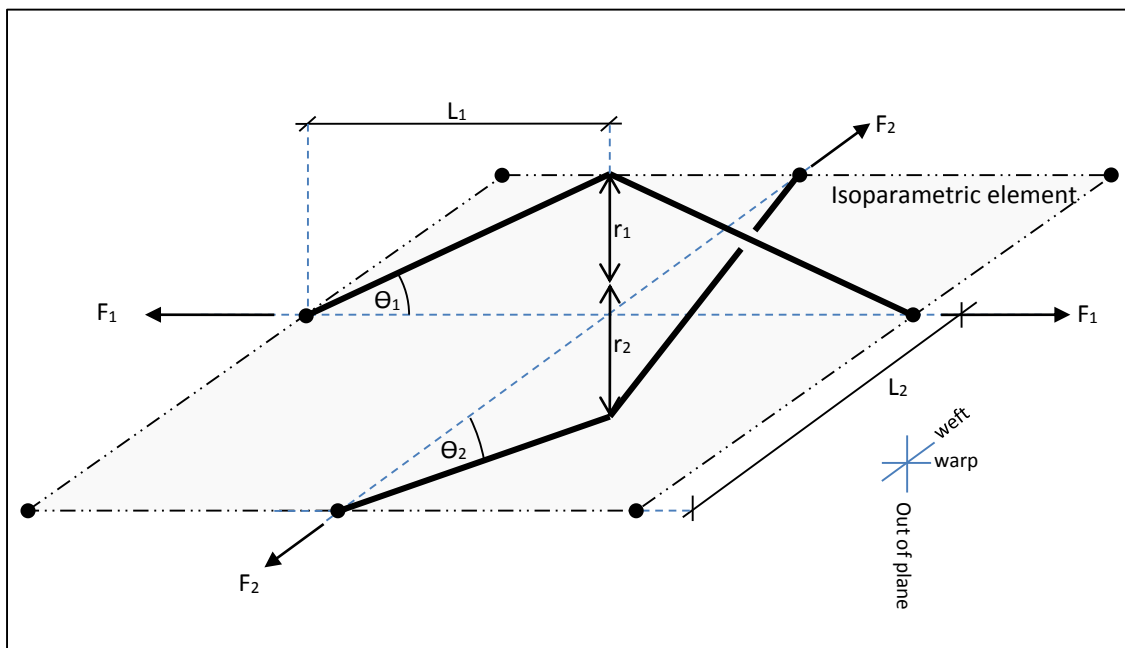
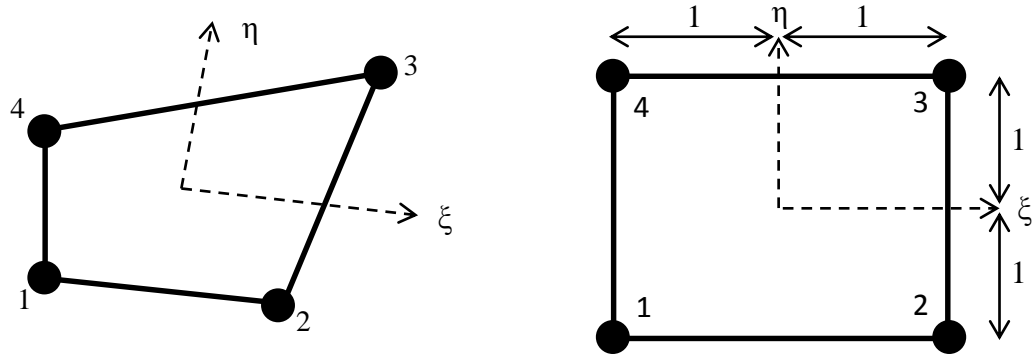


Figure 3-9: Fundamentals of the full sawtooth model with an Isoparametric Element representing the coating

The construction of the Plane Bilinear Isoparametric formulation that will be used to represent the coating is shown below:



Plane Isoparametric Element in xy space

Plane Isoparametric Element in $\xi\eta$ space

Figure 3-10: Plane Isoparametric Element in xy and $\xi\eta$ space modified from Cook *et al.* (1989)

For the Plane Stress Isoparametric Element there are two fields, the displacements u and v (Equation 3-66).

$$u = \sum N_i u_i, \quad v = \sum N_i v_i$$

*Displacements u and v are parallel to x and y **NOT** ξ and η

Equation 3-66

The Shape functions are then calculated and their derivatives with relation to η and ξ derived (Equation 3-67).

An alternate method of writing the derivatives is used below, such that the derivative of N_1 with respect to ξ is written as $N_{1,\xi}$ (Equation 3-67) (Cook *et al.*, 2002).

3. Predictive model

$$N_1 = \frac{(1-\xi)(1-\eta)}{4}, N_2 = \frac{(1+\xi)(1-\eta)}{4}, N_3 = \frac{(1+\xi)(1+\eta)}{4}, N_4 = \frac{(1-\xi)(1+\eta)}{4}$$

$$N_{1,\xi} = \frac{-1+\eta}{4}, \quad N_{2,\xi} = \frac{1-\eta}{4}, \quad N_{3,\xi} = \frac{1+\eta}{4}, \quad N_{4,\xi} = \frac{-1-\eta}{4}$$

$$N_{1,\eta} = \frac{-1+\xi}{4}, \quad N_{2,\eta} = \frac{-1-\xi}{4}, \quad N_{3,\eta} = \frac{1+\xi}{4}, \quad N_{4,\eta} = \frac{1-\xi}{4}$$

Equation 3-67

Once the shape functions have been calculated the strain-displacement relationship can be derived, with the addition of the displacements (Equation 3-68 and Equation 3-69).

$$\{\boldsymbol{\varepsilon}\} = \begin{Bmatrix} \varepsilon_x \\ \varepsilon_y \\ \gamma_{xy} \end{Bmatrix} = \begin{bmatrix} 1 & 0 & 0 & 1 \\ 0 & 0 & 0 & 1 \\ 0 & 1 & 1 & 0 \end{bmatrix} \begin{Bmatrix} u_{,x} \\ u_{,y} \\ v_{,x} \\ v_{,y} \end{Bmatrix}$$

$$\begin{Bmatrix} u_{,x} \\ u_{,y} \\ v_{,x} \\ v_{,y} \end{Bmatrix} = \begin{bmatrix} \Gamma_{11} & \Gamma_{12} & 0 & 0 \\ \Gamma_{21} & \Gamma_{22} & 0 & 0 \\ 0 & 0 & \Gamma_{11} & \Gamma_{12} \\ 0 & 0 & \Gamma_{21} & \Gamma_{22} \end{bmatrix} \begin{Bmatrix} u_{,\xi} \\ u_{,\eta} \\ v_{,\xi} \\ v_{,\eta} \end{Bmatrix}$$

$$\begin{Bmatrix} u_{,\xi} \\ u_{,\eta} \\ v_{,\xi} \\ v_{,\eta} \end{Bmatrix} = \begin{bmatrix} N_{1,\xi} & 0 & N_{2,\xi} & 0 & N_{3,\xi} & 0 & N_{4,\xi} & 0 \\ N_{1,\eta} & 0 & N_{2,\eta} & 0 & N_{3,\eta} & 0 & N_{4,\eta} & 0 \\ 0 & N_{1,\xi} & 0 & N_{2,\xi} & 0 & N_{3,\xi} & 0 & N_{4,\xi} \\ 0 & N_{1,\eta} & 0 & N_{2,\eta} & 0 & N_{3,\eta} & 0 & N_{4,\eta} \end{bmatrix} \{\mathbf{d}\}$$

Equation 3-68

$$[\Gamma] = \begin{bmatrix} \Gamma_{11} & \Gamma_{12} \\ \Gamma_{21} & \Gamma_{22} \end{bmatrix} = [J]^{-1} = \frac{1}{J} \begin{bmatrix} J_{22} & -J_{12} \\ -J_{21} & J_{11} \end{bmatrix}$$

$$[J] = \begin{bmatrix} J_{11} & J_{12} \\ J_{21} & J_{22} \end{bmatrix} = \begin{bmatrix} x_{,\xi} & y_{,\xi} \\ x_{,\eta} & y_{,\eta} \end{bmatrix} = \begin{bmatrix} \sum N_{i,\xi} x_i & \sum N_{i,\xi} y_i \\ \sum N_{i,\eta} x_i & \sum N_{i,\eta} y_i \end{bmatrix}$$

Equation 3-69

$$[k] = \int \int [B]^T \cdot [E] \cdot [B] \cdot t \cdot dx \cdot dy = \int_{-1}^1 \int_{-1}^1 [B]^T \cdot [E] \cdot [B] \cdot t \cdot J \cdot d\xi \cdot d\eta$$

Where J is the determinant of [J], [k] is the element stiffness matrix, [B] is the strain displacement matrix, t is the element thickness, and [E] is the material properties

Equation 3-70

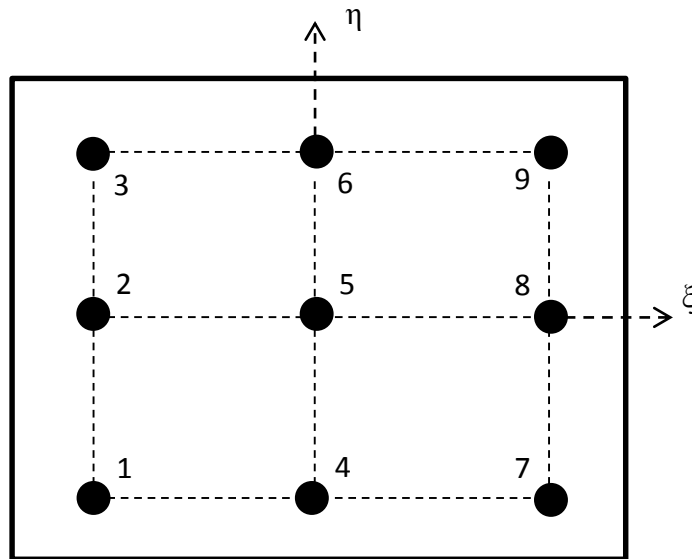
This is then integrated using nine point Gauss Quadrature (Equation 3-71 and Figure 3-11). As [k] is needed if the reactions, [r_e], are to be computed.

$$I \approx \frac{25}{81}(\vartheta_1 + \vartheta_3 + \vartheta_7 + \vartheta_9) + \frac{40}{81}(\vartheta_2 + \vartheta_4 + \vartheta_6 + \vartheta_8) + \frac{64}{81}\vartheta_5$$

(Cook *et al.*, 2002)

Where I is the integral, and ϑ_1 are the values at each node

Equation 3-71



Gauss point locations in a quadrilateral element using nine points
(order 3 rule)

Figure 3-11: Order three Gauss Point locations in a quadrilateral element: Reproduced from Cook *et al.* (1989)

The element is placed into the model (Figure 3-9), and the calculation of the shear stress 'τ' is achieved using [ε] and [E] (Equation 3-72).

$$[\boldsymbol{\varepsilon}] = [\boldsymbol{B}][\boldsymbol{d}]$$

$$[\boldsymbol{\sigma}] = [\boldsymbol{E}][\boldsymbol{\varepsilon}]$$

Equation 3-72

At this stage the shear stiffness of the fabric due to only the coatings deformation can be predicted and included in the design of a fabric. However, as shown by Liu *et al.* (2004) and other authors, the coating stiffness is not the only method by which fabrics respond to shear. Though the effect of the coating may be principal to the shear response (Testa and Yu, 1987) it has been deemed necessary to include other resistance mechanisms to ensure accuracy and allow for the design of the fabric's base cloth for shear. Therefore shear resistance between yarns will also be taken into account.

3.4.3.4. Shear force calculation due to friction between fibres

In addition to the coating response to in-plane shear a method for the calculation of the in-plane frictional forces between yarns, and its corresponding effect in resisting shear deformation was developed by Liu *et al.* (2004). This model considered how yarn lateral compaction and in-plane friction between yarns at cross-over can be used to calculate shear forces in an uncoated fabric, with equal warp and weft dimensions (Figure 3-12).

The model considers the in-plane moments produced by the resistances to shear deformation, and compares these to the in-plane shear forces that would produce a moment of equal magnitude to the resistance moment (Equation 3-73). The model developed by Liu *et al.* (2004) considers only a square fabric geometry. The method has been modified by Colman (2014) to include.

$$M_s = M_c + M_f$$

Equation 3-73

Where M_s is the total moment resisting shear force, M_c is the moment due to yarn compaction, M_f is the moment due to inter yarn friction

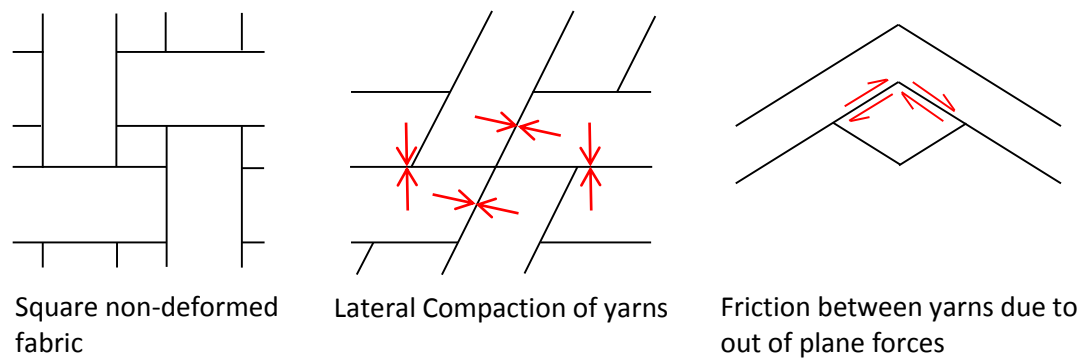


Figure 3-12: Equal geometry uncoated fabric, yarn lateral compaction, and yarn friction (Liu *et al.*, 2004)

However, as the fabrics to be considered are primarily coated fabrics we can surmise that it is unlikely that lateral compaction as considered by Liu *et al.* (2004) will be a principle resistance mechanism, once the coating is considered. For the purposes of this model the lateral compaction of yarns is considered to be either non-existent, as yarns are restrained by coating between them, or as having a minimal impact on shear stiffness. Therefore only friction between yarns at cross over will be considered in conjunction with the effect of the coating.

Liu *et al.* (2004) proposes formulae that can be used to calculate the moment due to friction between yarns on a unit cell of uncoated square fabric, however, as many fabrics to be considered will not have square geometry it is necessary to improve on these formulations. This has been achieved by Colman (2014), who considers a similar model to Liu *et al.* (2004), and refers to this methodology, but produces equations that can be used with any yarn geometry.

The yarn friction is considered over the area of the contact between the two yarns, and this is used to calculate the moment produced by the friction force. The area of interaction between the yarns is split into four areas (Figure 3-13). The effect of the friction in each of the areas is then considered, and its contribution to the moment produced by the friction is then calculated (Equation 3-74).

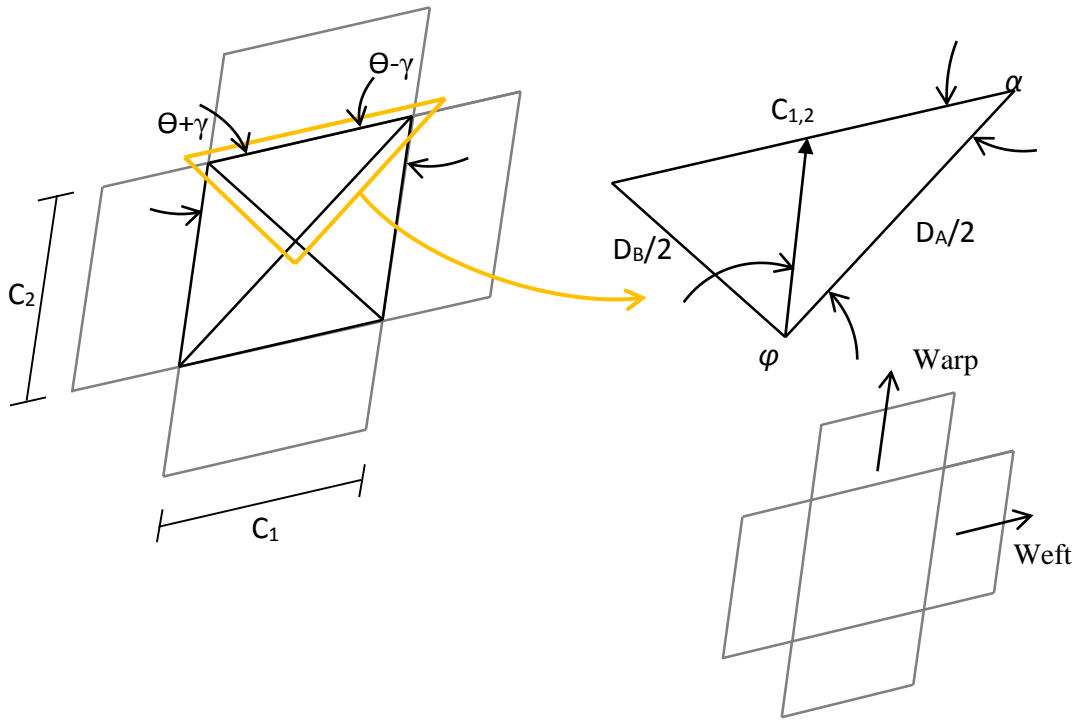


Figure 3-13: Moment due to inter yarn friction calculation (Colman, 2012)

$$\begin{aligned}
 M_F &= 2 \int_0^{\phi_A} \int_0^{\frac{D_A \sin(\alpha_A)}{2 \sin(\alpha_A + \phi)}} F_f R^2 dR d\phi + 2 \int_0^{\phi_B} \int_0^{\frac{D_A \sin(\alpha_B)}{2 \sin(\alpha_B + \phi)}} F_f R^2 dR d\phi \\
 &= 2 \int_0^{\phi_A} F_f \left[\frac{1}{3} R^3 \right]_0^{\frac{D_A \sin(\alpha_A)}{2 \sin(\alpha_A + \phi)}} d\phi + 2 \int_0^{\phi_B} F_f \left[\frac{1}{3} R^3 \right]_0^{\frac{D_A \sin(\alpha_B)}{2 \sin(\alpha_B + \phi)}} d\phi \\
 &= \frac{1}{12} F_f D_A^3 \sin^3(\alpha_A) \int_0^{\phi_A} \frac{d\phi}{\sin^3(\alpha_A + \phi)} + \frac{1}{12} F_f D_A^3 \sin^3(\alpha_B) \int_0^{\phi_B} \frac{d\phi}{\sin(\alpha_B + \phi)} \\
 \phi_{A,B} &= \cos^{-1} \left(\frac{D_A^2 + D_B^2 - 4c_{1,2}^2}{2D_A D_B} \right) \\
 \alpha_{A,B} &= \cos^{-1} \left(\frac{c_{1,2}^2 + D_A^2 - 2c_{2,1}^2}{2c_{1,2} D_A} \right) \\
 D_A &= \sqrt{c_1^2 + c_2^2 - 2c_1 c_2 \cos(\theta + \gamma)} \\
 D_B &= \sqrt{c_1^2 + c_2^2 - 2c_1 c_2 \cos(\theta - \gamma)}
 \end{aligned}$$

(Colman, 2014)

Once the moment due to friction has been calculated the shear force on the edge of the unit cell can also be calculated, and can then be used to calculate the shear stress over the entire unit cell.

3.4.3.5. *Shear force calculation*

The resisting moments have been calculated, but these moments must be related to shear stress and shear modulus. Shear stress is assumed to be equal across both sides of the unit cell which allows for the calculation of the shear forces, even given any variation of those forces on the unit cell. However, the moment due to the coating must first be calculated (Equation 3-75).

$$M_k = F_{sk2}L'_1 \cos \gamma + F_{sk1}L'_2 \cos \gamma$$

$$F_{sk2,1} = \tau_k 2L_{2,1}'$$

$$M_k = \tau_k 2L_2' L'_1 \cos \gamma + \tau_k 2L_1' L'_2 \cos \gamma$$

$$M_k = 4\tau_k L_2' L'_1 \cos \gamma$$

Equation 3-75

And the moment due to the imposed shear force must also be calculated (Equation 3-76 and Figure 3-14). As such two causes of shear resistance are identified and related to the point at which the resisting moment is acting (Figure 3-15).

$$M_S = F_{S2} \cdot (L_1') \cdot \cos(\gamma) + F_{S1} \cdot (L_2') \cdot \cos(\gamma)$$

Equation 3-76

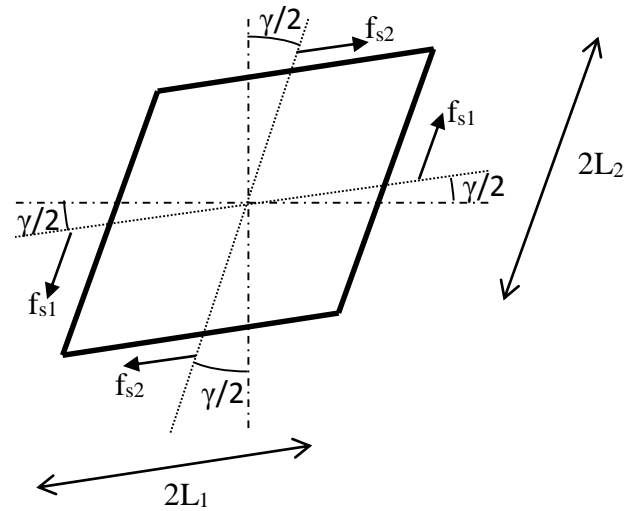


Figure 3-14: Calculation of shear force for a non-square geometry (Liu *et al.*, 2004) (Colman, 2014)

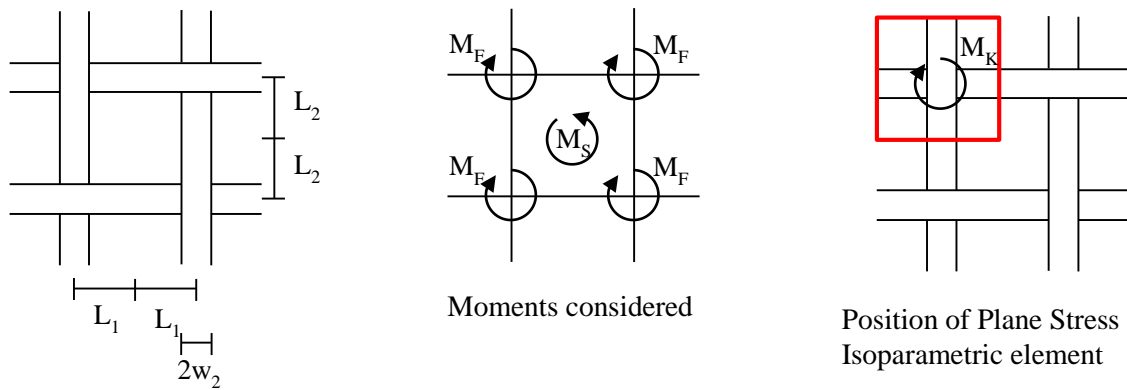


Figure 3-15: Review of the positions of the elements that make up the shear model.

The shear force and shear stress acting on the unit cell can be calculated by considering all of these moments. This is made more complex by the non-square geometry (Figure 3-16).

$$M_S = M_K + M_F$$

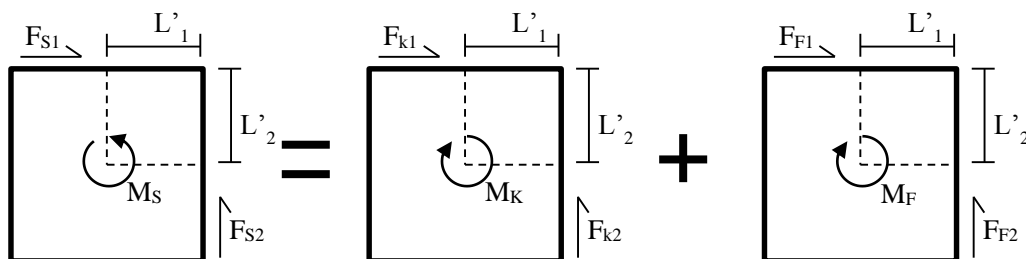


Figure 3-16: Calculation of the external shear force acting on the unit cell. Where M_S is the total moment resisting shear force, M_K is the moment due to the coating, M_F is the moment due to inter yarn friction

3. Predictive model

Referring back to the above assumption that shear stress is constant the shear stress is then calculated (Equation 3-77). The full derivation is in the appendix (§A.9).

$$\tau_s = \frac{F_{s1}}{2L'_2} \quad \text{Equation 3-77}$$

It is also necessary to calculate the shear modulus (Equation 3-78).

$$G_s = \frac{\tau_s}{\gamma_s} \quad \text{Equation 3-78}$$

It was decided that the shear modulus would be the principal concern for an engineer requiring a designed fabric, and thus this is the output of the model (or the target to which a fabric should be designed).

Once all these equations have been derived all the pieces are in place to implement the full optimisation routine (§3.5).

3.5. Implementation

The implementation of the formulae described in the previous section into a useable and complete optimisation routine is described in this section.

Initially the sawtooth model (not inverse) routine is quickly covered as this is the basis of the modelling method used. It is also used to corroborate the results produced from the optimisation routines through a finite difference check of the results obtained.

3.5.1. Sawtooth model

The following Equilibrium model is for the full sawtooth model with all deformation methods. To convert this to the equilibrium model used for the simple sawtooth model values of Y' simply need to be replaced with the initial value, Y .

The angles ($\theta_{1,2}'$) and the Yarn lengths ($Y_{1,2}'$) are the variables within the solver. These are placed in the matrix ' x ' (Equation 3-79). This allows the transfer of data between the solver and the instigating function. The initial (guess) values of ' x ' used are the values of the unstrained geometry. This reduces computation time by initialising the solver with an approximate solution.

$$\begin{Bmatrix} x_1 \\ x_2 \\ x_3 \\ x_4 \end{Bmatrix} = \begin{Bmatrix} \theta_1' \\ \theta_2' \\ Y_1' \\ Y_2' \end{Bmatrix}$$

Equation 3-79

The 'Fsolve' (MathWorks, 2012a) routine is used to find the solution to the equilibrium problem as defined by the equations and constraints (Figure 3-17). The calculations performed within the 'Fsolve' routine are also shown (Figure 3-17).

'Fsolve' makes use of "*Trust-Region Dogleg Method*" (MathWorks, 2014) which "*solves a linear system of equations to find the search direction*". The principle being to "*define a region around the current iterate within which they trust the model to be an accurate representation*" (Nocedal and Wright, 2006, p. 66). At this point "*a trial step 's' is computed by minimizing (or approximately minimizing) over N [the neighbourhood around the current point]*" (MathWorks, 2014). Should this new point be an improvement on the previous one the current point is updated. The program

documentation goes into great detail as to how exactly this is achieved, all of which is not reproduced here. The “*Trust-Region Dogleg*” is implemented by solving a merit function ‘ $m(d)$ ’ for a step ‘ d ’ using “*a convex combination of a Cauchy step (a step along the steepest descent direction) and a Gauss-Newton step for $f(x)$* ”. This briefly comprises approximating the function that is to be minimised at the current point with a new function. This is then minimised within the ‘trust region’, within which the new function is deemed to represent the original function to be minimised, and then the process is begun again.

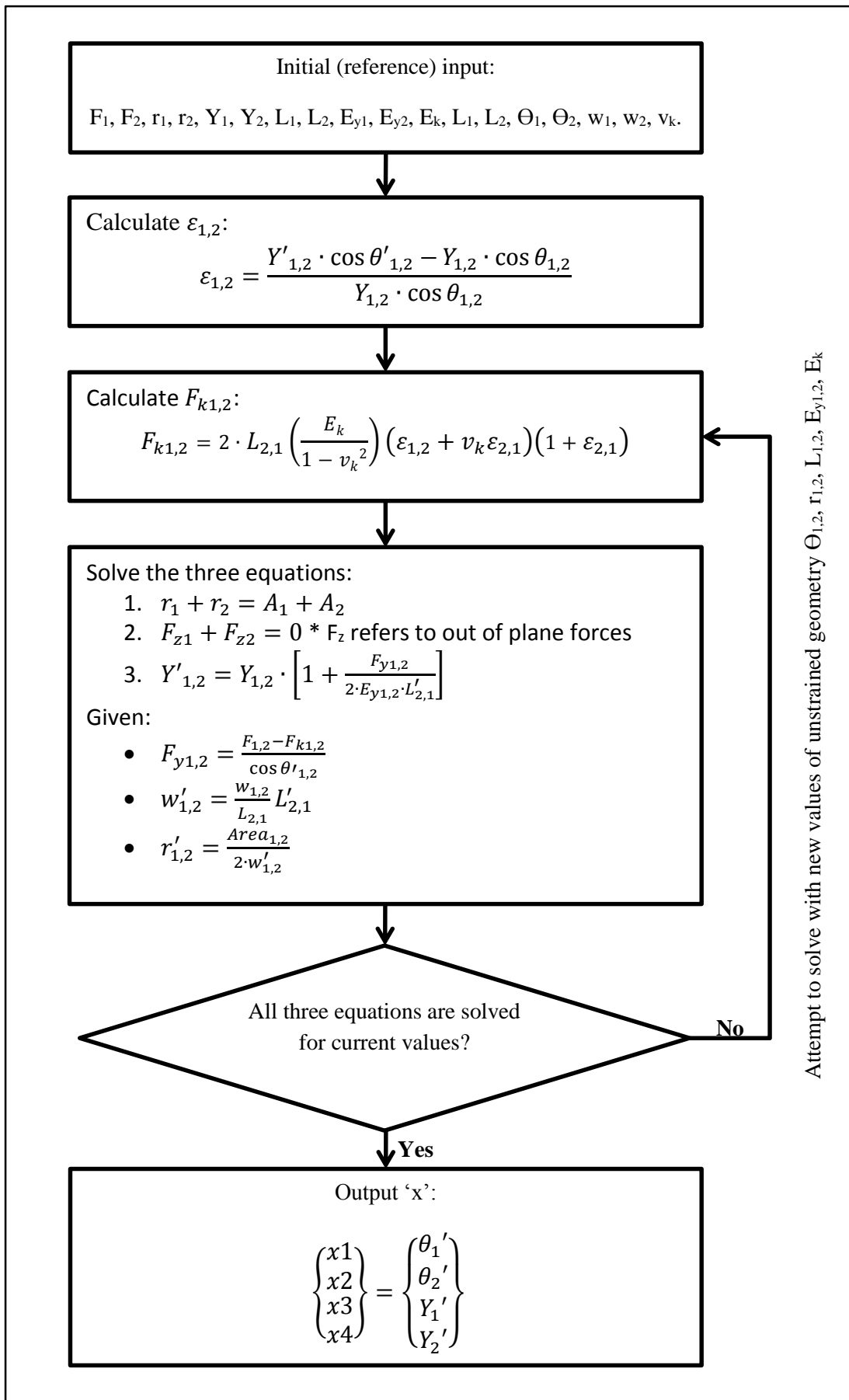


Figure 3-17: Overview of the process of solving the equilibrium sawtooth problem

The result of the sawtooth model can then be used to calculate the strain in the unit cell, and the mechanical properties of the fabric (§3.4.1).

3.5.2. Objective function

For the optimisation of the geometry for a designed fabric it was necessary to produce a reliable objective function. As such two optimisation functions were considered for use.

$$Obj = \sum_1^a (Target_a - Calculation_a)^2$$

Equation 3-80

$$Obj = \sum_1^a \left(\frac{Calculation_a}{Target_a} - 1 \right)^2$$

Equation 3-81

Where *Obj* is the objective function, *Target* is the target of the optimisation at '*a*', and *Calculation* is the calculated value of E_{11} , E_{22} , ν_{12} or ν_{21} for the current geometry at '*a*'.

It is apparent calculating the objective function in the former manner (Equation 3-80), whilst apparently the least computationally expensive of the two possible methods shown will give poor results due to the difference in possible values of Poisson's ratios and Young's moduli. This means that a 1% difference between a target Young's modulus and the calculated value might produce a result of approximately $(10^1)^2$ whilst the same difference between calculated and target Poisson's ratios might produce a result of approximately $(10^{-3})^2$. Therefore a variable weighting factor would be needed to ensure equal importance is given to each target. As such the second calculation method was utilised (Equation 3-81).

The values of the comparison between calculation and target are squared to remove the possibility of negative values affecting the minimisation, where a negative value might be seen as preferable to the algorithms even though it represents a deviation from the target. This introduces one further complication. The apparent error in the objective function is a squared relationship and so objective function values less than one appear to be a greater improvement than is actually the case.

3.5.3. Simple sawtooth

The inverse simple sawtooth is not discussed at length in this section as the model of particular interest is the full sawtooth, with which bespoke architectural fabrics for particular mechanical stiffnesses will be designed.

The routine used to minimise a problem for a specific geometry has been discussed in the Literature Review (§2.4.2.6), and was the 'Fmincon' (Kozola, 2009; Kozola, 2010; MathWorks, 2012a; Mathworks, 2012b) optimisation routine.

3.5.3.1. Optimisation methodology

The optimisation methodology for this version of the sawtooth model is detailed as a flow chart (Figure 3-18 and Figure 3-19). The method's accuracy was compared to finite difference calculations (§A.7).

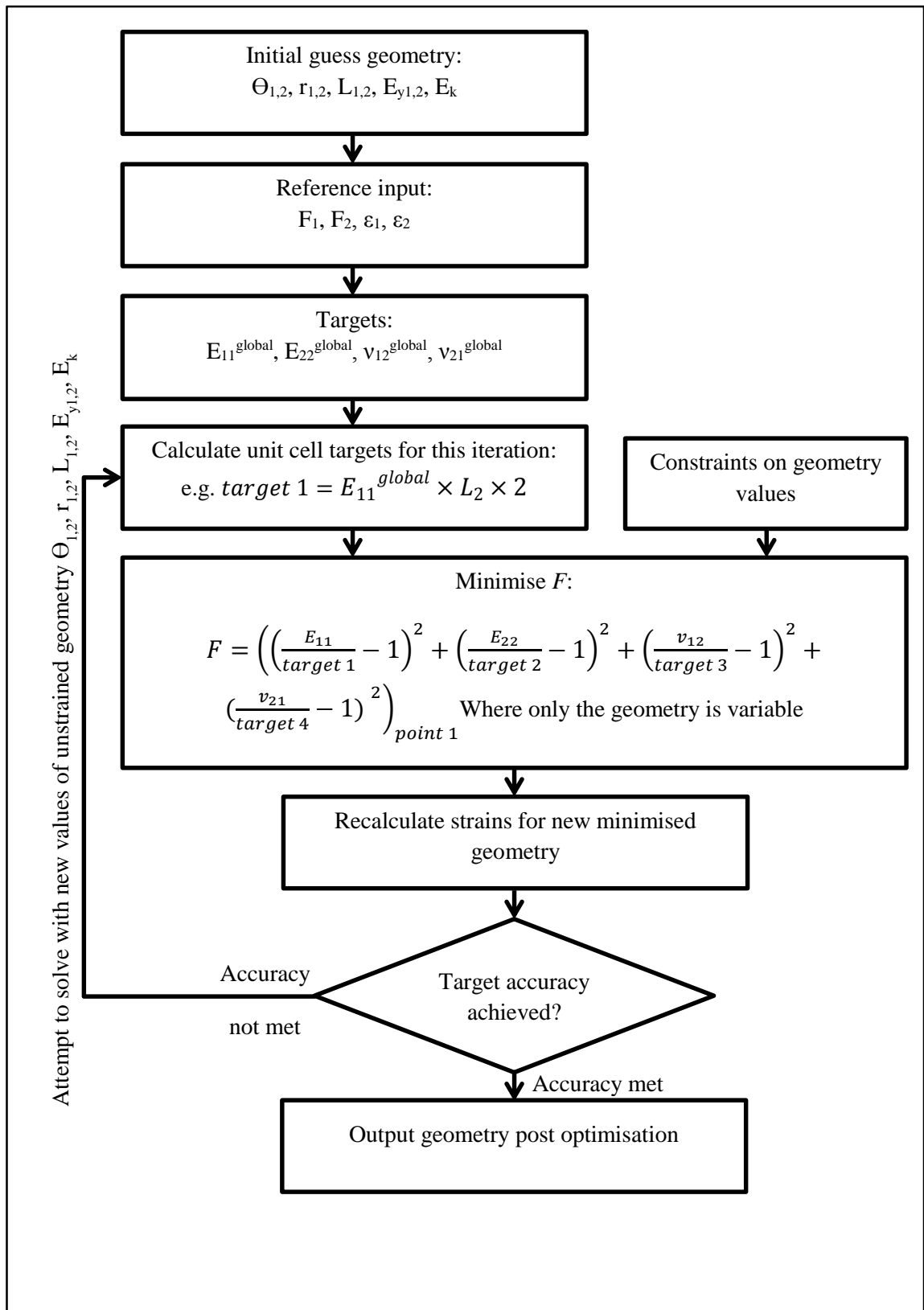


Figure 3-18: Overview of the geometry optimisation for the unit cell minimisation (for a whole fabric)

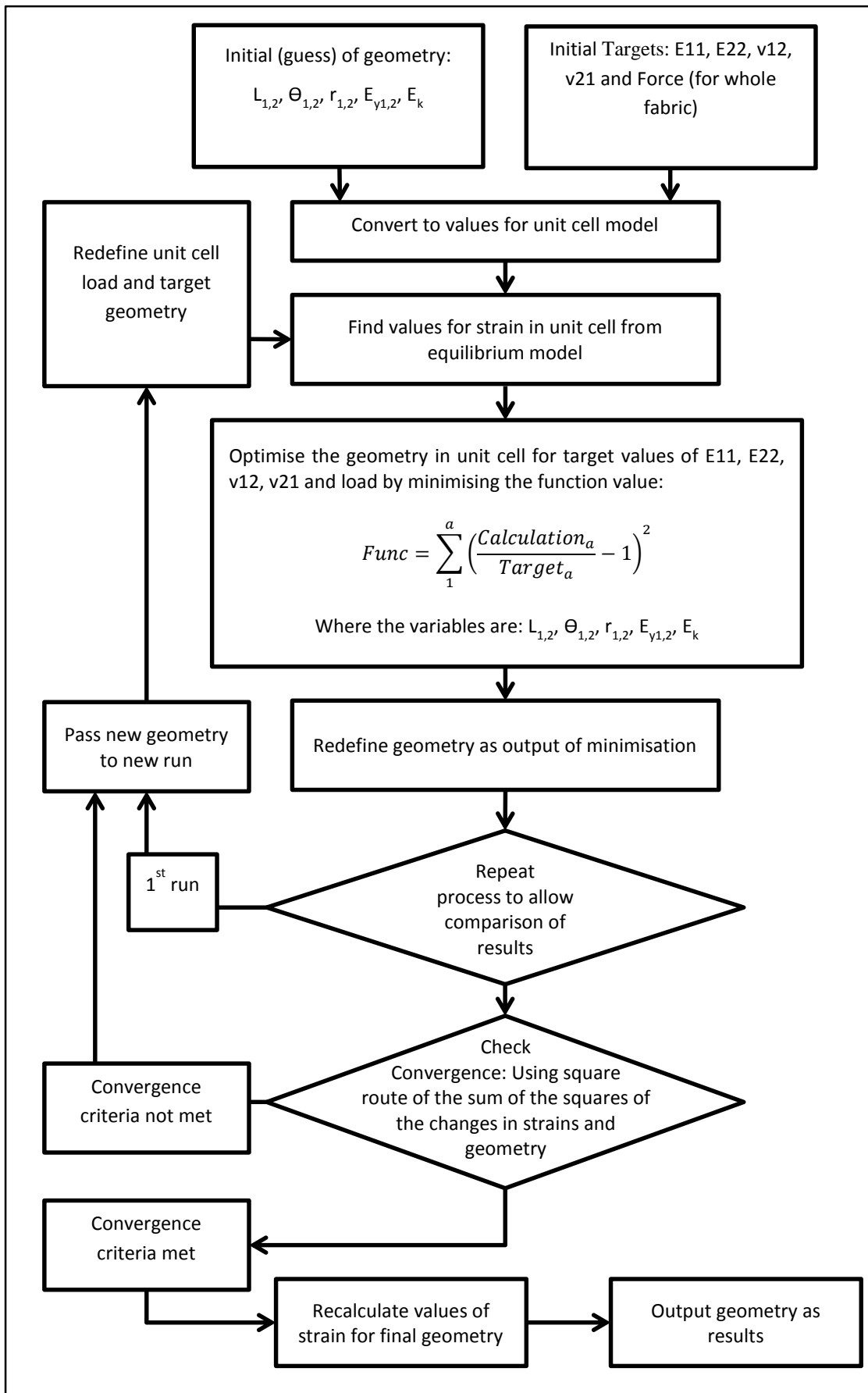


Figure 3-19: Simple sawtooth optimisation process overview

Many lessons were learned from the 'inverse simple sawtooth', and improvements were made for to the planned full sawtooth methodology. These were as follows:

- The objective function was modified to remove the unwanted weighting that occurred when both Poisson's ratios and Young's moduli were compared.
- The constraint functions were tested to ensure that the model was compliant.
- The need for multiple runs to determine accuracy was identified.
- The need to vary the step size when producing a numerical rather than analytical derivative, or when comparing the analytical derivatives to central finite difference calculations at the same point was noted and tested for.

3.5.3.2. Findings

This model produces the same results for any two equal ratios of load placed upon it. This is found because the magnitude of the load does not produce any deformation in the coating or the yarns. Therefore only the configuration of the model components changes when loaded.

As such when a 10:10 load, or 100:100 load is applied the result is exactly the same, with the simple model acting as a mechanical problem. This was not initially predicted, but when it became apparent that this was the case the reasons for this behaviour were evident.

3.5.4. Full sawtooth

The inverted full sawtooth model, or the predictive model for the design of fabrics, was considerably more complex than the initial simple model. It included a number of additional optimisation runs that allowed for the more complex optimisation problem.

3.5.4.1. Overview

The biggest change from the simple model, in terms of optimisation, was the inclusion of an initial pattern search routine which is used to locate a probable zone for the result to be located. This routine performs a number of searches, before locating the most likely position of a solution (a local minimum). This addition reduced the number of false starts in the optimisation routine, by focussing the following solver onto an area where there was likely to be a solution.

3. Predictive model

The gradient based solver could then focus on this 'area' without being drawn into local minima. The pattern search will find a close approximation to the true minimum, and then allow the gradient based solver to find the true minimum at this point.

the gradient based solver, if it began its search at point 'A' would find a 'solution' at one of the local minima, however, if informed by the pattern search grid, would begin its search at point 'B' and therefore find the true minima (Figure 3-20).

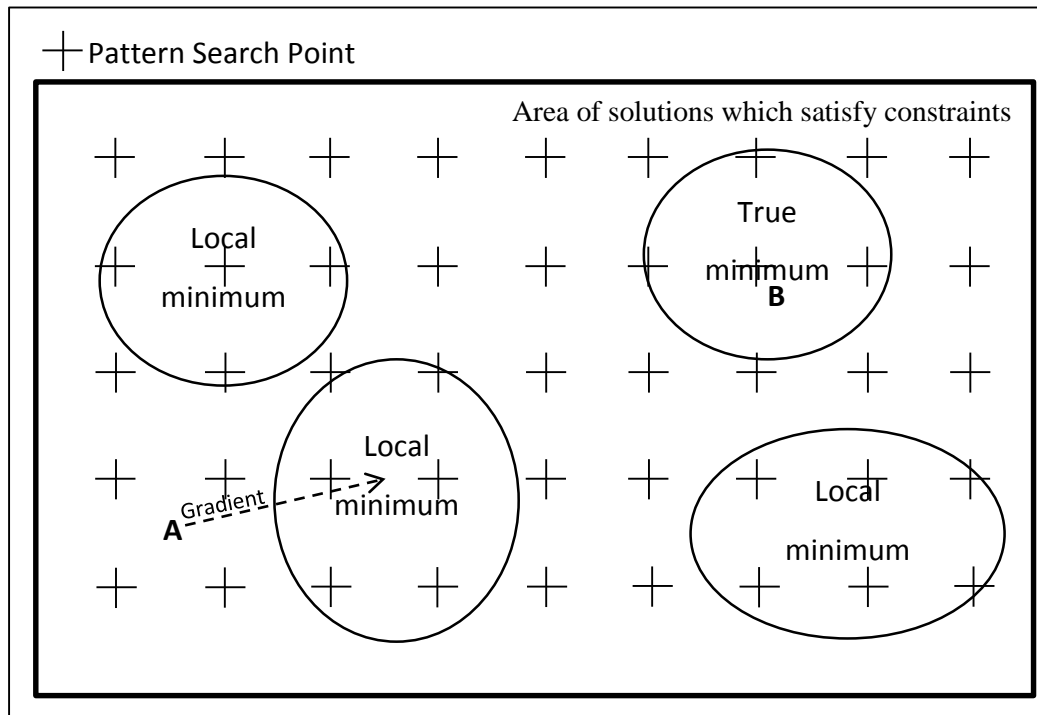


Figure 3-20: Use of pattern search to inform gradient based optimisation

The second principal change is that the optimisation allows for an over constrained search, or to put it another way, allows a solution to be found where no perfect solution exists by allowing the targets to vary a little from their user defined positions. The amount of allowable variation can be either chosen by a user or predefined within the algorithm.

The hypothesis here is that where a low number of targets are chosen then a front of possible solutions exists. For instance if only E_{11} at one load case was specified then a number of possible fabrics might be able to produce the required response, and the output result will be the one closest to the user defined initial search position (X_0). However, if twenty five targets are chosen then it is possible (and likely) that within the constraints placed on the function no possible solution can be found, and at this point

the targets must be allowed to move to place the required response plane into an achievable zone. How this works in practice is shown below (Figure 3-21).

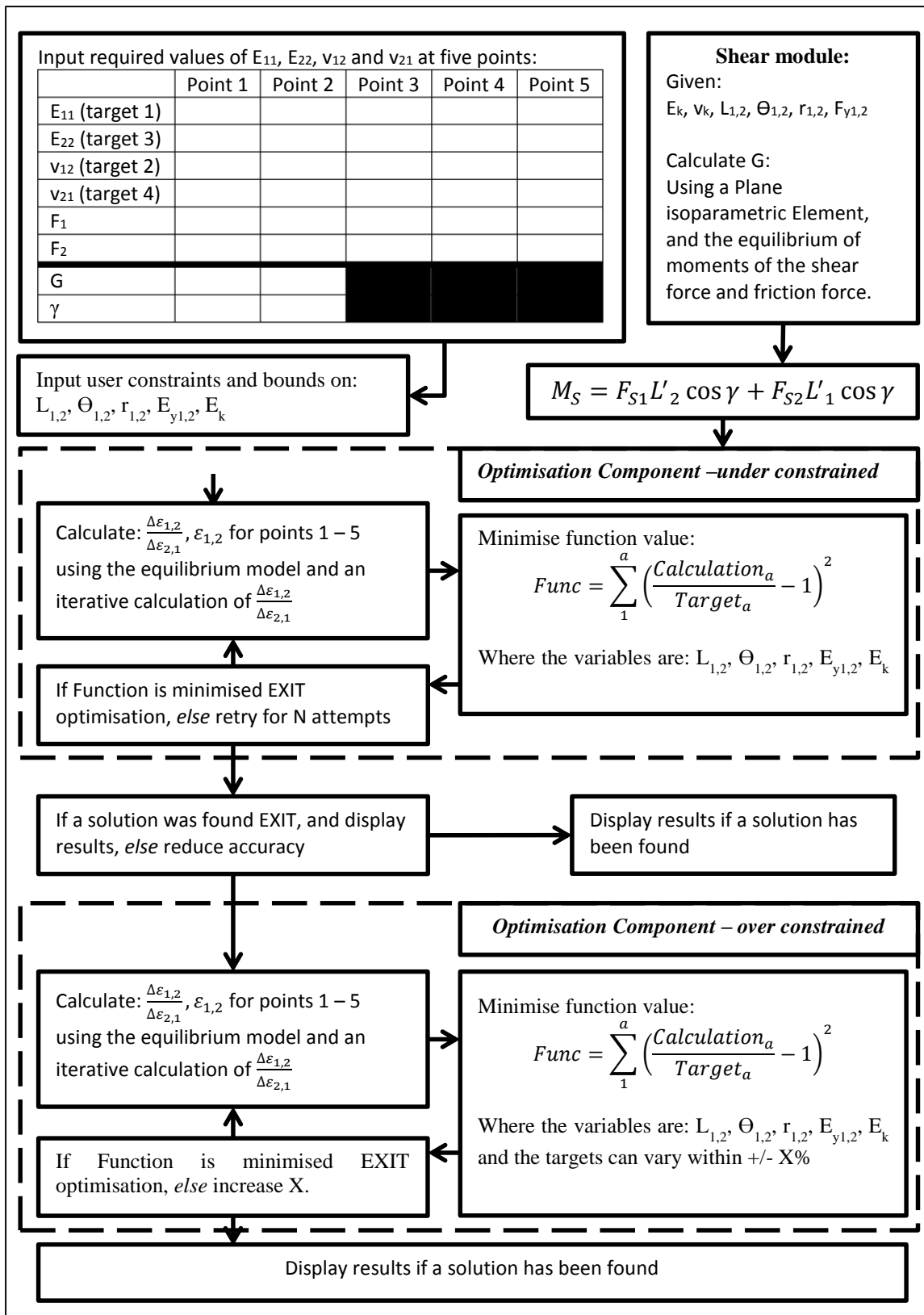


Figure 3-21: Overview of full sawtooth fabric design optimisation procedure

3.6. Yarn strength

Yarn strength is the final fabric parameter that is likely to be required for the design of a fabric. The sawtooth model cannot be used to predict fabric strength because it includes no consideration of the yarn strength or of the yarn build up. Initially it was hoped that a simple relationship between yarn tenacity and area might be found that would allow an approximation of yarn strength to be made from parameters available within the optimisation process. However, after some initial investigation it became apparent that this is not the case. Published yarn strengths are presented in two different ways (Figure 3-22 and Figure 3-23), with the yarn area calculated from photographs of yarn cross sections.. However, even within the confines of only polyester yarns it is apparent that no readily appreciable and easily accessible relationship exists, i.e. in the form $\frac{A}{L} \propto x$ where x is tensile strength.

It is however apparent that tenacity is very generally related to yarn area (Figure 3-22, Figure 3-23, Figure 3-24 and Figure 3-25). When a larger number of yarn types are considered it can be noted that whilst a general relationship appears apparent, no specific linear or non-linear relationship can be interpreted from the data (Figure 3-24 and Figure 3-25).

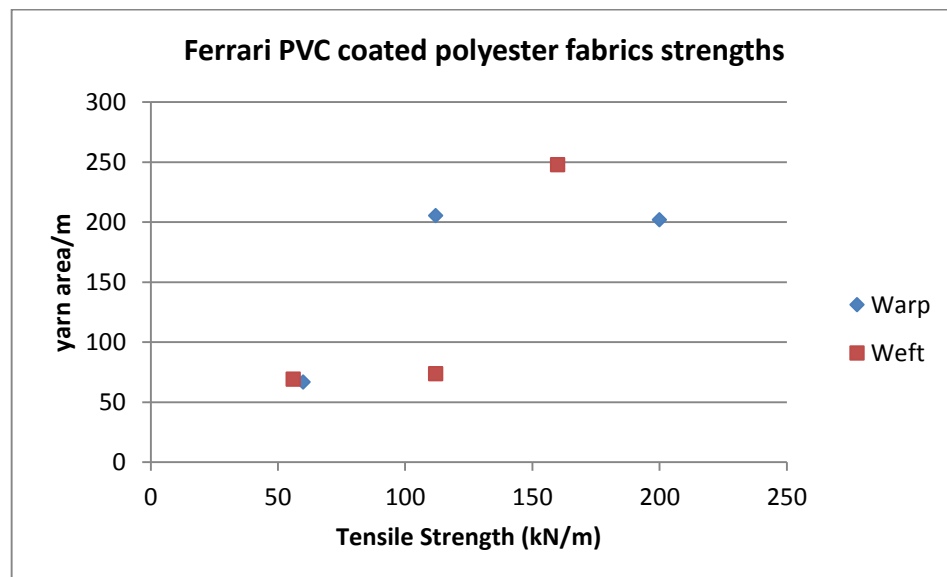


Figure 3-22: Published fabric strengths for Ferrari fabrics (Ferrari, 2013c; Ferrari, 2013a; Ferrari, 2013b)

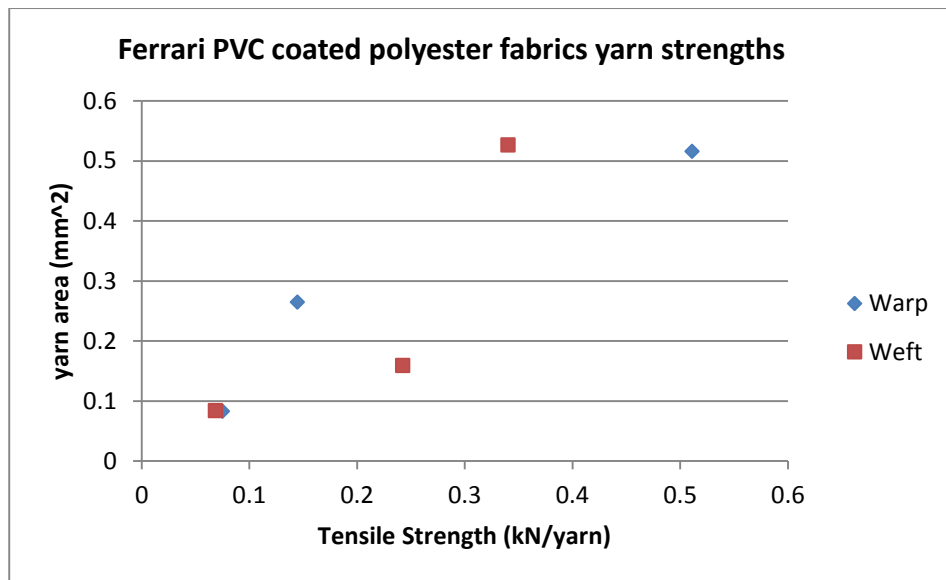


Figure 3-23: Inferred yarn strengths for Ferrari fabrics from published data (Ferrari, 2013c; Ferrari, 2013a; Ferrari, 2013b)

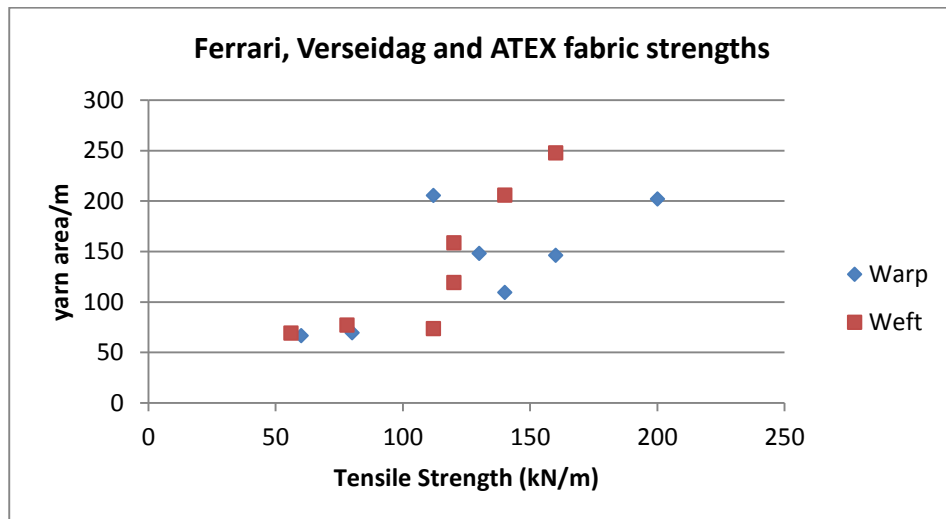


Figure 3-24: Published fabric strengths for Ferrari, Verseidag and ATEX fabrics (Verseidag, 2010a; Verseidag, 2010b; ATEX, 2013a; ATEX, 2013b; Ferrari, 2013c; Ferrari, 2013a; Ferrari, 2013b)

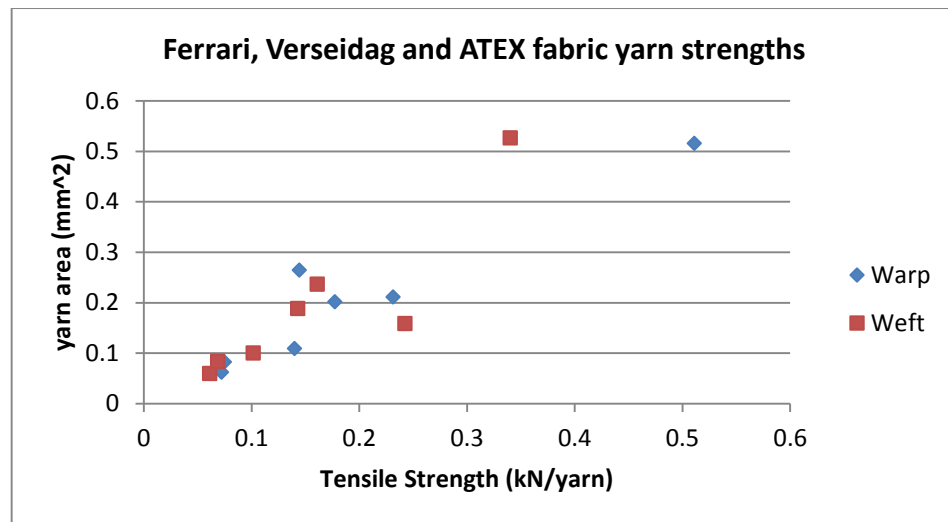


Figure 3-25: Inferred yarn strengths for Ferrari, Verseidag and ATEX fabrics from published data (Verseidag, 2010a; Verseidag, 2010b; Atex, 2013a; Atex, 2013b; Ferrari, 2013c; Ferrari, 2013a; Ferrari, 2013b)

Investigation reveals that the problem of yarn and fabric strength is far more complex than a simple relationship between material and yarn area. Ghosh (2005, p. 731) finds that *“yarn failure is strongly dependent on the yarn structure”* specifically the *“configuration, alignment and packing of the constituent yarns”*. Indeed it appears that even in the consideration of uncoated (i.e. without the inclusion of coating penetration) the problem is complex. Even where the tensile strength of a yarn might be predicted *“in actual practice, the yarns and fabric undergo stresses and strains that are substantially different from those applied in the standard testing conditions”* (Ghosh, 2005, p. 732). As such the prediction of the fabric tensile strength using yarn characteristics may be unwise.

Bogdanovich (2008, p. 248) states that *“obtaining full set of ultimate failure characteristics for each practical textile composite is a big challenge on its own”*, resulting in high cost testing. The Hierarchical *“3-D Mosaic Analysis”* presented by Bogdanovich (2008, p. 248) again would not be directly applicable to the model developed.

The *“Longitudinal tensile strength of twisted impregnated yarns”* can be described in terms of the twist angle, lateral pressure, twist wavelength, and other parameters of the yarn including its lateral compaction ratio and Poisson’s ratio (Singh and Naik, 2001, p. 350). Again, it can be seen from the required parameters that to describe tensile strength even of a yarn prior to consideration as part of a fabric whole would require a

3. Predictive model

step change in the level of complexity of the design process. This would include a series of parameters that would need to be tested for or which do not lend themselves to the design methodology as it stands.

Future work might extend the model developed to include yarn and fabric strength, however, owing to the importance of parameters that are outside of the scale considered, and which do not form a part of the model developed no further consideration of yarn strength will be made. It is noted that this does present a limit to the relevance of the model, though a design methodology for tensile strength might be found to be a project of equal or greater length than this one.

3.7. Model checking and initial validation

Three types of fabric are initially considered, a PVC polyester fabric, a PTFE glass-fibre fabric and a silicone glass-fibre fabric. All three are analysed using the sawtooth model to produce mechanical properties, and these results are then used to design the initial fabric. The design process has no knowledge of the fabric from which the targets came from except for the required mechanical properties (targets).

In addition to these tests the constraints and equilibrium equations are checked for the designed model.

Additional validation is carried out in the following sections (§5.3), where real fabric response parameters from biaxial test data are compared to fabrics designed to reproduce these.

3.7.1. Results for known feasible biaxial targets

To demonstrate the functionality of both the method of optimisation and the validity of the equations used an optimisation for a set of targets that were known to be feasible was performed for three different fabric geometries.

- F1202 PVC coated polyester fabric (§A.1)
- B18089 PTFE glass-fibre fabric (§A.1)
- ATEX3000 Silicone coated glass-fibre fabric (§A.1)

The feasible targets were produced from the sawtooth equilibrium model using a central finite difference method and recorded (Table 3-2). The resulting mechanical properties were also recorded (Table 3-3).

The optimisation routine had no prior knowledge of the geometry from which the targets were calculated. The initial 'starting geometry' was randomised. Randomising the starting geometry creates an artificially difficult situation for the optimisation routine. In most scenarios a 'close approximation' might originally be used to target the result. However, starting from a randomised geometry helps to demonstrate the model's utility.

F1202 PVC coated Polyester results for feasible targets:

Variable	Geometry from which targets are calculated	Optimised geometry
Θ_1 (Rad)	0.101	0.108
Θ_2 (Rad)	0.180	0.177
L_1 (mm)	0.645	0.691
L_2 (mm)	1.082	1.166
r_1 (mm)	0.157	0.169
r_2 (mm)	0.106	0.114
E_1 (kN/m)	880	879
E_2 (kN/m)	810	805
E_k (kN/m)	37	39
A_1 (mm)	0.066	0.075
A_2 (mm)	0.197	0.208
w_1 (mm)	0.859	0.949
w_2 (mm)	1.044	0.105
v_k	0.3	0.3

Table 3-2: Geometry used to find feasible targets and resultant optimised geometry for F1202 fabric

	Point 1	Point 2	Point 3	Point 4	Point 5
E_{11} (target 1) (kN/m)	543.5	691.1	632.1	403.5	806.1
E_{22} (target 3) (kN/m)	501.7	628.3	578.2	625.8	547.9
v_{12} (target 2)	0.419	0.276	0.331	0.309	0.250
v_{21} (target 4)	0.386	0.252	0.303	0.450	0.187
P_1 (kN/m)	10	20	15	10	20
P_2 (kN/m)	10	20	15	20	10
E_{11} (result 1) (kN/m)	543.1	691.3	632.1	403.4	806.2
E_{22} (result 3) (kN/m)	502.3	628.0	578.2	625.2	548.6
v_{12} (result 2)	0.419	0.277	0.331	0.309	0.250
v_{21} (result 4)	0.386	0.252	0.303	0.450	0.187

Table 3-3: Feasible targets found at the applied loads P1 and P2 and results for F1202 fabric

Optimisation function value: 8.22×10^{-6}

Equilibrium check: $A_1 + A_2 - (r_1 + r_2) = 4.4 \times 10^{-16} \approx 0$

The results of this fabric design are as predicted, a near perfect solution is found quickly (291 seconds) suggesting that the method works well. The equations therefore correlate to the sawtooth method which is known to correlate well with the biaxial response of real fabrics. It should be noted that the start point of the optimisation was not the geometry used to find the targets; this ensured that the method was in fact finding a solution, and not succeeding having been given the correct geometry as a start point. The method used to renew the initial guess point was also demonstrated with four runs having been attempted prior to a solution being found.

3. Predictive model

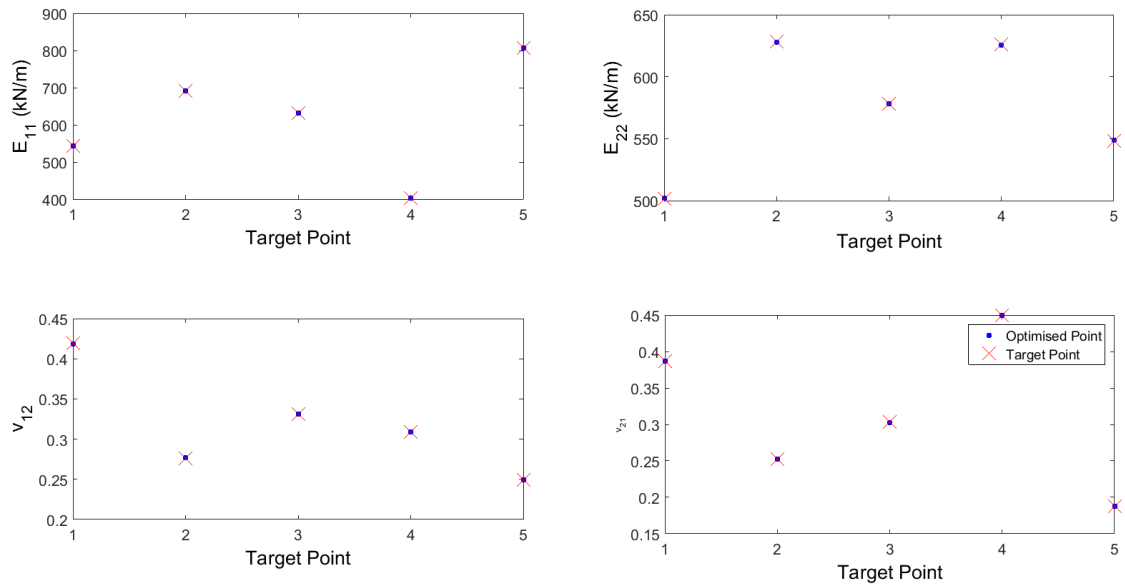


Figure 3-26: Results of the optimisation for the feasible solution of the F1202 PVC Polyester fabric

The optimisation for the feasible values of stiffness and Poisson's ratio produces good results (Figure 3-26). Target points 1 in the plots v_{12} and v_{21} results show some slight deviation from the targets. In reality this error is small, whilst observable in the figure, and equates to a difference of only 0.11%. This is as a result of the slight deviation from the original geometry that was found. A higher accuracy requirement on the solver may produce more accurate results, but would be more computationally expensive, taking longer. The current accuracy requirement is deemed adequate for this optimisation.

B18089 PTFE coated glass-fibre results for feasible targets:

Variable	Geometry from which targets are calculated	Optimised geometry
Θ_1 (Rad)	0.227	0.227
Θ_2 (Rad)	0.328	0.328
L_1 (mm)	0.500	1.265
L_2 (mm)	0.423	1.071
r_1 (mm)	0.127	0.321
r_2 (mm)	0.133	0.335
E_1 (kN/m)	4270	4270
E_2 (kN/m)	3970	3970
E_k (kN/m)	36	36
A_1 (mm)	0.116	0.292
A_2 (mm)	0.144	0.364
w_1 (mm)	0.373	0.945
w_2 (mm)	0.573	1.451
v_k	0.3	0.3

Table 3-4: Geometry used to find feasible targets and resultant optimised geometry for B18089 fabric

3. Predictive model

	Point 1	Point 2	Point 3	Point 4	Point 5
E_{11} (target 1) (kN/m)	332.22	555.90	446.97	292.54	774.90
E_{22} (target 3) (kN/m)	276.77	503.23	393.39	766.73	223.60
v_{12} (target 2)	0.999	0.890	0.936	0.509	1.634
v_{21} (target 4)	0.833	0.809	0.826	1.394	0.452
P_1 (kN/m)	10	20	15	10	20
P_2 (kN/m)	10	20	15	20	10
E_{11} (result 1) (kN/m)	332.22	555.90	446.97	292.54	774.90
E_{22} (result 3) (kN/m)	0.999	0.890	0.936	0.509	1.634
v_{12} (result 2)	276.77	503.23	393.39	766.73	223.60
v_{21} (result 4)	0.833	0.809	0.826	1.394	0.452

Table 3-5: Feasible targets found at the applied loads P_1 and P_2 and results for B18089 fabric

Optimisation function value: 9.47×10^{-11}

Equilibrium check: $A_1 + A_2 - (r_1 + r_2) = 9.25 \times 10^{-12}$

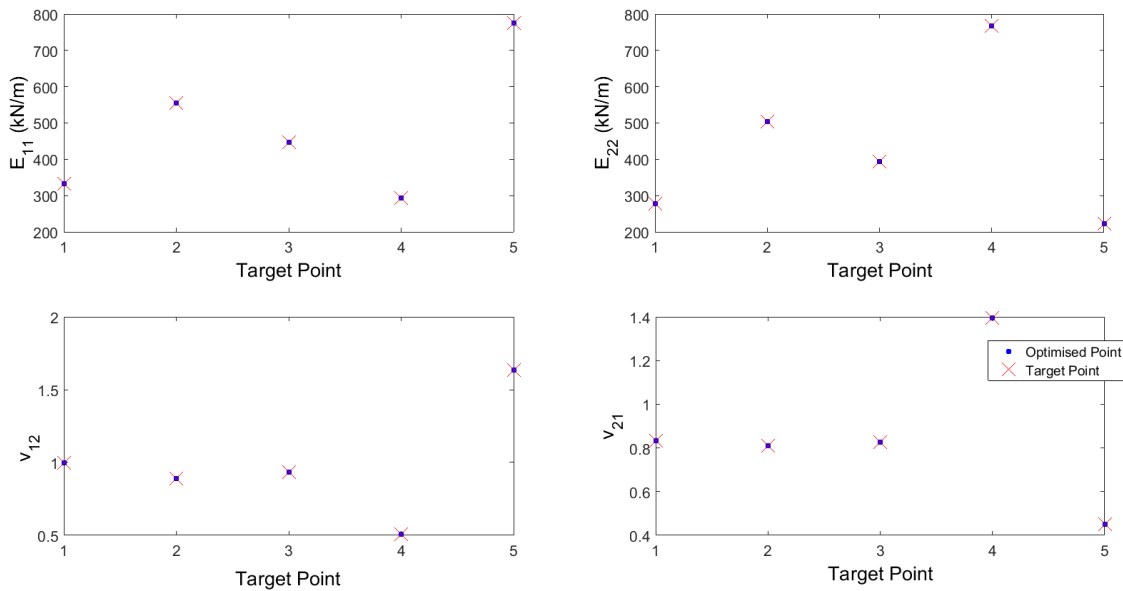


Figure 3-27: Results of the optimisation for the feasible solution of the B18089 PTFE glass-fibre fabric

3. Predictive model

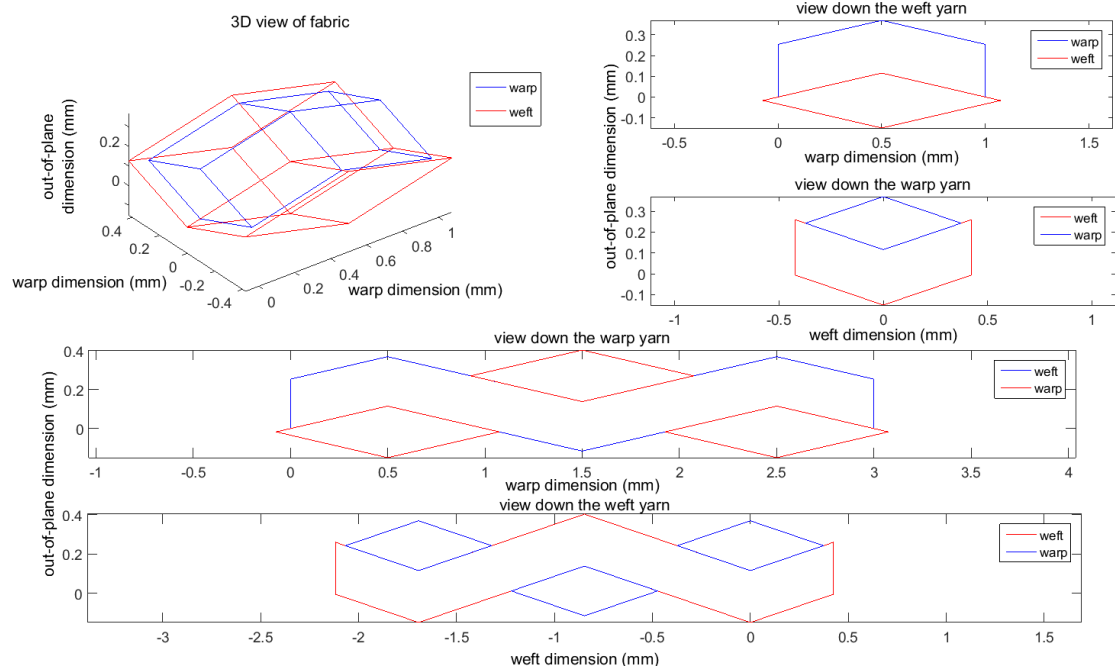


Figure 3-28: Original geometry of the B18089 PTFE glass-fibre fabric

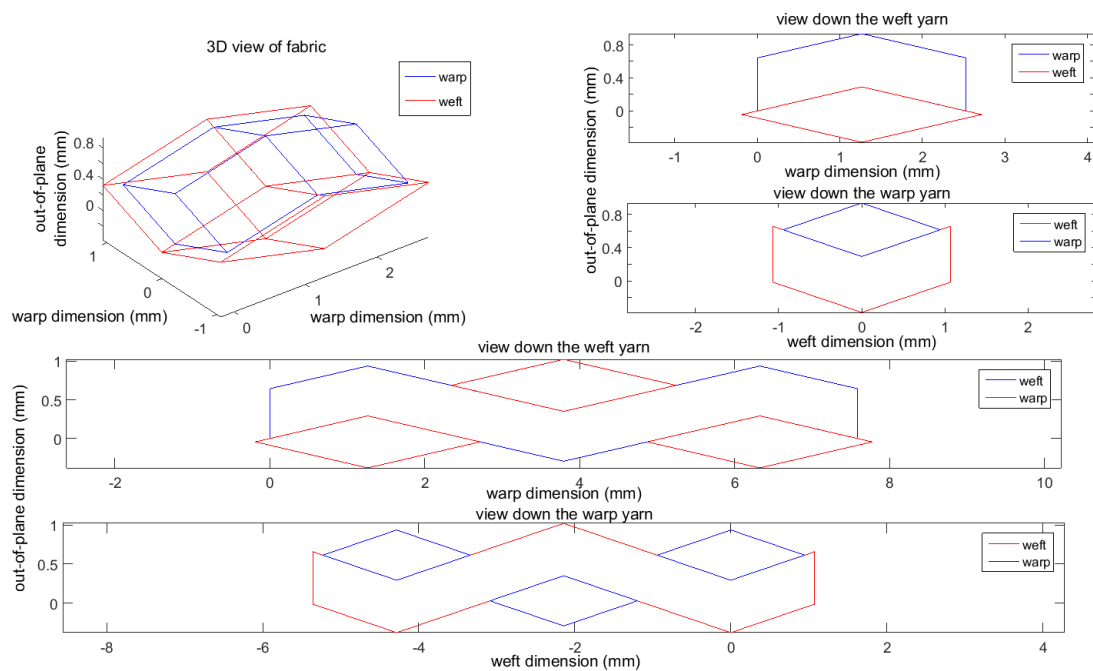


Figure 3-29: Optimised geometry of the B18089 PTFE glass-fibre fabric

A different solution for the targets produced for the B18089 fabric is found after the design process. This is discussed in more detail below.

B18089 PTFE coated glass-fibre results for feasible targets (with prior knowledge):

Variable	Geometry from which targets are calculated	Optimised geometry
Θ_1 (Rad)	0.227	0.227
Θ_2 (Rad)	0.328	0.328
L_1 (mm)	0.500	0.500
L_2 (mm)	0.423	0.423
r_1 (mm)	0.127	0.127
r_2 (mm)	0.133	0.133
E_1 (kN/m)	4270	4270
E_2 (kN/m)	3970	3970
E_k (kN/m)	36	36
A_1 (mm)	0.116	0.116
A_2 (mm)	0.144	0.144
w_1 (mm)	0.373	0.373
w_2 (mm)	0.573	0.390
v_k	0.3	0.3

Table 3-6: Geometry used to find feasible targets and resultant optimised geometry for B18089 fabric

	Point 1	Point 2	Point 3	Point 4	Point 5
E_{11} (target 1) (kN/m)	332.22	555.90	446.97	292.54	774.90
E_{22} (target 3) (kN/m)	276.77	503.23	393.39	766.73	223.60
v_{12} (target 2)	0.999	0.890	0.936	0.509	1.634
v_{21} (target 4)	0.833	0.809	0.826	1.394	0.452
P_1 (kN/m)	10	20	15	10	20
P_2 (kN/m)	10	20	15	20	10
E_{11} (result 1) (kN/m)	332.23	555.90	446.97	292.54	774.90
E_{22} (result 3) (kN/m)	0.999	0.890	0.936	0.509	1.634
v_{12} (result 2)	276.77	503.23	393.39	766.73	223.60
v_{21} (result 4)	0.833	0.809	0.826	1.394	0.452

Table 3-7: Feasible targets found at the applied loads P1 and P2 and results for B18089 fabric

Optimisation function value: 8.22×10^{-6}

Equilibrium check: $A_1 + A_2 - (r_1 + r_2) = 8.87 \times 10^{-10} \approx 0$

3. Predictive model

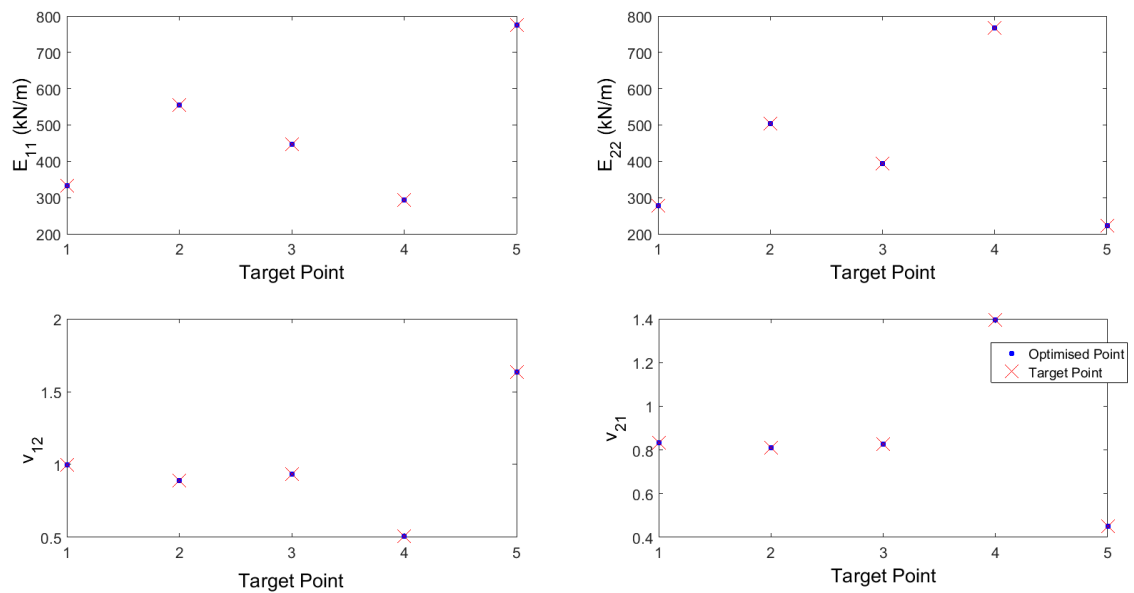


Figure 3-30: Results of the optimisation for the feasible solution of the B18089 PTFE glass-fibre fabric

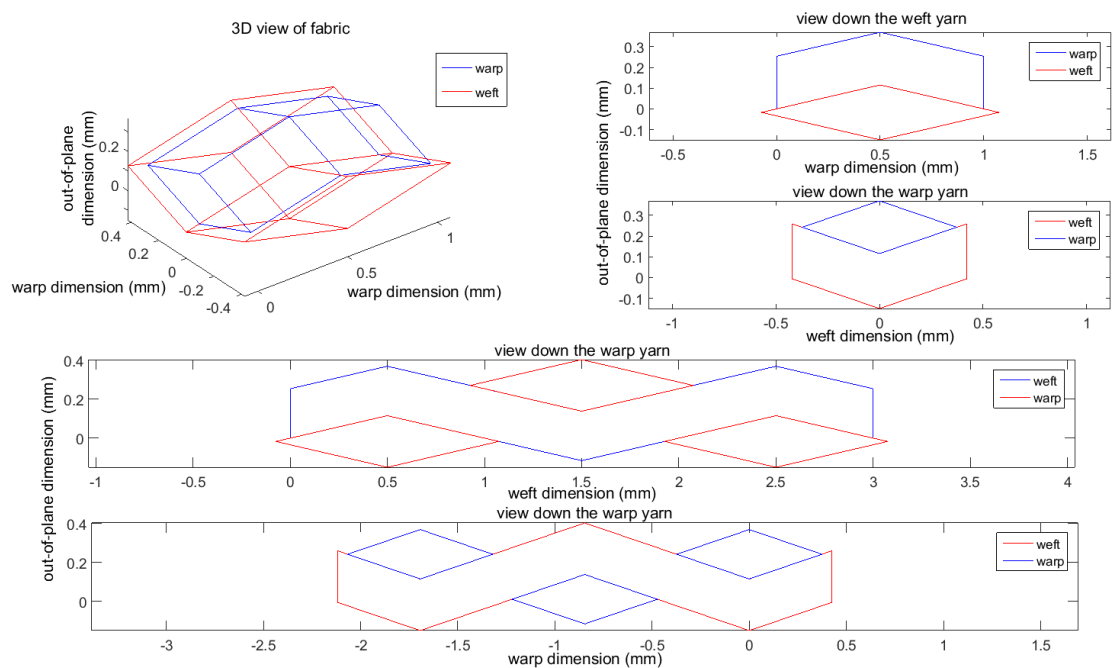


Figure 3-31: Optimised geometry of the B18089 PTFE glass-fibre fabric (Prior knowledge of original geometry)

The method does reproduce the initial geometry when it is given prior knowledge of the geometry from which the targets were derived (i.e. an initial geometry close to that of the original fabric is selected). This is probably because the steepest decent from the initial point found by the pattern search method directs the result towards a different solution. This is discussed in more detail below.

ATEX3000 Silicone coated glass-fibre results for feasible targets:

Variable	Geometry from which targets are calculated	Optimised geometry
Θ_1 (Rad)	0.181	0.181
Θ_2 (Rad)	0.184	0.183
L_1 (mm)	0.451	1.557
L_2 (mm)	0.391	1.353
r_1 (mm)	0.076	0.264
r_2 (mm)	0.079	0.272
E_1 (kN/m)	3120	3118.553877
E_2 (kN/m)	3190	3187.954473
E_k (kN/m)	12	10.33580805
A_1 (mm)	0.083	0.286
A_2 (mm)	0.073	0.250
w_1 (mm)	0.408	1.426
w_2 (mm)	0.434	1.483
v_k	0.3	0.3

Table 3-8: Geometry used to find feasible targets and resultant optimised geometry for ATEX3000 fabric

	Point 1	Point 2	Point 3	Point 4	Point 5
E_{11} (target 1) (kN/m)	531.98	899.56	729.56	499.95	1147.60
E_{22} (target 3) (kN/m)	0.819	0.693	0.750	0.414	1.221
v_{12} (target 2)	531.61	906.02	732.56	1339.14	406.38
v_{21} (target 4)	0.819	0.698	0.754	1.112	0.430
P_1 (kN/m)	10	20	15	10	20
P_2 (kN/m)	10	20	15	20	10
E_{11} (result 1) (kN/m)	531.42	900.12	729.66	499.03	1148.95
E_{22} (result 3) (kN/m)	0.819	0.692	0.750	0.413	1.222
v_{12} (result 2)	531.54	906.78	732.99	1340.71	405.81
v_{21} (result 4)	0.819	0.697	0.754	1.112	0.429

Table 3-9: Feasible targets found at the applied loads P1 and P2 and results for ATEX3000 fabric

Optimisation function value: 2.22×10^{-5}

Equilibrium check: $A_1 + A_2 - (r_1 + r_2) = 0$

3. Predictive model

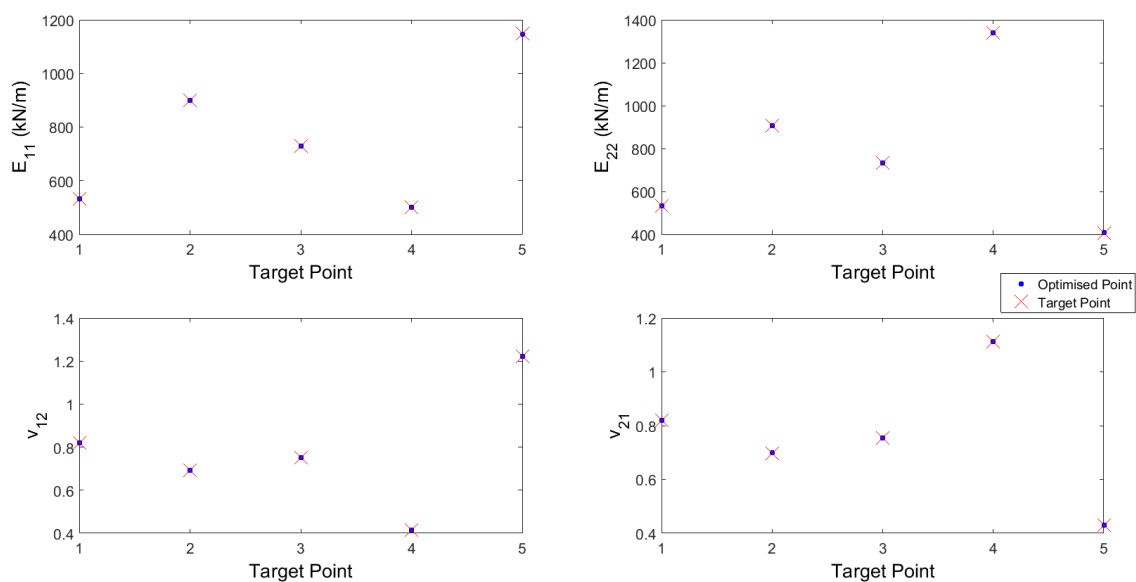


Figure 3-32: Results of the optimisation for the feasible solution of the ATEX3000 Silicone glass-fibre fabric

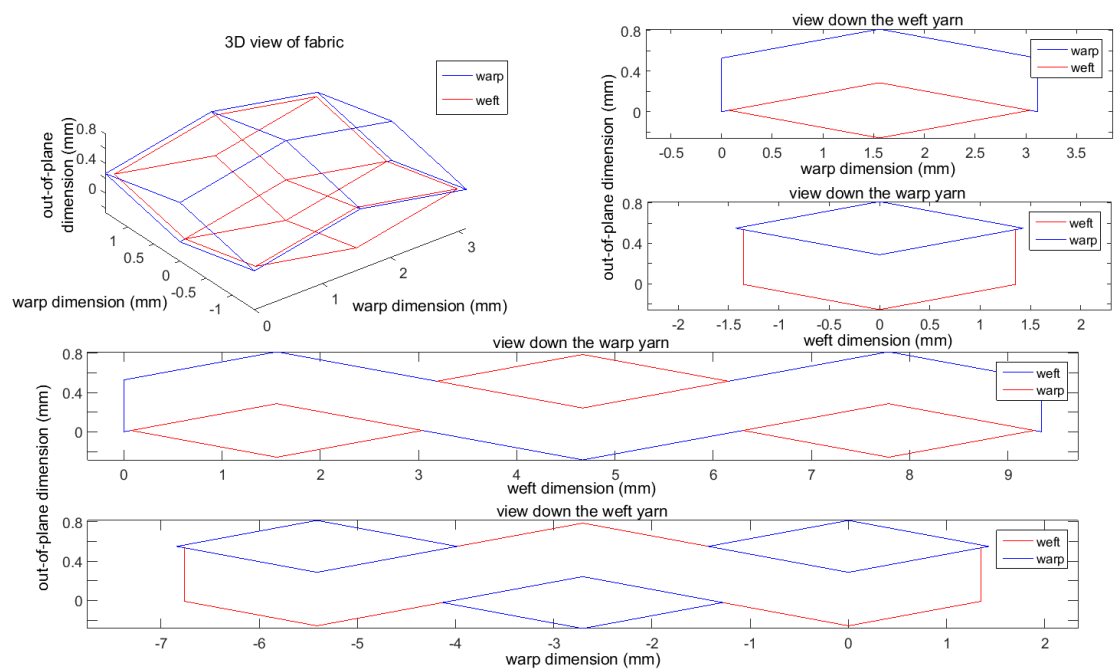


Figure 3-33: Original geometry of the ATEX3000 Silicone glass-fibre fabric

3. Predictive model

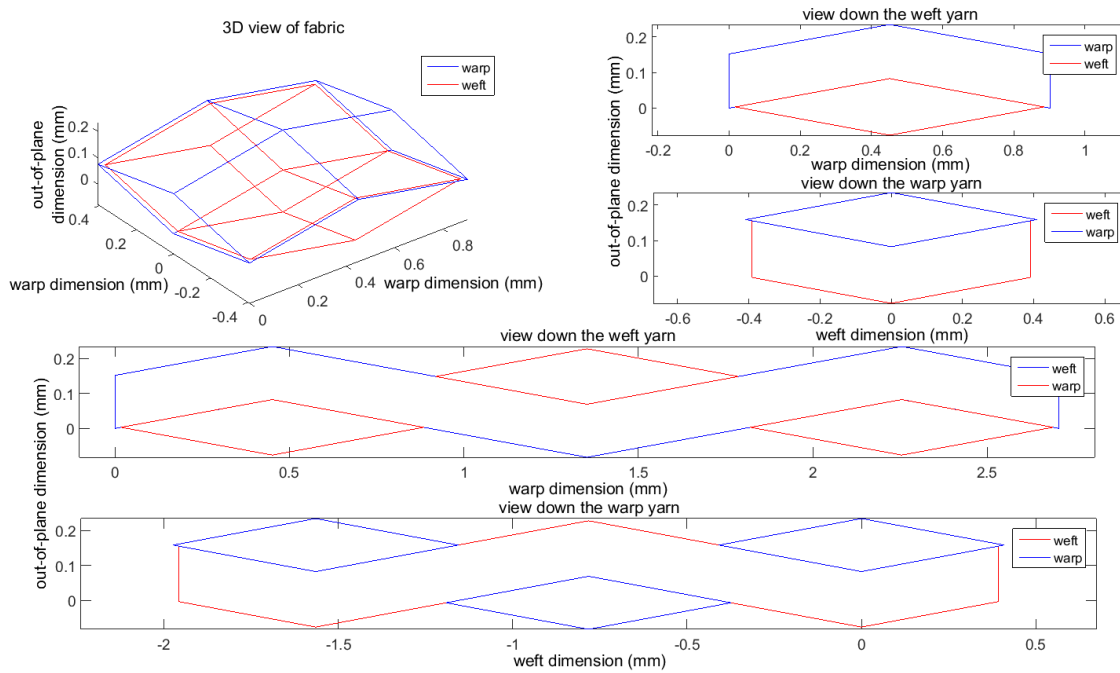


Figure 3-34: Optimised geometry of the ATEX3000 Silicone glass-fibre fabric

Again the method finds an alternate solution.

ATEX3000 Silicone coated glass-fibre results for feasible targets (with prior knowledge):

Variable	Geometry from which targets are calculated	Optimised geometry
Θ_1 (Rad)	0.181	0.181
Θ_2 (Rad)	0.184	0.184
L_1 (mm)	0.451	0.451
L_2 (mm)	0.391	0.391
r_1 (mm)	0.076	0.076
r_2 (mm)	0.079	0.079
E_1 (kN/m)	3120	3120
E_2 (kN/m)	3190	3190
E_k (kN/m)	12	12
A_1 (mm)	0.083	0.083
A_2 (mm)	0.073	0.073
w_1 (mm)	0.408	0.408
w_2 (mm)	0.434	0.434
v_k	0.3	0.3

Table 3-10: Geometry used to find feasible targets and resultant optimised geometry for ATEX3000 fabric

	Point 1	Point 2	Point 3	Point 4	Point 5
E_{11} (target 1) (kN/m)	531.98	899.56	729.56	499.95	1147.60
E_{22} (target 3) (kN/m)	0.819	0.693	0.750	0.414	1.221
v_{12} (target 2)	531.61	906.02	732.56	1339.14	406.38
v_{21} (target 4)	0.819	0.698	0.754	1.112	0.430
P_1 (kN/m)	10	20	15	10	20
P_2 (kN/m)	10	20	15	20	10
E_{11} (result 1) (kN/m)	531.98	899.56	729.56	499.95	1147.60
E_{22} (result 3) (kN/m)	0.819	0.693	0.750	0.414	1.221
v_{12} (result 2)	531.61	906.02	732.56	1339.14	406.38
v_{21} (result 4)	0.819	0.698	0.754	1.112	0.430

Table 3-11: Feasible targets found at the applied loads P1 and P2 and results for ATEX3000 fabric

Optimisation function value: 1.47×10^{-13}

Equilibrium check: $A_1 + A_2 - (r_1 + r_2) = 1.136 \times 10^{-10} \approx 0$

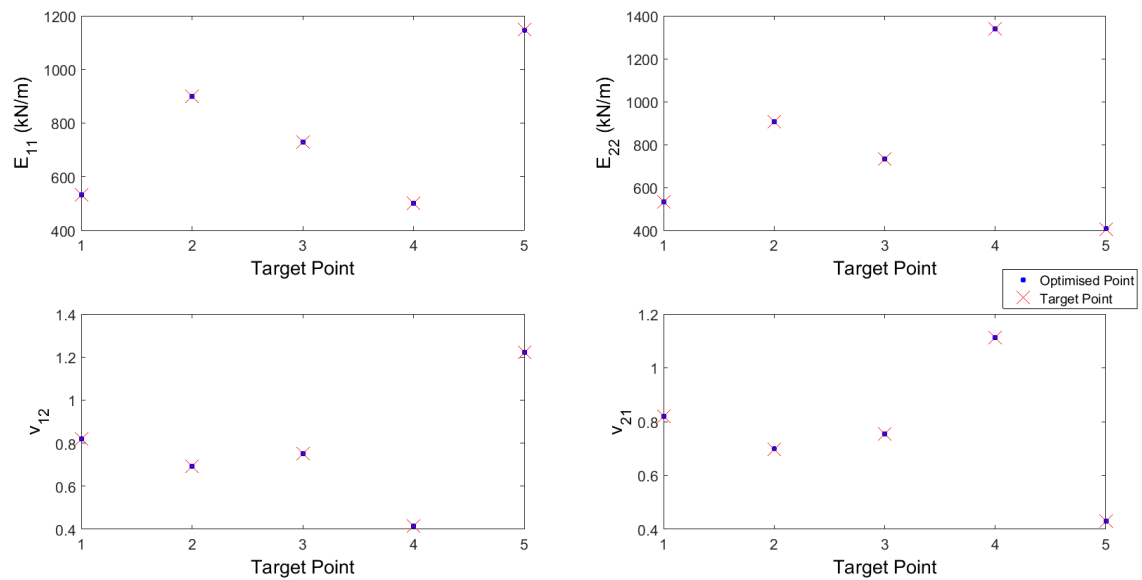


Figure 3-35: Results of the optimisation for the feasible solution of the ATEX3000 Silicone glass-fibre fabric

3. Predictive model

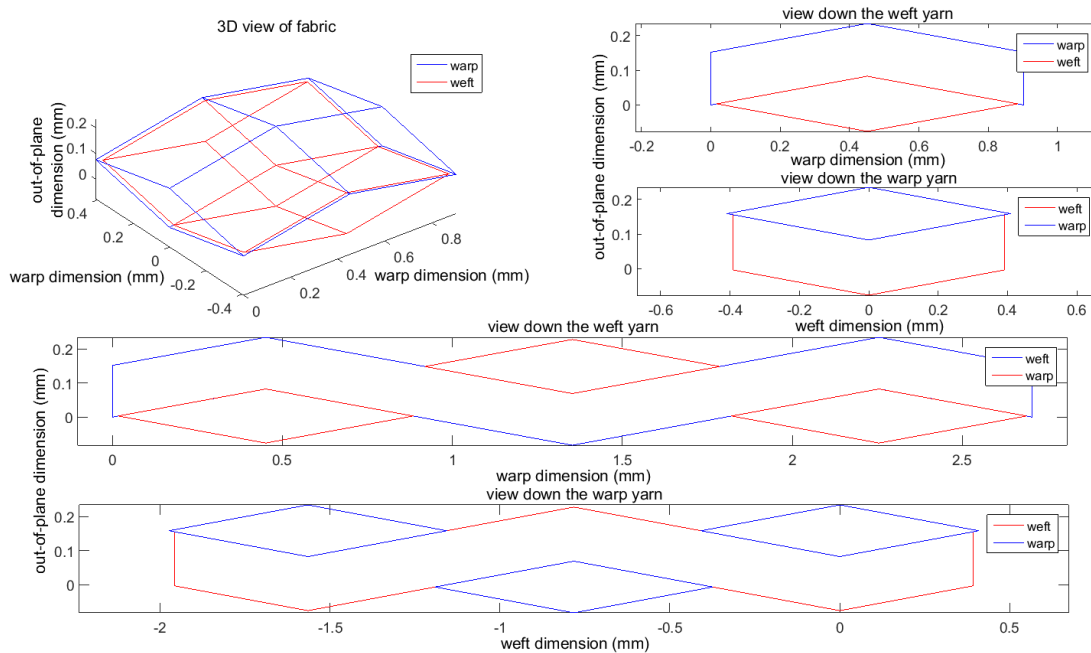


Figure 3-36: Optimised geometry of the ATEX300 Silicone glass-fibre fabric (Prior knowledge of original geometry)

The results for the PTFE glass-fibre fabric and Silicone glass-fibre fabric design process demonstrate how for each set of yarn target mechanical properties it is possible that more than one solution exists. For ‘original fabric geometries’ two sets of tests were carried out. The first followed the same principle as the PVC coated polyester fabric above, namely that the optimisation routine had no prior knowledge of the fabric geometry. This results in a solution different to the original geometry, but which still solves the equations produced earlier and thus will produce the required tensile stress-strain response at the stated loads. This occurs because there exists more than one solution within the bounds of the optimisation, and the starting point of the optimisation, which is randomised, leads to the solutions shown rather than the original geometry.

Next, to demonstrate that the solver can indeed find the original solution a starting point close to the original geometry is used, and in this case the solver finds a solution to the problems that matches the original geometry.

It is infeasible to attempt to find all possible solutions, where all possible starting points or at least a grid of starting points of indefinite fineness would need to be tested for. As such, it has been demonstrated that more than one solution to any problem may exist,

and as will be discussed in following chapters (§4.5) reducing the number of targets will increase the size of this volume of possible solutions.

It has been demonstrated that for feasible targets the solver produces results that appear to be visually viable. Further discussion of the applicability of this to real fabric biaxial test data follows in later chapters (§5.4).

Further results for optimisations were carried out and are summarised in Appendix 3 (§A.3).

3.7.2. Results for known feasible shear targets

The method for the calculation of the shear modulus was used in conjunction with data from a F1202 PVC polyester fabric to show the method's applicability. Similarly to the methodology above (§3.5.4) the shear modulus was calculated for a geometry to give a known feasible target. After this the optimisation routine was used to design a fabric for which the target is achieved without any prior knowledge of the original geometry from which the target was obtained.

Shear test data for a coated fabric demonstrating nonlinearity and hysteresis offers two problems for the design of a fabric (Figure 3-37). The first is how to represent the hysteresis? This is resolved by considering only the loading curve, as is done for plane stress fits to biaxial test data. Therefore whilst the frictional resistance of the fabric to unloading could be considered using this shear method this is not incorporated into the model.

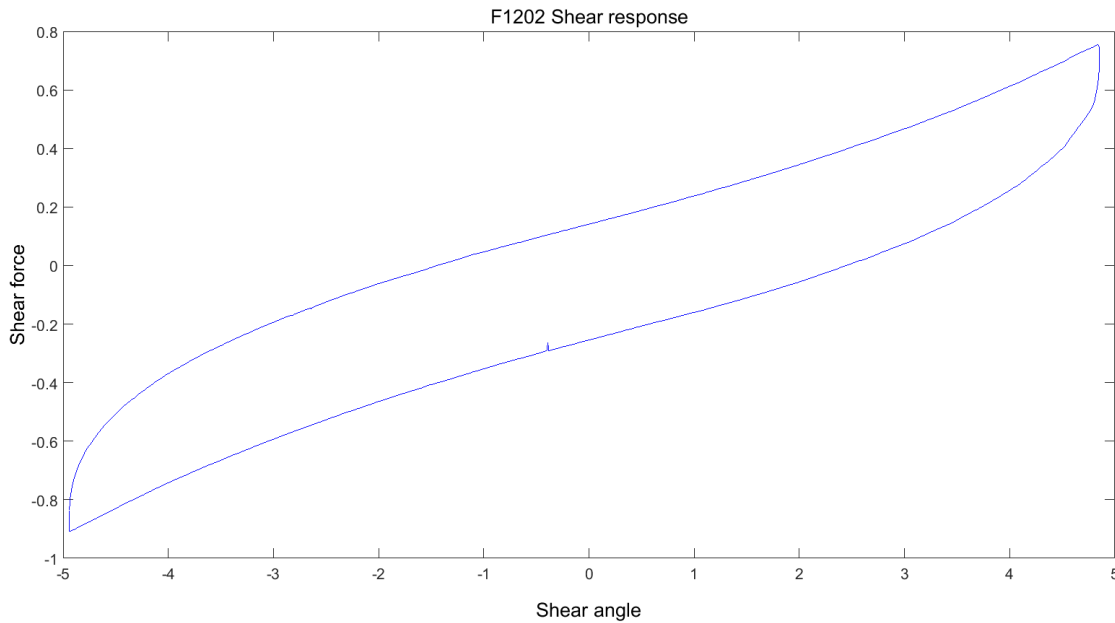


Figure 3-37: Shear response of a F1202 fabric up to a 50 shear angle

The second problem associated with the use of this data is where to take the shear modulus from? The MSAJ standard requires that the tip to tip displacements be used, with the gradient of a line between the two calculated (Membrane Structures Association of Japan, 1993; Colman *et al.*, 2014). Different stress ratios therefore produce different shear moduli, and as such “*Accounting for shear at different biaxial stress states should be considered for accurate prediction of material behaviour*” (Colman *et al.*, 2014, p. 170). Therefore the shear modulus for comparison is calculated as the gradient between the maximum and minimum points on the deformation.

A frictional coefficient of 0.3 as used by Liu *et al.* (2004) is used for all fabrics and weaves. This is probably unrealistic, though extensive testing would be needed to derive the coefficients for different fabric types and any associated variation within these. This is outside of the scope of this project.

Initially a series of targets were defined as shown in Table 3-12 using the F1202 fabric geometry. Two sets of target points were used corresponding to the load at which the shear response was calculated. Other target points were left unused.

	Point 1	Point 2
E_{11} (target 1) (kN/m)	543	691
E_{22} (target 3) (kN/m)	502	628
v_{12} (target 2)	0.419	0.276
v_{21} (target 4)	0.386	0.252
G (target) (kN/m)	17.35	10.90
γ (degrees)	3	5
P_1 (kN/m)	10	20
P_2 (kN/m)	10	10
E_{11} (result 1) (kN/m)	545	690
E_{22} (result 3) (kN/m)	501	629
v_{12} (result 2)	0.419	0.277
v_{21} (result 4)	0.387	0.252
G (result) (kN/m)	17.34	10.90

Table 3-12: Initial targets and results for the design of shear properties

The targets are chosen arbitrarily to demonstrate the applicability of the model to any geometry or target set.

Variable	Geometry from which targets are calculated	Optimised geometry
Θ_1 (Rad)	0.101	0.146
Θ_2 (Rad)	0.180	0.141
L_1 (mm)	0.645	1.049
L_2 (mm)	1.082	0.662
r_1 (mm)	0.157	0.088
r_2 (mm)	0.106	0.160
E_1 (kN/m)	880	892
E_2 (kN/m)	810	773
E_k (kN/m)	37	43
A_1 (mm)	0.066	0.154
A_2 (mm)	0.197	0.094
w_1 (mm)	0.859	0.619
w_2 (mm)	1.044	1.090
v_k	0.3	0.3

Table 3-13: Initial and optimised geometry for shear target optimisation

The design process (optimisation) resolves to a solution, though as with the sawtooth only tests (§3.7.1) this has not found the original geometry from which the targets were obtained. This is not a failure of the methodology but a demonstration of the multiple possible solutions available for a single set of targets, which here are much reduced from the larger more constraining sets above.

Lastly it now becomes apparent that the effect of the coating dominates the response of the fabric to shear deformation (Figure 3-38) as predicted by Testa and Yu (1987, p. 1636) who state that *“resistance to shear deformation arises almost entirely from the*

3. Predictive model

coating". This presents a problem when considering the design of a fabric. Essentially the method must choose a fabric coating almost entirely based on the shear requirements.

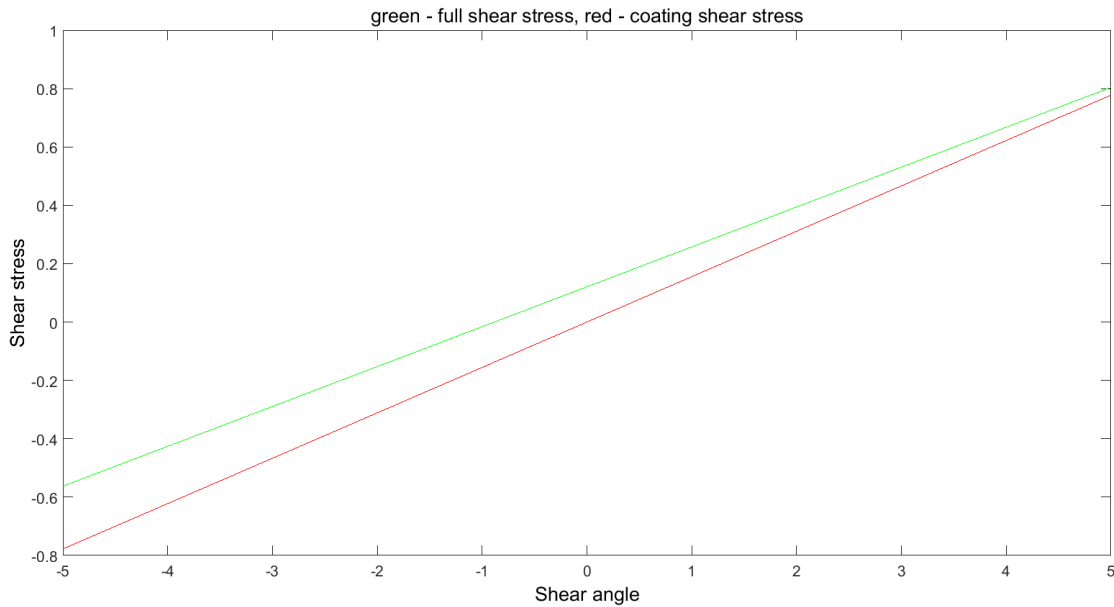


Figure 3-38: Comparison between coating only and coating and friction shear response (green-full shear response, red-coating only)

As such by selecting a coating the approximate value of the shear modulus can be defined using Equation 3-82. The problem with defining the coating in this fashion is that one of the nine geometric variables can no longer vary to the same degree.

$$G = \frac{E}{2(1 + \nu)}$$

Equation 3-82

Defining the shear characteristics therefore defines the shear stiffness.

3.7.3. Discussion of results

The model developed has been shown to work within the confines of a feasible solution. This will be tested further, used to analyse the variability of a fabric's response and its effect on real fabrics and compared to real fabric response surfaces in later chapters (§5.3).

The method developed offers close correlation between results for feasible targets. This good fidelity was predicted, as the optimisation equations were developed using the

sawtooth model, but demonstrates the utility of the method. The optimisation works by finding the solutions available from all possible response planes of the sawtooth model, and should eventually find a solution for targets that originally existed on this plane. This does, importantly, show that the method being employed to find the targets is working even if in some cases alternate solutions might be found.

Small amounts of error or inaccuracy between the produced and initial geometries in the test cases can be accounted for by considering that there might be some 'area' of viable solutions, however small, around the original solution. Alternatively increasing the required accuracy of the solution might reduce the error present in the calculation. Whilst the solution is found to a high degree of accuracy both the function value and the constraint function are rarely found to be zero at the proffered solution. This is a result of the use of an optimisation routine rather than finding an analytical solution. Where an analytical solution would give an exact value at the point of solution the optimisation routine only continues to the predefined tolerances.

The error in accuracy might have been predicted, but is, at this stage considered acceptable and allowable within the confines of the feasible solutions presented.

The shear component of the sawtooth optimisation model is not used further in this report because of the way using the shear design component largely selects the coating stiffness. As the coating's Poisson's ratio is fixed only the coating's Young's modulus affects the shear modulus significantly. Whilst how the component can be used has been demonstrated the actual usefulness of the component is therefore limited.

Further to this only one value of μ (the coefficient of friction between yarns at crossover) is available to the designer. The design of the fabric takes no account of how this value may vary for changing geometries, and work to account for this would be considerable and time consuming, well beyond the scope of this report similar to how the nonlinearity of yarn stiffness is overlooked (§3.5.4).

Lastly the shear stiffness generally used in industry is the gradient between the tips of the shear stress-angle graph, not the point shear used in this method. The method's use of the shear characteristics at a point will be more accurate than the interpolation of a line, however, such information could not be used in design and analysis packages.

3. Predictive model

Overall it must be concluded that whilst the shear design methodology can be used to design a fabric's shear stiffness its utility in further analysis is severely hampered, and it therefore will remain unused in further sections.

3.8. Conclusions

- Fabric mechanical properties can be accurately predicted from initial geometric properties by taking the derivative of the defining equations. These derivatives can then be used to design a bespoke architectural plane weave fabric for specific mechanical properties at prescribed loads.
- The accuracy of the optimisation method with regards to known feasible targets derived from the sawtooth model is excellent.
- The methodology is slower than hoped as the calculation of $\frac{\Delta \varepsilon_{1,2}}{\Delta \varepsilon_{2,1}}$ must be completed after each iteration. This also reduces the utility of the model by making further derivative calculations difficult. These are necessary for the development of the FORM methods discussed in the next chapter (§4).
- It has been demonstrated that for some targets multiple solutions exist and thus conversely it can be assumed that for other targets no solutions may exist (§3.7.2). The latter will be demonstrated in following chapters.
- Shear stiffness is dominated by the coating response (stiffness).

4. Variability and Robustness of Fabric Geometry and Constituent Parameters

4.1. Introduction

It can be understood intuitively that when the geometry or properties of a fabric are changed the response of the fabric to loads will also alter. This is seen in the different responses of alternative fabric types, or observed in models, by changing the input parameters. However, little investigation has been carried out into the effect of the variation that exists in an individual fabric properties on its response (§2.5).

This chapter first describes the effect of variation of different properties by using both Monte Carlo simulations and First Order Reliability Method (FORM) analysis. It also demonstrates that multiple solutions exist for various targets, and shows that the effect of varying different fabric properties is dependent on the property and the target considered. These analyses are also used to show how the previously developed model can be adapted to demonstrate the probability of a fabric's response failing certain performance criteria, i.e. that the fabric must respond to within 1% of a specified target 99% of the time. Lastly, the equations developed in the previous chapter (§3.4.3) are used to show how FORM may be used to optimise a fabric geometry to minimise its susceptibility to variation (or increase its robustness to variability).

4.2. Aim

To derive a method based on Monte Carlo simulations and FORM to simulate the effect of variation in geometry on the tensile response of plain weave architectural fabrics to inform a method to enable the design of fabrics that minimises sensitivities to variations in their constituent properties.

4.3. Objectives

- Produce methodologies for the analysis of the effect of material variability on the mechanical properties of a fabric using the FORM and Monte Carlo methods.
- Compare the FORM and Monte Carlo methodology results.
- Analyse how variation in fabric material properties affects the mechanical properties of a fabric.
- Produce a methodology to maximise the robustness of a fabric with respect to variation in its constituent parameters.
- Discuss the possible applications of the work to the design of fabric structures.

4.4. Chapter overview

The variability and robustness of fabric mechanical properties due to variation in geometry, yarn and coating stiffness are reviewed in this chapter. The chapter further presents:

- A methodology for the predictive simulation of the effect of variability on the mechanical properties of a fabric using the FORM and Monte Carlo methods.
- A discussion of how variation in a single property effects the mechanical properties of the fabric.
- A method to maximise the robustness of a fabric's design by refining its geometry, yarn, and coating properties.
- Data on the variability of the geometry of fabrics, and how they can be considered normally distributed.
- Simulations of the variation in response of fabrics to changes in their constituent properties.

4.5. Initial Assumptions

Distributions for the uncertain variables $\theta_{1,2}$ $L_{1,2}$ $r_{1,2}$ $E_{1,2}$ E_k (§3.4) are needed to analyse the effect of variation in these properties on the tensile response of fabrics.

The coating Poisson's ratio is not a design variable in the design process in the previous chapter (§3.4) and is considered constant (fixed) in this chapter also. The difficulty in specifying the Poisson's ratio of a coating, or analysing its variation in test specimens, puts a detailed analysis of this outside the scope of this thesis, as it is an entire component of the field of material science. Only three values of Poisson's ratio are identified in the literature review (§2.2.7.3), and whilst it is possible that some change in these may be possible with the addition of additives, no detailed information on how this might be achieved has been identified. The Poisson's ratio of a coating is defined at the point the type of coating is selected.

Statistical data regarding the distribution of the variables is discussed in terms of the mean, standard deviation, and coefficient of variation. The sample standard deviation and mean (Equation 4-2) differ from the population standard deviation and mean (Equation 4-1) in that they are derived from samples that have been subject to statistical analysis, and do not consider the entire population of possible results.

$$\begin{aligned} &\mu_{\theta_{1,2}} \mu_{L_{1,2}} \mu_{r_{1,2}} \mu_{E_{1,2}} \mu_{E_k} \\ &\sigma_{\theta_{1,2}} \sigma_{L_{1,2}} \sigma_{r_{1,2}} \sigma_{E_{1,2}} \sigma_{E_k} \\ &\sigma = C_v \mu \end{aligned}$$

Equation 4-1

where μ is the population mean, σ is the population standard deviation, and C_v is the coefficient of variation which relates the standard deviation to the mean. E.g. μ_{θ_1} defines the population mean of the out-of-plane angle of the warp yarn from the plane of the fabric.

$$\begin{aligned} &\bar{\theta}_{1,2} \bar{L}_{1,2} \bar{r}_{1,2} \bar{E}_{1,2} \bar{E}_k \\ &s_{\theta_{1,2}} s_{L_{1,2}} s_{r_{1,2}} s_{E_{1,2}} s_{E_k} \\ &s = C_v \bar{X} \end{aligned}$$

Equation 4-2

4. Variability and robustness

where \bar{X} is the sample mean, and s is the sample standard deviation.

Properties are considered to be normal and not skewed unless shown otherwise.

4.6. Normally distributed data

The normal density function for a random variable x is given by Equation 4-3 and an example of normally distributed data is shown in Figure 4-1 (Ayyub and McCuen, 1997):

$$f_x(x) = \frac{1}{\sigma\sqrt{2\pi}} \exp\left(-\frac{1}{2}\left[\frac{x-\mu}{\sigma}\right]^2\right) \quad -\infty < x < \infty \quad \text{Equation 4-3}$$

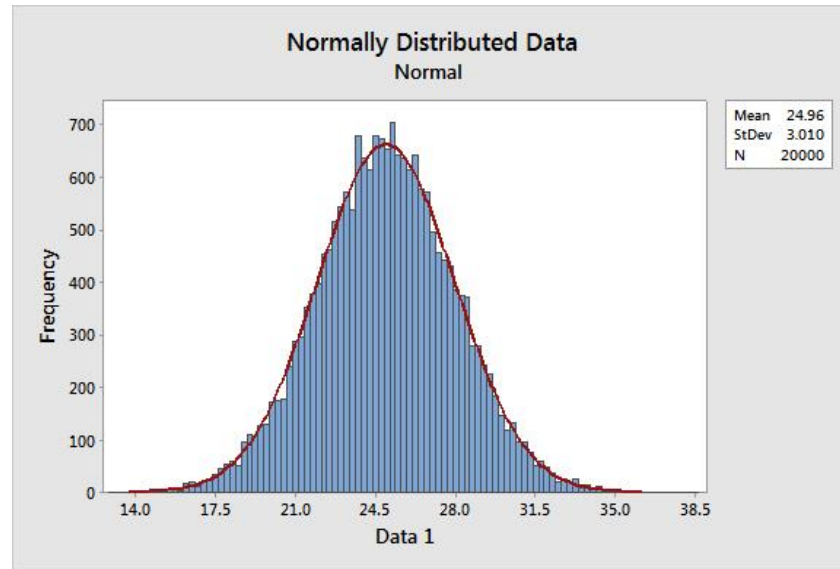


Figure 4-1: Normal Distribution (Mean = 24.96, standard deviation = 3.010)

Data is considered to be 'normally distributed' when it follows the normal distribution (Equation 4-3). However the degree of fit can vary, and is often described in terms of hypothesis testing in which an initial hypothesis as to a data set's distribution is made (i.e. normally distributed) which is then tested. The data used to produce Figure 4-1 can be represented in a probability plot (Figure 4-2) and a hypothesis test carried out on it to discover if it is indeed normally distributed. Two outer red lines denote a 95% confidence interval for the data (very close together with this highly normal data set, but clearly indicated in Figure 4-3) with the exact normal distribution for a data set sitting on the middle red line. For this data set the P-value (probability) is greater than 0.05 (the limit) and as such the hypothesis that the data is normally distributed can be accepted. Non-normal data can also be plotted in the same fashion, but will appear to be nonlinear in a similar plot.

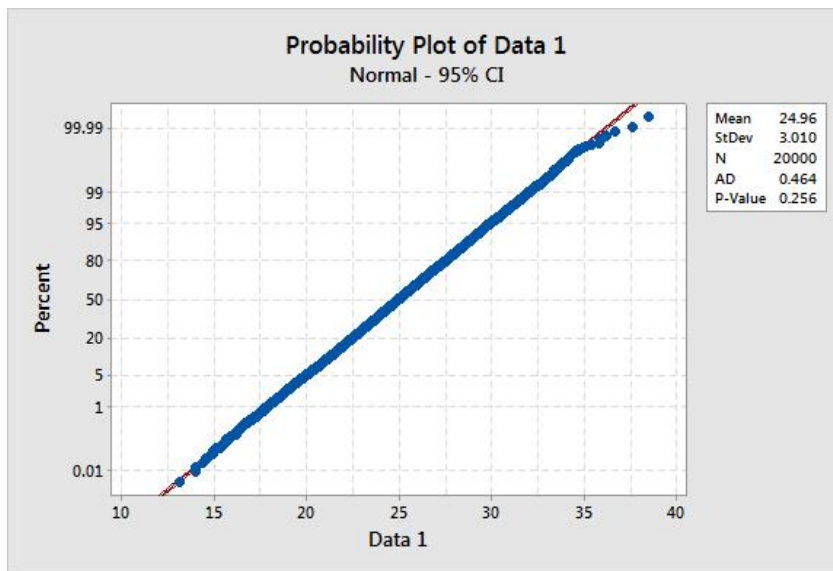


Figure 4-2: Probability plot of data used in Figure 4-1

To demonstrate the validity of using the normal distribution to represent fabric geometric variability, statistical data from an F1202 PVC coated polyester fabric was considered. The data was produced by Colman (2013) who measured the geometries of a wide range of fabrics. The variation in the amplitude of the warp yarn (Figure 4-3), the weft yarn thickness (Figure 4-4), and the warp out of plane angle (Figure 4-5) are shown below. Other distributions of the fabric's geometry can be found in the appendix (§A.4). Whilst the fit to the normal distribution is not perfect the P-value is consistently greater than 0.05, suggesting that the data can be considered normal. As such it is accepted that generally an untested (designed or unknown) fabric's geometric properties can be considered to be normally distributed.

Properties that are found to be non-normal in the variation analysis could be transformed to normal space using well understood and recognised transformations.

Whilst other fabrics may show better or worse fits a single assumption of a distribution, i.e. normality, must be made at this stage to allow for the model to continue to be predictive. It is impossible to analyse the distribution of the properties of a fabric that is to be designed, or has not been created, although if required other distributions could be used.

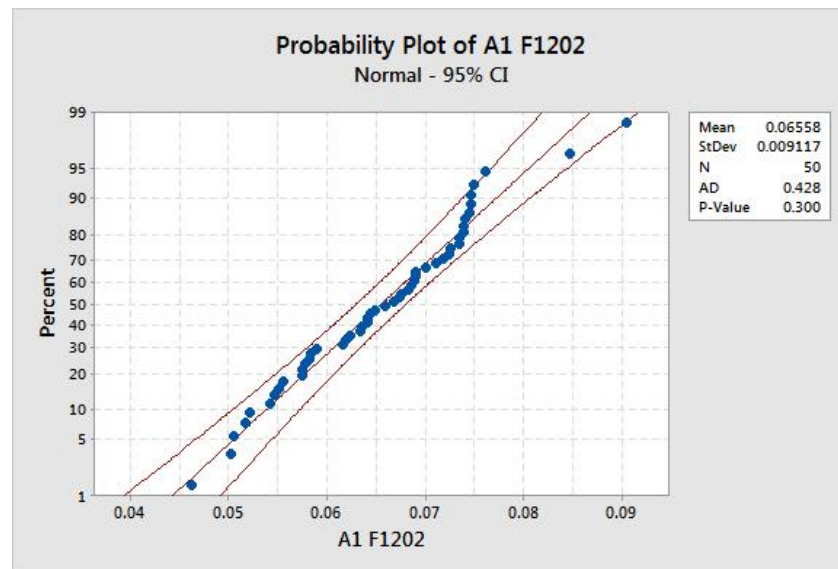


Figure 4-3: Probability plot of warp yarn amplitudes for an F1202 fabric

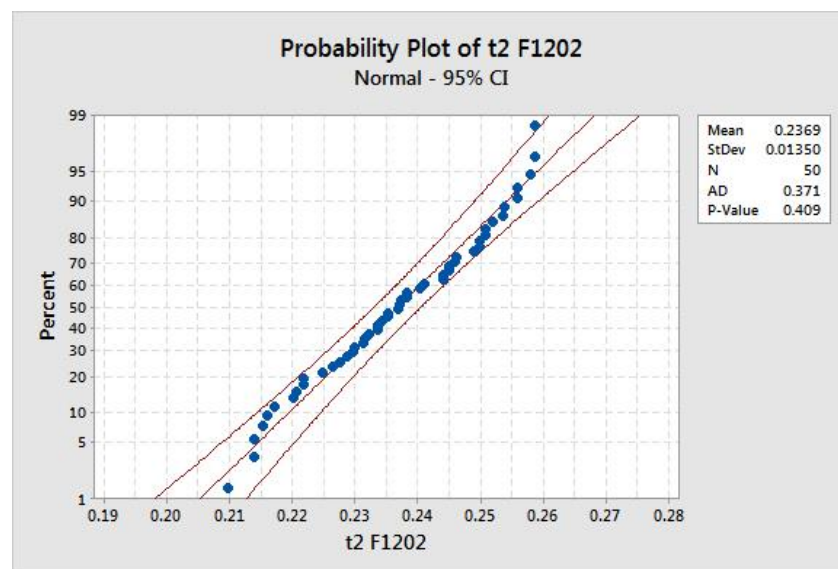


Figure 4-4: Probability plot of weft yarn thicknesses for an F1202 fabric

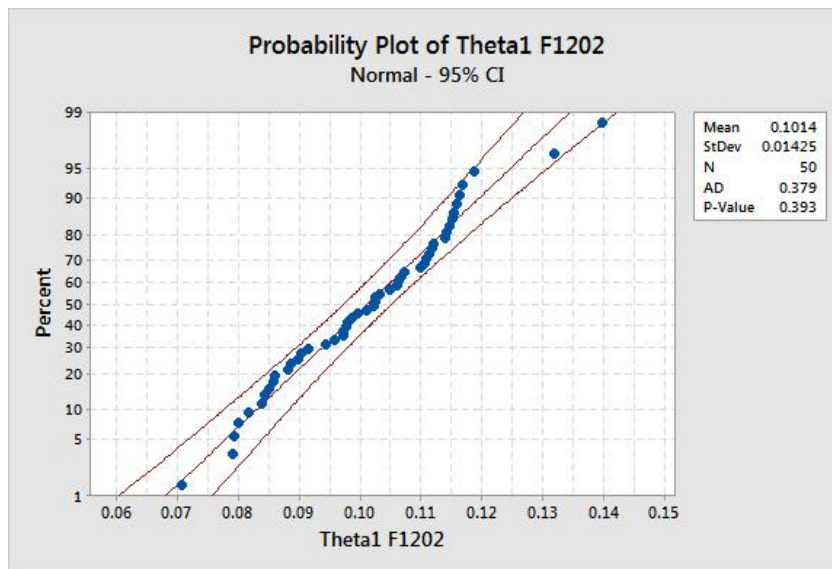


Figure 4-5: Probability plot of warp yarn out of plane angles for an F1202 fabric

The distributions show some variation away from the normal distribution as the data presented in Figure 4-3, Figure 4-4, and Figure 4-5 is not perfectly linear. Some deviation towards a linear distribution can be noted in the yarn thickness (t_1) and yarn angle (A_1) plots (Figure 4-3 and Figure 4-4) although both plots are still considered normal as the P-value is greater than 0.05. Linearly distributed data tested in this fashion appears as an s-curve, shown in Figure 4-6 (which shows 200 artificially generated linearly distributed data points between 0 and 1). Figure 4-6 also shows a situation where the data cannot be considered normally distributed as the P-value is less than 0.05.

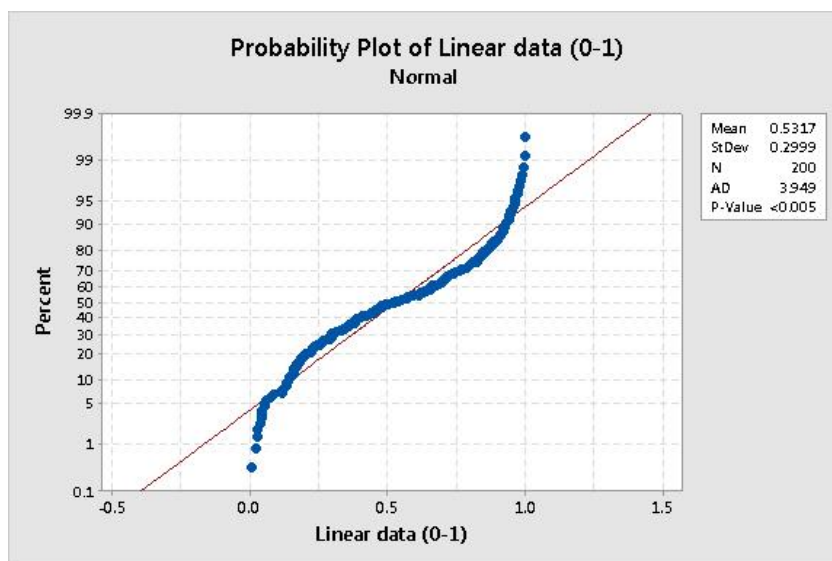


Figure 4-6: Linearly distributed data tested for normality (200 data points linearly distributed between 0 and 1)

4. Variability and robustness

There exists a special case of the normal distribution where the mean is zero and the standard deviation is one. This is referred to as the standard normal distribution and is important in that it is used in many of the following sections as an invariant measure. The use of invariant measures allows for the comparison of different data sets within a single simulation where the mean, standard deviation, or both might be different. Melchers (1999, p. 97) describes how a “*lack of invariance*” can occur where resistances and loads vary between different situations or “*because there are different ways in which the relationships between resistances and loads may be defined*”. As such it is desirable for a measure to be ‘invariant’ such that comparisons can be drawn. The first step to achieve this is “*to transform all variables to their standard normal form $N(0,1)$* ” (Melchers, 1999, p. 97).

The Hasofer-Lind transformation (Equation 4-4) can be used to convert normally distributed data to standard normal space where “*the joint probability density function $f_Y(y)$ is the standardised multivariate normal [...]; thus many well-known properties of this distribution can be applied*” (Melchers, 1999, p. 97). Melchers (1999) reproduces the equation from the work of Hasofer and Lind (1974).

$$Y_i = \frac{X_i - \mu_{X_i}}{\sigma_{X_i}}$$

Equation 4-4

4.7. Monte Carlo Methodology:

“The Monte Carlo method provides approximate solutions to a variety of mathematical problems by performing statistical sampling experiments” (Fishman, 1997, p. 1). The accuracy of this approximation increases with the number of points sampled, and it is also possible to vary the sampling methodology to increase the speed of the method by attempting to focus the sampled area to the failure plane, i.e with the use of ‘importance sampling’ (Melchers, 1999). However, the method used in this work is a ‘Coarse’ or ‘crude’ Monte Carlo method which is used to sample the entire space of the possible results as advanced Monte Carlo methods are outside of the scope of this thesis.

Using a coarse method has a specific advantage in this instance: Once a Monte Carlo analysis is completed, and the results of all the simulations have been obtained, the function values can be interrogated repeatedly to analyse different inequalities. Advanced (non-coarse) Monte Carlo simulations can only ever be used to interrogate results for a single inequality.

4.7.1. Methodology

The method used is that set out by Melchers (1999), with some small modifications to allow for its reproduction in MATLAB, and the use of fabric data.

For each variable two (linearly) randomly distributed numbers between 0 and 1 (r_1 and r_2) are selected. These are then used to create a *“pair of ‘exact’ independent standardised normal variates”*, u_1 and u_2 (Equation 4-5) (Box and Muller, 1958; Melchers, 1999, p. 68), such that,

$$r_1 = \text{random number 1; } 0 \leq r_1 \leq 1$$

$$r_2 = \text{random number 2; } 0 \leq r_2 \leq 1$$

$$u_1 = \sqrt{-2\ln(r_1)} \sin 2\pi r_2$$

$$u_2 = \sqrt{-2\ln(r_1)} \cos 2\pi r_2$$

Equation 4-5

These (Equation 4-5) are then be used to produce a pair of normally distributed data points for any variable where the standard deviation and the mean are known (Equation 4-6), using,

$$x_i = u_{1,2} \cdot \sigma_i + \mu_i \quad \text{Equation 4-6}$$

Equation 4-6 is applied for each of the nine basic variables listed in Equation 4-1 to give pairs of normal variates for each of the probabilistic variables considered in the unit cell.

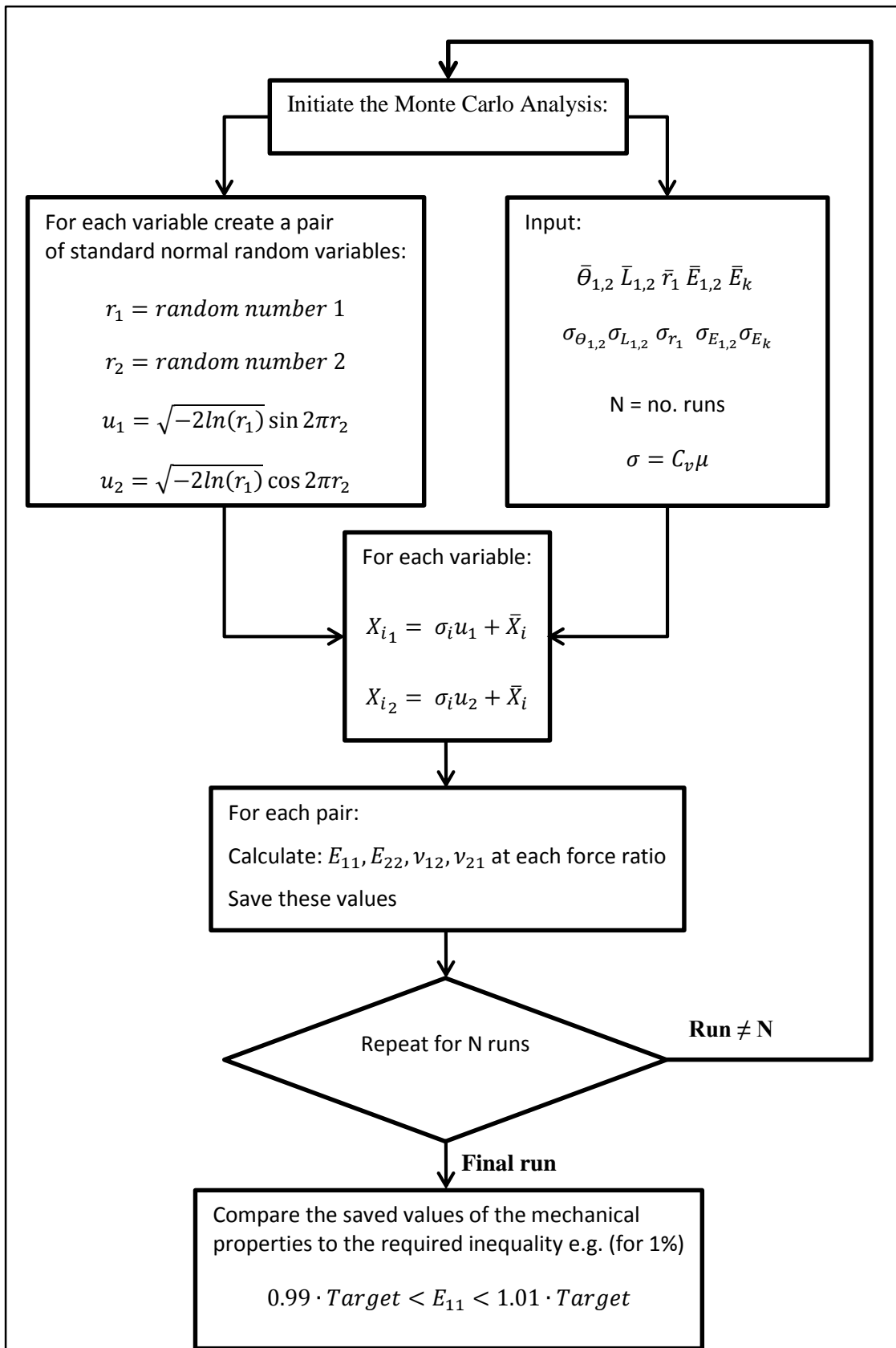
Varying the nine basic variables ($\theta_{1,2}$, $L_{1,2}$, $r_{1,2}$, $E_{1,2}$, E_k) produces a variation in the mechanical properties of the fabric (E_{11} , E_{22} , ν_{12} , and ν_{21}). It is therefore necessary to describe an inequality to define within what bounds a fabric might be required to perform, and to what extent the fabric might deviate from this. For instance 99% of a particular batch of fabric might be required to respond to within 1% of its published Young's Modulus at a certain level of stress such that Equation 4-7 holds.

$$P(E_{11,target} \cdot 0.99 < E_{11,result} < E_{11,target} \cdot 1.01) > 0.99 \quad \text{Equation 4-7}$$

Alternatively the probability of one of the mechanical properties might be needed where no results can be less than 5% of the target (Equation 4-8):

$$P(Target \cdot 0.95 < Result) = 1.0 \quad \text{Equation 4-8}$$

The data from a crude Monte Carlo simulation can be repeatedly interrogated to give the probability of a result satisfying different inequalities. The methodology used in the Monte Carlo analysis is laid out in Figure 4-7.

Figure 4-7: Method for the comparison of results to the failure criteria $0.99 \cdot \text{Target} < E_{11} < 1.01 \cdot \text{Target}$

4. Variability and robustness

The number of results required to meet a solution is checked by considering the variation in the mean of the results as the simulations progress. Figure 4-8 shows how the mean of the results varies as the number of iterations increases, whilst the mean and standard deviation can also be examined at intervals (Figure 4-9 and Figure 4-10). From these figures it is clear that the results for the test shown have converged to a solution. This simulation used arbitrary values of the coefficient of variation for each variable ($CoV = 0.1$), and calculated the probability that the resulting value of E_{11} would be greater than $0.9 \times E_{11,Target}$. Therefore the probability of failure indicated is the proportion of tests that did not satisfy this inequality.

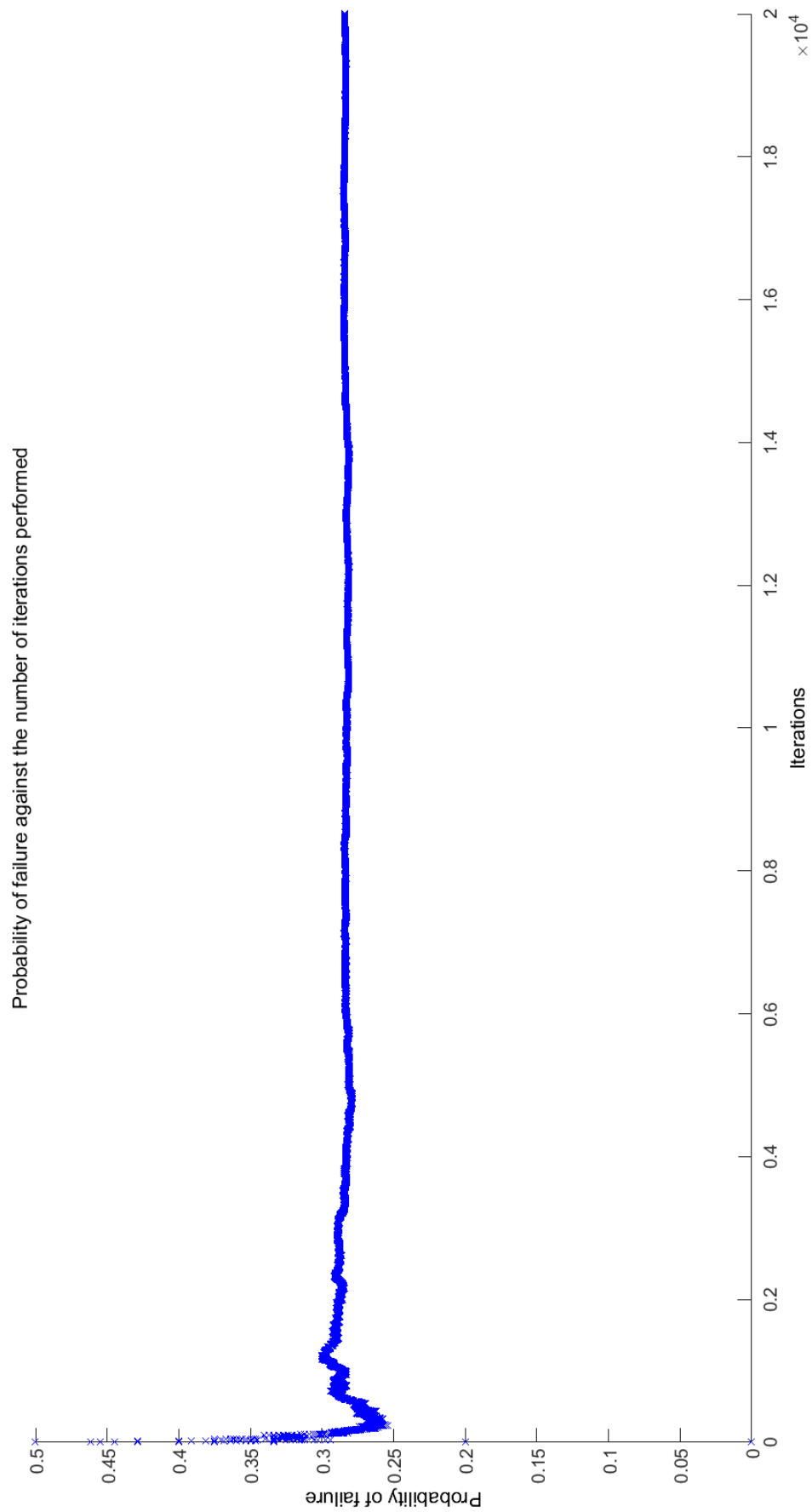


Figure 4-8: Convergence of Monte Carlo probability of failure

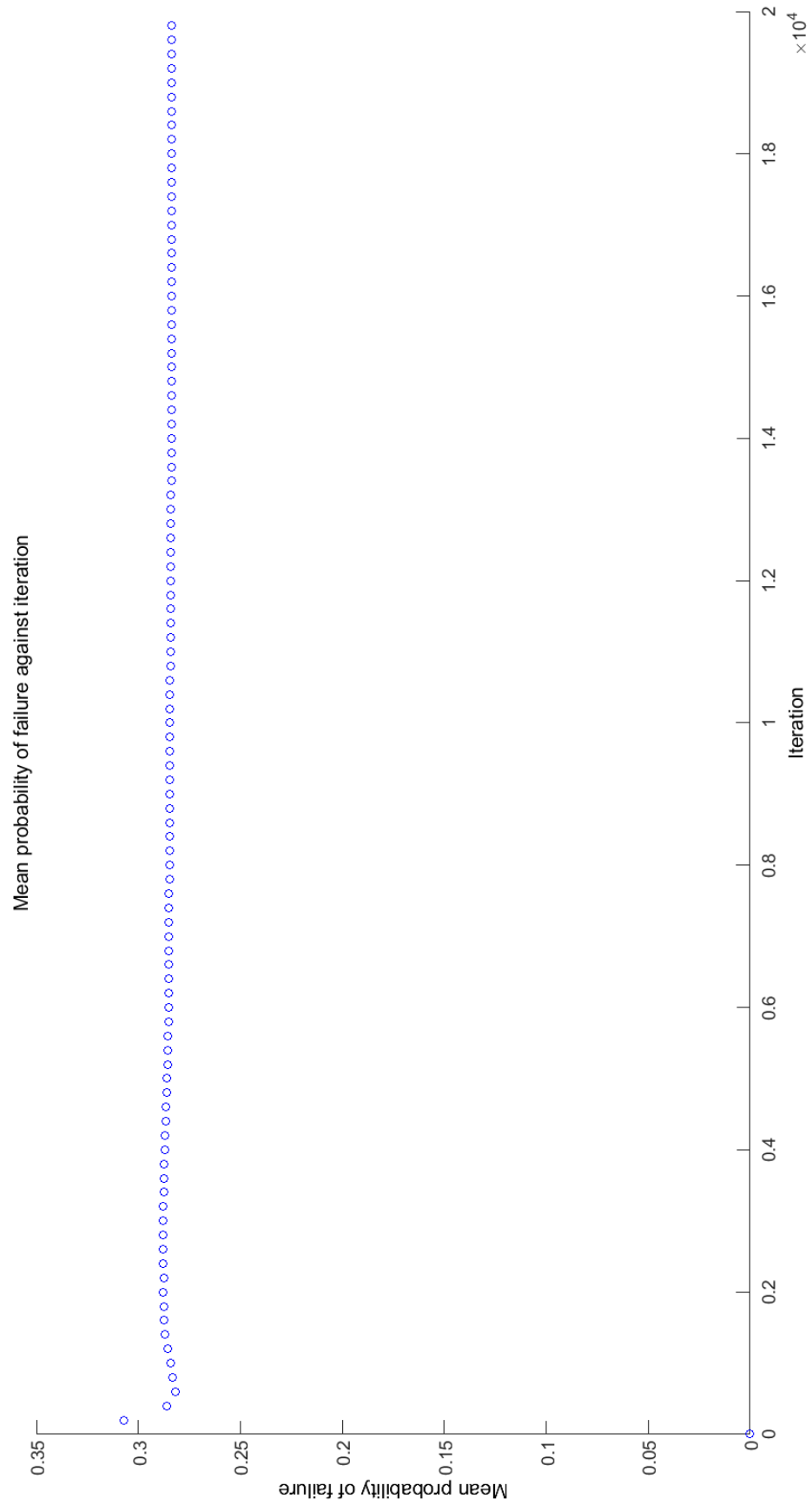


Figure 4-9: Mean probability of failure at increasing intervals

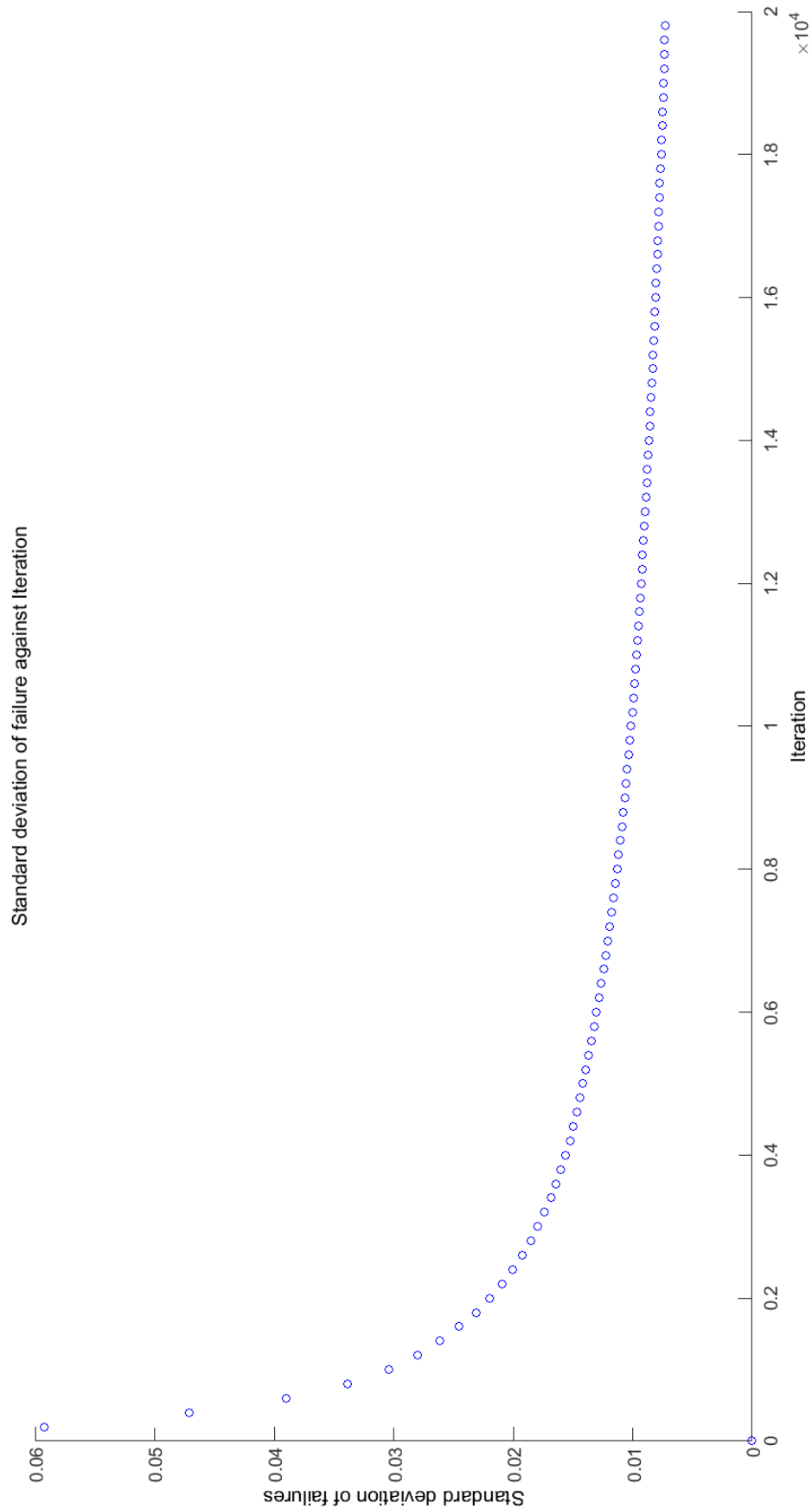


Figure 4-10: Mean standard deviation of failure at increasing intervals

In the results above both the mean and mean standard deviations of the data appear to have approached asymptotes after 20000 iterations, split into batches of 200 calculations. The mean standard deviation of failure gives a measure of the average of the standard deviations of failure at a point, looking at all the batches of 200 calculations. The high value of the probability of failure (approximately 30%) is indicative of an artificially high value of the coefficient of variation of each variable, when compared to the inequality used in the simulations.

4.7.2. Constraint compliant Monte Carlo

Using independently generated variables causes constraint violation during the simulation process. The randomly selected variables (amplitude, length, and radius) do not necessarily satisfy the equilibrium constraint. The interdependence of the first six variables causes error in the calculation of the probability of failure. In short, by allowing all variables to independently vary the equilibrium constraints are not being satisfied, leading to erroneous results. This led to the creation of the following statements:

- Any yarn or coating stiffness may be chosen, these are independent with relation to the equilibrium equation.
- Any three dependant variables ($\theta_{1,2}$, $L_{1,2}$, $r_{1,2}$) can be chosen using their statistical information and the normal distribution.
- Two further dependant variables ($\theta_{1,2}$, $L_{1,2}$, $r_{1,2}$) might be chosen using their statistical information and the normal distribution, but must be checked to ensure they do not violate the equilibrium constraint. In this case only where very large deviations from the mean are predicted is this necessary, but should always be checked for.
- The final variable is defined by the others.

The Monte Carlo analysis as presented includes three truly random dependant variables, θ_1 , θ_2 , and L_1 . The two partially random dependant variables are L_2 , and r_1 , and the fully dependant variable is r_2 , to allow the Monte Carlo algorithm to calculate probabilities whilst ensuring compliance with physical based constraints. However, the routine is designed to allow for any choice of variables to be placed in each category.

Variables that must be checked for compliance rarely violate the equilibrium constraints. This is because a very large variation from any originally valid fabric would be necessary

4. Variability and robustness

to prevent these values following a normal distribution. As such a check is applied, and where these variables do violate the equilibrium constraint the 'simulation' is abandoned, as infeasible. In practice, using reasonable variability data such as that produced from tests almost never generates such points.

Lastly, r_2 is defined as a function of the other variables (Equation 4-9), with its distribution defined by the interaction of the other variables in the equilibrium equation, where

$$r_2 = L_1 \tan \theta_1 + L_2 \tan \theta_2 - r_1 \quad \text{Equation 4-9}$$

This means that all the variables relating to the geometry of the fabric are related to each other by the value of r_2 . r_2 is therefore a deterministic variable that can be calculated by considering the variables $\theta_{1,2}$ $L_{1,2}$ r_1 , but does not appear within the objective function.

The objective function is therefore redefined as:

$$f(\theta_{1,2} L_{1,2} r_1 E_{1,2} E_k)$$

Equation 4-10

The Monte Carlo routine was then carried out as described in Figure 4-11.

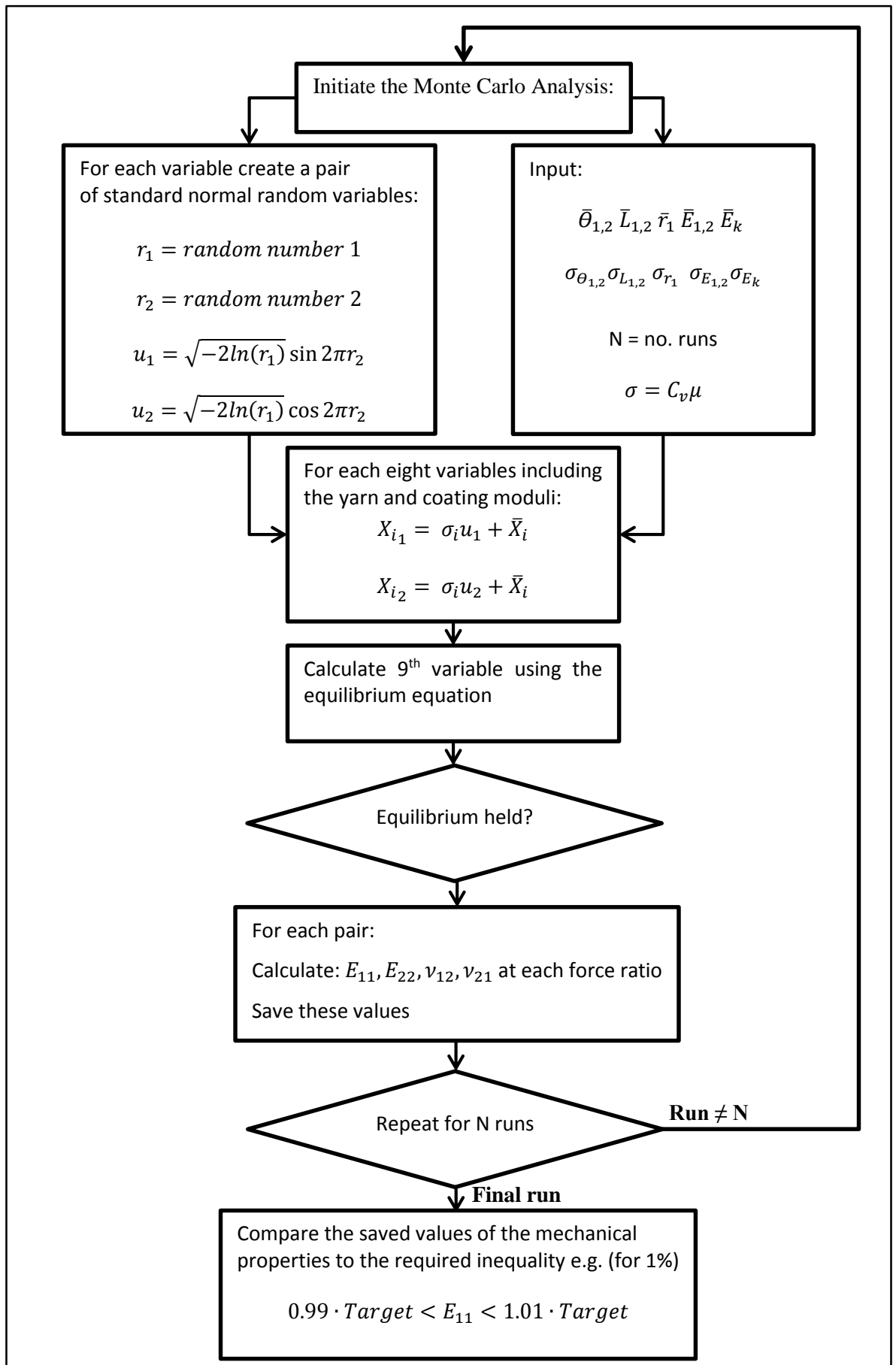


Figure 4-11: Method of Monte Carlo implementation

4.7.3. Analysis and discussion

The method presented (§4.7.1) allows for the analysis of both the probability a fabric will not react as predicted given variation in the geometric properties, and the analysis of how variation in a single variable affects a property. Within this section, assumed values of variation are used to demonstrate the effect of altering properties. Using assumed values of variation allows comparisons to be drawn between the effect of different amounts of variation that might be experienced in a fabric property without changing the fabric, and hence the relationship. Were only real values of fabric property variation used the effect of altering the property distribution could not be analysed. In the following discussion the geometry of a PVC coated polyester fabric (F1202) is used to demonstrate the effect of varying fabric geometry.

The probability of failure against feasible targets was analysed using the Monte Carlo method. This is carried out for a number of failure criteria detailed in Table 4-1 with relation to the inequalities detailed below (Equation 4-11). Each Monte Carlo analysis consists of 20,000 simulations, at the end of which six inequalities are tested for: that E_{11} should be greater than 90% or 99% of the target for E_{11} , that E_{11} should be less than 110% or 101% of the target for E_{11} , and that E_{11} should be between 99% and 101% or between 90% and 110% of the target value for E_{11} . The results of the simulations are tabulated in Table 4-1. Limiting variation to particular pairs of variables allows for the inspection of the effect of varying a particular property such as the out of plane angle on the value of E_{11} . The out of plane angle was shown to have the greatest effect on E_{11} in the tests carried out in Table 4-1.

Inequality 1:

$$(1 - x) \cdot Target < E_{11}$$

Inequality 2:

$$(1 - x) \cdot Target < E_{11} < (1 + x) \cdot Target$$

Inequality 3:

$$E_{11} < (1 + x) \cdot Target$$

Equation 4-11

where 'x' is the allowable deviation from the target (i.e. $x = 1\%, 2\%, 5\%, 10\%$).

Variation in unit cell properties (Cv)	Probability of not achieving inequality (P_f) of E_{11}		
	$0.9 \cdot E_{\text{target}} < E_{11}$	$0.9 \cdot E_{\text{target}} < E_{11} < 1.1 \cdot E_{\text{target}}$	$1.1 \cdot E_{\text{target}} > E_{11}$
$\Theta_{1,2}$ Cv = 0.1	0.040	0.059	0.099
$L_{1,2}$ Cv = 0.1	0.000	0.041	0.041
$E_{1,2}$ Cv = 0.1	0.050	0.030	0.081
All variables, Cv = 0.1	0.122	0.164	0.286
$\Theta_{1,2}$ Cv = 0.01	0.000	0.000	0.000
$L_{1,2}$ Cv = 0.01	0.000	0.000	0.000
$E_{1,2}$ Cv = 0.01	0.000	0.000	0.000
All variables, Cv = 0.01	0.000	0.000	0.000
	$0.99 \cdot E_{\text{target}} < E_{11}$	$0.99 \cdot E_{\text{target}} < E_{11} < 1.01 \cdot E_{\text{target}}$	$1.01 \cdot E_{\text{target}} > E_{11}$
$\Theta_{1,2}$ Cv = 0.1	0.437	0.871	0.433
$L_{1,2}$ Cv = 0.1	0.408	0.828	0.420
$E_{1,2}$ Cv = 0.1	0.433	0.857	0.424
All variables, Cv = 0.1	0.453	0.916	0.463
$\Theta_{1,2}$ Cv = 0.01	0.047	0.098	0.052
$L_{1,2}$ Cv = 0.01	0.012	0.029	0.018
$E_{1,2}$ Cv = 0.01	0.036	0.072	0.036
All variables, Cv = 0.01	0.141	0.291	0.150

Table 4-1: Monte Carlo predicted probability of failure at different failure criteria for feasible targets for an F1202 fabric (10000 runs = 20000 data sets)

As might be predicted where the failure criteria is higher a greater proportion of tests 'pass' reducing the probability of failure, and where the variation is lower the probability of failure is correspondingly low.

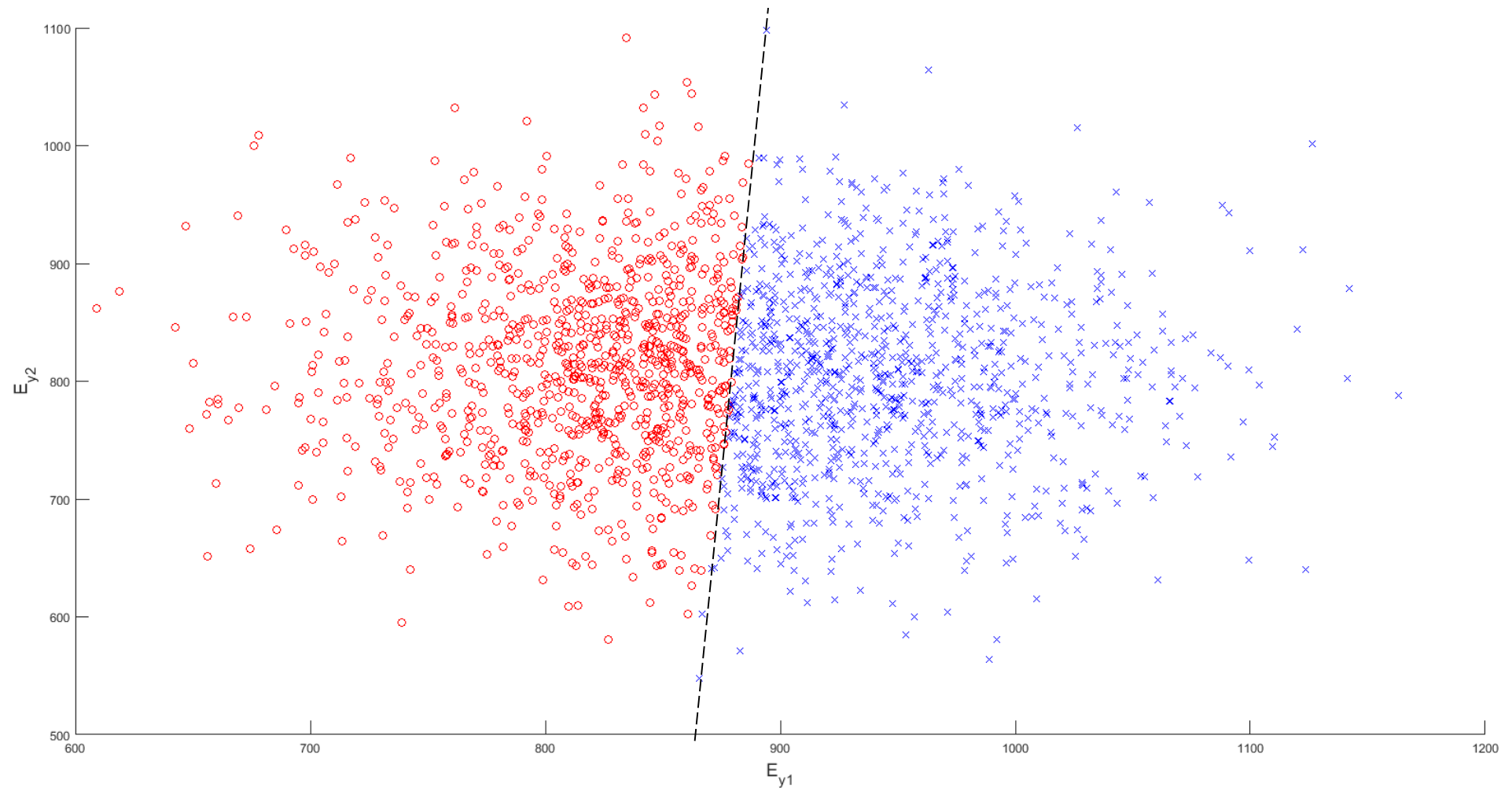


Figure 4-12: Monte Carlo results where only E_{y1} and E_{y2} are considered to vary with a coefficient of variation of 0.1 for the inequality $0.95Targ < E_{11}$ (red = failed, blue = success)

4. Variability and robustness

The line delineating failed and passed tests is found to be approximately straight (Figure 4-12, in which the red points are failed and the blue points have satisfied the inequality $0.95 E_{\text{Target}} < E_{11}$). The gradient of the delineating line provides information on the relative importance of the two different properties under consideration in determining the point of failure. Were the line to be at 45 degrees to either axis each property would have an equal effect on the point of failure. A curve would suggest that the effect is changing as the variables values change. The variable to which a particular inequality is most sensitive will be shown as the variable where the least variation in that variable causes greatest change to the result.

It is possible to begin to consider the sensitivities of the unit cell variables with relation to the Monte Carlo method. The change each variable causes with relation to a target value is considered, and then graphically displayed (Figure 4-13 and Figure 4-14). Figure 4-13 and Figure 4-14 show the effect of variation in one or two geometric properties on the value of E_{11} . The ‘tests’ described on the x-axis relate to the variables that are allowed to vary during a particular simulation. The variables varied in a ‘test’ can be found by relating the test number to row and column in Table 4-2. For instance, ‘test 38’ considered the variation of r_1 and E_2 .

Test	θ_1	θ_2	L_1	L_2	r_1	r_2	E_1	E_2	E_k
θ_1	1	-	-	-	-	-	-	-	-
θ_2	10	2	-	-	-	-	-	-	-
L_1	11	18	3	-	-	-	-	-	-
L_2	12	19	25	4	-	-	-	-	-
r_1	13	20	26	31	5	-	-	-	-
r_2	14	21	27	32	36	6	-	-	-
E_1	15	22	28	33	37	40	7	-	-
E_2	16	23	29	34	38	41	43	8	-
E_k	17	24	30	35	39	42	44	45	9

Table 4-2: Test definition for Figure 4-13 and Figure 4-14

From these simulations it is possible to observe the importance of changes in values, and consider how a reduction in the variability of one particular value might improve the robustness of an entire fabric. Additionally a variation in physical layout or geometry

4. Variability and robustness

might affect and improve the sensitivity of the fabric. The variation noted in pairs of tests 1 and 14, 2 and 21, 3 and 27 etc. is the same because the value of r_2 does not affect the calculation of the stiffness being considered, as it is defined by the other properties.

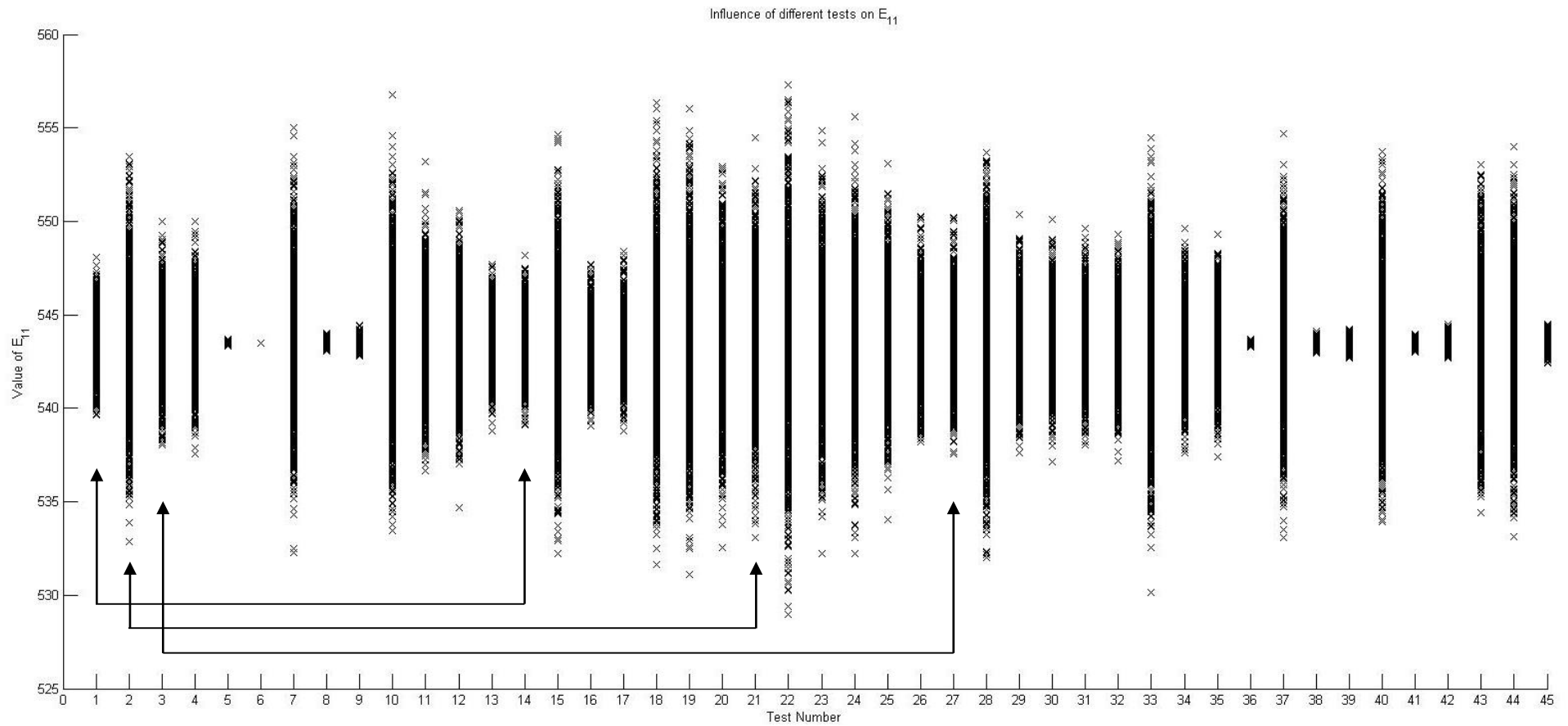


Figure 4-13: Sensitivity of E_{11} to variation in unit cell parameters ($C_v = 0.01$) for 'test' description see Table 4-2

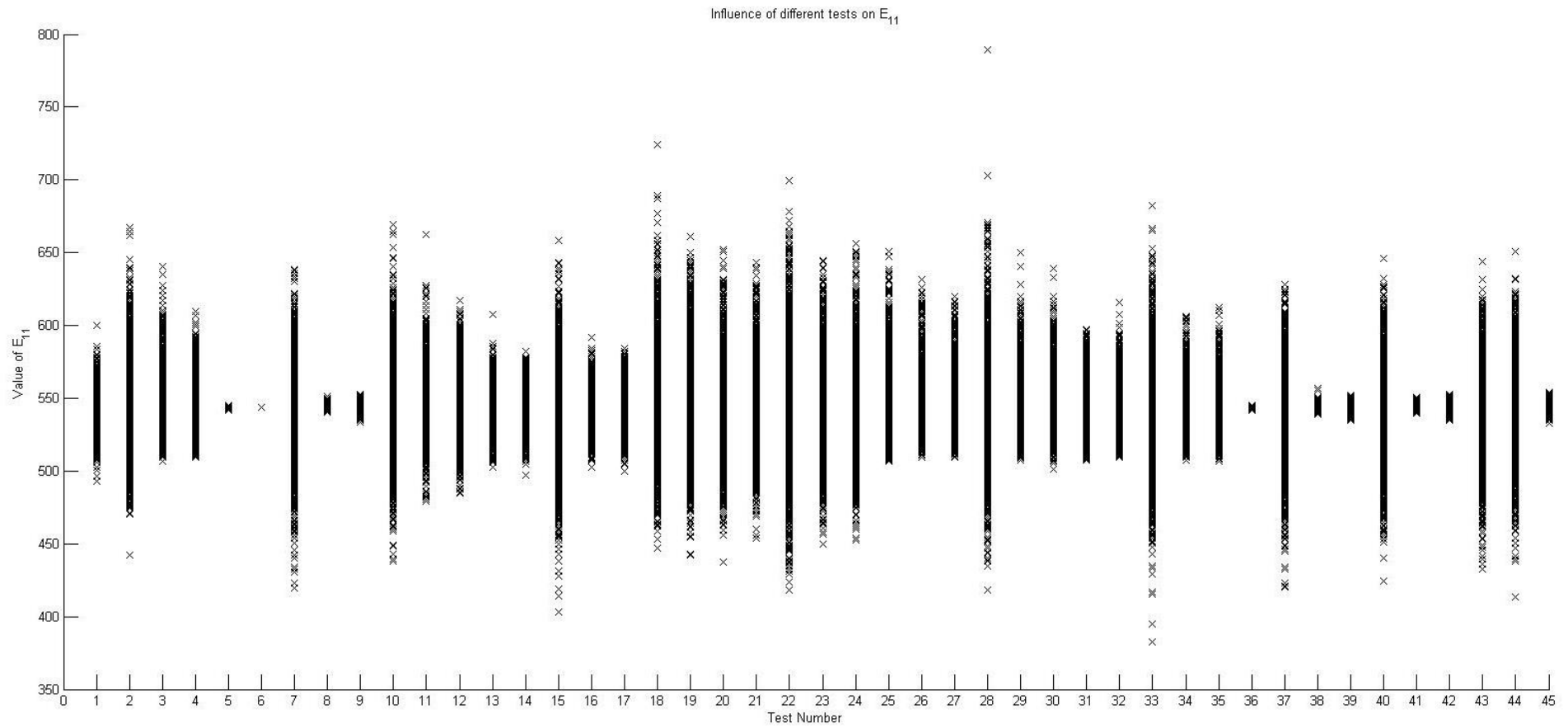


Figure 4-14: Sensitivity of E_{11} to variation in unit cell parameters ($C_v = 0.1$) for 'test' description see Table 4-2

4. Variability and robustness

Figure 4-13 and Figure 4-14 are plotted on different scales to ensure comparisons between 'tests' are possible. All the data in Figure 4-13 is normally distributed with the mean centred on the target value of E_{11} . The greatest variation in E_{11} is experienced during test 22, which considers variation in E_{y1} and θ_2 . E_{y1} is regularly associated with higher variation in E_{11} in the different simulations. The inclusion of r_2 does not produce an increase in the sensitivity of E_{11} .

Figure 4-14 continues to show that the mean of the calculated values of E_{11} is the target for the value of E_{11} (tests carried out on the data set confirm this). However, it is noticeable from the distributions that some of the simulations (using larger variations) appear to be non-normal as the data points are not evenly distributed around the mean. A number of the 'tests' are normal, such as 'test 14'. However 'test 3' amongst others shows non-normal distribution (Figure 4-15).

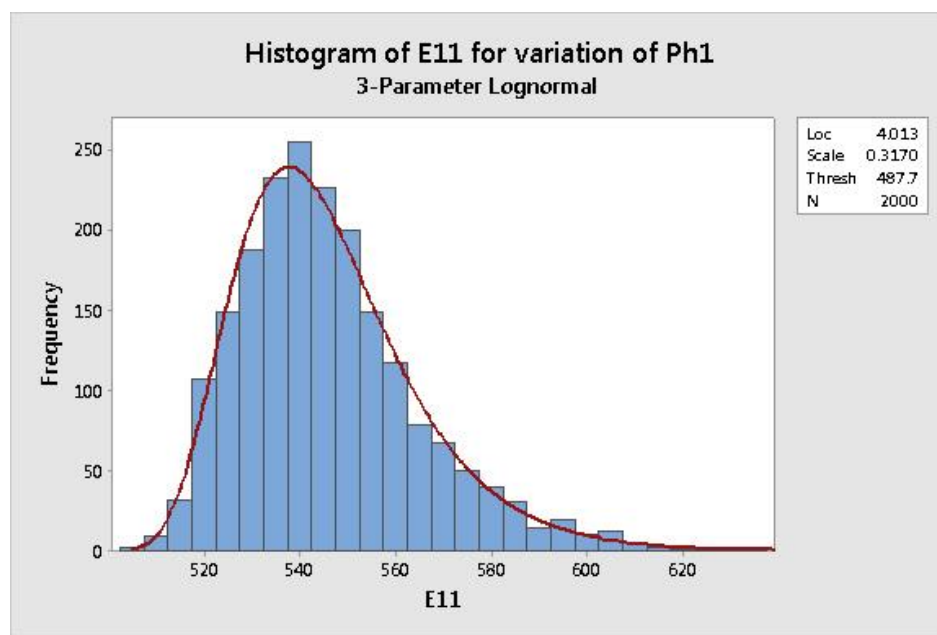


Figure 4-15: Histogram and Normal fit of 'test 3' data

The histogram (Figure 4-15) shows how the data is truncated at lower values of E_{11} . The introduction of the equilibrium equations to the Monte Carlo analysis may therefore be restricting complete normal behaviour across the entire data set where larger variation is present. This pattern is not repeated at lower values of variation. Real variation in the values of fabric geometries varies between a coefficient of variation of 0.125 and 0.011 (F1202). This degree of variation is not common across all fabric types. The variation observed in the B18089 fabric is at most 0.062. It is beyond the scope of this thesis to

4. Variability and robustness

create a predictive model that can predict the distribution a Monte Carlo test will produce at this time. A combination of normally distributed data should produce a normally distributed result (Melchers, 1999). However, the constraints on the function may be impairing this. A distribution must be selected without prior detailed knowledge of the fabric property under consideration. Whilst it is necessary to consider the implications of this it should not affect the usefulness of the method as a whole. The data is, by visual inspection, close to normal.

Additionally a comparison of how variables affect each other can be made with the Monte Carlo analysis, and demonstrate how the variation in one might be found to be considerably more important to the value of the target being considered than another for certain statistical distributions of properties. For example, it is readily apparent that a variable that varies very little will cause less variation in a target than one that varies more. However, what happens when two values of C_v are similar might not be readily apparent. This can be considered to some extent graphically using Monte Carlo data (Figure 4-16, Figure 4-17, Figure 4-18, Figure 4-19, and Figure 4-20). These figures show how the response of the mechanical property under inspection varies with variation in the unit cell properties. It is notable in Figure 4-18 that certain variables have a far larger effect on the value of E_{11} than the corresponding variable shown. E_{11} would appear to be approximately equally sensitive to L_2 and θ_1 (Figure 4-18) whilst it is considerably more sensitive to the same variation in E_2 .

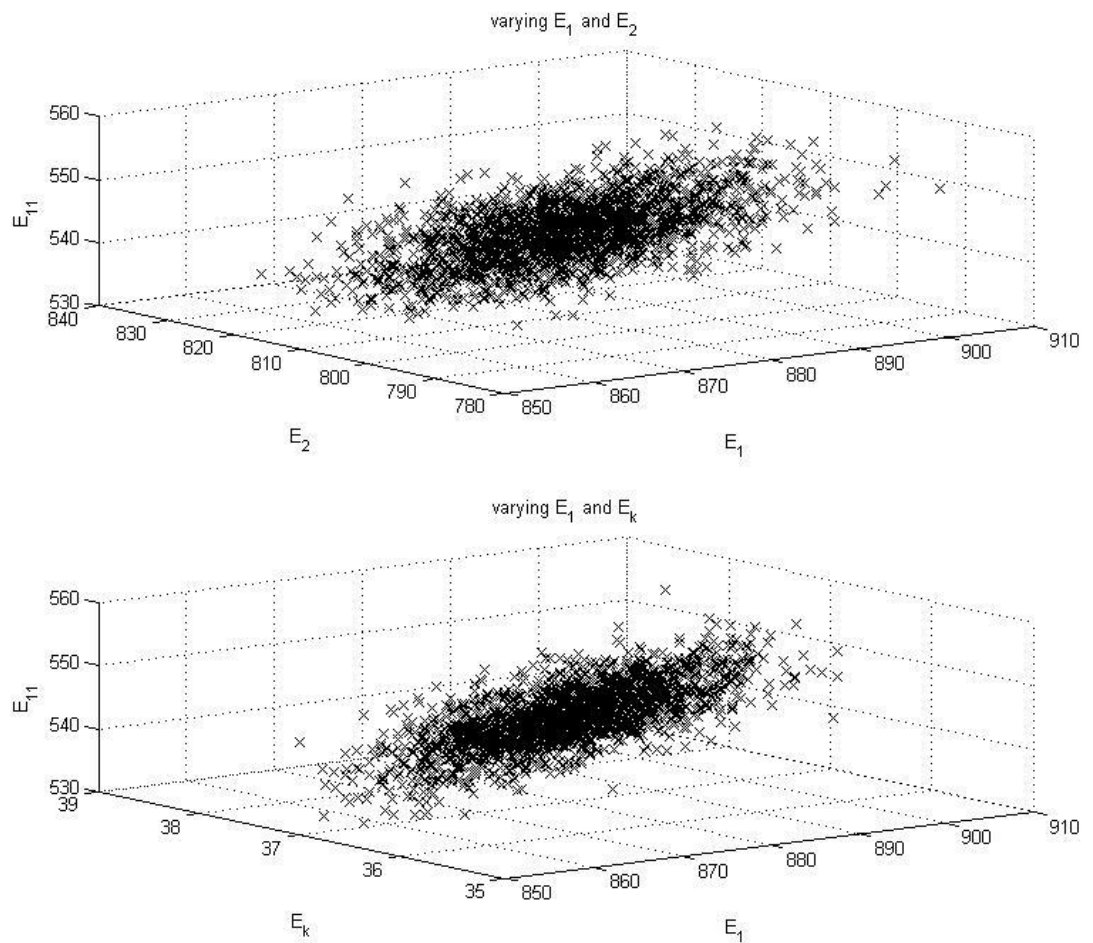


Figure 4-16: Effect of variation in E_{y1} with respect to E_{y2} and E_k on the value of E_{11} where the $C_v = 0.01$

4. Variability and robustness

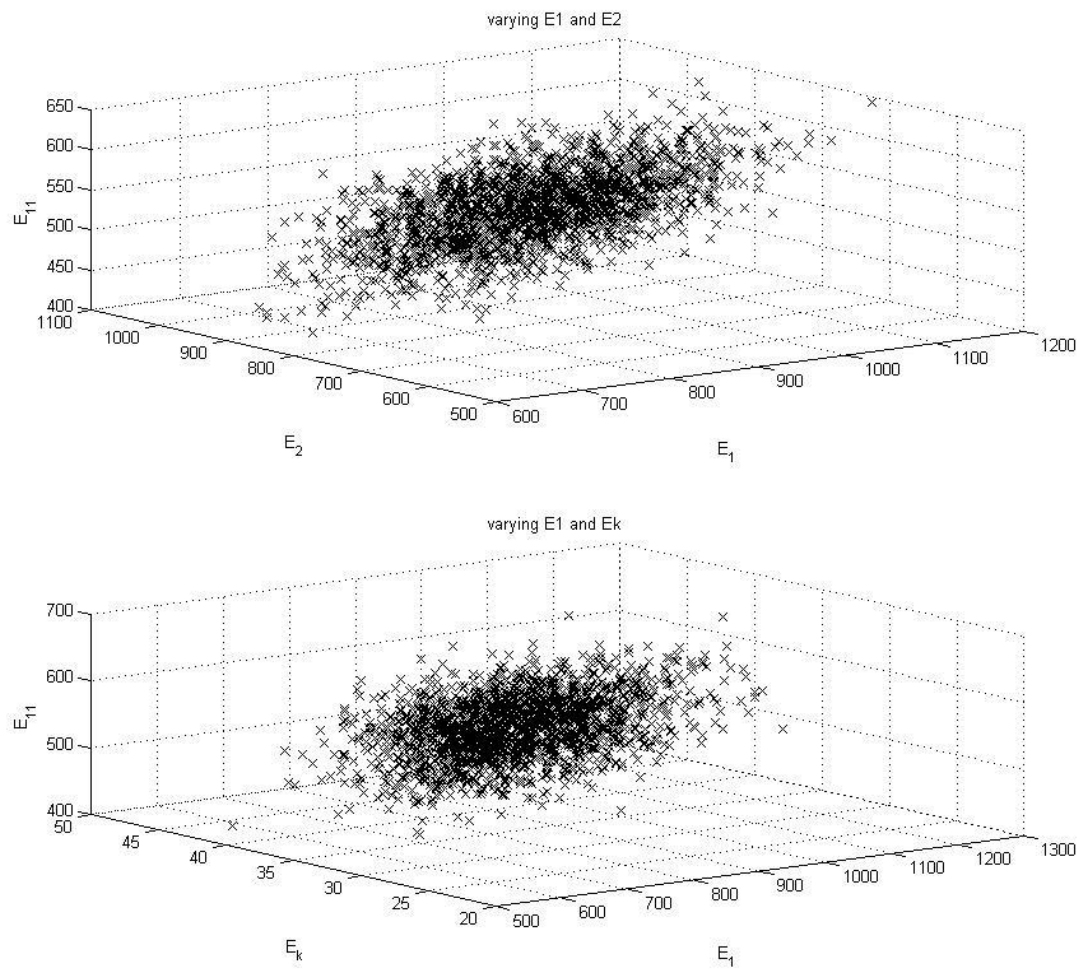


Figure 4-17: Effect of variation in E_{v1} with respect to E_{v2} and E_k on the value of E_{11} where the $C_v = 0.1$

4. Variability and robustness

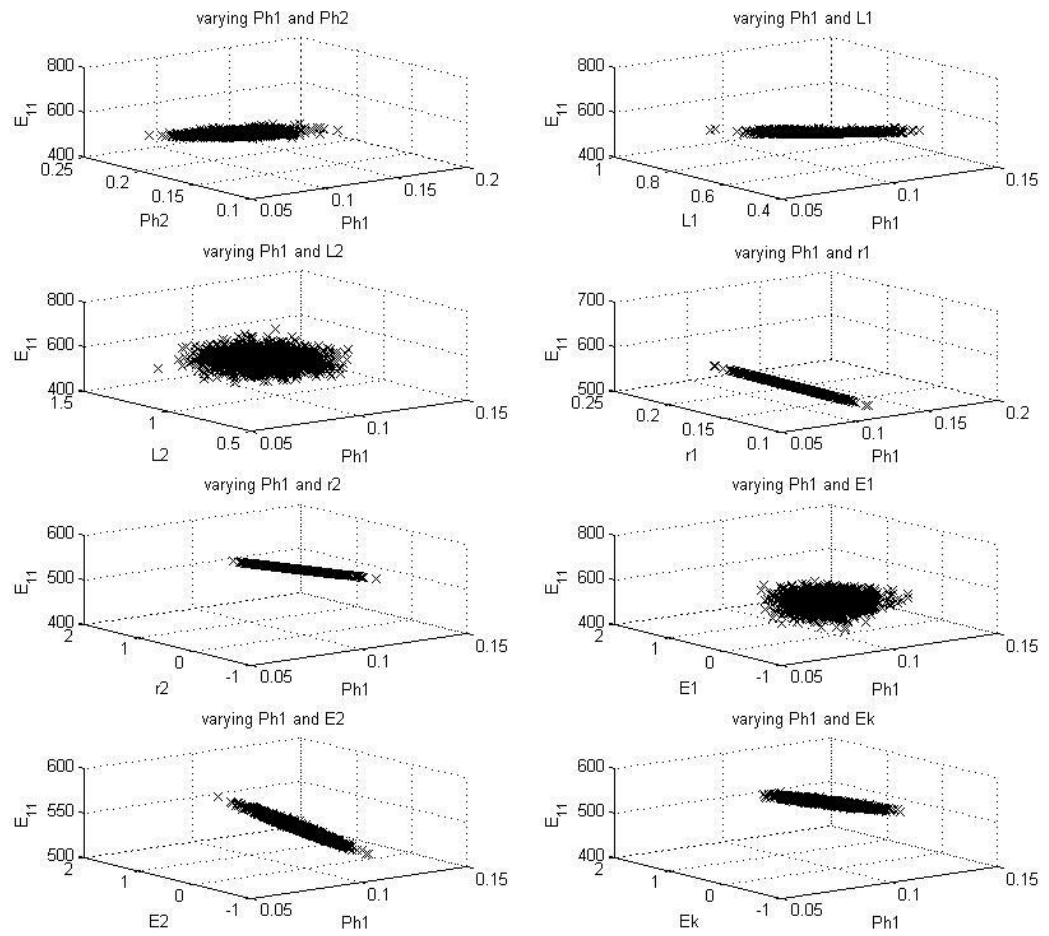


Figure 4-18: Effect of variation in θ_1 with respect to other variables on the value of E_{11} where the $C_v = 0.1$

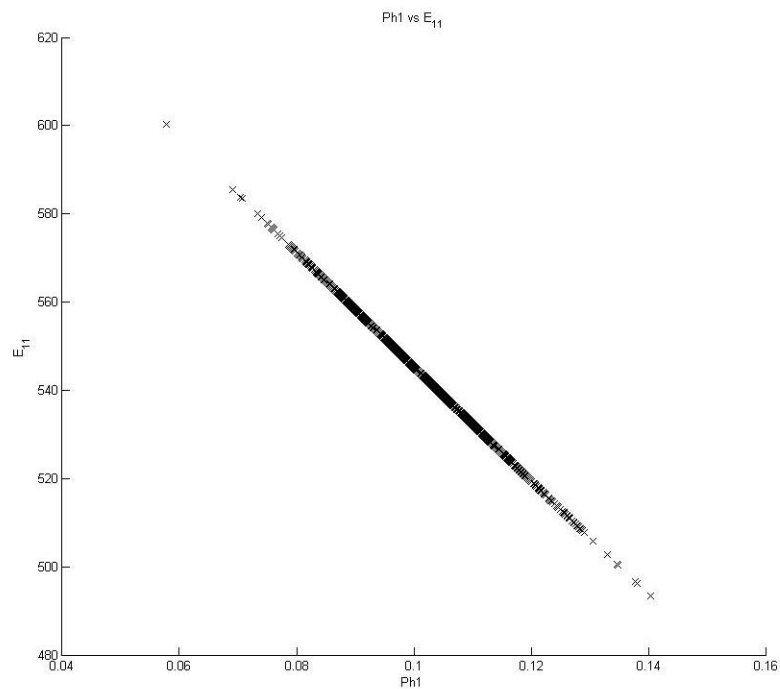


Figure 4-19: Effect of variation in θ_1 on the value of E_{11} where the $C_v = 0.1$

4. Variability and robustness

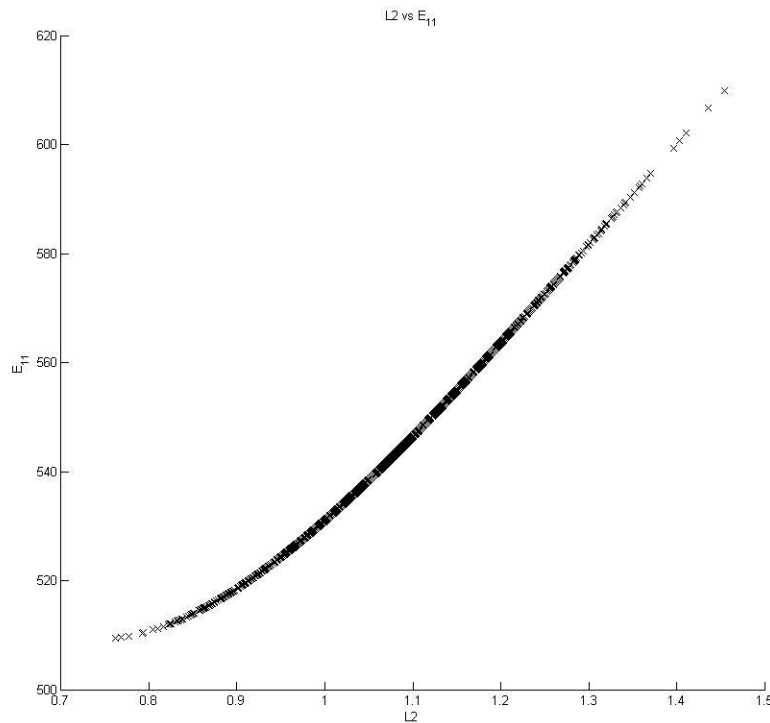


Figure 4-20: Effect of variation in L_2 on the value of E_{11} where the $C_v = 0.1$

Lastly the method demonstrates that a front of possible solutions exists for certain sets of targets. By considering the optimisation of a geometry for only one target (E_{11}), and allowing only two variables to vary (E_{y1} and E_{y2}) it is possible to demonstrate that multiple solutions exist by setting the inequality to Equation 4-21 (Figure 4-12) :

$$Target < E_{11}$$

Equation 4-12

As such, any point greater than the target will be identified, and any point on the failure plane will equal the target, producing a visualisation of the possible solutions (Figure 4-12). This mostly serves to demonstrate the assumptions proposed earlier in this thesis (§3.7), and might also demonstrate how no solution exists were the target is set to some unobtainable value.

4.8. FORM Methodology:

The FORM (First Order Reliability Method) is an analytical approximation method used to calculate the probability that an objective function does not produce a result within a predefined limit state. The accuracy of the method depends on the linearity of the limit state that is being approximated. The method computes the shortest distance to a failure plane from the origin (mean) which is then assumed to be linear and perpendicular to that point, thus allowing for the calculation of the approximate failure probability (Melchers, 1999). This method allows for a far quicker analysis of the failure probability, but importantly also includes the calculation of the sensitivities of the objective function. Error is introduced into the method with increasing nonlinearity of the limit state. Where the limit state is nonlinear the FORM method will likely provide an approximation of the failure probability unlike the Monte Carlo method which provides an exact probability if enough points are sampled.

The following methodology is used initially to verify the probability of failure of a fabric, it is the ability of the method to calculate the sensitivity of the function to variations in variables that is equally interesting. This leads to the proposition of a method to design fabrics for robustness to variation in addition to mechanical response (§4.10).

4.8.1. Background

The method used is similar to that proposed by Melchers (1999). For two variables the method is summarised as:

For two variables, using “*well-known properties of the bivariate normal distribution the marginal distribution is also normal*” (Melchers, 1999, p. 98), or the function of two normal distributions is also normal (Figure 4-21, Figure 4-22, and Figure 4-23). Therefore for a function, $g(x_1, x_2)$ transformed into standard normal space $g(y_1, y_2)$ (Equation 4-4), the point \underline{y}^* (Figure 4-22) is calculated as the shortest distance to the failure plane which equals β (Figure 4-21). β can then be used to calculate the probability of failure using standard normal tables $N(0,1)$.

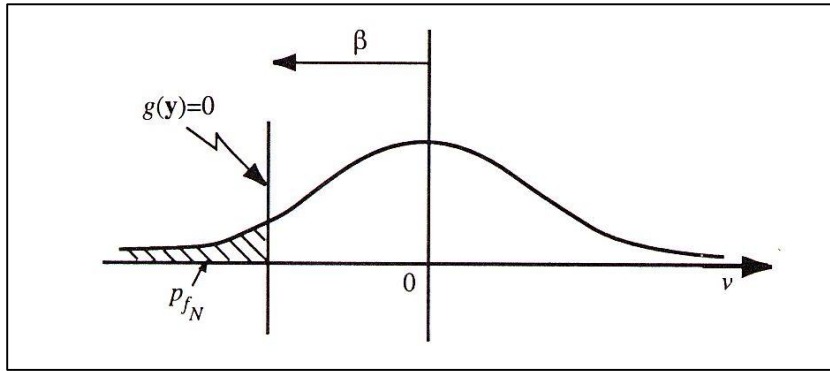


Figure 4-21: Marginal distribution in the space of the standardised normal variables (Melchers, 1999)

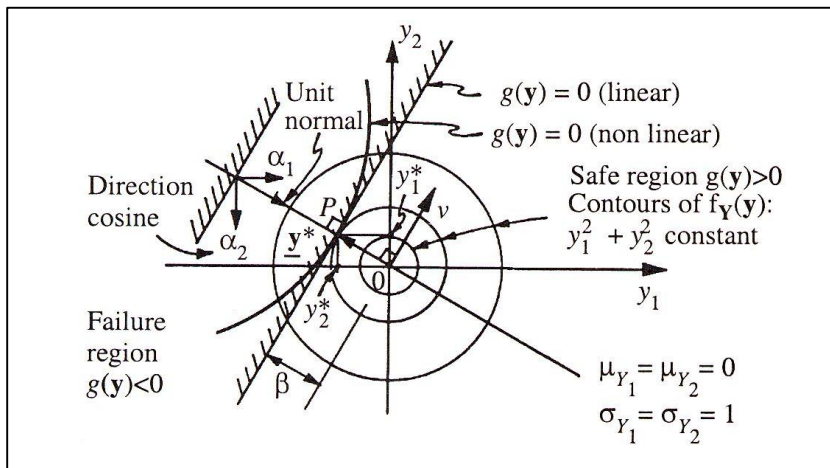


Figure 4-22: Probability density function contours and original (non-linear) and linearized limit state surfaces in the standard normal space (Melchers, 1999)

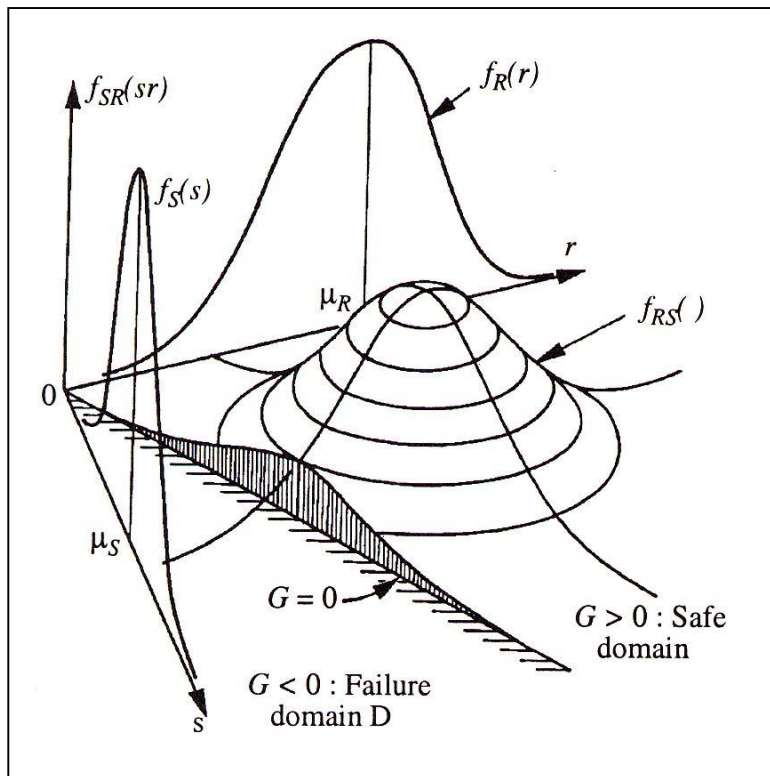


Figure 4-23: Two random variable joint density function $f_{RS}(r, s)$, marginal density functions f_R and f_S and failure domain D (Melchers, 1999)

4.8.2. Methodology

Eight variables (excluding r_2) are considered during the proposed FORM method.

More generally it might be stated that:

$$\beta = \min \left(\sum_{i=1}^{n=8} y_i^2 \right)^{1/2} = \min(\mathbf{y}^T \cdot \mathbf{y})^{1/2}$$

Equation 4-13

Y^* is considered to be the point of maximum likelihood for the failure plane (Figure 4-22), or the point on the failure plane that is closest to the origin in standard normal space. At this point the failure plane is perpendicular to the line intersecting the point of highest probability and the origin. Once Equation 4-13 is satisfied the probability of failure can be calculated using the value of β . The probability of failure can be calculated using the following series of equations (Melchers, 1999):

The direction components ' c ' of the outward normal ' l ' are calculated from the partial derivatives of ' g ' with respect to each variable ' y_i '.

$$c_i = \lambda \frac{\partial g}{\partial y_i}$$

Equation 4-14

where λ is an arbitrary constant.

The length of the outward normal (l) is calculated as the square route of the sum of the squares of c_i (Figure 4-22).

$$l = \left(\sum_i c_i^2 \right)^{1/2}$$

Equation 4-15

The direction cosines α_i can be calculated with respect to each variable ' y_i '. Each direction cosine gives the sensitivity of the function to variable ' y_i '.

$$\alpha_i = \frac{c_i}{l}$$

Equation 4-16

Thus the distance to the point of maximum likelihood from the mean of each variable can be calculated as y_i^* , which give the coordinates of the point of maximum likelihood:

$$y_i^* = -\alpha_i \beta$$

Equation 4-17

This is shown in normal space for two variables in Figure 4-22. Finally the equation for the linearized approximate failure plane might be written as:

$$g(y) = \beta + \sum_{i=1}^n \alpha_i y_i = 0$$

Equation 4-18

A method for the application of the FORM method to fabric geometry is summarised in 12 steps below and in Figure 4-26:

1. Obtain statistical information about the parameters of the unit cell.
2. Write the equations for the mechanical properties of a fabric E_{11} , E_{22} , ν_{12} , and ν_{21} (§3.4.3) in terms of y_i to transition to standard normal, $N(0,1)$, space:

$$y_i = \frac{X_i - \mu_{X_i}}{\sigma_{X_i}}$$

3. Write the mechanical property equations as inequalities to be solved where ' D ' is the allowable deviation (%allowable deviation/100).

$$g(y) = E_{11} - Target_{E_{11}} \cdot D$$

4. Derive the partial derivatives of $g(y)$ with respect to $y_i \forall i$.

$$\frac{\partial g(y)}{\partial y_i}$$

5. Choose an initial starting point y_i^0 at the mean values.
6. For y_i^0 calculate the strains and their numerical derivatives as required for the predictive model (§3.4.3.2):

$$\varepsilon_1, \varepsilon_2, \frac{\Delta \varepsilon_1}{\Delta \varepsilon_2}, \frac{\Delta \varepsilon_2}{\Delta \varepsilon_1}$$

7. Calculate the values of the partial derivatives derived in '4'.
8. Compute $g(y)$ at the current values of y_i the outward normal (l), shortest distance (β), and direction cosines (α).
9. Calculate the new values of y :

$$y_i^{n+1} = -\alpha_i \cdot \left(\beta + \frac{g(y)}{L} \right)$$

10. Return to '6' with new values of y_i .

11. Where β stabilises to a value, and $g(y) = 0$ exit and output probability of failure and point of highest probability.

$$p_f = 1 - \Phi(\beta)$$

12. Convert the design point back to X_i space from standard normal space using:

$$X_i = y_i \sigma_{X_i} + \mu_{X_i}$$

Note that the probability of failure is not β , as the shortest distance is calculated as the distance from the mean. As such β relates to the probability of success (Figure 4-24). The probability of failure is calculated as one minus the probability found using β and standard normal tables.

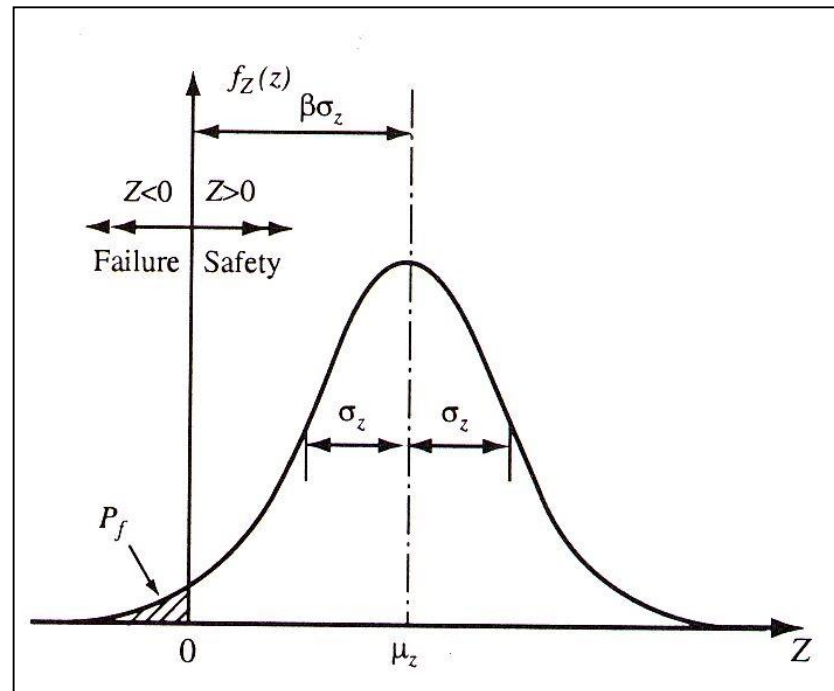


Figure 4-24: Distribution of safety margin $Z = R - S$ (Melchers, 1999)

The analysis produces fewer outputs that can be visualised without comparison to Monte Carlo simulations (§4.7). The value of the function $g(y)$, can be compared to the shortest distance β (Figure 4-25). Figure 4-25 shows the progress of the FORM method for a data set to the inequality $0.95 \cdot Target < E_{11}$ where the coefficients of variation are all set to 0.1. After 20 iterations the function $g(y)$ reaches zero, and the value of β , which has reached an asymptote, is approximately 1.5. Using standard normal tables the probability of failure can be calculated as 0.066 (Equation 4-19).

4. Variability and robustness

$$\Phi(-\beta) = 1 - \Phi(\beta) = 1 - \Phi(1.5) = 0.066 = p_f \quad \text{Equation 4-19}$$

Realistic values of β are in the order of 3 – 4.5, when used in design (§4.11) however, as partial factors and other sources of error are not being considered here values of the reliability index other than these are expected.

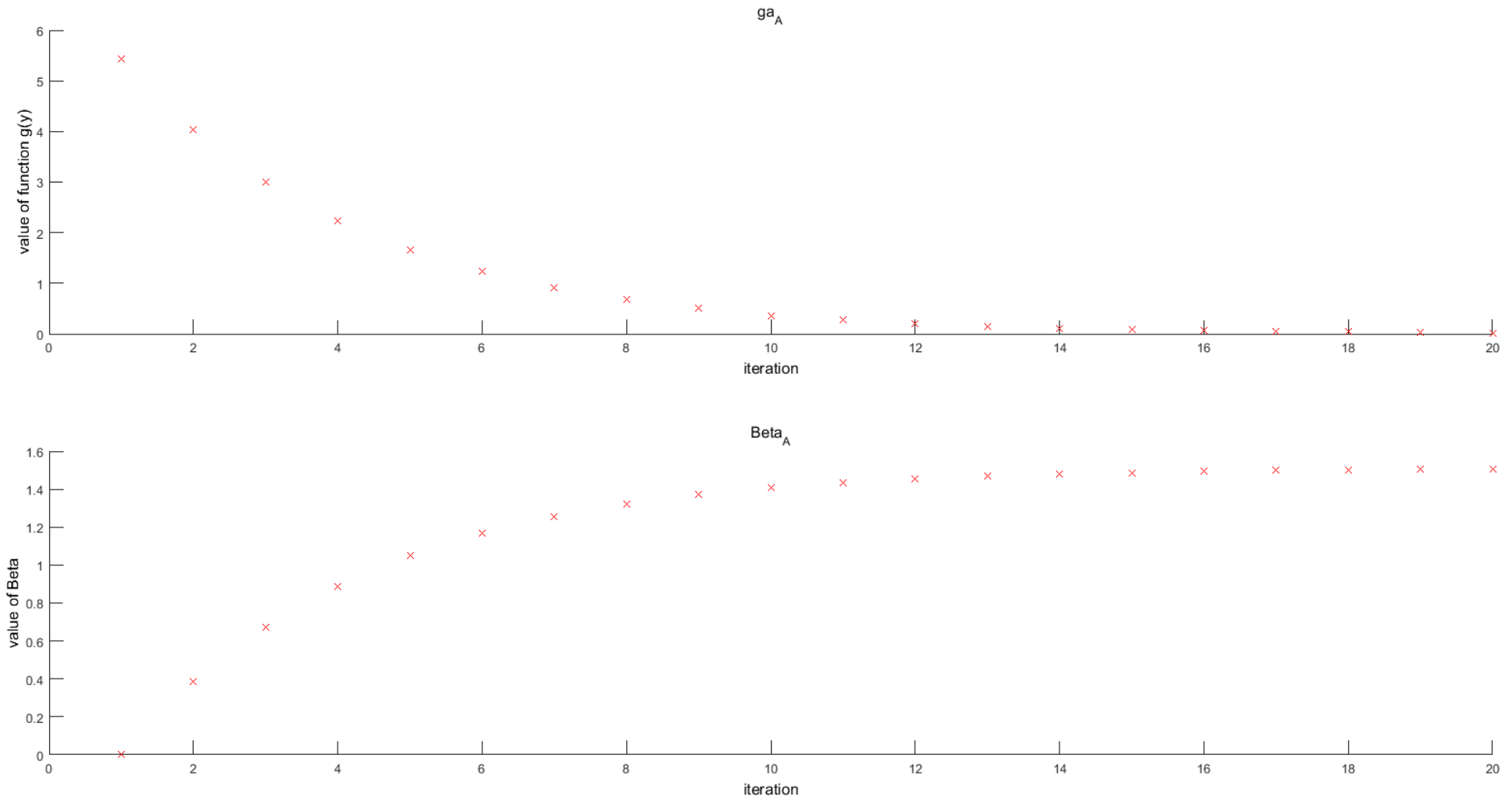


Figure 4-25: Comparison of the value of the shortest distance β and $g(y)$ as an optimisation progresses for the inequality $0.95 \times \text{Target} < E_{11}$ where $C_v = 0.01$ for all variables

4.8.3. Constraint compliant FORM

As discussed above (§4.7.2) the interdependence of variables leads to problems in the calculation of β . When all nine variables are allowed to vary independently a situation arises within the FORM method that cannot occur in the unit cell where equilibrium equations have to be complied with. The FORM method attempts to move each and every variable towards the point of maximum likelihood for the inequality under consideration. This results in noncompliance with the equilibrium equations as each variable moves independently.

The proposed solution redefines r_2 as a dependent variable as was done in the Monte Carlo method. Equation 4-9 as redefined in standard normal space can be produced (Equation 4-20).

$$r_2 = (y_3\sigma_{L_1} + \mu_{L_1}) \tan(y_1\sigma_{\theta_1} + \mu_{\theta_1}) + (y_4\sigma_{L_2} + \mu_{L_2}) \tan(y_2\sigma_{\theta_2} + \mu_{\theta_2}) - (y_5\sigma_r + \mu_{r_1})$$

Equation 4-20

Once this has been achieved the other variables can be assumed to be independent, as the dependence is encapsulated into a single variable. Therefore the solver now only solves for eight variables.

Whilst dependence like this normally adds some level of complexity to a model Melchers (1999, p. 27) suggests that where this is the case some *“dependence structure between dependant variables be known and expressed”* which is achieved using Equation 4-20. It should also be noted that this does limit the applicability of the method to some degree, as the end user of the method can no longer observe the effect of changing the variation associated with r_2 on the sensitivity of the function. The distribution of r_2 with relation to variation in other parameters is still obtainable (Equation 4-21). The calculation of the sensitivity of the objective function to the value of r_2 is unnecessary as the effect of variation in r_2 on the result is included within the response of the other variables, r_2 having been removed from the objective function.

4. Variability and robustness

The implicit sensitivities for r_2 could be calculated using Equation 4-21. The derivatives in Equation 4-21 are independently obtainable, and only the derivative $\frac{dg}{dr_2}$ is not available, being deterministic. This is not explored further at this stage.

$$r_2 = f(L_1, L_2, r_1, \theta_1, \theta_2) = L_1 \tan \theta_1 + L_2 \tan \theta_2 - r_1$$

$$\frac{dg}{dr_2} = \frac{\partial g}{\partial L_1} \cdot \frac{\partial L_1}{\partial r_2} + \frac{\partial g}{\partial L_2} \cdot \frac{\partial L_2}{\partial r_2} + \frac{\partial g}{\partial r_1} \cdot \frac{\partial r_1}{\partial r_2} + \frac{\partial g}{\partial \theta_1} \cdot \frac{\partial \theta_1}{\partial r_2} + \frac{\partial g}{\partial \theta_2} \cdot \frac{\partial \theta_2}{\partial r_2}$$

Equation 4-21

The methodology as completed is presented in Figure 4-26.

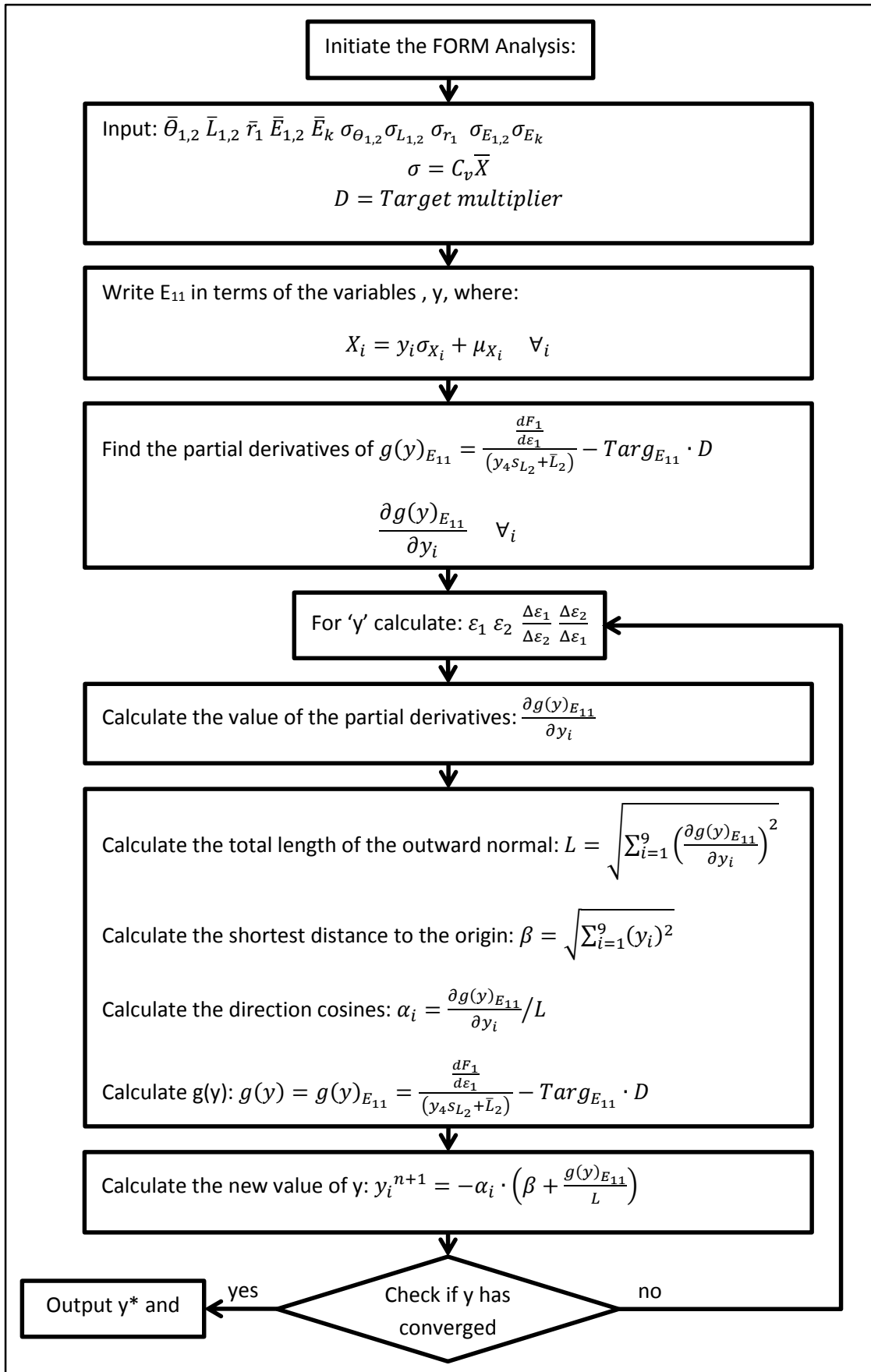


Figure 4-26: Method of FORM implementation

4.8.4. Example Results

As with the Monte Carlo analysis the FORM analysis was carried out at different levels of variation with respect to two tests (Equation 4-22) using the geometry of a PVC coated polyester fabric (F1202), the results of which are detailed in the table below. A comparison of these results with those of the Monte Carlo analysis is made in the following section. All the results of simulations below converged to a solution with 100 iterations or where the change in $g(y)$ was less than 1×10^{-8} between iterations. Direction cosines were produced relating to the point of maximum likelihood as part of the methodology. The value of β for each Probability of failure can be calculated using Equation 4-19.

Inequality 1:

$$(1 - x) \cdot Target < E_{11}$$

Inequality 2:

$$E_{11} < (1 + x) \cdot Target$$

Equation 4-22

Where 'x' is the allowable deviation from the mean.

Variation in unit cell properties (Cv)	Probability of failure (P_f) of E_{11}	
	$0.9 \cdot E_{target} < E_{11}$	$1.1 \cdot E_{target} > E_{11}$
$\Theta_{1,2}$ Cv = 0.1	0.041	0.059
$L_{1,2}$ Cv = 0.1	0.000	0.023
$E_{1,2}$ Cv = 0.1	0.050	0.030
All variables, Cv = 0.1	0.046	0.081
$\Theta_{1,2}$ Cv = 0.01	0.000	0.000
$L_{1,2}$ Cv = 0.01	0.000	0.000
$E_{1,2}$ Cv = 0.01	0.000	0.000
All variables, Cv = 0.01	0.000	0.000
	$0.99 \cdot E_{target} < E_{11}$	$1.01 \cdot E_{target} > E_{11}$
$\Theta_{1,2}$ Cv = 0.1	0.434	0.435
$L_{1,2}$ Cv = 0.1	0.406	0.411
$E_{1,2}$ Cv = 0.1	0.431	0.430
All variables, Cv = 0.1	0.440	0.441
$\Theta_{1,2}$ Cv = 0.01	0.049	0.051
$L_{1,2}$ Cv = 0.01	0.009	0.012
$E_{1,2}$ Cv = 0.01	0.040	0.038
All variables, Cv = 0.01	0.066	0.069

Table 4-3: FORM predicted probability of failure at different failure criteria for feasible targets for an F1202 fabric (5000 runs = 10000 data sets)

Table 4-3 summarises the results of a number of FORM simulations. The results show that larger values of variation, when compared to smaller allowable deviations from the target, produce higher failure probabilities. Where the inequalities limit deviation from

4. Variability and robustness

the target more, and large values of variation of constitutive property are used, the probability of failure approaches 50% (as high as possible for a FORM method considering a single sided inequality with Normally distributed data). This is because the probability of failure as defined if the inequality were set to require all data to be greater than the target would be equal to 50%, as half the normally distributed objective function would be less than the target.

A comparison is made between the Monte Carlo results and the results of the FORM method, discussed in detail below (§4.9).

4.9. Comparison of failure points

To compare the point y^* of the Monte Carlo analysis to the point produced in the FORM analysis it is necessary to estimate the point of maximum likelihood from Monte Carlo simulations where only two geometric properties are allowed to vary. Limiting the analysis to two variables allows for the 2D visualisation of the response surface, and thus the application of a fitted (quadratic polynomial) curve to the line delineating the passed and failed points. The minimum distance to the origin from the line is then calculated and the point on the curve that this relates to is noted as y^* from the Monte Carlo analysis. This is then compared to the output of a FORM simulation.

Considering the inequality:

$$0.95 \times Target < E_{11}$$

Equation 4-23

Whilst only varying the values of the out of plane angles ($\theta_{1,2}$) for an F1202 fabric is used to demonstrate how this is achieved. First a FORM analysis is carried out, and the point of maximum likelihood calculated (Table 4-4).

	Value	Direction Cosine
y_1	3.42E-01	-4.05E-01
y_2	7.73E-01	-9.14E-01

Table 4-4: Point of Maximum likelihood for an F1202 fabric compared to the inequality $0.95 \times Target < E_{11}$ where $C_v = 0.1$ for $\theta_{1,2}$ only

Once the point of maximum likelihood has been calculated from the FORM method a Monte Carlo analysis is carried out using the same properties as the FORM analysis. This produces Figure 4-27 and Figure 4-28.

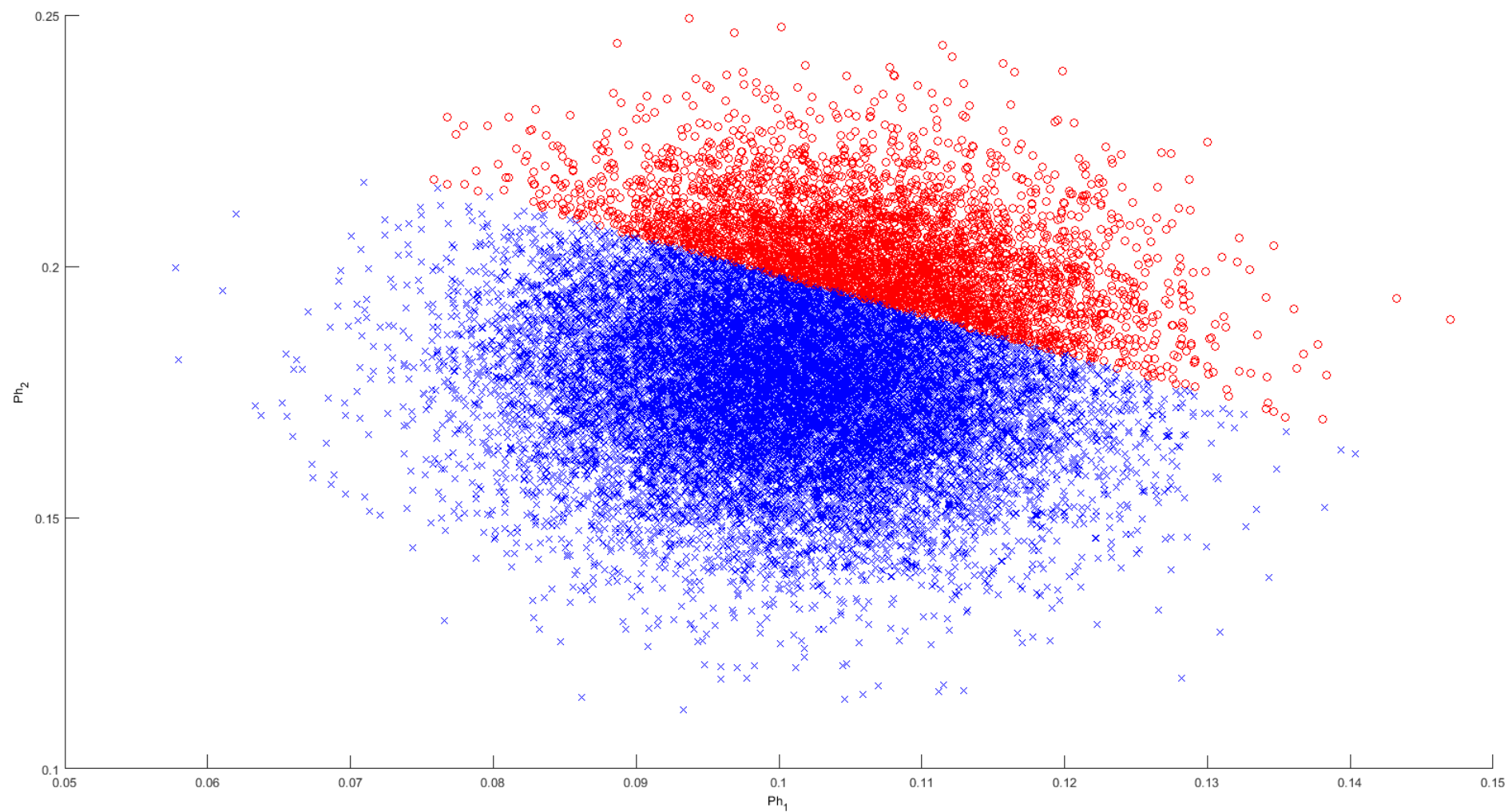


Figure 4-27: Monte Carlo results showing θ_1 and θ_2 where only θ_1 and θ_2 are considered to vary with a coefficient of variation of 0.1 for the inequality $0.95Targ < E11$ (red = failed, blue = success)

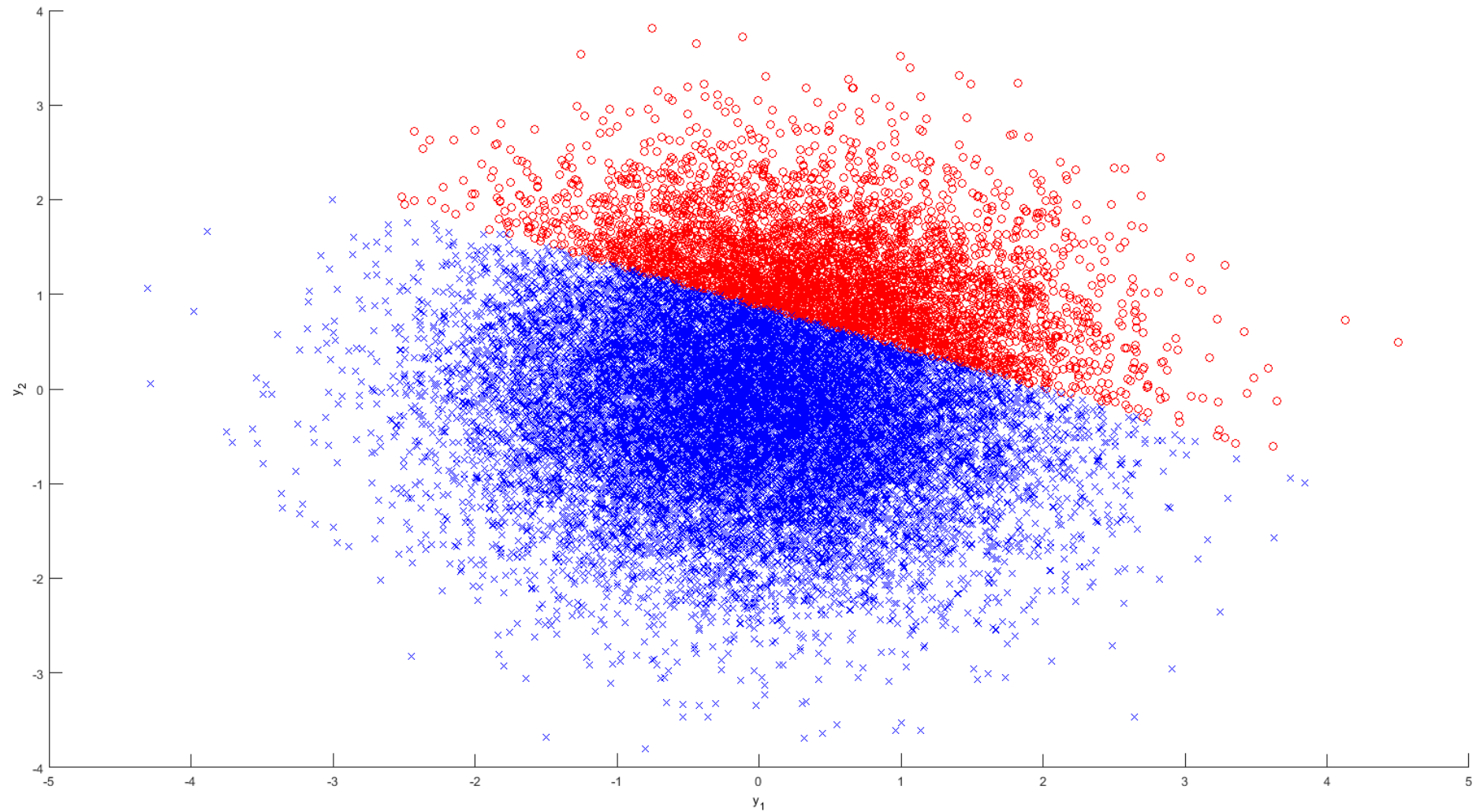


Figure 4-28: Monte Carlo results showing y_1 and y_2 where only θ_1 and θ_2 are considered to vary with a coefficient of variation of 0.1 for the inequality $0.95Targ < E11$ (red = failed, blue = success)

4. Variability and robustness

Figure 4-28 is used to calculate a quadratic equation for the line delineating the failed and passed points. Fitting a quadratic to manually selected points along the pass/fail boundary leads to:

$$y_2 = 0.0006829y_1^2 + -0.4607y_1 - 0.9078 \quad \text{Equation 4-24}$$

The script calculates the formula of the line, and calculates the point of maximum probability as the point closest to the mean (0,0). This allows the planes of failure to be visualised comparatively, demonstrating that both methods come to a similar conclusion (Figure 4-29) and allows the points of maximum likelihood to be visually compared (Figure 4-30).

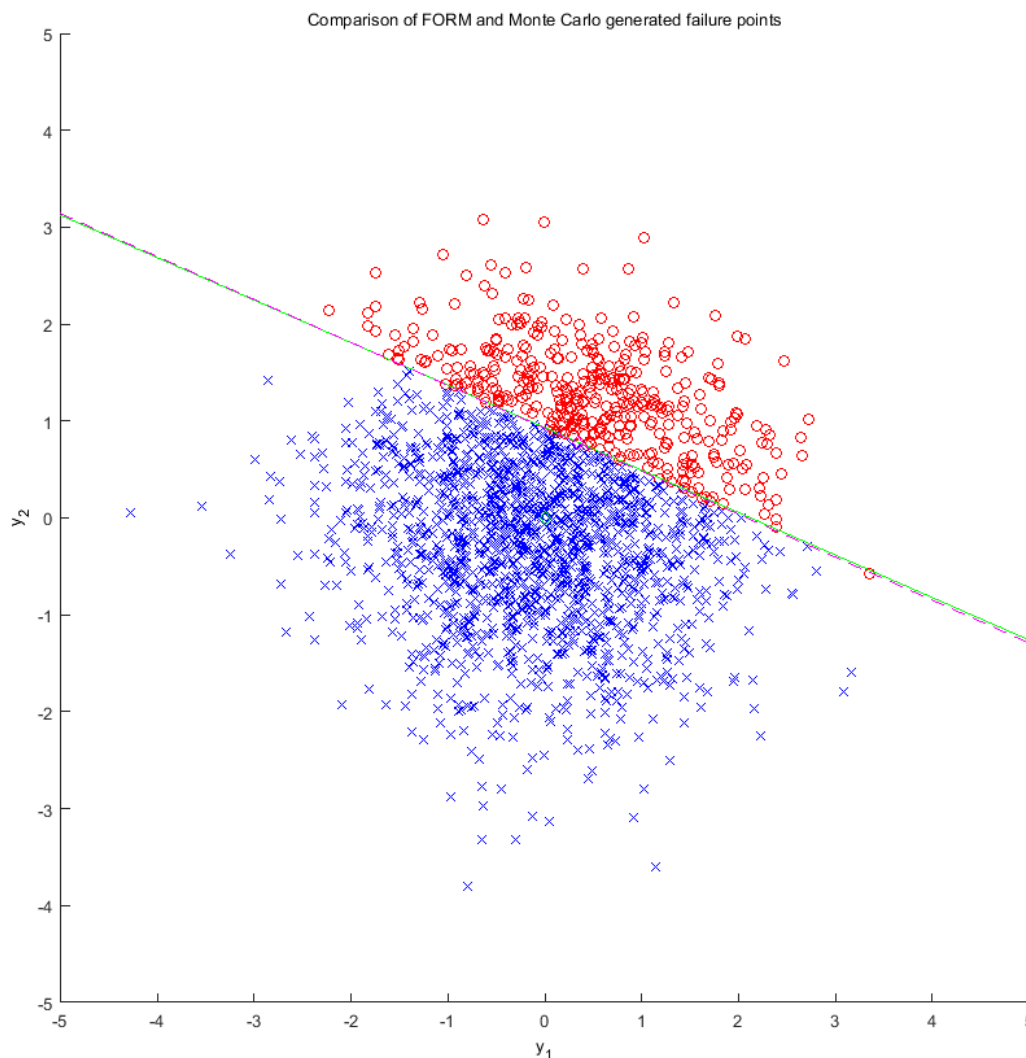


Figure 4-29: Comparison of FORM and Monte Carlo generated failure points (approximate point of likely failure Monte Carlo (green), and point of failure from FORM analysis (magenta))

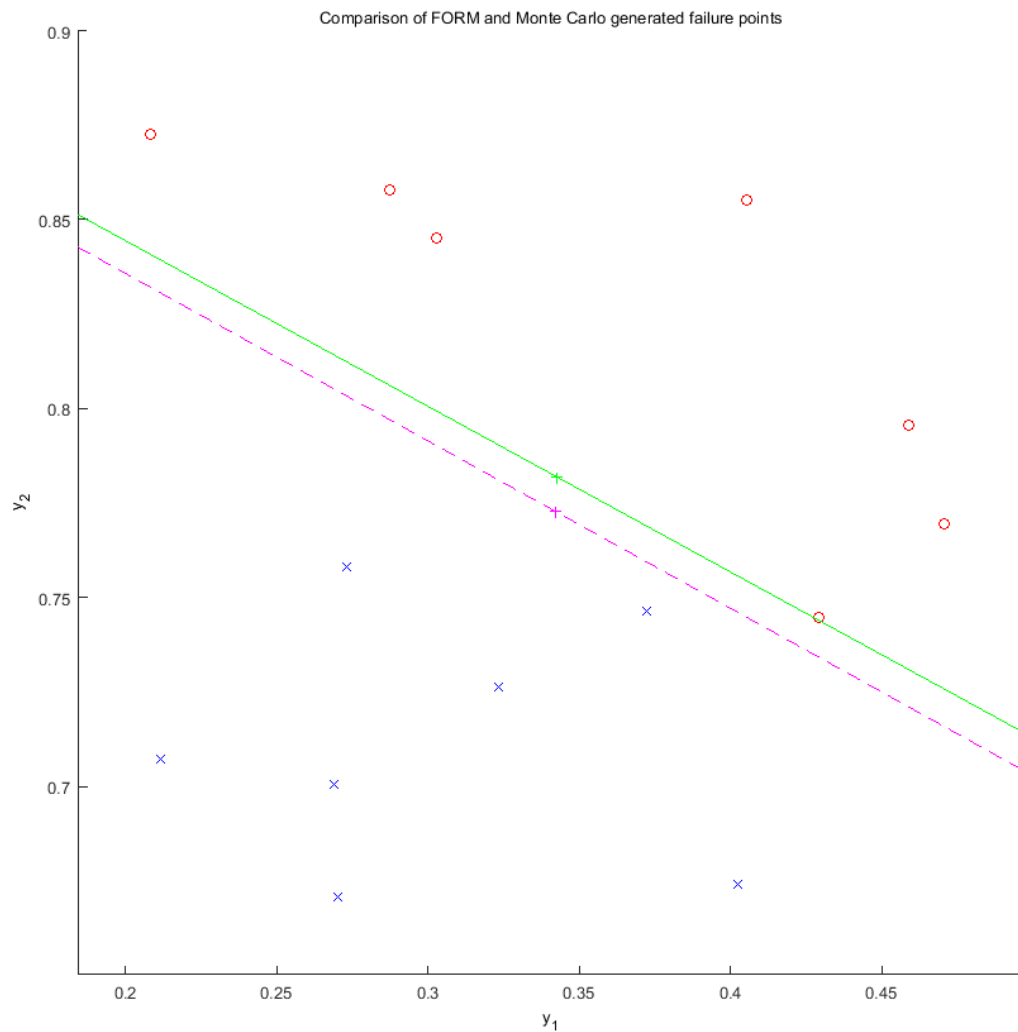


Figure 4-30: Comparison of FORM and Monte Carlo generated failure points zoomed to failure point (approximate point of likely failure Monte Carlo (green), and point of failure from FORM analysis (magenta)). Points of maximum likelihood are shown as '+'.

The value of the coefficient of x^2 compared to the other coefficients (Equation 4-24) and the values of y_1 and y_2 being less than one (meaning that they become smaller when squared) (Figure 4-30) suggests that the assumption of a linear failure plane for the joint density function is acceptable. The value is small compared to the other coefficients, and therefore affects the equation less. Figure 4-30 shows that the two points of maximum likelihood are not at precisely the same point. This is due to both the inaccuracy of the method of calculating the equation using a visual inspection of the failure line, and the inaccuracy of the FORM method when compared to the Monte Carlo method.

Comparing the points of maximum likelihood demonstrates the error that is experienced (Table 4-5):

4. Variability and robustness

	FORM	Monte Carlo	Direction Cosine (FORM)
y_1	0.342	0.345	-0.405
y_2	0.773	0.749	-0.914

Table 4-5: Comparison of point of Maximum likelihood for an F1202 fabric compared to the inequality $0.95x\text{Target} < E_{11}$ where $C_v = 0.1$ for $\theta_{1,2}$ only

The two methods confirm the point of maximum likelihood, and the two probabilities of failure are also similar: 0.201 (Monte Carlo), 0.199 (FORM).

The difference between Monte Carlo and FORM results are summarised in Table 4-6 for similar inequalities using the same initial geometry. Notably as more variation in the variables (that make up the unit cell) is introduced the methods differ to a greater degree.

Variation in unit cell properties (C_v)	Probability of failure (P_f) of E_{11}			
	Absolute difference	Absolute Percentage difference (%)	Absolute difference	Absolute Percentage difference (%)
	$0.9 \cdot E_{\text{target}} < E_{11}$		$1.1 \cdot E_{\text{target}} > E_{11}$	
$\theta_{1,2} C_v = 0.1$	0.00	2.64	0.00	0.64
$L_{1,2} C_v = 0.1$	0.00	200.00	0.02	46.16
$E_{1,2} C_v = 0.1$	0.00	1.15	0.00	2.42
All variables, $C_v = 0.1$	0.08	91.87	0.08	66.98
$\theta_{1,2} C_v = 0.01$	0.00	0.00	0.00	0.00
$L_{1,2} C_v = 0.01$	0.00	0.00	0.00	0.00
$E_{1,2} C_v = 0.01$	0.00	0.00	0.00	0.00
All variables, $C_v = 0.01$	0.00	0.00	0.00	0.00
	$0.99 \cdot E_{\text{target}} < E_{11}$		$1.01 \cdot E_{\text{target}} > E_{11}$	
$\theta_{1,2} C_v = 0.1$	0.00	0.67	0.00	0.43
$L_{1,2} C_v = 0.1$	0.00	1.14	0.01	1.99
$E_{1,2} C_v = 0.1$	0.00	0.42	0.01	1.24
All variables, $C_v = 0.1$	0.01	2.92	0.02	4.74
$\theta_{1,2} C_v = 0.01$	0.00	5.65	0.00	1.46
$L_{1,2} C_v = 0.01$	0.00	25.54	0.01	33.98
$E_{1,2} C_v = 0.01$	0.00	6.59	0.00	6.92
All variables, $C_v = 0.01$	0.08	74.37	0.08	72.65

Table 4-6: comparison of FORM and Monte Carlo failure probability to different failure criteria for feasible targets for an F1202 fabric (5000 runs = 10000 data sets)

From the data in Table 4-6 most of the FORM tests appear to produce similar results to the accurate Monte Carlo data. However, a number of tests display high percentage differences, some of which are far higher than are hoped for. Of immediate concern is the percentage difference of 200%. However, inspection of the results shows that this error occurs with a very low absolute difference between the FORM and Monte Carlo data. This is because of the high value of β at this point (5.89) resulting in a probability

4. Variability and robustness

of failure of 1.86×10^{-6} . To obtain a result comparable to this the Monte Carlo analysis has to run for a minimum of one hundred million simulations, to give an accuracy of three decimal places. The Monte Carlo analysis concluded that the probability of failure was zero. Therefore, whilst to five significant figures the result is accurate, a large percentage difference is shown. A number of other errors result from similar situations, however, it is clear that some do not.

A notable value of percentage difference of 6.59% between the FORM and Monte Carlo results for an inequality of $E_{11, \text{target}} \times 0.99 < E_{11}$ is also interesting. An analysis of the failure points shows them to be very similar (Figure 4-31, Figure 4-32).

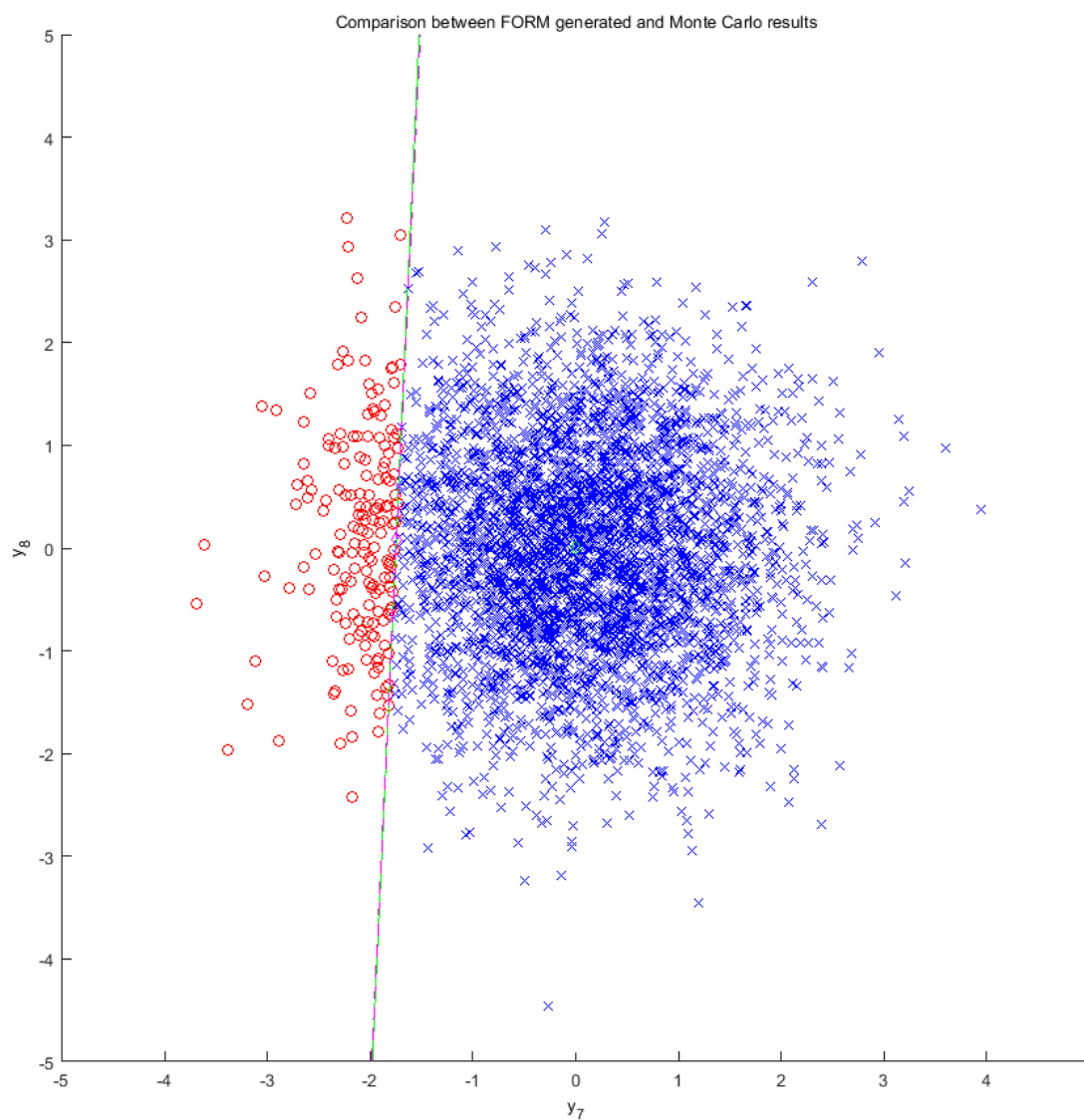


Figure 4-31: Comparison of FORM and Monte Carlo generated failure points (approximate point of likely failure Monte Carlo (green), and point of failure from FORM analysis (magenta))

4. Variability and robustness

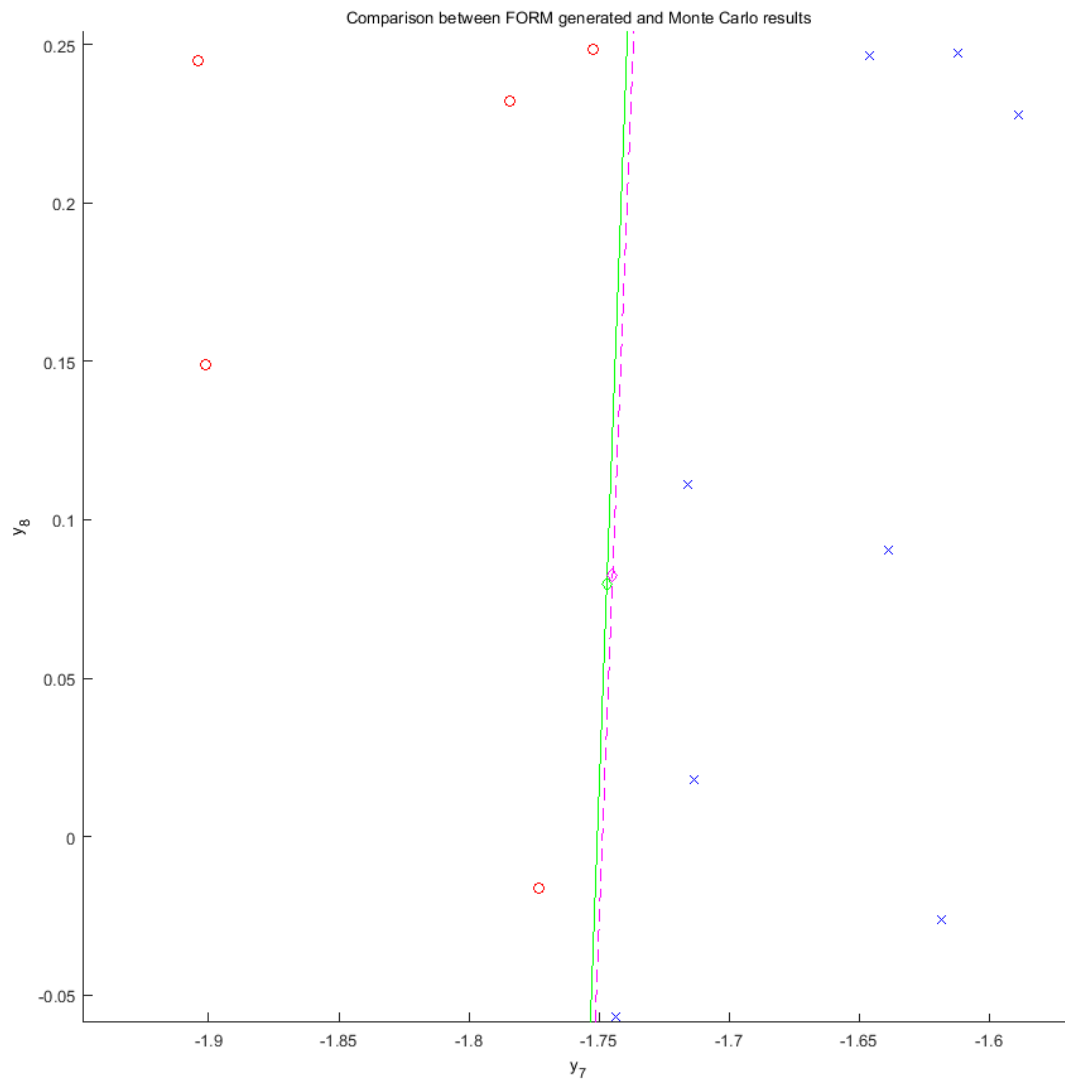


Figure 4-32: Comparison of FORM and Monte Carlo generated failure points zoomed to failure point (approximate point of likely failure Monte Carlo (green), and point of failure from FORM analysis (magenta)). Points of maximum likelihood are shown as '◇'.

Further, a check on the normality of the results (Figure 4-33) shows them to be normal, with some deviation at extreme values. It must therefore be the case that this small deviation has caused the error in the calculation of the probability of failure in the FORM method. Whilst the Monte Carlo method has accurately calculated the probability of failure based on the points counted the FORM method has assumed perfectly normal behaviour, and therefore slightly miscalculated the probability of failure.

Small errors in the FORM method when compared to the Monte Carlo method are to be anticipated, as the FORM method does not perfectly reproduce a Monte Carlo simulation.

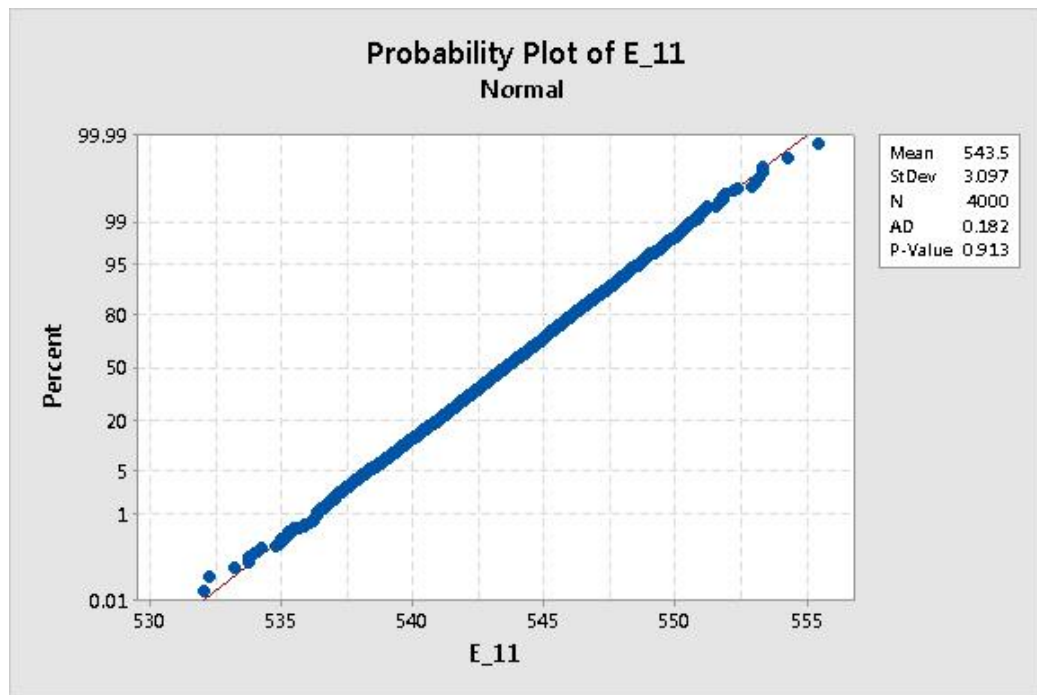


Figure 4-33: Normality test for the results of the Monte Carlo analysis for the inequality $E_{11,target} \times 0.99 < E_{11}$, where E_1 and E_2 varied only with a coefficient of variation of 0.01.

The cause of other errors, where the percentage difference is high, with a correspondingly large value of actual absolute error is therefore due to the problem encountered in §4.7.3. The interaction of the formulae under consideration, and the truncation of the data due to the equilibrium constraint produces non-normal results. In Figure 4-15 this was found to be 3 parameter lognormal. Non-normal, or slightly non-normal results, which when compared to the FORM analysis which is considering normally distributed data only (which is for the most case true) result in an error in the calculation of the FORM probability of failure.

Without carrying out a Monte Carlo analysis for each fabric and each set of variation parameters it is impossible to tell which fit will most accurately predict the response of a fabric. Though the results should generally be normally distributed due to the interaction of two normal curves. Therefore, to allow prediction of non-existent fabrics, or the robustness (§4.10) of existing fabrics without considerable outlay in time, it is necessary to assume normal distribution.

4.10. Robust design of a fabric

Robustness is signified by “*insensitivity to small deviations from the assumptions*” (Huber, 1981). It is desirable for fabrics to be robust to any small variations in fabric parameters. Therefore a modified FORM methodology is developed to enhance the robustness of designed fabrics by allowing small changes in fabric geometry to reduce the overall sensitivity of the designed fabric. Robustness can be interpreted as an attempt to find the minimum or maximum of a function with constraints on the probability of failure such that the result may not be the global minimum, but will be robust. The optimisation function might not be completely satisfied, but where the additional lack of sensitivity outweighs this a robust solution may be considered to have been found (Figure 4-34). Figure 4-34 shows how at point ‘B’, the global minimum, a small deviation from the design variables would result in a large deviation from the global minimum. However, at point ‘A’ very little change in the objective function would occur for an equivalent change in the design variables. Point ‘A’ is therefore the robust minimum, and preferential where the sensitivity of the objective function is more important than finding the global minimum.

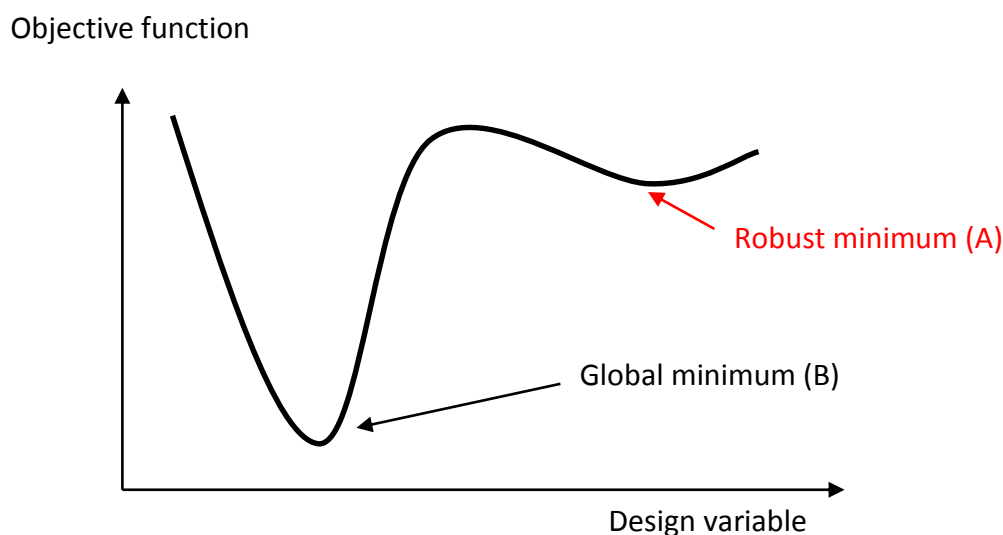


Figure 4-34: Comparing robust and global optimisation

Erfani and Utyuzhnikov (2012, p. 247) put the problem succinctly: “*In engineering design optimisation, the designer may prefer a use of robust solution to a more optimal one... Therefore a designer may demand a stable (or robust) configuration*”. As such, whilst a

4. Variability and robustness

robust and optimal solution may be desired, if it is unobtainable a robust solution or an optimal solution or some combination of the two might be sought. In addition the proposed method is able to predict the robustness of the designed fabric, unlike some methods which require experimental results to form conclusions (Erfani and Utyuzhnikov, 2012). A discussion on different methods of robust optimisation is made in the literature review (§2.5.2).

Previous work has looked at multi-objective robust optimisation in a number of different ways, like the work carried out by Kim *et al.* (2010, p. 3117) which optimises the “*maximum gradient of the objective function of interest with respect to uncertain variables*”. As such gradients are minimised, reducing the sensitivity of the overall design to that particular uncertain variable. This method is similar to the one presented for the robust design of fabrics except for a number of important distinctions. In the work by Kim *et al.* (2010) the uncertain variables alter a design geometry, whilst in the presented method the uncertain variables are considered to be the design variables. In addition the objective function, $g(y_i)$, becomes the minimisation of the gradients, whilst constrained by the design function, $f(y_i)$, and the system constraints, $h(y_i)$ and $j(y_i)$, which relate closely to the equations produced by Beyer and Sendhoff (2007) (§2.5.2). An overview of the method is presented below (Equation 4-25).

$$\begin{aligned}
 & \text{Min} \left[g(x) = \sum_{i=1}^n \left| \frac{\partial f(y_i)}{\partial y_i} \right| \right] \\
 & \text{subject to } f(y_i) = 0, \quad \text{if target is feasible} \\
 & \text{or Min } f(y_i), \quad \text{if target infeasible} \\
 & h(y_i) = 0, \quad \text{equilibrium equations} \\
 & j(y_i) \leq 0, \quad \text{overlap constraint} \\
 & \text{Min}(y_i) \leq y_i \leq \text{Max}(y_i)
 \end{aligned}$$

Equation 4-25

The method summarised above (Equation 4-25) minimises the function $g(x)$ to minimise the value of the sensitivities defined as the RMS of the derivatives, $\frac{\partial f(y_i)}{\partial y_i}$. Reducing the

4. Variability and robustness

RMS sum of the derivatives therefore reduces the effect that any change in a variable has on the function $f(y_i)$. Ensuring $f(y_i)$ is equal to zero, where $f(y_i) = \Sigma(\text{calculated}_i/\text{target}_i - 1)$, ensures that in the first instance the original targets of mechanical properties are still met. The equilibrium equation ensures that during optimisation the out-of-plane ‘amplitudes’ are equal to the sum of the yarn radii whilst the overlap constraint checks that yarns do not overlap each other.

In practice where more than one variable is under consideration, $g(x)$ becomes the absolute value of the sum of more than one set of partial derivatives relating to each target (E_{11} , E_{22} etc). Unlike Taguchi’s method which use DOE (Design of Experiment) methods (Beyer and Sendhoff, 2007) the optimisation routine used to calculate the optimum robustness is based on the previously used optimisation routines (Fsolve, PatternSearch, and Fmincon), a discussion of which was made in the literature review (§2.4.2.4).

The sensitivities are calculated using the sensitivity calculations described above (Equation 4-16). As such it is possible to change the sensitivities by altering the geometry. This is achieved by minimising the square of the absolute sum of the sensitivity calculations, whilst retaining the fabric in a condition that satisfies the targets, $f(y_i)$, which are now considered constraints. Some allowable variation in targets can be introduced, but in this demonstration of the method only two targets are considered which are both feasible. This ensures that a minimum of one or more possible solutions is possible, and that the sensitivity minimisation calculation is choosing the least sensitive geometry available. This least sensitive (most robust) geometry will satisfy the requirement that $(y_i) = 0$.

The method can also constrain the amount of deviation from an original geometry that is permitted by introducing the constraint $\text{Min}(y_i) \leq y_i \leq \text{Max}(y_i)$. This can limit the number of standard deviations that each individual variable can move from the mean, or original fabric.

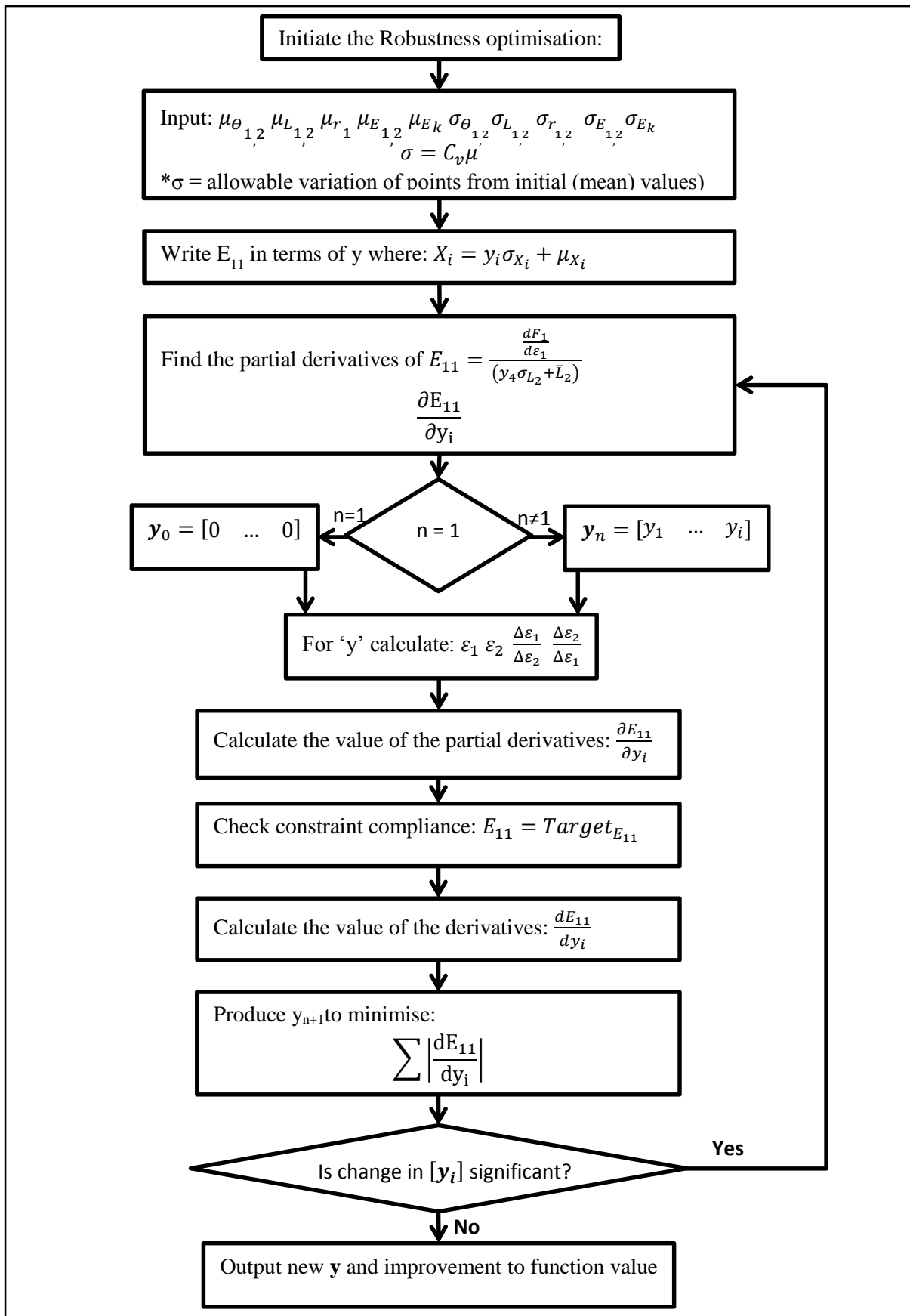
As with all reviewed methods of robust optimisation the presented method minimises a function with respect to some constraints (Beyer and Sendhoff, 2007; Schuëller and Jenson, 2008; Kim *et al.*, 2010) (Equation 4-26):

$$\text{Min } F = \{F_1(x), F_2(x), \dots, F_n(x)\}$$

Equation 4-26

$$\text{Subject to } g_j(x) \leq 0, \quad j = 1, 2, \dots, m$$

The method used to calculate the robust optimum solution is shown in detail below (Figure 4-35).

Figure 4-35: Methodology for robust design for a single target E_{11}

4. Variability and robustness

Two tests are carried out to verify the method presented in Figure 4-35: The first checks the robustness of an F1202 PVC coated polyester fabric when compared to two feasible targets (targets produced using the sawtooth method (§3.4.3), and the second checks the feasibility of an optimised fabric design other than that of the original fabric geometry to two feasible targets. Two feasible targets are used to reduce the computing time required for the considerably more complex and time consuming optimisation process. In addition this ensures that more than one possible solution exists, thus allowing for a more robust solution to be searched for whilst satisfying the target constraint. The amount of computing power required to run a sensitivity optimisation for a full set of twenty targets is currently unavailable. Two targets require between 4 and 8 hours to optimise, and the increase in time will not be linear. Therefore, to demonstrate the feasibility of the method it is carried out for two targets only.

Robustness of existing fabric considering two targets

An existing F1202 fabric geometry is tested for its sensitivity to individual geometric parameters (original), and then optimised for sensitivity to those parameters (robust optimised).

A coefficient of variation from the original geometry of 0.1 was chosen (this represents the variation that might be found in each property), and the allowable variation from the original targets was set to a single standard deviation ($-1 \leq y_i \leq +1$). This ensured that the new fabric design would be constrained to approximately the same 'space' as the original fabric geometry. Were the entire possible space of geometries to be searched for the most robust solution possible the number of standard deviations away from the mean geometry the model considers would have been set to infinity.

Before the robustness optimisation is carried out the original fabric geometry is produced using the method detailed in earlier chapters (§3.5.4), to allow for comparisons (Figure 4-36). A PVC coated polyester F1202 fabric geometry as described in the previous chapter was used as the basis for the test. The design variables ($Ph_{1,2}$ $L_{1,2}$ $r_{1,2}$ $E_{1,2}$ E_k) are then optimised to allow for the reduction of the fabric's total sensitivity to variation in them. The absolute sum of the original fabric sensitivities is 365.7.

The original geometry from which Figure 4-36 is created and the robustly optimised geometry are detailed in Table 4-7.

4. Variability and robustness

Fabric property	Original (F1202) geometry	Robustly optimised geometry
θ_1 (rad)	0.1014	0.1115
θ_2 (rad)	0.1805	0.1903
L_1 (mm)	0.6446	0.7090
L_2 (mm)	1.0817	0.9786
r_1 (mm)	0.1567	0.1411
r_2 (mm)	0.1062	0.1267
E_{y1} (kN/m)	880	955
E_{y2} (kN/m)	810	876
E_k (kN/m)	37	34

Table 4-7: Original and robustly optimised geometry for F1202 fabric.

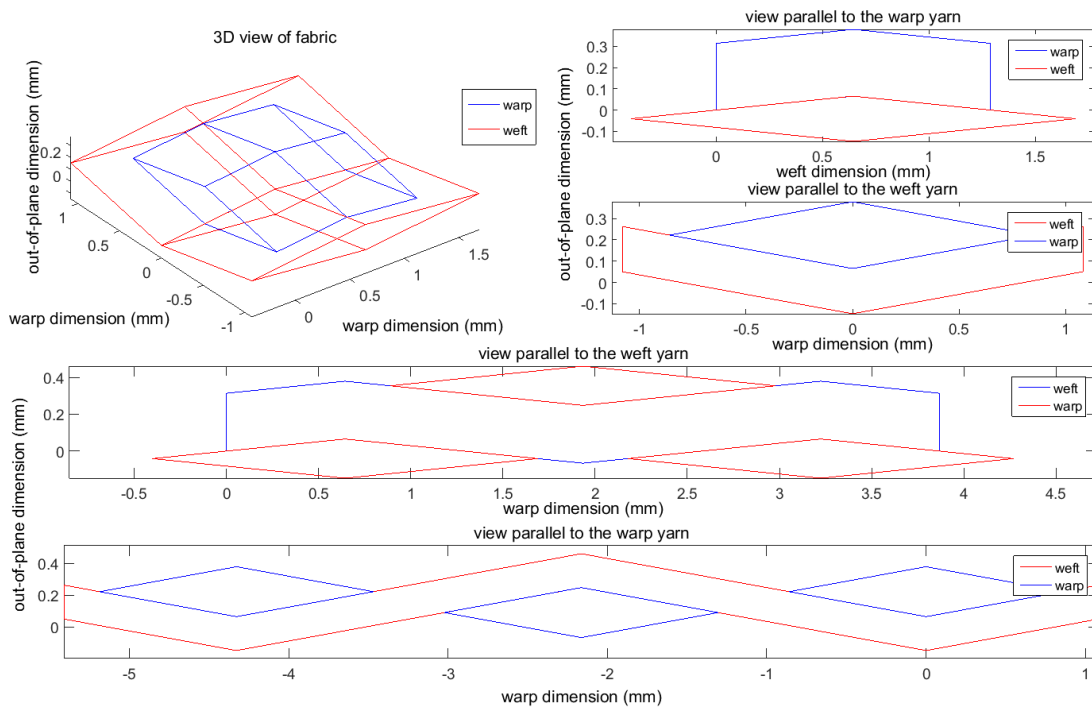


Figure 4-36: Original fabric geometry (F1202 PVC coated polyester)

4. Variability and robustness

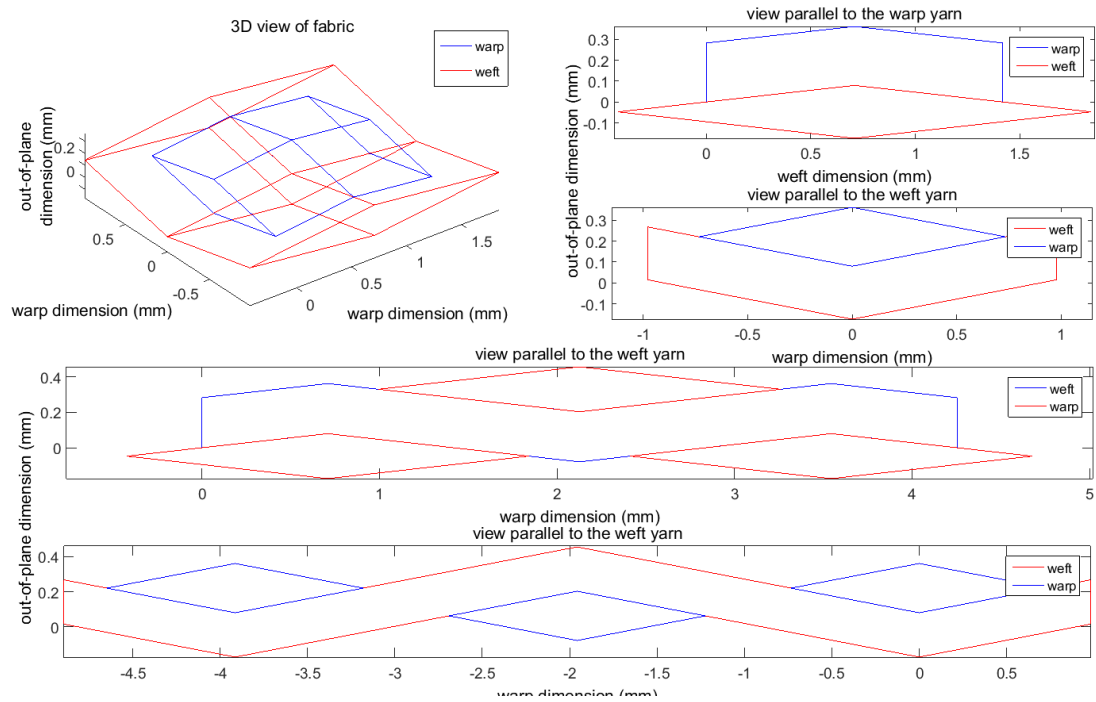
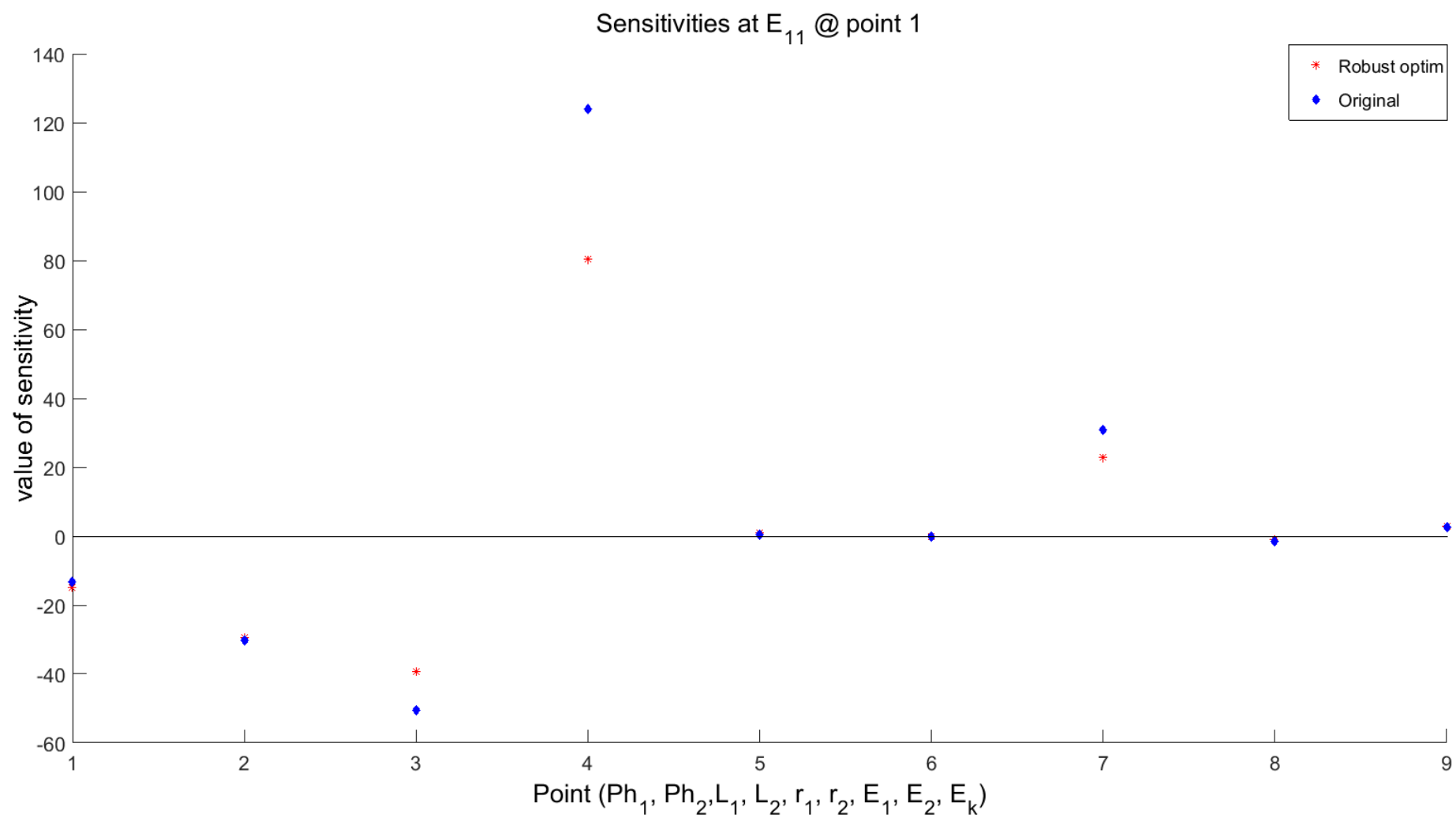
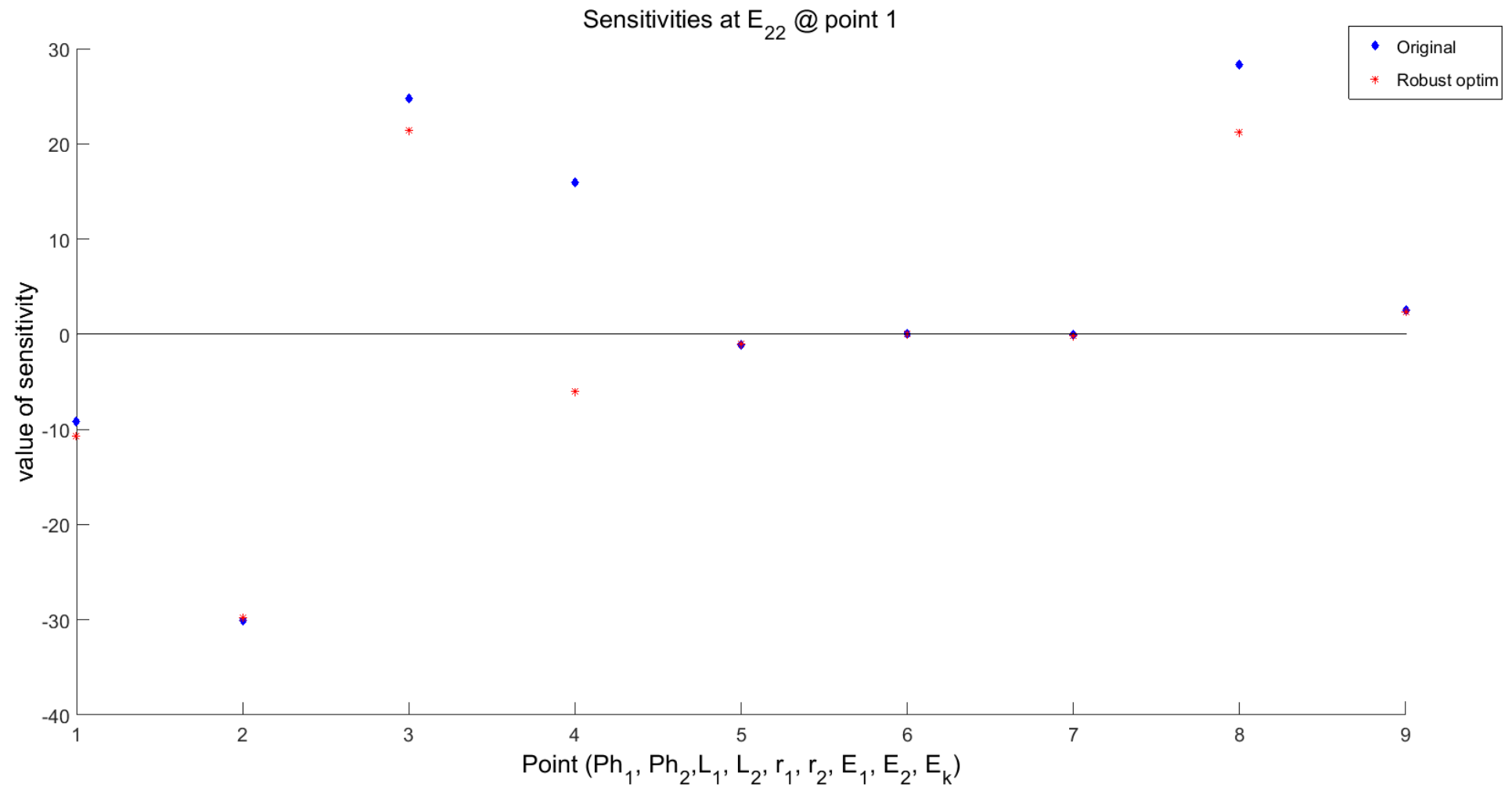


Figure 4-37: Robustly optimised fabric geometry for two targets (F1202 PVC coated polyester E₁₁ and E₂₂)

Figure 4-38: Sensitivities of the variables to the E_{11} target

Figure 4-39: Sensitivities of the variables to the E_{22} target

4. Variability and robustness

In the individual sensitivity figures (Figure 4-38, Figure 4-39, Figure 4-42, and Figure 4-43) the points on the x-axis relate to the geometry θ_1 to E_k respectively.

After the optimisation is carried out the new fabric's sum of sensitivities was 284.0 demonstrating an improvement of 22% from the original layout. It should however be noted that the fabric's similarity to the original is guaranteed by the limit placed on how much the geometry can vary (one standard deviation). Were a larger variation allowed a less sensitive geometry might have been produced. However, the geometry may have been less realistic.

The sensitivity of the targets to the individual unit cell properties are given in Figure 4-38 and Figure 4-39. A number of important points can be deduced from the figures:

- Firstly, the sensitivity to variation in the warp yarn out-of-plane angle (θ_1) is increased with respect to both E_{11} and E_{22} compared to the previous value of sensitivity, which leads to an overall reduction in the cumulative sensitivity by allowing change in the geometry of other points. Thus, increasing the robustness of the fabric as a whole has been achieved by increasing the fabric's sensitivity to the value of the out of plane angle. Increasing this sensitivity will allow for an alternate geometry which, overall, is less sensitive to variation.
- The radius of the weft yarn's sensitivity is zero in both instances. The sensitivity of the radius is encapsulated by the response of the other geometric variables.
- E_{11} is considerably more sensitive to the warp yarn stiffness than the weft yarn stiffness, whilst E_{22} is considerably more susceptible to variation in the weft yarn stiffness. This concurs with the Monte Carlo data (§4.7) where the target relating to E_{11} could be seen to be more sensitive to variation in E_{y1} . This also confirms the instinctive assumption that it would be the warp and weft yarn stiffness's that most affect the value of E_{11} and E_{22} respectively.
- At low loads (10:10kN/m) the geometry is found to be the cause of most sensitivity, confirming the observations of Dimitrov and Schock (1986).

Robustness of designed fabric considering two targets

An existing F1202 fabric geometry is tested for its sensitivity to individual geometric parameters (original), a fabric is then designed to reproduce its response (optimised), and then optimised for sensitivity to those parameters (robust optimised).

A fabric designed to reproduce the response of the of the original F1202 fabric using the method presented in the previous chapter (§3.5.4.1) is also tested, and the robustness of this fabric design is then optimised. One solution that was found is detailed below (Figure 4-40). The other variables in the test were the same as those set out above.

Fabric property	Original (F1202) geometry	Optimised geometry	Robustly optimised geometry
θ_1 (rad)	0.1014	0.1728	0.1812
θ_2 (rad)	0.1805	0.2347	0.2525
L_1 (mm)	0.6446	1.3969	1.4602
L_2 (mm)	1.0817	1.1222	1.2299
r_1 (mm)	0.1567	0.2719	0.2872
r_2 (mm)	0.1062	0.2402	0.2976
E_{y1} (kN/m)	880	6945	7031
E_{y2} (kN/m)	810	6945	7024
E_k (kN/m)	37	26	30

Table 4-8: Original and robustly optimised geometry for F1202 fabric.

The designed fabric has selected a very stiff (glass fibre type) yarn, but this does not interfere in the process of robustly optimising this new geometry.

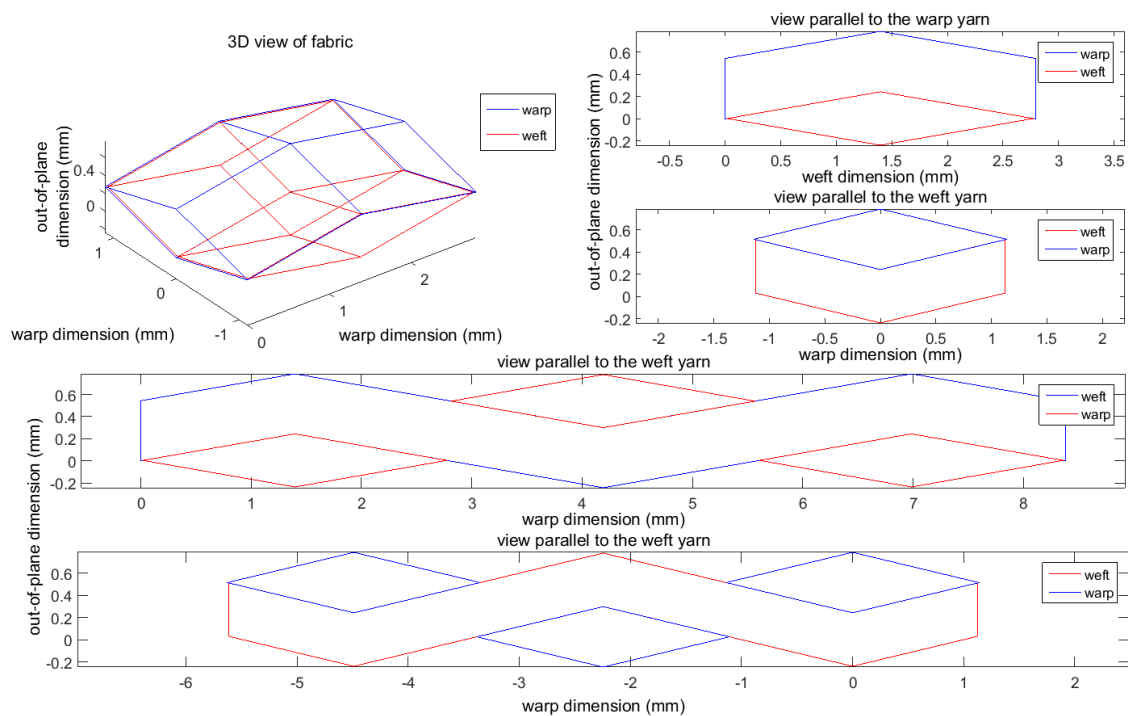


Figure 4-40: Designed fabric geometry for two targets (F1202 PVC coated polyester E_{11} and E_{22})

4. Variability and robustness

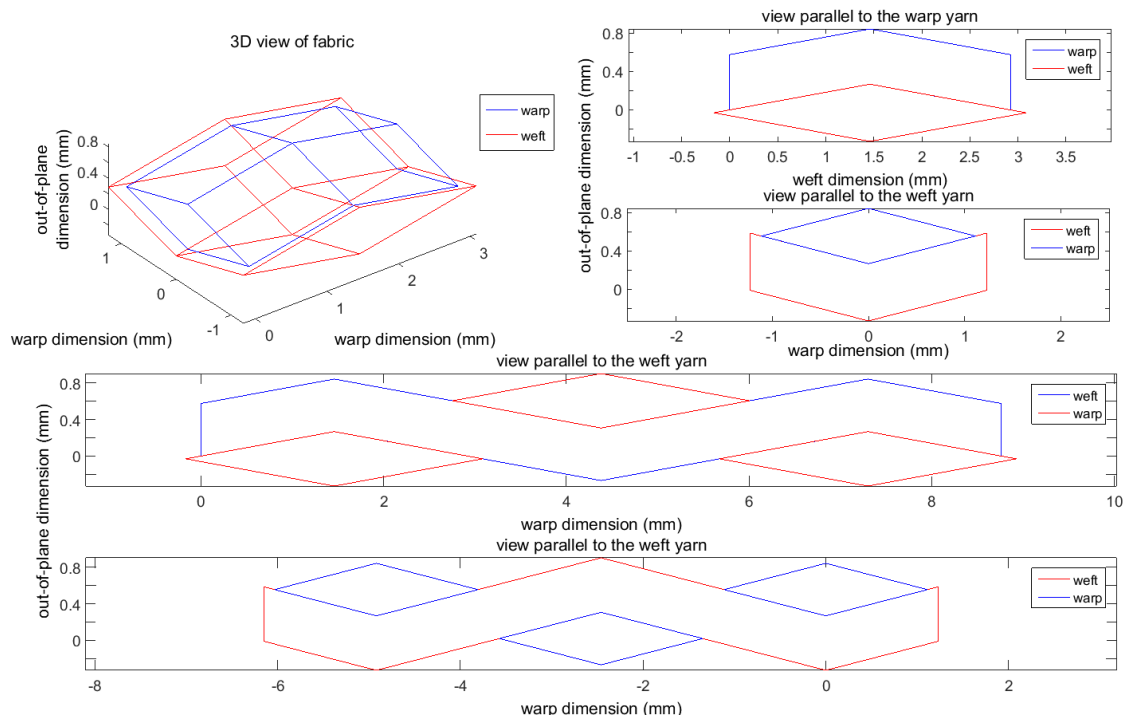
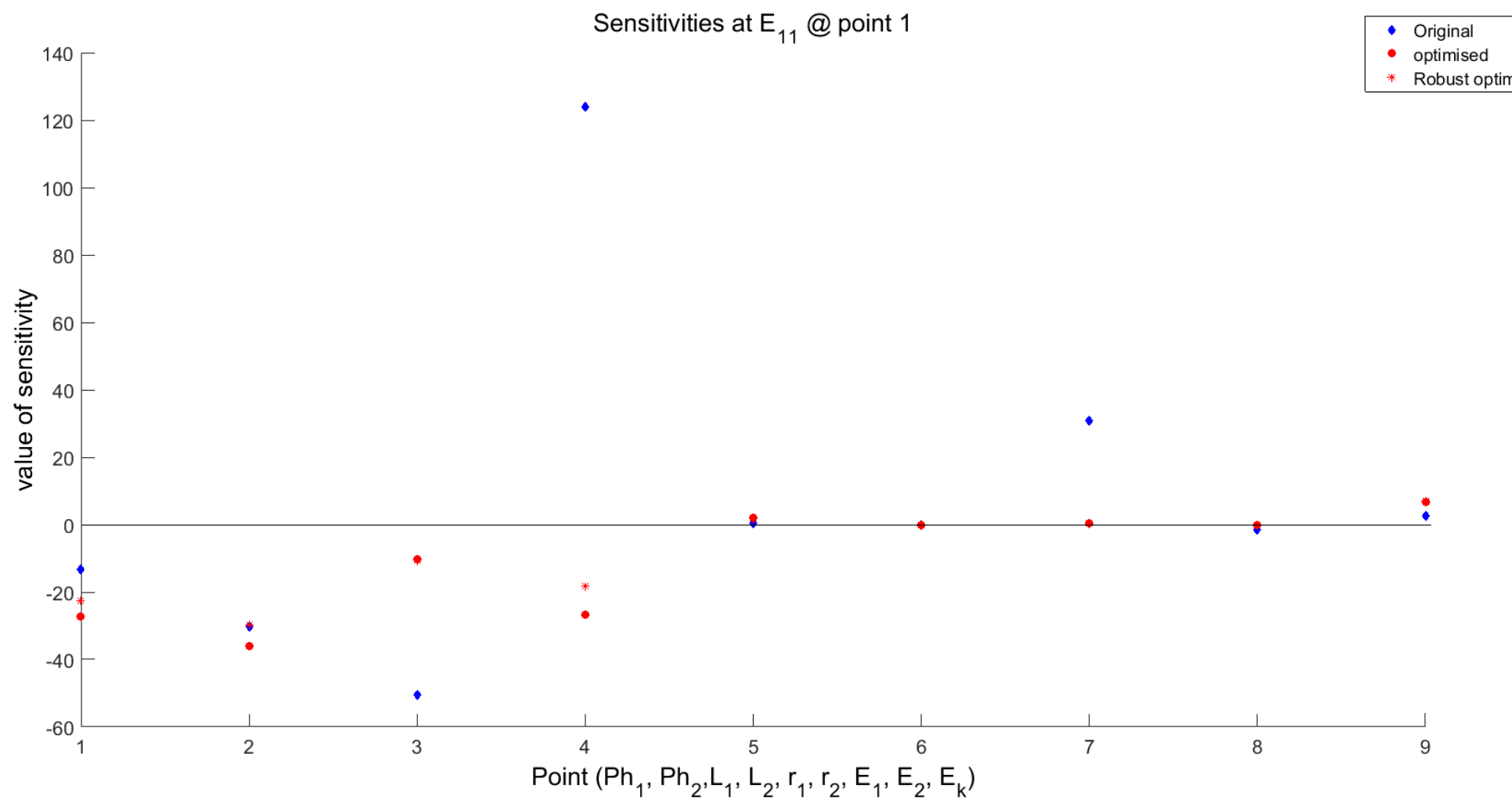
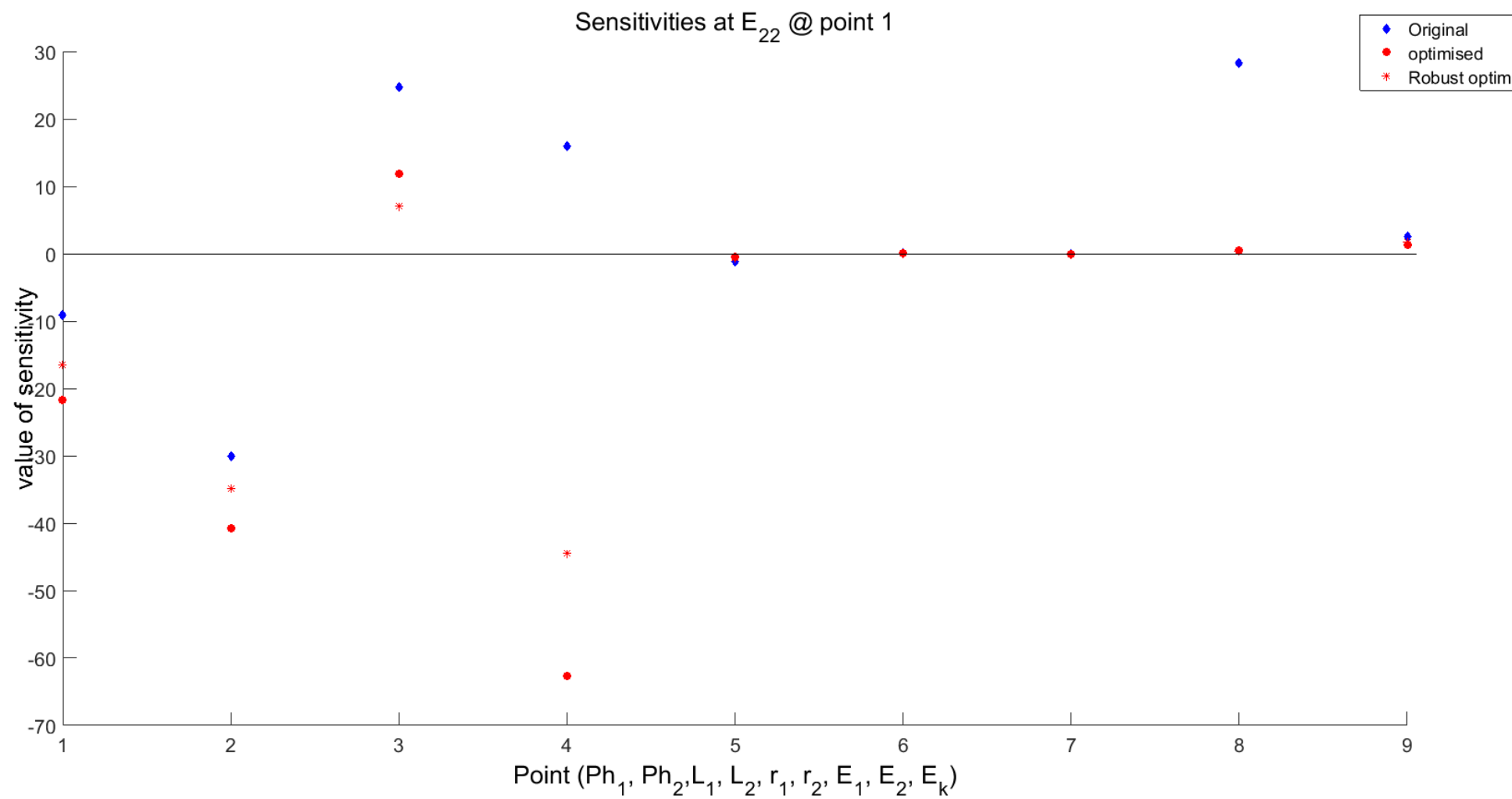


Figure 4-41: Robustly optimised fabric geometry for two targets (Optimised designed geometry)

Figure 4-42: Sensitivities of the variables to the E_{11} target

Figure 4-43: Sensitivities of the variables to the E_{22} target

4. Variability and robustness

Here the optimised geometry actually demonstrated a lower sensitivity to variation in properties than the original geometry from which the targets were produced (249). The principal improvement is the removal of the high sensitivity of E_{11} to r_1 . The new geometries are far less sensitive to r_1 . A number of new properties show higher values of sensitivity than the original fabric, which is then improved upon with the robust optimisation, producing a fabric with a combined sensitivity of 196, a considerable improvement on the original fabric. This has however been achieved by, for the most part, reducing the sensitivity of the stiffness to the value of L_2 to which the design appeared particularly sensitive. The function is actually more sensitive to some variables than the original geometry was. However the overall effect is to drastically reduce the fabric's overall sensitivity to variation in the design variables.

4.11. Discussion of application to the reliability index

The partial safety method derives the values of the partial factors and the ψ factors in one of two ways; either through the use of statistical data and methods, or calibration of long standing tradition and knowledge (BSI, 2006). Where the former is used the reliability index ' β ' is stipulated to "*ensure that no relevant limit state has been exceeded*" (BSI, 2006, p. 90). The reliability index is defined as the shortest distance to the limit state (Figure 4-44), where the probability of failure can be calculated in accordance with Equation 4-27.

$$p_f = \Phi(-\beta)$$

Equation 4-27

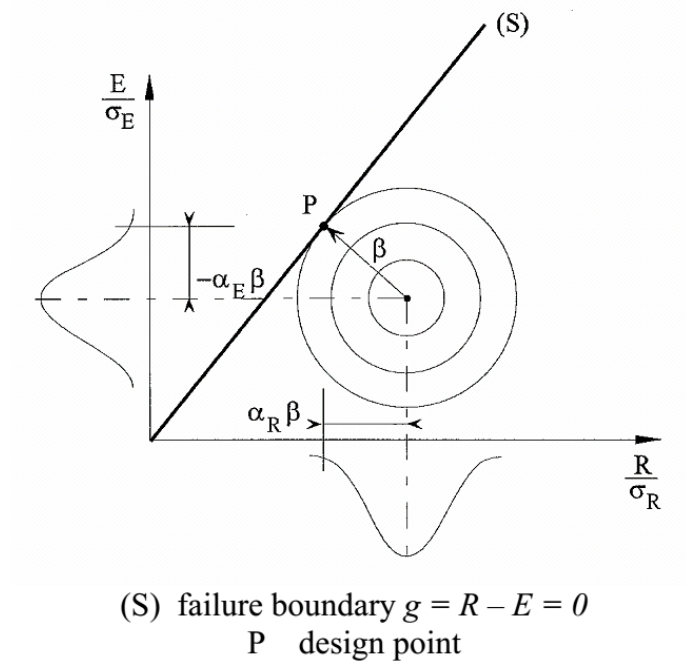


Figure 4-44: Design point and reliability index β according to the first order reliability method (FORM) for normally distributed uncorrelated variables (BSI, 2006)

Eurocode BS EN 1990:2002 appendix C (BSI, 2006) requires that for different design situations a different value of the reliability index is satisfied (Table 4-9). In the ultimate design case this will normally be 3.8, and in design terms equates to the use of the factors 1.35 (for permanent actions), 1.5 (for variable actions) and other factors.

4. Variability and robustness

Limit State	Target reliability index	
	1 year	50 years
Ultimate	4.7	3.8
Fatigue		1.5 to 3.8 ²⁾
Serviceability (irreversible)	2.9	1.5
1) See Annex B 2) Depends on degree of inspectability, reparability and damage tolerance.		

Table 4-9: Target reliability index β for Class RC2 structural members ¹⁾ (BSI, 2006)

The factors accompanying material properties are calculated for known variability in the material. Concrete is found to be more variable in its constitutive properties than steel, for instance, as the nature of in-situ casting reduces the surety of the finished product. Similarly as discussed by Forster and Mollaert (2004) in the Tensinet Design Guide the material factors applied to fabrics are very high. This is due to the high degree of uncertainty regarding the performance of architectural fabric.

Increasing the factors used in material, loading, or other calculations during the design process therefore creates a situation where “*no relevant limit state has been exceeded*” (BSI, 2006, p. 90) . Or put another way the reliability index is restrained to a value greater than 3.8. Where there is a high variability in a particular resistance or action that affects the structures response it must be adequately factored to ensure that the reliability index remains above 3.8.

Figure 4-45 (BSI, 2006) shows how the different actions and uncertainty in material properties from the two factors γ_F (action and effect) and γ_M (material). Using detailed data on the uncertainty of the fabric’s material properties it should therefore be possible to reduce the value of γ_m , and similarly using detailed knowledge of how a fabric responds should decrease the value of γ_{Rd} . The probability of the effect (E) exceeding the design resistance can be calculated using Equation 4-28.

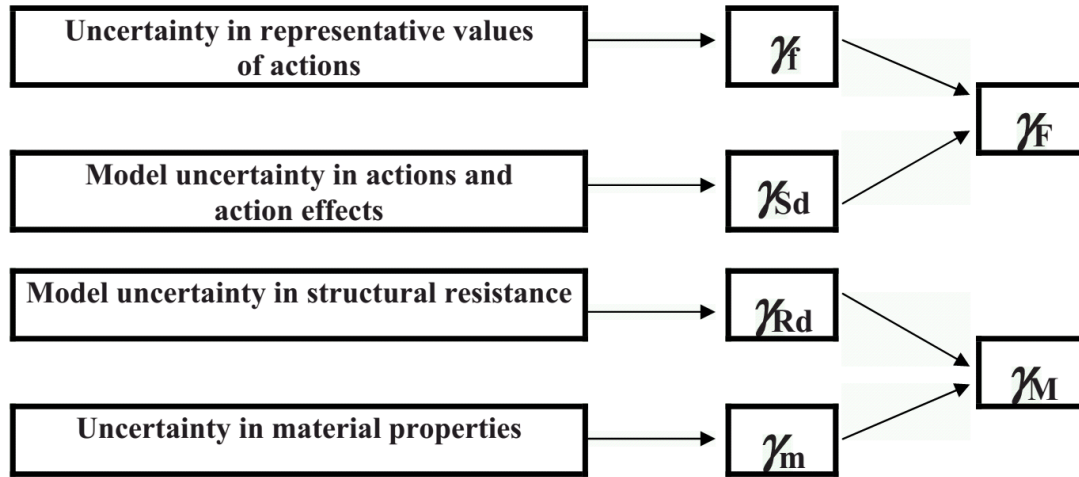


Figure 4-45: relationship between individual partial factors (BSI, 2006)

$$P(E > E_d) = \Phi(+\alpha_E\beta)$$

$$P(R \leq R_d) = \Phi(-\alpha_R\beta)$$

Equation 4-28

Where:

β is the target reliability index

α_E and α_R , with $|\alpha| \leq 1$, are the values of the FORM sensitivity factors. The value of α is negative for unfavourable actions and action effects, and positive for resistances.

A full methodology for how this might be applied in practice is beyond the scope of this project, however a discussion of how it can be applied is detailed below:

For a particular fabric the probability of success must result in a value of $\beta \geq 3.8$. The “uncertainty in representative values of actions” and the “uncertainty in actions” (BSI, 2006, p. 97) is fixed and defined BS EN 1991. Therefore the reduction in factors must be achieved in the consideration of material properties and structural resistance.

The fabric coating and yarn property variability can be determined using testing (§4.7). Therefore the variation in resistance (stiffness) remains to be calculated. This can be achieved using Monte Carlo simulations (Figure 4-46) or the FORM method. Knowledge of the distribution and variation in structural resistance is therefore available.

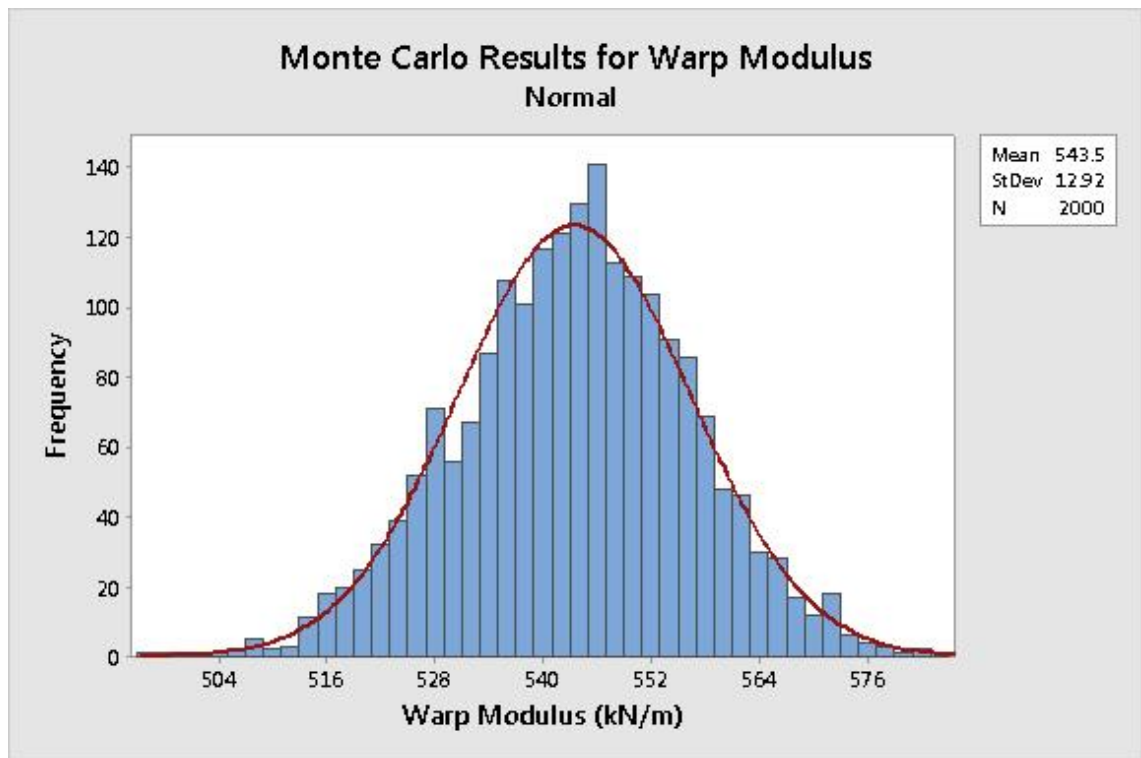


Figure 4-46: Probability density function from Monte Carlo data where r_2 and θ_1 were varied with $C_v = 0.1$.

The method would briefly comprise:

- Information required: Mean and standard deviation of fabric yarn and coating properties.
- Intermediate information: Mean and standard deviation of the objective function (stiffness).
- Result: Value of β for the variation in fabric yarn and coating properties at different load cases for required confidence interval.

The calculation of the value of β for the variation in fabric yarn and coating properties is then modified by partial factors to ensure that a sufficient level of confidence is maintained. In practice this will involve increasing the resistance of the fabric by reducing its allowable load or extension. Once this has been achieved the value of β should be greater than or equal to 3.8, i.e there is a 0.000723 probability of the fabric not satisfying the design.

This should result in more efficient designs where lower safety factors are utilised in the design and construction process. Reducing the sensitivity of the fabric to variation in the model variables will further help reduce the necessary factors. However, it is

4. Variability and robustness

conceivable that this could result in a higher safety factor if a fabric is unusually susceptible to variation.

4.12. Conclusions

This chapter has presented both a Monte Carlo and a FORM method for the predictive simulation of the effect of variability on the mechanical properties of fabrics. Both the methods produced required the calculation of one variable directly from the values of the others to ensure the compliance with the equilibrium constraint. This process results in the encapsulation of the variability of one variable into the response of the fabric through the variation in the others. Ensuring the compliance of the simulations to the constraints discussed in the previous chapter is necessary to ensure the model's validity. Without compliance with the constraint equations it is possible that yarns could exist in the same space, overlapping, or that the yarns could become disassociated from each other. Additionally, without compliance with these constraints, the derivatives that allow for the calculation of the mechanical properties of a fabric can no longer be expected to produce accurate results. The use of these equations presupposes that the equilibrium constraints have been complied with. One problem with this method is that the normal distributions of calculated mechanical properties when using higher values of variation (C_v) cannot be guaranteed. However, to ensure a predictive method is presented a distribution for the objective function must be assumed to allow the calculation of the probability of failure in the FORM method. The Monte Carlo method, however, does not require this information.

A comparison between the FORM and Monte Carlo methods shows considerable variation between the results obtained from the two methods in some simulations. This is due to the assumption of normality in the FORM method, where non-normal results may be present. Without carrying out a Monte Carlo analysis for each fabric and each set of variation parameters it is impossible to tell which fit will most accurately predict the response of a fabric. Though the results should generally be normally distributed due to the interaction of two normal curves. Therefore, to allow prediction of non-existent fabrics, or the robustness (§4.10) of existing fabrics without considerable outlay in time, it is necessary to assume normal distribution.

Variation in a single basic variable affects the mechanical properties of the whole fabric to a greater or lesser extent depending on the property under consideration and the basic variable being investigated. Monte Carlo tests (§4.7.3) showed that variation in the output produced by individual basic variables could be visualised graphically (Figure 4-13)

4. Variability and robustness

and that the effect of each variable on the result was not constant. The fabric was noted to be more sensitive to variation in some variables than others, namely L_1 and L_2 when considering E_{22} and E_{11} respectively. The FORM methodology allowed for the quantification of this sensitivity. Finally the robust optimisation method allows the values of these sensitivities, and their effect on a fabric to be optimised to reduce the overall effect the variables have on a fabric.

The method to maximise the robustness of a fabric's design produces considerable improvement in the sensitivity of a fabric to variation in its geometric properties and the mechanical properties of the coating and yarns. This can result in the increasing of the sensitivity of a fabric of a fabric to a particular variable, with a corresponding greater improvement across other variables. The complex nonlinear behaviour of fabrics means that without the method developed it would be impossible to optimise a fabric in such a way using only Monte Carlo or FORM results.

Both the Monte Carlo and FORM methods rely on the use of data that is normally distributed. Data on the variability of the geometry of fabrics, and how they can be considered normally distributed was presented at the beginning of the chapter. Normal distributions best fit the available data, demonstrated by the probabilities presented.

5. Model Validation

5.1. Model validation

The model validation is split into three distinct parts: First a discussion of testing methodologies is made. This includes a discussion of uniaxial and biaxial testing, a review of the method of processing biaxial data, the creation of a method for the testing of individual yarns for elastic moduli, a review of the tensile strengths of fabrics, and a method for the calculation of target values of elastic constants at multiple biaxial stress states.

This is followed by comparisons of the model to results for known feasible targets (targets which have been derived from sawtooth simulations of fabric biaxial stress-strain response). This demonstrates how the model can find fabric geometries that reproduce target values of Young's Modulus and Poisson's ratio which are not always the same as the original geometry from which the targets are derived. However, it is also demonstrated that the model, when sufficiently constrained, finds the original geometry form which the targets were derived.

Following this a comparison of designed fabrics to real fabric geometry and biaxial stress-strain response is made. Real target values of elastic constants at multiple biaxial stress states are used as the input for the predictive design model, and real fabric geometries are compared to the output. Unfortunately this is less successful than when the model is compared to known feasible targets, and a discussion of the reasons for this is also made. A real measured fabric geometry is also used as the input for the robust fabric geometry optimisation method described in the previous chapter (§4.10). Statistical data regarding the fabric geometry is also used rather than assumed values of variation.

5.2. Methodology for testing of fabrics

5.2.1. Uniaxial testing

Uniaxial testing (Figure 5-1) is used to test a fabric's response under loading in only one direction, normally along the warp yarns, along the weft yarns and at 45° to each in a bias test (Colman, 2014). In this project uniaxial testing is used to measure the yarn modulus by testing only one yarn direction at a time, and thus removing the crimp in that yarn (Dimitrov and Schock, 1986). At this point the response of the fabric will be largely that of the yarns in one direction only, and therefore the yarn modulus can be calculated from the stress-strain response of the specimen (Figure 5-1). This works because the stiffness of the coating is considerably less than that of the yarn. Uniaxial testing was carried out by Colman (2014). Uniaxial tests often include multiple repeats of loading and unloading, which produces hysteresis, as demonstrated below (Figure 5-1).

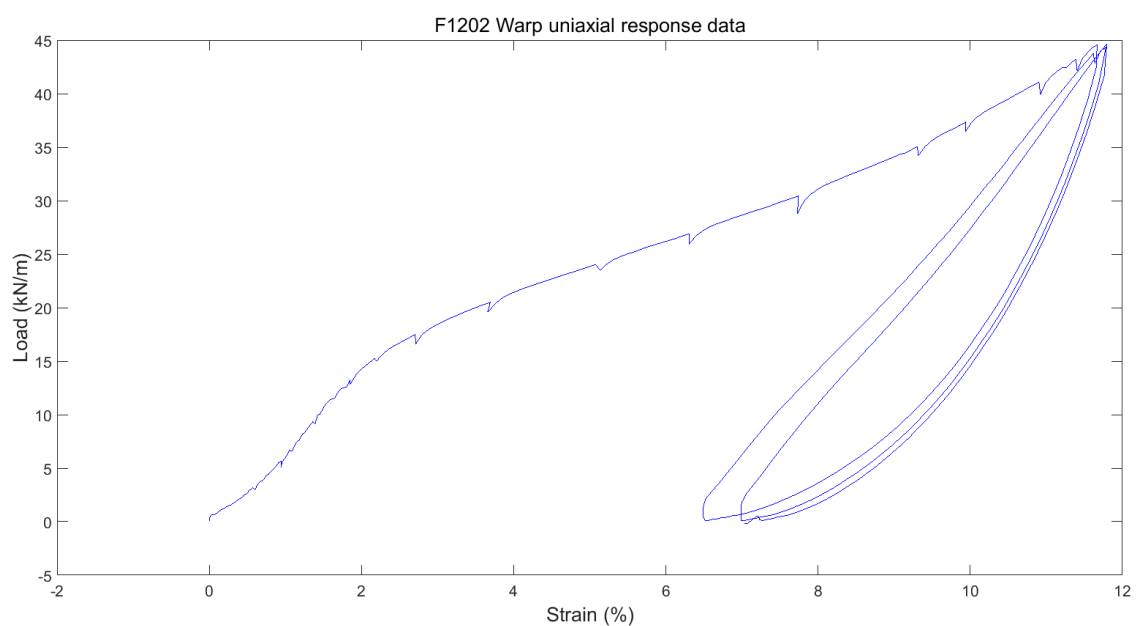


Figure 5-1: Uniaxial stress strain curve, showing hysteresis in the fabric response under repeated loading (F1202 Warp data (Colman, 2013b))

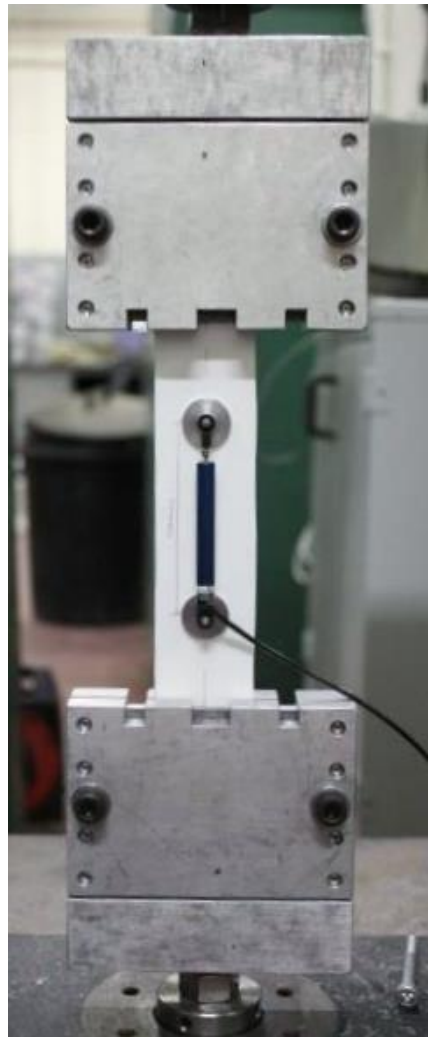


Figure 5-2: Uniaxial testing equipment for stress-strain response reproduced from (Newcastle_University, 2012)

5.2.1.1. *Uniaxial testing methodology*

The following is the abbreviated methodology for the uniaxial testing of a fabric for the calculation of uniaxial stiffness, not tensile strength (which is described in BS EN ISO 1421 1998 Determination of tensile strength and elongation at break (BSI, 1998)) or seam strength (which is described in BS 3424 Part 33 Method 36 - seam strength (BSI, 1996)).

The uniaxial test for stress-strain response uses a flat jaw with grooves to minimise slippage of the sample (Figure 5-2). The sample (200mm in length) is tested in a constant rate of extension testing machine (INSTROM) at a rate of 100mm/min, although this can be varied (Figure 5-3). An LVDT (linear variable differential transformer – strain measurement device) is placed along the centre line of the sample to give accurate strain read outs. This method limits the amount of displacement that can be recorded

to 35mm as the LVDT will not extend beyond this. The data in Figure 5-1 for instance demonstrates uniaxial fabric hysteresis after the removal of initial fabric creep.

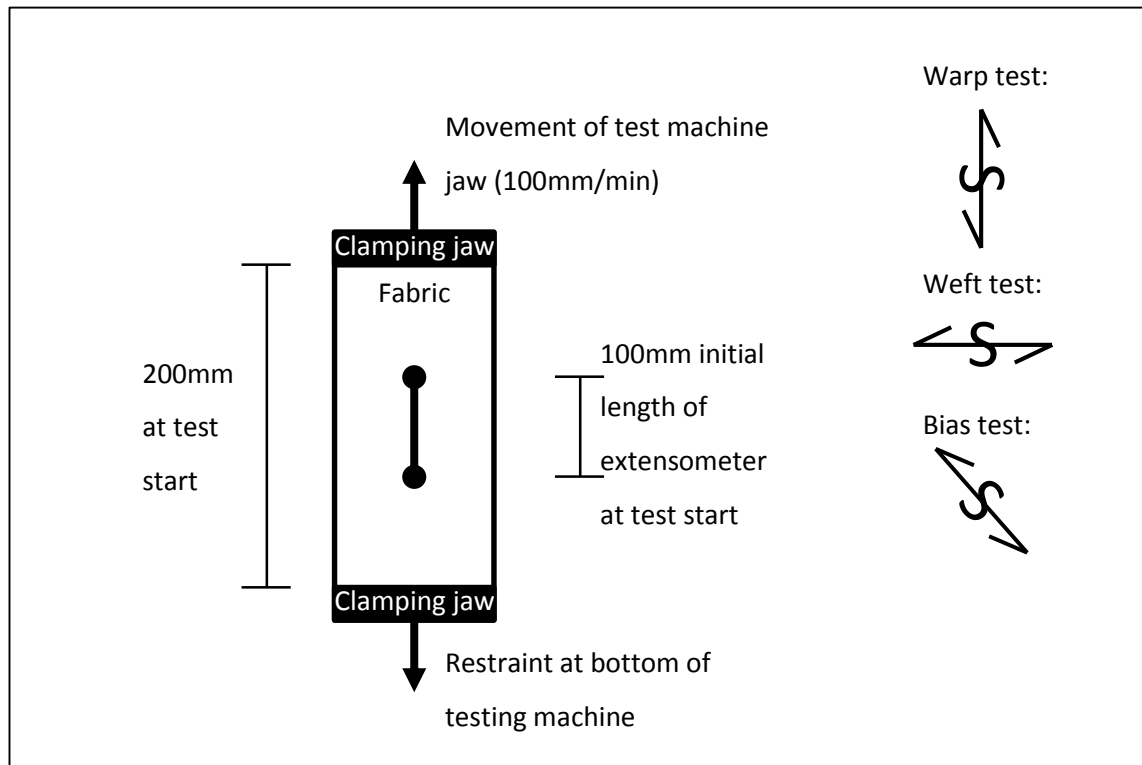


Figure 5-3: Uniaxial test setup

Uniaxial testing has been used to calculate the yarn and coating stiffnesses used in previous chapters.

5.2.2. Biaxial testing

Biaxial testing is used to produce a fabric's stress-strain behaviour in both the warp and weft directions. The advantage of Biaxial testing is that a more realistic response of the fabric is obtained as *"uniaxial tensile tests subject a material to loads that hardly ever occur in practice"* (Menges and Meffert, 1976, p. 12). Fabrics are almost always under biaxial or biaxial and shear stress during normal operation, meaning that the response to biaxial loading is more relevant to real world situations.

The biaxial test apparatus used at Newcastle University (Figure 5-4) tests *"cruciform specimens"* which *"are cut in line with the warp and fill yarns, not necessarily orthogonally"* (Bridgens and Gosling, 2008, p. 3). As fabrics resist loads in the direction of the yarns this allows for the bowing of yarns to be taken into account (§2.2.6), and

avoids the introduction of shear forces by ensuring that stress is acting only in the direction of the yarns.

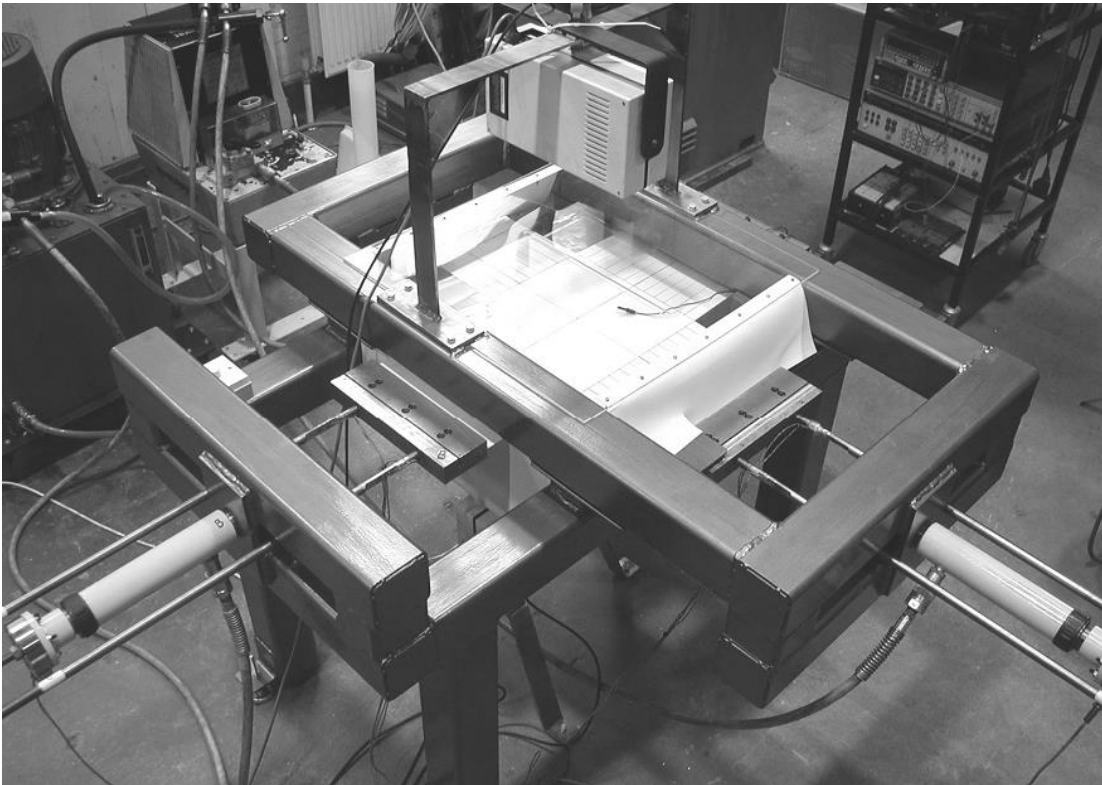


Figure 5-4: Biaxial test apparatus used at Newcastle University, reproduced from: (Bridgens and Gosling, 2008)

Test data used in this report uses a newer biaxial test rig than that pictured in Figure 5-4, which includes automated controls.

5.2.2.1. *Biaxial testing methodology*

A test specimen is cut to the required dimensions for the testing rig to be used. In Newcastle this involves a 300mm by 300mm test specimen cut to account for non-orthotropic yarns with 300mm arms as shown in Figure 5-5. LVDTs are attached to record the strain in the specimen; with one positioned in the warp direction, one in the weft direction, and one at 45° to the other two. The sample is then installed in the testing rig, with slack manually removed from the sample. A prestress is then applied to the sample, and prior to each iteration a set of 1:1 loads are applied to remove any conditioning from the sample (Membrane Structures Association of Japan, 1995; Bridgens and Gosling, 2008).

5. Model validation

A standard test protocol can then be carried out (Figure 5-6). This procedure of applying *“prestress followed by mechanical conditioning provides repeatable stress-strain data for medium to long term structural design”* (Bridgens and Gosling, 2008, p. 4). The profile used in this report runs three cycles of each of the following load ratios; 1:1, 2:1, 1:1, 1:2, 1:1, 1:0, 1:1, 0:1, 1:1 as described in the MSAJ testing method (Membrane Structures Association of Japan, 1995, p. 2). Each load ratio is run three times as shown in Figure 5-6. Other test profiles have also been developed such as the one shown in Figure 5-7 from the Tensinet Design Guide (Forster and Mollaert, 2004), or the radial load regime developed by Bridgens and Gosling (2008) which is designed to populate the entire stress space with strain data (Figure 5-8).

The MSAJ test method returns the test sample to an original 1:1 ratio after each iteration which ensures repeatability of results by beginning each test from a similar load history. Load history has been shown to affect load response, as such it is important to control this during testing with two load cycles required to settle the response (Jackson *et al.*, 2009).

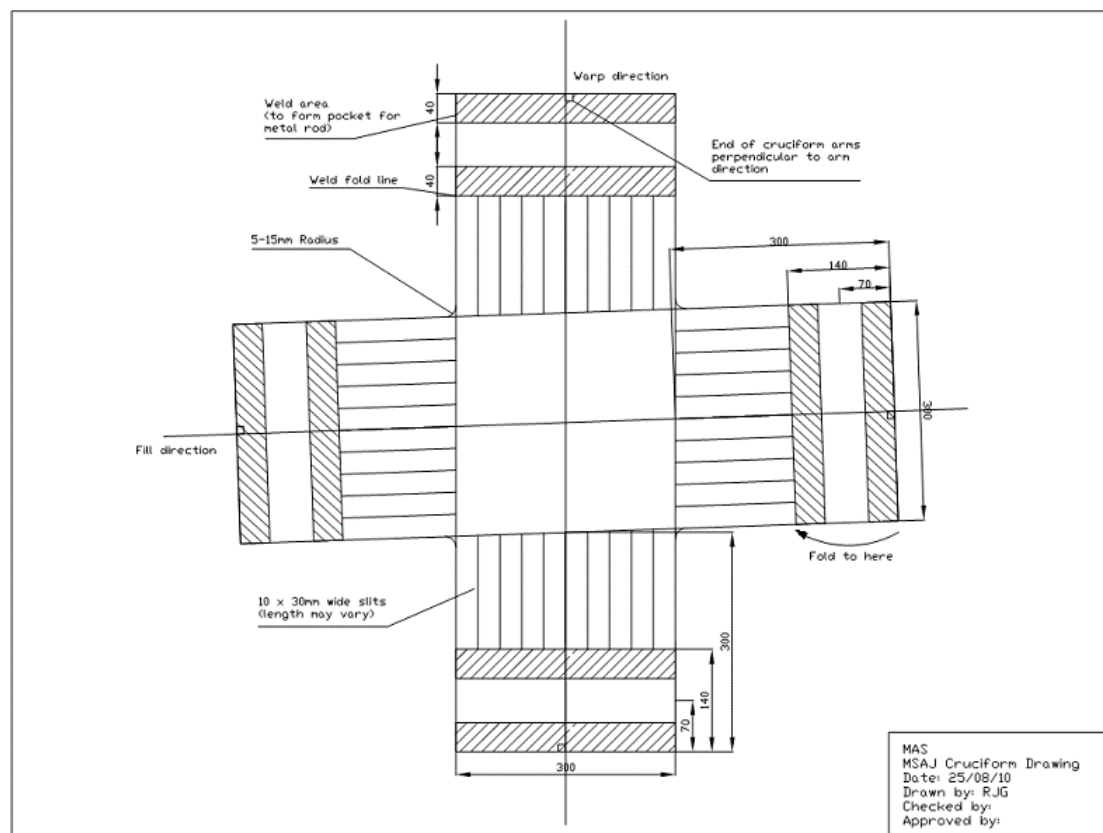


Figure 5-5: MSAJ cruciform specification (Membrane Structures Association of Japan, 1995)

5. Model validation

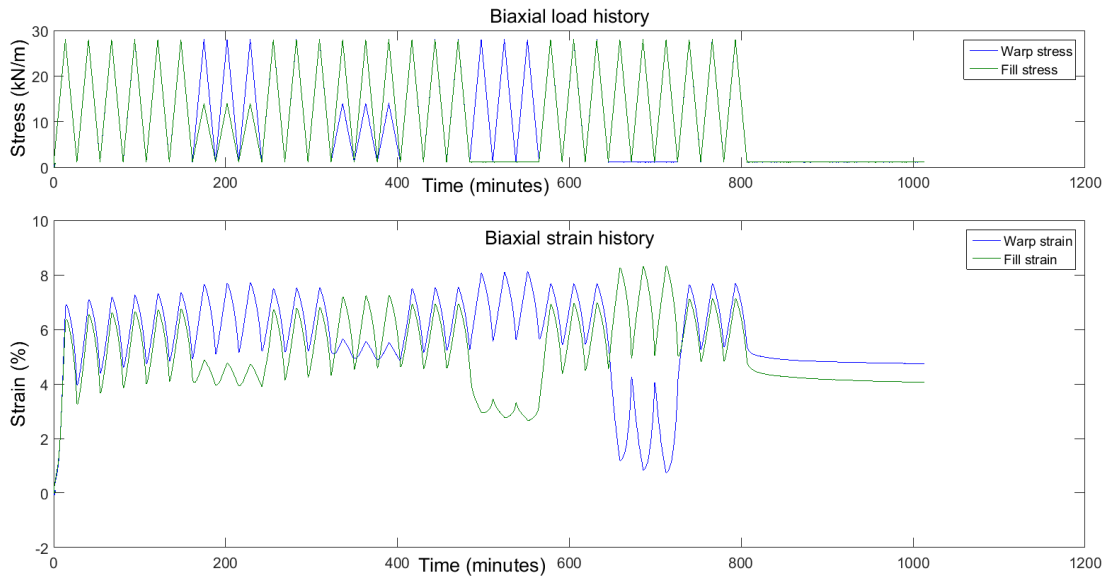


Figure 5-6: Example biaxial response for F1202 fabric

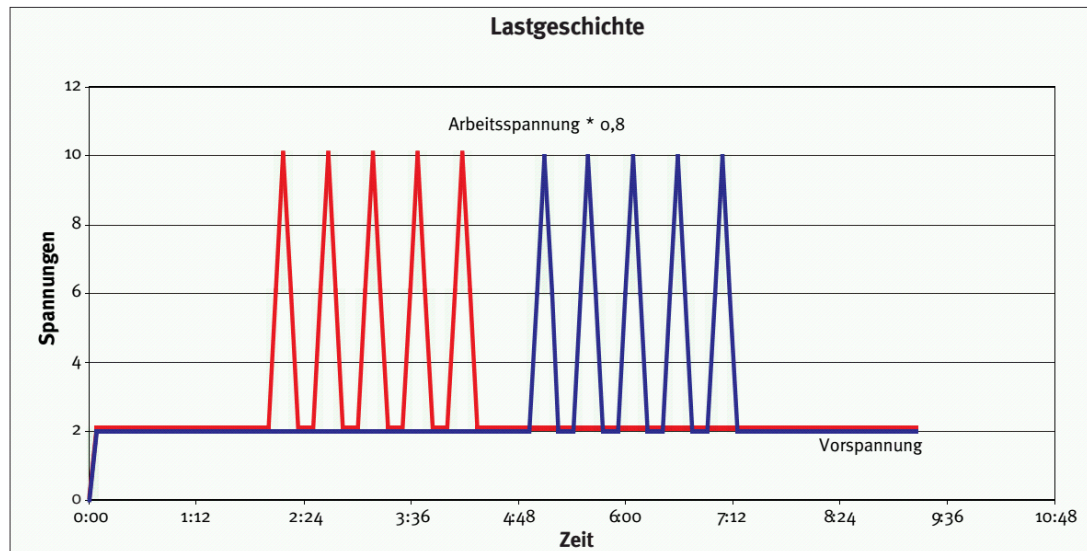


Figure 5-7: Characteristic load history, red = stress in warp direction, blue is the stress in the weft direction from the Tensinet Design Guide (Forster and Mollaert, 2004)

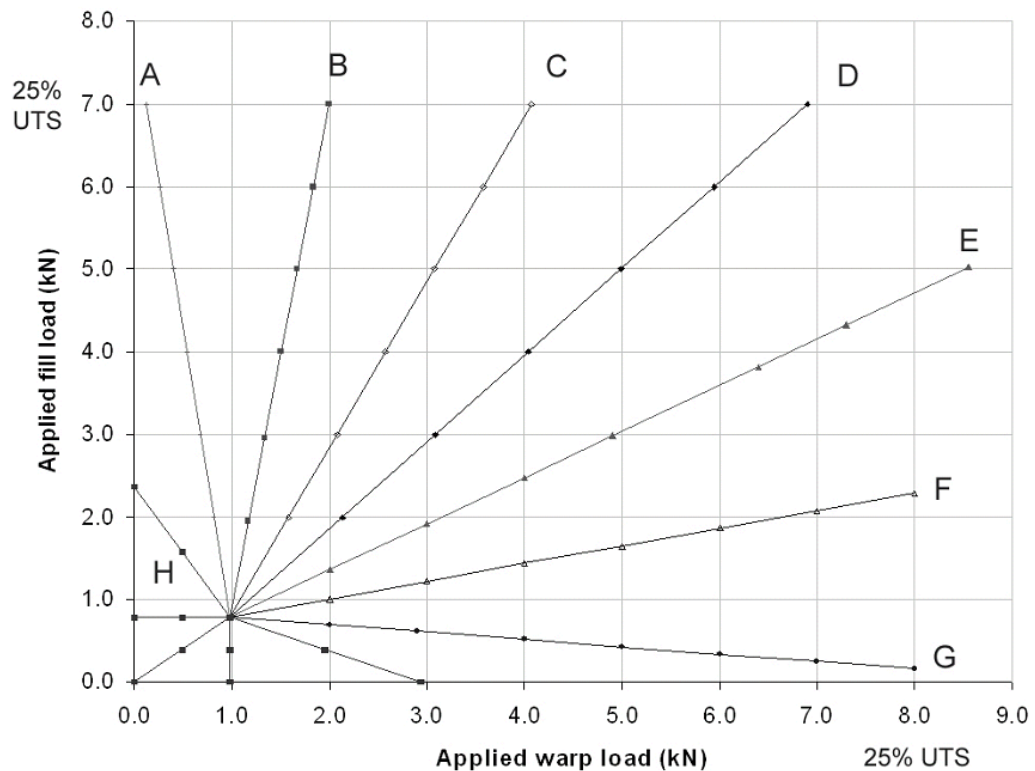
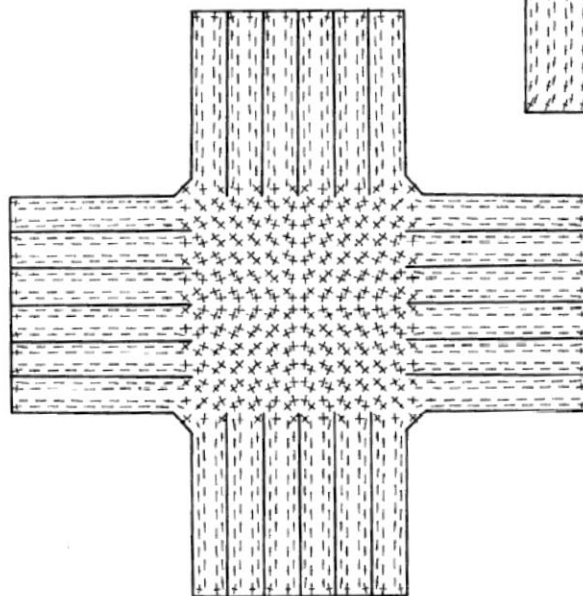
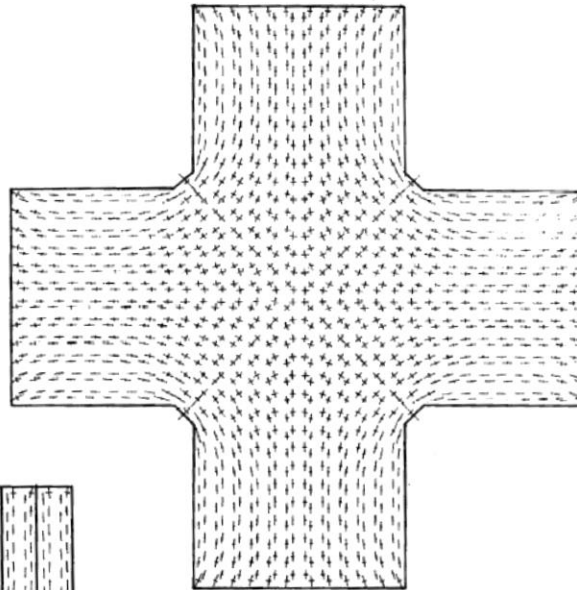


Figure 5-8: Radial load regime (Bridgens and Gosling, 2008, p. 4)

The slits in the arms (Figure 5-5) ensure that the stress developed at the centre of the specimen is closer to that applied to the specimen. Without the slits deformation occurs in the arms, resulting in only 72% of applied stress at the centre of the sample. With slits in the arms this is increased to 92% (Membrane Structures Association of Japan, 1995). Figure 5-9 shows a finite element representation of a cruciform specimen with and without slits in the arms. When no slits are present some biaxial stress can be seen in the arms of the sample, which results in deformation, resulting in decreased stress at the centre of the sample.

Commentary fig.-3
Plot of principal stresses of an
isotropic elastic specimen
without slits (Load ratio 1:1)



Commentary fig.-4 Plot of principal stresses of an isotropic
elastic specimen with slits (Load ratio 1:1)

Figure 5-9: Finite element representation of stress distribution in the cruciform specimen (Membrane Structures Association of Japan, 1995)

5.2.2.2. *Determination of elastic constants from biaxial test data*

Biaxial data is initially processed as follows and utilises a MatLab code produced at Newcastle University to process biaxial data based on the MSAJ standard (Membrane Structures Association of Japan, 1995):

- Initial low loads (i.e. manual loading) can be removed
- Initial strains can be zeroed at the start of the profile
- Data is then trimmed to remove excessive data points at the end of the profile

- Cycles are then identified automatically
- At this point response plots can be produced for individual cycles
- Elastic constants can then be calculated using strain or stress minimisation

Elastic constants are calculated using differential stress or strain minimisation to ‘fit’ a plane stress representation to the biaxial data from which elastic constants are then calculated. The method uses differential minimisation to find the best fit plane stress representation of elastic constants to the biaxial response data. Conceptually both stress and strain minimisation are similar as both minimise the difference between a plane stress surface and test data to give a best fit surface. However, stress minimisation minimises the error between a plane stress surface and measured stresses, whilst strain minimisation minimises the error between the surface and the measured strains. The different methods can have marked differences in outcome, as will be shown later (Table 5-1). The methods consider both constrained and unconstrained formulations, i.e. that the relationship in Equation 5-1 (Jones and Pickett, 2005) holds for constrained minimisation, whilst it is not a requirement of the unconstrained minimisation.

$$\frac{\nu_{21}}{E_2} = \frac{\nu_{12}}{E_1}$$

Equation 5-1

where ν_{21} and ν_{12} are the Poisson’s ratios in the warp-weft, and weft-warp directions respectively, and E_2 and E_1 are the fabric stiffnesses in the weft and warp directions respectively.

The reciprocal relationship (Equation 5-1) does not necessarily hold for fabrics as they are not a homogeneous material (§2.2.7.3) (Gosling and Bridgens, 2008) i.e. the *“interaction of warp and fill yarns and the behaviour of the twisted yarn structure mean that [fabrics] are better described as a mechanism”* (Gosling and Bridgens, 2008, p. 220). It is possible with testing to show that the Poisson’s ratio can also be greater than 0.5, not possible in simple homogeneous materials. As such the unconstrained minimisations do not require that the reciprocal relationship is fulfilled. Loss of energy where the reciprocal equation is not held can be accounted for in the friction between and within yarns, and permanent deformation (Gosling and Bridgens, 2008).

5. Model validation

The equations for the unconstrained and constrained stress and strain minimisation can be found in the appendix (§A.10).

The constrained differential strain minimisation calculates the inverse of '**M**' (Equation A-31) and multiplies this by '**N**' (Equation A-32) to give the elastic constants (Equation A-33).

The coefficient of determination or ' R^2 ' value for the constrained differential strain minimisation is then calculated using the methodology described in the literature review (§2.5.1) (Ayyub and McCuen, 1997).

The unconstrained strain minimisation and constrained and unconstrained stress minimisation routines are also described (Equation A-35 to Equation A-43) (Membrane Structures Association of Japan, 1995).

In the minimisation equations **E**(1) etc. is the first value in the matrix **E**[...]. E_x and E_y are the warp and weft stiffnesses respectively, and ϵ_x and ϵ_y are the warp and weft strains respectively.

5. Model validation

Examples of the results as calculated for a PVC coated polyester fabric (Ferrari Preconstraint F1202 PVC-polyester) (§A.1) are shown below (Table 5-1). From this the difference between constrained and unconstrained minimisation becomes clearer. The unconstrained minimisation generally produces a higher R^2 value although given that the fit is less constrained this might be expected. There is also a marked variation in the Poisson's ratios which have a far greater variation in the unconstrained variation than their constrained counterparts. Given the highly nonlinear nature of fabric response and the non-homogeneity of the material it is possible that a ratio of greater than 0.5 might be produced (Gosling and Bridgens, 2008). Mechanical interaction between warp and weft yarns and crushing of yarns may result in a situation where the extension of one yarn produces an equivalent contraction in the other direction that is larger than can be accounted for if the Poisson's ratio is limited to 0.5. There is also variation in the value of Young's modulus produced (up to 282kN/m in the warp direction), which again is due to the type of optimisation carried out.

Analysis	E_x (kN/m)	E_y (kN/m)	ν_{xy}	ν_{yx}	R^2
Constrained, Differential Strain Min	894	788	0.483	0.426	0.877
Constrained, Differential Stress Min	602	873	0.534	0.368	0.833
Unconstrained, Differential Strain Min	792	889	0.255	0.675	0.902
Unconstrained, Differential Stress Min	651	875	0.291	0.580	0.918

Table 5-1: Example elastic constants calculated using a Plane Stress Representation (F1202 fabric)

Whilst the above plane stress equations can be used to calculate the elastic constants it is necessary for the purposes of this project to find distinct values of elastic constants at specific points on a response surface. For instance, the data shown in Table 5-1 makes no distinction between the modulus at 10kN/m:10kN/m (Warp:Weft) and at 30kN/m:10kN/m. A visual inspection of the 3D graphical representation of the response data shows that whilst the results for a plane stress representation may represent a best fit to all the fabric data they do not necessarily represent the variation across the surface (Figure 5-10 and Figure 5-11). The surface is clearly nonlinear, and the stiffness varies across the surface.

5. Model validation

As a visual aid a four degree polynomial fit is applied to the test results (i.e. it follows the form set out in Equation 5-2). To ensure the quality of interpolation between data points of the stress-stress-strain surface a number of cuts are then taken through the surface along the warp and weft directions with the points they intercept included in the diagram to demonstrate that no unexpected variations in surface occur (Figure 5-12 and Figure 5-13). Whilst the first subplot for both figures appears to show a lack of data points at high loads this is because the cut runs parallel to one of the testing directions, not crossing it. R^2 values are not used because the fit's profile between data points could not be controlled. The difference in R^2 values between a third and fourth order polynomial is discussed with relation to Figure 5-14 below.

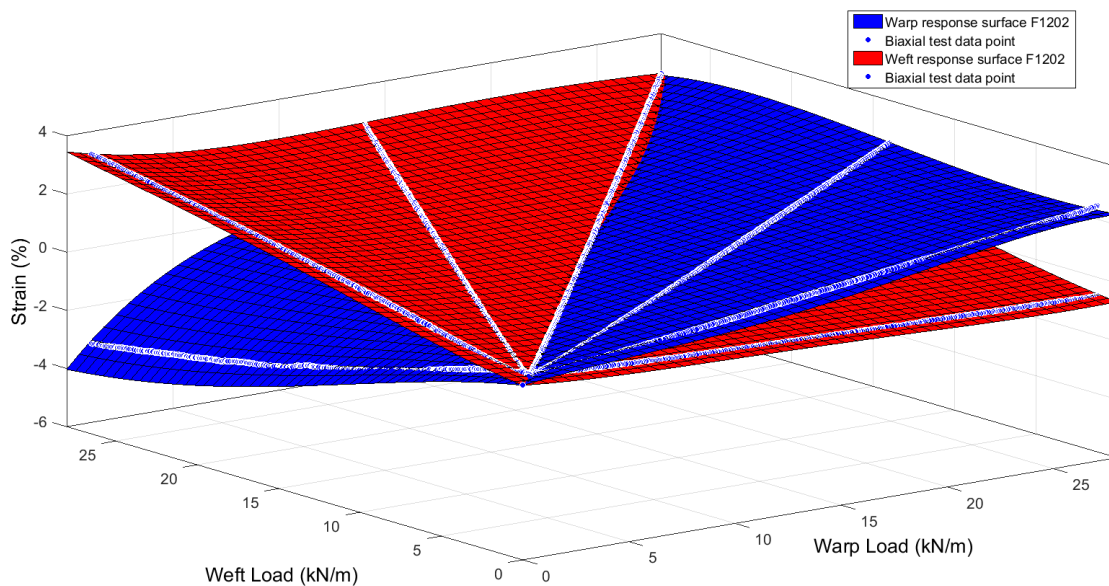


Figure 5-10: 3D representation of F1202 response data with biaxial data points which appear as the white lines in the figure. The data was obtained using a biaxial testing machine at Newcastle University.

5. Model validation

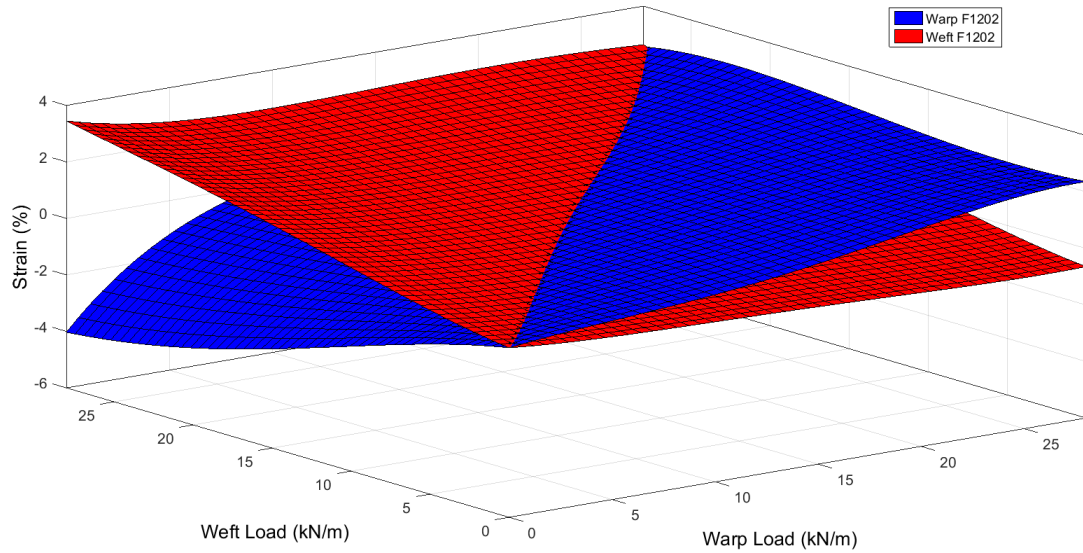


Figure 5-11: 3D representation of F1202 response data without biaxial data points. The data was obtained using a biaxial testing machine at Newcastle University.

$$f(x, y) = p_{00} + p_{10}x + p_{01}y + p_{20}x^2 + p_{11}xy + p_{02}y^2 + p_{30}x^3 + p_{21}x^2y + p_{12}xy^2 + p_{03}y^3 + p_{40}x^4 + p_{31}x^3y + p_{22}x^2y^2 + p_{13}xy^3 + p_{04}y^4$$

Equation 5-2

Where p_{xy} is a constant coefficient

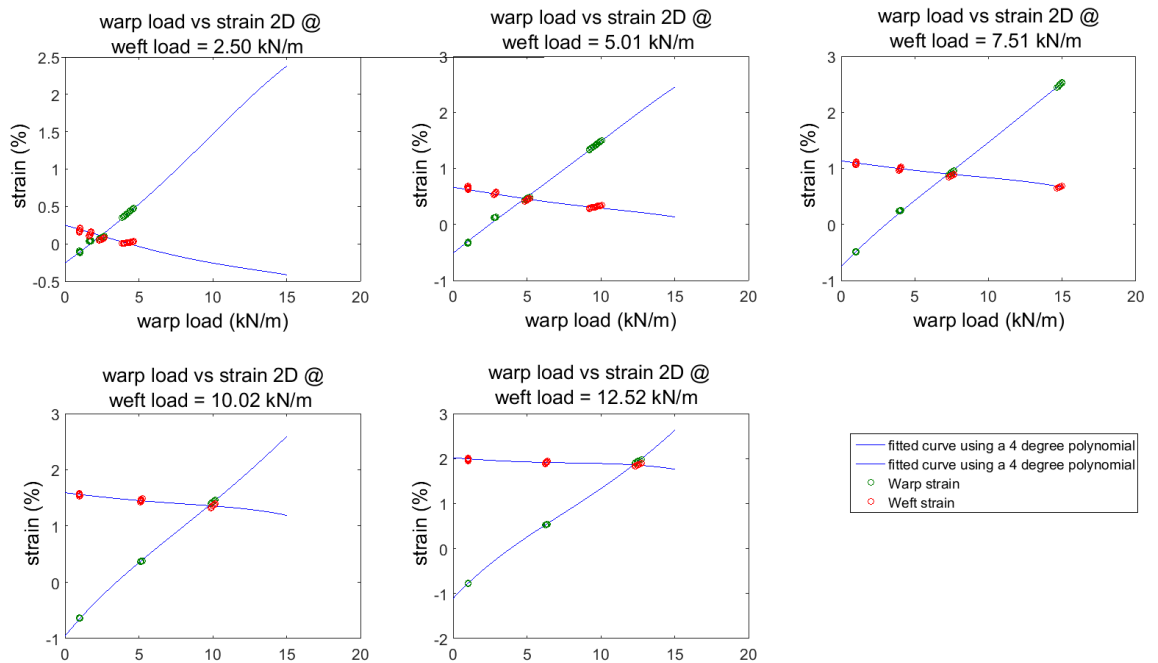


Figure 5-12: F702 cut through the surface for surface fit checking along the weft direction

5. Model validation

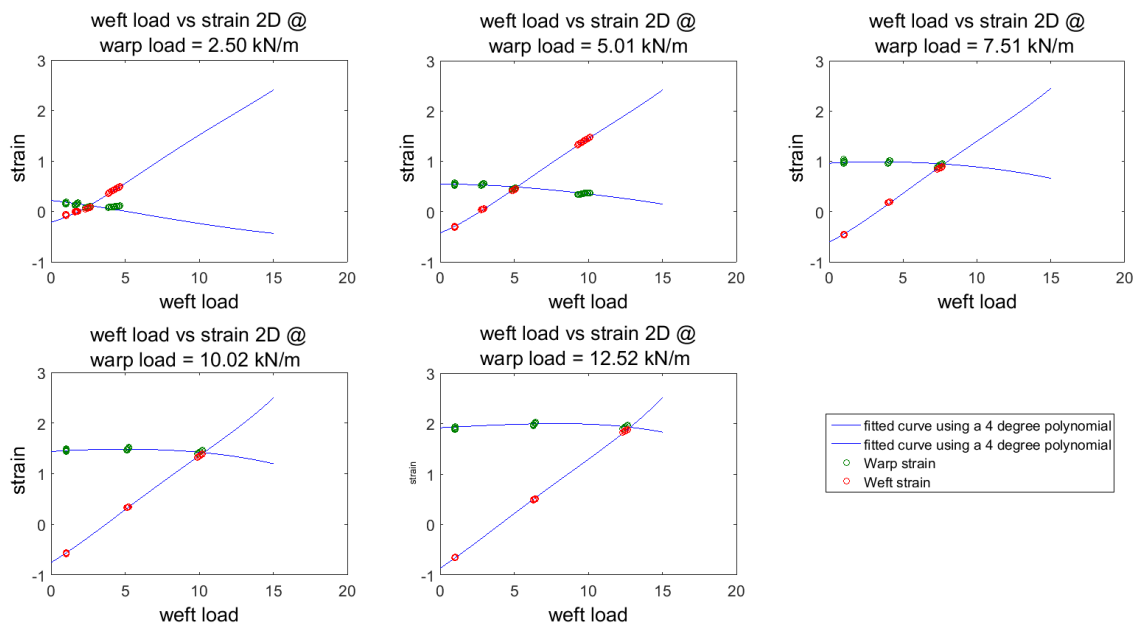


Figure 5-13:F702 cut through the surface for surface fit checking along the warp direction

The elastic constants calculated for a PTFE B18089 PTFE coated glass fibres fabric (§A1) show a different set of results to those for the PVC coated polyester fabric (Table 5-1). The values of R^2 for differential stress minimisation are very poor (Table 5-2), and this is discussed below. These results are clearly erroneous, and show that stress minimisation is less reliable than the strain minimisation method. Figure 5-14 shows a 3D representation of the data. The R^2 values for the fit in Figure 5-14 are 0.996 and 0.997 in the warp and weft direction respectively. This is reduced to 0.97 if a third order polynomial is used, a small but appreciable difference.

Analysis	E_x	E_y	ν_{xy}	ν_{yx}	R^2
Constrained, Differential Strain Min	1448	997	1.137	0.783	0.099
Constrained, Differential Stress Min'	522	583	-0.044	-0.039	859017
Unconstrained, Differential Strain Min	1397	1022	1.049	0.849	0.098
Unconstrained, Differential Stress Min	549	560	-0.110	0.015	858745

Table 5-2: Example elastic constants calculated using a Plane Stress Representation (B18089 fabric)

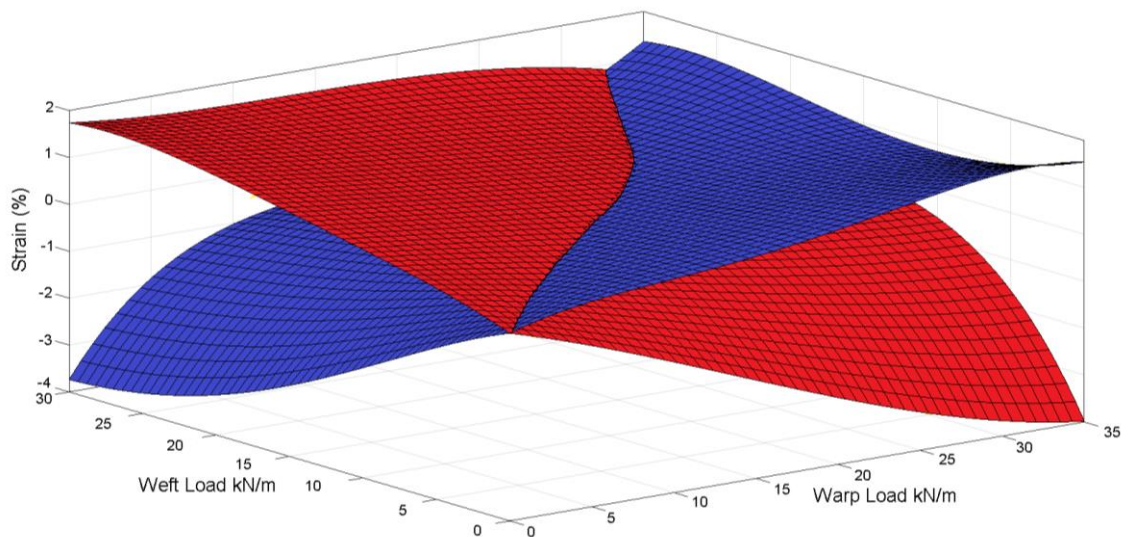


Figure 5-14: 3D representation of B18089 response data without biaxial response data points shown in the figure

The PTFE glass-fibre fabric (Figure 5-14) is clearly less well represented by a plane stress relationship, with the sharp downward curves at more extreme ratios of stress-strain (1:0 for instance). A Plane stress relationship might adequately describe the stress – stress-strain surface at the centre of the plot, but this would underestimate stiffness at the edges.

A method was developed to calculate elastic constants at specific points on a surface to allow for a comparison between biaxial test data and simulated designed fabric response data. For this section a PVC coated polyester Ferrari Precontraint F702 (§A.1) fabric will be used as the example fabric. As the response for this fabric fits the plane stress formulation well this will demonstrate just how much variation can be found even in fabrics where the fit is good. The F702 fabric produces a very flat response surface. Notably the R^2 value for the fabric (Table 5-3) is far higher than that shown earlier for the F1202 fabric. There is also far less variation between different analysis methods (and between different directions) in the values of the elastic constants.

5. Model validation

Analysis	E_x (kN/m)	E_y (kN/m)	ν_{xy}	ν_{yx}	R^2
Constrained, Differential Strain Min	572	575	0.323	0.325	0.962
Constrained, Differential Stress Min'	558	564	0.300	0.297	0.942
Unconstrained, Differential Strain Min	573	574	0.327	0.321	0.962
Unconstrained, Differential Stress Min	558	564	0.304	0.293	0.942

Table 5-3: Elastic constants calculated using a Plane Stress representation (F702 fabric)

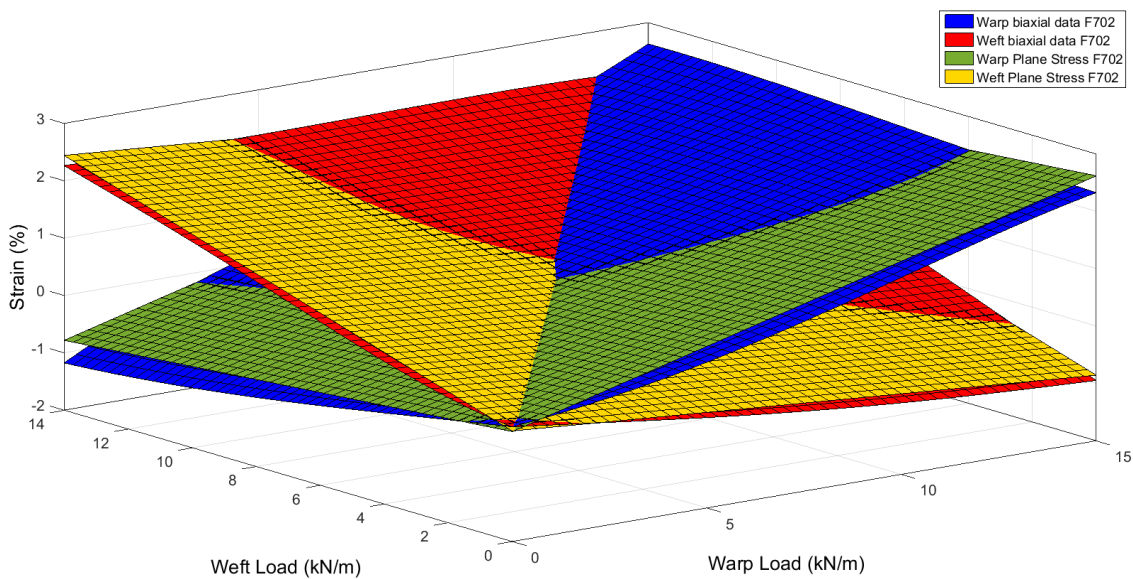


Figure 5-15: 3D representation of F702 response data without biaxial data points including the plane stress representation of the surface using unconstrained strain minimisation elastic constants

Even where the R^2 value is high (0.962) the plane stress representation does not perfectly represent the fabric response. The solution chosen to this was to create a series of small planes for specific points on the surface, in the following example the points are evenly spread across the range of loads, but there is no requirement for this to be so. At the chosen point on the surface a small area of the surface is considered, the size of which will be discussed below, for this small area an individual plane stress representation is made. The small area is defined as a sample of the total biaxial data for which mechanical properties can be found. The small area is populated with data points (again the number of which is discussed below) and the plane stress formulation applied to these data points. From this the elastic constants can be found as has been shown below (Figure 5-17, Figure 5-16). Where more than one of these areas is used to

calculate targets for fabric design the method will be referred to as the multiple point target method.

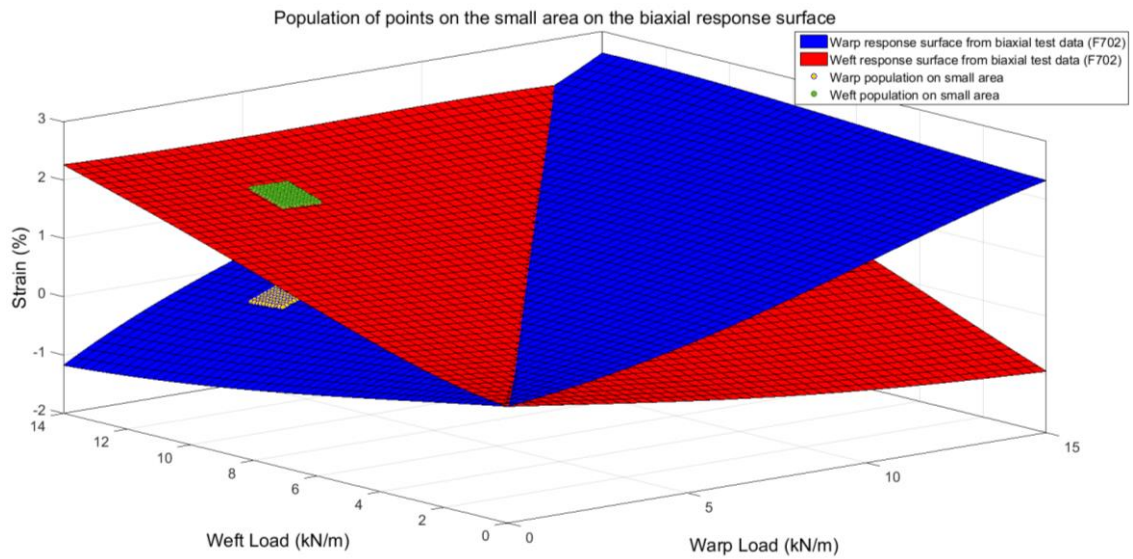


Figure 5-16: Data points in relation to biaxial test response surface, showing how a smaller area of points fits to the test data better than the larger are shown above

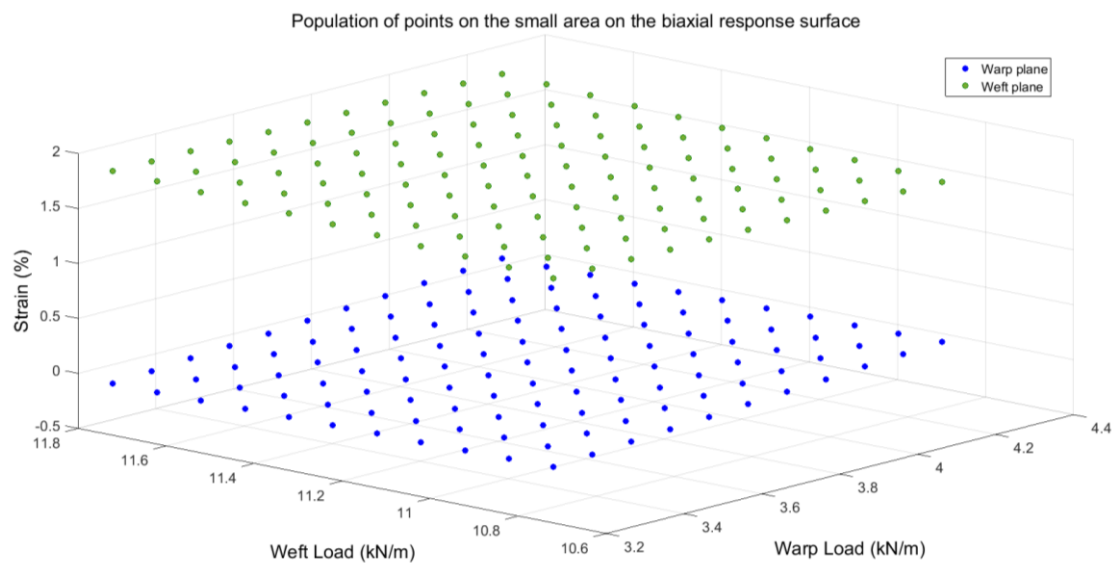


Figure 5-17: Data points produced to populate the small surface area to be represented by the plane stress surface

Initially each plane was created using all four differential minimisation methods, however, it became apparent that the differential stress minimisation was not producing accurate results, with clearly erroneous values of R^2 being produced. After an investigation of the individual parameters of the calculation it was noted that $\det(\mathbf{M})$ was approximately zero in the stress minimisation method. As such the matrix \mathbf{M} was singular, and therefore the inverse of \mathbf{M} , \mathbf{M}^{-1} , was ill conditioned, and would be very

5. Model validation

sensitive to small errors, thus producing the erroneous results. This is problematic because in the differential stress minimisation changes in the strain are exceptionally small, especially in PTFE glass-fibre fabrics. This is because the total change in strain (which may have only been in the order of 2.5% (0.025) to begin with) is distributed across perhaps 1000 points (if a logging rate of 2s is used). Thus the change between individual points may be in the order of 2.5×10^{-5} . In PTFE fabrics the strain experienced is less due to the stiffness of the glass fibre yarns, and the original flatter geometry. This is particularly problematic when only a small area, as used to calculate point elastic constants, is considered as less points of a smaller change are used. This is shown in Figure 5-18, where the top two plots show how the strain minimisation results sit on top of the biaxial test data. However, the bottom two plots show that the stress minimisation results are distinct from biaxial test data that they should represent.

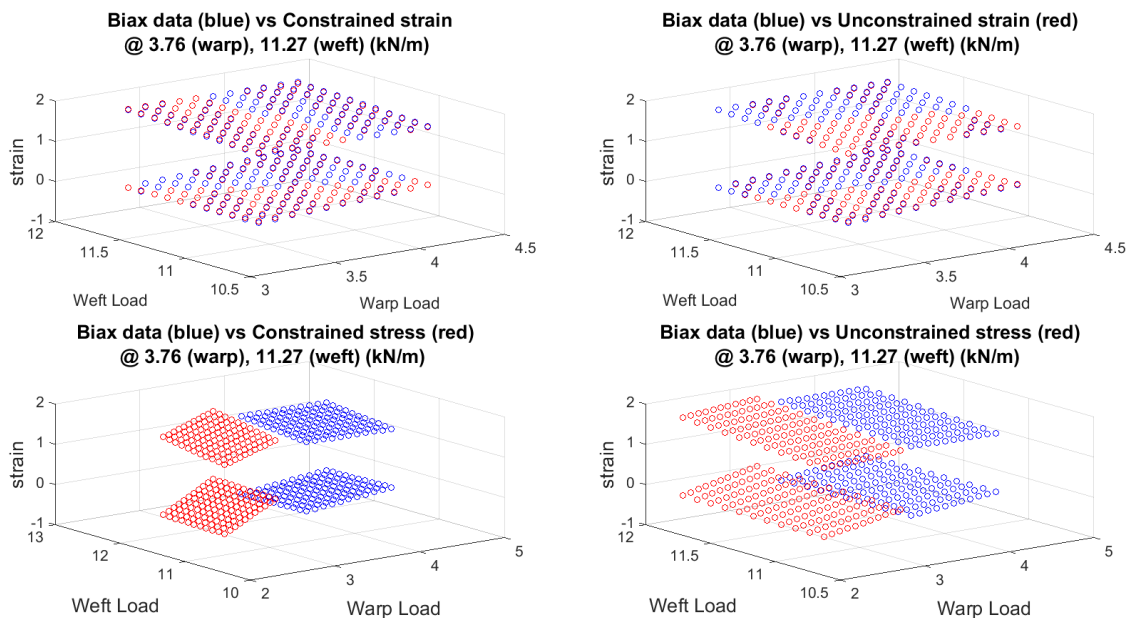


Figure 5-18: Comparison of constrained and unconstrained differential strain and stress minimisation results. Blue—fabric biaxial stress-stress-strain response surface points, red – constrained/unconstrained differential stress/strain results. For a f702 fabric at 3.76kN/m (warp), 11.27kN/m (weft)

Therefore differential stress minimisation is only applicable where changes in strain are observed to be comparatively large. The difference in magnitude between the determinants of the stress and strain matrices for **M** is of the order 10^{18} . It is noted that the stress minimisation becomes more accurate where there is a greater slope, normally where the load ratio is 1:1.

5. Model validation

Because stress minimisation can produce erroneous results it was decided that only differential strain minimisation will be used for further work on the 'patch' used to calculate elastic constants.

The area and number of points that were needed to give accurate elastic constants was derived from a variation study. The study looked at the 'area' the points inhabited (range of loads in the warp and weft directions), the number of points, and the density of the points used in the 'patch' (selection of biaxial data under consideration) and the effect of varying these on the value of the elastic constants produced. Again a F702 PVC polyester fabric is used in this section.

The results are shown below where the area of the 'patch' was found to be the most important factor for the calculation of the elastic constants for the multiple point target method, whilst the density appeared to show some correlation to the value of resultant elastic constants the number of points showed no correlation. Examples of the results are given below (Figure 5-19 through to Figure 5-25).

Variable	Target point 1	Target point 2	Target point 3	Target point 4	Target point 5
P_x (kN/m)	3.8	3.8	7.5	11.2	11.2
P_y (kN/m)	3.8	11.2	7.5	3.8	11.2
E_x (kN/m)	698	441	569	644	487
E_y (kN/m)	651	620	568	481	528
ν_{xy}	0.585	0.122	0.325	0.460	0.233
ν_{yx}	0.433	0.459	0.281	0.028	0.302

Table 5-4: Target values of elastic constants at specified stress states produced from the F702 fabric using unconstrained differential strain minimisation

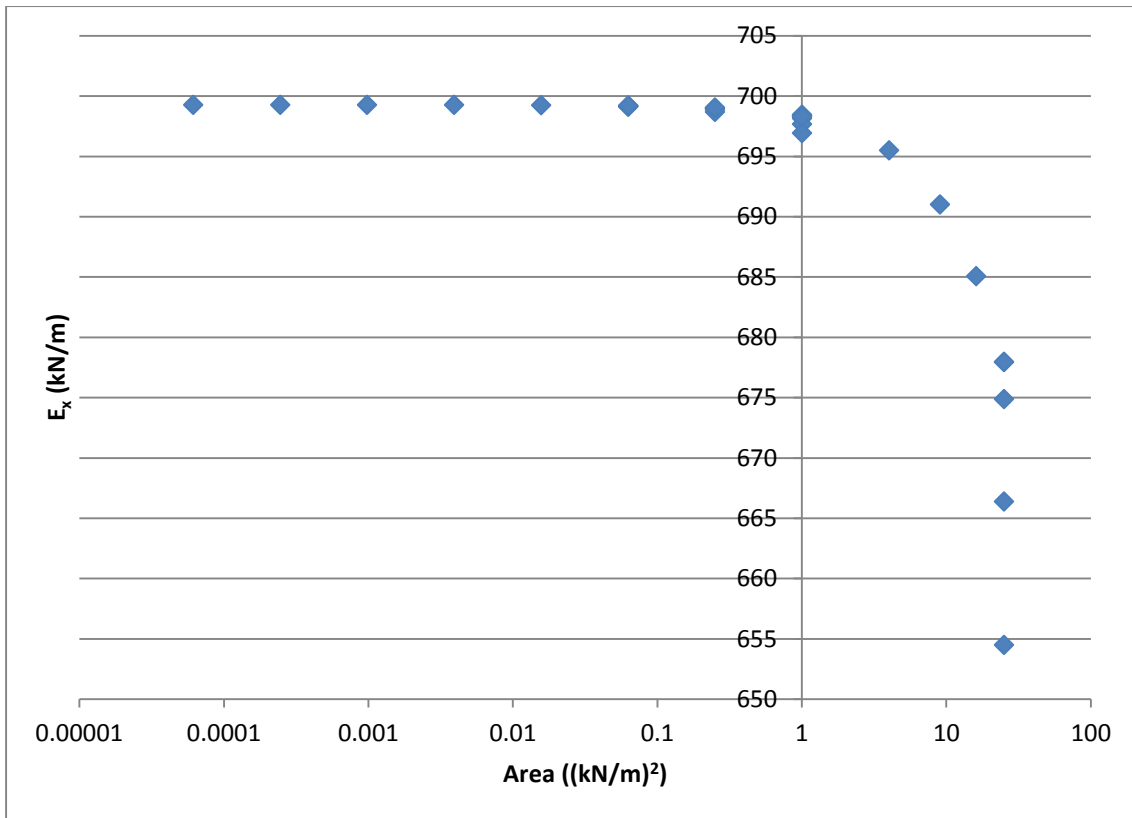


Figure 5-19: Area of 'patch' plotted against E_x at target point 1

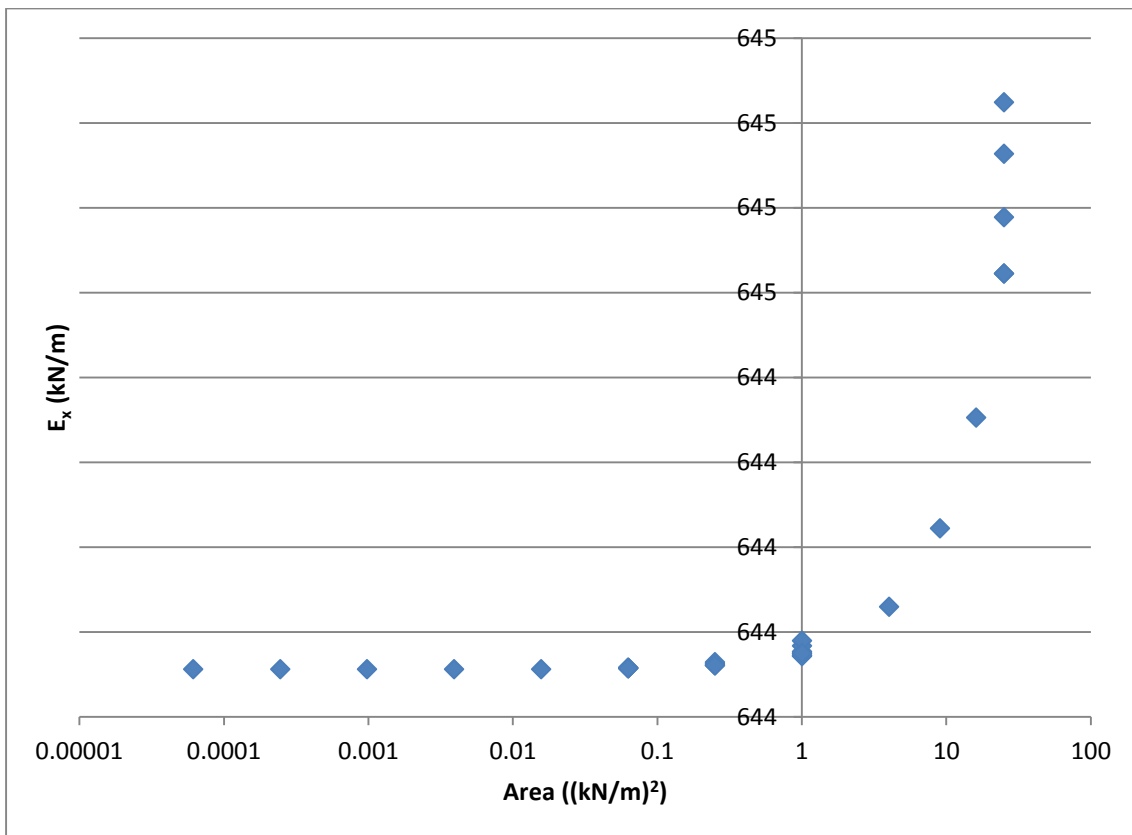


Figure 5-20: Area of 'patch' plotted against E_x at target point 4

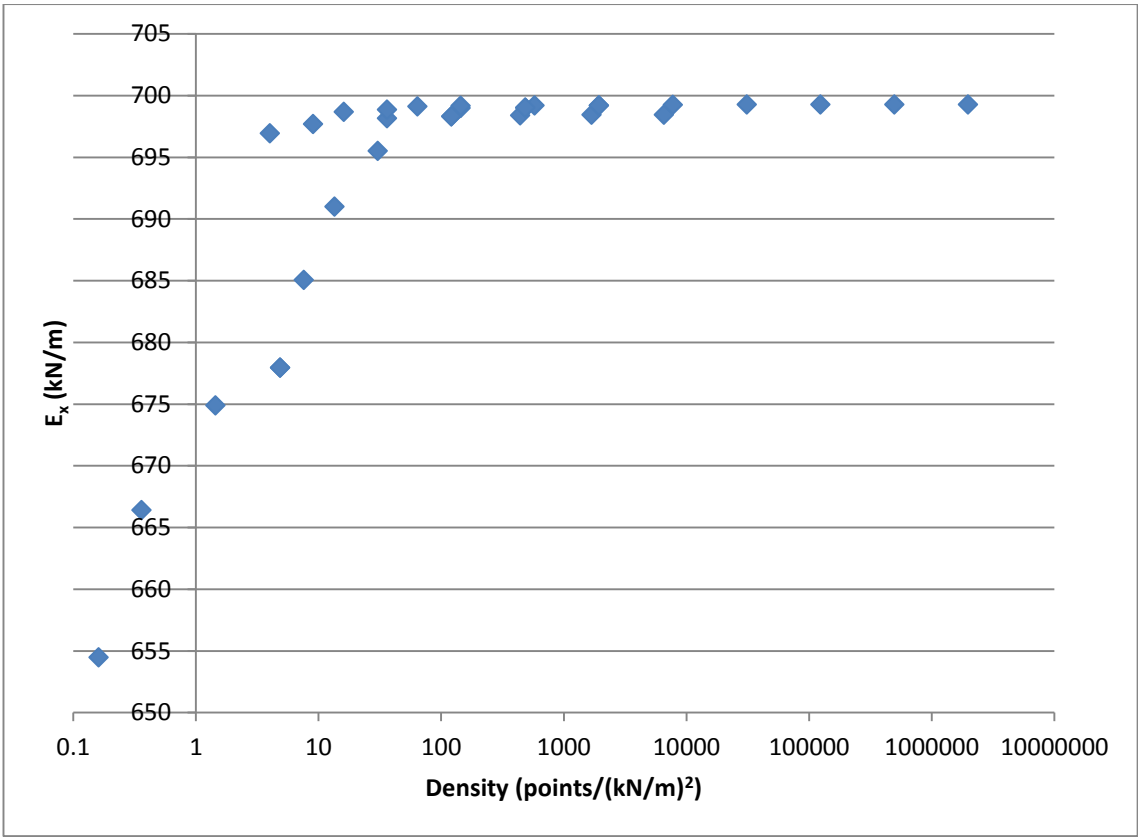


Figure 5-21: Density of 'patch' plotted against E_x at target point 1

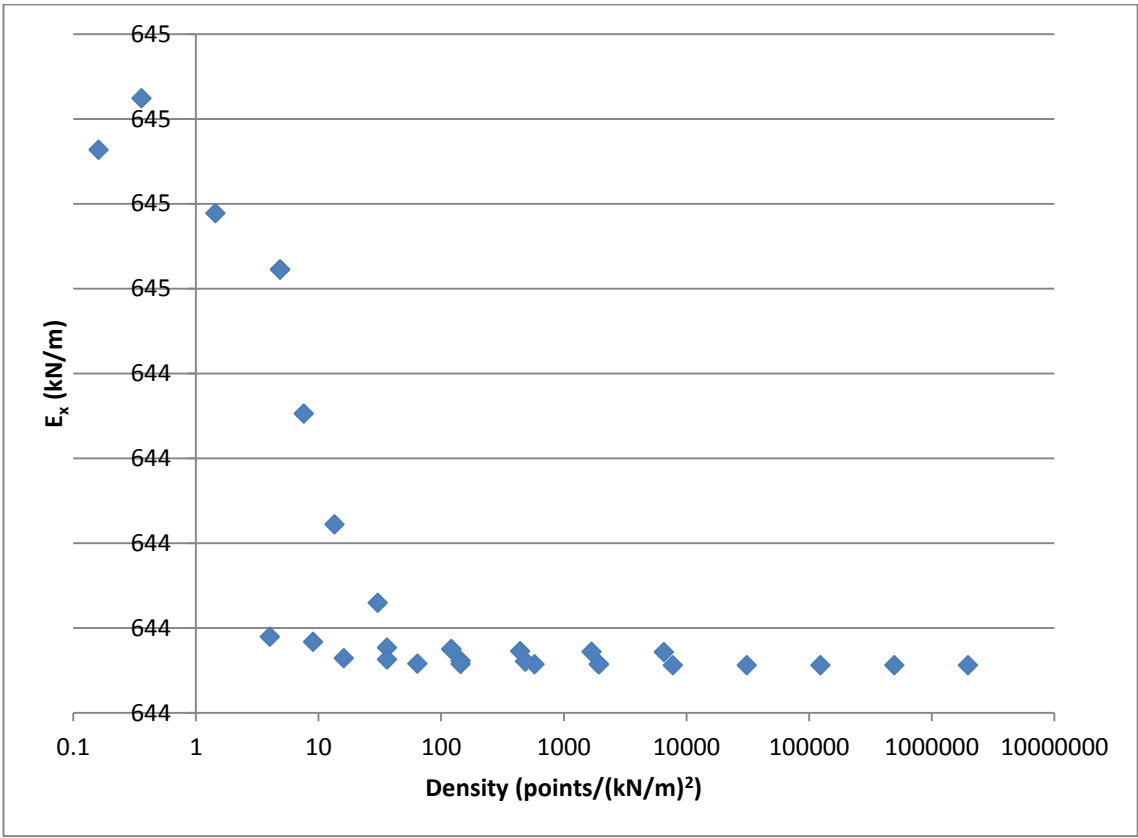


Figure 5-22: Density of 'patch' plotted against E_x at target point 4

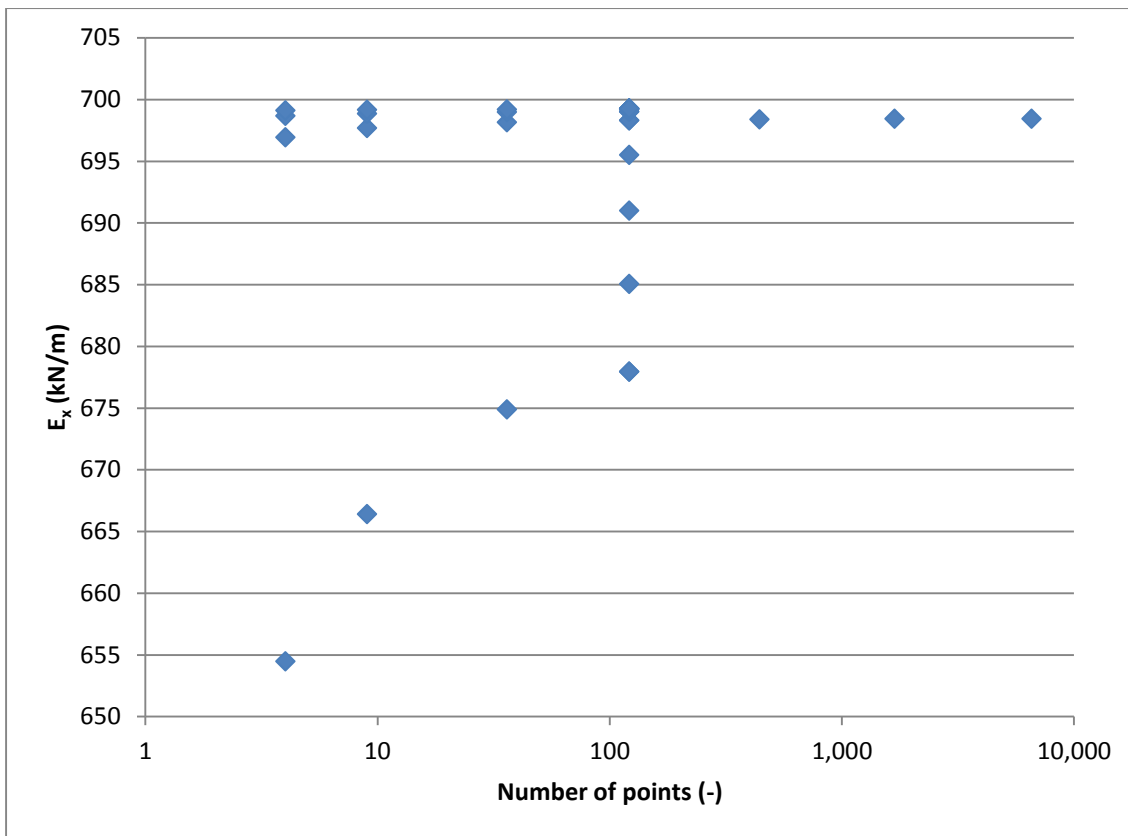


Figure 5-23: Number of points in the 'patch' plotted against E_x at target point 1

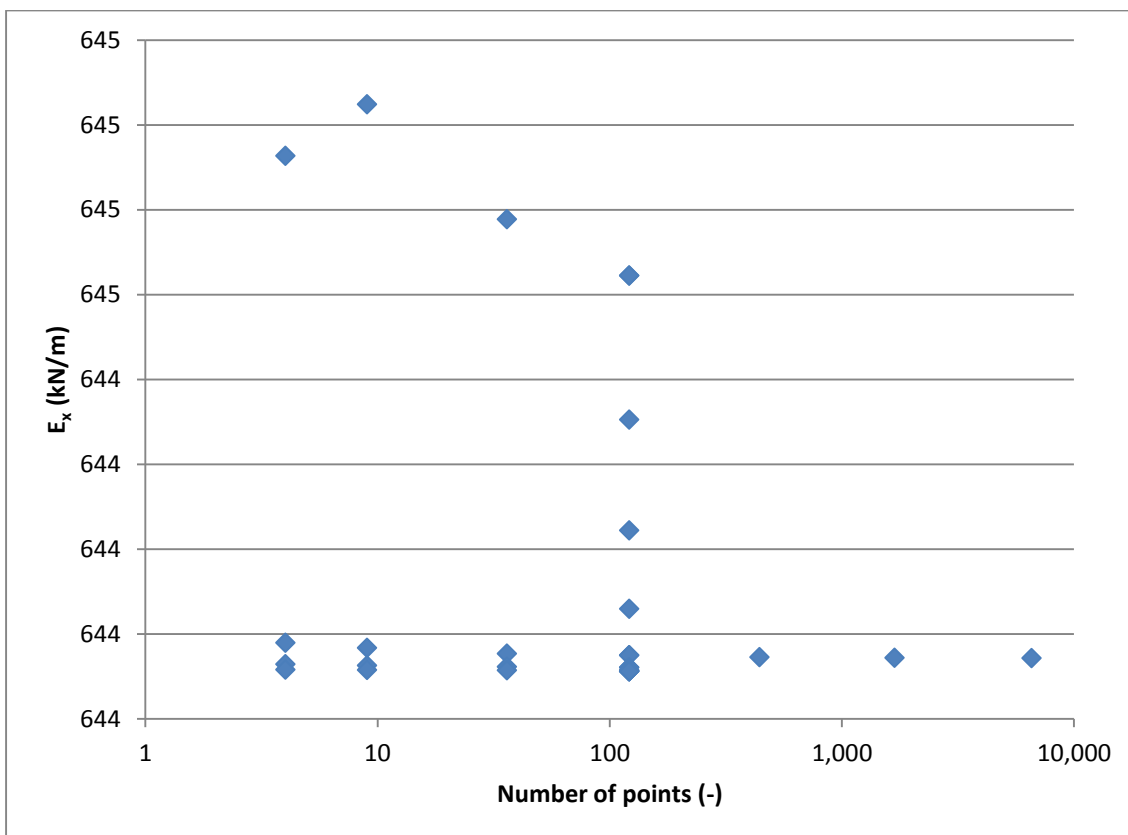


Figure 5-24: Number of points in the 'patch' plotted against E_x at target point 14

The R^2 value is investigated with respect to the density (Figure 5-26). Logarithmic scales were used to avoid clustering at small values, which also demonstrates how the value of the elastic modulus changes with variation in area. A smaller area is found to generally produce a less variable result, with the hypotenuse occurring at approximately $0.1(\text{kN/m})^2$ (the area being the area on stress-stress-strain response surface considered, the axis of which are kN/m). Additionally the optimum density seems to consistently occur at approximately 70 points/ $(\text{kN/m})^2$.

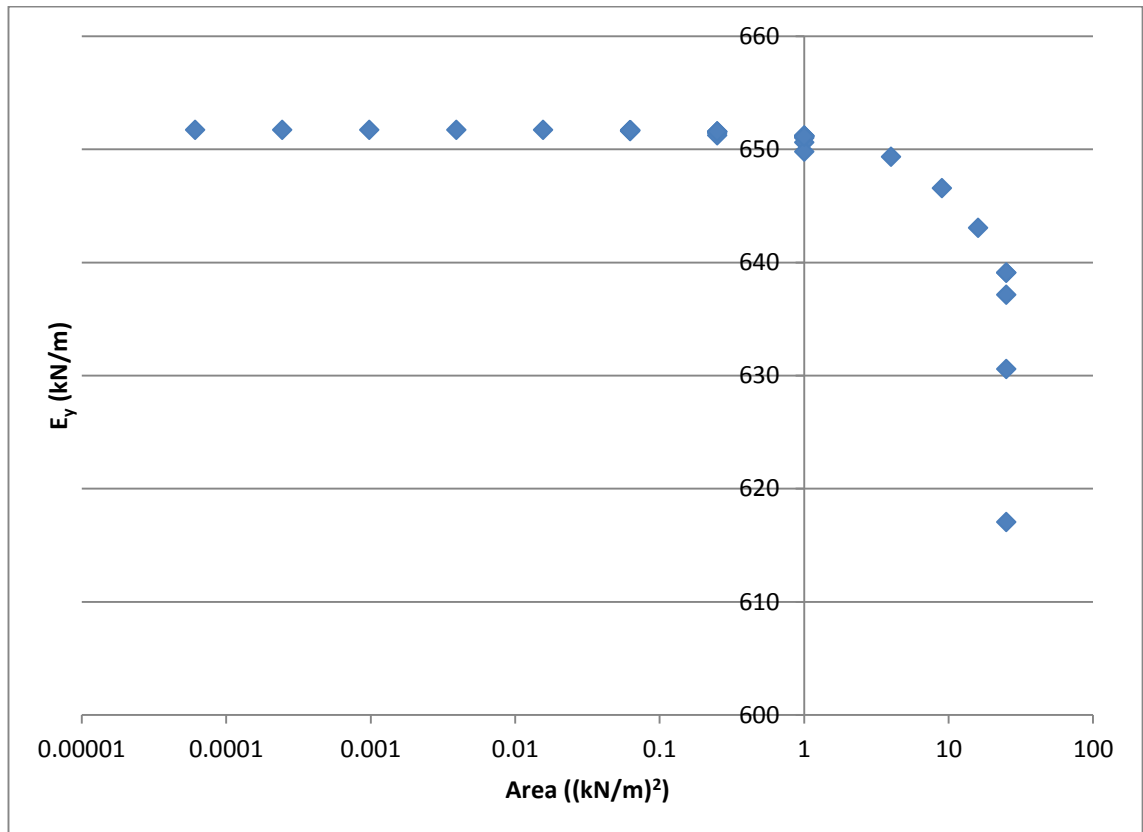


Figure 5-25: Area of 'patch' plotted against E_y at target point 1

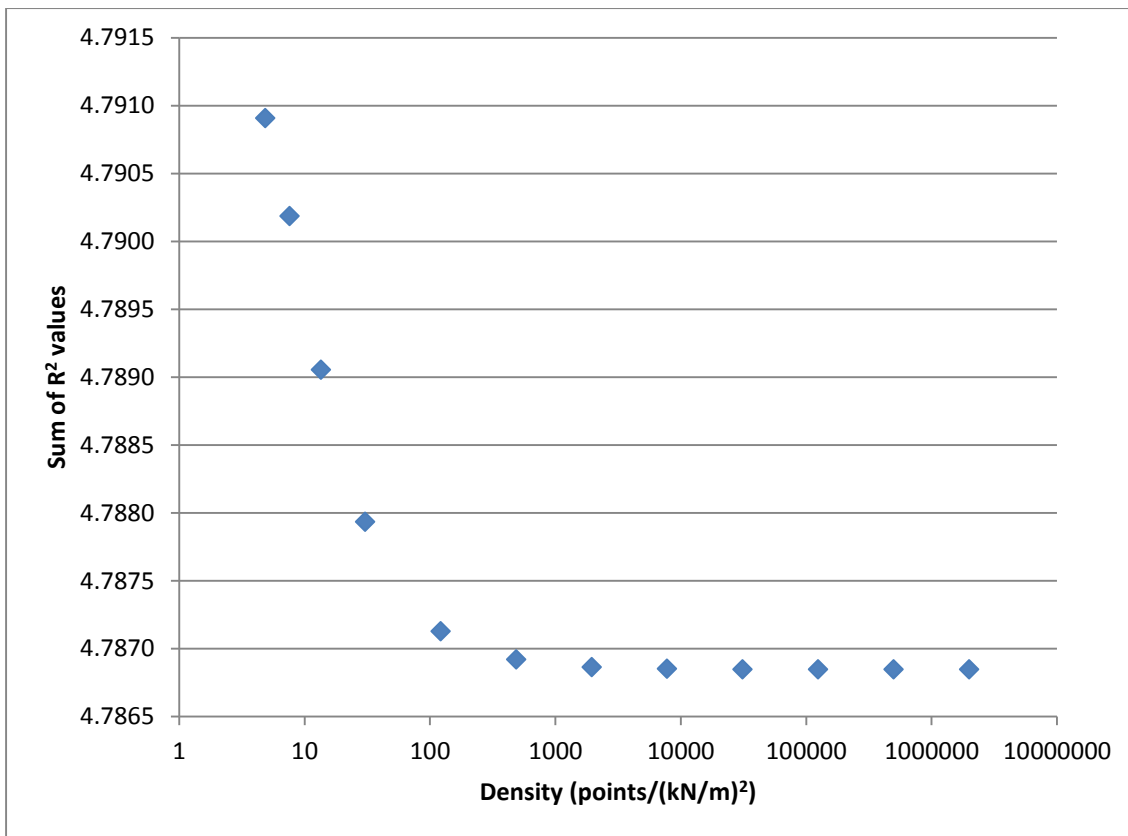


Figure 5-26: Sum of R² plotted against the density of points for the plane stress representing the whole fabric

The maximum total R² value appears to occur at a lower density, however, this does not necessarily mean that the lower densities will give improved results. In this instance a reduced density reduces the number of points, thus allowing a better fit. For instance the lowest possible density would have only four points to which a fit would need to be made, whereby error might be reduced, whilst the interior of the ‘four points’ might show, if investigated, a larger error. Thus the hypotenuse occurs at approximately 1×10^2 (points/(kN/m)²) where R² appears to be stabilised. This value is similar to the 70 value identified earlier, and solidifies the choice of density to be used.

The final result of the process is a series of graphs (Figure 5-27 and Figure 5-28) which show how the value of stiffnesses changes with relation to the area of the patch being considered, the number of points, and the density of points. There is some coupling between the different tests, most obvious in Figure 5-23 where two distinct curves are visible. This is because, whilst generally more points are better, the graph includes data for increased numbers of points at different patch areas. Therefore, where the patches are small to begin with, area (the least coupled response) is already low. This is similar

in other figures, where the density is low in Figure 5-22, and E_x is already approximately optimal, a small enough area is being considered to give the required value of E_x .

A set of target values for the elastic properties that can be used as the target properties for fabric design are also produced. For this particular fabric these are given in Table 5-4 which includes the loads (P) as well as the elastic constants.

In addition a PTFE coated glass-fibre fabric is also considered (Figure 5-29 and Figure 5-30) with each plane shown at the target loads that have been spaced evenly on the response surface. When the PVC coated polyester fabric's response surfaces are compared to the PTFE coated glass-fibre fabric's surfaces it is easier to acknowledge why a single plane stress representation does not adequately represent fabric response. Whilst the PVC coated polyester fabric appears to be fairly well represented by the plane stress representation the PTFE coated glass-fibre fabric shows considerably greater variation in the position of the planes (Table 5-5).

A numerical comparison between the results of a plane stress representation and the multiple point target generation is made using the data in Table 5-5. Considering only the results of the stiffness in the warp (x) direction it is clear that the plane stress representation overestimates stiffness at the 10kN:30kN loads by 93% and underestimates it at targets 3 and 4 by 30 and 34% respectively. Further, the Poisson's ratios whilst higher than 0.5 as discussed earlier in this section (§5.2.2.2) and in the literature review (§2.2.7.3) are in error by up to 200% (Target 4).

This clearly demonstrates how multiple targets are necessary for fabric design, and how the use of single values from plane stress representations can give misleading results because the expected stiffness might be up to 93% less than predicted using the plane stress representation. Bridgens *et al.* (2009) considers how variation in stiffness might affect the displacement of a hypar structure under different loading conditions. Using a broad comparison to these results it is possible to see that where the height/side length is 0.2 a difference of +500kN/m (target 3) might result in a reduced deflection of approximately 100mm, and a difference of -1000kN/m might result in a difference in predicted deflections of approximately 100mm. When ponding and serviceability criteria are considered this might result in serious problems should this data be used to

5. Model validation

design a structure (an additional 100mm deflection might result in a clash between supporting structure and the fabric). These multiple targets are used as the targets for the design process for fabrics below (§5.3.2), allowing a fabric to be designed for accurate fabric properties rather than the approximation offered by the plane stress method.

It is important that accurate targets and high quality data are available to ensure the design model is able to reproduce fabric geometries. Without multiple targets, and using the plane stress representation, the model as developed (§3.3) will be unlikely to reproduce fabric geometries, as the targets would not fully represent the stress-strain characteristics of the fabric under consideration.

Method	Analysis		E_x (kN/m)	E_y (kN/m)	ν_{xy}	ν_{yx}
Plane Stress	Constrained, Differential Strain Min		1706	969	1.27	0.72
	Unconstrained, Differential Strain Min'		1578	1016	1.07	0.84
Multiple targets	Unconstrained, Differential Strain Min	Target 1 (10:10)	1380	952	0.80	0.72
		Target 2 (10:30)	819	1556	0.14	1.29
		Target 3 (20:20)	2261	1287	0.72	0.58
		Target 4 (30:10)	2416	619	1.83	0.28
		Target 5 (30:30)	1279	1115	0.63	0.87
	Constrained, Differential Strain Min	Target 1 (10:10)	1570	879	1.05	0.59
		Target 2 (10:30)	977	1191	0.74	0.91
		Target 3 (20:20)	2646	1189	1.01	0.46
		Target 4 (30:10)	1979	656	1.44	0.48
		Target 5 (30:30)	1569	960	0.99	0.61

Table 5-5: Comparison of plane stress and multiple target representations of biaxial data (PTFE coated glass-fibre – B18059). The values (10:10) etc. refer to the warp:weft load respectively in kN/m

5. Model validation

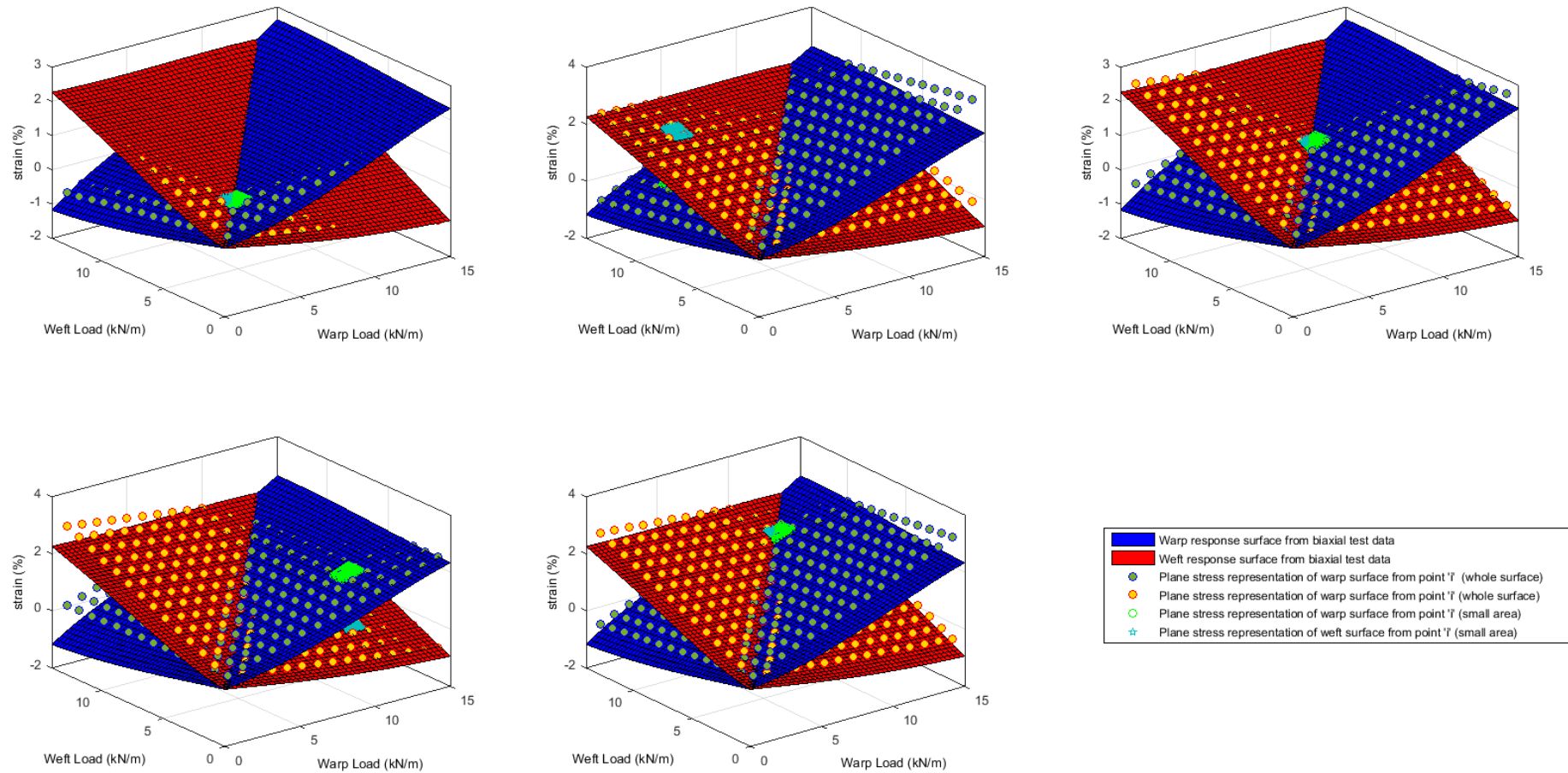


Figure 5-27: Plane stress response surfaces for each selected point on the surface for a PVC coated polyester fabric (F702) (using unconstrained strain minimisation) visualisation 1

5. Model validation

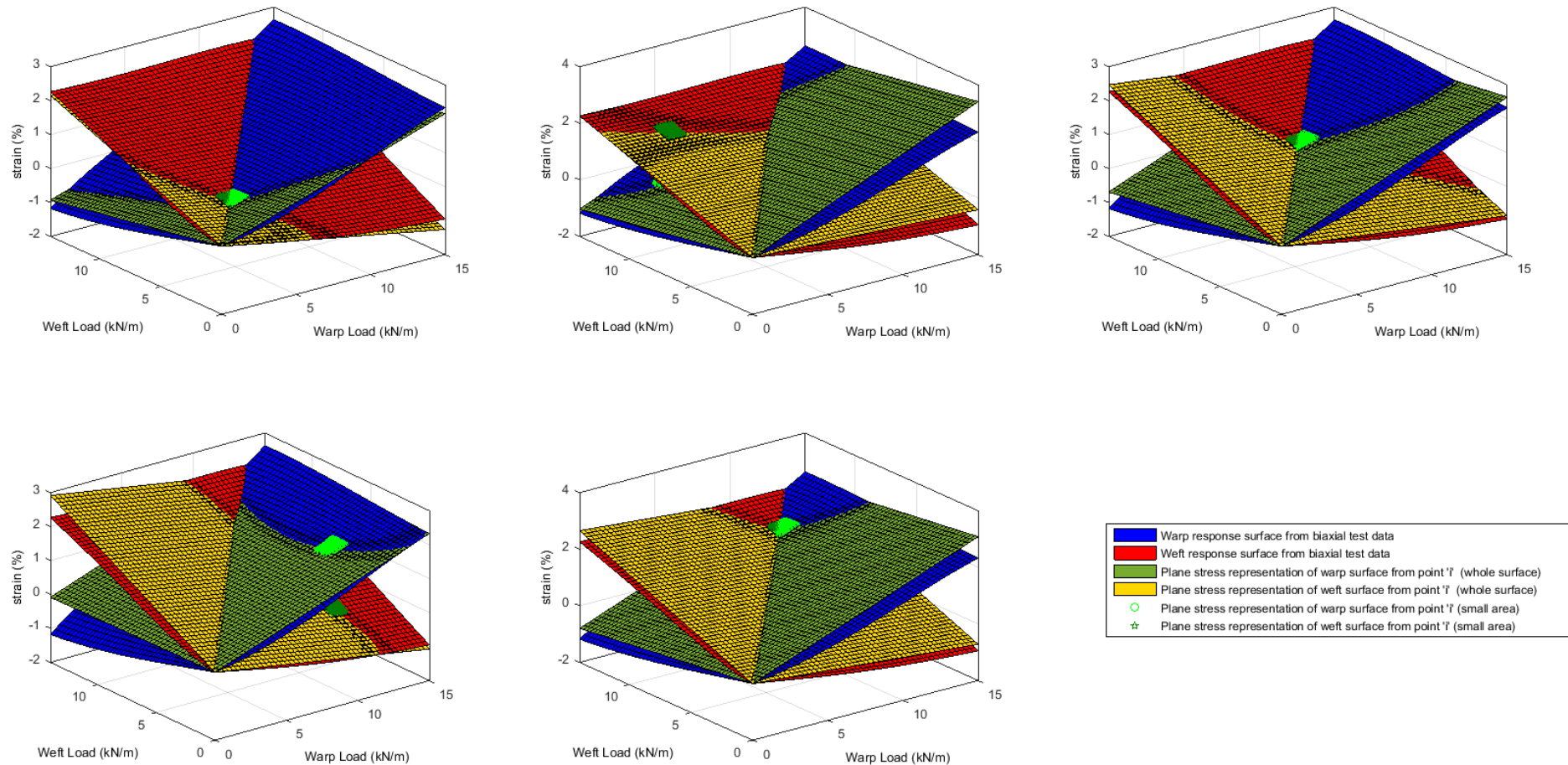


Figure 5-28: Plane stress response surfaces for each selected point on the surface for a PVC coated Polyester fabric (F702) (using unconstrained strain minimisation) visualisation 2

5. Model validation

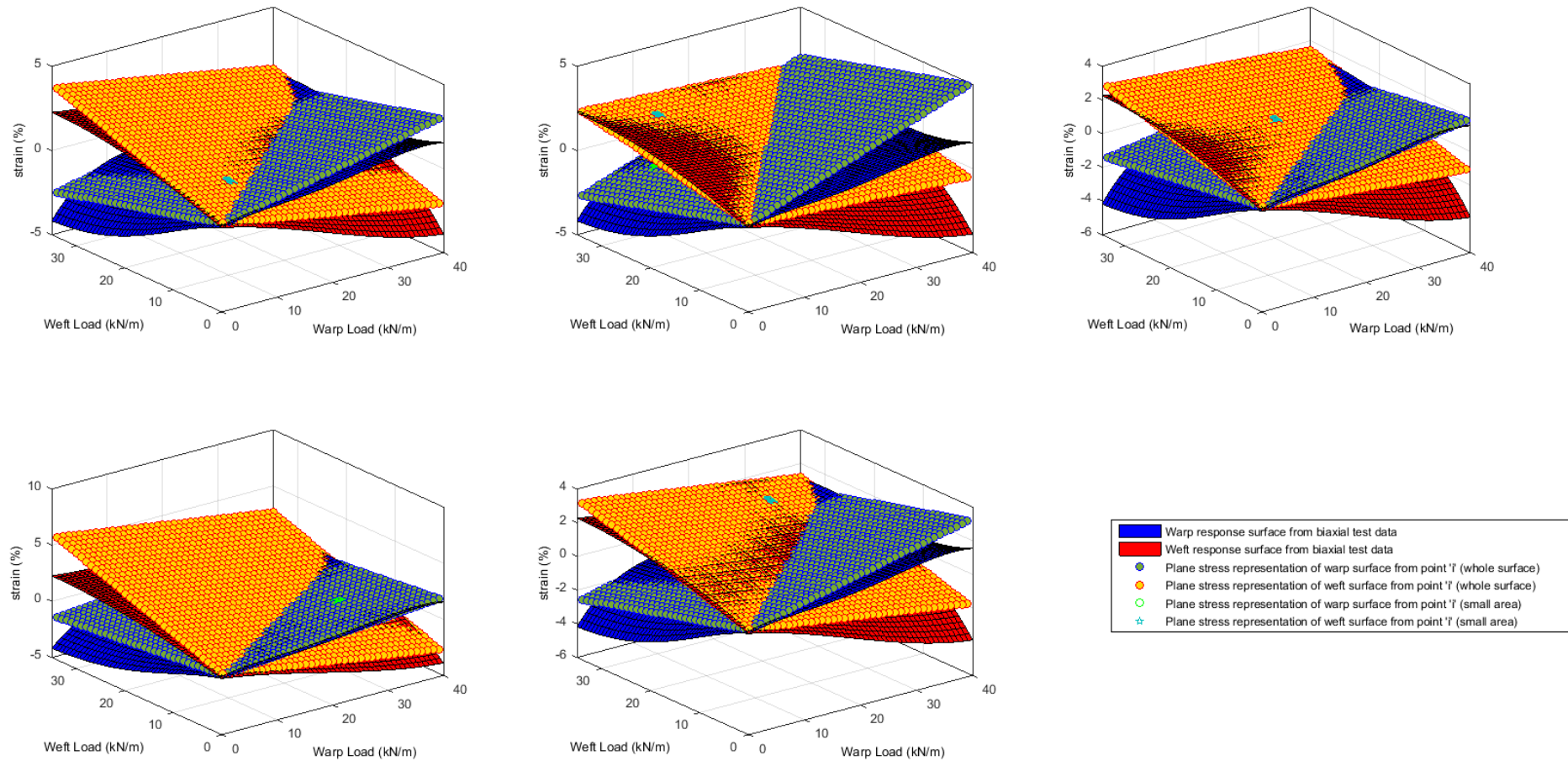


Figure 5-29: Plane stress response surfaces for each selected point on the surface for a PTFE coated glass-fibre fabric (B18059) (using unconstrained strain minimisation) visualisation 1

5. Model validation

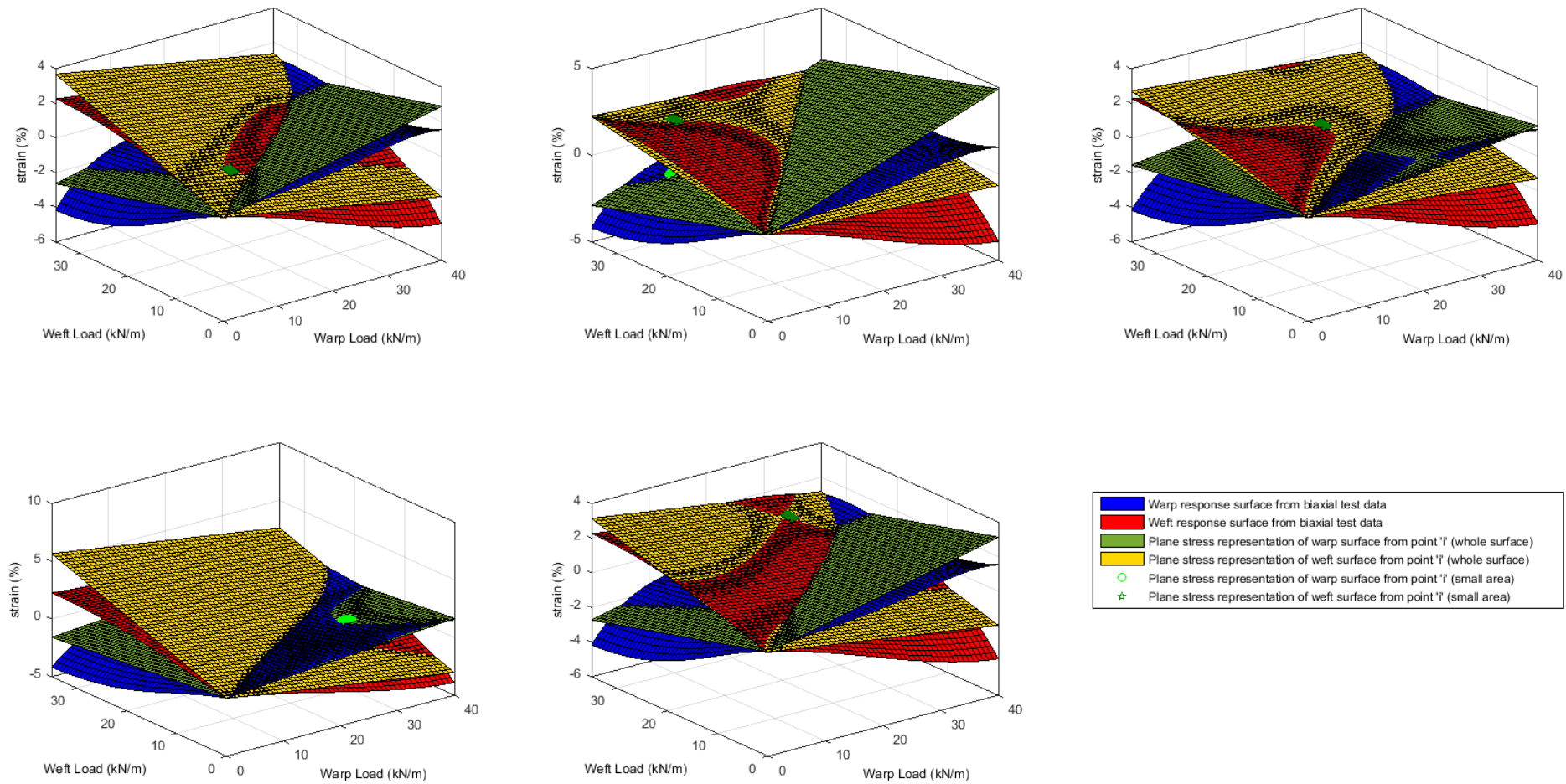


Figure 5-30: Plane stress response surfaces for each selected point on the surface for a PTFE coated glass-fibre fabric (B18059) (using unconstrained strain minimisation) visualisation 2

5.2.3. Yarn mechanical properties

Testing of yarns to determine mechanical properties is necessary to produce the yarn moduli that are used to carry out fabric design. There are numerous inherent problems associated with the testing of yarns for stiffness values.

5.2.3.1. *Yarn properties from uniaxial tests*

A 200x50mm sample is tested using LVDT strain measurements at a rate of 100mm/min. The yarn directions are aligned along and orthogonal to the loading direction respectively, when preparing the sample the yarn directions need to be noted and the edges of the sample aligned with the yarns (for a fabric with orthogonal yarns). LVDTs are attached to the sample along its centre line using pins at a separation of 100mm. Flat tensile jaws are used to clamp a 380x 50mm sample between a gauge length of 200mm. LVDTs cannot be used to record extension beyond 35mm and as such need to be removed if extensions are required to go beyond this point.

After the test the stress-strain curves for the fabric are available such as those presented earlier (§5.2.1) or in the literature review (§2.3.2.3) where Dimitrov and Schock (1986) identify how the stress-strain curve can be used to identify yarn stiffness. The yarn response can then be characterised in terms of kN/m or if necessary with knowledge of the yarn spacing in terms of N/yarn or even kN/m² if the cross-sectional areas of yarns are known.

There are specific advantages to using uniaxial testing for yarn properties. Yarns tested in-situ (as part of a fabric) are being tested under the conditions that occur when resisting loads in structural situations, with the same crushing or crimping factors. However, given that there will always be some crimp in the tested fabric, and some transfer of energy to friction between yarns it is also possible to see that this testing method is not truly determining the actual yarn response. Of principal importance for this report is the inability of the uniaxial test method to produce statistical distributions of mechanical properties for individual yarns for use in the robustness optimisation method (§5.4.4). This is because the contribution of an individual yarn within a fabric cannot be distinguished from that of the other yarns in a strip test, and cannot therefore

be measured. This means that any statistical distributions obtained from uniaxial tests are not applicable to the individual yarns.

To calculate coating stiffness a bias-cut test (§5.2.1.1) can be carried out using the same procedure as for a normal uniaxial test but the yarns are aligned at 45 degrees to the loading direction, meaning that the cut is also carried out at 45 degrees to the yarn direction.

This means that no two yarn ends of a single yarn are within the jaws, and the load is therefore only carried by the coating. In this situation the coating stiffness can be calculated.

5.2.3.2. *Testing of single yarns*

The testing of individual yarns for mechanical properties is necessary to provide a useful comparison to the properties obtained through uniaxial testing and provide a second source of input for modelling. Specifically relevant as mentioned above was the need for accurate statistical information about the distributions of yarn moduli. The Robust Fabric design method (§4.10) requires as its input data about the coefficients of variation of individual unit cell properties. For geometric properties this has been achieved using the results of photogrammetry, however, no distributions regarding individual yarns are available.

Testing was carried out using the ASTM International standards (ASTM, 2014), with references to British standards (BSI, 2014) and the Membrane Structures Association of Japan (Membrane Structures Association of Japan, 1995). No standard has been found relating specifically to the testing of yarns that have been removed from an architectural fabric. The ASTM Standard Test Method for Tensile Properties of Yarns by the Single-Strand Method is used as the basis for the testing procedure as “*most yarns can be tested by this test method*” (ASTM, 2010, p. 2). Some variation is introduced that relates specifically to the types of yarns tested and the data needed, for instance, whilst the standard requires a time to break of 20 seconds a constant rate of extension will be used that is consistent with uniaxial tests. This variation is used to allow useful comparisons to be made to uniaxial test results. Varying the testing rate may have introduced or reduced creep in the yarn, making comparisons of data less viable. This variation is

allowed for within the standard which specifies that alternate speeds are provided for within the standard (ASTM, 2010).

Initially a series of tests are carried out on a virgin yarn to identify errors and problems with the methodology, after which tests are carried out on stripped yarns from fabrics:

A virgin (as manufactured) polyester yarn was tested in accordance with the testing schedule laid out in the appendix (A.11 Table A-6). The test was performed to check the accuracy of the testing method and to ensure that unexpected problems and procedural errors were identified prior to the use of yarns stripped out of fabrics which are time consuming to produce. The yarn tested was a 'Tersuisse Multifils SA' PES (Polyester) fibre from a spool available at the time of testing (Federation, 2014). It was chosen for its immediate availability rather than any specific properties, with a large quantity available multiple tests could be carried out quickly with only minimum preparation time.

The yarn has a linear mass density of 1100 dtex and a fibre count of 192.

A number of deviations from the standard were made:

- An extension rate of 100mm/min is used to allow a comparison to be made between uniaxial test data and the yarn tests.
- Breakages at grips are not considered to be as detrimental to the test as specified in the standard as the yarn extension characteristics are under investigation not the breaking strength. The extension properties will be more accurately investigated with flat jaws than capstans or other clamping methods as extension within the capstan cannot be accurately accounted for and would contribute to the apparent extension of the specimen within the gauge length.
- Flat faced jaws are constructed by using the toothed jaws used in the uniaxial tests, and shown in Figure 5-2, with an intermediate PVC Polyester layer to give cohesion to the jaws clamping the yarns and stop the yarns breaking due to the jaw teeth.

The results of the virgin yarn test are shown in Figure 5-31.

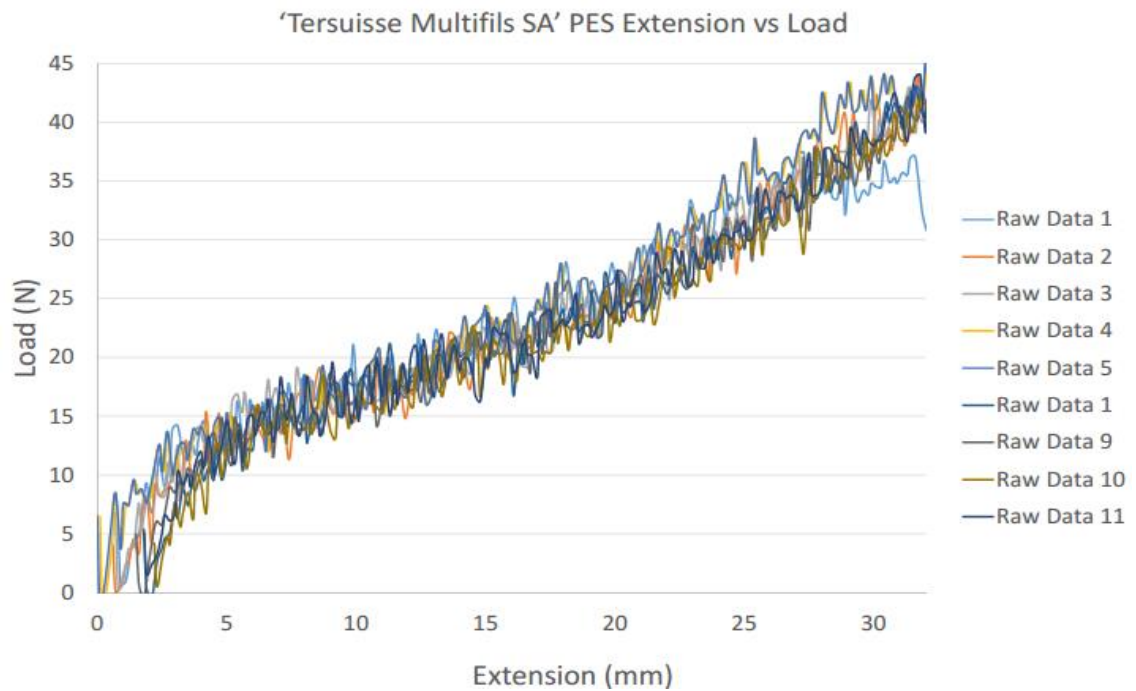


Figure 5-31: Results of the virgin yarn (Tersuisse Multifils SA) tests with outliers removed

The tests used to produce Figure 5-31 used a 250kN load cell which gave a low resolution on the relatively low loads the yarns were tested at, resulting in the poor quality curves presented. The curves are consistent with the response shown in the literature review (§2.2.2). Further to this, once redundant results had been removed, principally the two results for yarns that failed at very low loads, responses appear to be repeatable. From this it can be concluded that the testing procedure appears to work. However, the further tests carried out on a 50kN load cell gave a far higher resolution resulting in a smoother curve for all following results.

The yarns also failed across the length of the yarn, with some clustering towards the jaws which suggested that whilst the jaws had an effect on the point of failure this was only the case at high loads, and was not effecting the test prior to failure.

5.2.3.3. *Yarn properties from stripped yarns*

The method of yarn extraction (sometimes hereafter referred to as stripping or ravelling) is based on ASTM (2012) D3883-04 and the detailed yarn testing methodology is covered in the appendix (§A.11). Examples of the ravelling process are shown in Figure 5-32 and Figure 5-33.

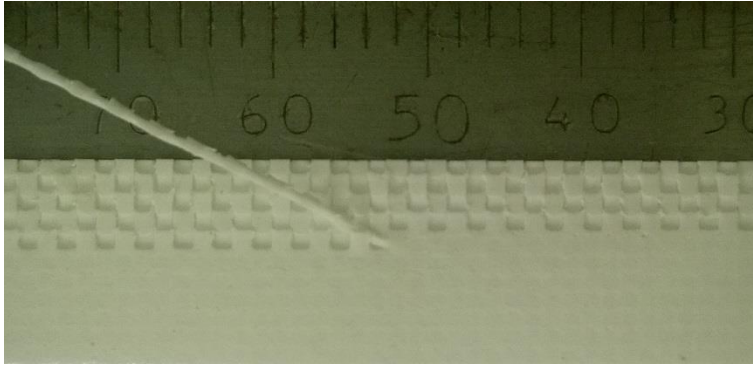


Figure 5-32: Yarn ravelling on a sample of PVC coated polyester fabric



Figure 5-33: Yarn ravelling on a sample of PTFE coated glass-fibre fabric

The testing equipment is shown in Figure 5-34, the yarns are aligned centrally, and cohesion is maintained using the intermediate PVC layer, which cushions the yarn against the pressure of the teeth.

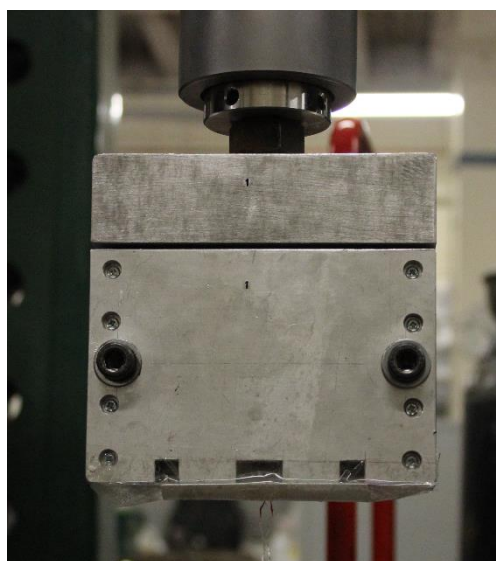


Figure 5-34: Testing equipment including failed F1202 yarn

5. Model validation

Examples of the results produced are shown below. A minimum of 13 tests were carried out in each direction (warp and weft) to ensure a sufficient sample. If any single yarn slipped excessively during testing or failed at a low load more tests were carried out to produce 13 data sets. Considerably more tests than are shown in the following figures were carried out however for brevity these results are summarised in Table 5-7.

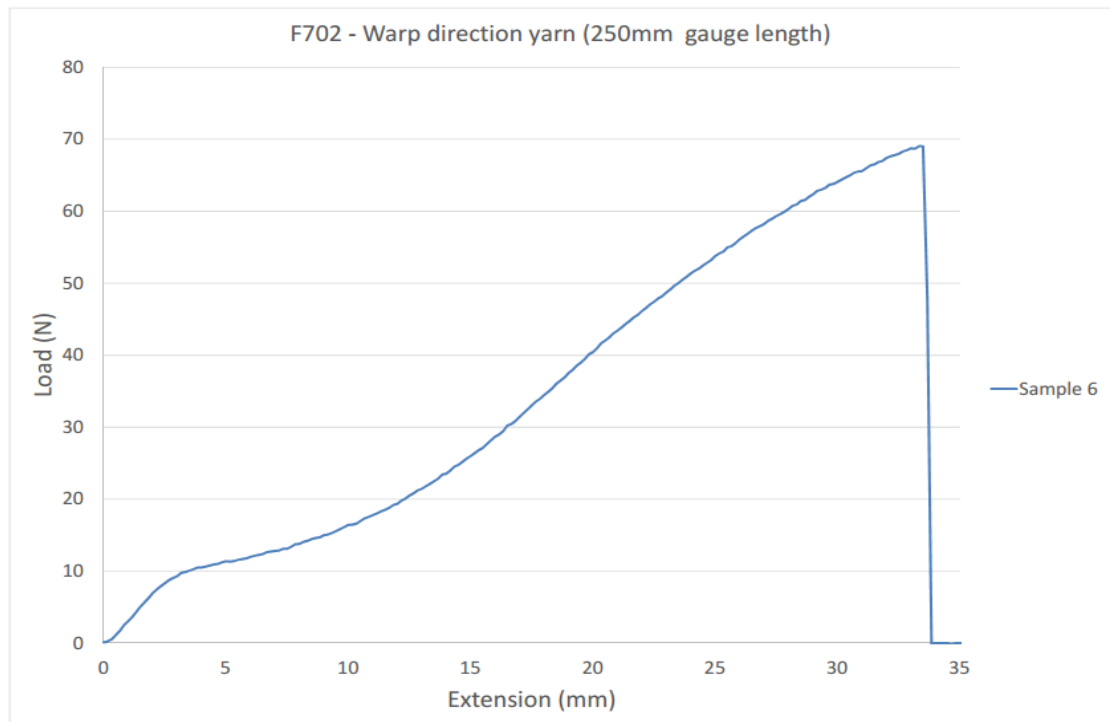


Figure 5-35: Example result for PVC polyester fabric F702 in the warp direction

The polyester yarn (Figure 5-35) shows a similar response to the virgin yarn (as they are both polyester) and to the initial uniaxial response (Figure 5-1). It is also similar to the polyester force-extension curve shown in the literature review (§2.2.1). An initial higher stiffness followed by a period of relatively low stiffness, returning to approximately the original stiffness again prior to failure. This response posed some problems for the calculation of a linear modulus, which is discussed below (Figure 5-38).

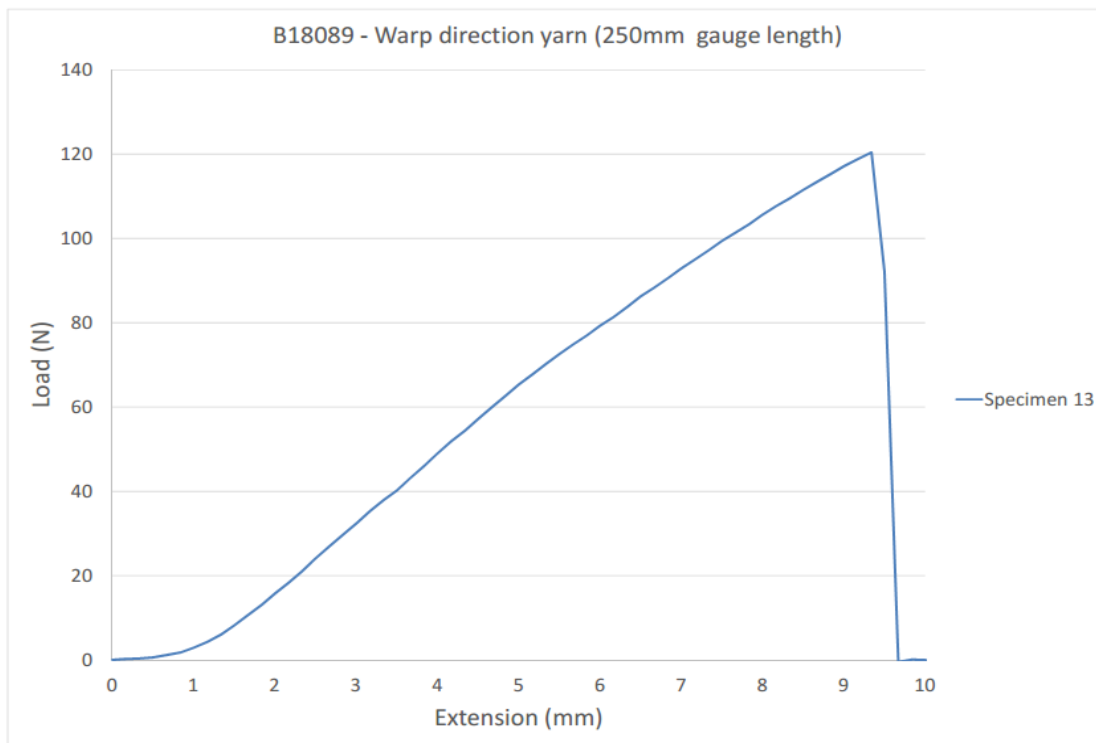


Figure 5-36: Example results for PTFE glass-fibre fabric B18089 in the warp direction

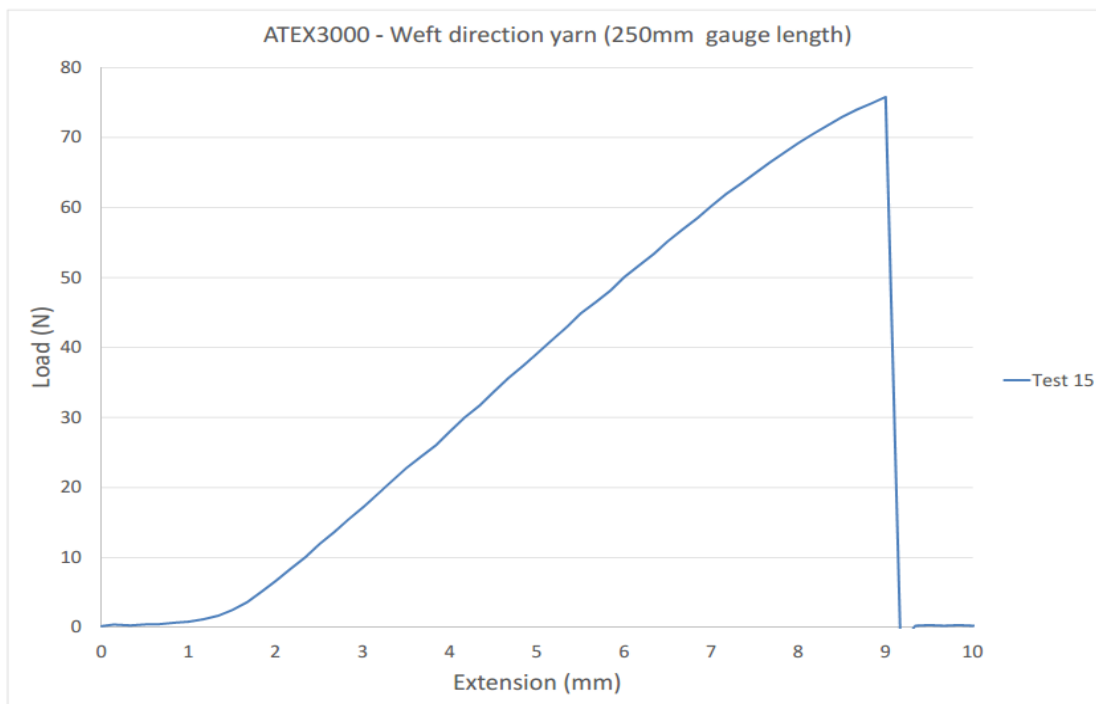


Figure 5-37: Example results for Silicone glass-fibre fabric ATEX3000 in the weft direction

The calculation of the modulus for the glass-fibre yarns is far simpler due to the linear response of the yarn. A small amount of curvature in the load extension graph might be noted (especially at high loads), this could be caused by the twist imparted to the

5. Model validation

filaments in the yarn. In the glass-fibre yarns a small degree of initial extension at almost no load was always noted. This is caused by the crimp that remained in the yarn after it was removed from the fabric increasing the length of the specimen slightly whilst no initial load is placed on the yarn.

Repeatability was excellent with the calculated coefficients of variation for the data low and in the order of 0.021 – 0.07. Visual inspection confirms the repeatability of the results except where some outlier exists. Outliers generally occurred where the yarn slipped in the jaws, or where the yarn failed prematurely, which may have been caused by damage in the yarn, possibly occurring during ravelling. The one exception to this was the consideration of the F1202 fabric yarns in the warp direction.

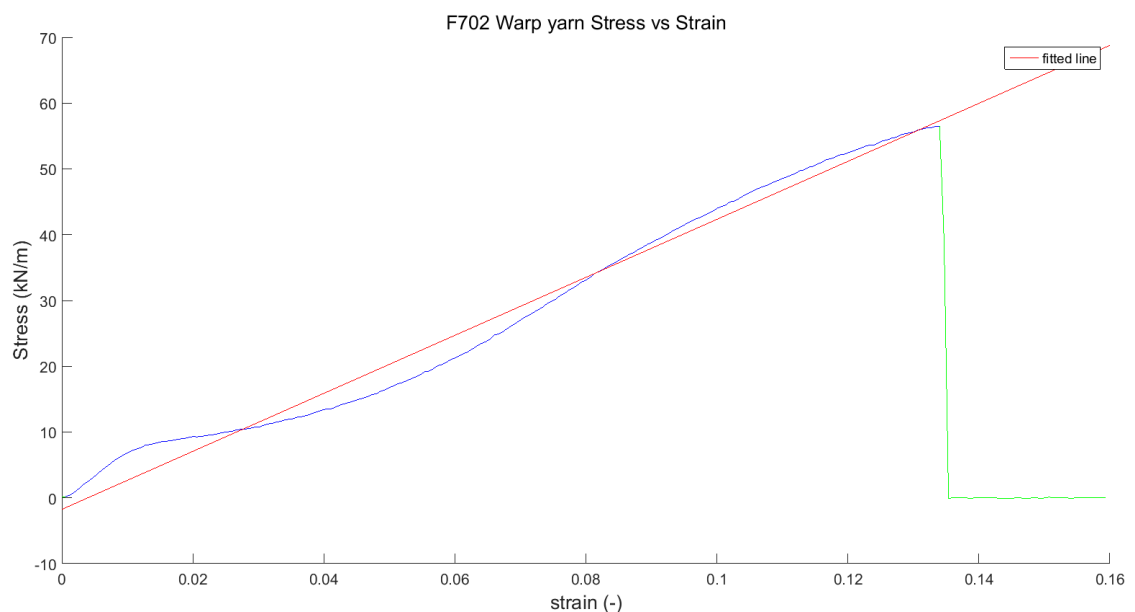


Figure 5-38: Example of method of calculation of modulus for polyester yarns (F702 Warp) (blue = curve utilised for calculation, green = available data, red = fitted curve)

5. Model validation

Specimen	Point on Curve	Calculated Modulus (kN/m)
3	Initial stiffness	732
	Early low stiffness	153
	Mid extension stiffness	606
	Late stiffness	352
5	Initial stiffness	772
	Early low stiffness	165
	Mid extension stiffness	629
	Late stiffness	384
6	Initial stiffness	769
	Early low stiffness	161
	Mid extension stiffness	600
	Late stiffness	309
7	Initial stiffness	781
	Early low stiffness	169
	Mid extension stiffness	617
	Late stiffness	368

Table 5-6: Comparison of yarn modulus for different curve segments for selected tests (tests 1, 2, and 4 were removed as anomalous)

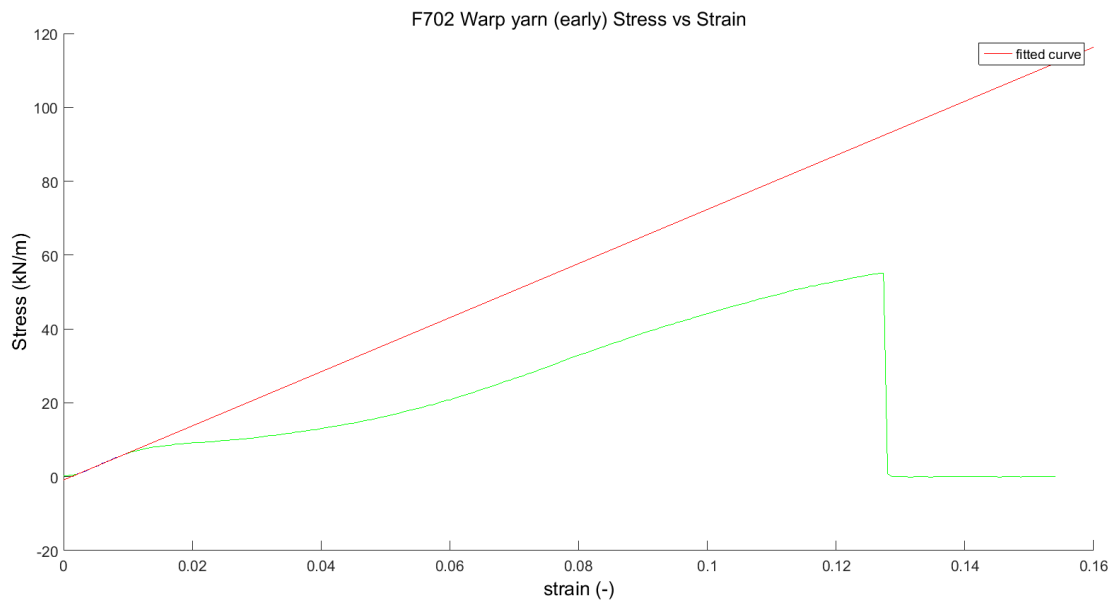


Figure 5-39: Calculation of yarn modulus as calculated for the early response from F702 (warp) yarn response curve (blue = curve utilised for calculation, green = available data, red = fitted curve)

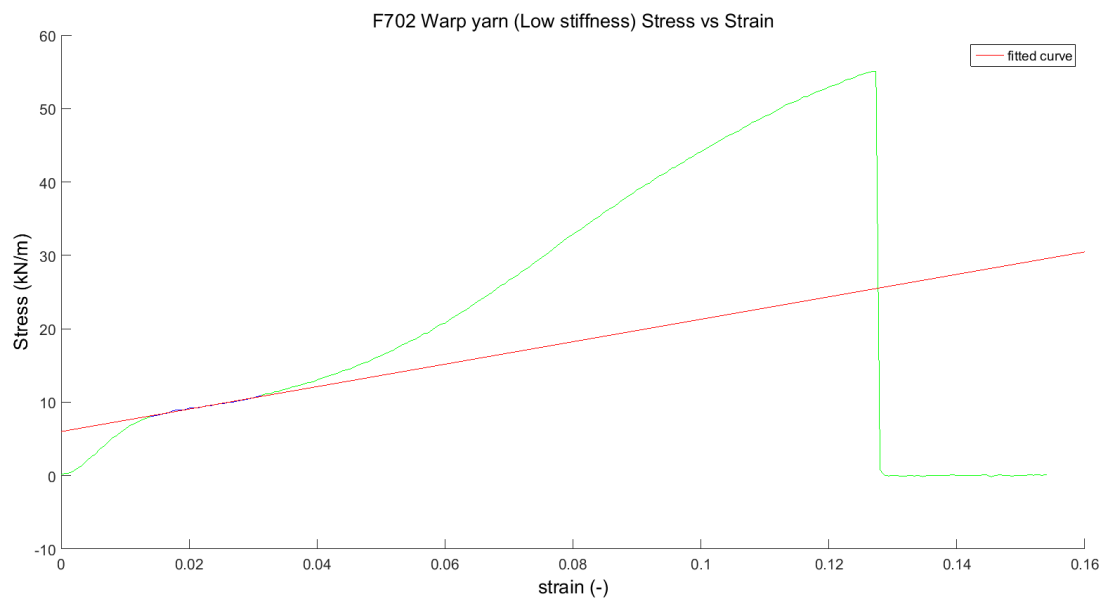


Figure 5-40: Calculation of yarn modulus as calculated for the low stiffness response from F702 (warp) yarn response curve (blue = curve utilised for calculation, green = available data, red = fitted curve)

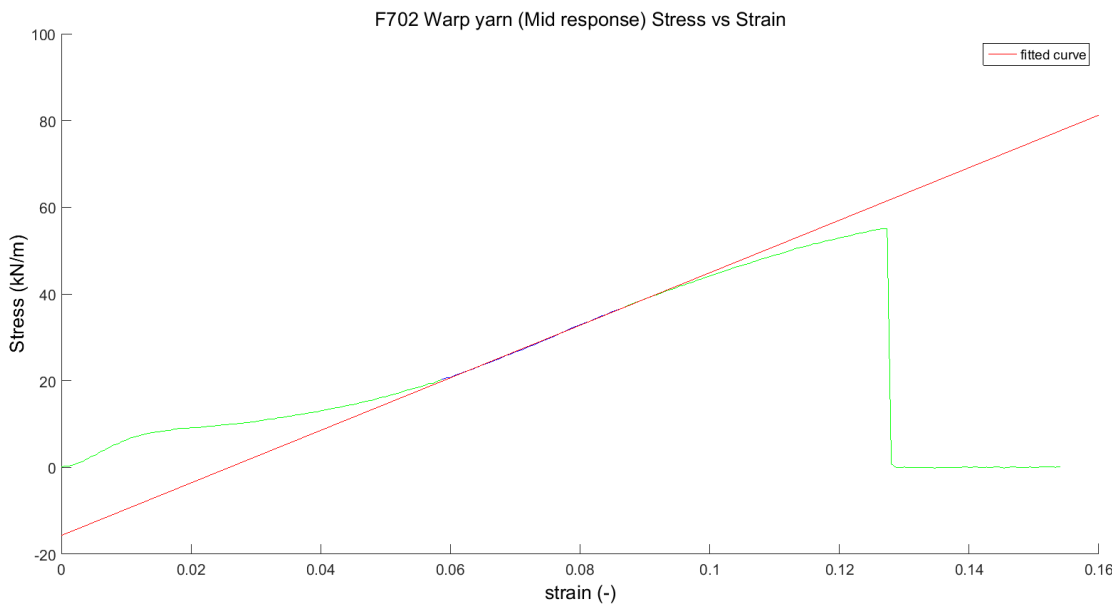


Figure 5-41: Calculation of yarn modulus as calculated for the mid response from F702 (warp) yarn response curve (blue = curve utilised for calculation, green = available data, red = fitted curve)

5. Model validation

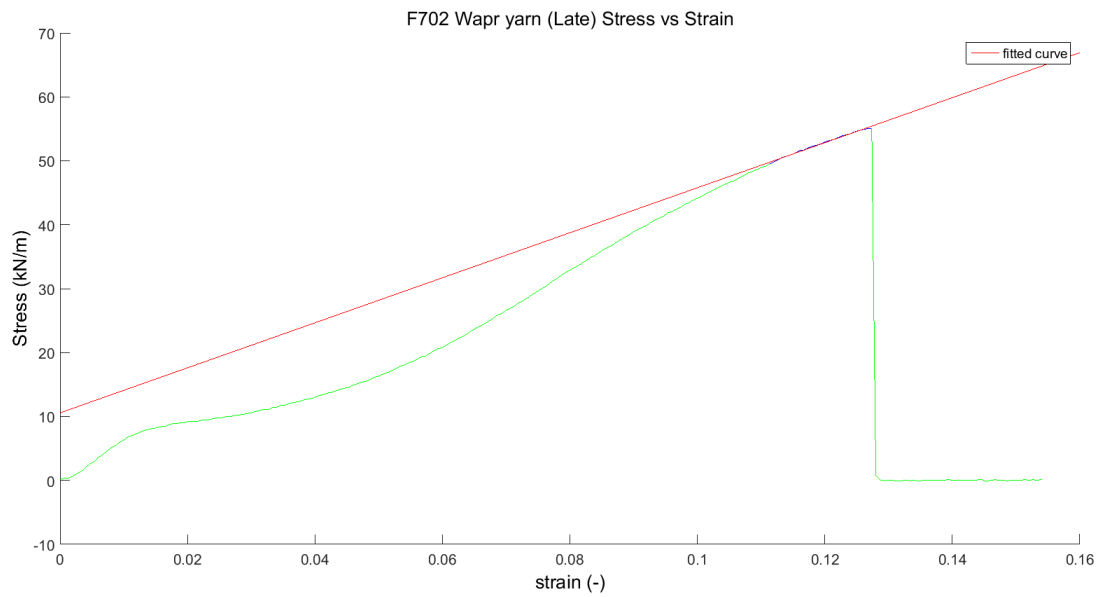


Figure 5-42: Calculation of yarn modulus as calculated for the late response from F702 (warp) yarn response curve (blue = curve utilised for calculation, green = available data, red = fitted curve)

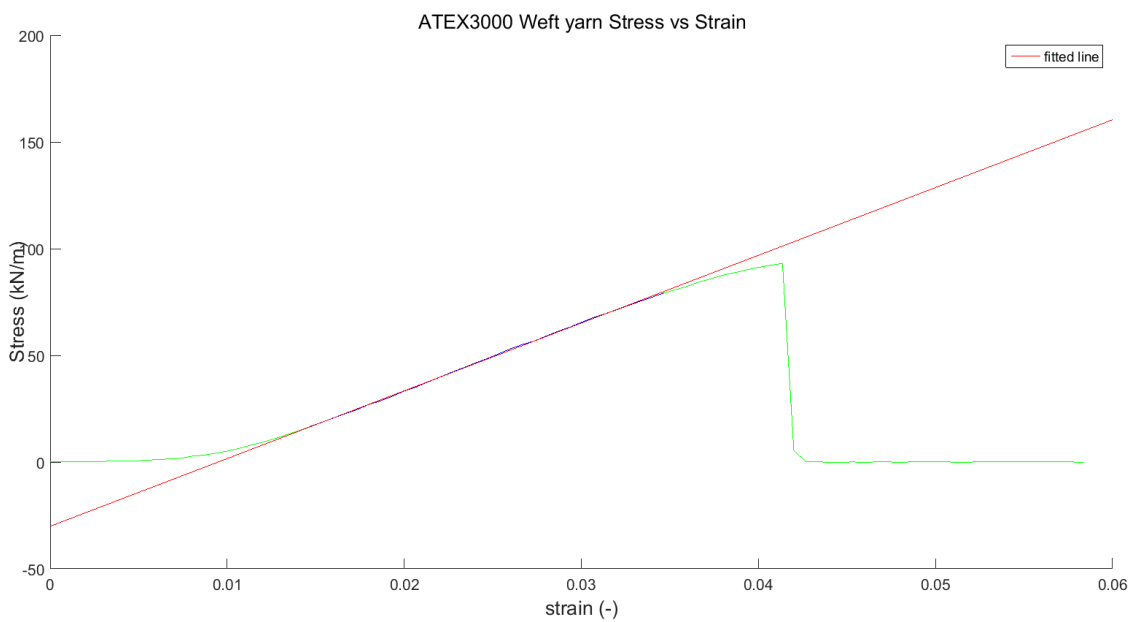


Figure 5-43: Example of method of calculation of modulus for glass-fibre yarns (ATEX3000 weft) (blue = curve utilised for calculation, green = available data, red = fitted curve)

Fabric Type	Direction	Mean	Standard deviation	Variance	Coefficient of variation	Number of samples used
ATEX3000	Warp	3222	67.6	4574	0.021	12
	Weft	2875	116.1	13485	0.040	12
ATEX5000	Warp	5525	215.8	46587	0.039	13
	Weft	5149	273.7	74915	0.053	13
B18089	Warp	4438	327.6	107300	0.074	13
	Weft	3705	238.9	57052	0.064	11
B18059	Warp	6812	227.9	51923	0.033	13
	Weft	5302	195.3	38153	0.037	13
F702	Warp	444	9.1	84	0.021	9
	Weft	382	14.2	202	0.037	13
F1202	Warp	729	50.7	2568	0.070	7
	Weft	617	46.3	2142	0.075	14

Table 5-7: Yarn test summary; showing the calculated values of stiffness using the central portion of the response

Generally results showed low values of variation with coefficients of variation being consistently less than or equal to 0.075 exemplified by the data used to calculate the ATEX3000 yarn elastic properties (Figure 5-44). Visual inspections demonstrates that the gradients appear similar, and the coefficient of variation found for the data bears this out (0.021). Compare this with the results for the F1202 warp yarn and there is clearly a difference in the repeatability of the tests (the tests were carried out under the same conditions) (Figure 5-45). Firstly, the tests show failures at high loads due to slips of the clamping equipment or partial failure of the specimen. After this was noted a further seven repeats were carried out in an attempt to find a solution to this, but were unsuccessful in doing so. The tests are therefore considered to have failed at the slip point, with data beyond this being unused. Using teeth to stop slippage was shown to cause failure at lower loads, whilst capstans were ruled out as they do not allow for the accurate calculation of stiffness. Capstans spread the load of the yarn across a wider area using a curved surface to spread the load in the yarn before it is clamped. This means that extension across the surface of the capstan cannot be accurately determined, rendering head displacements unusable.

The data in Figure 5-45 shows a high degree of spread, with a wide range of gradients. The coefficient of variation of all these gradients with the exception of sample 6 was actually found to be 0.20, which is unacceptable for use in this model as it suggests that there is a 20% dispersion in the data. After the investigation of the data a second change

5. Model validation

in gradient mid curve was found in the data, and noted at around 15mm extension. It is therefore hypothesised here that some further deformation mechanism is occurring in those yarns not grouped with the steepest seven.

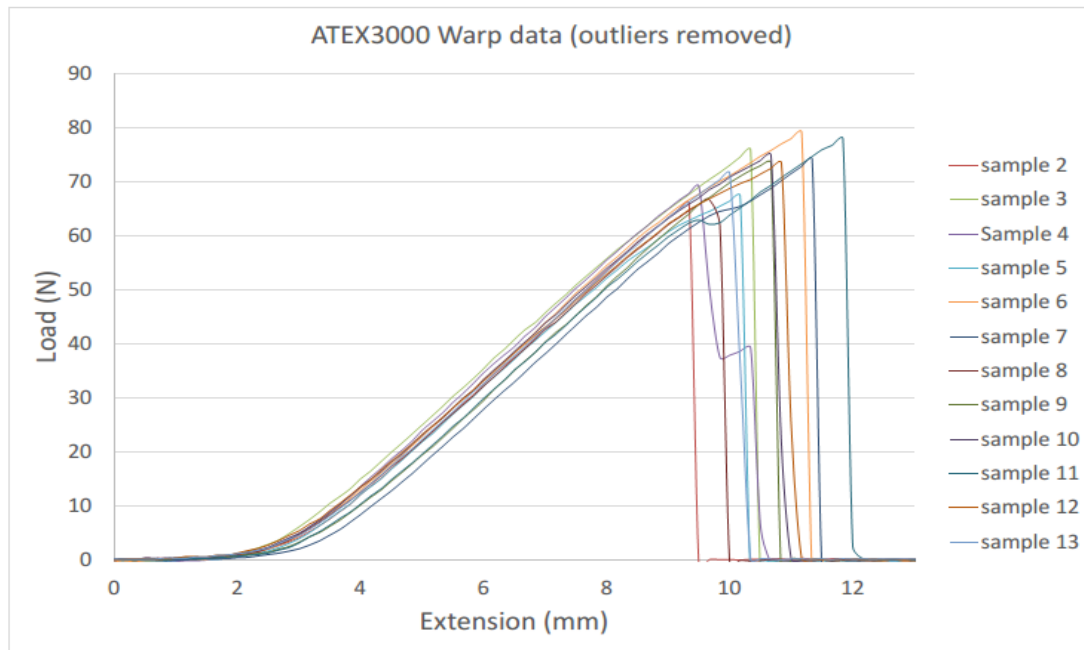


Figure 5-44: Example of repeatability of results from ATEX3000 warp data with outliers removed

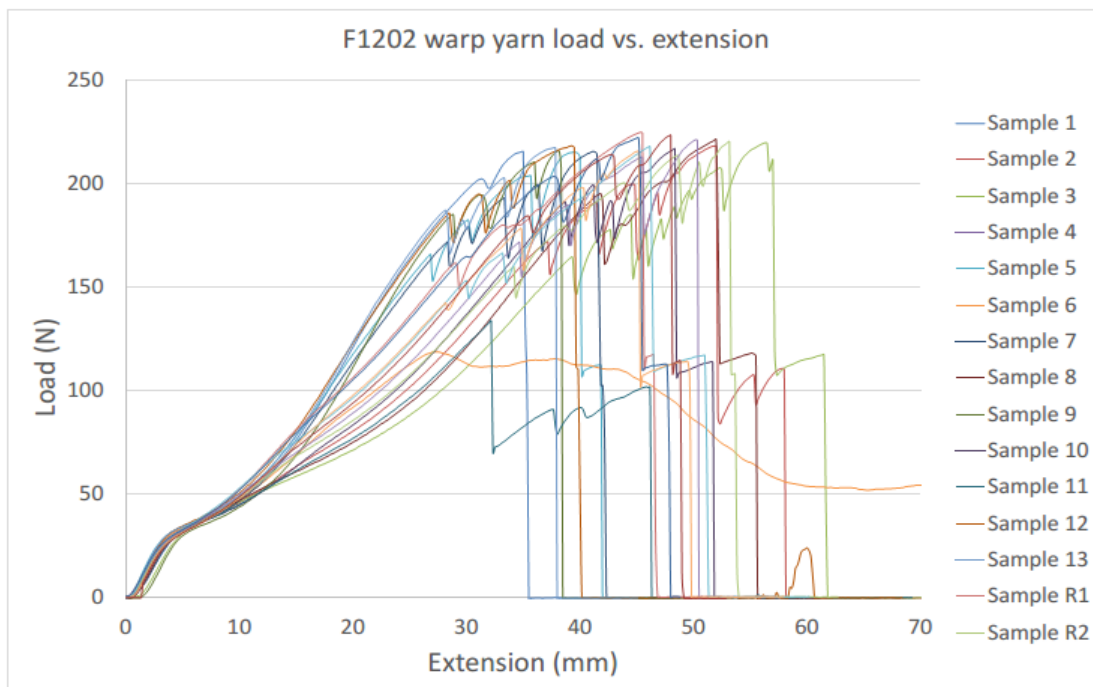


Figure 5-45: All data produced from the F1202 tests in the warp direction

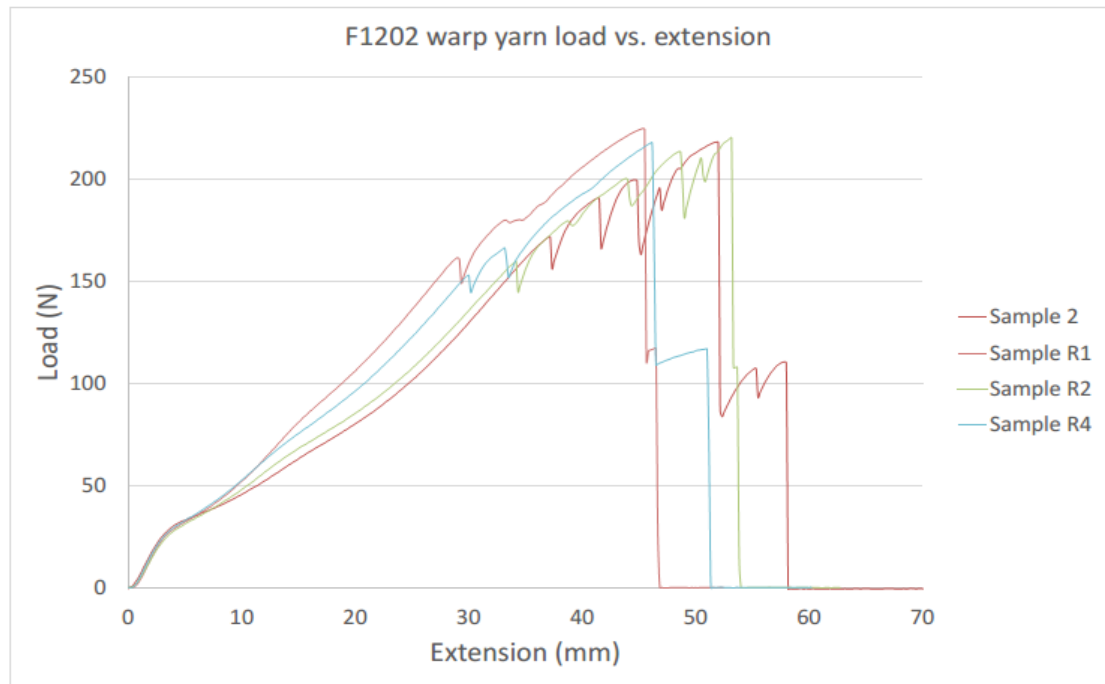


Figure 5-46: A selection of samples of F1202 warp data with the second change in gradient visible

The F1202 warp yarn shows considerable discretisation of two plies once removed from the fabric, which can also be seen in cross sections of the fabric in situ (Figure 5-47). The second extension to failure after the initial failure is caused by the continued extension of the second ply demonstrating that both plies are acting individually to some extent (Figure 5-46 and Figure 5-45). Lastly, Figure 5-48 shows how the yarn has failed at two distinct points, and how the yarn has split into its two constituent plies during the testing (the red marks indicate the centre of the sample). Given this information it is concluded that the high variation in the yarns response is likely to be due to the two plies of the yarn becoming uncoupled and acting separately. This decrease in stiffness at approximately 10-15mm extension, preceded by an area of high repeatability up to approximately 10mm extension, is therefore not typical of what would happen in a yarn in-situ. Where the yarn is still restrained as part of a whole fabric this uncoupling would not occur at these loads, as such only those tests where the uncoupling does not occur were used in the calculation of the yarn extension characteristics.

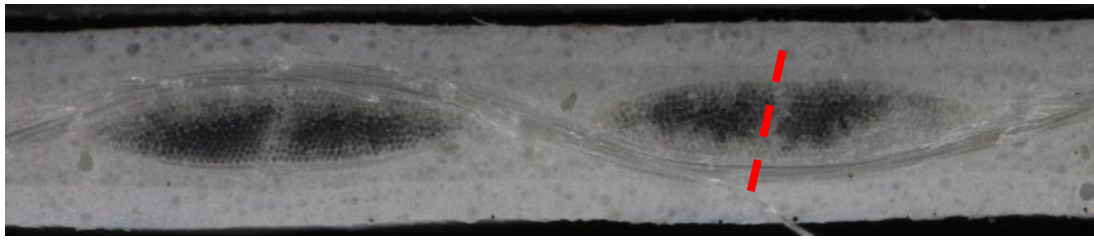


Figure 5-47: Cross section of F1202 warp yarn showing the two discrete plies (Colman, 2013a)



Figure 5-48: F1202 warp yarn after failure

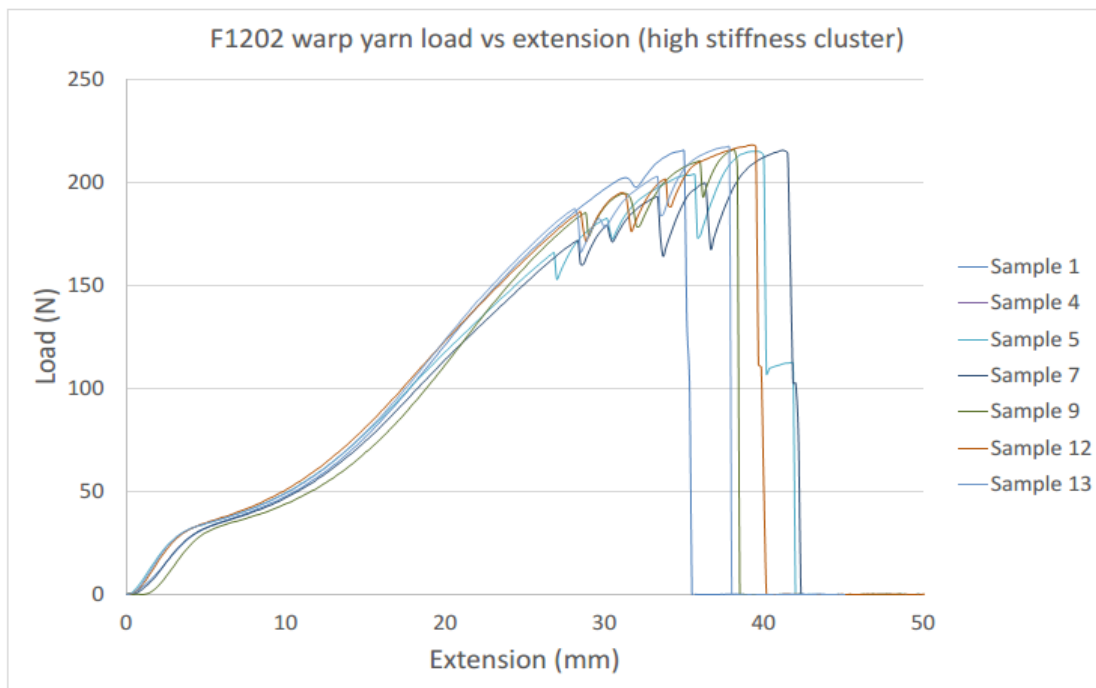


Figure 5-49: Results used for calculation of F1202 (warp) mechanical properties

The results whilst clearly not as visually repeatable as those shown for the ATEX 3000 fabric are a clear improvement on the wide spread shown for all the data. As such it was deemed reasonable to use this data in further calculations.

A comparison to previously carried out uniaxial tests (Colman, 2014) was also made (Table 5-8):

Fabric Type	Direction	Yarn test result (kN/m)	Upper yarn test value (kN/m)	Lower yarn test value (kN/m)	Uniaxial strip test result (kN/m)
ATEX3000	Warp	3222	3357	3087	3120
	Weft	2875	3107	2643	3190
ATEX5000	Warp	5525	5957	5093	4110
	Weft	5149	5696	4601	6300
B18089	Warp	4438	5094	3783	4270
	Weft	3705	4183	3228	3970
B18059	Warp	6812	7268	6356	4610
	Weft	5302	5693	4911	4770
F702	Warp	444	462	426	485
	Weft	382	411	354	425
F1202	Warp	729	830	627	880
	Weft	617	710	525	810

Table 5-8: Comparison of single yarn test results to previously carried out uniaxial tests for yarn modulus

The uniaxial data used in Table 5-8 was produced by Colman (2014) and was generated using straight portion of the uniaxial response from uniaxial strip tests (§5.2.1) (similar to Figure 5-41), and includes the coating response (i.e. it has not been removed).

The upper and lower values of the yarn test results are calculated as the 95% confidence bounds, or two standard deviations up and down from the calculated mean. The yarn tests for the PVC polyester fabric appear to underestimate the yarn stiffness if compared to the uniaxial tests, whilst the glass fibre yarns both over and underestimate the value. However, as discussed above the values calculated for individual yarns are likely to be the true values of the stiffness of the yarns, whilst the results of the uniaxial tests will be affected by other factors.

Firstly, if some crimp remains in the yarns under uniaxial testing then the calculated value of stiffness may be underestimated as some portion of the extension is due to further yarn straightening and the yarn length will in reality be longer than predicted. Both these would reduce the value of the calculated stiffness. Further the yarn crushing caused by the interaction between the yarns may affect the yarn, possibly causing bending in the tested yarn, or inducing further stress. Coating and the transverse yarns will also offer some resistance to extension in the alternate direction, and it is possible

that in the case of the PVC coated fabrics this is more profound. A visual inspection of PVC coated polyester fabric cross-sections, in comparison to other fabric cross sections, does seem to show a higher degree of coating impregnation, which may result in the coating having a greater effect on tensile strength. Yarns may have been damaged during ravelling, reducing their stiffness, whilst this may have been more profound in some fabrics, or directions than in others.

In short, it is difficult to prove whether either set of values are correct. The accuracy of the resulting analysis from the results is the defining consideration.

5.2.4. Tensile strength

Tensile strength has not been measured for this report, but might be measured as per BS EN ISO 1421:1998 (BSI, 1998). Tensile strength would be better measured using capstans, where the clamping force should be spread more evenly reducing the number of breaks at clamp, found to be generally between half and three quarters of tests for elongation response above. The use of capstans however would not be applicable to testing for elongation characteristics, as discussed above.

5.3. Validation study

Comparisons of the model output using known feasible targets have been made in previous chapters (§3.7), and a short review of those findings is made in this section (§5.3.1). Further validation studies are then carried out using biaxial test data processed using the method discussed earlier (§5.2.2.2). These compare the method's output to real test data, and demonstrate how the design methodology operates when posed with test data. A fabric geometry is also robustly designed using statistical data collected on the about the fabric's properties.

5.3.1. Comparison to known feasible targets

The model was implemented with known feasible targets used as the input for the optimisation in an earlier chapter (§3.7). Known feasible targets were derived from the sawtooth equilibrium equations using a central finite difference method at target values of stress, i.e. 10kN:10kN. Four targets (E_{11} , E_{22} , ν_{12} , ν_{21}) were calculated at each target value of biaxial stress. These targets were then used as the input for the fabric design (optimisation) method.

The output of the method demonstrated that the optimisation of the defining equations was able to calculate a fabric geometry that reproduced the target values of stiffness and Poisson's ratio at the specified loads. However, the optimised geometry was not always that of the original fabric from which the targets had been derived using the central finite difference method. A new fabric was often designed that should adequately reproduce the required targets at the specified loads. To check that the model could also reproduce the original fabric from which the targets had been derived a further optimisation was carried out where a geometry similar to that of the original fabric was used as the initial guess point. In this situation the original fabric geometry was reproduced by the model. It was hypothesised that multiple, or zero, solutions may exist for any set of targets at specified loads, and this was shown to be the case in the previous chapter (§4).

The reason the fabric design methodology selected a geometry other than that of the original fabric from which the targets were derived is due to the optimisation method employed following a steepest gradient approach. If a point is selected by the pattern

search method that appears to be a possible solution then the optimisation will use this point as the initial start point and follow the steepest gradient to a solution. In this case the steepest gradient leads not to the original geometry, but to another geometry.

The methodology for the design of a fabric was therefore shown to be adequately designing fabric geometries for multiple targets at different loads.

5.3.2. Fabric design for five sets of targets

For the validation study three fabrics will be 'designed' using targets obtained using the multiple point target method discussed earlier (§5.2.2.2). The method follows the procedure laid out below:

1. Biaxial test data is imported and processed using the method described in §5.2.2.2.
2. Plane Stress Elastic constants are derived from the data for reference
3. Point (plane stress) targets are produced using the method described earlier (§5.2.2.2) at equidistant intervals on the fabric's surface to give five sets of four targets.
4. An attempt is made to produce a fabric that would respond in the same way as the fabric from which the original targets were obtained using the model.
5. Where the targets cannot be adequately met variation in the targets is allowed using the best optimised geometry from the previous step.
6. Incremental steps in variation are allowed in targets, up to 75% variation from the original targets.
7. If a solution is found at any point the solver will end and display the results

Initially test data for a F702 PVC coated polyester fabric is analysed using the method described in 5.2.2.2 and the targets obtained from that analysis are shown in Table 5-9. After the targets are calculated an attempt is made to design a fabric that satisfied the targets, which it was found could not be achieved. This was repeated a number of times from different initial start points to ensure that a local minima had not been found during the optimisation process.

	Point 1	Point 2	Point 3	Point 4	Point 5
E_{11} (target 1) (kN/m)	698	441	569	644	487
E_{22} (target 3) (kN/m)	0.585	0.122	0.324	0.460	0.233
v_{12} (target 2)	651	620	568	481	528
v_{21} (target 4)	0.433	0.459	0.281	0.028	0.302
P_1 (kN/m)	3.76	3.76	7.51	11.27	11.27
P_2 (kN/m)	3.76	11.27	7.51	3.76	11.27

Table 5-9: Targets from PVC coated Polyester fabric F702

The targets in Table 5-9 vary from those that would have been used if a single plane stress representation had been used. The values for a standard plane stress representation are given in Table 5-1. Most notable is the very low Poisson's ratio (target 4 at point 4). This will be due to the specifics of the surface at this point, not captured by the standard plane stress method which would have led to the use of a considerably higher ratio.

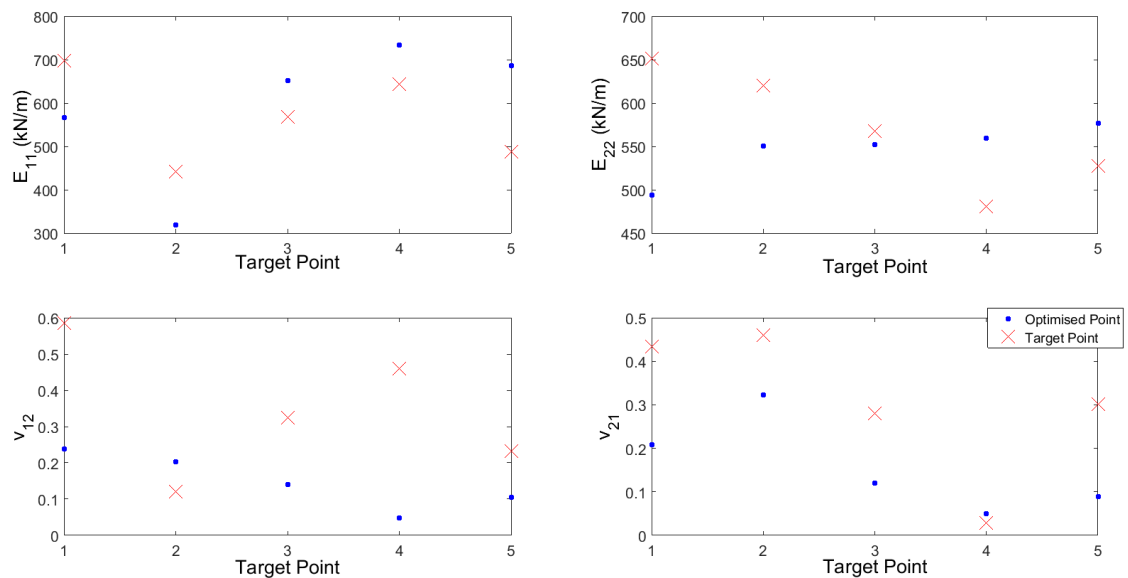


Figure 5-50: Results of fabric design without variation in targets for F702 targets (1)

5. Model validation

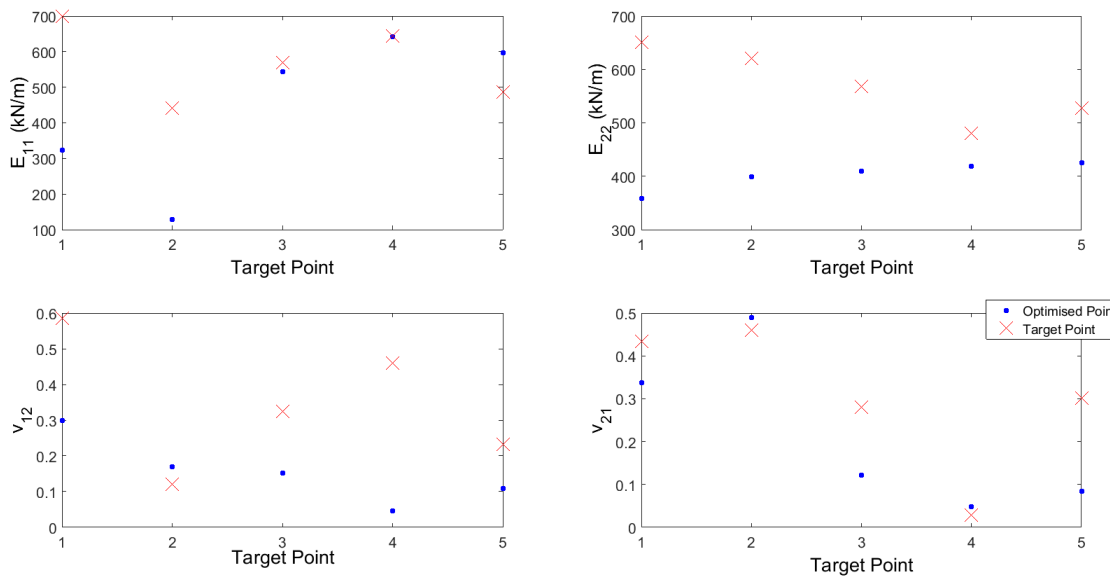


Figure 5-51: Results of fabric design without variation in targets for F702 targets (2)

The results for the initial design to the F702 fabric targets show poor correlation to the biaxial test results with only one target being achieved in the second test (Figure 5-51) at the fourth target point for E_{11} . The solver is unable to find the original geometry nor produce a geometry that satisfies the targets (Figure 5-51 and Figure 5-50). Shown are two different results of the optimisation, using different initial guesses. As the method continues to search for better solutions after a local minima has been found by randomising its start point more than one local minima can be found. To test the entire possible data space for a best local minima would take a large amount of computing power or time as each of these sets of results required approximately four hours to find. Testing the entire space would require a grid search of indefinite fineness to be used; if only 10 values of each property were tested this would require 4×10^9 hrs. Whilst the method would allow the user to carry this out if needed (computing power and memory notwithstanding) it is not considered to be viable where no perfect solution is found. Both sets of results have similar objective function values (4.19 and 4.49 respectively), with this being no real indication of the quality of the result.

Whilst the optimisation did not reproduce the original fabric this might be expected given that the original model did not perfectly reproduce fabric response. This is discussed in more detail later.

After the initial optimisation the routine attempts to design a fabric that satisfies the targets, given some quantity of allowable variation in the target values. In this example the targets are allowed to vary in steps of 5% (steps of 10% are shown in Figure 5-52).

5. Model validation

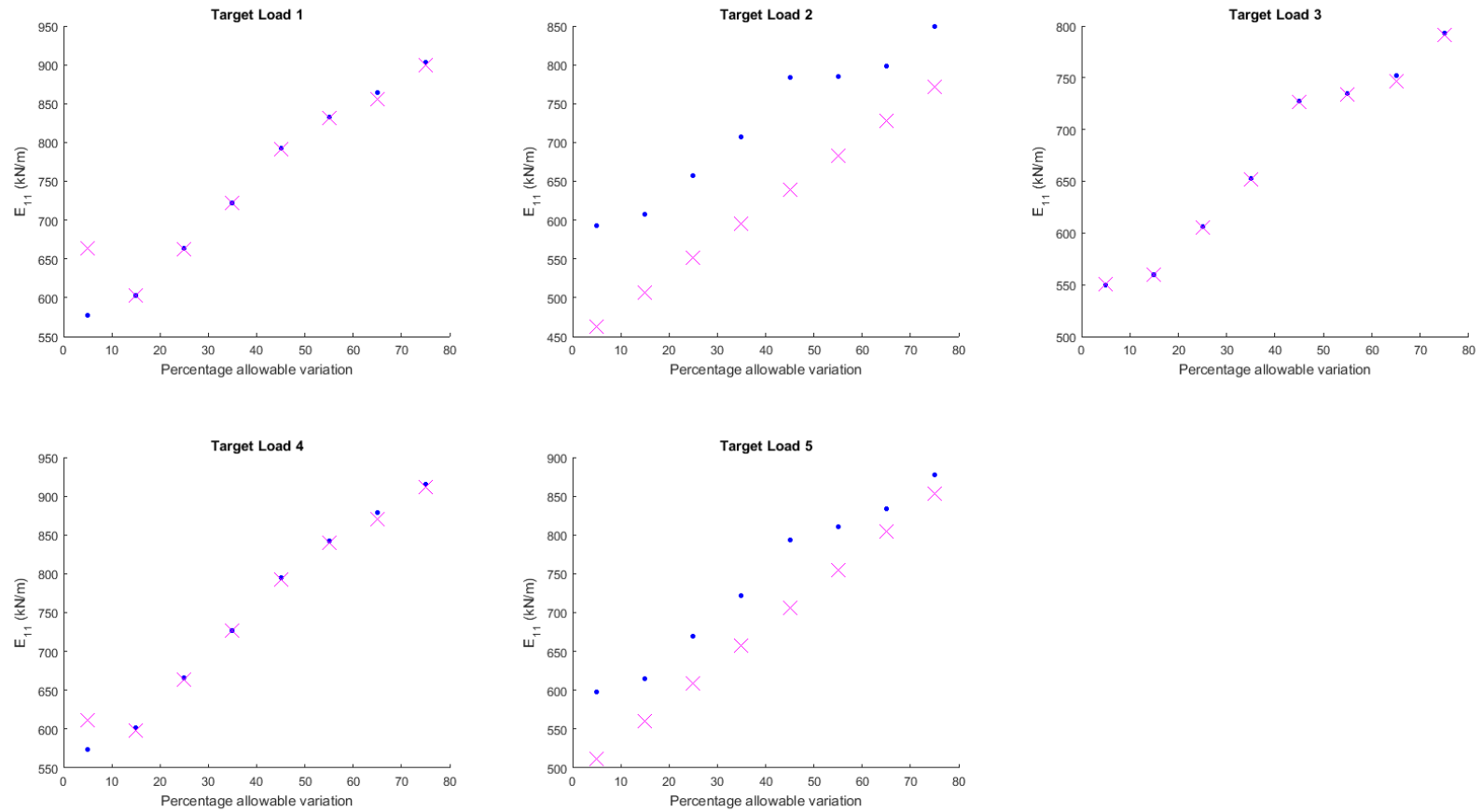


Figure 5-52: Target (X) and designed fabric (.) stiffnesses at increasing values of allowable variation from original targets

5. Model validation

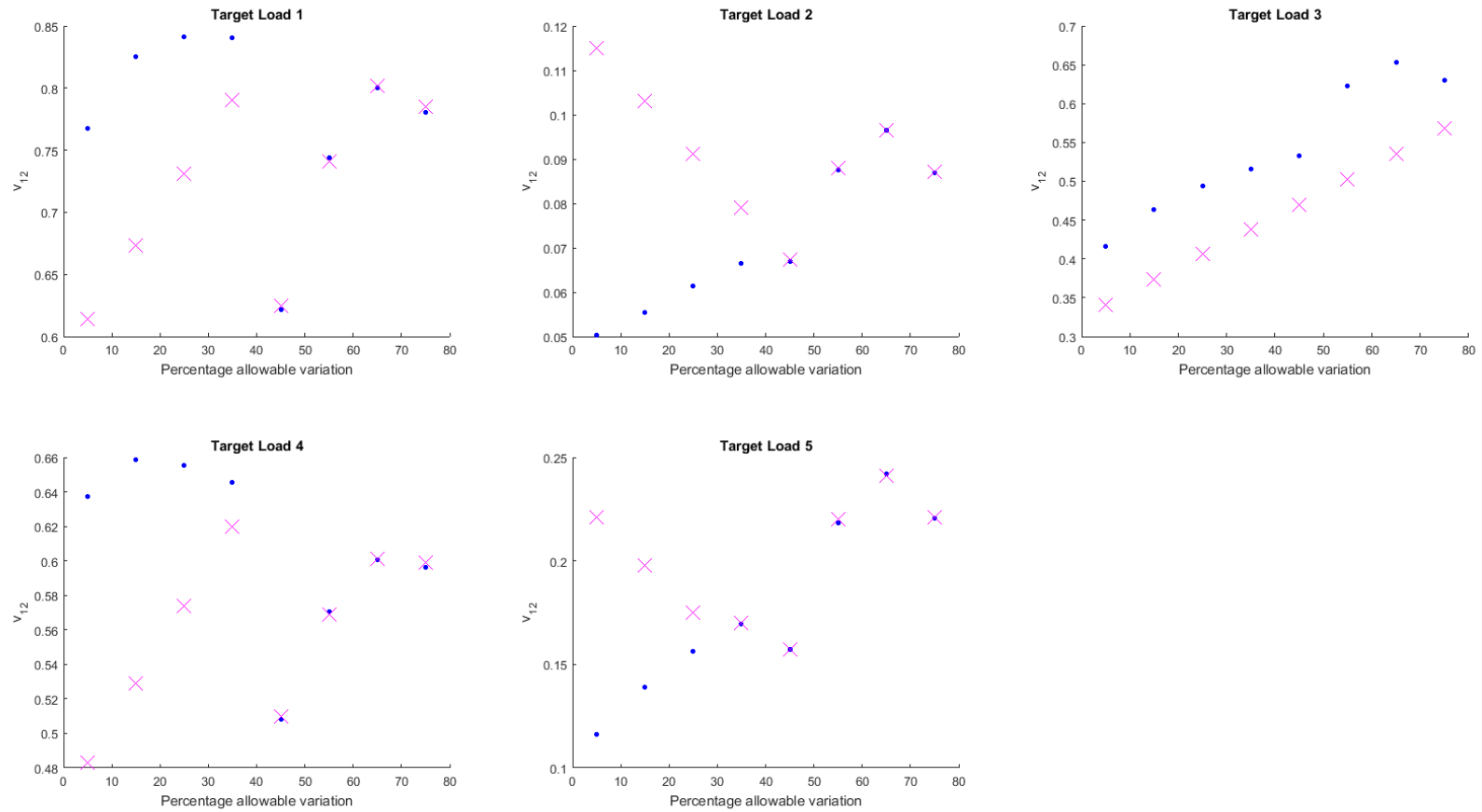


Figure 5-53: Target (X) and designed fabric (.) Poisson's ratios at increasing values of allowable variation from original targets

5. Model validation

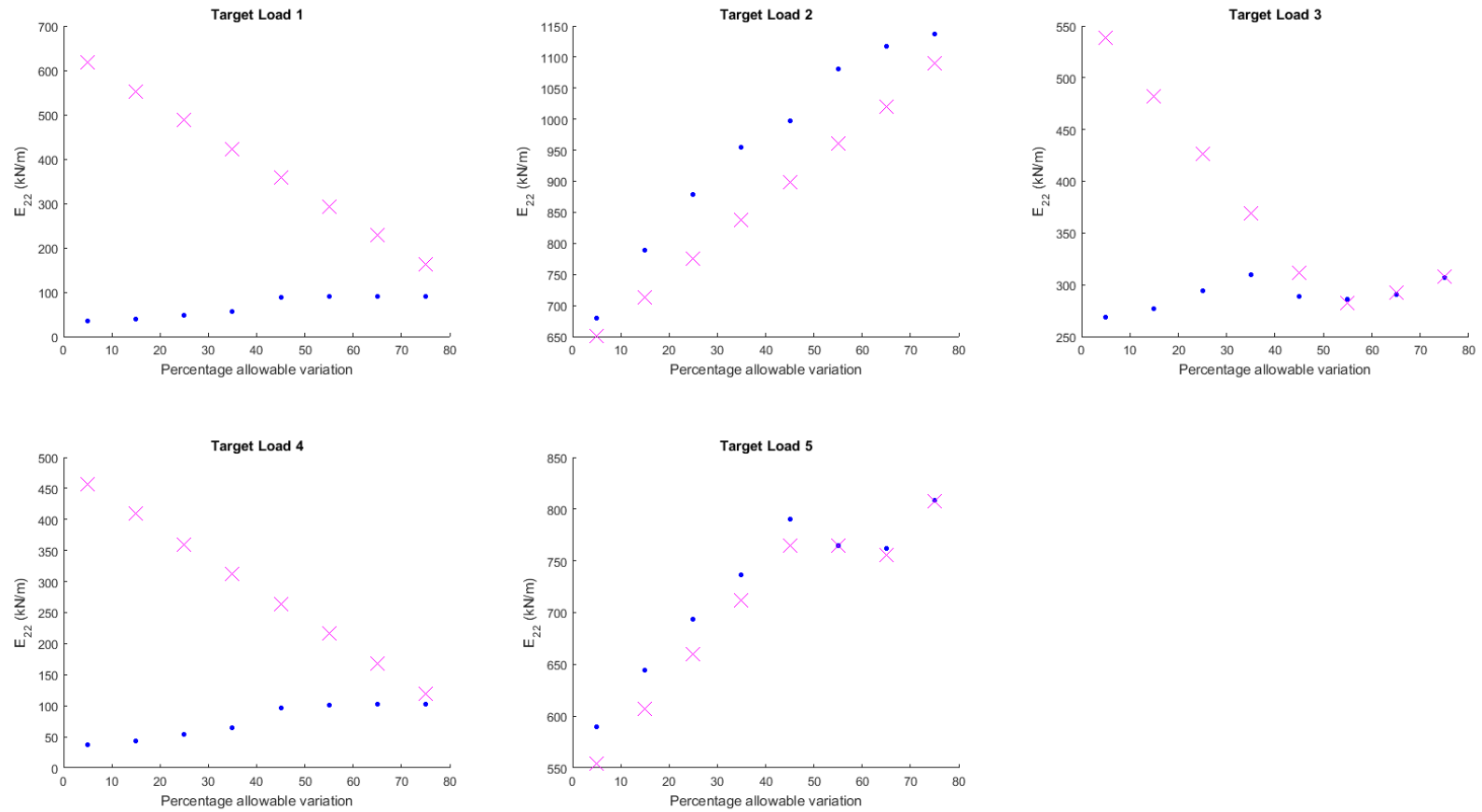


Figure 5-54: Target (X) and designed fabric (.) stiffnesses at increasing values of allowable variation from original targets

5. Model validation

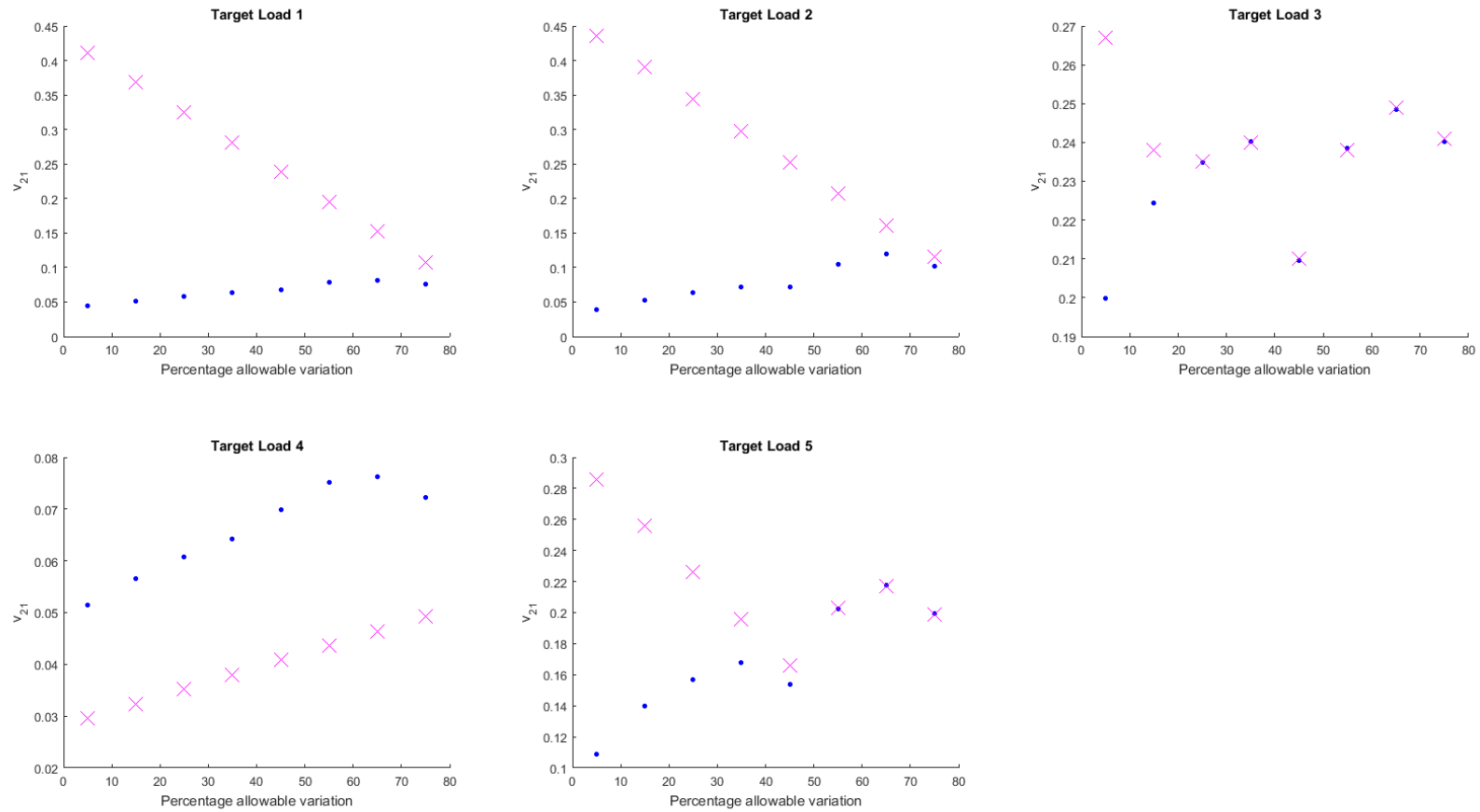


Figure 5-55: Target (X) and designed fabric (.) Poisson's ratios at increasing values of allowable variation from original targets

It has been observed that generally the limiting factor when optimising the geometry is the worst initial estimate. As the geometry has already been optimised to try to achieve the targets its value does change noticeably during this phase, however, targets move towards the elastic constants of the designed fabric. This is shown in detail in Figure 5-52 to Figure 5-55.

Some targets are quickly met, whilst others prove more challenging. The optimised point does on occasion move away from the target, demonstrating how the routine is minimising error across the entire optimisation. In this case even after a variation in target of 75% was allowed not all targets were met.

A visual inspection of the optimised geometry (designed geometry) shown suggests that it does not appear to demonstrate a feasible fabric design (Figure 5-56). However, were a very thin and flat yarn used in conjunction with a more normally sized yarn it might be possible to recreate something similar to this. Some improvement to this is made in the following sections where a fabric robust to variation is considered, but at this stage the model might be considered to have failed to design a valid fabric. This is one reason the robust optimisation is necessary. Further constraints on the yarn geometry might be possible to reduce the possibility of unreproducible fabric designs occurring where unrealistic fabric geometries are produced. What is, and is not, an unrealistic fabric geometry is subjective, as the geometry produced fulfils all the criteria given to the model (i.e. that the yarns are within the maximum and minimum thicknesses described in the literature review (§2.2.2)). The geometry uses realistic thicknesses of yarns, but combines them in a fashion that appears to show an inappropriate solution. It is possible that with further study a relationship for realistic fabric geometry might be produced, and this used to constrain the fabric design. However, this would further restrict and constrain the design process, which may result in further reductions in the accuracy of the optimisation to the biaxial targets.

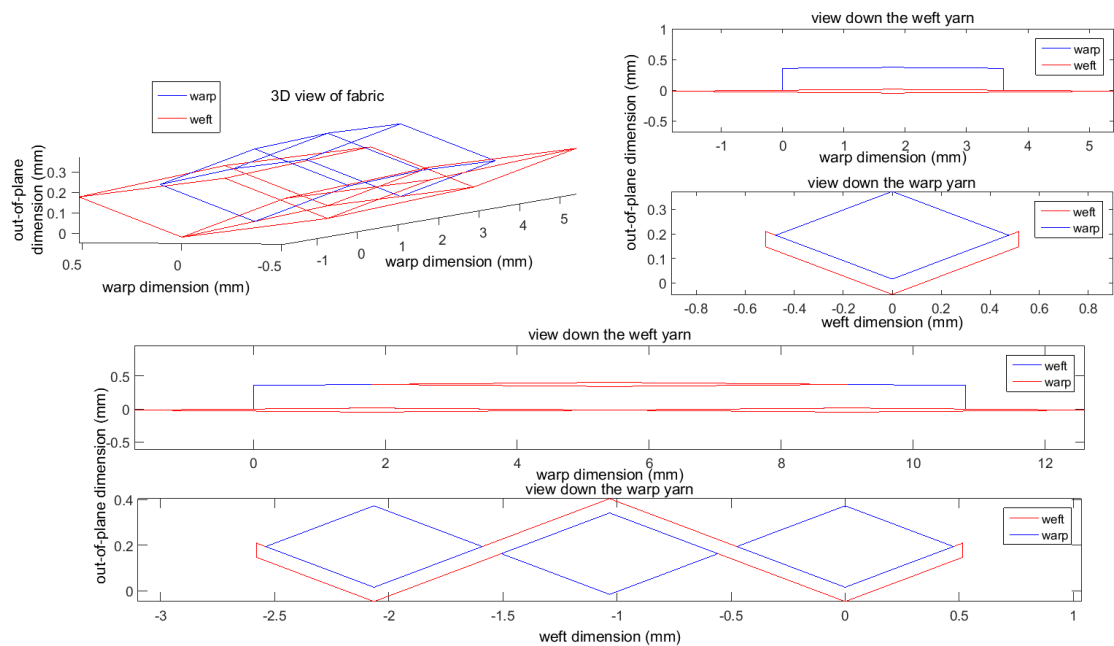


Figure 5-56: Geometry of the designed fabric (F702 targets)

The results for a B18059 PTFE coated glass-fibre fabric are now considered below.

	Point 1	Point 2	Point 3	Point 4	Point 5
E_{11} (target 1) (kN/m)	1380	819	2261	2416	1279
E_{22} (target 3) (kN/m)	0.800	0.139	0.720	1.826	0.626
v_{12} (target 2)	952	1556	1287	619	1115
v_{21} (target 4)	0.719	1.288	0.576	0.279	0.868
P_1 (kN/m)	10	10	20	30	30
P_2 (kN/m)	10	30	20	10	30

Table 5-10: Targets from PTFE coated glass-fibre fabric B18059

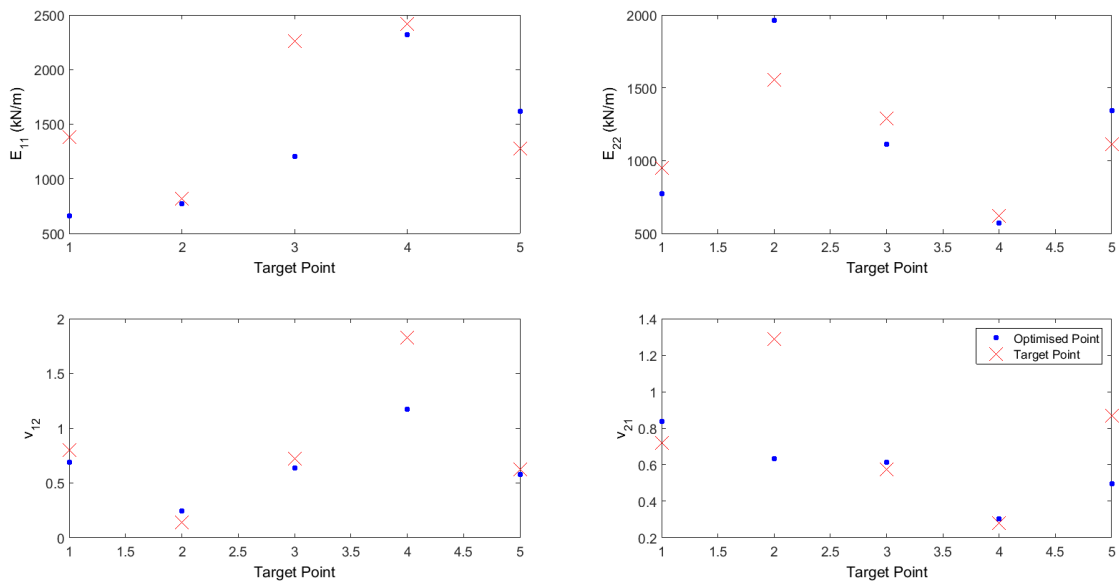


Figure 5-57: Results of fabric design without variation in targets for B18059 targets

5. Model validation

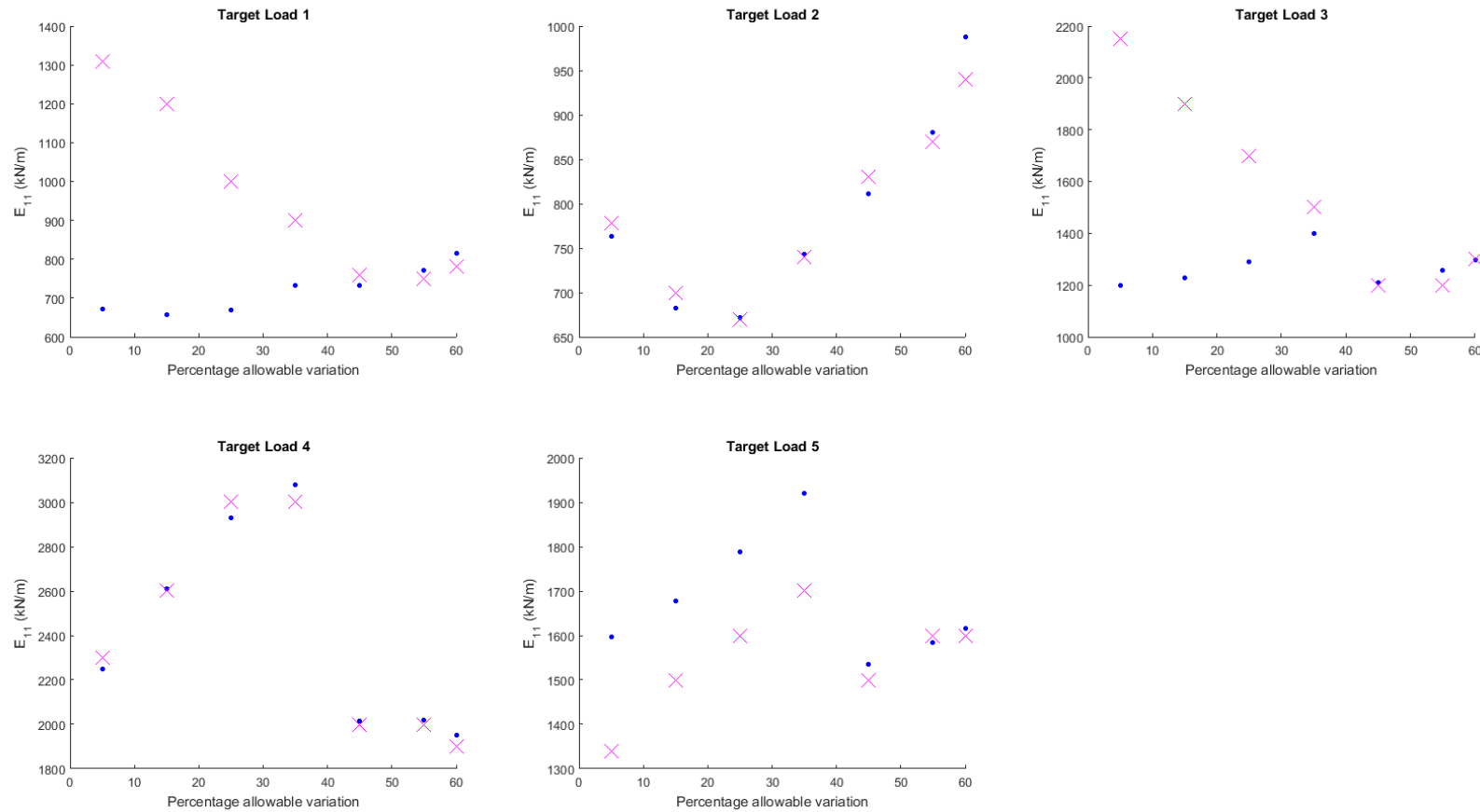


Figure 5-58: Target (X) and designed fabric (.) stiffnesses at increasing values of allowable variation from original targets

5. Model validation

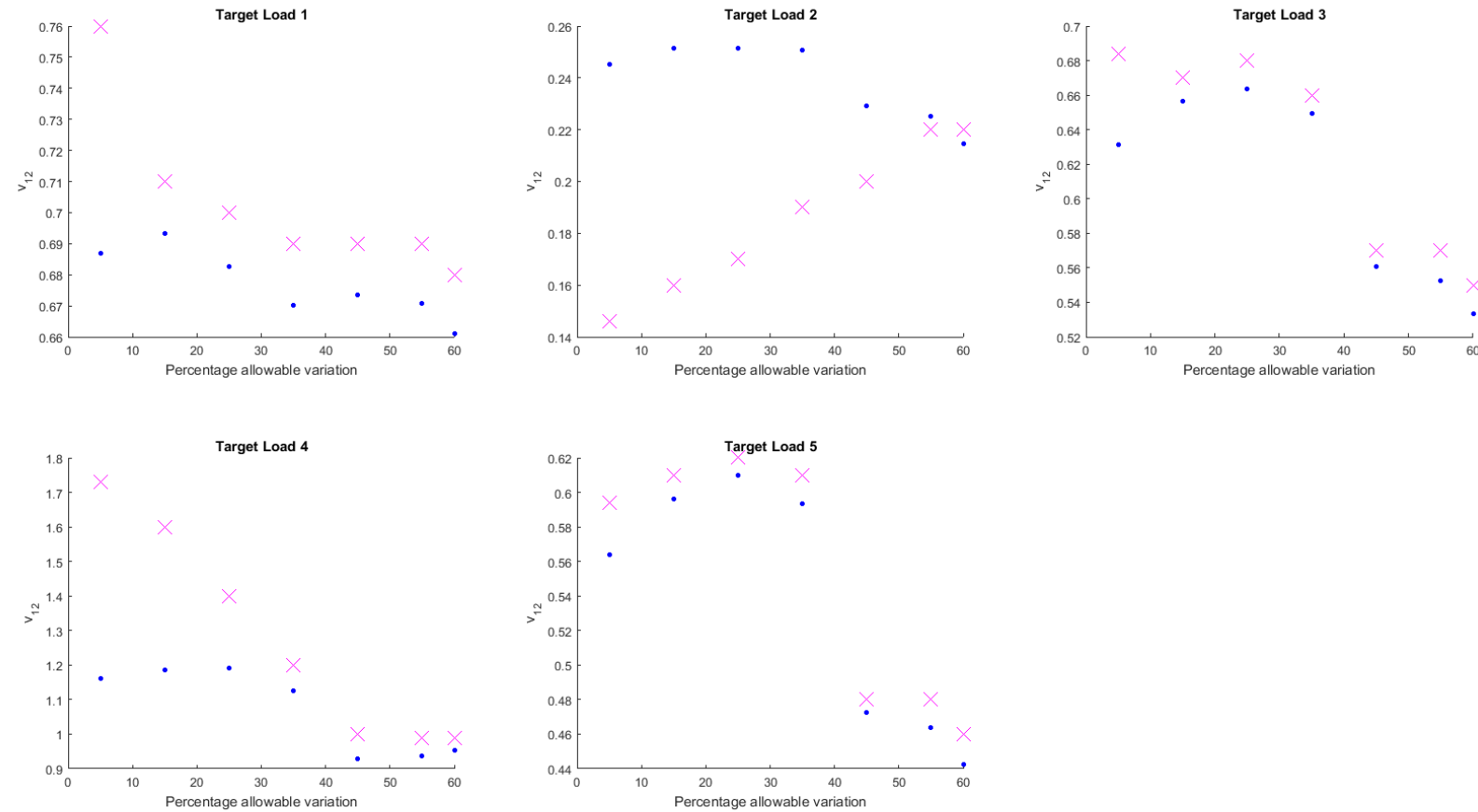


Figure 5-59: Target (X) and designed fabric (.) Poisson's ratios at increasing values of allowable variation from original targets

5. Model validation

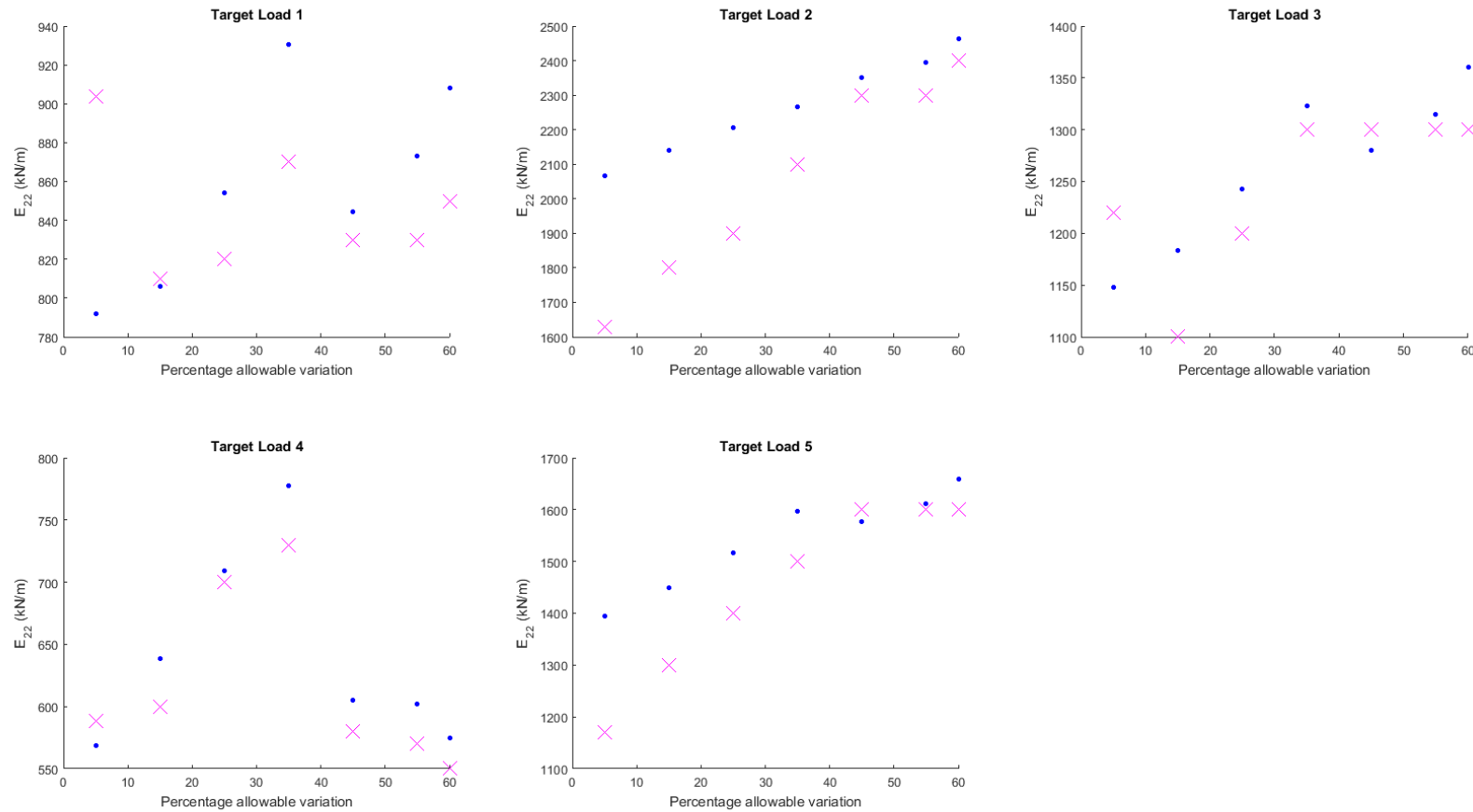


Figure 5-60: Target (X) and designed fabric (.) stiffnesses at increasing values of allowable variation from original targets

5. Model validation

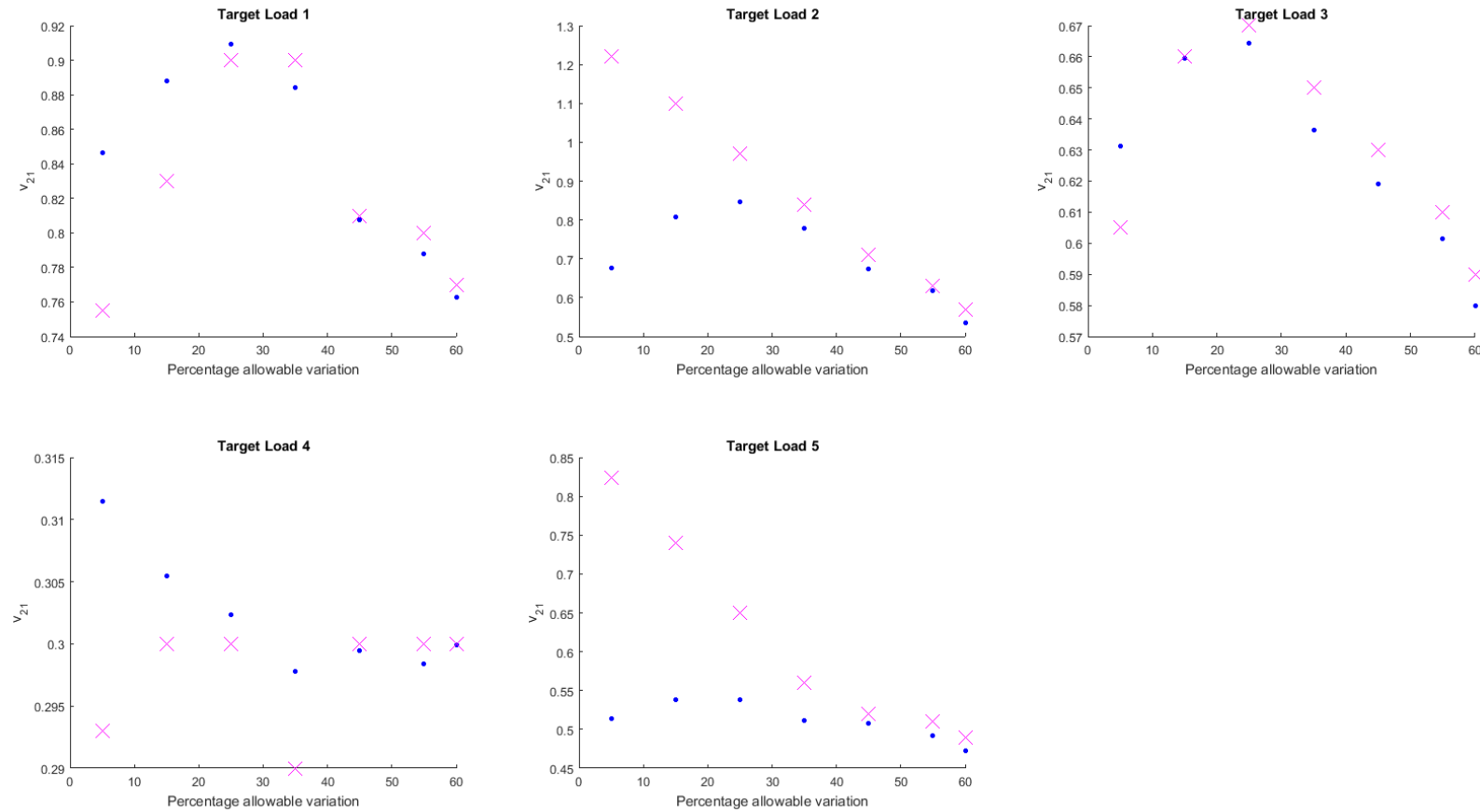


Figure 5-61: Target (X) and designed fabric (.) Poisson's ratios at increasing values of allowable variation from original targets

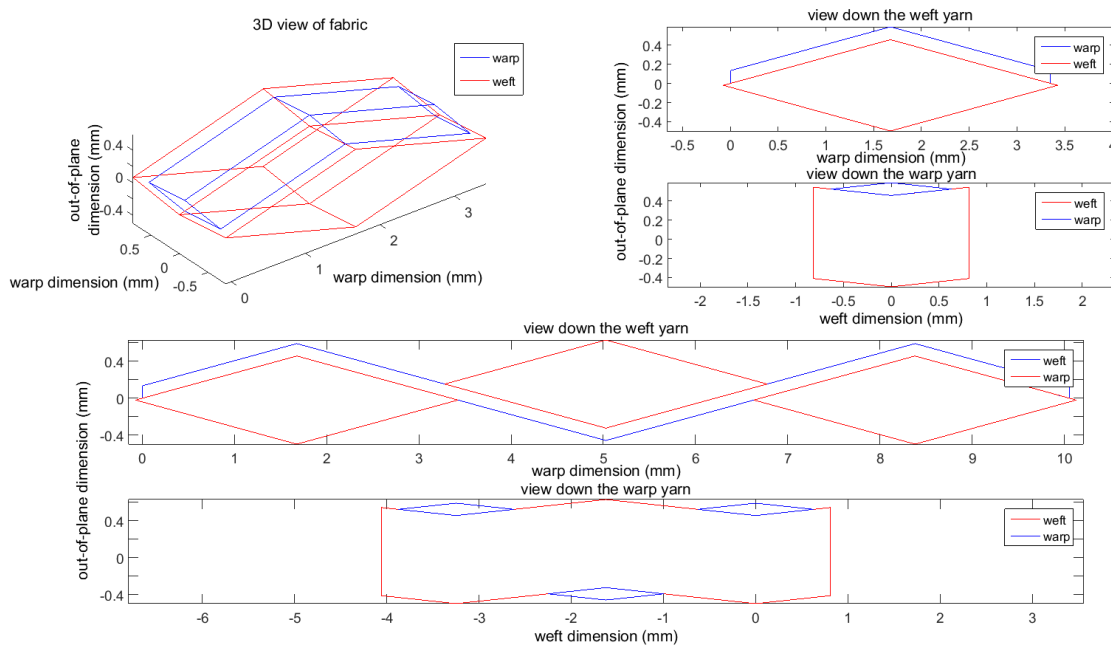


Figure 5-62: Geometry of the designed fabric (B18059 targets)

The results for the B18059 fabric are visually more appealing, and appear to more accurately match the targets at lower levels of variation. This may be due to the more linear response of the yarns in a glass fibre fabric, coupled with the higher values of fabric stiffness. Higher values of fabric stiffness should lead to greater allowable variation as the model allows targets to move by a fraction of the target.

The results for an ATEX 3000 are detailed below.

	Point 1	Point 2	Point 3	Point 4	Point 5
E_{11} (target 1) (kN/m)	617	365	1138	969	959
E_{22} (target 3) (kN/m)	1.061	0.320	0.586	2.246	0.898
ν_{12} (target 2)	409	804	816	209	662
ν_{21} (target 4)	0.630	1.266	0.564	0.227	0.561
P_1 (kN/m)	3.76	3.76	7.52	11.28	11.28
P_2 (kN/m)	3.76	11.28	7.52	3.76	11.28

Table 5-11: Targets from Silicone coated glass-fibre fabric ATEX 3000

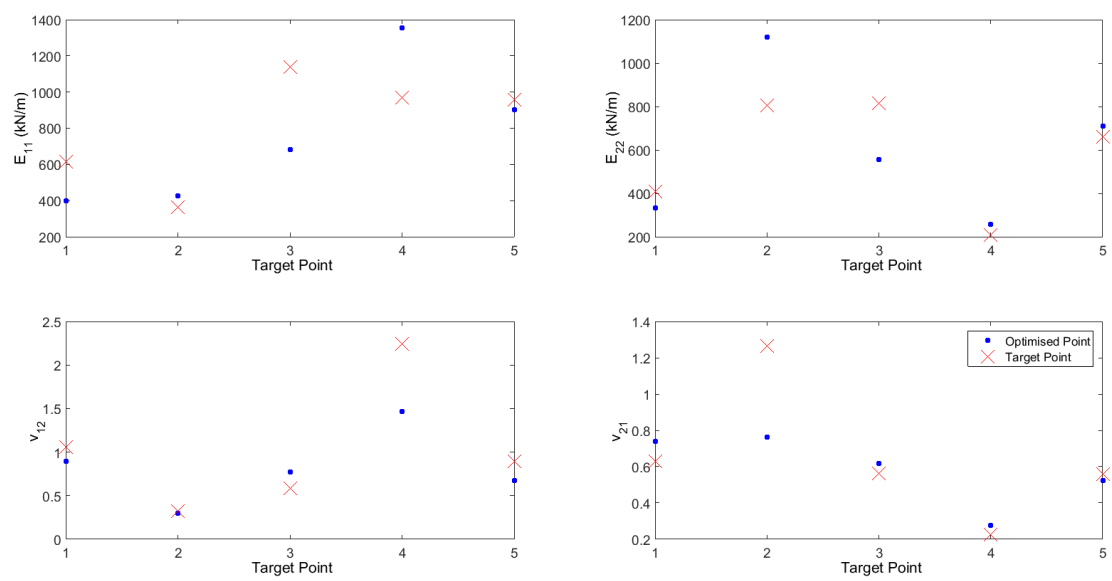


Figure 5-63: Results of fabric design without variation in targets for ATEX3000 targets

5. Model validation

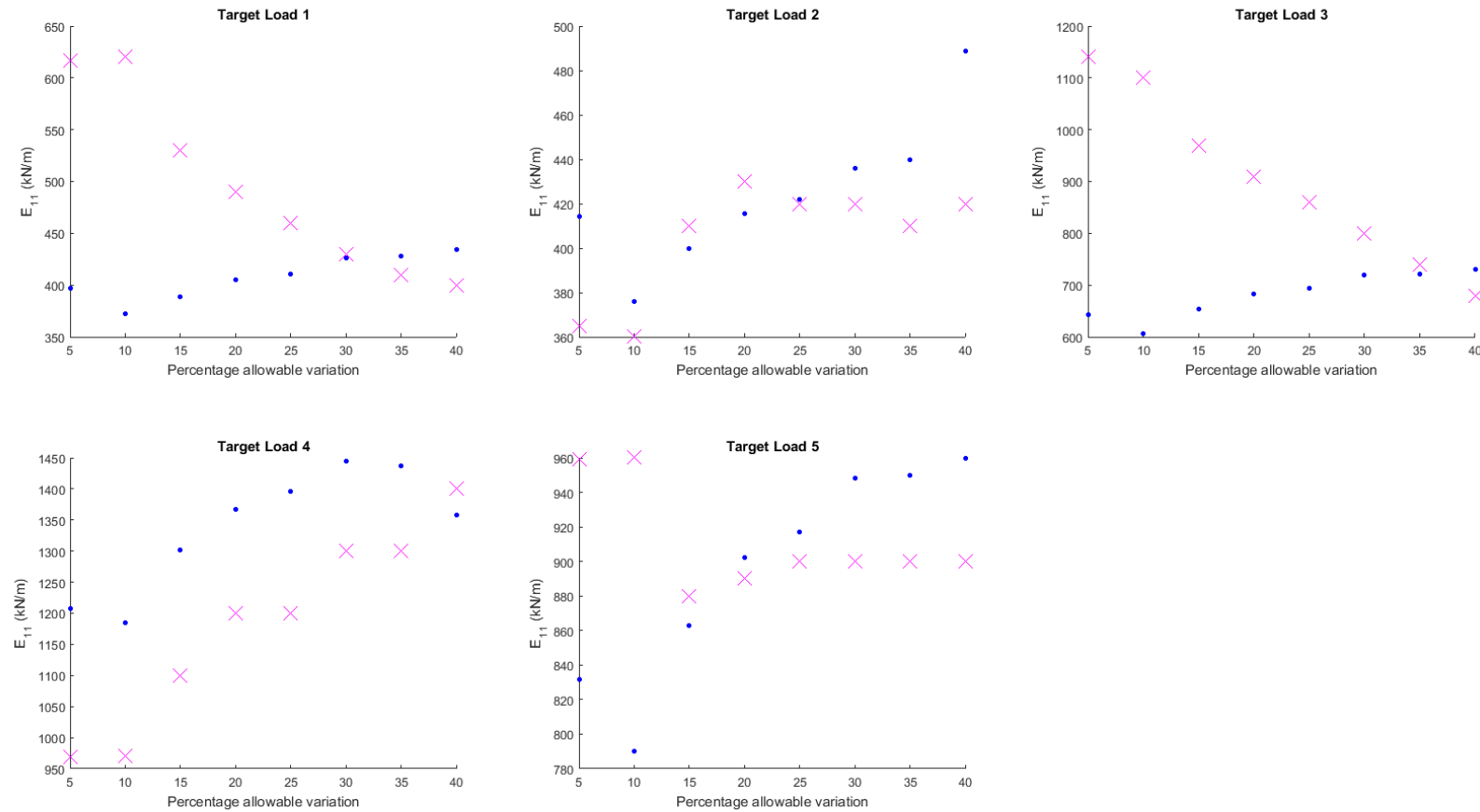


Figure 5-64: Target (X) and designed fabric (.) stiffnesses at increasing values of allowable variation from original targets

5. Model validation

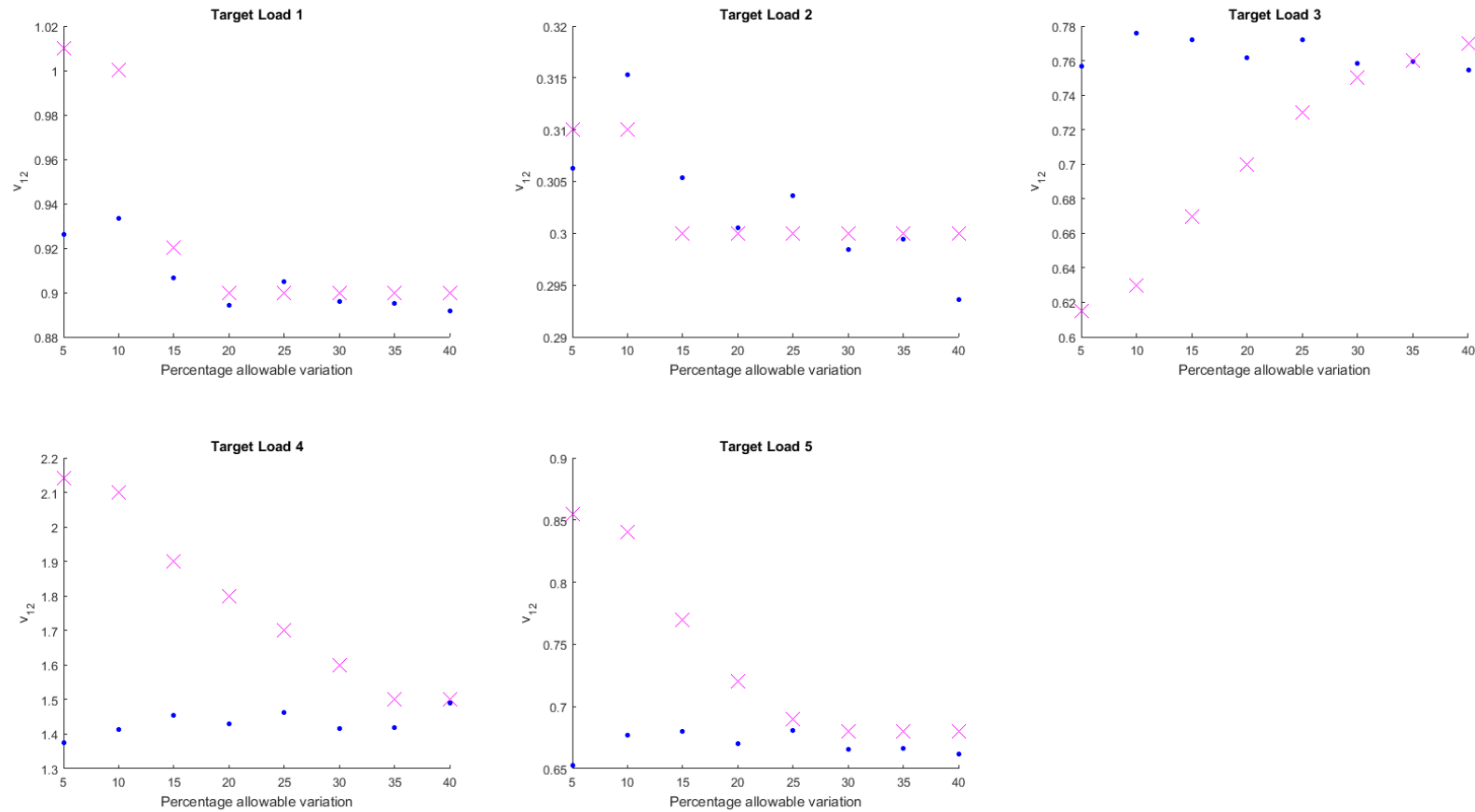


Figure 5-65: Target (X) and designed fabric (.) Poisson's ratios at increasing values of allowable variation from original targets

5. Model validation

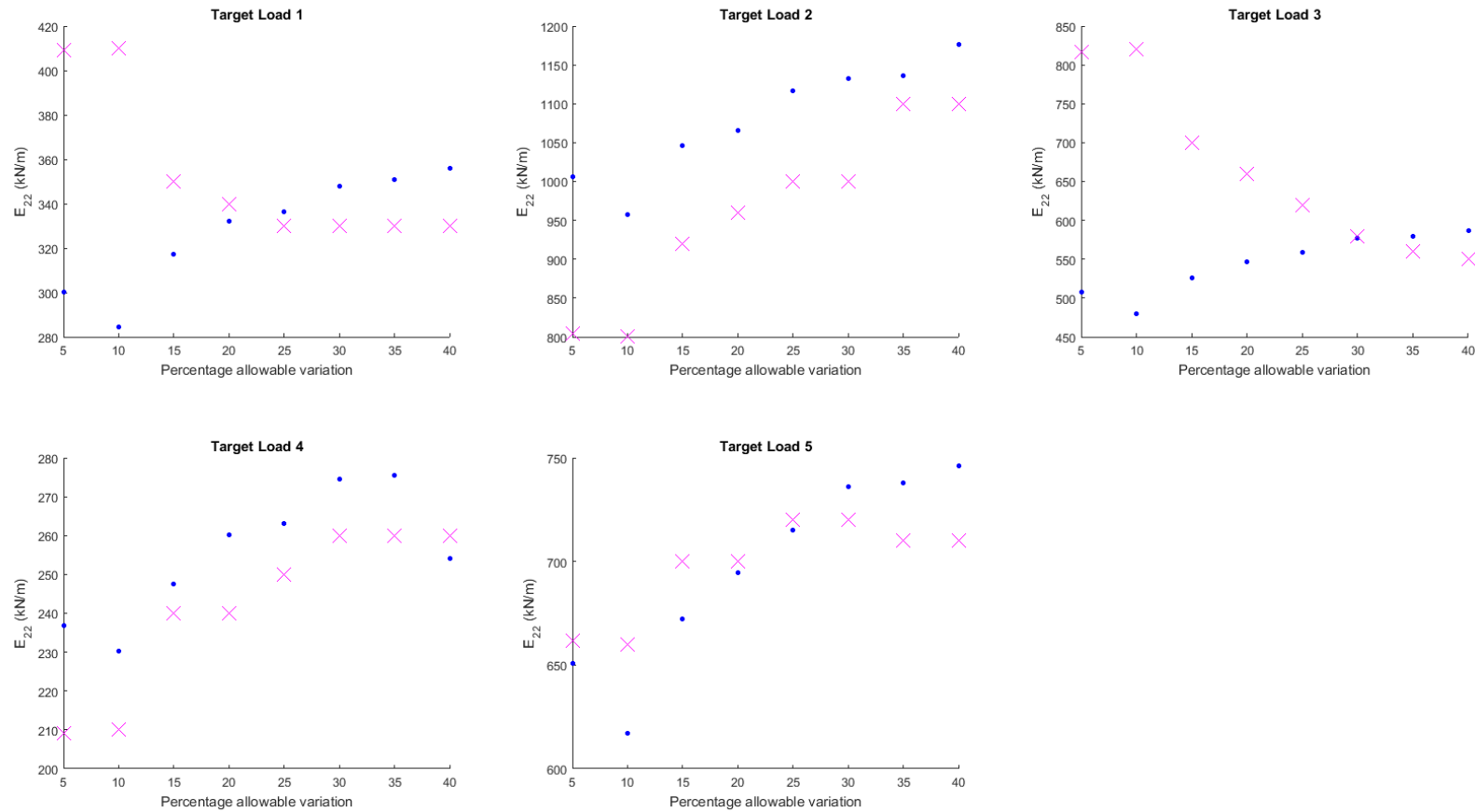


Figure 5-66: Target (X) and designed fabric (.) stiffnesses at increasing values of allowable variation from original targets

5. Model validation

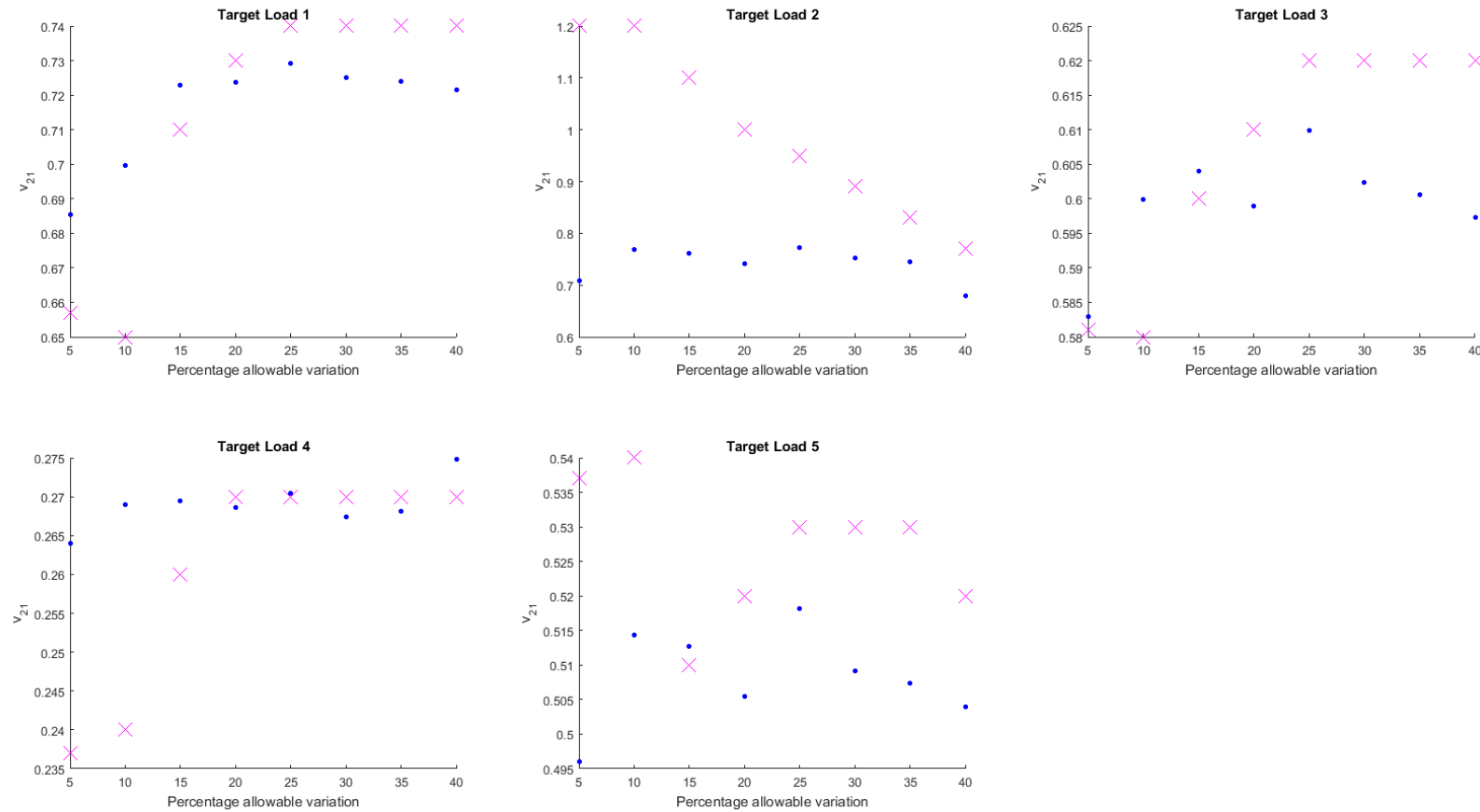


Figure 5-67: Target (X) and designed fabric (.) Poisson's ratios at increasing values of allowable variation from original targets

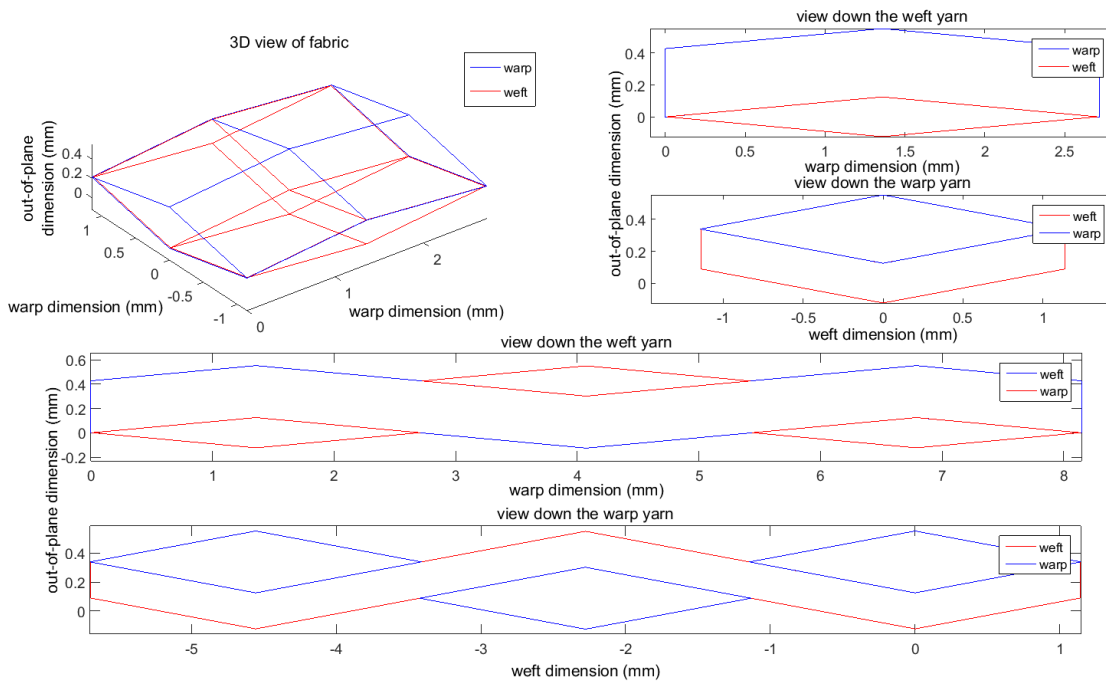


Figure 5-68: Geometry of the designed fabric (ATEX3000 targets)

Failure to reproduce the fabric geometry from which the targets were produced appears to be endemic with neither the 'zero variation' nor 'target variation allowed' optimisation routines reproducing the original fabric geometry. In some ways this might be expected as the original sawtooth model as produced by Bridgens and Gosling (2008) did not perfectly reproduce fabric stiffnesses. Probable reasons for this and discussion is made below (§5.3.4) however it should be noted that without any knowledge of the original fabric the model does achieve in two of the above optimisations (ATEX 3000, B18059) a possible fabric design. In this regard the model succeeds.

5.3.3. Reducing model constraint by reducing the number of targets:

It is possible to demonstrate that the model solves the optimisation problem in fewer steps and with less variation when fewer targets are specified for the fabric to be designed to. The fabric used in this section is a F1202 PVC coated polyester, from which targets were derived from biaxial test data as specified above (§5.2.2.2). Four, eight and twelve targets were all designed for.

Principally this demonstrates how additional targets further constrain the model, leading to a considerably more over constrained situation where further variation in targets has to be allowed for.

	Point 1	Point 2	Point 3	Point 4	Point 5
E_{11} (target 1) (kN/m)	944	413	1021	1151	801
E_{22} (target 3) (kN/m)	1049	947	979	877	883
v_{12} (target 2)	0.45	0.16	0.28	0.40	0.21
v_{21} (target 4)	0.58	0.90	0.23	0.05	0.39
P_1 (kN/m)	7	7	14	21	21
P_2 (kN/m)	7	21	14	7	21

Table 5-12: Targets for PVC coated polyester F1202 fabric

The test for four targets optimised to a result dissimilar to the original geometry after an allowable variation of just five percent (Figure 5-69). However, a solution was found that appears to be considerably more feasible (visually) than those found earlier (§5.3.2).

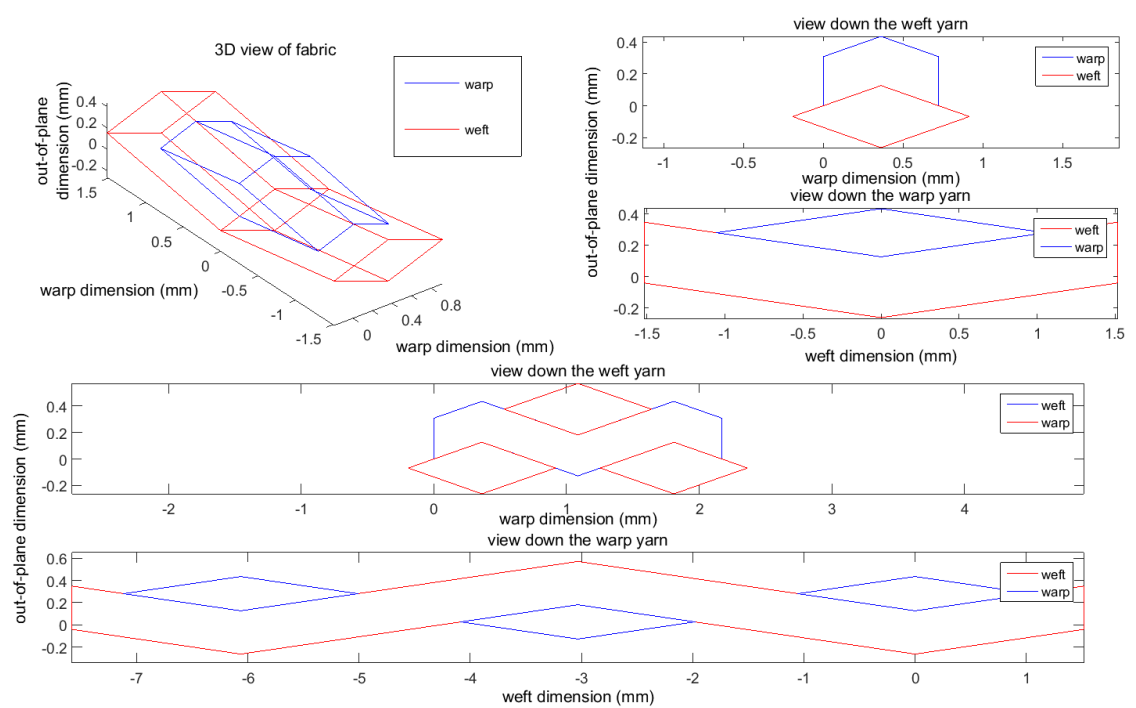


Figure 5-69: Designed Geometry for four targets (F1202)

5. Model validation

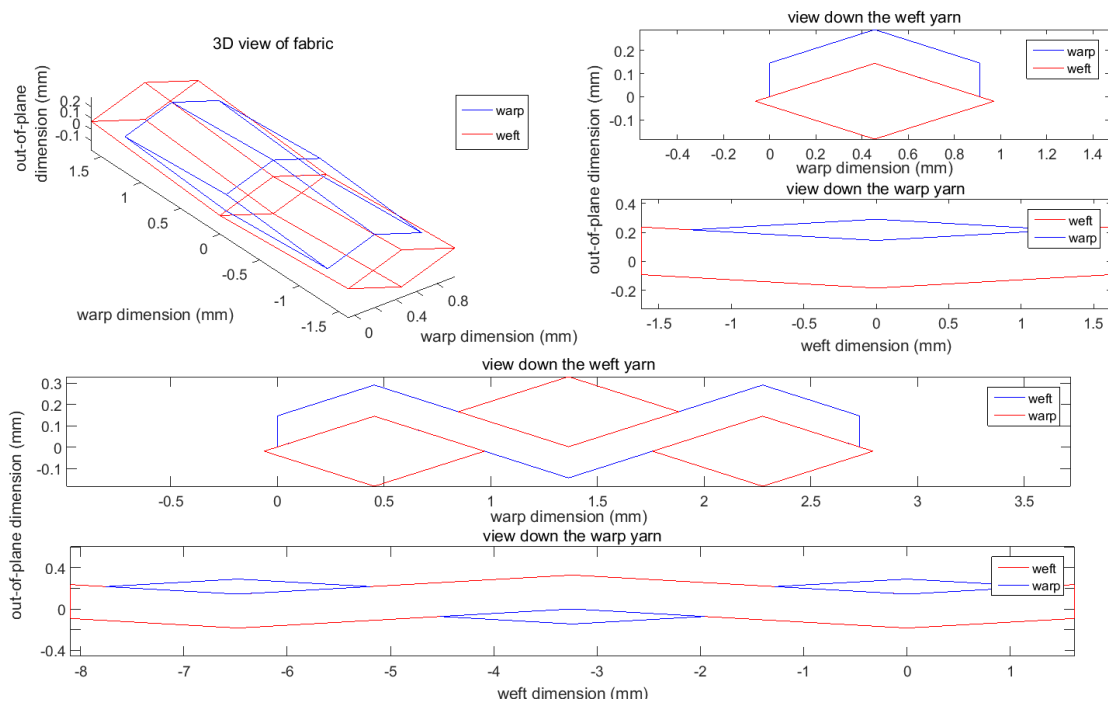


Figure 5-70: Designed Geometry for eight targets (F1202)

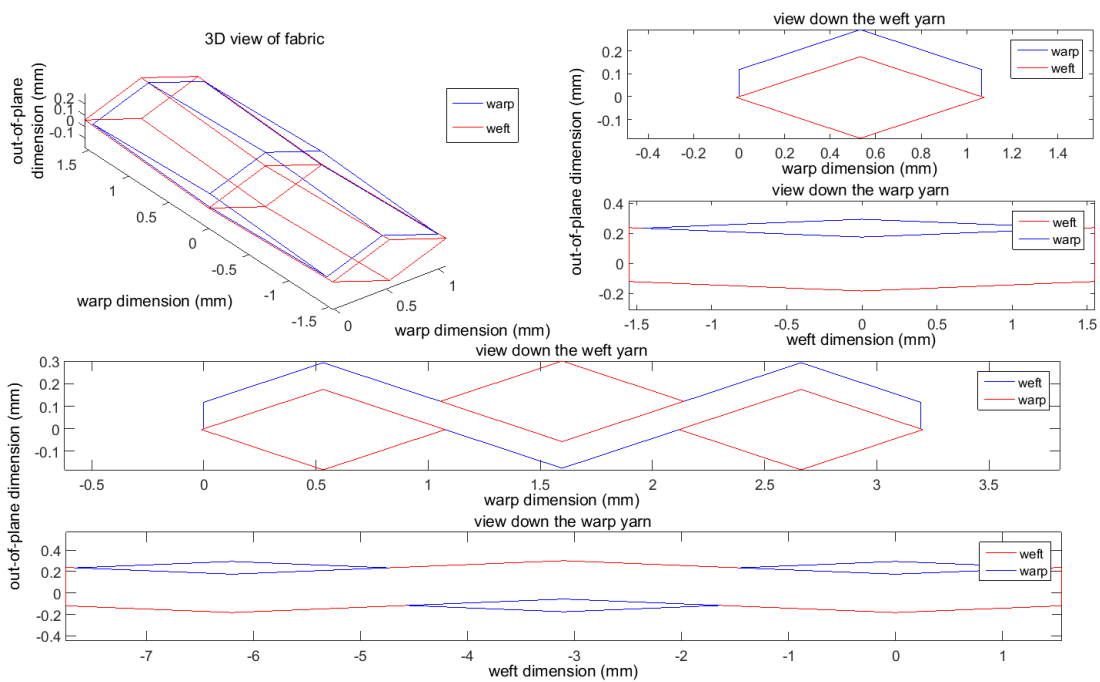


Figure 5-71: Designed Geometry for twelve targets (F1202)

Whilst both the optimisation for eight and twelve targets resulted in a designed fabric after an allowable variation of 25% none of the designed fabrics represented the original fabric from which the targets were measured. Notably the fabric's geometry becomes less (visually) realistic as more targets are included, and in this case this may be in part

due to the very low value of warp stiffness required for the second set of targets deforming the results. As the design becomes more over constrained it appears that the results deviate further from feasible designs, a possible further limiting factor on the methodology.

5.3.4. Discussion of designed fabrics

It has been demonstrated that whilst the model will accurately design a fabric that is known to be feasible, i.e. the targets were produced from the sawtooth model using a central finite difference method, it will fail to reproduce the geometry of a fabric using the targets generated from biaxial testing of that fabric. A number of reasons for this are discussed below:

Firstly the original sawtooth model did not perfectly predict the response of a fabric under biaxial loads (Figure 5-72). The sawtooth model provides a reasonable prediction of fabric behaviour with the model's deviation from the mean of the strain range of a real fabric being between 5.3 and 5.9% (Bridgens and Gosling, 2008) (Figure 5-72). This presents a problem, namely that the fabric that is designed when targets are taken from the biaxial data would not be represented perfectly by the sawtooth model. Whereas upon visual inspection the surfaces in Figure 5-72 appear similar, and the response appears to be adequately modelled the fabric design model is, in essence, attempting to design a fabric that may not exist within any possible sawtooth response region. As such the model deviates from the original targets attempting to find a solution in the spectrum available to the sawtooth response, within the constraints presented by the user.

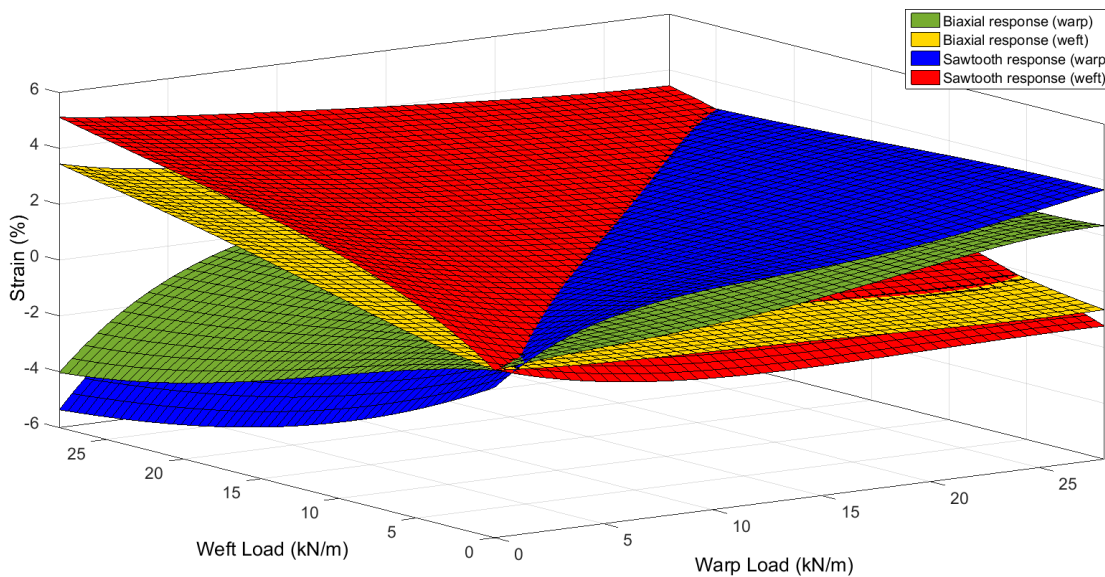


Figure 5-72: Response surfaces for the sawtooth model and measured response for one geometry (F1202)

Following this it is apparent that the model is over constrained at large numbers of targets as the targets must vary to allow for a solution to be found. The model is over constrained in two ways, firstly the number of targets prohibits the movement of the response planes. This is in contrast to, say, where only one target exists the response plane will perfectly satisfy the target. And the second source of constraint is the model parameters, namely that the fabric must be flat ($A_1 + A_2 = r_1 + r_2$) and the constraints on the yarn width and loads. These must be maintained for the model to work, but constrain the solution. The final form of constraint is on the model parameters. These are greater than the value of the maximum and minimum values exhibited in testing, but this does limit the solution.

Whilst the model may be over constrained it has been demonstrated that more than one solution has been found for feasible targets generated from the sawtooth model. It is therefore likely that the problems exist in the creation of targets from real fabrics that are not truly represented by the sawtooth model.

To attempt to define this the following hypothesis is made; that a unique solution that is not perfectly represented by a model cannot be found by the inverse of that model:

The principle is that that a predictive model, when set to model a response, may not perfectly reproduce that original behaviour, but may adequately reproduce it to some tolerance. In this situation the model has knowledge of the original properties of the system it is modelling. And as such approximately reproduces the behaviour.

However, if the inverse of the model is taken, and used to attempt to reproduce the original situation that the predictive model was representing it cannot achieve a perfect result because the model never perfectly represented the original behaviour. As such the inverse model, if allowed, will attempt to find a solution in the 'space' of possible solutions that it can interrogate. Therefore the inverse model will find the best fit to the targets within the space the predictive model considers, and this may look nothing like the original geometry, but satisfy the targets and constraints placed on the model.

For instance, as above, the sawtooth model reproduces the response of the fabric to an adequate degree, however, when the inverse model is used it fails to reproduce the original fabric. This is because the inverse model is attempting to find a solution to the problem in the 'space' of results available to the sawtooth model, in which the original targets may never have existed, and certainly didn't exist for that geometry.

This problem may be specific to predictive models of this level of complexity, given that non-predictive models use factors to increase the accuracy of the original model. As such factors might 'direct' the model to a solution. Less complex models might have fewer variables to begin with, or simply be more accurate, leading to more readily obtained targets.

5.3.5. Robust fabric design

In this section an existing fabric is redesigned to improve its robustness to changes in its constituent geometry. This aims to demonstrate the feasibility of applying the robust design methodology to real, existing fabrics. If applicable this would allow small changes to fabrics currently in use to be made in order to improve their robustness. The method differs from that used earlier (§4.10) in that the original geometry used is measured from an F702 fabric. The new, robustly designed, F702 fabric cannot be tested to demonstrate its robustness characteristics as producing a bespoke fabric is beyond the scope of this project. The fabric is not being redesigned as has been carried out in section

5.3.2. However, it is being altered slightly (up to one standard deviation) from its existing geometry.

Two targets (E_{11} and E_{22}) are used to demonstrate how the method can be applied. The fabric's geometric property variation and yarn and coating stiffness variation are defined from test results (Table 5-13).

	Mean value	Coefficient of variation
θ_1 (degrees)	0.102	0.108
θ_2 (degrees)	0.125	0.078
L_1 (mm)	0.624	0.019
L_2 (mm)	0.611	0.019
r_1 (mm)	0.079	0.033
r_2 (mm)	0.062	0.034
E_1 (kN/m)	444	0.021
E_2 (kN/m)	382	0.037
E_k (kN/m)	33	0.056

Table 5-13: Variation in geometry used in the robust optimisation of an F702 fabric

The results of the optimisation (the new robustly designed F702 fabric) are shown in Table 5-14 and the individual sensitivities are shown in Figure 5-74 and Figure 5-75. An improvement is made to the sum of the sensitivities from the original 108.9 to the optimised 102.6, an improvement of 5.8%. This improvement is significant. The geometry, due to the limit on the overall change that can be made to it, is similar to that of the original fabric. The new fabric also appears to be reproducible upon a visual inspection of Figure 5-73.

	Result
θ_1 (degrees)	0.098
θ_2 (degrees)	0.135
L_1 (mm)	0.630
L_2 (mm)	0.606
r_1 (mm)	0.080
r_2 (mm)	0.065
E_1 (kN/m)	438
E_2 (kN/m)	392
E_k (kN/m)	33.6

Table 5-14: F702 robustly optimised geometry

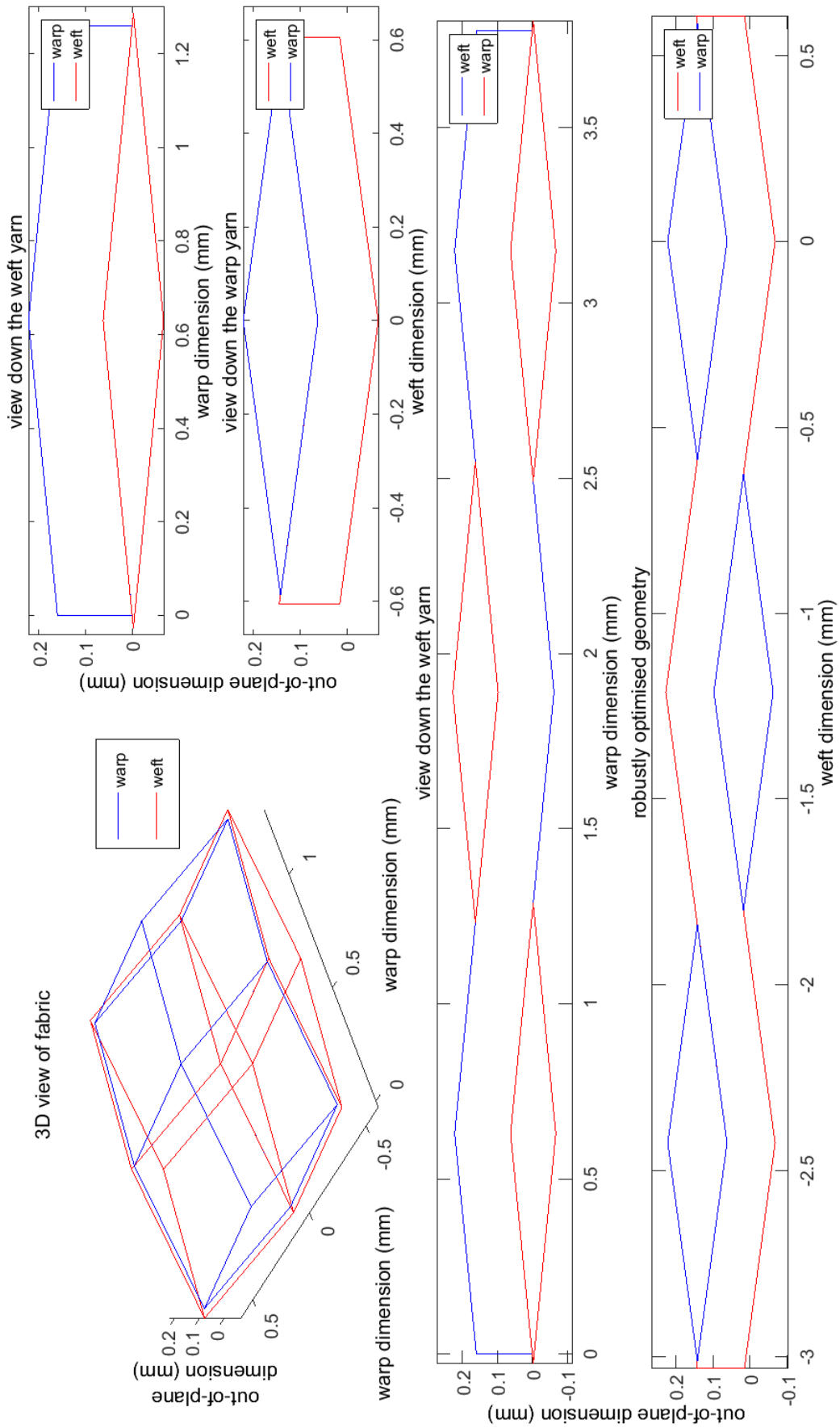


Figure 5-73: Geometry of the robustly optimised F702 fabric

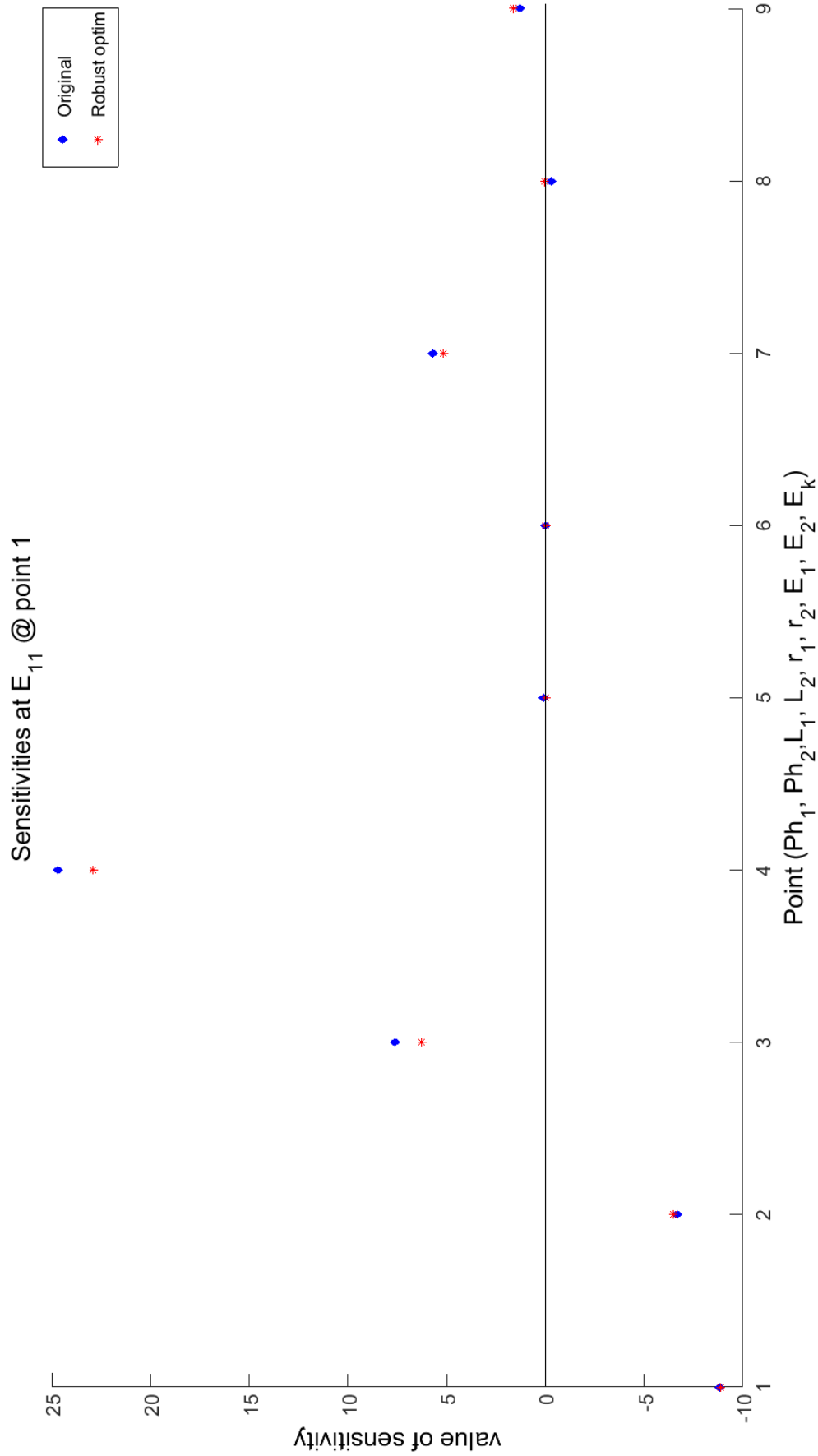


Figure 5-74: Comparison of original F702 and robustly optimised fabric sensitivities to E_{11}

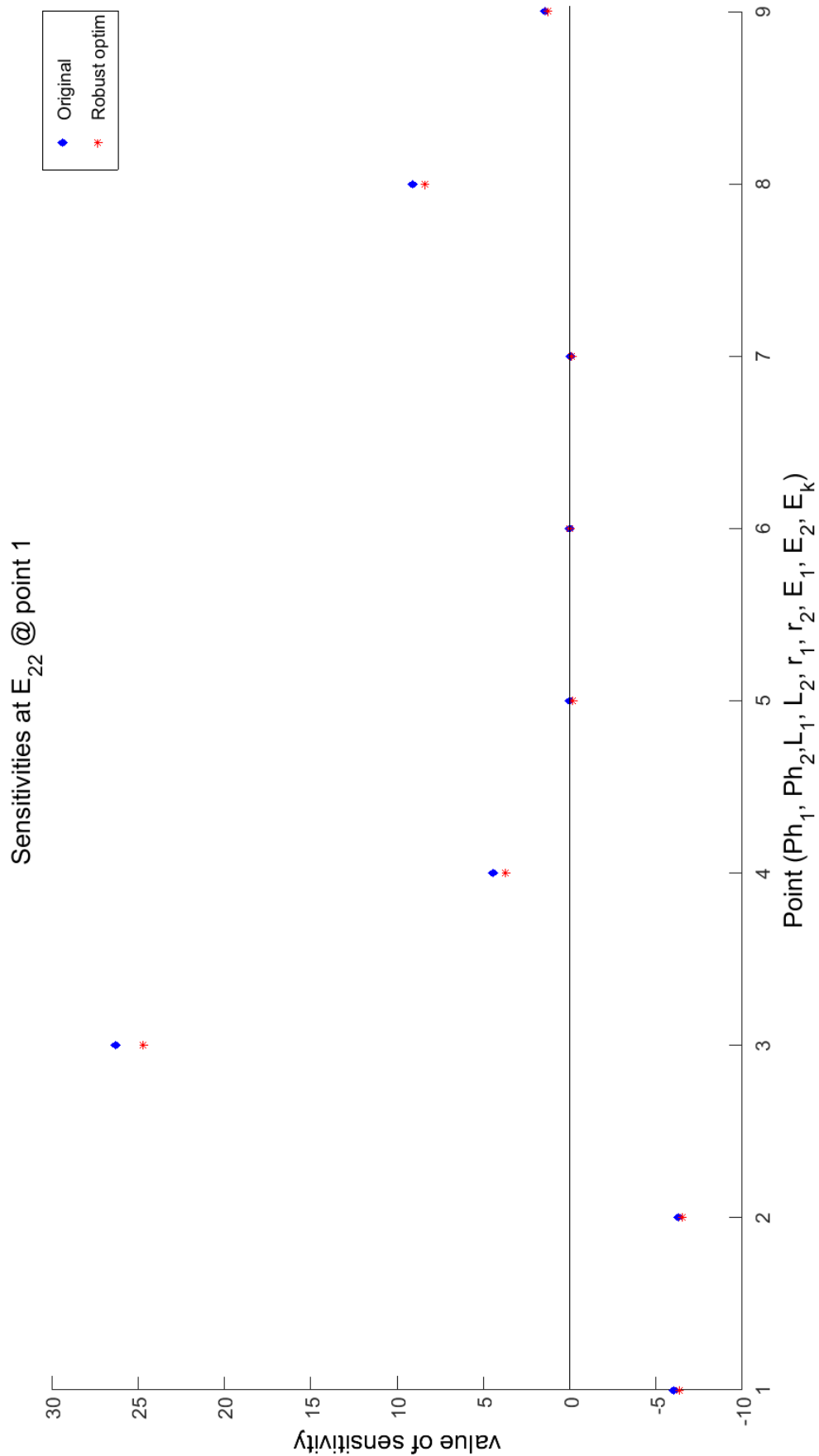


Figure 5-75: Comparison of original F702 and robustly optimised fabric sensitivities to E_{22}

A number of the geometric properties have become more sensitive to variation, however, as was shown in the previous chapter (§4.10), small increases in the susceptibility of the stiffness to one geometric property can mean that the overall sensitivity of the fabric to such variabilities is reduced.

5.3.5.1. Discussion

The suggested geometry cannot be tested to check that the reduction in sensitivity described is actually achieved. It is evident that small changes to the geometry of a fabric can reduce the sensitivity of that fabric to variation in those properties. It is also evident that this can be achieved by increasing the sensitivity of the fabric to some parts of its geometry, whilst the overall effect is to reduce the overall sensitivity of the fabric to variation in its geometry. Information such as this may serve to allow for small improvements to the robustness of fabrics currently in production whilst maintaining their overall appearance and response. This could be a cost effective way to improve a fabric without resorting to long term expensive testing of multiple samples.

Further work will need to be carried out on this method prior to its use in this field however.

6. Conclusions and Recommendations for future work

6.1. Research Summary

This research has been primarily concerned with the creation of a methodology for the design of bespoke architectural fabrics for particular loading conditions. A model has been produced that is capable of designing a fabric for specific values of Young's modulus, Poisson's ratio and shear modulus. This necessitates the specification of the loads at which the target values are required, and in the case of the shear stiffness the angle to which the fabric will deform (§3.4.3). These have then been implemented alongside a variability analysis to show how a fabric can be designed for not only mechanical properties but also reliability characteristics (§4.10).

The literature review (§2.3) identified a number of models that might have been used as the basis of an inverse model, but most of these were not used as the basis of the inverse methodology due to their representative nature, the unquantified accuracy of the model, or the lack of any coating consideration. The sawtooth model as previously developed by Bridgens and Gosling (2008) was selected as the basis of the inverse modelling process as it fit most closely to the stipulated requirements: It is predictive, includes a consideration of coating, and is made up of equations that can be differentiated. Most startling, and notable by absence, is the lack of any previous work on the design of architectural fabrics using numerical methods other than those discussed by Behera and Muttagi (2002) and Bartle *et al.* (2013) which focus on the use of neural networks. This is an oversight this report has aimed to resolve.

6.2. Conclusions

The aim of this research was to develop a predictive inverse material model for coated woven fabrics that was robust with respect to variability in material properties and could be used to design bespoke architectural fabrics with specific properties at different loading conditions. This has been achieved with the creation of the inverse sawtooth method (§3.4.3) for which a design methodology is developed which utilises the model (§3.5.4) and the extension of this to incorporate robust design principles (§4.10). Each objective is reviewed below, with a summary of the conclusions that have been drawn from the relevant chapters.

To complete a full and in depth review of the state of the art of fabric modelling, design and analysis:

The literature review identified the most relevant fabric type (plain-weave), which has been the focus of this report, and the various components of a fabric composite were identified. A yarn level unit cell model was chosen which was shown to give accurate prediction of fabric stress-strain behaviour without the incorporation of the complex detail required for fibre and filament modelling (§2.3.2.3). The sawtooth model was chosen as the basis of the inverse model (§2.3.2.4) due its predictive nature and the published accuracy of the model (Bridgens and Gosling, 2008, p. 13). In addition the model included a method for the inclusion of coating properties, unlike a number of reviewed models.

Formulate an inverse material model:

The inverse material model was successfully formulated (§3.4.3.2), and demonstrated how the mechanical properties of a fabric can be calculated from the initial geometry and loaded state of the fabric (§3.7.1). However a full and complete analytical model was found to be unobtainable, meaning that the model retained a numerical component (§3.4.3.2). The lack of completely analytical derivatives increases the complexity of the model programme, and leads to considerable additional computing power being required when a solution to the derived equations is calculated; up to four hours is needed to run a fabric design. Further, calculating gradients slows the robust design methodology such that only two mechanical properties can reasonably be robustly optimised simultaneously (§4.10).

6. Conclusions and recommendations

The derived equations were initially compared to targets derived from a central finite difference method using the sawtooth model from which they were formulated (§3.7.1). This ensured that the fabric design methodology was initially attempting to design a feasible fabric, i.e. one that could be modelled accurately with the sawtooth model. The results of this were encouraging with the model finding solutions to fabric design problems (§3.7.1). At this stage it also became apparent that for any individual set of targets more than one possible fabric geometry might be applicable as a solution. This was further confirmed using a Monte Carlo analysis to show that for one target, considering only two variables, a plane of possible solutions can be identified (§4.7.3).

It has been reasoned that for an increasing number of targets the number of possible solutions will decrease as the model becomes more constrained, while conversely for a small number of targets the model will find a solution from a large number of possible solutions (§5.3.4). The over constraint of the model becomes considerably more apparent when real targets are designed for (§5.3.2). Where no solution could be found the design method was programmed such that a relaxation in the required accuracy of the solver might allow a less than optimal solution to be found (§3.5.4.1).

Incorporate variability of material parameters into the model and assess sensitivity of the resultant design:

FORM (§4.8) and Monte Carlo (§4.7) methods were used to analyse how a fabric's mechanical properties respond to variability, whilst a sensitivity analysis was incorporated into the design methodology (§4.10). The analysis of particular components of the unit cell and how the sensitivity of the overall composite is affected by variance in unit cell properties enabled the creation of a robust design methodology (§4.10). The individual geometric properties of the fabric were shown to affect the fabric's mechanical responses to differing degrees, and for the first time the effect these properties have on fabric response can be accurately quantified at any stress state for geometry (§4.10).

The robust design methodology demonstrates how, for the first time, it is possible to minimise the sum total of the sensitivities of a fabric's mechanical properties to variation in individual unit cell properties. Whilst the methods employed do not show exact correlation to each other they demonstrate how individual property sensitivities can be

reduced (or increased) whilst reducing the overall sensitivity of a fabric, producing a more robust fabric design (§4.10). This can be used as a cheap alternative to extensive testing when initially trying to design a robust fabric.

Complete a validation study:

A methodology for the ravelling and testing of individual yarns was developed to enable the calculation of individual yarn stiffnesses from which statistical data regarding yarn stiffnesses can be obtained (§5.2.3). A method to calculate plane stress constants at discrete points on a fabric's biaxial stress-stress-strain response surface was also devised to enable multiple targets to be found at separate stress states (§5.2.2.2). With relation to this the cause of the stress minimisation method's inability to accurately describe fabric plane stress constants for some fabrics was also identified (§5.2.2.2). Where the strains experienced by a fabric are small $\det(\mathbf{M})$ approaches zero, and as such \mathbf{M} becomes singular, meaning that the inverse of \mathbf{M} is ill-conditioned.

The validation studies demonstrate that the inverse sawtooth method for the design of fabrics, whilst accurate when compared to material models, is unusable with regards to the design of real fabrics (§5.3.2). The reason for this becomes apparent when the methodology is considered: The fabric design method is excellent at designing a 'sawtooth fabric'. This means that the method can perfectly design any fabric that exists in the 'space' that the sawtooth model represents. However, the sawtooth model does not perfectly represent the response of real fabrics (though it does it well) (Bridgens and Gosling, 2008). The result of this is that the inaccuracy inherent in the predictive model is translated to the design of the fabric. Or, to put it succinctly, the design methodology is not actually designing a real fabric, but something very close. Therefore given the complex nonlinear interactions that govern fabric response the result of the design is visually considerably different to the fabric from which the biaxial test results used as targets were obtained (§5.3.4).

In hindsight a considerably more accurate model may be necessary in future to adequately allow for the prediction of real fabric response. Alternatively the equations derived in this thesis (§3.4.3.2) could be used to produce fabric response surfaces, or as part of neural network optimisations, possibly within the 'knowledge base' described by (Behera and Muttagi, 2002, p. 318) (§2.1.2).

6. Conclusions and recommendations

Whilst the inability of the model to reproduce real fabrics detracts from its utility it is hoped that future work might result in a solution to this being found (§6.3).

To attempt a structural design study using an FE simulation of a true structural design case:

A structural design study using FE simulation will be necessary to demonstrate the applicability of the methodologies developed. However, whilst a structural design study was considered, the limitations of current finite element modelling software, which can only utilise a single set of fabric properties (i.e. one set of plane stress constants) meant that it was found to be unfeasible at this time (§1.3). Using separate FE simulations with differing values of elastic constants was considered, but abandoned because the deformation of the fabric prior to it reaching the load at which the constants become relevant would be incorrect. This will be an important part of any future work if software capable of carrying it out is available (§6.3).

6.3. Recommendations for future work

Inclusion of a yarn model

The accuracy of the model might be improved by the inclusion of a constitutive yarn model to replace the assumption of linear elastic yarn response, which has been shown to only be the case for glass-fibre yarns (§2.2, 5.2.3.4). This would also enable the designer to select particular yarn geometry and materials that could then be analysed for response characteristics. The model developed by Madhavan and Naik (2000) might form the basis of such a component. In addition the tear strength of fabrics might be analysed in an integrated fashion by considering the tear strength of the yarns that make up the fabric (Nurwaha and Wang, 2011).

Sinusoidal model

At the inception of this work it was initially hoped that a sinusoidal model might provide the basis of the governing equations discussed in detail in the previous chapters (§3.4). However, sinusoidal models available at the time were not presented in an appropriate manner, nor had been shown to be accurate enough to be used in the presented work (Wang, 2002; Bridgens and Gosling, 2008). Since that time the work by Colman (2014) has produced a more complex and accurate model that might form the basis for a considerable improvement to the presented work.

The inclusion of a geometry that is closer to that of real fabrics presents the possibility of a more natural design process. The use of a more accurate model should remove (in part) some of the inherent inaccuracy that became apparent in the presented model when biaxial test data was considered. As the ground work governing how the defining equations might be produced has been covered in detail in this thesis (§3.4) the implementation of the sinusoidal model into this methodology should be a simpler process.

Powerful computing

More powerful computing will be needed if the method presented is to become any more complex than that presented in this report. Already the sensitivity calculation requires considerable computing time (up to eight hours) due to the high number of variables considered (§4.10). If this were to increase due to the inclusion of a yarn

material model then the computing power of a standard desktop computer may not be adequate for the task, and networked servers may be necessary.

Non-rectangular Geometry

Non-rectangular geometry has been eluded to in this report when the isoparametric finite element was introduced (§3.4.3.3). However, no detailed consideration of non-perpendicular unit cell geometry has been made in this thesis. This, and its effect on the shear properties of a fabric are necessary in future work.

Non-plain weave fabrics

It should be possible to extend the model to non-plane weave geometries by using formulae that define these geometries as the base for the derivatives calculated rather than the sawtooth model. The application of other material geometries to the method should enable the use of the inverse model in different industrial sectors, such as clothing or sail design, and possibly in the design of rigid composites such as wind turbine blades (Sørensen, 2009). The latter might require significant alteration to the presented model. Solid rigid composites, for instance, will undoubtedly have to take account of out-of-plane deformations which this model makes no reference to, and include higher stresses, with lower strains (§2.6.1).

Improvement to the shear model

Improvements to the shear model would enable more accurate modelling of fabric shear response, and allow some uncoupling between shear stiffness and the coating stiffness. At this time the coating dominates the shear response (§3.7.2), and this limits the applicability of the model to the design of fabrics for shear stiffness to the selection of a coating which will in turn decide the shear stiffness of the fabric. Future work like that carried out by Liu *et al.* (2004) will hopefully allow for improvements in this area to be made.

Use in a finite element program

Incorporation of the design methodology into a finite element model will enable the design of a fabric for conditions required by a structural engineer (§5.4). For instance, where an engineer might currently require a certain deflected shape, and have to choose a fabric from those available from manufacturers, the program can offer

suggestions as to the necessary geometry. Alternatively the program may design a fabric that would perform as required within the finite element model.

Structural design case study

A structural design study using a working and operational methodology would be able to demonstrate the applicability of future fabric models to use in the design environment (§5.4). This would have to incorporate a finite element modelling program that was able to consider multiple stiffnesses, or include the response surfaces that can be produced using the sawtooth model. This could then be used to show how a designed fabric could be utilised in construction to maximise crimp interchange at low (installation) loads, but provide the correct response at higher loads, as suggested for a conic structure (§1.3).

7. Glossary

All glossary entries refer to the TensiNet European Design Guide for Tensile Surface Structures (Forster, Mollart, et al, 2004), the Oxford English Dictionary, (Oxford_University_Press, 2004), or the ASTM standard terminology documents (ASTM, 2012; ASTM, 2013).

Anticlastic

An Anticlastic surface has Gaussian Curvature less than zero. Locally, Anticlastic surfaces are Saddle shaped. Most Boundary Tensioned Membrane Structures are composed of Anticlastic surfaces.

ASTM

American Society for Testing and Materials.

Biaxial

In the context of Lightweight Structures the term Biaxial is typically used in connection with the elastic behaviour of the Membrane surfaces. Biaxial Membrane stresses are measured using biaxial material tests. In some cases uniaxial tests are also performed.

Boundary

The terms Boundary and Border are synonymously used to refer to both the complete Boundaries of Tensile surface structural Components, as well as the individual Boundary sections.

BSI

British Standards Institute.

Cable Net

Surface Structures composed of netting fabricated from Cables. Cable Nets are classified as being either regular or irregular depending on their mesh geometry. Early Cable Net structures were usually regular and often waterproofed by cladding with semi-rigid materials. Currently Cable Nets are typically used for zoo aviaries as well as the reinforcement of Pneumatic Cushions.

Cable

A flexible Tensile Component.

Catenary

The pure geometrically defined shape of a Cable or chain hanging under self-weight only. Sometimes the expression is, loosely, used to describe any flexible Boundary or Funicular shape.

CRE

Continuous Rate of Extension – normally relating to a tensile testing machine.

Creep

Slow deformation when a fabric is stressed resulting in semi-permanent deformation.

Crimp

The bending of the yarns in a Textile. Weft yarns typically have higher levels of Crimp compared to the Warp.

Dimensional Stability

The maintenance of a fabric's pattern and weave structure.

Double Curvature

A surface with Gaussian Curvature not equal to zero has Double Curvature.

Dynamic Relaxation

Popular method used for the Form finding, Load Analysis and Cutting Pattern Generation of Lightweight Structures.

Fabric

In textiles, a planar structure consisting of yarns or fibres.

Fill

American name for the weft of a textile.

Finite Element

A numerical solution method for problems (Cook *et al.*, 2002) which discretises these into solvable elements.

Foil

Strictly the term Foil refers to a metallic membrane. However, it is now the most commonly used term for all Isotropic structural Membranes including the popular ETFE Films.

Form finding

The process of determining the Force-Equilibrant Prestress shape.

Gaussian Curvature

The Gaussian Curvature K of a surface is equal to the product of the two principal curvatures k_1 and k_2 , $K = k_1 \cdot k_2$.

Hydrophobic

Repels or is repelled by water.

Isotropic

A material whose mechanical properties are similar in all directions is termed Isotropic. Conversely if the material's mechanical properties vary with respect to loading orientation, it is termed **Anisotropic**. The Coated Textiles typically used for architectural Membrane Structures are strongly elastically Anisotropic, while ETFE Foils are nearly Isotropic.

Linear density

The measure of the mass of yarn per unit length.

Melt spinning

A method of rapid solidification of liquids (i.e. glass) using a cooled spinning drum or wheel.

Membrane

A Surface Structure with no bending resistance and thereby capable of resisting only tensile forces.

Mesh

Expression used during the Computational Modelling of structures to describe the connected collection of Finite Elements

representing the surfaces and other structural Components.

MSAJ

Membrane Structures Association of Japan.

Orthotropic

A material is Orthotropic if it is Anisotropic with the axes of Anisotropy oriented normally. The woven Textiles typically used for Textile architecture have Orthotropic Anisotropy.

Ply Yarn

A yarn made up of more than one yarn spun together.

Poisson's ratio

Material constant relating the elastic behaviour between orthogonal directions. Sometimes used to model the Crimp interchange behaviour of Coated Textile.

Prestress

The Stress carried by a structure when subject to no externally applied loading.

Prestress Ratio

The ratio between the Prestress levels in the Warp and Weft directions of a Textile Structure. More generally, the ratio between the principal Prestress values of a Membrane Structure.

PTFE

A synthetic polymer:
Polytetrafluoroethylene

PVC

A synthetic polymer: Polyvinyl chloride

Ravel

To remove a yarn from a fabric.

Soap Film

Physical Modelling technique used to determine Constant Stress forms by exploiting the energy minimising behaviour of soap films.

Stiffness

In general engineering, the material constant used to represent Stiffness is Young's Modulus E . E is defined as the ratio between the Stress and Strain of an elastically linear material. Due to the complex microstructure of the Coated Textile and rope materials typically used for Tensile Architecture, Stiffness

is more usually measured and specified together with the cross sectional area.

The combination of the material Stiffness constant E with the area A is referred to as the EA Value. In the case of Textile, EA values are specified for a unit width.

Strain

Ratio of the extension under load of a structural member to the unstressed length.

Stress

The usual engineering definition for Stress is force per unit area. Due to the complex non-uniform nature of the Coated Textile materials used for tensile architecture, Textile Stresses are usually expressed as force per unit width.

Tenacity

The measure of the strength of a fibre or yarn.

tex

Measure of linear density, (1 tex = 1 g/km).

Textile

Fabric material usually woven from orthotropic oriented yarns.

8. References

- Aernouts, J., Couckuyt, I., Crombecq, K. and Dirckx, J.J.J. (2010) 'Elastic characterization of membranes with a complex shape using point indentation measurements and inverse modelling', *International Journal of Engineering Science*, 48(6), pp. 599-611.
- Alagirusamy, R. and Das, A. (2010) *Technical textile yarns industrial and medical applications*. Boca Raton, Oxford: CRC Press; Woodhead Pub.
- Arain, F.A., Tanwari, A., Hussain, T. and Malik, Z.A. (2012) 'Multiple response optimization of rotor yarn for strength, unevenness, hairiness and imperfections', *Fibers and Polymers*, 13(1), pp. 118-122.
- ASTM (2007) D2591 – 07 (Reapproved 2013) - Standard Test Method for Linear Density of Elastomeric Yarns (Short Length Specimens).
- ASTM (2010) D2256.618817-1-Standard Test Method for Tensile Properties of Yarns by the Single-Strand Method.
- ASTM (2012) D3883–04 (Reapproved 2012) Standard Test Method for Yarn Crimp and Yarn Take-up in Woven Fabrics.
- ASTM (2012) 'D3775–12-Standard Test Method for Warp (End) and Filling (Pick) Count of Woven Fabrics'.
- ASTM (2013) D123 – 13a - Standard Terminology Relating to Textiles.
- ASTM (2013a) D123 – 13a - Standard Terminology Relating to Textiles.
- ASTM (2013b) D4849 – 13 - Standard Terminology Related to Yarns and Fibers.
- ASTM (2014) ASTM International. Available at: <http://www.astm.org/> (Accessed: 14/07/2014).
- Atex (2013a) ATEX3000 TRL Technical specifications.
- Atex (2013b) ATEX5000 TRL Technical specifications.
- Ayyub, B.M. and McCuen, R.H. (1997) *Probability, statistics, & reliability for engineers*. Boca Raton: CRC Press.
- AZO Materials (2014) *Silicone Rubber Properties [Data sheet]*. Available at: <http://www.azom.com/properties.aspx?ArticleID=920> (Accessed: 07/10/2014).

- Badel, P., Vidal-Sallé, E. and Boisse, P. (2007) 'Computational determination of in-plane shear mechanical behaviour of textile composite reinforcements', *Computational Materials Science*, 40(4), pp. 439-448.
- Bartle, N., Gosling, P.D. and Bridgens, B.N. (2013) 'A neural network material model for the analysis of fabric structures', Paper presented at the TensiNet Symposium: [Re]Thinking lightweight structures. Istanbul, Turkey.
- Behera, B.K. and Muttagi, S.B. (2002) 'Engineering design of woven fabrics - A recent approach', *Indian Journal of Fibre & Textile Research*, 27(3), pp. 315-322.
- Beyer, H.-G. and Sendhoff, B. (2007) 'Robust Optimization - A comprehensive survey', *Computer methods in applied mechanics and engineering*, 196, p. 28.
- Bigaud, D. and Hamelin, P. (1997) 'Mechanical properties prediction of textile-reinforced composite materials using a multiscale energetic approach', *Composite Structures*, 38(1-4), pp. 361-371.
- Blum, R. and Bögner, H. (2002) 'Evaluation Method for the Elastic Moduli', *Tensinews*, 3(3), p. 3, Tensinet [Online] (Accessed: 2013).
- Bogdanovich, A.E. (2008) 'Recent Advances in Textile Composites - Proceedings of the 9th International Conference on Textile Composites _TOPIC VI 3D TEXTILE COMPOSITES_ MECHANICAL BEHAVIOUR'.
- Boisse, P., Gasser, A., Hagege, B. and Billoet, J.-L. (2005a) 'Analysis of the mechanical behavior of woven fibrous material using virtual tests at the unit cell level', *Journal of Materials Science*, 40(22), pp. 5955-5962.
- Boisse, P., Long, A.C. and Robitaille, F. (2005b) 'Design and manufacture of textile composites - Chapter 2', in Long, A.C. (ed.) *Design and manufacture of textile composites*. Boca Raton, FL Cambridge: CRC Press ; Woodhead, pp. 62 - 110.
- Box, G.E.P. and Muller, M.E. (1958) 'A Note on the Generation of Random Normal Deviates', pp. 610-611.
- Bridgens, B., Gosling, P., Patterson, C., Rawson, S. and Hove, N. (2009) 'Importance of material properties in fabric structure design and analysis', *Proceedings of the International Association for Shell and Spatial Structures (IASS) Symposium 2009*.
- Bridgens, B.N. (2005) *Architectural fabric properties: determination, representation & prediction*. University of Newcastle upon Tyne.

- Bridgens, B.N. and Gosling, P.D. (2004) 'Direct stress–strain representation for coated woven fabrics', *Computers & Structures*, 82(23-26), pp. 1913-1927.
- Bridgens, B.N. and Gosling, P.D. (2008) 'A predictive fabric model for membrane structure design', *Textile Composites and Inflatable Structures II*, (8), pp. 35-50.
- Bridgens, B.N., Gosling, P.D. and Birchall, M.J.S. (2004) 'Membrane material behaviour: concepts, practice & developments', *The Structural Engineer*, 82(14), pp. 28 -33.
- BSI (1971) BS 481: Part 1 : 71: BS 481 Specification for Industrial Wire Mesh. British Standards Institute: British Standards Institute.
- BSI (1982) BS 3424-5, 1982, Testing coated fabrics, Part 5, Determination of tear strength.
- BSI (1984) BS 2862: 1984: BS 2862: 1984. Methods for determination of number of threads per unit length. BSI.
- BSI (1996) BS 3424 Part 33 Method 36 - seam strength.
- BSI (1998) BS EN ISO 1421, 1998, Determination of tensile strength and elongation at break.
- BSI (1998a) BS EN 1875-3, 1998, Determination of tear strength - trapezoidal method.
- BSI (1998b) BS EN ISO 1421, 1998, Determination of tensile strength and elongation at break.
- BSI (2003) BS EN 13895_2003_Textiles_ Monofilaments_ Determination of tensile properties.
- BSI (2003) BS EN ISO 4674-1, 2003, Determination of tear resistance.
- BSI (2006) Eurocode — Basis of structural design. BSI.
- BSI (2007) Structural Eurocodes - Extracts from the structural Eurocodes for students of structural design. London: BSI.
- BSI (2014) British Standards Online. Available at: <https://bsol.bsigroup.com/> (Accessed: 14/07/2014).

- Buckenham, P. (1997) 'Bias-extension Measurements on Woven Fabrics', *Journal of the Textile Institute*, 88(1), pp. 33-40.
- Bulut, Y. and Sular, V. (2013) 'Manufacturing and sewing performance of polyurethane and polyurethane/silicone coated fabrics', *Materials and Manufacturing Processes*, 28(1), pp. 106-111.
- Campbell, F.C. (2010) *Structural Composite Materials*. ASM International.
- Champault, G., Polliand, C., Dufour, F., Zioli, M. and Behr, L. (2009) 'A "self-adhering" prosthesis for hernia repair: experimental study', *Hernia*, 13(1), pp. 49-52.
- Chen, Y., Lloyd, D.W. and Harlock, S.C. (1995) 'Mechanical Characteristics of Coated Fabrics', *Journal of the textile Institute*, 86(4), pp. 690-700.
- Chilton, J. and Velasco, R. (2005) 'Design and manufacture of textile composites - Chapter 12', in Long, A.C. (ed.) *Design and manufacture of textile composites*. Boca Raton, FL Cambridge: CRC Press; Woodhead, pp. 424 - 436.
- Colman, A. (2012) 'A pragmatic approach to determining the mechanical behaviour of structural fabrics'.
- Colman, A. (2013a) Fabric cross section images.
- Colman, A. (2013b) Uniaxial Response Data.
- Colman, A. (2014) Determination and prediction of the mechanical behaviour of architectural fabrics. Newcastle University.
- Colman, A.G., Bridgens, B.N., Gosling, P.D., Jou, G.T. and Hsu, X.Y. (2014) 'Shear behaviour of architectural fabrics subjected to biaxial tensile loads', *Composites Part A: Applied Science and Manufacturing*, 66, pp. 163-174.
- Concise Oxford English Dictionary (2004) Great Clarendon Street Oxford: Oxford Press.
- Cook, R.D., Malkus, D.S. and Plesha, M.E. (1989) *Concepts and applications of finite element analysis*. 3rd edn. New York: Wiley.
- Cook, R.D., Malkus, D.S., Plesha, M.E. and Witt, R.J. (2002) *Concepts and applications of finite element analysis*. 4th edn. Wiley.

- Croft, T., Davison, R. and Hargreaves, M. (2001) Engineering mathematics: a foundation for electronic, electrical, communications, and systems engineers. 3rd edn. Harlow, England; New York: Prentice Hall.
- Day, A.S. (1986) 'Stress strain Equations for non-linear behaviour of coated woven fabrics', Shells, Membranes and Space Frames, Proceedings IASS Symposium, Osaka, 1986, 2.
- Dimitrov, N. and Schock, H.J. (1986) 'Study on the Load-Extension Behavior of Coated Fabrics with special reference to PTFE-Coated Glass-Fibre Fabric, Using the Meffert Model'.
- Durville, D. (2010) 'Simulation of the mechanical behaviour of woven fabrics at the scale of fibers', International Journal of Material Forming, 3(2), pp. 1241-1251.
- Erfani, T. and Utyuzhnikov, S.V. (2012) 'Control of robust design in multiobjective optimization under uncertainties', Struct Multidisc Optim, 45, pp. 247-256.
- Farboodmanesh, S., Chen, J., Mead, J.I., White, K.D., Yesilalan, H.E., Laoulache, R. and Warner, S.B. (2005) 'Effect of Coating Thickness and Penetration on Shear Behavior of Coated Fabrics', Journal of Elastomers and Plastics, 37(3), pp. 197-227.
- Faurholdt, T.G. (2000) 'Inverse modelling of constitutive parameters for elastoplastic problems', The Journal of Strain Analysis for Engineering Design, 35(6), pp. 471-478.
- Federation, S.T. (2014) Swiss Textile Federation members list. Available at: http://www.swisstextiles.ch/cms/front_content.php?idcat=1&idart=1&lang=2.
- Ferrari (2013a) Precontraint 702T2 Technical specifications.
- Ferrari (2013b) Precontraint 1002S, 1202S, 1302S, 1502S Technical specifications.
- Ferrari (2013c) Precontraint 1202T2 Technical specifications.
- Ferrari, S. (2014) What is Précontraint Serge Ferrari composite material? (Accessed: 12/2014).
- Fillon, M. and Glavatskih, S.B. (2008) 'PTFE-faced centre pivot thrust pad bearings: Factors affecting TEHD performance', Tribology International, 41, pp. 1219–1225.
- Fishman, G.S. (1997) Monte Carlo: concepts, algorithms, and applications. Corr. 2nd print. edn. New York: Springer.

- Forster, B. and Mollaert, M. (2004) European Design Guide for Tensile Surface Structures. <http://www.tensinet.com/>: TensiNet.
- Gajewski, T. and Garbowski, T. (2014) 'Calibration of concrete parameters based on digital image correlation and inverse analysis', *Archives of Civil and Mechanical Engineering*, 14(1), pp. 170-180.
- Gasser, A., Boisse, P. and Hanklar, S. (2000) 'Mechanical behaviour of dry fabric reinforcements. 3D simulations versus biaxial tests', *Computational Materials Science*, 17(1), pp. 7-20.
- Gerdeen, J.C., Lord, H.W. and Rorrer, R.A.L. (2006) *Engineering design with polymers and composites*. London: Taylor & Francis.
- Ghosh, A. (2005) 'Analysis of Spun Yarn Failure. Part I: Tensile Failure of Yarns as a Function of Structure and Testing Parameters', *Textile Research Journal*, 75(10), pp. 731-740.
- Glaessgen, E.H., Pastore, C.M., Griffint, O.H. and Birger, A. (1996) 'Geometrical and finite element modelling of textile composites, Composites ', *Composites Part B*, 27B, pp. 43-50.
- Gosling, P. and Bridgens, B. (2008) 'Material Testing & Computational Mechanics – A New Philosophy For Architectural Fabrics', *INTERNATIONAL JOURNAL OF SPACE STRUCTURES*, 23(4).
- Gosling, P.D., Bridgens, B.N., Albrecht, A., Alpermann, H., Angeleri, A., Barnes, M., Bartle, N., Canobbio, R., Dieringer, F., Gellin, S., Lewis, W.J., Mageau, N., Mahadevan, R., Marion, J.M., Marsden, P., Milligan, E., Phang, Y.P., Sahlin, K., Stimpfle, B., Suire, O. and Uhlemann, J. (2013) 'Analysis and design of membrane structures: Results of a round robin exercise', *Engineering Structures*, 48, pp. 313-328.
- Grosberg, P. and Park, B.J. (1966) 'The Mechanical Properties of Woven Fabrics Part V: The Initial Modulus and the Frictional Restraint in shearing of Plain Weave Fabrics', *Textile Research Journal*, 66, pp. 420-431.
- Gunawan, S. and Azarm, S. (2004a) 'Multi-objective robust optimization using a sensitivity region concept', *Structural and Multidisciplinary Optimization*, 29(1), pp. 50-60.

- Gunawan, S. and Azarm, S. (2004b) 'Non-Gradient Based Parameter Sensitivity Estimation for Single Objective Robust Design Optimization', *Journal of Mechanical Design*, 126(3), p. 395.
- Happold, E., Ealey, T.A., Liddell, W.I., Pugh, J.W. and Webster, R.H. (1987) 'Discussion: The design and construction of the Diplomatic Club, Riyadh', *The structural engineer: journal of the Institution of Structural Engineers*, 65A(10), pp. 377-382.
- Hasofer, A.M. and Lind, N.C. (1974) 'Exact and Invariant Second-Moment Code Format', *Journal of the Engineering Mechanics Division-Asce*, 100(1), pp. 111-121.
- Hearle, J.W.S. (1969) 'Theory of the extension of continuous filament yarns', *Structural Mechanics of Fibres, Yarns and Fabrics*, 1, p. 37.
- Hendricks Franssen, H.J., Alcolea, A., Riva, M., Bakr, M., van der Wiel, N., Stauffer, F. and Guadagnini, A. (2009) 'A comparison of seven methods for the inverse modelling of groundwater flow. Application to the characterisation of well catchments', *Advances in Water Resources*, 32(6), pp. 851-872.
- Horrocks, A.R. and Kandola, B.K. (2005) 'Design and manufacture of textile composites - Chapter 9', in Long, A.C. (ed.) *Design and manufacture of textile composites*. Boca Raton, FL Cambridge: CRC Press; Woodhead, pp. 330 - 364.
- Houtman, R. and Orpana, M. (2000) 'Materials for Membrane Structures', *Bauen mit Textilien Heft*, 4, pp. 1 - 7.
- Huber, P.J. (1981) *Robust statistics*. New York: Wiley.
- Jackson, A.L., Bridgens, B.N. and Gosling, P.D. (2009) 'A new biaxial and shear protocol for architectural fabrics', *Proceedings of the International Association for Shell and Spatial Structures (IASS) Symposium 2009, Valencia Evolution and Trends in Design, Analysis and Construction of Shell and Spatial Structures*.
- Jones, F.R. (1994) *Handbook of polymer-fibre composites*. Burnt Mill, Harlow, Essex: Longman Scientific & Technical.
- Jones, I.A. and Pickett, A.K. (2005) 'Design and manufacture of textile composites - Chapter 8', in Long, A.C. (ed.) *Design and manufacture of textile composites*. Boca Raton, FL Cambridge: CRC Press; Woodhead, pp. 292 - 330.

- Kageyama, M., Kawabata, S. and Niwa, M. (1988) 'The Validity of a Linearizing Method for Predicting the Biaxial-Extension Properties of Fabrics', *Journal of the Textile Institute*, 79(4), pp. 543-567.
- Kato, S., Yoshino, T. and Minami, H. (1999) 'Formulation of constitutive equations for fabric membranes based on the concept of fabric lattice model', *Engineering Structures*, 21(8), pp. 691-708.
- Kawabata, S., Niwa, M. and Kawai, H. (1973) 'Finite-Deformation Theory of Plain-Weave Fabrics .1. Biaxial-Deformation Theory', *Journal of the Textile Institute*, 64(1), pp. 21-46.
- Kemp, A. (1957) 'An Extension of Peirce's Cloth Geometry to the Treatment of Non-circular Threads', *Journal of the Textile Institute Transactions*, 49(1), p. 5.
- Kharazi, A.Z., Fathi, M.H. and Bahmany, F. (2010) 'Design of a textile composite bone plate using 3D-finite element method', *Materials & Design*, 31(3), pp. 1468-1474.
- Kim, N.-K., Kim, D.-H., Kim, D.-W., Kim, H.-G., Lowther, D.A. and Sykulski, J.K. (2010) 'Robust Optimization Utilizing the Second-Order Design Sensitivity Information', *IEEE TRANSACTIONS ON MAGNETICS*, 46(8).
- Kostikov, V. (1995) *Fibre science and technology*. Chapman and Hall.
- Kozola, S. (2009) 'Recorded Webinar: Tips and Tricks- Getting Started Using Optimization with MATLAB ' Tips and Tricks. 03/2012. MathWorks. Available at: www.mathworks.co.uk.
- Kozola, S. (2010) 'Recorded Webinar: Speeding up Optimization Problemns With Parallel Computing '. 03/2012. MathWorks. Available at: www.mathworks.co.uk.
- Lawrence, C.A. (2003) *Fundamentals of Spun Yarn Technology*. CRC Press. Available at: http://www.NCL.eblib.com/EBLWeb/patron?target=patron&extendedid=P_214650_0 & (Accessed: 04/09/2012).
- Liu, L., GORCZYCA, J.L. and SHERWOOD, J.A. (2004) 'Modeling of Friction and Shear in Thermostamping of Composites - Part II', *Journal of Composite Materials*, 38(21), pp. 1931-1947.
- Lomov, S., Verpoest, I. and Robitaille, F. (2005) 'Design and manufacture of textile composites - Chapter 1', in Long, A.C. (ed.) *Design and manufacture of textile composites*. Boca Raton, FL Cambridge: CRC Press; Woodhead, pp. 1 - 62.

Long, A.C. (2005) Design and manufacture of textile composites. Boca Raton, FL
Cambridge: CRC Press; Woodhead.

Lucas, L.J. (1983) 'Mathematical Fitting of Modulus-Strain Curves of Poly(Ethylene-Terephthalate) Industrial Yarns', Textile Research Journal, 53(12), pp. 771-777.

Madhavan, V. and Naik, N.K. (2000) 'Twisted impregnated yarns: elastic properties', The Journal of Strain Analysis for Engineering Design, 35(2), pp. 83-91.

Margolis, J.M. (1985) Engineering thermoplastics: properties and applications. New York: Dekker.

MathWorks (2012a) MATLAB - Product Documentation - R2012b. Available at: www.Mathworks.co.uk/help/ (Accessed: 03/2012).

Mathworks (2012b) MATLAB and Simulink for Technical Computing. Available at: <http://www.mathworks.co.uk/> (Accessed: 2012).

MathWorks (2014) MATLAB - Product Documentation - R2014a. Available at: www.Mathworks.co.uk/help/ (Accessed: 09/2012).

Matsudaira, M. and Kawabata, S. (1998) 'A study of the mechanical properties of woven silk fabrics. Part II Analysis of the Shearing Properties of Woven Fabrics', Journal of the Textile Institute, 3, pp. 476-489.

McIntyre, J.E. (ed.) (2000) Synthetic Fibres: nylon, polyester, acrylic, polyolefin. Woodhead Publishing Limited.

McKeen, L.W. (2009) 'The Effect of Creep and Other Time Related Factors on Plastics and Elastomers (Second Edition)', in 2nd edn. <http://www.sciencedirect.com/science/book/9780815515852>: Elsevier, pp. 373-381.

Melchers, R.E. (1999) Structural reliability: analysis and prediction. 2nd edn. Chichester: John Wiley.

Membrane Structures Association of Japan, M. (1993) MSAJ Testing Method for In-Plane Shear Stiffness of Membrane Materials.

Membrane Structures Association of Japan, M. (1995) MSAJ Testing Method for Elastic Constants with commentary.

- Menges, G. and Meffert, B. (1976) 'Mechanical Behaviour of PVC-Coated Polyester Fabrics under Biaxial Stress', *German Plastics*, 66(11).
- Menges, P.D.-I.G. and Meffert, D.-I.B. (1976) 'Mechanical Behaviour of PVC-Coated Polyester Fabrics under Biaxial Stress', *German Plastics*, 66(11).
- Minami, H. (2006) 'A Multi-Step Linear Approximation Method for Nonlinear Analysis of Stress and Deformation of Coated Plain-Weave Fabric', *Journal of Textile Engineering*, 52(5), pp. 189-195.
- Minami, H., Yamamoto, C., Segawa, S. and Kono, Y. (1997) 'A Method for Membrane Material Nonlinear Stress Analysis Using Multi-step Linear Approximation', *IASS International Symposium '97 on Shell & Spatial Structures*: 10 - 14 November.
- Newcastle_University (2012) *MASys (Measurement & Analysis Systems) Guide to testing structural fabrics*. Newcastle University.
- Nguyen, M., Herszberg, I. and Paton, R. (1999) 'The shear properties of woven carbon fabric', *Composite Structures*, 47(1–4), pp. 767-779.
- Nocedal, J. and Wright, S.J. (2006) *Numerical optimization*. 2nd edn. New York; London: Springer.
- Nurwaha, D. and Wang, X. (2011) 'Prediction of rotor spun yarn strength using support vector machines method', *Fibers and Polymers*, 12(4), pp. 546-549.
- Oasys (2014) *Oasys GSA product information*. Available at: <http://www.oasys-software.com> (Accessed: 31/01/2014).
- Ognedal, A.S., Clausen, A.H., Polanco-Loria, M., Benallal, A., Raka, B. and Hopperstad, O.S. (2012) 'Experimental and numerical study on the behaviour of PVC and HDPE in biaxial tension', *Mechanics of Materials*, 54, p. 13.
- O'Hara, G.P. (1983) *Mechanical Properties of Silicone Rubber*. <http://www.dtic.mil/dtic/>.
- Osswald, T.A. and Menges, G. (1996) *Materials science of polymers for engineers*. Munich; New York Cincinnati: Hanser ;Hanser/Gardner.
- Page, J.R. and Wang, J. (2000) 'Prediction of shear force and an analysis of yarn slippage for a plain-weave carbon fabric in a bias extension state', *Composites Science and Technology*, 60, pp. 977-986.

- Palaniswamy, N.K. and Mohamed, A.P. (2005) 'Effect of single yarn twist and ply to single yarn twist ratio on strength and elongation of ply yarns', *Journal of Applied Polymer Science*, 98(5), pp. 2245-2252.
- Pan, N. (1996) 'Analysis of Woven Fabric Strengths: Prediction of Fabric Strength Under Uniaxial and Biaxial Extensions', *Composites Science and Technology*, 56(56), pp. 311 - 327.
- Pargana, J.B., Lloyd-Smith, D. and Izzuddin, B.A. (2000) 'Advanced Material Model for the Analysis of Tensioned Fabric Structures'.
- Pargana, J.B., Lloyd-Smith, D. and Izzuddin, B.A. (2007) 'Advanced material model for coated fabrics used in tensioned fabric structures', *Engineering Structures*, 29(7), pp. 1323-1336.
- Pargana, J.B., Lloyd-Smith, D. and Izzuddin, B.A. (2010) 'Fully integrated design and analysis of Tensioned Fabric Structures: Finite elements and case studies', *Engineering Structures*, 32(4), pp. 1054-1068.
- Pavlidou, S., Mai, S., Zorbas, T. and Papaspyrides, C.D. (2003) 'Mechanical Properties of Glass Fabric/Polyester Composites: Effect of Silicone Coatings on the Fabrics', *Journal of Applied Polymer Science*, 91, pp. 1300 - 1308.
- Peirce, F.T. (1937) 'Geometry of cloth structure', *Textile Institute -- Journal*, 28(3), pp. 45-96.
- Rao, M.P., Pantiuk, M. and Charalambides, P.G. (2008) 'Modeling the Geometry of Satin Weave Fabric Composites', *Journal of Composite Materials*, 43(1), pp. 19-56.
- Sanders, D.L. and Kingsnorth, A.N. (2012) 'Prosthetic mesh materials used in hernia surgery', *Expert Rev Med Devices*, 9(2), pp. 159-179.
- Scheidbach, H., Tamme, C., Tannapfel, A., Lippert, H. and Kockerling, F. (2004) 'In vivo studies comparing the biocompatibility of various polypropylene meshes and their handling properties during endoscopic total extraperitoneal (TEP) patchplasty - An experimental study in pigs', *Surgical Endoscopy and Other Interventional Techniques*, 18(2), pp. 211-220.
- Schuëller, G.I. and Jenson, H.A. (2008) 'Computational methods in optimization considering uncertainties - An overview', *Computational Methods Applied Mechanical Engineering*, 198, pp. 2-13.

- Sergent, F., Desilles, N., Lacoume, Y., Bunel, C. and Marie, J.P. (2009) 'Experimental biomechanical evaluation of polypropylene prostheses used in pelvic organ prolapse surgery', *International Urogynecology Journal*, 20(5), pp. 597-604.
- Singh, M.N. and Naik, N.K. (2001) 'Twisted impregnated yarns: transverse tensile strength', *The Journal of Strain Analysis for Engineering Design*, 36(4), pp. 347-357.
- Skelton, J. (1980) 'Mechanical Properties of Coated Fabrics', pp461-469
- Skelton, J. and Freeston, W.D. (1971) 'Mechanics of Elastic Performance of Textiles Part XIX: The Shear Behaviour of Fabrics Under Biaxial Load', *Textile Research Journal*, 41(11), pp. 420-431.
- Sørensen, B.F. (2009) ICCM17 Edinburgh Conference.
- Stubbs, N. and Fluss, H. (1980) 'A space-truss model for plain-weave coated fabrics'.
- Sun, H. and Pan, N. (2005) 'Shear deformation analysis for woven fabrics', *Composite Structures*, 67(3), pp. 317-322.
- Tan, K.Y. and Barnes, M. (1984) 'Numerical Representation of Stress/Strain Relations for Coated Fabrics'.
- Tarfaoui, M., Drean, J.Y. and Akesbi, S. (2001) 'Predicting the stress-strain behavior of woven fabrics using the finite element method', *Textile Research Journal*, 71(9), p. 790.
- Testa, R.B. and Yu, L.M. (1987) 'Stress-Strain Relation for Coated Fabrics', *Journal of Engineering Mechanics-Asce*, 113(11), pp. 1631-1646.
- Testa, R.B., Stubbs, N. and Spillers, W.R. (1978) 'Bilinear Model for Coated Square Fabrics', *Journal of the Engineering Mechanics Division-Asce*, 104(5), pp. 1027-1042.
- Uetani, K., Fujiwara, J. and Ohsaki, M. (2002) 'A Simple Viscoelastic Membrane Material Model for Cutting Pattern Optimization'.
- Verseidag (2005) Verseidag Duraskin Brochure.
- Verseidag (2010a) B18059 Technical specifications.
- Verseidag (2010b) B18089 Technical specifications.

- Verseidag (2011) Versedag Website [Web Page]. Available at:
<http://www.verseidag.de/en/en/technology/production/production>.
- Wallenberg, F.T. and Bingham, P.A. (eds.) (2010) *Fiberglass and Glass Technology*. Springer Science+Business Media.
- Wang, F.-M. (2002) 'Prediction Method for Tensile Property of Woven Fabrics in Lower Loads', *Journal of Dong Hua University*, 19(2).
- Wilcox, R.R. (2005) *Introduction to robust estimation and hypothesis testing*. 2nd edn. Amsterdam ; Boston: Elsevier/Academic Press.
- WOO, K., SUH, Y.W. and WHITCOMB, J.D. (2002) 'Phase Shift Effect on the Stress Distribution for Satin Weave Composites', *Journal of Composite Materials*, 36(271).
- Wu, Y. and Wu, A. (2000) *Taguchi Methods for Robust Design*.
- Yang, W. and Xiao, R. (2013) 'Multiobjective Optimization Design of a Pump–Turbine Impeller Based on an Inverse Design Using a Combination Optimization Strategy', *Journal of Fluids Engineering*, 136(1), p. 014501.
- Zimlik, D.A., Kennedy, J.M., Hirt, D.E. and Reese, G.P. (2000) 'Determining Mechanical Properties of Yarns and Two-Ply Cords from Single-Filament Data: Part II: Comparing Model and Experimental Results for PET', *Textile Research Journal*, 70(12), pp. 1097-1105.

A. Appendix

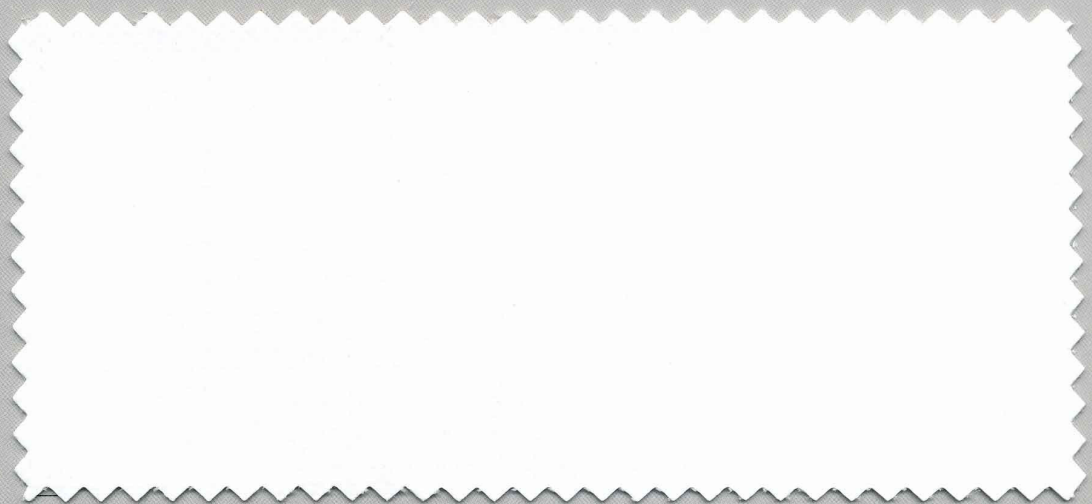
A. 1. Appendix A: Fabric data sheets

Textile Architecture



www.ferrari-architecture.com

PRECONSTRAINT[®]
702T2 back
PVDF



702 - 1746

FERRARI
architecture



Technical properties	Precontraint® 702 T2 back PVDF	Standards
Yarn	PES HT 1100 Dtex	TERSUISSE
Weight	750 g/m ² - 22 oz/sqyd	EN ISO 2286-2
Width	178 cm	(-1mm/+1mm)
Tensile strength (warp/weft)	300/280 daN/ 5 cm 340/330 Lbs	EN ISO 1421 ASTM D 751-00 Cut Strip Method
Tear resistance (warp/weft)	30/28 daN 85/82 Lbs	DIN 53.363 ASTM D 751-00 Trapezoid Tear Method
Adhesion	10 daN/5 cm	EN ISO 2411
Flame retardancy	M2/NF P92-507 • B1/DIN 4102-1 • BS 7837 • Test 2/NFPA 701 CSFM T19 • Group 1/AS/NZS 3837 • ASTM E84 • VKF 5.2/SN 198898	
Surface treatment	Fluotop® T2 (High concentration PVDF)	
Back side treatment	Weldable PVDF (for a better resistance to pollution of the back side of the fabric)	
Product application	Static & permanent structures	

702T2 back PVDF capitalizes on the excellent PVDF weathering and without changing the making up process allows a better aesthetical performance of the membrane under any shape and from any angle.

The technical data here above are average values with a +/- 5% tolerance.

Additional information

Coating thickness at the top of the yarns	240 µ	
Total thickness	0,56 mm	
Light transmission	14%	NFP 38-511
White index	82%	CIE: International Light Commission
Thermal values	ASHRAE standard 74-1988	EN ISO 410
Transmission	Ts 9%	Ts 10%
Reflexion	Rs 76%	Rs 79%
Absorption	As 15%	As 11%
Shading coefficient	g 15%	g 13%
Visible transmission	-	Tv 8%
Visible reflexion	-	Rv 88%
UV transmission	T-UV 0%	Eppeley Solar & Sky U-V radiometer
Global thermal conductivity*	Vertical position: U = 5,6W/m ² °C Horizontal position: U = 6,4W/m ² °C	
Acoustical weakening index	14 dBA	ISO 717
Extreme working temperatures	- 30°C/+70°C	in static position
Quality management system		ISO 9001

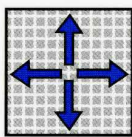
* Those data are obtained by calculation through simulations of the average conditions of use, those values must be considered as approximation.

The buyer of our products is fully responsible for their application or their transformation concerning any possible third party. The buyer of our products is responsible for their implementation and installation according to the standards, use and customs and safety rules of the countries where they are used. Concerning the contractual warranty, please refer to the text of our warranty.

The values here above mentioned are the results of tests performed in conformity with the use and customs in terms of studies, they are given as an indication in order to allow our customers to make the best use of our products. Our products are subjects to evolutions due to technical progress, we remain entitled to modify the characteristics of our products at any time. The buyer of our products is responsible to check that the here above data are still valid.



Précontraint
Ferrari®



Dimensional
stability



Long life



Easy
maintenance



U.V.
resistant



Guarantee
10 years



100%
recyclable textile

100% recyclable

Ferrari® developed the Taxyloop® technology specifically for the recycling of composite PVC membranes and textiles. Through the management of its end-of-life products Ferrari® is committed to sustainable development.
www.taxyloop.com

Sustainable development

Ferrari® development is based on strict adherence to good safety and environmental practices, that include an understanding of Life Cycle Analysis (ACV), selection of the best materials, and eco-design.
The Company obtained its first ISO 14001 certification in 2003.

Specification Service

The Ferrari® specification service is available to inform you, advise you and suggest innovative solutions for your specific requirements.

To detail your project, fill in a form on:
www.ferrari-architecture.com

FERRARI



FERRARI SA - FRANCE
BP 54
38352 La-Tour-du-Pin Cedex
Tel: +33 (0)4 74 97 66 49
Fax: +33 (0)4 74 83 59 71

STAMOID AG
A Ferrari Group Company
CH 8193 Eglisau - Switzerland
Tel: +41 (0)44 868 26 26
Fax: +41 (0)44 868 27 27

FERRARI TEXTILES CORP
Pompano Beach, FL, USA
Tel: (954) 942-3600
Fax: (954) 942-5555

FERRARI CHINA OFFICE
Shanghai, China
Tel: 0086 21 62814886
Fax: 0086 21 62946165

Textile Architecture



www.ferrari-architecture.com


PRECONSTRAINT[®]
1202T2 back
PVDF



1202 - 1746

FERRARI
architecture



Technical properties	Preconstraint® 1202 T2 back PVDF	Standards
Yarn	PES HT 1100 Dtex/1670 Dtex	TERSUISSE 
Weight	1050 g/sqm - 31 oz/sqyd (1250 g/m²*)	EN ISO 2286-2
Width	178 cm	(-1mm/+1mm)
Tensile strength (warp/weft)	560/560 daN/ 5 cm 565/565 Lbs	EN ISO 1421 ASTM D 751-00 Cut Strip Method
Tear resistance (warp/weft)	80/65 daN 130/110 Lbs	DIN 53.363 ASTM D 751-00 Trapezoid Tear Method
Adhesion	12 daN/ 5 cm	EN ISO 2411
Flame retardancy	B1/DIN 4102-1 • BS 7837 • Test 2/NFPA 701 CSFM T19 • Group 2/AS/NZS 3837 • VKF 5.2/SN 198898	
Surface treatment	Fluotop® T2 (High concentration PVDF)	
Back side treatment	Weldable PVDF (for a better resistance to pollution of the back side of the fabric)	
Product application	Static & permanent structures	

1202T2^{back} PVDF capitalizes on the excellent PVDF weathering and without changing the making up process allows a better aesthetical performance of the membrane under any shape and from any angle.

The technical data here above are average values with a +/- 5% tolerance.

Additional information

Coating thickness at the top of the yarns	270 µ	
Total thickness	0,78 mm	
Light transmission	10%	NFP 38-511
White index	82%	CIE: International Light Commission
Thermal values	ASHRAE standard 74-1988	EN ISO 410
Transmission	Ts 7%	Ts 7%
Reflexion	Rs 77%	Rs 79%
Absorption	As 16%	As 14%
Shading coefficient	g 13%	g 11%
Visible transmission	-	Tv 5%
Visible reflexion	-	Rv 87%
UV transmission	T-UV 0%	Eppley Solar & Sky U-V radiometer
Global thermal conductivity**	Vertical position: U = 5,6W/m² °C Horizontal position: U = 6,4W/m² °C	
Acoustical weakening index	15 dBA	ISO 717
Extreme working temperatures	- 30°C/+70°C	in static position
Quality management system		ISO 9001

* M2 only available on special order at 1250 g/m².

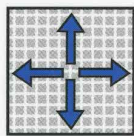
** Those data are obtained by calculation through simulations of the average conditions of use, those values must be considered as approximation.

The buyer of our products is fully responsible for their application or their transformation concerning any possible third party. The buyer of our products is responsible for their implementation and installation according to the standards, use and customs and safety rules of the countries where they are used. Concerning the contractual warranty, please refer to the text of our warranty.

The values here above mentioned are the results of tests performed in conformity with the use and customs in terms of studies, they are given as an indication in order to allow our customers to make the best use of our products. Our products are subjects to evolutions due to technical progress, we remain entitled to modify the characteristics of our products at any time. The buyer of our products is responsible to check that the here above data are still valid.



Préconstraint
Ferrari®



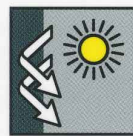
Dimensional
stability



Long life



Easy
maintenance



U.V.
resistant



Guarantee
15 years



100%
recyclable textile

100% recyclable

Ferrari® developed the Taxyloop® technology specifically for the recycling of composite PVC membranes and textiles. Through the management of its end-of-life products Ferrari® is committed to sustainable development.
www.taxyloop.com

Sustainable development

Ferrari® development is based on strict adherence to good safety and environmental practices, that include an understanding of Life Cycle Analysis (ACV), selection of the best materials, and eco-design.
The Company obtained its first ISO 14001 certification in 2003.

Specification Service

The Ferrari® specification service is available to inform you, advise you and suggest innovative solutions for your specific requirements.

To detail your project, fill in a form on:
www.ferrari-architecture.com

FERRARI



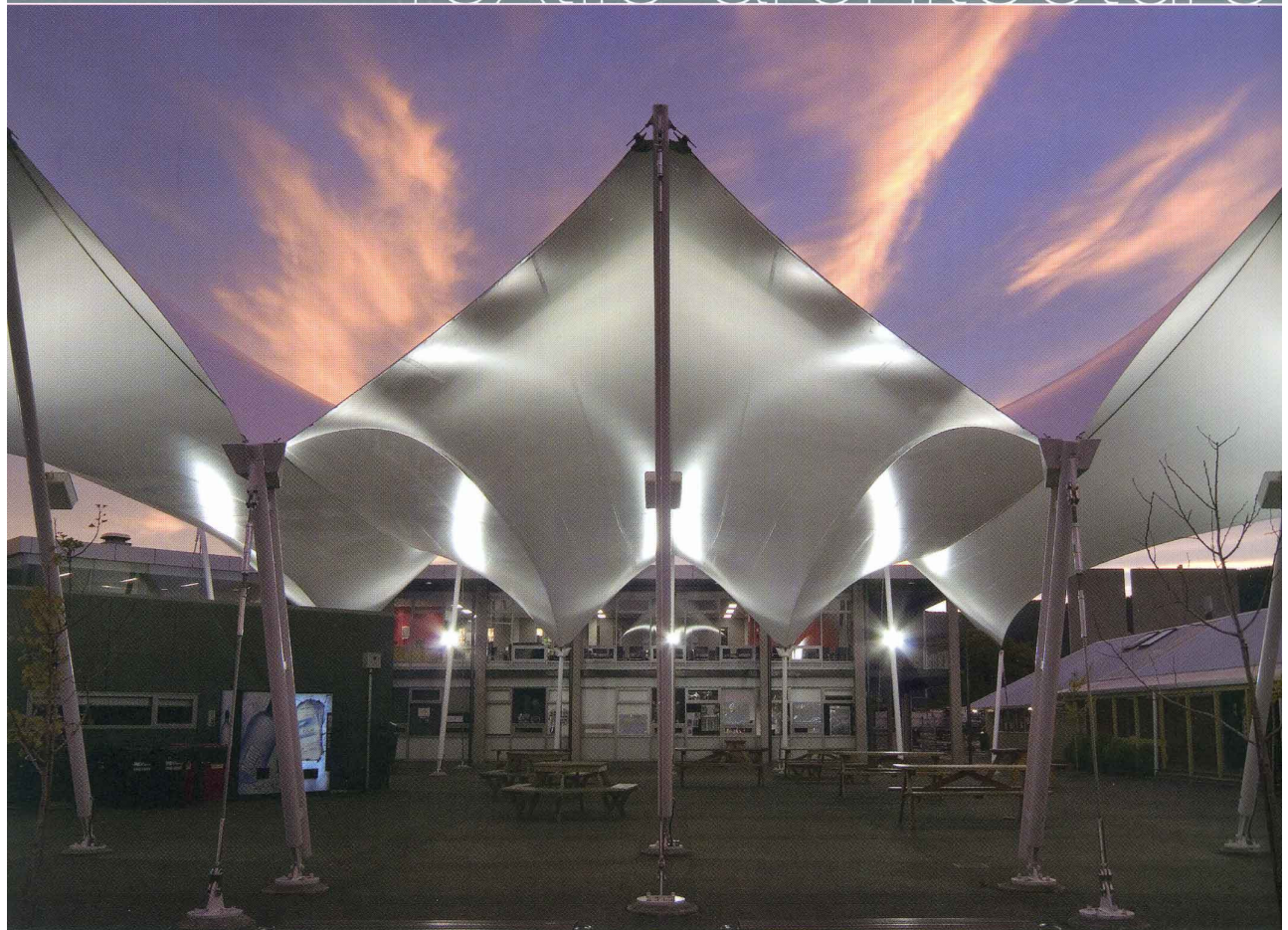
FERRARI SA - FRANCE
BP 54
38352 La-Tour-du-Pin Cedex
Tel: +33 (0)4 74 97 66 49
Fax: +33 (0)4 74 83 59 71

STAMOID AG
A Ferrari Group Company
CH 8193 Eglisau - Switzerland
Tel: +41 (0)44 868 26 26
Fax: +41 (0)44 868 27 27

FERRARI TEXTILES CORP
Pompano Beach, FL, USA
Tel: (954) 942-3600
Fax: (954) 942-5555

FERRARI CHINA OFFICE
Shanghai, China
Tel: 0086 21 62814886
Fax: 0086 21 62946165

Textile architecture



www.ferrari-architecture.com

PRECONSTRAINT®


1002S • 1202S • 1302S • 1502S • back
PVPF

FERRARI
architecture



Textile architecture

PRECONTRAIN[®]

1002S-1202S-1302S-1502S-

Technical properties	Précontraint [®] 1002 S back PVDF	Précontraint [®] 1202 S back PVDF	Précontraint [®] 1302 S back PVDF	Précontraint [®] 1502 S back PVDF	Standards
Yarn	1100 Dtex PES HT	1100 / 1670 Dtex PES HT	1100/2200 Dtex PES HT	1670/2200 Dtex PES HT	
Weight	1050 g/m ² / 31 oz/sqyd	1050 g/m ² (1250 g/m ²)* / 31 oz/sqyd	1350 g/m ² / 40 oz/sqyd	1500 g/m ² / 44 oz/sqyd	EN ISO 2286-2
Width	180 cm	180 cm	180 cm	180 cm	(-1mm/+1mm)
Tensile strength (warp/weft)	420/400 daN/ 5 cm	560/560 daN/ 5 cm	800/700 daN/ 5 cm	1000/800 daN/ 5 cm	EN ISO 1421
Tear resistance (warp/weft)	55/50 daN	80/65 daN	120/110 daN	160/140 daN	DIN 53.363
Adhesion	12 daN/ 5 cm	12 daN/ 5 cm	13 daN/ 5 cm	15 daN/ 5 cm	EN ISO 2411
Flame retardancy	M2/NF P 92-507 • B1/DIN 4102-1 BS 7837 • M2/UNE 23.727 SITAC/ETA/SIS 650082 VKF 5.2/SN 198898 • Test 2/NFPA 701 CSFM T19 • ASTM E84 Class C/ASTM E 108	B1/DIN 4102-1 • BS 7837 CSFM T 19 • SITAC/SIS 650082 VKF 5.2/SN 198898 Test 2/NFPA 701	B1/DIN 4102-1 • BS 7837 CSFM T 19 • SITAC/SINTEF/SIS 650082 VKF 5.3/SN 198898 Test 2/NFPA 701 B1/ONORM B 3800-1	B1/DIN 4102-1 • BS 7837 SITAC/SINTEF/ETA/SIS 650082 Test 2/NFPA 701 • CSFM T 19	
Surface treatment	Formula S: calibrated PVDF alloy				
Reverse side treatment	Weldable PVDF (for better resistance to pollution on the reverse side of the fabric).				

PVDF back treatment cashes in on the excellent anti-ageing qualities of fluoropolymer and, without modifying fabric making-up procedures, enables better-looking finishes for all sorts of fabrics, seen from any angle

The figures in the above data-sheet are average values, with a tolerance of +/- 5%.

Additional informations

Coating thickness at the top of the yarns	350 µ		270 µ		300 µ		300 µ		
Total thickness	0,78 mm		0,78 mm		1,02 mm		1,14 mm		
White index**	82 %		82 %		82 %		82 %		CIE: Commission Internationale de l'éclairage
Light transmission**	7,5 %		10 %		5,5 %		5,5 %		NFP 38-511
Thermal values**	ASHRAE 74 1988	ISO EN 410	ASHRAE 74 1988	ISO EN 410	ASHRAE 74 1988	ISO EN 410	ASHRAE 74 1988	ISO EN 410	
Solar Transmission	Ts 6 %	Ts 6 %	Ts 7 %	Ts 6 %	Ts 5 %	Ts 4,5 %	Ts 5 %	Ts 4 %	
Solar Reflection	Rs 78 %	Rs 80 %	Rs 77 %	Rs 80 %	Rs 78 %	Rs 78 %	Rs 78 %	Rs 81 %	
Solar Absorption	As 16 %	As 14 %	As 16 %	As 14 %	As 17 %	As 17,5 %	As 17 %	As 15 %	
Shading coefficient	g 12 %	g 10 %	g 13 %	g 10 %	g 11 %	g 8,5 %	g 11 %	g 8 %	
Visible transmission	T-UV 0%		T-UV 0%		T-UV 0%		T-UV 0%		Eppley Solar & Sky U-V radiometer
Global thermal conductivity									
Vertical position	U= 5,6W/m2/°C		U= 5,6W/m2/°C		U= 5,6W/m2/°C		U= 5,6W/m2/°C		
Horizontal position	U= 6,4W/m2/°C		U= 6,4W/m2/°C		U= 6,4W/m2/°C		U= 6,4W/m2/°C		
Acoustical weakening index	Rw: 15 dBA Tolerance +/- 1 dBA		Rw: 15 dBA		Rw: 16 dBA		Rw: 17 dBA		ISO 717
Extreme working temperatures	- 30°C/+ 70°C		- 30°C/+ 70°C		- 30°C/+ 70°C		- 30°C/+ 70°C		In static position
Quality management system							ISO 9001		

* M2 classification is only available on request. Specially manufactured at 1250 g/sqm - ** White value 8126S only.

Those data are obtained by calculation through simulations of the average conditions of use, those values must be considered as approximation.

The buyer of our products is fully responsible for their application or their transformation concerning any possible third party. The buyer of our products is responsible for their implementation and installation according to the standards, use and customs and safety rules of the countries where they are used.

Concerning the contractual warranty, please refer to the text of our warranty. The values here above mentioned are the results of tests performed in conformity with the use and customs in terms of studies, they are given as an indication in order to allow our customers to make the best use of our products. Our products are subject to evolutions due to technical progress, we remain entitled to modify the characteristics of our products at any time. The buyer of our products is responsible to check that the here above data are still valid.

100% recyclable

Ferrari[®] developed the Taxyloop[®] technology specifically for the recycling of composite PVC membranes and textiles. Through the management of its end-of-life products Ferrari[®] is committed to sustainable development.
www.taxyloop.com

Sustainable development

Ferrari[®] development is based on strict adherence to good safety and environmental practices, that include an understanding of Life Cycle Analysis (ACV), selection of the best materials, and eco-design. The Company obtained its first ISO 14001 certification in 2003.

Specification Service

The Ferrari[®] specification service is available to inform you, advise you and suggest innovative solutions for your specific requirements.

To detail your project, fill in a form under:
www.ferrari-architecture.com

FERRARI



FERRARI SA - FRANCE
BP 54
38352 La-Tour-du-Pin Cedex
Tel: +33 (0)4 74 97 41 33
Fax: +33 (0)4 74 83 59 71

STAMOID AG
A Ferrari Group Company
CH 8193 Eglisau - Switzerland
Tel: +41 (0)44 868 26 26
Fax: +41 (0)44 868 27 27

FERRARI TEXTILES CORP
Pompano Beach, FL, USA
Tel: +1(954) 942-3600
Fax: +1(954) 942-5555

FERRARI CHINA OFFICE
Shanghai, China
Tel: 0086 21 62814886
Fax: 0086 21 62946165

■ PVDF treatment — unique know-how

Ferrari® is a precursor in PVDF treatments for architectural textile membranes. The technology has been available for over 15 years and is available in a very extensive range to meet many performance requirements.

For PVDF to really come into its own as an anti-ageing agent with anti-pollution adhesion features a calibrated formulation concentration is required. As Formule S is a weldable formulation it is easier to fabricate, and comes in a wide range of colours.



America's Cup China Team - Valencia - Spain

■ Formula S and back PVDF



Water treatment plant - Valenton - France

- **Maintenance and cleaning** are easy because Formula S contains a calibrated surface concentration of PVDF fluoropolymer. Moreover, PVDF treatment on the back of PVDF cashes in on the excellent anti-ageing qualities of fluoropolymer and, without modifying fabric making-up procedures, enables better-looking finishes for both sides of fabrics, seen from any angle.

- **Welding performance:** with simple HF welding, assembled sections stand up to high temperatures while bearing considerable tension.

- **Colour range:** Formula S back PVDF is possible in the Précontraint® 502 range of colour shades (except for aluminium and "metallic"). Other colour shades upon request after studying the UV behaviour.

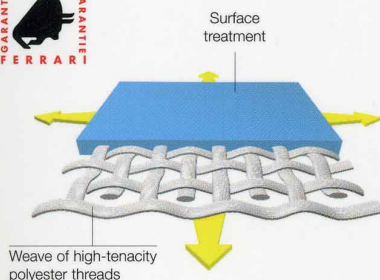


Hotel Al Shark - Doha - Qatar



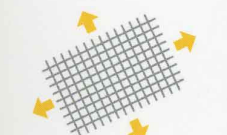
Gymnasium - Espo - Finland

Exclusive **Précontraint® Ferrari®** technology

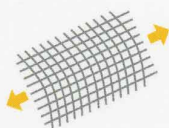


Worldwide patented Ferrari® Précontraint® technology consists of prestressing the textile base cloth both before and during all the coating operations. Unlike traditional textiles Ferrari® Précontraint® membranes are subjected to regular, balanced tension both warpwise and weftwise that results in similar elongation characteristics in both directions.

This gives – very considerable dimensional stability – limited creep over time – longer life – performance homogeneity from batch to batch.



Ferrari® Précontraint textiles respect the weft yarn direction which stays identical from one batch to the other.



Conventional coated textiles exhibit serious deformation of the weft yarn which in addition vary greatly from one batch to the other.



Précontraint® textiles have very low crimp, that is similar in both warp and weft direction.



Conventional coated textiles presents a high level a crimp in the weft direction.

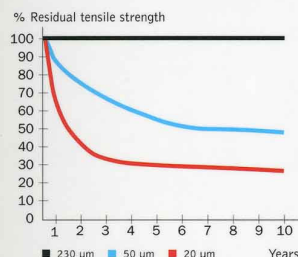


Précontraint® 702



Type I classic coated textile

- **Longevity:** because Ferrari® Précontraint membranes have thicker coating at the top of the yarns, they keep their qualities of mechanical resistance for a long time—a key factor in the long life of your installations.



An independent ENKA study of three textiles (all the same material but with different degrees of coating thickness at the top of the yarns). Exposure to in natural conditions over a period of 10 years in Florida, USA.



Airbus hangar, 1982
Germany — Précontraint® 1302
Resistance to traction after 22 years:
Warp 97 % - Weft 84 %



Exhibition marquee, 1982
Port Saint Louis — Précontraint® 1302
Resistance to traction after 18 years:
Warp 86 % - Weft 76 %

- **Homogeneity:** Major textile architectural projects or those that are targeting a level of standardization for industrial applications, are carried out using modules or panels that are reproduced in several units. It is therefore essential that the compensation calculations and cutting plans made from a set of values are reliable for all the fabric batches used. The Précontraint® technology guarantees this uniformity.

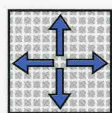
- **Limited creep:** The Précontraint® technology controls the weft direction and significantly reduces the creep phenomenon which appears to be 3 to 4 times higher with conventional fabrics. With Précontraint® textiles, the initial shape of the membranes is therefore controlled and maintained over time.

Technical features **PRECONTRAIN®**

1002S • 1202S • 1302S • 1502S • BECK



Précontraint®
Ferrari®



Dimensional
stability



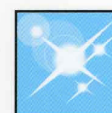
Long life



U.V.
resistant



Flame
retardant



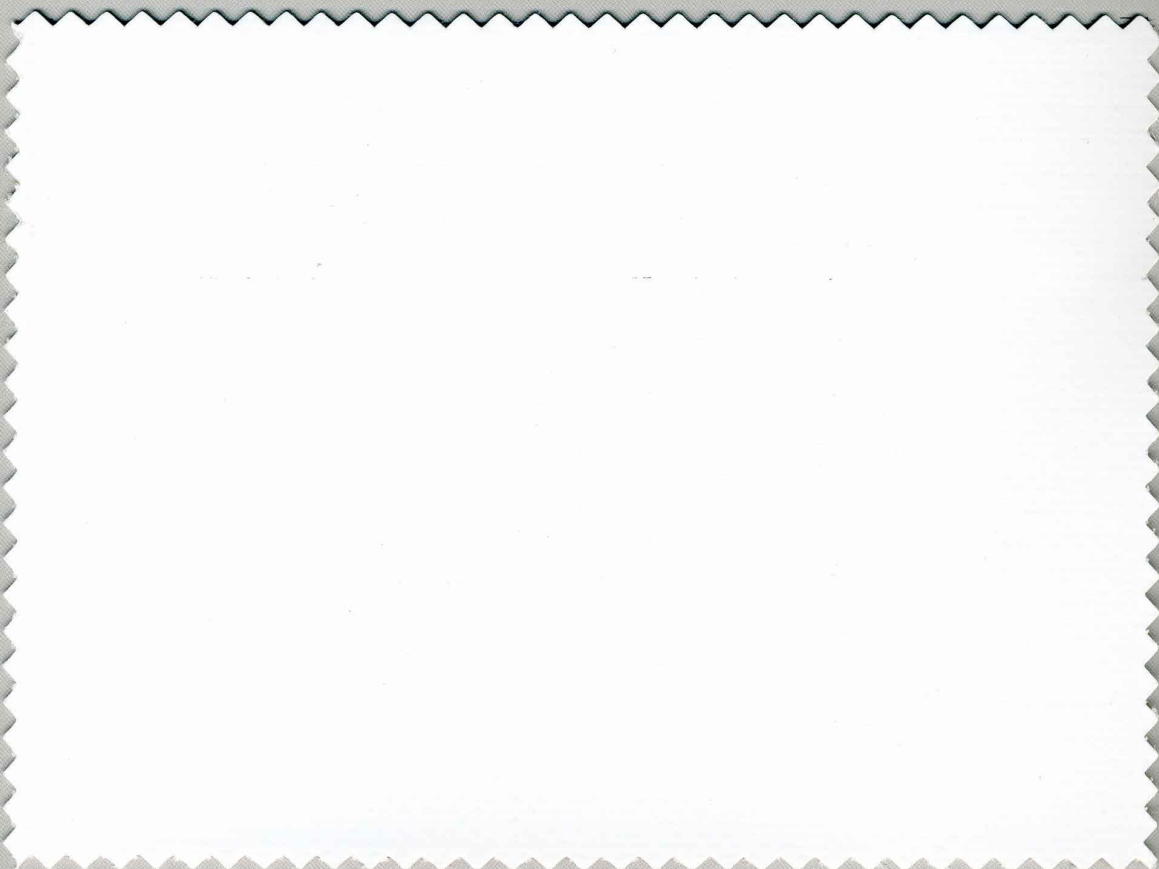
Easy
maintenance



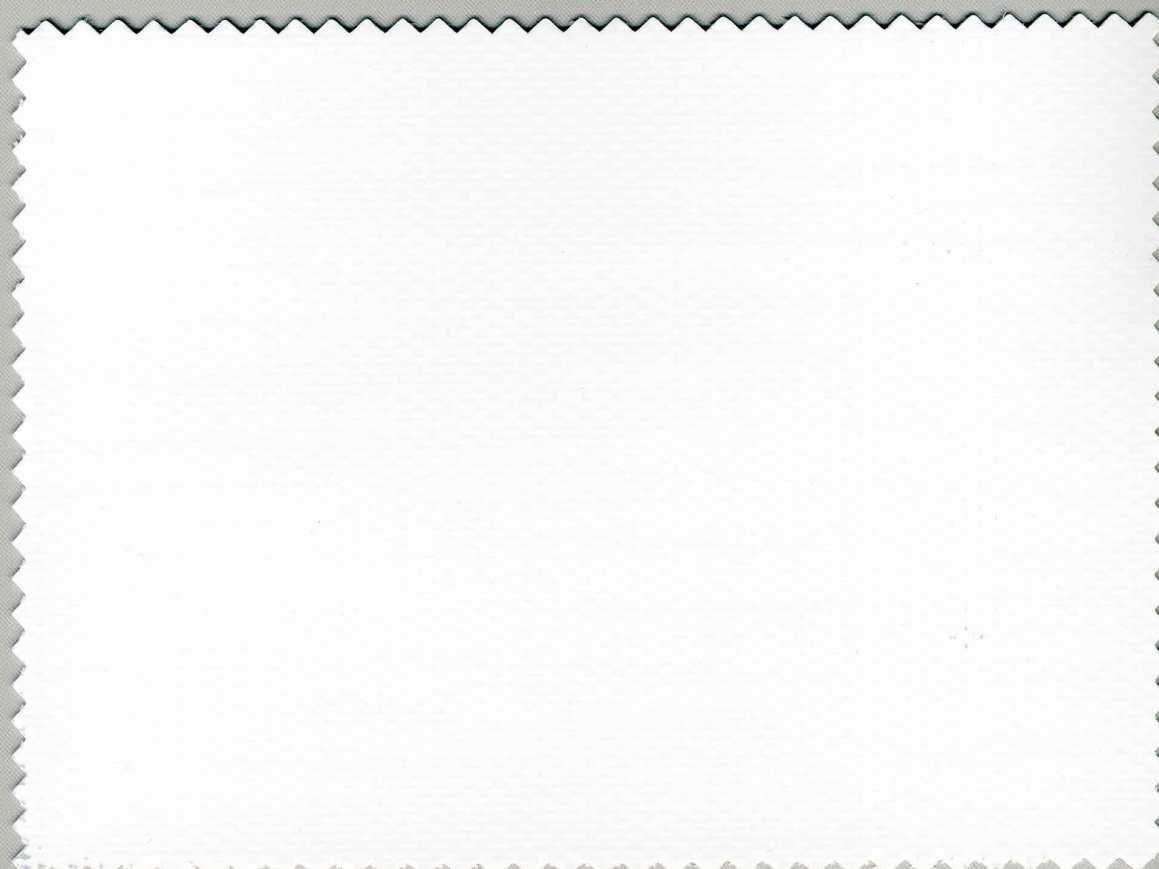
100% recyclable
textile



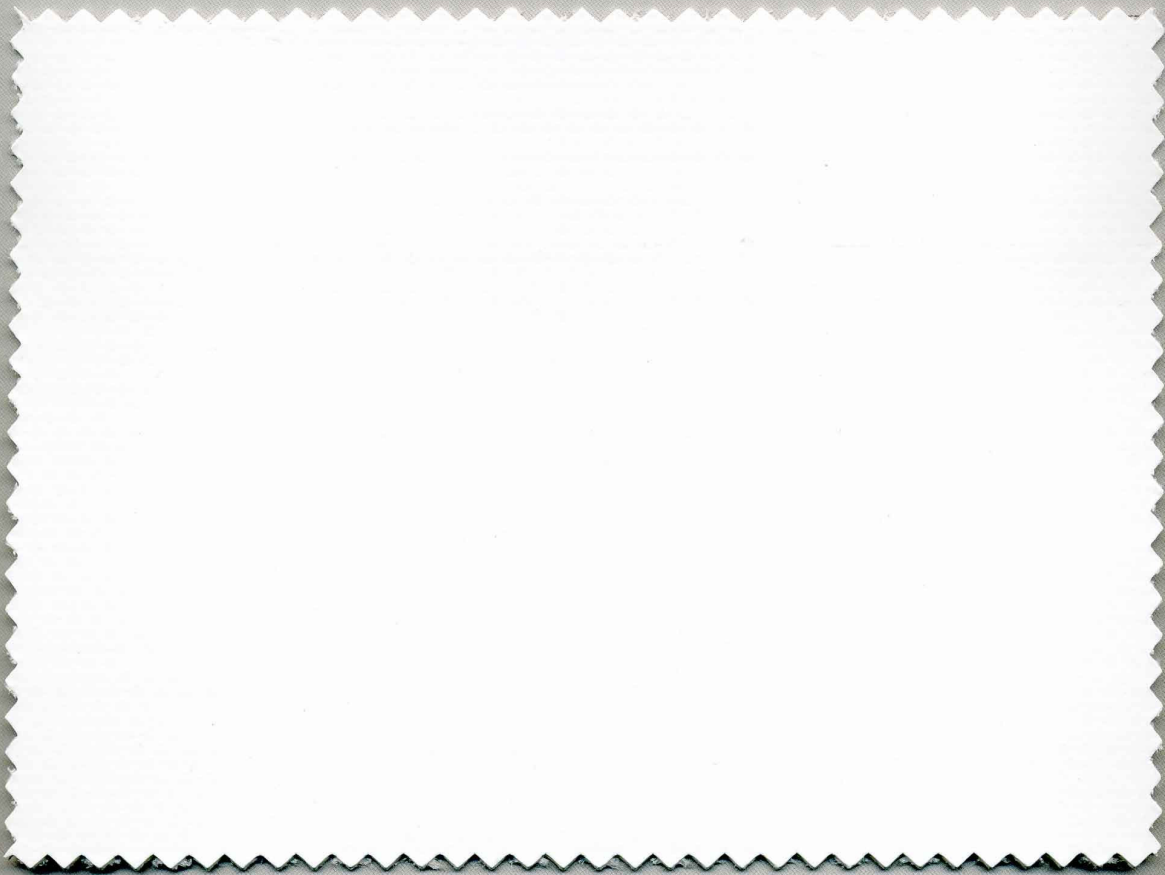
12 year
guarantee



1002-8126S back PVDF



1202-8126S back PVDF



1302-8126S back PVDF

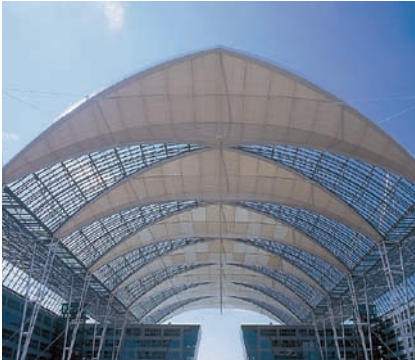


1502-8126S back PVDF

White Précontraint® 8126 S: standard products (in stock),
Précontraint® 502 range of colours: production to order.
Adjustments of welding parameters are necessary.

duraskin®

B 18059



**VERSEIDAG-INDUTEX GmbH
Deutschland**

Industriestrasse 56, 47803 Krefeld
Postfach 10 23 13, 47723 Krefeld
Phone +49 2151 876-0
Fax +49 2151 876-291
e-mail duraskin@vsindutex.de

**Office Shanghai
China**

Room 1002, No.333 Jingang Road
Shanghai 201206, P.R. China
Phone/Fax +86 21 5865 2805
Mobile +86 1350 168 5081
e-mail long@duraskin.cn

**VERSEIDAG seemee (U.S.) Inc.
USA**

4 Aspen Drive
Randolph, New Jersey 07869
Phone +1 973 252 1189
Fax +1 973 252 1109
e-mail info@seemeeus.com

**VERSEIDAG-INDUTEX GmbH-MENA
Jordan**

1st Floor – Offices No. (101–103)
219-Al Madina Al Munawara Street
P.O. Box 1909, Amman 11941, Jordan
Phone +962 6 554 5981
Fax +962 6 554 5982
e-mail mbahsh@vsindutex.jo

**VERSEIDAG seemee UK Ltd.
UK**

Collingwood House, Alington Road
Eynesbury, St. Neots
PE19 6YH Cambridgeshire
Phone +44 1480 213700
Fax +44 1480 213609
e-mail info@seemeeuk.com

www.vsindutex.de

Membranen PTFE
Membranes PTFE
Membranes PTFE
Membranas PTFE

DE	Typ IV	B 18059
Trägergewebe		Glasfaser EC 3/4
Beschichtung		PTFE – Polytetrafluorethylen
Flächengewicht (g/m ²)	DIN EN ISO 2286-2	1550
Breite (cm)	DIN EN ISO 2286-1	470
Höchstzugkraft (N/5 cm)	DIN 53354	Kette/Schuss 8000/7000
Weiterreißkraft (N)	DIN 53363	Kette/Schuss 500/500
Haftung (N/5 cm)	DIN 53357	100
Transluzenz bei 550 nm (%)	DIN 5036	11
Brandverhalten	DIN 4102	B1*

Hinweis: Produkt ist nicht zu vernähen, sondern mit Heizbalken zu verschweißen. *Weitere Zertifikate erhältlich auf Anfrage. Änderungen, die dem technischen Fortschritt dienen, behalten wir uns vor. Werte ohne Toleranzangaben sind Nennwerte mit einer Toleranz von $\pm 5\%$. Die Angaben entsprechen unserem heutigen Kenntnisstand und sollen ohne Rechtsverbindlichkeit informieren. Transluzenz bezieht sich auf ausgebleichte Version.

UK	Type IV	B 18059
Base fabric		Glass fibre EC 3/4
Coating		PTFE – polytetrafluoroethylene
Total weight (g/m ²)	DIN EN ISO 2286-2	1550
Width (cm)	DIN EN ISO 2286-1	470
Tensile strength (N/5 cm)	DIN 53354	warp/weft 8000/7000
Tear resistance (N)	DIN 53363	warp/weft 500/500
Adhesion (N/5 cm)	DIN 53357	100
Translucency at 550 nm (%)	DIN 5036	11
Flame retardancy	DIN 4102	B1*

Note: Product must not be sewn, but hot-bar welded. *Additional certificates available on request. Subject to change regarding technical upgrades. Values indicated without tolerance levels are nominal values with a tolerance range $\pm 5\%$. All data presented here is given to the best of our current knowledge for guidance purposes and is not legally binding. Translucency refers to bleached version.

F	Type IV	B 18059
Tissu support		Fibre de verre EC 3/4
Enduction de base		PTFE – Polytétrafluoréthylène
Poids total (g/m ²)	DIN EN ISO 2286-2	1550
Largeur (cm)	DIN EN ISO 2286-1	470
Résistance à la eupture (N/5 cm)	DIN 53354	chaîne/trame 8000/7000
Résistance à la déchirure (N)	DIN 53363	chaîne/trame 500/500
Adhésion (N/5 cm)	DIN 53357	100
Translucidité à 550 nm (%)	DIN 5036	11
Réaction au feu	DIN 4102	B1*

Remarque : le produit ne doit pas être cousu mais soudé à l'aide d'une électrode chaude. *D'autres certificats sont disponibles sur demande. Sous réserve de toutes modifications dans le cadre d'améliorations techniques. Les valeurs mentionnées sans tolérance sont des valeurs nominales avec une tolérance de $\pm 5\%$. Les indications correspondent à notre savoir actuel et sont données à titre informatif sans obligation juridique. La translucidité se rapporte à la version blanchie.

ESP	Tipo IV	B 18059
Tejido base		Fibra de vidrio EC 3/4
Revestimiento		PTFE – Politetrafluoretileno
Peso total (g/m ²)	DIN EN ISO 2286-2	1550
Ancho (cm)	DIN EN ISO 2286-1	470
Resistencia a la rotura (N/5 cm)	DIN 53354	urdimbre/trama 8000/7000
Resistencia al desgarro (N)	DIN 53363	urdimbre/trama 500/500
Adherencia (N/5 cm)	DIN 53357	100
Translucidez en 550 nm (%)	DIN 5036	11
Ignifugación	DIN 4102	B1*

Nota: El producto no debe ser cosido, sino soldado con barra caliente. *Otros certificados obtenibles previa petición. Reservado el derecho a realizar modificaciones destinadas al avance técnico. Los valores sin datos de tolerancias obedecen a valores nominales con una tolerancia de $\pm 5\%$. Los datos se corresponden con nuestro estado actual de conocimiento y su finalidad es informar sin vinculación legal. La translucidez hace referencia a la versión blanqueada.



duraskin®

B 18089



**VERSEIDAG-INDUTEX GmbH
Deutschland**

Industriestrasse 56, 47803 Krefeld
Postfach 10 23 13, 47723 Krefeld
Phone +49 2151 876-0
Fax +49 2151 876-291
e-mail duraskin@vsindutex.de

**Office Shanghai
China**

Room 1002, No.333 Jingang Road
Shanghai 201206, P.R. China
Phone/Fax +86 21 5865 2805
Mobile +86 1350 168 5081
e-mail long@duraskin.cn

**VERSEIDAG seemee (U.S.) Inc.
USA**

4 Aspen Drive
Randolph, New Jersey 07869
Phone +1 973 252 1189
Fax +1 973 252 1109
e-mail info@seemeeus.com

**VERSEIDAG-INDUTEX GmbH-MENA
Jordan**

1st Floor – Offices No. (101–103)
219-Al Madina Al Munawara Street
P.O. Box 1909, Amman 11941, Jordan
Phone +962 6 554 5981
Fax +962 6 554 5982
e-mail mbahsh@vsindutex.jo

**VERSEIDAG seemee UK Ltd.
UK**

Collingwood House, Alington Road
Eynesbury, St. Neots
PE19 6YH Cambridgeshire
Phone +44 1480 213700
Fax +44 1480 213609
e-mail info@seemeeuk.com

www.vsindutex.de

Membranen PTFE
Membranes PTFE
Membranes PTFE
Membranas PTFE

DE	Typ III	B 18089
Trägergewebe		Glasfaser EC 3/4
Beschichtung		PTFE – Polytetrafluorethylen
Flächengewicht (g/m ²)	DIN EN ISO 2286-2	1150
Breite (cm)	DIN EN ISO 2286-1	470
Höchstzugkraft (N/5 cm)	DIN 53354	Kette/Schuss 7000/6000
Weiterreißkraft (N)	DIN 53363	Kette/Schuss 500/500
Haftung (N/5 cm)	DIN 53357	80
Transluzenz bei 550 nm (%)	DIN 5036	14
Brandverhalten	DIN 4102	B1*

Hinweis: Produkt ist nicht zu vernähen, sondern mit Heizbalken zu verschweißen. *Weitere Zertifikate erhältlich auf Anfrage. Änderungen, die dem technischen Fortschritt dienen, behalten wir uns vor. Werte ohne Toleranzangaben sind Nennwerte mit einer Toleranz von $\pm 5\%$. Die Angaben entsprechen unserem heutigen Kenntnisstand und sollen ohne Rechtsverbindlichkeit informieren. Transluzenz bezieht sich auf ausgebleichte Version.

UK	Type III	B 18089
Base fabric		Glass fibre EC 3/4
Coating		PTFE – polytetrafluoroethylene
Total weight (g/m ²)	DIN EN ISO 2286-2	1150
Width (cm)	DIN EN ISO 2286-1	470
Tensile strength (N/5 cm)	DIN 53354	warp/weft 7000/6000
Tear resistance (N)	DIN 53363	warp/weft 500/500
Adhesion (N/5 cm)	DIN 53357	80
Translucency at 550 nm (%)	DIN 5036	14
Flame retardancy	DIN 4102	B1*

Note: Product must not be sewn, but hot-bar welded. *Additional certificates available on request. Subject to change regarding technical upgrades. Values indicated without tolerance levels are nominal values with a tolerance range $\pm 5\%$. All data presented here is given to the best of our current knowledge for guidance purposes and is not legally binding. Translucency refers to bleached version.

F	Type III	B 18089
Tissu support		Fibre de verre EC 3/4
Enduction de base		PTFE – Polytétrafluoréthylène
Poids total (g/m ²)	DIN EN ISO 2286-2	1150
Largeur (cm)	DIN EN ISO 2286-1	470
Résistance à la rupture (N/5 cm)	DIN 53354	chaîne/trame 7000/6000
Résistance à la déchirure (N)	DIN 53363	chaîne/trame 500/500
Adhésion (N/5 cm)	DIN 53357	80
Translucidité à 550 nm (%)	DIN 5036	14
Réaction au feu	DIN 4102	B1*

Remarque : le produit ne doit pas être cousu mais soudé à l'aide d'une électrode chaude. *D'autres certificats sont disponibles sur demande. Sous réserve de toutes modifications dans le cadre d'améliorations techniques. Les valeurs mentionnées sans tolérance sont des valeurs nominales avec une tolérance de $\pm 5\%$. Les indications correspondent à notre savoir actuel et sont données à titre informatif sans obligation juridique. La translucidité se rapporte à la version blanchie.

ESP	Tipo III	B 18089
Tejido base		Fibra de vidrio EC 3/4
Revestimiento		PTFE – Politetrafluoretileno
Peso total (g/m ²)	DIN EN ISO 2286-2	1150
Ancho (cm)	DIN EN ISO 2286-1	470
Resistencia a la rotura (N/5 cm)	DIN 53354	urdimbre/trama 7000/6000
Resistencia al desgarro (N)	DIN 53363	urdimbre/trama 500/500
Adherencia (N/5 cm)	DIN 53357	80
Translucidez en 550 nm (%)	DIN 5036	14
Ignifugación	DIN 4102	B1*

Nota: El producto no debe ser cosido, sino soldado con barra caliente. *Otros certificados obtenibles previa petición. Reservado el derecho a realizar modificaciones destinadas al avance técnico. Los valores sin datos de tolerancias obedecen a valores nominales con una tolerancia de $\pm 5\%$. Los datos se corresponden con nuestro estado actual de conocimiento y su finalidad es informar sin vinculación legal. La translucidez hace referencia a la versión blanqueada.



- TRL (translucent)
- Matt or gloss
- Unlimited colour range
- Bi-colour / Metallic & blackout
- Perforated
- Aero coating
- Highly translucent up to 41%
- Blocks out harmful UV light
- Fire resistant
- Temperature range -50°C / +200°C
- Long life span 25 years +
- Weatherproof & hydrophobic
- Flexible & crease resistant
- Non toxic & PVC free
- Recyclable and sustainable



Think Green
Think Atex

APPLICATIONS		TYPE I		
Atex 3000 TRL - A popular fabric for architects combining excellent tensile strength in conjunction with high translucency for interior or external applications. Perfect for light weight tensile membrane structures and shade sails.				
BASE FABRIC				
Yarn		Glass-fibre	100%	
Weight			340 (g/m²)	DIN EN 5384
Weave style			Plain	
COATED FABRIC		WITH ANTI-WICK TREATMENT		
Coating		Clear Silicone Elastomer	100%	
Tensile strength	Warp Weft	> 4000 (N/5cm) > 3900 (N/5cm)	80 (kN/m) 78 (kN/m)	ISO 1421 ISO 1421
Trapezoidal tear	Warp Weft		> 190N > 190N	
Crease resistance			> 92%	ASTM D4851
Total weight			605 (g/m²)	DIN EN 5384
Thickness			0.45 mm	
Standard Widths			2000/2500/3000 mm	
Bi-Axial Mechanical properties			Available on request	
Acoustic attenuation			Available on request	
OPTICAL VALUES		Solar	Standard D65	
Transmission		38.0%	41.0%	DIN EN 410
Reflection		44.0%	41.0%	DIN EN 410
Absorption		17.0%	18.0%	DIN EN 410
FABRICATION				
Sewing (PTFE yarn) Welding (silicone tape)*		Tensile > 2000 (N/5cm)	Peel 180° > 150 (N/5cm)	
CHARACTERISTICS				
Temperature Range			-50° to + 200°C	
Capillary Rise		with Anti-wick treatment	<5 (mm/24h)	DIN 53 925
FIRE RATING				
UK DE			Class 0 B1	BS 476:Part 6:1989,Part 7:1997 DIN 4102

* depending on equipment, must be in accordance with specified adhesive tape grade and coordinated parameters.
(Company may change these specifications from time to time subject to a programme of continuous improvement.)
This data sheet is for guidance only.

Valmiera Glass UK Ltd

Sherborne, Dorset, DT9 3RB, England

Tel: +44 1935 813 722 Fax: +44 1935 811 822 Email: atex@valmiera-glass.com

www.atex-membranes.com

Regional Atex sales offices in: Germany, Italy, India, Australia, France, Brazil



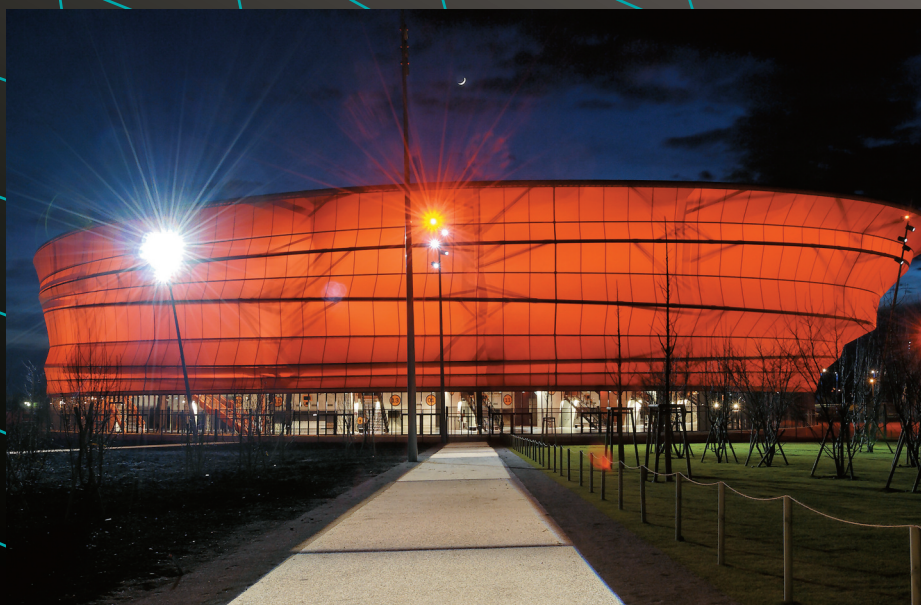
VALMIERA GLASS®



INDUSTRIAL FABRICS
Association International



- TRL (translucent)
- Matt or gloss
- Unlimited colour range
- Bi-colour / Metallic
- Blackout
- Aero coating
- Highly translucent up to 21%
- Blocks out harmful UV light
- Fire resistant
- Temperature range -50°C / +200°C
- Long life span 25 years +
- Weatherproof & hydrophobic
- Flexible & crease resistant
- Non toxic & PVC free
- Recyclable and sustainable



Think Green
Think Atex

APPLICATIONS		TYPE III		
Atex 5000 TRL - A high strength textile adapted for large scale tensile membrane structures. This mid-weight fabric offers outstanding weather protection.				
BASE FABRIC				
Yarn		Glass-fibre	100%	
Weight			685 (g/m²)	DIN EN 5384
Weave style			Plain	
COATED FABRIC		WITH ANTI-WICK TREATMENT		
Coating		Clear Silicone Elastomer	100%	
Tensile strength	Warp Weft	> 6500 (N/5cm) > 6000 (N/5cm)	130 (kN/m) 120 (kN/m)	ISO 1421 ISO 1421
Trapezoidal tear	Warp Weft		> 550N > 550N	
Crease resistance			> 99%	ASTM D4851
Total weight			1165 (g/m²)	DIN EN 5384
Thickness			0.80 mm	
Standard Widths			2000/2500/3000 mm	
Bi-Axial Mechanical properties			Available on request	
Acoustic attenuation			Available on request	
OPTICAL VALUES		Solar	Standard D65	
Transmission		18.5%	21.0%	DIN EN 410
Reflection		68.5%	75.0%	DIN EN 410
Absorption		13.0%	4.0%	DIN EN 410
FABRICATION				
Sewing (PTFE yarn) Welding (silicone tape)*		Tensile > 4000 (N/5cm)	Peel 180° > 150 (N/5cm)	
CHARACTERISTICS				
Temperature Range			-50° to + 200°C	
Capillary Rise		with Anti-wick treatment	<5 (mm/24h)	DIN 53 925
FIRE RATING				
UK DE			Class 0 B1	BS 476:Part 6:1989,Part 7:1997 DIN 4102

* depending on equipment, must be in accordance with specified adhesive tape grade and coordinated parameters.
(Company may change these specifications from time to time subject to a programme of continuous improvement.)
This data sheet is for guidance only.

Valmiera Glass UK Ltd

Sherborne, Dorset, DT9 3RB, England

Tel: +44 1935 813 722 Fax: +44 1935 811 822 Email: atex@valmiera-glass.com

www.atex-membranes.com

Regional Atex sales offices in: Germany, Italy, India, Australia, France, Brazil



VALMIERA GLASS®



INDUSTRIAL FABRICS
Association International



A. 2. Appendix B: Conference Paper: A Predictive model for the design of functional textiles

A PREDICTIVE MODEL FOR THE DESIGN OF FUNCTIONAL TEXTILES

STRUCTURAL MEMBRANES 2013

C.N.ILIFFE*, B.N.BRIDGENS* AND P.D.GOSLING*

* School of Civil Engineering and Geosciences
University of Newcastle upon Tyne
Newcastle upon Tyne, NE1 7RU, UK
Email: ben.bridgens@ncl.ac.uk, web page: <http://www.ncl.ac.uk/ceg/>

Key words: Predictive model, material design, woven fabric, textile, biaxial, yarn geometry, composite, fabric.

Summary: This report proposes a method for the design of a fabric for specified mechanical properties at multiple biaxial-stress states.

1 INTRODUCTION

Functional textiles have a wide variety of uses including large scale roof structures ^[1], medical applications ^[2], and as reinforcement for composite materials. Functional textiles are typically manufactured based on simplified engineering requirements (e.g. weight and uniaxial strength), with other properties (such as detailed analysis of stiffness) determined retrospectively through physical testing. The work presented here demonstrates a methodology for the design of bespoke functional textiles to meet detailed engineering requirements, with the focus on the biaxial response of flexible coated woven fabrics. The method employed uses a semi-analytical optimisation routine to determine the optimum fabric geometry and constituent material properties for detailed material stiffness requirements.

Previously developed mechanical ‘unit cell’ models have been shown to provide a good prediction of the response of architectural plain-weave fabrics under biaxial load, and have therefore formed the basis of the work ^[3, 4]. The derivatives of the unit cell equilibrium equations have been determined and this allows the fabric parameters to be optimised for a detailed set of biaxial and shear stiffness requirements at different stress levels. Initial validation using the model to design feasible, known fabrics has shown good results and demonstrated the potential utility of this approach.

2 SCOPE AND METHODOLOGY

2.1 Biaxial response

Coated architectural fabrics are employed in biaxial stress states and have “*negligible bending or compression stiffness*” ^[5] meaning loads are resisted through tension, and as such

the model was required to work with biaxial input and output parameters. Therefore the response characteristics under biaxial load are considered to be the Young's moduli in both warp and weft directions (E_{11} and E_{22}) and the Poisons ratios of the fabric (ν_{12} and ν_{21}).

Whilst shear response under biaxial load “*is crucial in order to build double-curvature tensioned structures*”^[6] the shear modulus (G) is not considered in the current version of this model as the response has been found to be dominated by the coating stiffness, currently modelled as linear. It is proposed that later versions of this model will include a module for the consideration of shear effects.

2.1 Sawtooth modelling

The sawtooth model developed by Menges and Meffert^[7] and further developed and used by Bridgens^[3, 4] was the basis of the work. It was chosen as it allowed for the possibility of truly predictive design, as the equations contain no factors that need to be derived through testing, and the equations themselves lend themselves to differentiation.

The method considers a unit cell of fabric as shown in Figure 3, and idealises this as a set of two orthotropic yarns that are perpendicular, as shown in Figure 1 and Figure 2.

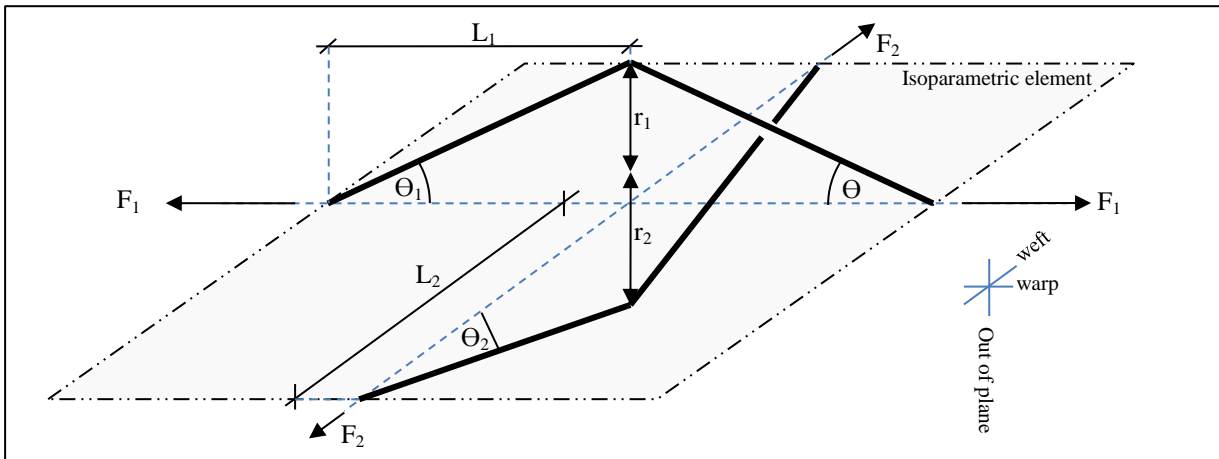


Figure 1: Fundamentals of the full sawtooth model with an Isoparametric Element representing the coating

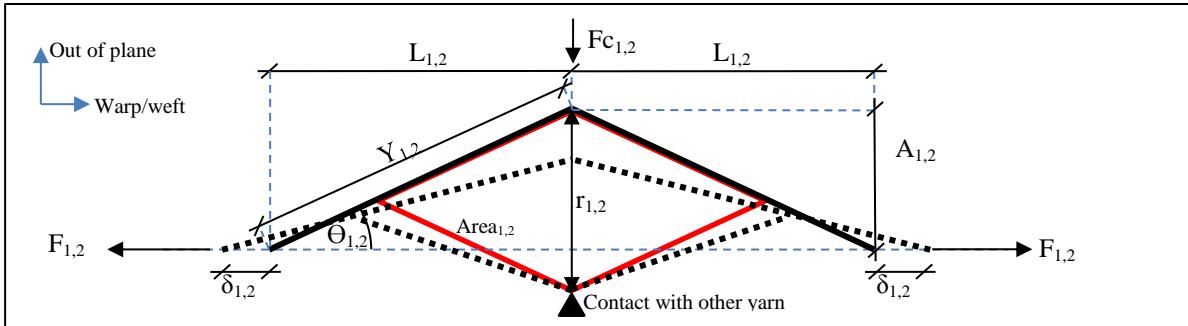
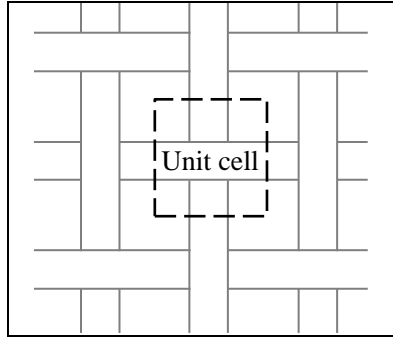


Figure 2: Further definitions within the unit cell

Figure 3: Unit Cell representation (Plain Weave)^[3, 4]

Unlike the previously developed models the coating is represented by a single Isoparametric Plane Stress element as described by Cook, Malkus and Plesha^[8]. This change was made in preparation for the analysis of shear response and the possibility of non-perpendicular geometry. The equations defining the response of the unit cell are therefore published as:

$$F_{k1,2} = 2 \cdot L_{2,1} \left(\frac{E_k}{1 - \nu_k^2} \right) (\varepsilon_{1,2} + \nu_k \varepsilon_{2,1}) (1 + \varepsilon_{2,1}) \quad , \quad (1)$$

$$Y'_{1,2} = Y_{1,2} \left[1 + \frac{F_{y1,2}}{2E_{y1,2}L'_{2,1}} \right] \quad ,$$

$$Area_{1,2} = 2w_{1,2}r_{1,2} \quad ,$$

$$w'_{1,2} = \frac{w_{1,2}}{L_{2,1}} L'_{2,1} \quad ,$$

$$r'_{1,2} = \frac{Area_{1,2}}{2 * w'_{1,2}} \quad ,$$

[3, 4]

constrained by the following equations which ensure geometric continuity and force equilibrium:

$$(r_1 + r_2) = (A_1 + A_2) \quad , \quad (2)$$

$$F_{c1} = F_{c2} \quad ,$$

$$F_{1,2} = F_{y1,2} \cos \theta'_{1,2} + F_{k1,2} \quad ,$$

[3, 4]

where the subscripts 1 and 2 refer to the warp and weft directions respectively. The subscripts k and y refer to the coating and yarn respectively. The apostrophe refers to a value after deformation. Other terms included are the yarn radius (r), the yarn length (L) (1/4 the yarn wavelength), force (F), yarn amplitudes (A), yarn widths (w) (1/2 the yarn width), the yarn cross-sectional area (Area), Young's Moduli (E), and yarn length (Y) (includes out-of plane distance).

3 RESULTS AND DISCUSSION

3.1 Construction of defining equations

Once the equations defining the unit cell are available it is possible to calculate the response characteristics of the fabric numerically, employing a finite difference method.

However, numerical perturbation does not lend itself to optimisation, which is necessary to design a bespoke fabric. To produce equations that can be used in conjunction with optimisation routines it is necessary to find the derivatives $\frac{dF_{1,2}}{d\varepsilon_{1,2}}$ (for $E_{11,22}$) and $\frac{dF_{1,2}}{d\varepsilon_{2,1}}$ (for $E_{12,21}$). The derivative $\frac{dF_{1,2}}{d\varepsilon_{1,2}}$ refers to the Young's modulus of the unit cell, and must be converted to the value for the whole fabric as shown in equation 3. The derivative $\frac{dF_{1,2}}{d\varepsilon_{2,1}}$ is needed to produce the Poisson's ratios, as shown in equation 4.

$$E_{11,22}^{unit\ cell} = E_{11,22}^{global} \times L_{2,1} \times 2 \quad (3)$$

$$-\frac{v_{12}}{E_{11}} = \frac{1}{E_{12}} \quad (4)$$

[1]

To find the derivatives the applied force was determined in terms of the unit cell variables, and strain as shown in equation 5. Equations 6 through 9 are then necessary to calculate further derivatives.

$$F_{1,2} = \frac{(F_{2,1} - F_{k2,1}) \left((r'_{1,2} + r'_{2,2}) - L_{1,2}(1 + \varepsilon_{1,2}) \tan \theta'_{1,2} \right)}{L_{2,1}(1 + \varepsilon_{2,1}) \tan \theta'_{1,2}} + F_{k1,2} \quad (5)$$

$$F_{k1,2} = 2 \cdot L_{2,1} \left(\frac{E_k}{1 - v_k^2} \right) (\varepsilon_{1,2} + v_k \varepsilon_{2,1})(1 + \varepsilon_{2,1}) \quad (6)$$

$$r'_{1,2} = \frac{r_{1,2}}{(1 + \varepsilon_{2,1})} \quad (7)$$

$$\theta'_{2,1} = \cos^{-1} \left((1 + \varepsilon_{2,1}) \cos \theta_{2,1} - \left(\frac{(F_{2,1} - F_{k2,1})}{2E_{2,1}L_{1,2}(1 + \varepsilon_{1,2})} \right) \right) \quad (8)$$

$$\theta'_{1,2} = \tan^{-1} \left(\frac{(r'_{1,2} + r'_{2,2}) - L_{2,1}(1 + \varepsilon_{2,1}) \tan \theta'_{2,1}}{L_{1,2}(1 + \varepsilon_{1,2})} \right) \quad (9)$$

To calculate the full derivatives it is necessary to find the partial derivatives for all the variables. There are numerous variables that are inter-related with relation to the defining equations expressed earlier (equations 1 and 2). As such equations 10 and 11 represent the

calculation that needs to be performed to produce the required derivatives.

$$\frac{dF_{1,2}}{d\varepsilon_{1,2}} = \frac{\partial F_{1,2}}{\partial \varepsilon_{1,2}} + \frac{\partial F_{1,2}}{\partial \theta'_{1,2}} \cdot \frac{\partial \theta'_{1,2}}{\partial \varepsilon_{1,2}} + \frac{\partial F_{1,2}}{\partial r'_{1,2}} \cdot \frac{\partial r'_{1,2}}{\partial \varepsilon_{1,2}} + \frac{\partial F_{1,2}}{\partial r'_{2,1}} \cdot \frac{\partial r'_{2,1}}{\partial \varepsilon_{1,2}} + \frac{\partial F_{1,2}}{\partial \varepsilon_{2,1}} \cdot \frac{\partial \varepsilon_{2,1}}{\partial \varepsilon_{1,2}} + \frac{\partial F_{1,2}}{\partial F_{k1,2}} \cdot \frac{\partial F_{k1,2}}{\partial \varepsilon_{1,2}} + \frac{\partial F_{1,2}}{\partial F_{k2,1}} \cdot \frac{\partial F_{k2,1}}{\partial \varepsilon_{1,2}} \quad (10)$$

$$\frac{dF_{1,2}}{d\varepsilon_{2,1}} = \frac{\partial F_{1,2}}{\partial \varepsilon_{2,1}} + \frac{\partial F_{1,2}}{\partial \theta'_{1,2}} \cdot \frac{\partial \theta'_{1,2}}{\partial \varepsilon_{2,1}} + \frac{\partial F_{1,2}}{\partial r'_{1,2}} \cdot \frac{\partial r'_{1,2}}{\partial \varepsilon_{2,1}} + \frac{\partial F_{1,2}}{\partial r'_{2,1}} \cdot \frac{\partial r'_{2,1}}{\partial \varepsilon_{2,1}} + \frac{\partial F_{1,2}}{\partial \varepsilon_{1,2}} \cdot \frac{\partial \varepsilon_{1,2}}{\partial \varepsilon_{2,1}} + \frac{\partial F_{1,2}}{\partial F_{k1,2}} \cdot \frac{\partial F_{k1,2}}{\partial \varepsilon_{2,1}} + \frac{\partial F_{1,2}}{\partial F_{k2,1}} \cdot \frac{\partial F_{k2,1}}{\partial \varepsilon_{2,1}} \quad (11)$$

Unfortunately it can be shown that due to the interdependence of the variables it is not possible to produce a fully analytical answer to equations 10 and 11. To produce useable equations one value must be calculated iteratively, as shown in equation 12. This must be calculated independently using the equilibrium model each time a new value is required.

$$\frac{\delta \varepsilon_{1,2}}{\delta \varepsilon_{2,1}} = \frac{\Delta \varepsilon_{1,2}}{\Delta \varepsilon_{2,1}} \quad (12)$$

Whilst this is now a semi-analytical method the equations derived do still allow for optimisation to be used to design a bespoke fabric.

3.2 The method of optimisation

MATLAB^[9] was used to produce an optimisation script for the minimisation of the defining equations. Internal functions were used to optimise the equations for a set of targets produced. The optimisation methodology is briefly summarised in Figure 4. The method initially uses a pattern search algorithm to refine the search ‘area’, and then uses an internal MATLAB search routine to find the “*minimum of [a] constrained nonlinear multivariable function*”^[10]. If no perfect solution can be found then the script implements a gradually varying allowance of variation from the targets to allow a solution to be found. This could be changed to allow for accurate optimisation for some important targets, and ‘as close as possible’ optimisation for other targets of less significance to the designer.

Using a function that allows for multiple constraints is used to incorporate the constraint equations (equations 2). If no perfect solution is found then bounds are placed on the targets, and these are allowed to vary by a percentage. This allows the script to find results where no realistic solution would be possible.

Five sets of targets are used in the current model to demonstrate how the method can be used to design for multiple material properties for a single fabric at different loads. More targets could be implemented, however the current number demonstrates the method’s utility without making any solution too difficult, or computationally expensive to find. The ‘Shear Module’ shown is currently in development.

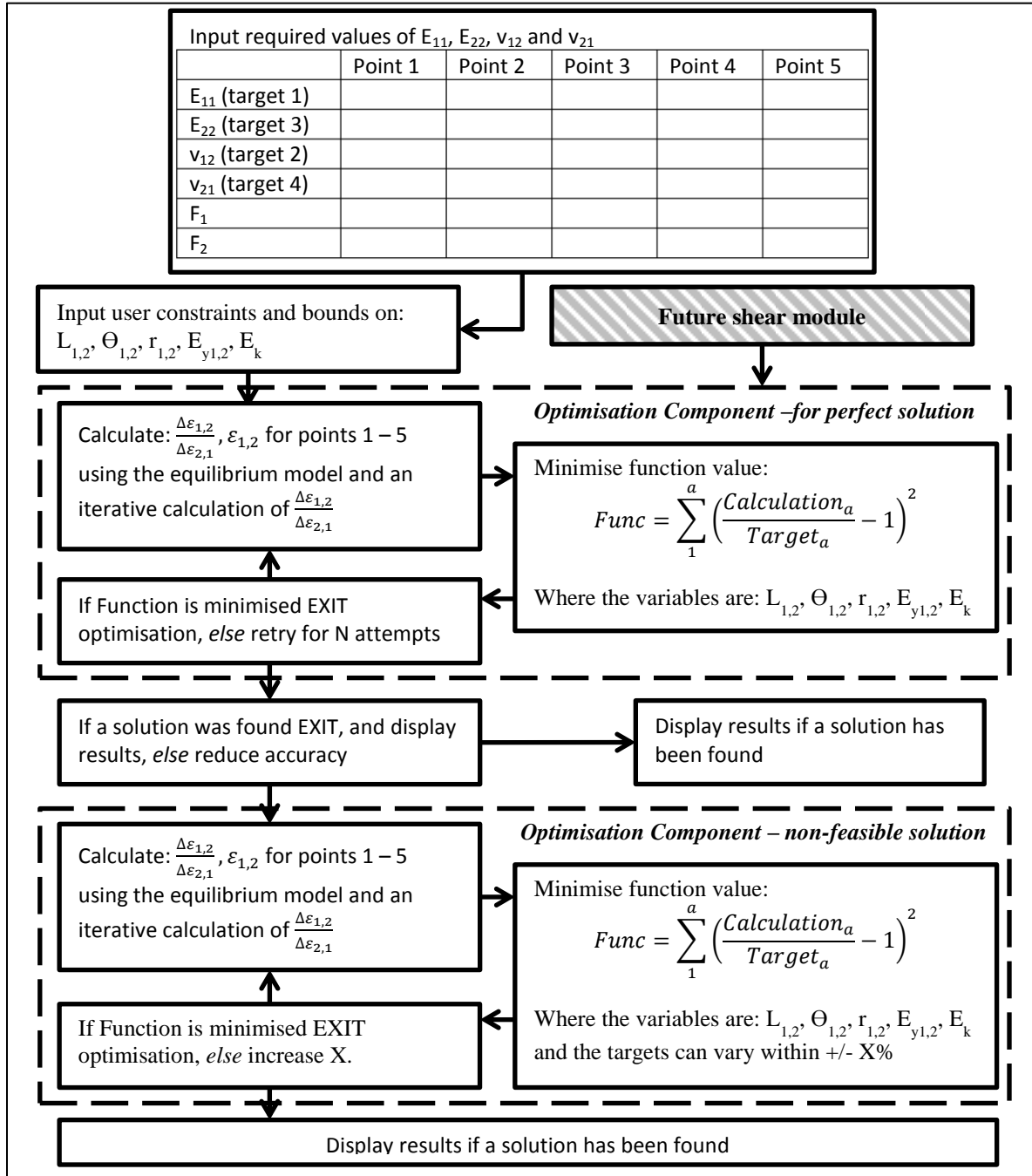


Figure 4: Flow chart to describe the optimisation process

3.3 Results for known feasible targets

To demonstrate the functionality of both the method of optimisation and the validity of the equations used an optimisation for a set of targets that were known to be feasible was performed.

The feasible targets were produced with the equilibrium model using a central finite difference method from the geometry shown in Table 1. The results of this finite difference method are shown in Table 2.

Table 1: Geometry used to find feasible targets and resultant optimised geometry

Variable	Geometry from which targets are calculated	Optimised geometry
A_1 (mm)	0.069	0.071
A_2 (mm)	0.207	0.190
Θ_1 (Rad)	0.106	0.116
Θ_2 (Rad)	0.189	0.183
L_1 (mm)	0.645	0.605
L_2 (mm)	1.082	1.022
r_1 (mm)	0.162	0.152
r_2 (mm)	0.114	0.107
w_1 (mm)	0.786	0.824
w_2 (mm)	0.673	0.920
E_1 (kN/m)	860	859
E_2 (kN/m)	710	703
E_k (kN/m)	30	33
v_k	0.3	0.3

Table 2: Feasible targets found at the applied loads P1 and P2.

	Point 1	Point 2	Point 3	Point 4	Point 5
E_{11} (target 1) (kN/m)	514	662	602	377	777
E_{22} (target 3) (kN/m)	444	554	510	551	484
v_{12} (target 2)	0.434	0.288	0.344	0.317	0.261
v_{21} (target 4)	0.374	0.241	0.291	0.431	0.180
P_1 (kN/m)	10	20	15	10	20
P_2 (kN/m)	10	20	15	20	10

The results of this are as expected, a near perfect solution is found quickly suggesting the equations appear to correlate well to the sawtooth method which is known to correlate well with the response of real fabrics. It should be noted that the start point of the optimisation was not the geometry used to find the targets; this ensured that the method was in fact finding a solution, and not succeeding having been given the correct geometry.

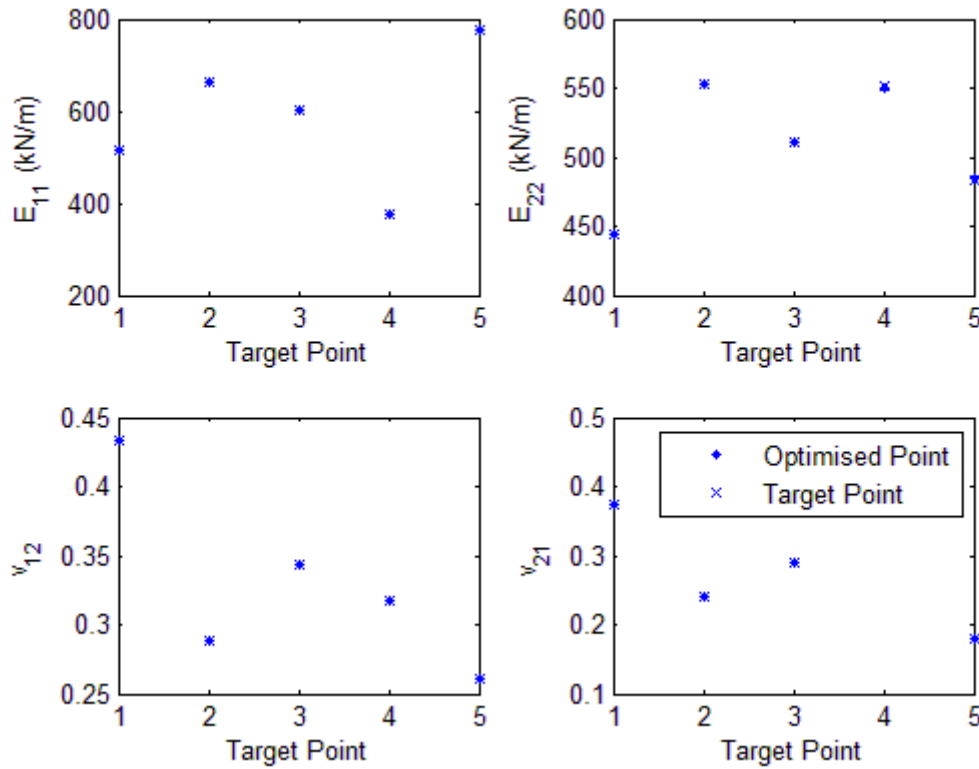


Figure 5: Results of the optimisation for the feasible solution

The optimisation for the feasible values of stiffness and poisons ratio produces good results (Figure 5). Target points 4 and 5 in the plot of E_{22} results show some slight deviation from the targets. In reality this small error, whilst observable in the figure, equates to a difference of 0.89kN/m and 0.90kN/m respectively. This is as a result of the slight deviation from the original geometry that was found. A higher accuracy requirement on the solver may produce more accurate results, but would be more computationally expensive, taking longer.

3.4 Comparison with measured fabric parameters

Target values of stiffness and poisons ratio were calculated from biaxial test data produced from a fabric with the geometry set out in Table 1. The targets are shown in Table 3, along with the numerical results of the optimisation. The points to be analysed were chosen from areas on the response surface that did not include flattening in one of the principle directions. This flattening leads to unexpectedly large or small results when analytical or numerical derivatives of the surface are calculated to give targets. Therefore similar targets to those used in the previous test could not be used in this instance.

Table 3: Measured targets found at the applied loads P1 and P2

		Point 1	Point 2	Point 3	Point 4	Point 5
Targets	E_{11} (kN/m)	700	799	794	668	596
	E_{22} (kN/m)	748	875	799	681	621
	v_{12}	0.218	0.170	0.197	0.114	0.138
	v_{21}	0.305	0.288	0.234	0.379	0.412
Results	E_{11} (kN/m)	552	652	604	611	591
	E_{22} (kN/m)	676	811	746	837	829
	v_{12}	0.248	0.153	0.196	0.145	0.152
	v_{21}	0.331	0.203	0.261	0.204	0.220
% differences	E_{11}	-21.1	-18.5	-24.0	-8.5	-0.8
	E_{22}	-9.6	-7.3	-0.5	22.9	33.4
	v_{12}	13.9	-10.1	-6.6	27.0	10.1
	v_{21}	8.6	-29.7	11.6	-46.3	-46.5
Applied Load	P_1 (kN/m)	10	20	14	12	10
	P_2 (kN/m)	10	20	14	16	14

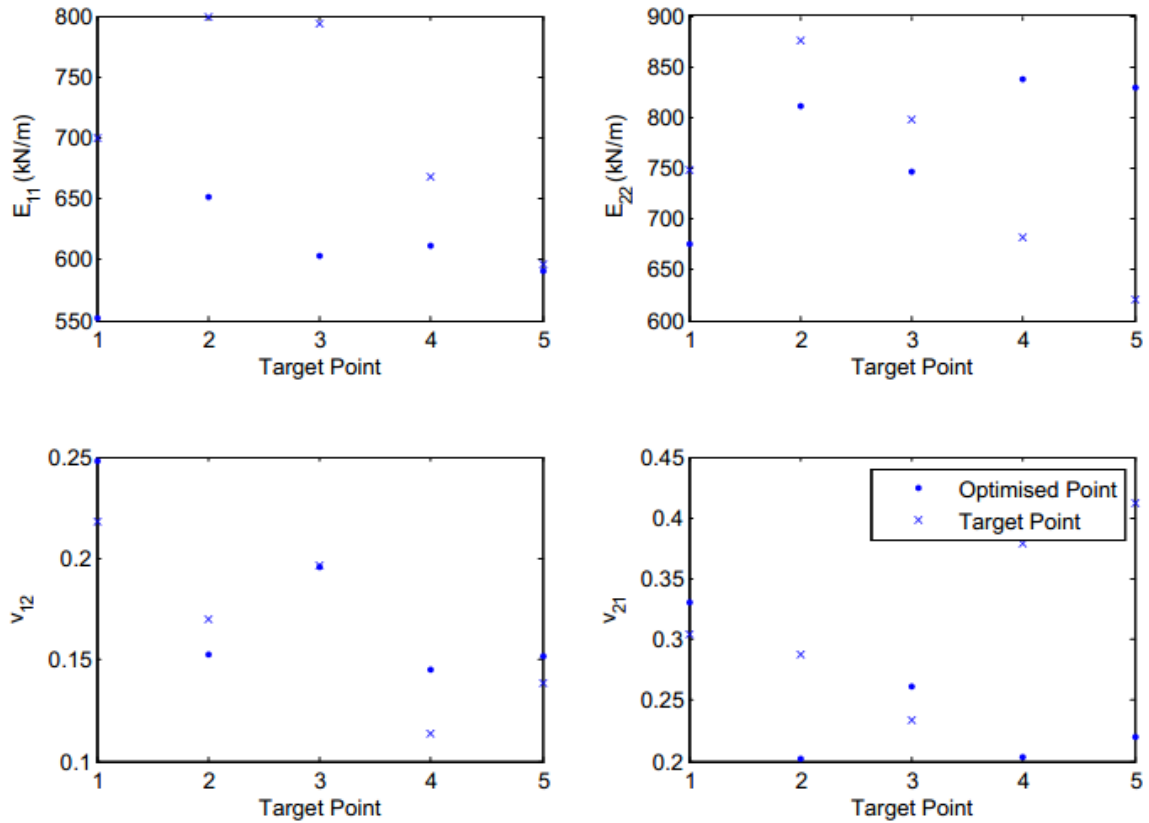


Figure 6: Results of the optimisation for the measured targets

No perfect solution could be found through the optimisation for the measured targets (Figure 6). Although no perfect solution could be found Figure 6 does show how close the

solutions found were to the targets. Table 4 shows the geometric solution found against the geometry of the original fabric.

Table 4: Optimised geometry for measured targets

Variable	Geometry from which targets are calculated	Optimised geometry
A_1 (mm)	0.069	0.428
A_2 (mm)	0.207	1.861
Θ_1 (Rad)	0.106	0.316
Θ_2 (Rad)	0.189	0.130
L_1 (mm)	0.645	1.039
L_2 (mm)	1.082	0.210
r_1 (mm)	0.162	0.033
r_2 (mm)	0.114	0.334
w_1 (mm)	0.786	0.254
w_2 (mm)	0.673	1.021
E_1 (kN/m)	860	925
E_2 (kN/m)	710	946
E_k (kN/m)	30	19
v_k	0.3	0.3

The optimised geometry is clearly not the same as the geometry of the fabric from which the targets were derived. The original set of targets may be unobtainable for the sawtooth method with the constraints currently placed on the solution. The constraints (maximum and minimum values of geometric properties, and the constraints on the deformation stated in equation 2) currently being used are very broad to encompass extremes of realistic fabrics. These would be further constrained for more specific and realistic designs.

When the targets are allowed to vary slightly (5%) from the initial input targets a far more successful optimisation is performed.

6 DISCUSSION

The sawtooth model provides a reasonable prediction of fabric behaviour with the model's deviation from the mean of the strain range of a real fabric being between 5.3 and 5.9%^[4] (Figure 7).

The method developed offers close correlation between results for feasible targets. This good fidelity was predicted, as the optimisation equations were developed using the sawtooth model, but demonstrates the utility of the method. Therefore the optimisation works by finding the solutions available from all possible response planes of the sawtooth model, and should eventually find a solution for targets that originally existed on this plane. This does, importantly, show that the method being employed to find the targets is working.

The error found in the optimised geometry for the targets measured from biaxial data can be explained by the difference in the response planes of the real fabric and the sawtooth's prediction of that fabric's response. Figure 7 shows the difference in the response planes of sawtooth and the real fabric when a sawtooth model is run using the geometry of the real fabric. These two sets of response planes, whilst similar, are clearly not the same. Over and under prediction of strain will also affect result.

It was unlikely at the outset that the solver would find a solution that perfectly matched the real fabric's geometry. It is also therefore possibly the case that no feasible solution exists for the sawtooth model where the targets stated in Table 3 could be achieved within the constraints placed on the model. Future work will be needed to demonstrate how much inaccuracy is inherent in the process, and therefore must be expected when attempting to design the geometry of 'real' fabrics.

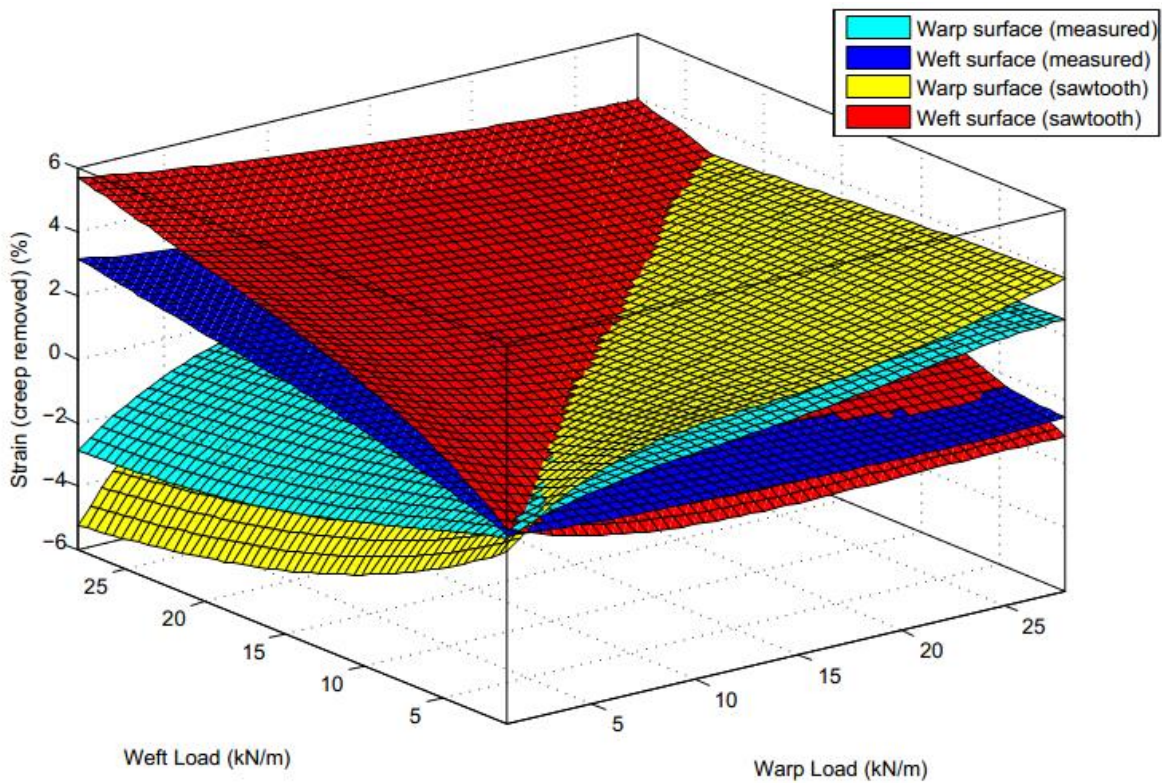


Figure 7: Response surfaces for the sawtooth model and measured response for one geometry

5 CONCLUSIONS

- The accuracy of the optimisation method with regards to known feasible targets derived from the sawtooth model is good.
- The methodology is slower than hoped as the calculation of $\frac{\Delta\epsilon_{1,2}}{\Delta\epsilon_{2,1}}$ must be completed after each iteration.

- The accuracy of the optimisation method with regards measured targets derived from real fabric data is acceptable at this stage of development. The actual accuracy of the optimised geometry for the new targets is unknown as it is not currently possible within the bounds of this work to produce a bespoke fabric to be tested.
- It is possible that for some targets multiple solutions exist and that for others no solutions exist. The latter has been shown through the results of the measured target optimisation, but the former is as of yet unproven.
- Allowing small amounts of variation from the target may drastically improve the model's utility and allow for a Pareto front of possible solutions to be found.

6 FURTHER WORK

Further work is on-going to allow the optimum design of a fabric's shear response characteristics as well as biaxial response to loads. The inherent uncertainty in the manufacturing process, and the discrete nature of some parameters, will also be considered and methods for the calculation of the effect of such variability incorporated into future models. In addition it is necessary to further check the inherent inaccuracy of the model when compared to real results obtained through tests. Other possible implications of the model must be further investigated. And the effect of varying one parameter on the optimised result will also be investigated.

7 REFERENCES

- [1] B. N. Bridgens, P. D. Gosling and M. J. S. Birchall (2004) 'Membrane material behaviour: concepts, practice & developments', *The Structural Engineer*.
- [2] A. Z. Kharazi, M. H. Fathi and F. Bahmany (2010) 'Design of a textile composite bone plate using 3D-finite element method', *Materials & Design*, 31(3), pp. 1468-1474.
- [3] B. N. Bridgens (2005) *Architectural fabric properties : determination, representation & prediction*. University of Newcastle upon Tyne.
- [4] B. N. Bridgens, & Gosling, P. D. (2008) 'A predictive fabric model for membrane structure design', *Textile Composites and Inflatable Structures II*, (8), pp. 35-50.
- [5] B. Bridgens, P. Gosling, C. Patterson, S. Rawson and N. Hove (2009) 'Importance of material properties in fabric structure design and analysis', *Proceedings of the International Association for Shell and Spatial Structures (IASS) Symposium 2009*.
- [6] C. Galliot and R. H. Luchsinger (2010) 'The shear ramp: A new test method for the investigation of coated fabric shear behaviour – Part II: Experimental validation', *Composites Part A: Applied Science and Manufacturing*, 41(12), pp. 1750-1759.
- [7] P. D.-I. G. Menges and D.-I. B. Meffert (1976) 'Mechanical Behaviour of PVC-Coated Polyester Fabrics under Biaxial Stress', *German Plastics*, 66(11).
- [8] R. D. Cook, D. S. Malkus and M. E. Plesha (1989) *Concepts and applications of finite element analysis*. 3rd edn. New York: Wiley.
- [9] Mathworks (2012) *MATLAB and Simulink for Technical Computing*. Available at: <http://www.mathworks.co.uk/> (Accessed: 2012).
- [10] MathWorks (2012) *MATLAB - Product Documentation - R2012b*. Available at: www.Mathworks.co.uk/help/ (Accessed: 03/2012).

A. 3. Appendix C: Further results for optimisation to known feasible targets (§3.7.1)

A.3.1. PVC coated Polyester

Variable	Geometry from which targets are calculated	Optimised geometry (without knowledge of original geometry)	Optimised geometry (with knowledge of original geometry)
Θ_1 (Rad)	0.102	0.102	0.102
Θ_2 (Rad)	0.125	0.125	0.125
L_1 (mm)	0.624	1.112	0.624
L_2 (mm)	0.611	1.088	0.611
r_1 (mm)	0.079	0.140	0.079
r_2 (mm)	0.062	0.111	0.062
E_1 (kN/m)	485	485	485
E_2 (kN/m)	425	425	425
E_k (kN/m)	33	33	33
A_1 (mm)	0.064	0.114	0.064
A_2 (mm)	0.077	0.137	0.077
w_1 (mm)	0.624	1.112	0.624
w_2 (mm)	0.608	1.083	0.608
v_k	0.3	0.3	0.3

Table A-1: Geometry used to find feasible targets and resultant optimised geometry for F702 fabric

	Point 1	Point 2	Point 3	Point 4	Point 5
E_{11} (target 1) (kN/m)	403	465	441	393	479
E_{22} (target 3) (kN/m)	362	414	394	426	352
v_{12} (target 2)	0.26	0.18	0.21	0.18	0.19
v_{21} (target 4)	0.23	0.16	0.18	0.17	0.17
P_1 (kN/m)	10	20	15	10	20
P_2 (kN/m)	10	20	15	20	10
Results without prior knowledge of geometry					
E_{11} (result 1) (kN/m)	403	465	441	393	479
E_{22} (result 3) (kN/m)	362	414	394	426	352
v_{12} (result 2)	0.26	0.18	0.21	0.18	0.19
v_{21} (result 4)	0.23	0.16	0.18	0.17	0.17
Results with prior knowledge of geometry					
E_{11} (result 1) (kN/m)	403	465	441	393	479
E_{22} (result 3) (kN/m)	362	414	394	426	352
v_{12} (result 2)	0.26	0.18	0.21	0.18	0.19
v_{21} (result 4)	0.23	0.16	0.18	0.17	0.17

Table A-2: Targets and resultant properties of a designed F702 fabric

A.3.2. PTFE coated glass-fibre

Variable	Geometry from which targets are calculated	Optimised geometry (without knowledge of original geometry)	Optimised geometry (with knowledge of original geometry)
Θ_1 (Rad)	0.283	0.281	0.283
Θ_2 (Rad)	0.364	0.366	0.364
L_1 (mm)	0.724	1.203	0.724
L_2 (mm)	0.575	0.962	0.575
r_1 (mm)	0.202	0.341	0.202
r_2 (mm)	0.228	0.375	0.228
E_1 (kN/m)	4610	4426	4610
E_2 (kN/m)	4770	5008	4770
E_k (kN/m)	54	54	54
A_1 (mm)	0.210	0.348	0.210
A_2 (mm)	0.219	0.369	0.219
w_1 (mm)	0.529	0.889	0.529
w_2 (mm)	0.784	1.300	0.784
v_k	0.3	0.3	0.3

Table A-3: Geometry used to find feasible targets and resultant optimised geometry for B18059 fabric**A.3.3. Silicon coated glass-fibre**

Variable	Geometry from which targets are calculated	Optimised geometry (without knowledge of original geometry)	Optimised geometry (with knowledge of original geometry)
Θ_1 (Rad)	0.260	0.260	0.260
Θ_2 (Rad)	0.233	0.232	0.233
L_1 (mm)	0.682	1.187	0.682
L_2 (mm)	0.595	1.037	0.595
r_1 (mm)	0.159	0.277	0.159
r_2 (mm)	0.164	0.285	0.164
E_1 (kN/m)	4110	4110	4110
E_2 (kN/m)	6300	6300	6300
E_k (kN/m)	21	21	21
A_1 (mm)	0.182	0.316	0.182
A_2 (mm)	0.141	0.246	0.141
w_1 (mm)	0.671	1.169	0.671
w_2 (mm)	0.614	1.070	0.614
v_k	0.3	0.3	0.3

Table A-4: Geometry used to find feasible targets and resultant optimised geometry for ATEX5000 fabric

A. 4. Appendix D: Additional distributions of fabric geometry

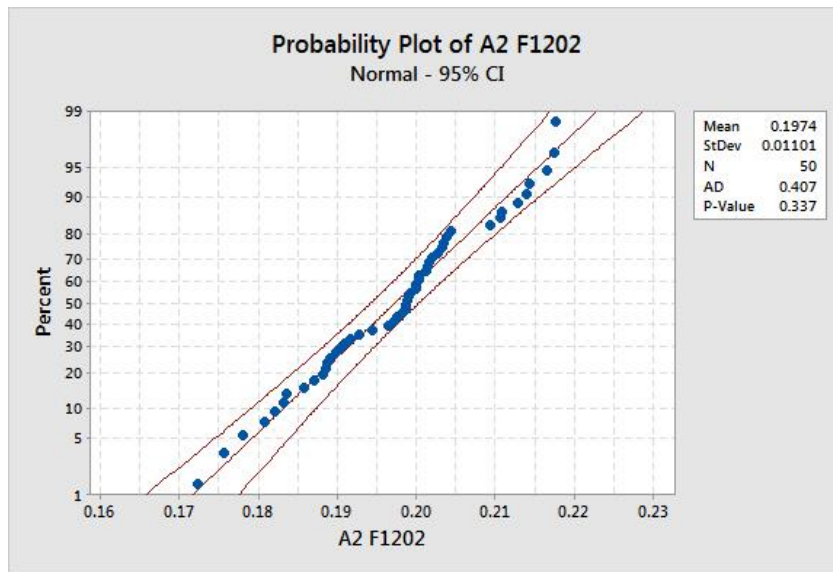


Figure A-1: Probability plot of weft yarn amplitudes for an F1202 fabric

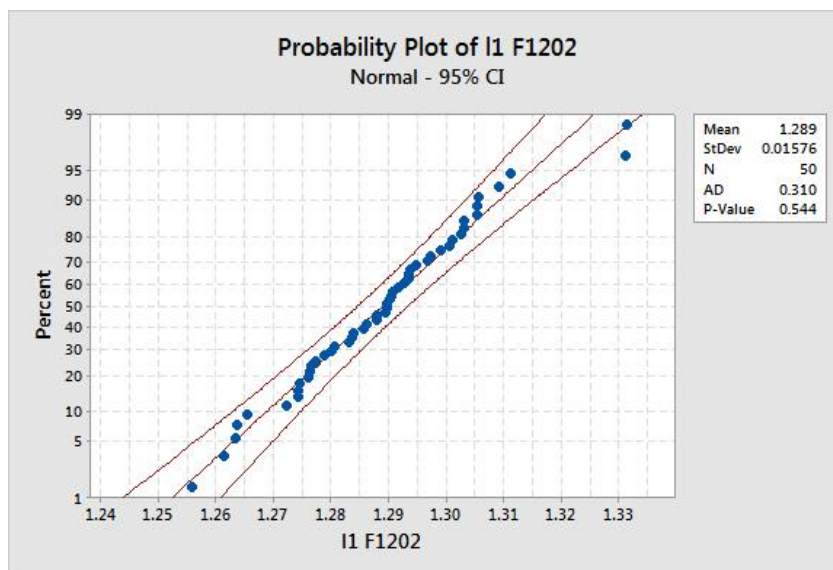


Figure A-2: Probability plot of warp yarn half wavelengths for an F1202 fabric

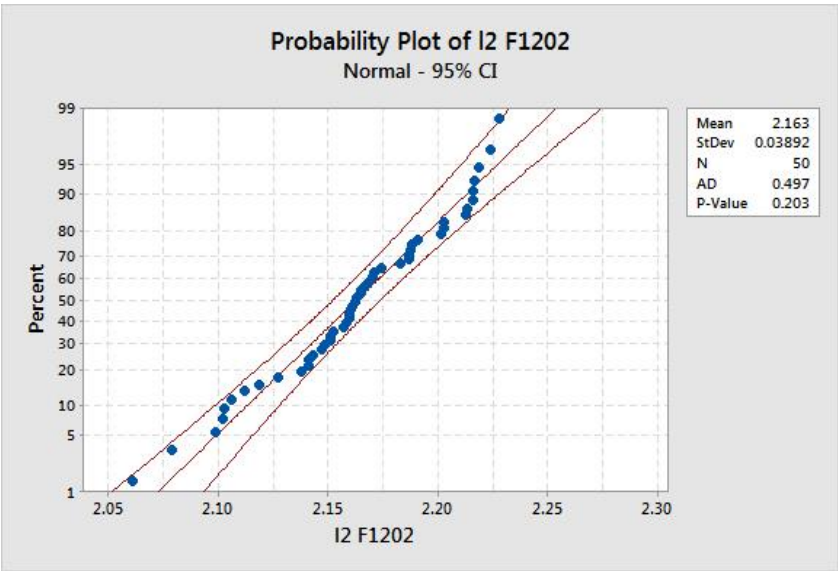


Figure A-3: Probability plot of weft yarn half wavelengths for an F1202 fabric

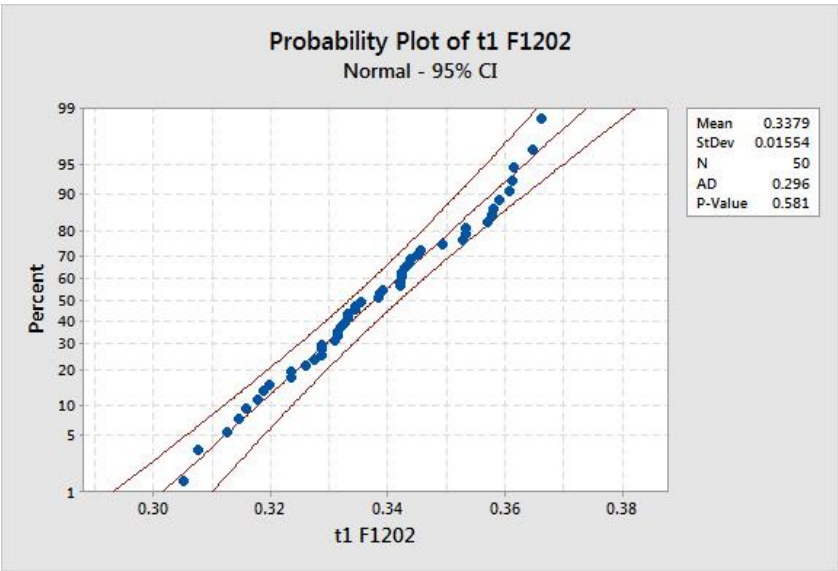


Figure A-4: Probability plot of warp yarn thicknesses for an F1202 fabric

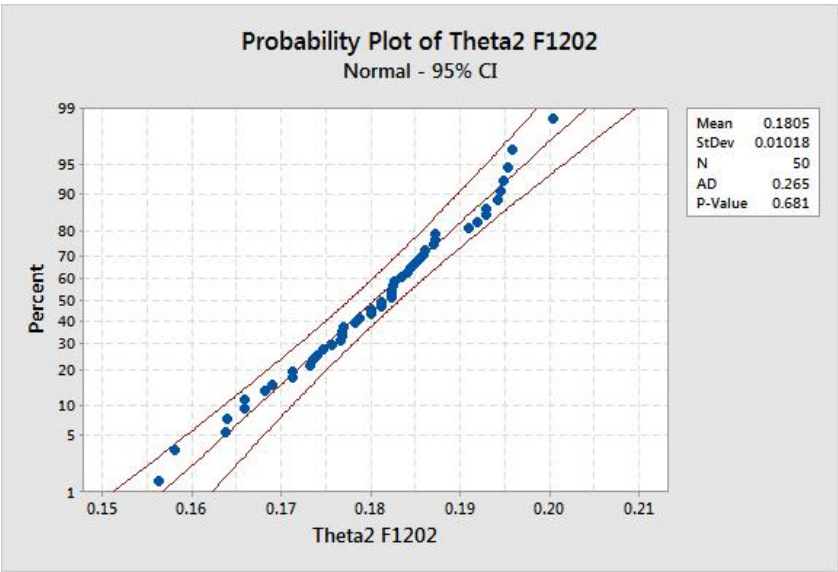


Figure A-5: Probability plot of weft yarn out of plane angles for an F1202 fabric

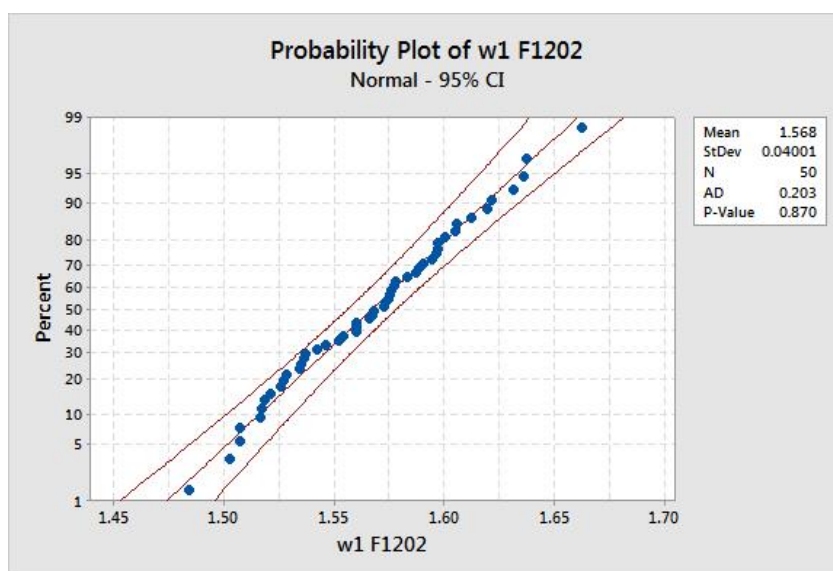


Figure A-6: Probability plot of warp yarn widths for an F1202 fabric

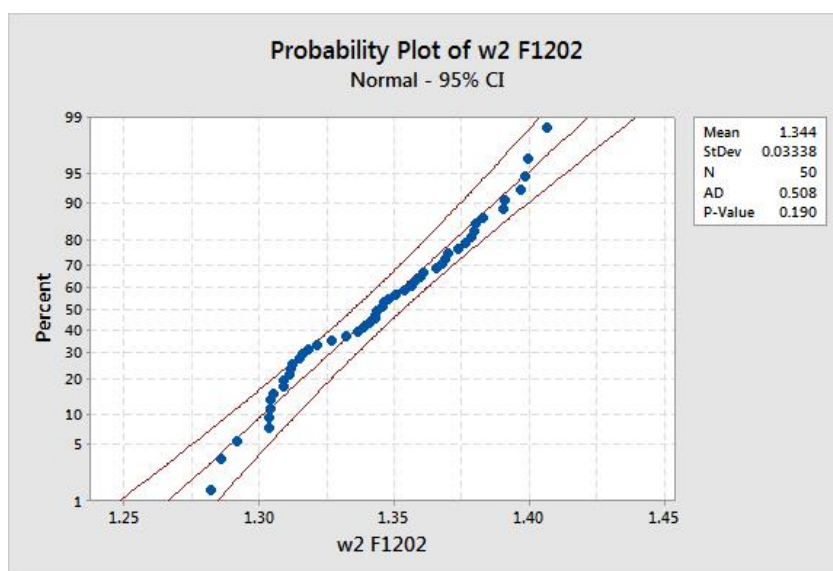
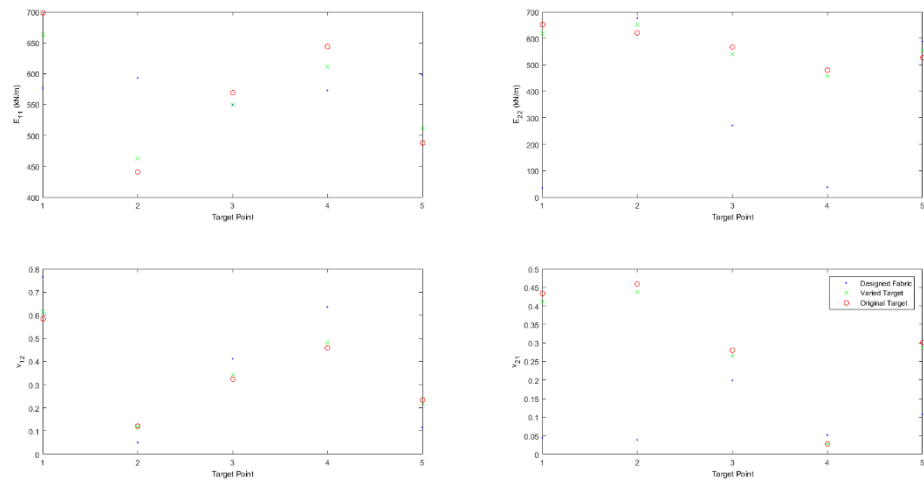


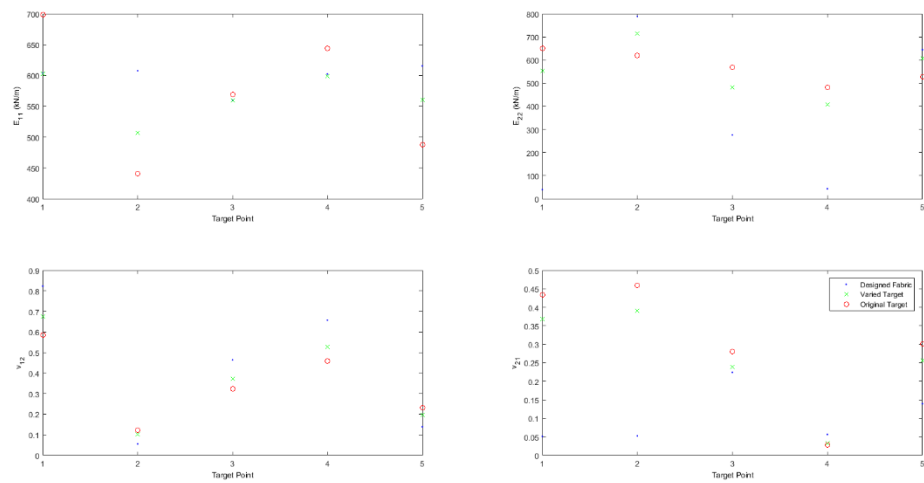
Figure A-7: Probability plot of weft yarn widths for an F1202 fabric

A. 5. Appendix E: Alternative visualisation of fabric design to targets obtained from biaxial test results (§5.3.2)

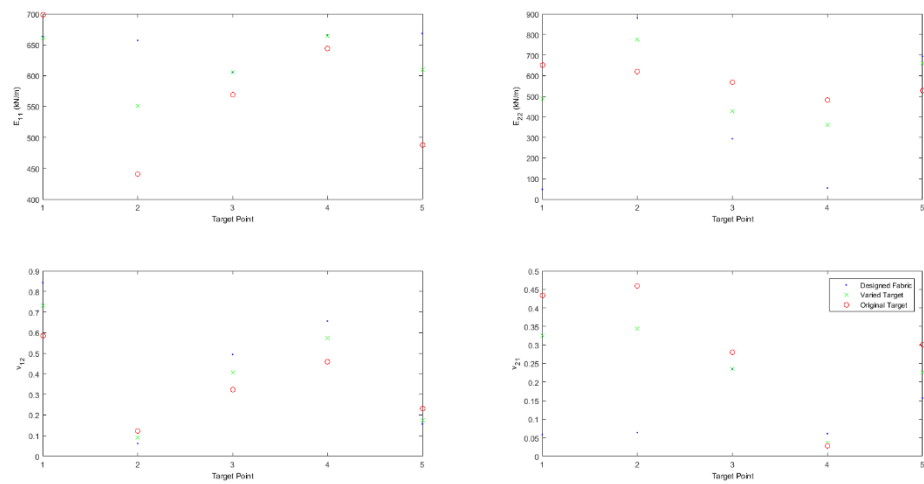
a)



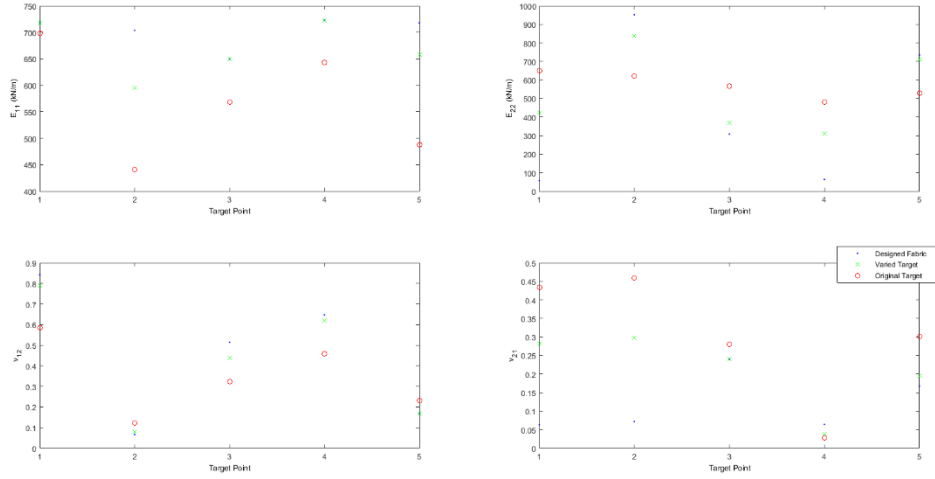
b)



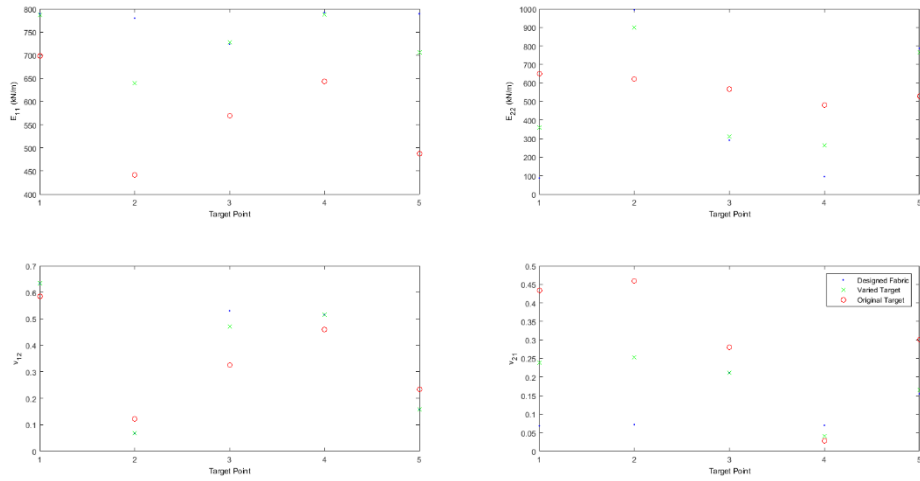
c)



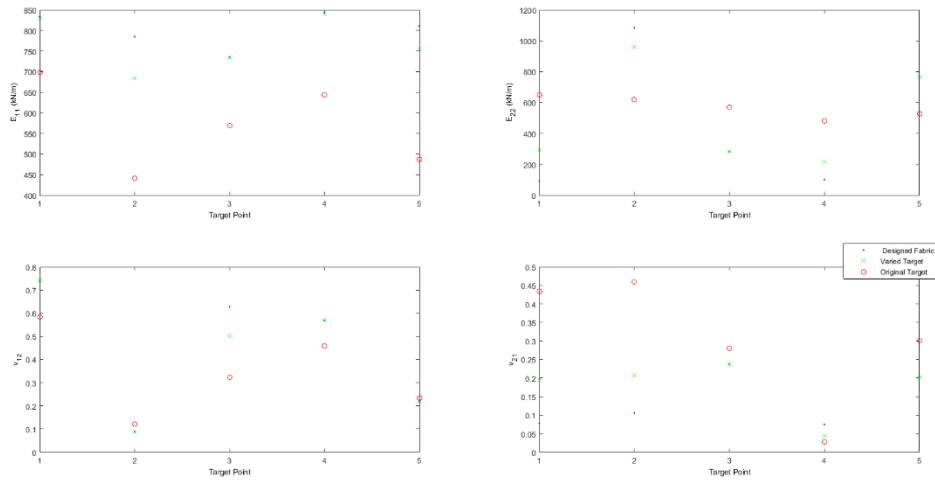
d)



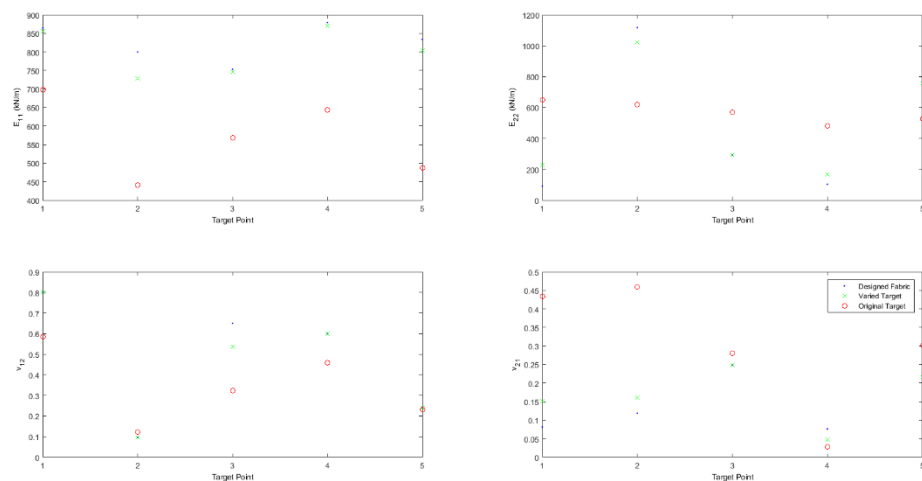
e)



f)



g)



h)

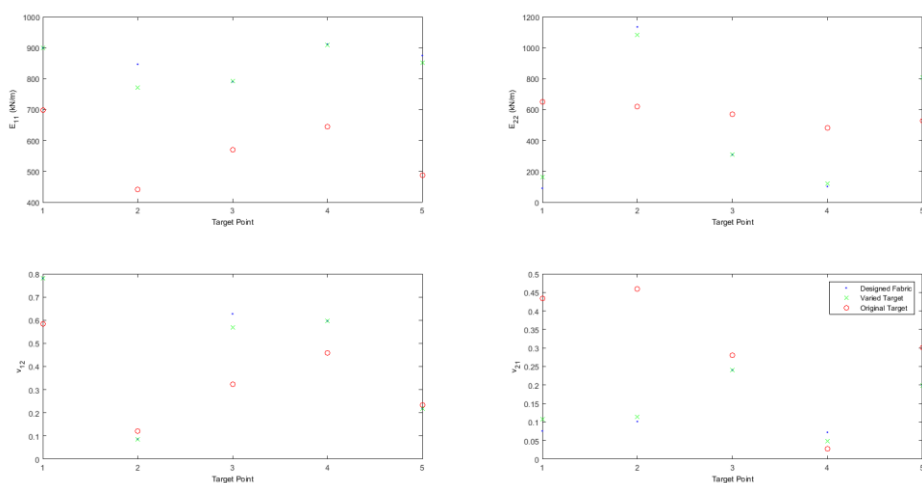


Figure A-8: Variable target optimisation for biaxial targets from a F702 fabric. a) 5% variation, b) 15% variation, c) 25% variation, d) 35% variation, e) 45% variation, f) 55% variation, g) 65% variation, h) 75% variation.

A. 6. Appendix F: Spring and Arm case formula derivations

Considering the deformation of triangle ABE (Equation A-1) with inextensible members gives:

$$\frac{L_0}{\cos \theta} = \frac{L_0 + \delta}{\cos \theta'} \quad \text{Equation A-1}$$

Original length BE is equal to the deformed length BE plus the change in length BE (Δ):

$$L_0 \tan \theta = \Delta + (L_0 + \delta) \tan \theta' \quad \text{Equation A-2}$$

By substituting in the equation for 'k' (Equation A-14), and considering the vertical resultant force at B the deflection of the spring (Δ) can then be written as:

$$L_0 \tan \theta = \Delta + (L_0 + \delta) \tan \theta' = \frac{F \tan \theta'}{k} + (L_0 + \delta) \tan \theta' \quad \text{Equation A-3}$$

$$\Delta = \frac{F_{\text{vertical at B}}}{k} \quad \text{Equation A-4}$$

The displacement of the system to the load can now be calculated as follows:

If a right angled triangle exists then Pythagoras holds.

The length of the hypotenuse is unchanged between the loaded and unloaded case. Thus for the initial situation:

$$\left(\frac{L_0 + \delta}{\cos \theta'} \right)^2 = \left(\frac{F \tan \theta'}{k} + (L_0 + \delta) \tan \theta' \right)^2 + (L_0)^2$$

*Note all $F = f(\theta', \delta)$

Equation A-5

Hence:

$$F = \frac{k}{\tan \theta'} \left[\left(\frac{\delta + L_0}{\cos \theta'} \right)^2 - L_0^2 \right]^{0.5} - k(\delta + L_0)$$

Equation A-6

And it follows that:

$$\theta' = \cos^{-1} \left(\frac{(L_0 + \delta) \cos \theta}{L_0} \right) \quad \text{Equation A-7}$$

Thus the Derivatives can be calculated:

$$\frac{dF}{d\delta} = \frac{\partial F}{\partial \delta} + \frac{\partial F}{\partial \theta'} \cdot \frac{\partial \theta'}{\partial \delta} \quad \text{Equation A-8}$$

Considering the partial derivative of F (Equation A-6) with respect to δ gives:

$$\frac{\partial F}{\partial \delta} = \frac{k \cdot (2L_0 + 2\delta)}{2Q \cdot \cos^2 \theta' \cdot \tan \theta'} \quad \text{Equation A-9}$$

And similarly the partial derivative of F (Equation A-10) with respect to θ' gives:

$$\frac{\partial F}{\partial \theta'} = \frac{k \cdot \sin \theta' \cdot (L_0 + \delta)^2}{Q \cdot \tan \theta'} - \frac{k \cdot Q \cdot (\tan^2 \theta' + 1)}{\tan^2 \theta'} \quad \text{Equation A-10}$$

Where 'Q' is equal to the square route of the 'hypotenuse' minus the 'adjacent' or the distance BE (Equation A-11):

$$Q = \left(\left(\frac{\delta + L_0}{\cos \theta'} \right)^2 - L_0^2 \right)^{0.5} \quad \text{Equation A-11}$$

And similarly the partial derivative of θ' (Equation A-12) with respect F to gives:

$$\frac{\partial \theta'}{\partial \delta} = \frac{(-) \cos \theta}{L_0 \left(1 - \left(\frac{\cos^2 \theta (L_0 + \delta)^2}{L_0^2} \right) \right)^{0.5}} \quad \text{Equation A-12}$$

Therefore the full derivative of the force with respect to the deformation is:

$$\begin{aligned} \frac{dF}{d\delta} &= \frac{\partial F}{\partial \delta} + \frac{\partial F}{\partial \theta'} \cdot \frac{\partial \theta'}{\partial \delta} = \\ &= \frac{\left[\cos \theta \left\{ \frac{k(\tan^2 \theta' + 1) \cdot Q}{\tan^2 \theta'} - \frac{k \sin \theta' (L_0 + \delta)^2}{\cos^3 \theta' \tan \theta' \left(1 - \left(\frac{\cos^2 \theta (L_0 + \delta)^2}{L_0^2} \right) \right)^{0.5}} \right\} \right]}{\left[L_0 \left(\frac{1 - (\cos^2 \theta' (L_0 + \delta)^2)}{L_0^2} \right)^{0.5} \right]} + \frac{k(2L_0 + 2\delta)}{(2 \cos^2 \theta' \tan \theta' \cdot Q)} - k \end{aligned} \quad \text{Equation A-13}$$

$$k = \frac{E \cdot A}{L_{y0}} \quad \text{Equation A-14}$$

Where E and A are the spring constants and L_{y0} is the initial length of the spring between D and B.

A. 7. Appendix G: Spring and Arm case method and validation

A.7.1. Spring and arm method

The validity of the method using the derived equation is demonstrated by solving the equations within MATLAB (Mathworks, 2012b) for an initial geometry and comparing calculated derivatives to results calculated using a central finite difference method (Figure A-9).

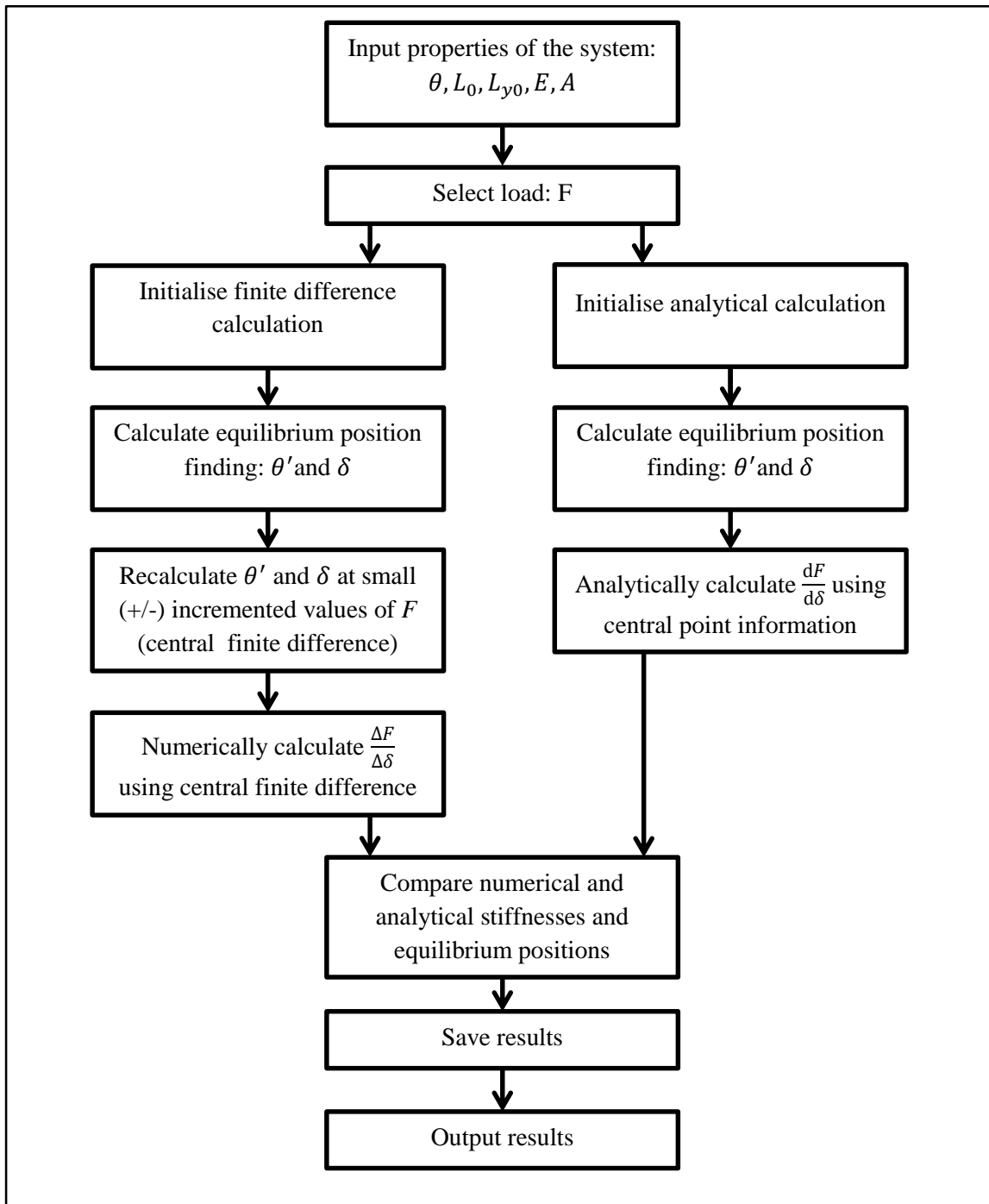


Figure A-9: Flow chart for validation of 'spring and arm model'

The result obtained using this method are discussed below (§A.7.2). This methodology is the foundation for the comparisons between the inverse model and sawtooth model presented in this report where multiple stress states are compared using finite difference calculations.

A.7.2. Spring and arm model validation

For the validation of the derivative arbitrary values were chosen for the initial geometry, though the initial angle (θ) and Length (L_0) which were chosen to allow for a sufficient deflection to occur (1.5% of the original length). The maximum load was chosen after an incremental increase in load was applied to the model for which the selected value produced an accurate maximum displacement to three decimal places. One thousand individual points were tested between the minimum and maximum load (giving 1002 points).

The analytical model's calculation of $dF/d\delta$ shows excellent correlation with data obtained numerically using the central finite difference calculation (Figure A-11).

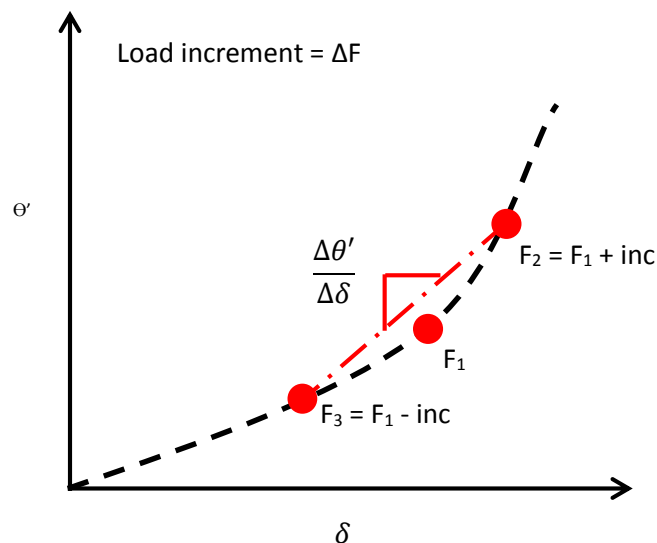


Figure A-10: Central Finite Difference method as used in the simple sawtooth

The accuracy of the derivative calculation $dF/d\delta$ (or the stiffness of the model) is verified by comparison to the finite difference calculations (Figure A-11). The displacement approaches an asymptote of 0.108 (Figure A-11-A) as can be predicted from the original length and angle (Equation A-15):

$$\delta_{max} = \frac{L_0}{\cos \theta} - L_0$$

$$7.1079 - 7 \approx 0.108 = \delta_{max}$$

This demonstrates that the model is accurately calculating the maximum displacement.

Percentage errors are low (order $\times 10^{-4}$), however the error grows rapidly as the force approaches the maximum (Figure A-11-B). At very high loads the increment used to calculate the finite difference becomes far smaller in comparison to the force applied, creating rounding errors and errors in the calculation of the numerically calculated stiffness value. This is compounded by the very small displacements that are being compared to very large forces introducing further errors (i.e. a very large number divided by a very small number). This is an example of how this model has informed the more complex models used later on, in future models calculations of finite difference use a varying factor to ensure this does not occur. The error that occurs due to this follows the same pattern as the percentage error, resulting in larger errors at high loads (Figure A-11-D).

The linear $y=x$ relationship demonstrates that the analytical and numerical calculations of the stiffness are in fact equal (Figure A-11-C). The small percentage error is not noticeable as a deviation from this relationship.

Initially it was hypothesised that the second term in the calculation of the full derivative ($\partial F / \partial \theta' \cdot \partial \theta' / \partial \delta$) might have a minimal impact on the calculated result, and might therefore be excluded from the final calculation of the stiffness. If this applied to 'spring and arm' case model it may also have applied to the sawtooth model, and would have meant that the calculation of the derivative would have been quicker, and less computationally expensive. The results show that without the second term the calculated derivative would be two orders of magnitude away from the correct value at the highest applied load (Figure A-12). The maximum error is calculated to be 7.6×10^{07} and as such the hypothesis was disproved, and all partial terms will be investigated in the inverse sawtooth modelling.

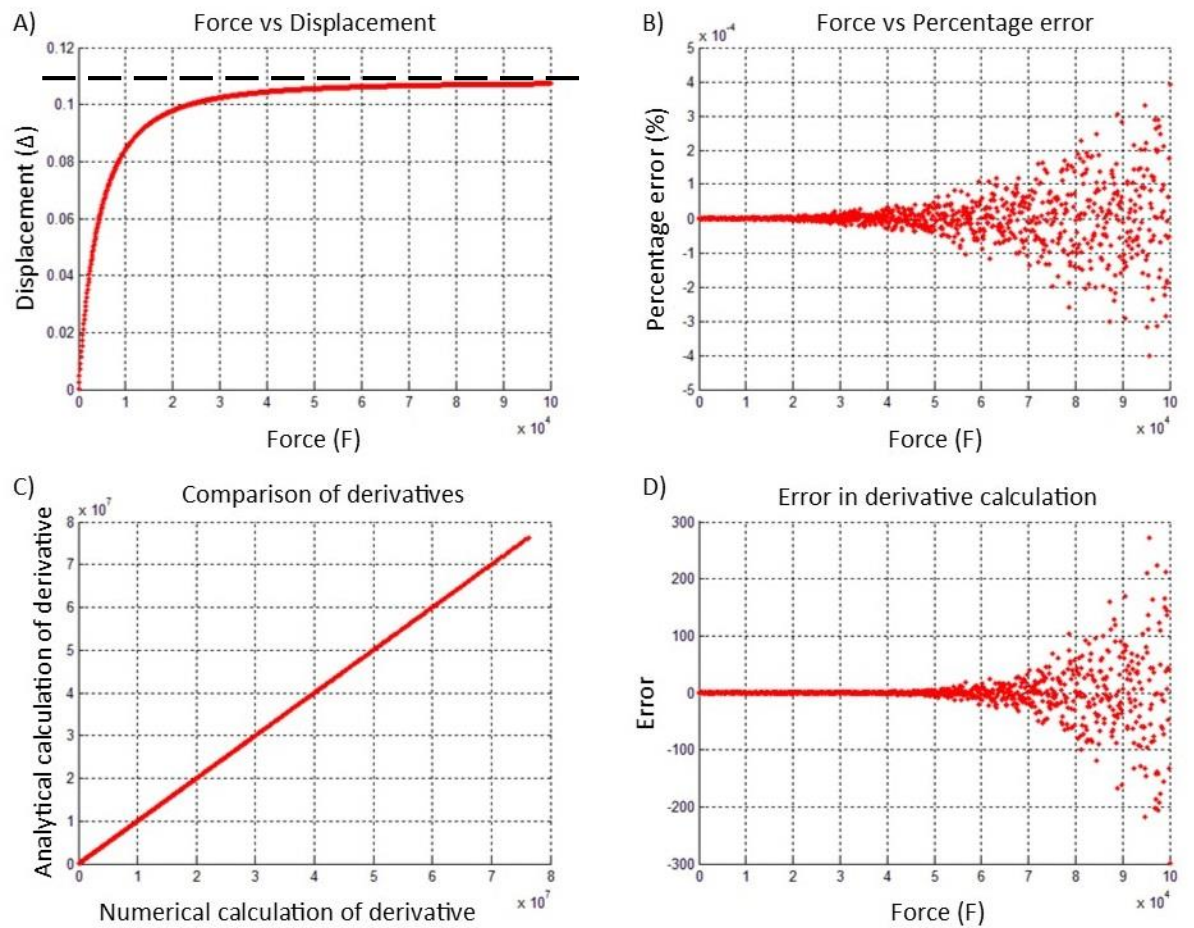


Figure A-11: Results of verification test on the 'spring and arm' case. A) Force vs Displacement with the asymptote at 0.108. B) Force vs Percentage error. C) Comparison of derivatives. D) Error in derivative calculation

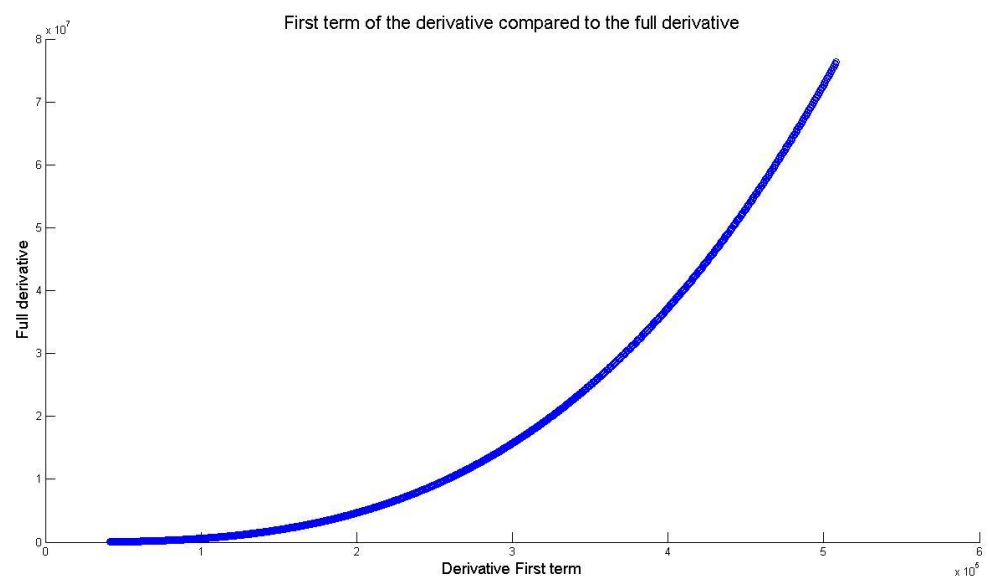


Figure A-12: Comparison of the full derivative to the first term of the derivative

Term	Input value (no units)	Description
F_{\max}	100000	The maximum value of force applied
F_{\min}	0	The minimum value of force applied
ΔF	0.01	The increment applied to F for finite difference calculations
Points	1002	The number of values of force tested
F_{inc}	100	The change in the force between test points
k	1250	The spring constant
θ	$\pi/18^{\circ}$	The angle between the bar and the x-axis
L_0	7	Half the initial length between the two rollers

Table A-5: Input data used to obtain the results in Figure A-11

A. 8. Appendix H: Simple sawtooth derivations

The derivation of a single formula that relates the force applied (F) to the out of plane angle ($\theta'_{1,2}$) and strain ($\varepsilon_{2,1}$):

$$a) \quad F_{1,2} = f(F_{2,1}, r_1, r_2, L_{1,2}, L_{2,1}, \varepsilon_{1,2}, \varepsilon_{2,1}, \theta'_{1,2})$$

$$b) \quad (r_1 + r_2) - (A_1 + A_2) = 0$$

$$c) \quad A_{1,2} = (L_{1,2} + \delta_{1,2}) \tan \theta'_{1,2}$$

$$d) \quad F_{c1} - F_{c2} = 0$$

$$e) \quad F_{c1,2} = F_{1,2} \tan \theta'_{1,2}$$

Substituting e) into d) and rearranging gives f).

$$f) \quad \frac{F_1 \tan \theta'_1}{F_2} = \tan \theta'_2$$

Substituting b) into c) gives g).

$$g) \quad \tan \theta'_2 = \frac{(r_1 + r_2) - (L_1 + \delta_1) \tan \theta'_1}{(L_2 + \delta_2)}$$

And substituting f) into g) gives a formulation for $F_{1,2}$ including no opposite yarn angle.

$$h) \quad 1 = \frac{F_2((r_1 + r_2) - (L_1 + \delta_1) \tan \theta'_1)}{(L_2 + \delta_2) F_1 \tan \theta'_1}$$

$$i) \quad F_1 = \frac{F_2((r_1 + r_2) - (L_1 + \delta_1) \tan \theta'_1)}{(L_2 + \delta_2) \tan \theta'_1}$$

$$j) \quad \delta_{1,2} = \varepsilon_{1,2} \cdot L_{1,2}$$

Finally substituting the displacement for the strain gives k)

$$k) \quad F_{1,2} = \frac{F_{2,1}((r_1 + r_2) - (L_{1,2} + (\varepsilon_{1,2} \cdot L_{1,2}))) \tan \theta'_{1,2}}{(L_{2,1} + (\varepsilon_{2,1} \cdot L_{2,1})) \tan \theta'_{1,2}}$$

Equation A-16

Once this has been achieved it is necessary to show that $\theta'_{1,2}$ can be defined in terms of only initial geometry and strain, as shown below (Equation A-17):

$$l) \quad \theta'_{1,2} = f(L_{1,2}, \varepsilon_{1,2}, \theta_{1,2})$$

$$m) \quad Y_{1,2} = \text{constant} = \frac{L_{1,2}}{\cos \theta_{1,2}} = \frac{L_{1,2} + \delta_{1,2}}{\cos \theta'_{1,2}}$$

Rearranging m) and replacing the displacement with the strain (j) gives a definition of the new yarn angle in terms of only the strain and original unit cell geometry.

$$n) \quad \theta'_{1,2} = \cos^{-1} \left(\frac{(L_{1,2} + (\varepsilon_{1,2} \cdot L_{1,2})) \cos \theta_{1,2}}{L_{1,2}} \right) = f(\varepsilon_{1,2})$$

Equation A-17

Finally it is necessary to show that $\varepsilon_{2,1}$ can be defined in terms of only initial geometry and $\varepsilon_{1,2}$ (Equation A-18).

The strain must be written as a function of original geometry and the

o) strain in the opposite direction.

$$\varepsilon_{2,1} = f(L_{1,2}, L_{2,1}, \varepsilon_{1,2}, \theta_{1,2}, \theta_{2,1})$$

Substituting c) into b) gives p).

$$p) \quad (r_1 + r_2) - (L_1 + \delta_1) \tan \theta'_{1,2} = (L_2 + \delta_2) \tan \theta'_{2,1} = \frac{(L_2 + \delta_2) \sin \theta'_{2,1}}{\cos \theta'_{2,1}}$$

And substituting m) into p) gives q).

$$q) \quad (r_1 + r_2) - (L_1 + \delta_1) \tan \theta'_{1,2} = \frac{L_2 \sin \theta'_{2,1}}{\cos \theta_{2,1}}$$

Rearranging q) gives:

$$r) \quad \frac{((r_1 + r_2) - (L_1 + \delta_1) \tan \theta'_{1,2}) \cos \theta_{2,1}}{L_2} = \sin \theta'_{2,1}$$

Which rearranged gives:

s)

$$\sin^{-1} \left(\frac{((r_1 + r_2) - (L_1 + \delta_1) \tan \theta'_1) \cos \theta_2}{L_2} \right) = \theta'_2$$

And further rearranging the first two components of p) gives:

$$\theta'_2 = \cos^{-1} \left(\frac{(L_2 + (\varepsilon_2 \cdot L_2)) \cos \theta_2}{L_2} \right)$$

t)

Making s) equal to t) and rearranging gives strain in terms of the original geometry and the out of plane yarn angle.

u) $\varepsilon_{2,1} =$

$$\frac{\cos \left(\sin^{-1} \left(\frac{((r_1 + r_2) - (L_{1,2} + (\varepsilon_{1,2} \cdot L_{1,2})) \tan(\theta'_{1,2})) \cos \theta_{1,2}}{L_{2,1}} \right) \right)}{\cos \theta_{2,1}} - 1 \quad \text{Equation A-18}$$

With the above equations it is possible to produce the derivatives $dF_{1,2}/d\varepsilon_{1,2}$ and $dF_{1,2}/d\varepsilon_{2,1}$, which can then be used to optimise a set of initial geometries for a set of targets. The derivatives are shown below:

$$\frac{dF_1}{d\varepsilon_1} = \frac{\cos \theta_1 \left(\frac{F_2 a (\tan^2 \theta'_1 + 1)}{b \tan \theta'_1} + \frac{F_2 (\tan^2 \theta'_1 + 1) (r_1 + r_2 - a \tan \theta'_1)}{b \tan^2 \theta'_1} \right)}{c} - \frac{F_2 L_1}{b} + \frac{F_2 a \cos \theta_1 \cos \theta_2 (r_1 + r_2 - a \tan \theta'_1) * \left(r_1 + r_2 - \frac{L_1 c}{\cos \theta_1} \right)}{L_2 c b^2 e \tan \theta'_1} \quad \text{Equation A-19}$$

$$\frac{dF_2}{d\varepsilon_2} = \frac{\cos \theta_2 \left(\frac{F_1 b (\tan^2 \theta'_2 + 1)}{a \tan \theta'_2} + \frac{F_1 (\tan^2 \theta'_2 + 1) (r_1 + r_2 - b \tan \theta'_2)}{a \tan^2 \theta'_2} \right)}{d} - \frac{F_1 L_2}{a} + \frac{F_1 b \cos \theta_1 \cos \theta_2 (r_1 + r_2 - b \tan \theta'_2) \left(r_1 + r_2 - \frac{L_2 d}{\cos \theta_2} \right)}{L_1 d a^2 f \tan \theta'_2} \quad \text{Equation A-20}$$

$$\frac{dF_2}{d\varepsilon_1} = \frac{F_1 \cos \theta_1 \cos \theta_2 \left(r_1 + r_2 - \frac{L_1 c}{\cos \theta_1} \right)}{L_2 c e} - \frac{F_1 L_1 (r_1 + r_2 - b \tan \theta'_2)}{a^2 \tan \theta'_2} -$$

$$\frac{a \cos \theta_1 \cos^2 \theta_2 \left(\frac{F_1 b (\tan^2 \theta'_2 + 1)}{a \tan \theta'_2} + \frac{F_1 (\tan^2 \theta'_2 + 1) (r_1 + r_2 - b \tan \theta'_2)}{a \tan^2 \theta'_2} \right) \left(r_1 + r_2 - \frac{L_1 c}{\cos \theta_1} \right)}{L_2^2 c e \left(1 - \frac{\cos^2 \theta_2 \left(L_2 - \frac{L_2 \cos \theta_2 - L_2 e}{\cos \theta_2} \right)^2}{L_2^2} \right)^{\frac{1}{2}}}$$

Equation A-21

$$\frac{dF_1}{d\varepsilon_2} = \frac{F_2 \cos \theta_1 \cos \theta_2 \left(r_1 + r_2 - \frac{L_2 d}{\cos \theta_2} \right)}{L_1 d f} - \frac{F_2 L_2 (r_1 + r_2 - a \tan \theta'_1)}{b^2 \tan \theta'_1} -$$

$$\frac{\cos^2 \theta_1 \cos \theta_2 b \left(\frac{F_2 a (\tan^2 \theta'_1 + 1)}{b \tan \theta'_1} + \frac{F_2 (\tan^2 \theta'_1 + 1) (r_1 + r_2 - a \tan \theta'_1)}{b \tan^2 \theta'_1} \right) \left(r_1 + r_2 - \frac{L_2 d}{\cos \theta_2} \right)}{L_1^2 d f \left(1 - \frac{\cos^2 \theta_1 \left(L_1 - \frac{L_1 \cos \theta_1 - L_1 f}{\cos \theta_1} \right)^2}{L_1^2} \right)^{\frac{1}{2}}}$$

Equation A-22

Where the values a, b, c, d, e, and f are calculated separately (Equation A-23, Equation A-24, Equation A-25, Equation A-26, Equation A-27, and Equation A-28 respectively).

$$a = (L_1 + L_1 \varepsilon_1)$$

Equation A-23

$$b = (L_2 + L_2 \varepsilon_2)$$

Equation A-24

$$c = \left(1 - \frac{a^2 \cos^2 \theta_1}{L_1^2} \right)^{\frac{1}{2}}$$

Equation A-25

$$d = \left(1 - \frac{b^2 \cos^2 \theta_2}{L_2^2} \right)^{\frac{1}{2}}$$

Equation A-26

$$e = \left(1 - \frac{\cos^2 \theta_2 \left(r_1 + r_2 - \frac{L_1 c}{\cos \theta_1} \right)^2}{L_2^2} \right)^{\frac{1}{2}}$$

Equation A-27

$$f = \left(1 - \frac{\cos^2 \theta_1 \left(r_1 + r_2 - \frac{L_2 d}{\cos \theta_2} \right)^2}{L_1^2} \right)^{\frac{1}{2}}$$

Equation A-28

A. 9. Appendix I: Derivation of Shear Stress

$$a) \quad M_S = F_{S1}L'_2 \cos \gamma + F_{S2}L'_1 \cos \gamma = M_K + M_F$$

Dividing a) by the cosine of the shear angle gives:

$$b) \quad F_{S1}L'_2 + F_{S2}L'_1 = \frac{M_K + M_F}{\cos \gamma}$$

Shear stress is constant on both edges:

$$c) \quad \tau_1 = \tau_2 = \tau_S$$

And therefore can be rewritten in terms of shear force

$$d) \quad \tau = \frac{F_{S1}}{2L'_2} = \frac{F_{S2}}{2L'_1}$$

Rearranging the last two parts of d) produces e)

$$e) \quad F_{S2} = \frac{F_{S1}L'_1}{L'_2}$$

And the shear force in the opposite direction can be calculated by rearranging b).

$$f) \quad F_{S1} = \frac{M_K + M_F}{\left(L'_2 + \frac{(L'_1)^2}{L'_2}\right) \cos \gamma}$$

$$g) \quad \tau_S = \frac{F_{S1}}{2L'_2}$$

Equation A-29

Lastly it is necessary to calculate the shear modulus (Equation A-30).

$$G_S = \frac{\tau_S}{\gamma_S}$$

Equation A-30

A. 10. Appendix J: Stress and strain minimisation equations

Constrained strain minimisation:

$$M = \begin{bmatrix} \sum_{i=1}^n 2\sigma_x^2 & \sum_{i=1}^n 2\sigma_x\sigma_y & 0 \\ \sum_{i=1}^n 2\sigma_x\sigma_y & \sum_{i=1}^n 2(\sigma_x^2 + \sigma_y^2) & \sum_{i=1}^n 2\sigma_x\sigma_y \\ 0 & \sum_{i=1}^n 2\sigma_x\sigma_y & \sum_{i=1}^n 2\sigma_y^2 \end{bmatrix}$$

Equation A-31

$$N = \begin{bmatrix} \sum_{i=1}^n 2\sigma_x\epsilon_x \\ \sum_{i=1}^n 2(\sigma_x\epsilon_y + \sigma_y\epsilon_x) \\ \sum_{i=1}^n 2\sigma_y\epsilon_y \end{bmatrix}$$

Equation A-32

$$E = M^{-1} \cdot N$$

$$E_x = \frac{1}{E(1)}$$

$$E_y = \frac{1}{E(3)}$$

$$v_{xy} = -\frac{E(2)}{E(1)}$$

$$v_{yx} = -\frac{E(2)}{E(3)}$$

Equation A-33

$$R^2 = 1 - \frac{UV}{TV} = \frac{\sum_{i=1}^n (\epsilon_i - \hat{\epsilon}_i)^2}{\sum_{i=1}^n (\epsilon_i - \bar{\epsilon})^2}$$

Equation A-34

Unconstrained strain minimisation:

$$M = \begin{bmatrix} \sum_{i=1}^n 2\sigma_x^2 & 0 & \sum_{i=1}^n 2\sigma_x\sigma_y & 0 \\ 0 & \sum_{i=1}^n 2\sigma_x^2 & 0 & \sum_{i=1}^n 2\sigma_x\sigma_y \\ \sum_{i=1}^n 2\sigma_x\sigma_y & 0 & \sum_{i=1}^n 2\sigma_y^2 & 0 \\ 0 & \sum_{i=1}^n 2\sigma_x\sigma_y & 0 & \sum_{i=1}^n 2\sigma_y^2 \end{bmatrix}$$

Equation A-35

$$N = \begin{pmatrix} \sum_{i=1}^n 2\sigma_x\epsilon_x \\ \sum_{i=1}^n 2\sigma_x\epsilon_y \\ \sum_{i=1}^n 2\sigma_y\epsilon_x \\ \sum_{i=1}^n 2\sigma_y\epsilon_y \end{pmatrix}$$

Equation A-36

$$\mathbf{E} = \mathbf{M}^{-1} \cdot \mathbf{N}$$

$$E_x = \frac{1}{\mathbf{E}(1)}$$

$$E_y = \frac{1}{\mathbf{E}(4)}$$

$$\nu_{xy} = -\frac{\mathbf{E}(2)}{E_x}$$

$$\nu_{yx} = -\frac{\mathbf{E}(3)}{E_y}$$

Equation A-37

Constrained stress minimisation:

$$M = \begin{bmatrix} \sum_{i=1}^n 2\varepsilon_x^2 & \sum_{i=1}^n 2\varepsilon_x\varepsilon_y & 0 \\ \sum_{i=1}^n 2\varepsilon_x\varepsilon_y & \sum_{i=1}^n 2(\varepsilon_x^2 + \varepsilon_y^2) & \sum_{i=1}^n 2\varepsilon_x\varepsilon_y \\ 0 & \sum_{i=1}^n 2\varepsilon_x\varepsilon_y & \sum_{i=1}^n 2\varepsilon_y^2 \end{bmatrix}$$

Equation A-38

$$N = \begin{pmatrix} \sum_{i=1}^n 2\sigma_x\varepsilon_x \\ \sum_{i=1}^n 2(\varepsilon_x\sigma_y + \varepsilon_y\sigma_x) \\ \sum_{i=1}^n 2\sigma_y\varepsilon_y \end{pmatrix}$$

Equation A-39

$$\mathbf{E} = \mathbf{M}^{-1} \cdot \mathbf{N}$$

$$v_{xy} = \frac{\mathbf{E}(2)}{\mathbf{E}(1)}$$

$$v_{yx} = \frac{\mathbf{E}(2)}{\mathbf{E}(3)}$$

$$V = (1 - v_{xy}v_{yx})$$

$$E_x = \mathbf{E}(1) \cdot V$$

$$E_y = \mathbf{E}(3) \cdot V$$

Equation A-40

Unconstrained stress minimisation:

$$M = \begin{bmatrix} \sum_{i=1}^n 2\varepsilon_x^2 & 0 & \sum_{i=1}^n 2\varepsilon_x\varepsilon_y & 0 \\ 0 & \sum_{i=1}^n 2\varepsilon_x^2 & 0 & \sum_{i=1}^n 2\varepsilon_x\varepsilon_y \\ \sum_{i=1}^n 2\varepsilon_x\varepsilon_y & 0 & \sum_{i=1}^n 2\varepsilon_y^2 & 0 \\ 0 & \sum_{i=1}^n 2\varepsilon_x\varepsilon_y & 0 & \sum_{i=1}^n 2\varepsilon_y^2 \end{bmatrix}$$

Equation A-41

$$N = \begin{pmatrix} \sum_{i=1}^n 2\sigma_x\varepsilon_x \\ \sum_{i=1}^n 2\sigma_y\varepsilon_x \\ \sum_{i=1}^n 2\sigma_x\varepsilon_y \\ \sum_{i=1}^n 2\sigma_y\varepsilon_y \end{pmatrix}$$

Equation A-42

$$\mathbf{E} = \mathbf{M}^{-1} \cdot \mathbf{N}$$

$$\nu_{xy} = \frac{\mathbf{E}(2)}{\mathbf{E}(1)}$$

$$\nu_{yx} = \frac{\mathbf{E}(3)}{\mathbf{E}(4)}$$

$$V = (1 - \nu_{xy}\nu_{yx})$$

$$E_x = \mathbf{E}(1) \cdot V$$

$$E_y = \mathbf{E}(4) \cdot V$$

Equation A-43

Ref	Description	Notes
D2256/D2256M 9.3	<p>Yarn preparation:</p> <p>Yarn Stripping is unnecessary as yarn is from a spool. Remove the initial 1000mm to ensure yarn is fresh and unspoil.</p> <p>Cut yarn to length of 430mm (250mm + distance in contact with clamps [2 x 90mm]).</p>	length in clamps calculated as (380-200)/2
D2591-07 D2256/D2256M – 10.1.	<p>Yarn linear density:</p> <p>The yarn linear density is not needed as it is known. The initial load is calculated in accordance with D2256/D2256M – 10.1 and will be</p> $1100 \text{ dtex} = 110 \text{ tex}$ $110 \text{ tex} \times \frac{0.5cN}{\text{tex}} = 55cN = 0.55N$	
D2256/D2256M 4.2 6.1 10.- 9.2.1 9.2 11.1 12.- 12.2.2 12.4 7.- 13 – 18	<p>Yarn testing for PES yarns:</p> <ol style="list-style-type: none"> 1. Use Configuration A, Condition 1 (straight yarn with moisture content equal to that in the environment) 2. Set up the CRE (continuous rate of extension) machine with reference to 6.1 (recording rate) using clamps with flat faced jaws [Not capstan-, drum-, or snubbing-type clamps]. 3. Results are recorded from head displacements and load recorded from load cells attached to the upper jaw of the INSTRON CRE machine. 4. The test specimen is loaded as per 10.1 (the specimen is handled to avoid damage or change of twist to the sample). 5. The CRE is operated at 100mm/minute as an alternative to a failure at 20s (9.2.1 and 9.1 respectively). As there is no need to compare data to different machines or laboratories at this time the justification for the use of a 20s to failure rate of extension is less important. 100mm/min is used to compare results to uniaxial tests. 6. Test conditions shall be as 11.1 (carried out in ambient air). 7. Initially a test will be carried out with flat faced jaws. If failure occurs repeatedly at jaws as described in '12'. If 24% break at jaws as described in 12.2.2 a new test method shall be considered. 8. Yarn extension shall be measured to three significant figures. 9. Yarns are marked at their contact with the jaws and centre to allow for the observation of 	<p>Head displacements are used to give yarn extensions.</p> <p>NOTE 1</p>

D578/D578M 27.2 EN 13895:2003 5.2	<p>movement within the jaws during the test. This is done using a red marker pen. This is not considered to have had any effect on the test.</p> <p>10.Repeats: 7.3 suggests that 3 specimens be taken for each laboratory sample, however, as there is only one sample available yarns will be taken from both warp and weft directions. 10 useable tests will be made in each direction. A useable test will be a test where failure does not occur at the jaws, and the sample does not slip.</p> <p>11.Calculations of modulus shall be carried out as per 2256/D2256M 13 – 18.</p> <p>Note 1: it is possible that the test specimen improvement method stated in D578/D578M 27.2 could be used to secure the yarns more satisfactorily in flat jaws.</p> <p>Note 2: This specification for testing monofilaments also allows for the use of flat faced clamps where no slippage occurs. (EN 13895:2003)</p>	NOTE 2
--	--	--------

Table A-6: Method of testing virgin yarns (ASTM, 2007; ASTM, 2010; ASTM, 2013a; ASTM, 2013b)

Yarn ravelling methodology:

Ref	Description	Notes
D2256/D2256M 9.3	A fabric sample should be prepared of at least the dimensions in warp/weft of the yarn required. In this instance the dimension must be at least 430mm.	
D3883-04	Place bench marks of the required length on the fabric, then ravel several yarns from the cut edge, such that they contain the bench marks. During ravelling the angle between the ravelled yarn and the fabric is kept to the minimum possible to pull the yarn loose, such that the yarn is not damaged. Additionally an effort is made to keep the twist in the yarn that existed prior to ravelling. Pulling of the yarn is carried out with pliers. The section that was gripped in the pliers is always considered to be damaged and removed during cutting. The sample is then cut to 430mm lengths within the bench marks. Due to removal of crimp the yarn is longer than the original bench marks after ravelling.	
	The samples are then secured in a tray, and the type and direction of sample noted. Samples are kept straight and unstrained, and secured using a small	No masking tape ever interacts

	quantity of masking tape at the extremities of the sample.	with the central testing area.
--	--	--------------------------------

Table A-7: Method of yarn ravelling

Ravelled yarn test methodology:

Ref	Description	Notes
D2256/D2256M 9.3	Yarn Stripping: Cut fabric to length of 430mm (250mm + distance in contact with clamps [2 x 90mm]). Pull out yarns as per the methodology in Table A-7: Method of yarn ravelling. Following the ravelling cut the sample down again to allow for additional length due to crimp.	Ref: length in clamps calculated as $(380-200)/2$
D2591-07 8.2 9.- 9.6 9.7.1 D2256/D2256M – 10.1.	Yarn Linear Density: Precondition yarns for a minimum 4hrs Calculation method will be invalid with residual coating on yarns, therefore a specimen of 430mm will be weighed as per section 9.6. Again given the variation expected in mass due to coating there is expected to be a difference between the expected nominal densities. Therefore four additional specimens will be measured and the Linear density calculated from the mean. This will be used to calculate the initial load used in D2256/D2256M – 10.1.	Linear density was not calculated as it was deemed unnecessary for the purposes of this model
D2256/D2256M 4.2 6.1 10.- 9.2.1 9.2 11.1 12.- 12.2.2 12.4 7.-	Yarn testing for PET yarns: 1. Using Configuration A, Condition 1 2. Set up CRE machine with reference to 6.1 using clamps with flat faced jaws [Not capstan-, drum-, or snubbing-type clamps]. 3. Results shall be recorded from head displacements and load recorded from load cells attached to the jaws, or if unavailable from the INSTRON recorded load. 4. The test specimen shall be loaded as per 10.1. 5. The CRE shall operate at 100mm/minute as an alternative to a failure at 20s (9.2.1 and 9.1 respectively). As there is no need to compare data to different machines or laboratories at this time the justification for the use of a 20s to failure rate of extension is less important. 100mm/min is used to compare results to uniaxial tests. 6. Test conditions shall be as 11.1 7. Initially a test will be carried out with flat faced jaws. If failure occurs repeatedly at jaws as described in '12', if 24% break at jaws as described in 12.2.2 a new test method shall be considered. 8. Yarn extension shall be measured to three significant figures.	Head displacements and a 50kN load cell are used

13 – 18 D578/D578M 27.2 EN 13895:2003 5.2	<p>9. Yarns were marked at their contact with the jaws and centre to allow for the observation of movement within the jaws using a red marker pen. This is not considered to have had any effect on the test.</p> <p>10.Repeats: 7.3 suggests that 3 specimens be taken for each laboratory sample, however, as there is only one sample available yarns will be taken from both warp and weft direction. 10 useable tests will be made in each direction.</p> <p>11.Calculations of modulus shall be carried out as per 2256/D2256M 13 – 18.</p> <p>Note 1: it is possible that the test specimen improvement method stated in D578/D578M 27.2 could be used to secure the yarns more satisfactorily in flat jaws.</p> <p>Note 2: This specification for testing monofilaments also allows for the use of flat faced clamps where no slippage occurs. (EN 13895:2003)</p>	NOTE 1 NOTE 2
D578/D578M	<p>Yarn testing for Glass yarns:</p> <ol style="list-style-type: none"> 1. After PET testing has been completed it will be evident whether or not flat faced jaws can be used. If this is the case the carry out the test as above, with reference to D578/D578M. 2. If test slips in jaws where another method of clamping has not been used then use the method described in 27.2. 3. Otherwise follow the procedure above. 4. An effort should be made to limit the possibility of inhaling or skin contact with glass-fibres, however, as they are bound in a fibre bundle and impregnated with coating the possible hazard is considered low. 	
	<p>Capstan clamps:</p> <p>Will be unusable as slippage around the clamp will lead to misleading extension characteristics.</p>	
Annex B	<p>Bollard Clamps:</p> <p>A bollard clamp such as that described in annex B may be applicable to problems with clamping.</p>	

Table A-8: Method of yarn (BSI, 2003), (ASTM, 2010), (ASTM, 2007), (ASTM, 2013a), (ASTM, 2013b)